The impact of the liver microenvironment on the immune checkpoint regulator PD-L1 in liver metastasis of pancreatic cancer

Dissertation

zur Erlangung des Doktorgrades
der Mathematisch-Naturwissenschaftlichen Fakultät
der Christian-Albrechts-Universität zu Kiel

Silje Victoria Beckinger

Kiel, 2023

First Reviewer:	Prof. Dr. rer. nat. Susanne Sebens
Second Reviewer:	Prof. Dr. rer. nat. Hinrich Schulenburg
Disputation:	14.09.2023

Preface

Parts of this dissertation have already been published. The respective manuscripts are attached in the appendix.

1. **Beckinger S***, Daunke T*, Aldag L, Krüger S, Heckl S, Wesch D, Schäfer H, Röcken C, Rahn S, Sebens S. Hepatic myofibroblasts exert immunosuppressive effects independent of the immune checkpoint regulator PD-L1 in liver metastasis of pancreatic ductal adenocarcinoma. Front Oncol. 2023 May 3;13. doi:10.3389/FONC.2023.1160824
   *These authors share first authorship.

2. **Group Young Researchers In Inflammatory Carcinogenesis*,** Wandmacher AM, Mehdorn AS, Sebens S. The Heterogeneity of the Tumor Microenvironment as Essential Determinant of Development, Progression and Therapy Response of Pancreatic Cancer. *Cancers (Basel)*. 2021;13(19):4932. Published 2021 Sep 30. doi:10.3390/cancers13194932
   *Group members (in alphabetical order) share first authorship: Aldag L, **Beckinger S**, Daunke T, Philipp LM, Surrow A, Yesilyurt UU

Zusammenfassung

Mit einer 5-Jahres-Überlebensrate von weniger als 5 % ist das duktale Pankreasadenokarzinom (PDAC) eine der tödlichsten bösartigen Erkrankungen. In den meisten Fällen wird das PDAC in einem lokal fortgeschrittenen oder metastasierten Stadium diagnostiziert, wobei die Leber das Hauptorgan der Metastasierung darstellt und hepatische Myofibroblasten (HMF) eine zentrale Rolle spielen. Da PDAC Patient*innen mit Lebermetastasen eine noch schlechtere Prognose aufweisen, ist es wichtig, die Mechanismen, die der Metastasierung in der Leber unterliegen, besser zu verstehen und wirksame Behandlungsmöglichkeiten zu entwickeln. Die Behandlung mit Immun-Checkpoint-Inhibitoren, die z. B. *programmed cell death ligand 1* (PD-L1) oder den Rezeptor *programmed cell death protein 1* (PD-1) blockieren, hat die Therapie von vielen Krebsarten revolutioniert, allerdings noch nicht beim PDAC. Ob und wie sich die PD-L1-Expression auf die Immunevasion, insbesondere bei Lebermetastasen auswirkt, ist noch wenig bekannt. Ziel dieser Studie war es daher, weitere Erkenntnisse über die Auswirkungen der Mikroumgebung der Leber, insbesondere HMF, auf PDAC Zellen und $CD8^+$ T-Zellen im Zusammenhang mit der Immunevasion zu gewinnen, wobei der Schwerpunkt auf der Rolle von PD-L1 lag.

Immunhistochemische Färbungen von Lebergewebeschnitte von PDAC Patient*innen zeigten, dass die Tumormikroumgebung während des metastatischen Wachstums umstrukturiert wird. HMF stellen eine präsente Stromapopulation in Lebermetastasen dar, mit deutlichen Unterschieden in der räumlichen Verteilung in kleinen ($\leq$ 1500 µm) und großen (> 1500 µm) Metastasen, wobei große Metastasen im Vergleich zu kleinen Metastasen einen höheren Anteil an HMF aufwiesen. Die PD-L1-Expression befand sich hauptsächlich an der Invasionsfront oder war in großen Metastasen gleichmäßig verteilt, während kleine Metastasen entweder keine PD-L1-Expression oder nur eine schwache Expression in der Mitte aufwiesen. Doppelfärbungen zeigten, dass PD-L1 vorwiegend von Stromazellen, insbesondere HMF und Makrophagen, exprimiert wird. Kleine Lebermetastasen ohne oder mit geringer PD-L1-Expression enthielten mehr $CD8^+$ T-Zellen im Tumorzentrum, während große Metastasen mit stärkerer PD-L1 Expression weniger $CD8^+$ T-Zellen enthielten, die sich meist an der Invasionsfront befanden. In 2D Kulturen verstärkten $CD8^+$ T-Zellen die Zelloberflächenexpression von PD-L1 auf humanen Pankreasgangepithelzellen, hepatischen Sternzellen (HSC) und HMF. HSC und HMF steigerten die Aktivierung und den Effektor-Phänotyp von $CD8^+$ T-Zellen, allerdings wurde der Aktvierung- und Effektor-Phänotyp nicht durch die Behandlung mit Durvalumab verstärkt.

In einem 3D-Kultur-Sphäroid-Modell, bei dem zwei verschiedene PDAC Zelllinien mit unterschiedlichen PD-L1 Zelloberflächenexpressionen und unterschiedlichen Verhältnissen von HMF verwendet wurden, wurden der Anteil und die Verteilung von PDAC Zellen und HMF sowie deren PD-L1 Expression in kleinen und großen Leber PDAC Metastasen nachgeahmt. In den mit HMF angereicherten Sphäroiden

nahm die Größe der PDAC-Sphäroide zu, was auf eine verstärkte Proliferation von PancTu1 und Panc89 Zellen hinweist. In Übereinstimmung mit den *in situ* Ergebnissen waren HMF die Hauptquelle der PD-L1 Expression und verstärkten die Zelloberflächenexpression von PD-L1 auf beiden PDAC Zelllinien. HMF beeinträchtigten die Freisetzung von Effektormolekülen durch $CD8^+$ T-Zellen und die Induktion von Zelltod der PDAC Zellen, eine Wirkung, die von der Menge der HMF, aber auch von den PDAC Zellen abhing. Trotz der beträchtlichen PD-L1 und PD-1 Expression in den verschiedenen Sphäroidmodellen führte die Behandlung mit den PD-1 bzw. PD-L1 Inhibitoren Pembrolizumab und Durvalumab zu keiner Verstärkung des Effektor-Phänotyps der $CD8^+$ T-Zellen, was mit dem nicht erhöhten PDAC Zelltod unter beiden Sphäroidbedingungen übereinstimmt. $CD8^+$ T-Zellen, die mit Gemcitabin vorbehandelten, PancTu1 und Panc89 Sphäroiden kokultiviert wurden, wiesen eine geringere Zellexpression von PD-1 und Aktivierungsmarkern auf. Außerdem war die Konzentration der Effektormoleküle in den Überständen der $CD8^+$ T-Zellen verringert. Die Vorbehandlung mit Gemcitabin wirkte sich unterschiedlich auf die Induktion des PDAC Zelltods durch $CD8^+$ T-Zellen aus. In PancTu1 Sphäroiden war die Induktion des Zelltods durch $CD8^+$ T-Zellen beeinträchtigt, insbesondere in HMF-angereicherten PancTu1 Sphäroiden, während in Panc89 Sphäroiden die Induktion des Zelltods verstärkt wurde. Die kombinierte Behandlung mit Gemcitabin und entweder Durvalumab oder Pembrolizumab hatte jedoch keinen Einfluss auf den Effektor-Phänotyp der $CD8^+$ T-Zellen und auf die Induktion des PDAC-Zelltods.

Die Ergebnisse dieser Arbeit weisen auf eine räumliche Umstrukturierung von HMF, $CD8^+$ T-Zellen und PD-L1-Expression während der Progression von PDAC Lebermetastasen hin. Darüber hinaus beeinträchtigen HMF den Effektor-Phänotyp von $CD8^+$ T-Zellen, aber die PD-L1/PD-1-Achse spielt dabei offenbar eine untergeordnete Rolle, was darauf hindeutet, dass die Immunevasion von PDAC Lebermetastasen auf anderen immunsuppressiven Mechanismen beruht.

Summary

With a 5-year survival rate of under 5 %, pancreatic ductal adenocarcinoma (PDAC) is one of the most fatal malignancies. In the European Union, PDAC represents the 4th most common cause of cancer-related deaths. Lacking specific symptoms, PDAC is mostly diagnosed at a locally advanced or metastatic stage, with the liver representing the main site of metastases and hepatic myofibroblasts (HMF) playing a pivotal role in metastatic outgrowth. To date, the only curative treatment is an R0 resection of the primary tumor. Since PDAC patients with liver metastases have an even worse prognosis, it is important to better understand the mechanisms underlying metastatic progression in the liver and to identify effective treatment options. Treatment with immune checkpoint inhibitors, e.g., targeting programmed cell death-ligand 1(PD-L1) or its receptor programmed cell death protein-1 (PD-1), has improved the therapy of many cancers but so far failed in PDAC. However, whether and how PD-L1 expression impacts immune evasion, especially in liver metastases, is still poorly understood, as they are not routinely resected in PDAC patients. Therefore, this study aimed to gain further insights into the impact of the liver microenvironment, particularly of HMF, on PDAC cells and $CD8^+$ T cells in the context of immune evasion, focusing on PD-L1.

Immunohistochemical stainings of liver tissue sections of PDAC patients revealed that the tumor microenvironment is remodeled during metastatic outgrowth. HMF represent an abundant stroma population in liver metastases, with clear differences in the spatial distribution in small (≤ 1500 µm) and large (> 1500 µm) metastases, large metastases showed a higher abundance of myofibroblasts compared to small metastases. PD-L1 expression was mainly located at the invasion front or evenly distributed in large metastases, while small metastases either lacked PD-L1 expression or mostly showed weak expression in the center. Double stainings revealed that PD-L1 is predominantly expressed by stromal cells, especially HMF and macrophages. Small liver metastases with no or low PD-L1 expression comprised more $CD8^+$ T cells in the tumor center, while large metastases exhibiting stronger PD-L1 expression comprised fewer $CD8^+$ T cells being mostly located at the invasion front. In 2 D cultures, $CD8^+$ T cells enhanced the cell surface expression of PD-L1 on pancreatic ductal epithelial cells and hepatic stromal cells. Haptic stromal cells enhanced the activation and the effector phenotype of $CD8^+$ T cells, however, treatment with Durvalumab did not enhance these effects.

In a 3D culture spheroid model using two PDAC cell lines with different PD-L1 cell surface expressions and different ratios of HMF adequately mimicked the proportion and distribution of PDAC cells and HMF as well as their PD-L1 expression observed in small and large hepatic PDAC metastases.

Here, in HMF-enriched spheroids, the size of PDAC spheroids was increased, indicating an enhanced cell growth of PancTu1 and Panc89 cells. In line with the *in situ* findings, HMF were the main source of PD-L1 expression and further enhanced cell surface expression of PD-L1 on both PDAC cell lines. HMF

impaired the release of effector molecules by $CD8^+$ T cells and the induction of PDAC cell death, an effect dependent on the amount of HMF but also of PDAC cells. Despite the considerable PD-L1 and PD-1 expression in the different spheroid models, treatment with PD-1 and PD-L1 inhibitors Pembrolizumab and Durvalumab, respectively, did not boost the effector phenotype of $CD8^+$ T cells in line with not increased PDAC cell death under either spheroid condition. $CD8^+$ T cells cocultured with Gemcitabine pre-treated PancTu1 and Panc89 spheroids showed lower cell surface expression of PD-1 and activation markers. Further, the concentration of effector molecules in the supernatants of $CD8^+$ T cells was reduced. Pre-treatment with Gemcitabine differently affected the induction of PDAC cell death by $CD8^+$ T cells. In PancTu1 spheroids, induction of cell death by $CD8^+$ T cells was impaired, especially in HMF-enriched PancTu1 spheroids, while in Panc89 spheroids cell death induction was enhanced. However, combinational treatment of Gemcitabine and either Durvalumab or Pembrolizumab did not affect the effector phenotype of $CD8^+$ T cells and induction of PDAC cell death. Overall, the findings of this thesis indicate a spatial reorganization of HMF, $CD8^+$ T cells, and PD-L1 expression during progression of PDAC liver metastases. Furthermore, HMF potently impair the effector phenotype of $CD8^+$ T cells but the PD-L1/PD-1 axis apparently plays a minor role in this scenario, suggesting that immune evasion of PDAC liver metastases relies on other immunosuppressive mechanisms.

List of Abbreviations

ABCG2	ATP-binding cassette subfamily G member 2
AC	Activation culture
ANOVA	Analysis of variance
AP-1	Activation protein-1
APC	Allophycocyanin
APCs	Antigen presenting cells
αSMA	α-smooth muscle actin
ATRA	All-trans retinoic acid
BPE	Bovine pituitary extract
BSA	Bovine serum albumin
°C	Degree Celsius
CAF	Cancer-associated fibroblast
CC	Cocultures
ccK18	Caspase-cleaved Keratin 18
CCL	Chemokine (C-C) motif ligand
CD	Cluster of Differentiation
cDNA	Complementary deoxyribonucleic acid
CHMP	Committee for Medicinal Products for Human Use
cm	Centimeter
cm^2	Square centimeter
DAG	Diacylglycerol
CTC	Circulating tumor cell
CTG	CellTracker Green
CTL	Cytotoxic T lymphocyte
CTLA-4	Cytotoxic T lymphocyte-associated protein-4
CTV	CellTrace Violet
CXCL	chemokine (C-X-C motif) ligand
CXCR	chemokine (C-X-C motif) receptor
DC	Dendritic cell
ddH_2O	Double distilled water
DMEM	Dulbecco's Modified Eagle Medium
DMSO	Dimethyl sulfoxide

DNA	Deoxyribonucleic acid
DTC	Disseminated tumor cell
ECM	Extracellular matrix
EDTA	Ethylenediaminetetraacetic acid
EGF	Epidermal Growth Factor
EGFR	Epidermal Growth Factor receptor
EMA	European Medicine Agency
EMT	Epithelial-Mesenchymal-Transition
EpCam	Epithelial cell adhesion molecule
FACS	Fluorescence activated cell sorting
FCS	Fetal calf serum
FFPE	Formalin-fixed and paraffin embedded
FGF	Fibroblast Growth Factor
FITC	Fluorescein isothiocyanate
FoV	Fields of View
FoxP3	Forkhead box protein 3
FSC	Forward scatter
FSP1	Fibroblast-specific protein1
g	Gram
Gamma/delta T cell	γ/δ T cell
GAPDH	Glyceraldehyde 3-phosphate dehydrogenase
G-CSF	Granulocyte-colony stimulating actor
HEPES	4-(2-hydroxyethyl)-1-piperazineethansulfonic acid
hHSteC	Human hepatic stellate cells
HGF	Hepatocyte Growth Factor
HMF	Hepatic myofibroblast
HSC	Hepatic stellate cell
iCAF	Inflammatory cancer-associated fibroblast
ICI	Immune checkpoint inhibitor
IF	Immunofluorescence
IFNγ	Interferon-gamma
IgG	Immunoglobulin G
IHC	Immunohistochemistry
IL	Interleukin

ITAM	Immunoreceptor tyrosine-based activation motif
Itk	Inducible T cell kinase
IPMN	Intraductal papillary mucinous neoplasms
LAT	Linker for activation of T cells
Lck	Lymphocytes protein tyrosine kinase
L-Gln	L-Glutamine
µg	Microgram
µl	Microliter
µm	Micrometer
MACS	Magnetic Cell Sorting
MAM	Metastasis-associated macrophage
MCN	Mucinous cystic neoplasms
M-CSF	Macrophage-colony stimulating factor
MDSC	Myeloid-derived suppressor cell
MFI	Median fluorescence intensity
mg	Milligram
MHC	Major histocompatibility complex
min	Minutes
ml	Milliliter
mM	Millimolar
MMP	Matrix metalloproteinases
MyCAF	Myofibroblastic cancer-associated fibroblast
NFAT	Nuclear factor of activated T cells
NF-κB	Nuclear factor-kappa B
ng	Nanogram
NK cell	Natural killer cell
NSCLC	Non-small cell lung cancer
PanCK	Pan-Cytokeratin
PanIN	Pancreatic intraepithelial neoplasia
PBMC	Peripheral blood mononuclear cell
PBS	Phosphate-buffered saline
PD-1	Programmed cell death protein-1
PDAC	Pancreatic ductal adenocarcinoma
PDEC	Pancreatic ductal epithelial cell

PDGF	Platelet derived growth factor
PD-L1	Programmed cell death-ligand 1
PE	Phycoerythrin
Pe-Cy7	Phycoerythrin-Cyanine7
Pen/Strep	Penicillin and Strepomycin
PFA	Paraformaldehyde
pg	Picogram
PI	Propidium Iodide
PI3-K	Phosphoinositide 3-kinase
PIP_3	Phosphatidylinositol 4,5-trisphosphate
PLC-γ	Phospholipase C-gamma
PSC	Pancreatic stellate cell
qPCR	Quantitative real-time polymerase chain reaction
RNA	Ribonucleic acid
rpm	Rounds per minute
RPMI	Roswell Park Memorial Institute
RT	Room temperature
SD	Standard Deviation
sFas	Soluble Fas
sFasL	Soluble Fas Ligand
SSC	Side scatter
TAM	Tumor-associated macrophage
TCM	T cell medium
TCR	T cell Receptor
TGF-β1	Transforming Growth Factor-Beta 1
T_H	T helper
TIGIT	T cell immunoreceptor with Ig and ITIM domains
TIM3	T cell immunoglobulin and mucin domain-containing protein 3
TNFα	Tumor Necrosis Factor alpha
TME	Tumor microenvironment
T_{Reg}	Regulatory T cell
U	Units
µg	Microgram

UK	United Kingdom
ULA	Ultra-low attachment plates
µm	Micrometer
USA	United States of America
vs	versus
v/v	Volume per volume
VEGF	Vascular Endothelial Growth Factor
xg	Force of gravity
ZAP70	Zeta-chain associated protein kinase 70
2D	Two-dimensional
3D	Three-dimensional

Table of Contents

1 Introduction

1.1 PDAC

1.1.1 Epidemiology

Pancreatic ductal adenocarcinoma (PDAC) is the 14th leading cancer type worldwide. In 2020, the number of new cases was 495,773, representing 2.6 % of all cancer diagnoses. Compared to other types of cancer the incidence rate is low, however, it is on rank 7 in cancer-related deaths worldwide. In 2020, 466,003 patients died of PDAC (4.7 % of all cancer-related deaths), which is nearly as high as the incidence that year. The incidence rate is higher in males compared to females, at 5.7 and 4.1 cases per 100,000 people, respectively [1]. At a 5-year survival rate of under 5 %, PDAC is one of the most fatal malignancies [2]. In the European Union, PDAC represents the 4th most common cause of cancer-related deaths and is estimated to become the 3rd leading cause of cancer-related death, even exceeding breast cancer [3]. Due to unspecific symptoms and a lack of screening methods, 80 % of patients are diagnosed at a locally advanced or metastatic stage [4,5]. To date, the only curative treatment is the R0 resection of the locally restricted primary tumor, which is only possible in a minority of patients. Thus, for most patients, only palliative treatment options remain. However, even the patients undergoing an R0 resection often relapse and develop metastases shortly after or even during adjuvant therapy. The median survival is 17 – 23 months after surgery [6]. If early liver metastasis develops (within 6 months after surgery), the median overall survival is reduced to only 9 months [7].

There are several risk factors known for PDAC. First, the risk of developing PDAC highly increases with age. Most patients are diagnosed between the ages of 60 to 80 years, with half of all patients diagnosed at over 70 years old [8]. Around 10 % of all cases have a hereditary background [4,9], with common hereditary germline mutations in *BRCA1/BRCA2* (hereditary breast and ovarian cancer), *STK11* (Peutz-Jeghers syndrome), and *p16INK4A* (familial atypical multiple mole melanoma syndrome) [4,10,11]. Further, mutations in the gene *PRSS1* (hereditary pancreatitis) increase the risk of developing PDAC. Acute and chronic pancreatitis increases the risk for PDAC, but in many cases also leads to PDAC diagnosis at earlier stages [12,13]. Additionally, lifestyle-associated factors increase the risk for PDAC development, e.g., smoking, heavy alcohol abuse, obesity, and diabetes mellitus [14]. Especially smoking increased the risk by 2.0-fold [15].

1.1.2 Pathology

The pancreas can be divided into an exocrine and an endocrine part. The exocrine part of the pancreas constitutes about 80 % of the cellular organ mass, is composed of acinar and ductal cells, and secrets digestive enzymes into the duodenum. The endocrine part is formed by the islets of Langerhans. The Langerhans islets are composed of different cell types and produce metabolically relevant hormones, which are released into the blood [16]. Over 95 % of all pancreatic tumors arise from the exocrine part and PDAC accounts for 90 % of all pancreatic cancers [17].

PDAC shows a stepwise progression from normal ductal epithelium to duct lesions and finally to invasive ductal adenocarcinoma [18]. During progression, different precursor lesions can be identified: intraductal papillary mucinous neoplasms (IPMN), mucinous cystic neoplasms (MCN), and pancreatic intraepithelial neoplasia (PanIN). PanIN are the most common type among precursor lesions. In 2001, Hruban *et al.* classified the PanIN precursor lesions into three grades according to their epithelial abnormalities. The grades are called PanIN-1A/B, PanIN-2, and PanIN-3 (Figure 1) [19]. The physiological duct epithelium of the pancreas is organized in a flat monolayer and its nuclei show basal localization. PanIN-1A lesions are flat and PanIN-1B lesions are papillary, but their nuclei still show basal localization. PanIN-2 (intermediate grade) show frequent papillae and nuclear atypia, like pleomorphism. Further, hyperplasia is observed. PanIN-3 (high grade), also called *carcinoma in situ,* are characterized by a high grade of hyperplasia, partly multilayer epithelium, and pleomorphisms. PanIN-3 lesions maintain contact with the basement membrane [20]. During the progression of the lesions, multiple genetic alterations, especially in oncogenes and tumor suppressor genes, occur. The earliest genetic alteration, already found in PanIN-1A lesions, is the activation of the *kras* gene. Mutation of the *kras* gene is found in 90 % of PDAC and is essential for PDAC development [20,21]. Further, *HER2/neu* is overexpressed in early lesions [22]. A PDAC mouse model showed that mutation of *kras* and overexpression of *HER2/neu* are necessary for progression [23]. During progression, the tumor suppressor genes *p16 (≈90 %), p53 (≈70 %),* and *SMAD4 (≈ 60 %)* become inactivated [20].

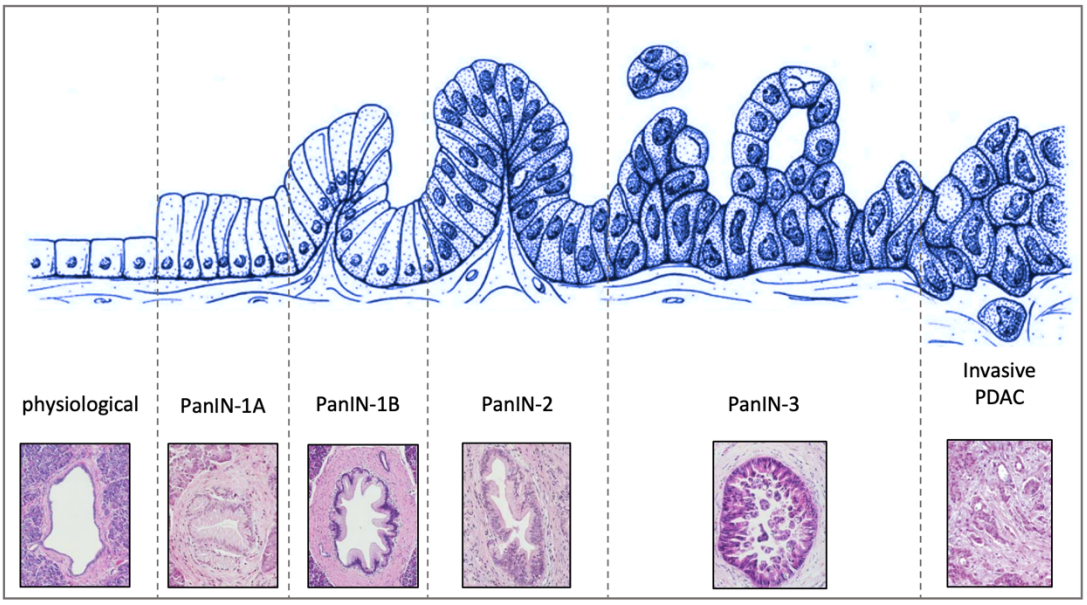

Figure 1: Pancreatic ductal adenocarcinoma (PDAC) shows a stepwise progression from pancreatic intraepithelial neoplasia (PanIN). Schematic illustrations of the different PanIN grades and further presentative images of hematoxylin and eosin staining of PanIN stages and invasive PDAC. Adapted from [24].

1.1.3 Current therapies for PDAC

As mentioned above, achieving an R0 resection is the only curative treatment option for PDAC patients, however, only a minority of patients are eligible for an operation, as the tumor must be locally confined. R0 resection is followed by adjuvant chemotherapy. The selection of the chemotherapeutic drugs depends on the patient's general health condition. If patients are in good health condition, they receive FOLFIRINOX, which is a combination of four different agents (5-Fluorouacil, Leucovorin, Irinotecan, and Oxaliplatin). If the general health condition is reduced, patients receive the cytostatic drug Gemcitabine or 5-Fluorouacil or a combination of Gemcitabine with Capecitabine [25]. FLOFIRINOX as an adjuvant therapy option increases the disease-free survival from 12.8 months to 21.6 months compared to monotreatment with Gemcitabine [26]. However, FLOFIRINOX has more side effects and therefore, most patients still receive Gemcitabine as the standard therapy. Patients with non-resectable PDAC and metastases only receive palliative chemotherapy, which can improve survival and quality of life [27]. Here, different agents alone or in combination are used, depending on the general health condition, progression of the disease, and potential side effects.

Gemcitabine is a nucleoside antimetabolite, which is phosphorylated into triphosphate in the cell. Gemcitabine triphosphate is similar to deoxycytidine and is therefore inserted into the deoxyribonucleic acid (DNA), disrupting the DNA synthesis, and finally causing cell death [28]. However, many patients develop chemoresistance within weeks [29]. The therapeutic options are

quite rare and treatment response is minimal in PDAC patients, therefore it is of outmost importance to investigate underlying drug resistance in order to develop more effective treatment options.

1.2 Tumor stroma

In the last years, the tumor microenvironment (TME) has become of great interest, as it takes an active part during the development and progression of tumors and in their therapy resistance. The PDAC stroma makes up 80 - 90 % of the whole tumor mass [29]. To gain more information about tumor biology and to develop new therapies, it is essential to unravel stromal heterogeneity within the TME and its impact on tumor progression.

The TME consists of immune cells, cancer-associated fibroblasts (CAFs), endothelial cells, and a high amount of extracellular matrix (ECM) molecules (Figure 2).

In the following sections, tumor-associated macrophages (TAMs) will be introduced briefly, and tumor-infiltrating lymphocytes and CAFs in more detail as there are the dominating stromal cell population in PDAC stroma.

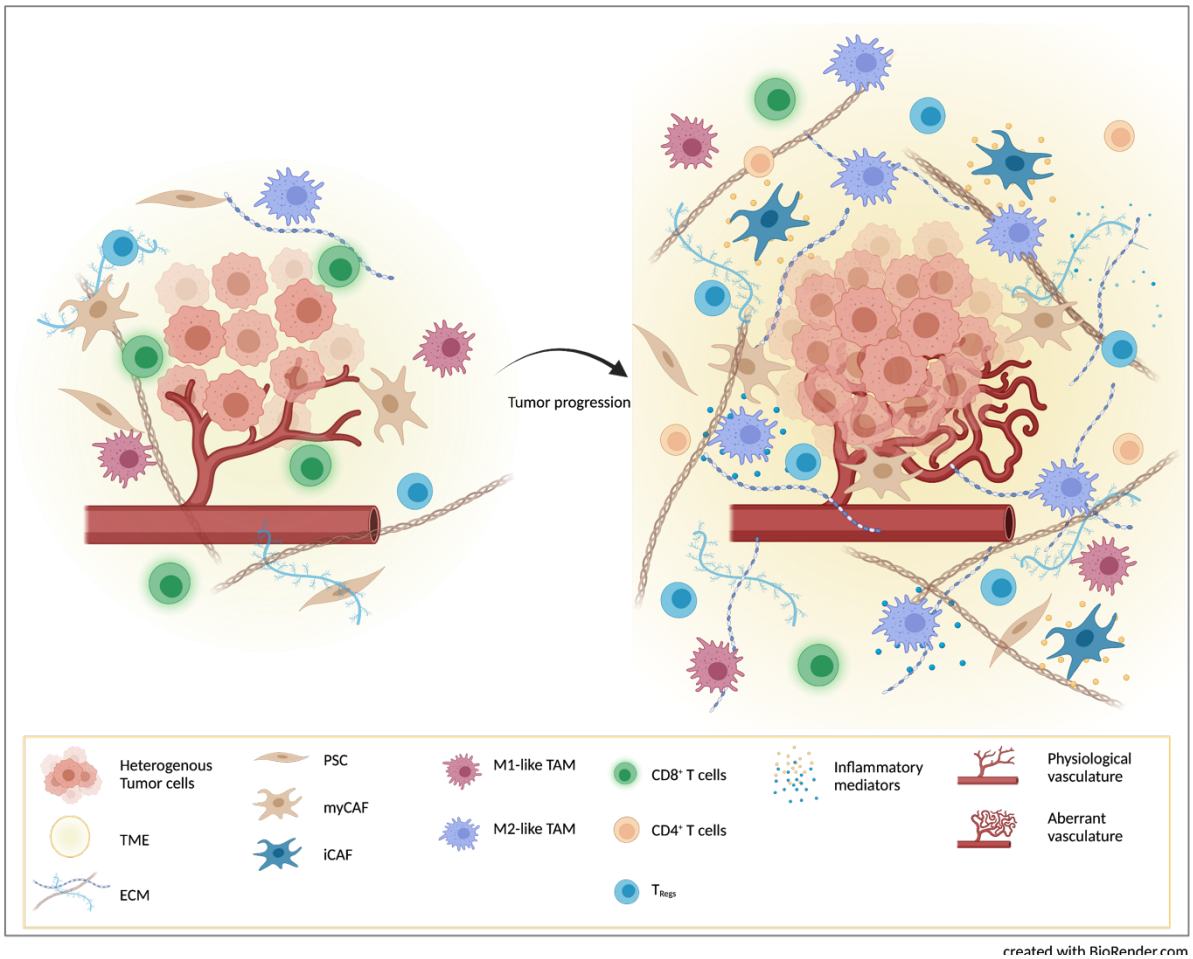

Figure 2: Heterogeneous tumor stroma in pancreatic ductal adenocarcinoma (PDAC). During tumor progression, the tumor microenvironment (TME) undergoes alterations, involving (i) activation of stellate cells and transdifferentiation into carcinoma-associated fibroblasts (CAFs) with different phenotypes (myCAFs, iCAFs), (ii) alteration of the extent and composition of the extracellular matrix (ECM), (iii) enrichment of immunosuppressive and tumor-promoting immune cells, e.g., tumor-associated macrophages (TAMs) with different phenotypes (M1-like TAMs versus M2-like TAMs), cytotoxic T cells (CTLs) and regulatory T cells (T_{Regs}), (iv) formation of new and modified blood vessels. Overall, this TME heterogeneity is an essential driver of PDAC development and progression. Adapted from [30].

1.2.1 Tumor-associated macrophages

Besides CAFs and T lymphocytes, TAMs are also found in high numbers in many tumor entities representing the most abundant leucocyte population in the TME [31], also applying to PDAC [32]. Importantly, in dependence on environmental factors, monocytes/macrophages acquire different phenotypes exerting distinct functional effects. According to a simplified model, macrophages can differentiate into M1-like and M2-like macrophages. While Interferon-gamma (IFNγ) and bacterial lipopolysaccharide promote polarization of pro-inflammatory M1-like macrophages, Interleukin (IL)-4, IL-13, IL-10, and Transforming Growth Factor-beta TGF-β foster an anti-inflammatory M2-like

phenotype [33,34]. Thus, the composition of the TME (e.g., oxygen level, amount and type of other stromal or tumor cells) impacts the phenotype and effector function of macrophages and promotes the switch from one type to another. This process also occurs under physiological conditions. As outlined later, CAFs promote an immunosuppressive environment by recruiting monocytes and promoting the accumulation of M2-polarized macrophages [30].

M1-like macrophages secrete different pro-inflammatory cytokines like IL-12, IL-23, and M2-like macrophages secrete anti-inflammatory cytokines such as IL-10, TGF-β, and Tumor Necrosis Factor alpha (TNFα) to prevent T cells from effectively exerting their anti-tumor functions and further to induce Epithelial-Mesenchymal-Transition (EMT) [30].

TAMs in PDAC predominantly exhibit a M2-like phenotype. These are associated with diverse pro-tumoral effects, including the promotion of tumorigenesis, immunosuppression, metastasis acceleration, and chemotherapeutic resistance [30]. In primary PDAC, a high infiltration of macrophages, particularly $CD163^+$ macrophages (a marker for M2-like macrophages), is observed [32,35], indicating an M2-type which has been associated with a poor prognosis and decreased survival [36].

1.2.2 Cancer-associated fibroblasts

The most abundant inflammatory stromal cells in PDAC are myofibroblasts, also termed CAFs. CAFs are abundant in primary PDAC as well as in metastases, e.g., in the liver [30].

Exposure to stressful conditions, including exogenous toxins, surgical intervention, inflammatory injury, hypoxia, or mediators released by immune cells, promotes the proliferation and activation of pancreatic stellate cells (PSC) in the primary tumor or hepatic stellate cells (HSC) in the liver into myofibroblasts which is associated with increased alpha-smooth muscle actin (αSMA) expression. Stimuli leading to the transdifferentiation and activation of myofibroblasts are TGF-β, Platelet-Derived Growth Factor (PDGF), and IL-6 [30,37,38].

Myofibroblasts produce elevated amounts of ECM proteins at an altered composition, resulting in fibrosis and causing desmoplastic stroma. This fibrotic ECM is composed of fibronectin as well as collagen type I, III, and IV [39]. Meanwhile, it is well known that CAFs can exhibit different phenotypes and different CAF populations have been discovered in recent years. In the pancreas, major subgroups are myofibroblastic CAFs (myCAFs) and inflammatory CAFs (iCAFs). MyCAFs, which are tumor-adjacent and express high levels of αSMA, are activated in a TGF-β-dependent manner. In contrast, iCAFs are localized distant from the tumor, express low αSMA levels, and exhibit rather tumor-promoting and immunosuppressive properties by secreting inflammatory cytokines, like IL-6, chemokine (C-X-C motif) ligand (CXCL) 12, and Granulocyte-Colony Stimulating Factor (G-CSF) [30,40,41].

As outlined above, CAFs are the major source of ECM in the TME. ECM proteins, like collagen, cause a stiffened matrix, stimulating accelerated cell cycle progression in tumor cells and thus fuels tumor growth [42,43]. Moreover, the dense stroma acts as a physical barrier for drugs and immune cells [30,41].

Besides the ECM mediated effects, CAFs exert several direct effects on the tumor. CAFs promote an immunosuppressive TME by selecting tumor-promoting immune cells and inhibiting tumor-suppressive ones. Hence, increased PD-L1 and PD-L2 expression was demonstrated on activated CAFs [44]. Multiple studies showed their capability of excluding cytotoxic T cells (CTLs) from tumor islands and inhibiting T cell activity in multifaceted ways [44–46]. While preventing CTLs functions, CAFs recruit immunosuppressive immune cells, like myeloid-derived suppressor cells (MDSCs) and monocytes, and promote monocyte differentiation into M2-like macrophages via Macrophage-Colony Stimulating Factor (M-CSF) [30,47–49]. Furthermore, CAFs can enhance cell growth [50], vascularization via Vascular Endothelial Growth Factor (VEGF) [51], induce EMT, thereby facilitating PDAC cell dissemination and metastasis, and promote apoptosis and a drug-resistant phenotype in PDAC in a paracrine manner [30,52–54].

1.2.3 Tumor-infiltrating lymphocytes

Different T cell populations can be found in the TME of the primary tumor and metastases of PDAC patients. Owing to their different effector phenotypes, T cells essentially impact the process of tumor and metastasis formation in several ways. In general, an increase of immunosuppressive T cells can be observed during PDAC development, while tumor-directed immune functions are impaired and/or even lost [30]. Key players in the immune response against tumor cells are $CD8^+$ T cells. Accordingly, several studies showed that a high infiltration of $CD8^+$ T cells is associated with longer overall survival of PDAC patients [30]. However, $CD8^+$ T cells are often exhausted in PDAC, characterized by a high expression of immune checkpoint molecules, like programmed cell death protein-1 (PD-1) and cytotoxic T lymphocyte-associated protein-4 (CTLA-4) [55]. Further, different cell populations, like tumor cells and gamma/delta (γ/δ) T cells within the tumor stroma inhibit $CD8^+$ T cells by expressing high levels of the immune checkpoint molecule programmed cell death-ligand 1 (PD-L1) [56].

Rahn et al. showed that $CD8^+$ T cells are predominantly present in the TME and less in close proximity to PDAC cells [35]. One reason for this can be seen in the desmoplastic stroma containing high amounts of ECM molecules, which acts as a physical barrier for immune cells and in particular for $CD8^+$ T cells [30]. Similar findings were reported in liver metastases. Accordingly, in a KPC mouse model, small metastatic lesions in the liver showed a high $CD8^+$ T cell infiltration compared to large metastatic lesions [57].

For optimal $CD8^+$ T cell survival and effector function, $CD4^+$ T helper (T_H) cells are pivotal. In line with this finding, a high infiltration of $CD8^+$ T cells together with $CD4^+$ T cells correlates with a better prognosis for PDAC patients [30]. $CD4^+$ T cells are another very heterogeneous T cell population, as they can differentiate into diverse subsets (T_H1, T_H2, T_H17, and T_{Reg}). The differentiation of T_H0 helper cells into the different subsets depends on cytokines (IL-12, IL-4, TGF-β, IL-6, and IL-2) in the microenvironment. The different subsets are characterized by the release of distinct cytokines and therefore show divergent impacts on other cells in the TME. These effects can be either tumor-promoting or tumor-suppressing [58].

T_H1 cells are regarded as tumor-suppressing as they exert various immune response activating functions, for example, the release of IFNγ, which promotes the recruitment of T lymphocytes, M1-like macrophages, and Natural Killer (NK) cells, and IL-2 which activates $CD8^+$ T cells. On the other hand, IFNγ also induces PD-L1 expression on tumor cells, T lymphocytes, myofibroblasts, and macrophages, thereby supporting CTLs inhibition and immune escape in PDAC [30].

However, PDAC cells and the TME rather promote differentiation of T_H2 cells by TGF-β and IL-10. T_H2 cells are regarded as immune-suppressing and thereby tumor-promoting [30,59], mainly because of the release of cytokines like IL-4, IL-6, IL-10, and IL-13 [60]. IL-4 and IL-10 foster the differentiation of monocytes into M2-like macrophages, IL-4 and IL-13 trigger the collagen synthesis by myofibroblasts, thereby contributing to ECM remodeling, and IL-4 and IL-13 have been shown to enhance the growth of PDAC cells [30,61]. High plasma levels of T_H2 cytokines in patients with resectable PDAC are associated with shorter survival [30].

Furthermore, PDAC tissues contain higher numbers of T_H17 cells compared to normal pancreatic tissue, associated with shorter median survival of PDAC patients. T_H17 cells are regarded mainly as tumor-promoting because this T cell subset is characterized by an elevated release of IL-17, IL-21, and IL-22. Notably, IL-17 has been shown to enhance the initiation and progression of PanIN, thus being a trigger in early pancreatic tumorigenesis [30].

Another important immunosuppressive cell population in PDAC tissues is regulatory T cells (T_{Regs}). Especially in PDAC, T_{Regs} are mostly located in the stroma. Furthermore, Hiraoka et al. demonstrated a significant increase in the number of T_{Regs} during the progression from early PanIN to an invasive PDAC. Additionally, a high prevalence of T_{Regs} in PDAC is significantly correlated with distant metastases, advanced tumor stage, as well as poorer prognosis [62,63]. Here, CAF-derived TGF-β can induce the conversion of $CD4^+$ $CD25^-$ T cells into T_{Regs}. It was also shown that Forkhead box protein 3 (FoxP3) expressing tumor cells recruit T_{Regs} by chemokine (C-C) motif ligand (CCL) 5 [64]. Shen et al. argued that PDAC cell-derived exosomes induce an enrichment of T_{Regs} and overexpression of immune checkpoint molecules PD-1, PD-L1, CTLA-4, and T cell immunoglobulin and mucin domain-containing protein 3 (TIM3) [65].

First attempts have been undertaken to consider this T cell heterogeneity to provide a rationale for patient stratification and optimized treatment choice. Depending on the number of infiltrating lymphocytes, tumors have been categorized into immunological subtypes: T cell inflamed ("hot tumors") or non-T cell inflamed ("cold tumors"). Owing to the low T cell infiltration, especially of $CD8^+$ T cells, PDAC is mostly characterized as a cold tumor. Importantly, immunotherapies are often ineffective in "cold" tumors explaining their common failure in PDAC [30,66,67].

Overall, the tumor stroma in PDAC is quite heterogeneous. The broad impact of tumor-infiltrating T lymphocytes, CAFs, and TAMs on PDAC progression, immune modulation, and drug resistance, targeting the TME have emerged as attractive targets for PDAC therapy [30].

1.3 T lymphocytes

As mentioned above, T lymphocytes are an important cellular component in the tumor stroma. T lymphocytes are white blood cells derived from hematopoietic stem cells in the bone marrow. In the thymus, lymphoid progenitors mature into T lymphocytes. During development, these cells are called thymocytes. In the beginning, thymocytes are called double-negative and neither express T cell receptor (TCR)/CD3 complex nor CD8 or CD4. First, transcription factors are activated through Notch signaling, leading to the rearrangement of the TCR. Here, thymocytes develop into two T cell subsets, characterized by the expression of either an α/β TCR or a γ/δ TCR. Afterward, double-negative develop into double-positive α/β thymocytes by expressing both coreceptors CD8 and CD4. Then, double-positive α/β thymocytes undergo positive selection. Here, the cells are exposed to thymus stromal cells that present self-antigens on either major histocompatibility complex (MHC) I or II. Only thymocytes that bind to either MHC survive, the others undergo apoptosis. In addition, double-positive become single-positive α/β thymocytes by binding to MHC I, CD4 expression is downregulated and vice versa. Finally, the thymocytes undergo negative selection. Here, single-positive α/β thymocytes are confronted with dendritic cells (DCs) and macrophages, presenting self-antigens on the MHC complex. Thymocytes that bind to the MHC complex undergo apoptosis, to prevent the development of autoreactive T cells. Mature T cells, either CD4 or CD8 T positive, leave the thymus and migrate through the lymphatic system [68,69].

1.3.1 Activation of T lymphocytes

The key players in an immune response are CTLs. For activation of naïve T cells, three signals are needed. Activation occurs in secondary lymphoid organs, e.g., in the lymph node. Here, antigen presenting cells (APCs), like DCs or macrophages present processed antigens on the MHC complex.

Intracellular antigens are generally presented on MHC I and extracellular ones on MHC II, however, intracellular antigens can also be presented on MHC II by cross-presentation [69].

For activation of T cells, the TCR/CD3 complex on T cells binds to the MHC on APC. The binding of the coreceptor CD4 on $CD4^+$ T cells is restricted to MHC II, while the binding of the coreceptor CD8 on $CD8^+$ T cells is restricted to MHC I (Figure 3). The α/β-chain of the TCR recognizes the antigen on the MHC and binds to it [70]. The binding of the TCR to MHC leads to an activation signaling cascade. First, the immunoreceptor tyrosine-based activation motif (ITAM) of the TCR/CD3 complex is phosphorylated by lymphocytes protein tyrosine kinase (Lck). Then, zeta-chain associated protein kinase 70 (Zap70) is recruited and binds to ITAM and phosphorylates SLP-76 and linker for activation of T cells (LAT). Inducible T cell kinase (Itk) activates the enzyme phospholipase C-gamma (PLC-γ), which in turn recruits the second messengers inositol-1,4,5-trisphosphate (IP_3) and diacylglycerol (DAG). These signaling pathways lead to the activation of the transcription factors Activation protein-1 (AP-1), Nuclear Factor of activated T cells (NFAT), and Nuclear Factor-kappa B (NF-κB), which initiate the upregulation of genes determining the T cell effector phenotype [69–72]. The binding of the coreceptor (CD8 or CD4) on MHC leads to an increase of Lck and therefore to the phosphorylation of ITAM, reinforcing the signaling cascade [72].

Afterwards, a second costimulatory signal is needed for survival. Costimulatory signals amplify the antigen receptor signals. The best-studied costimulatory signal is the interaction between CD80/CD86 on APCs with CD28 on T cells (Figure 3). After binding of CD28 to either CD80 or CD86, Lck phosphorylates the cytoplasmatic domain (YMNM motif) of CD28. Phosphorylation drives the activation of phosphoinositide 3-kinase (PI3-K) and subsequently the production of phosphatidylinositol 4,5-trisphosphate (PIP_3). High concentrations of PIP_3 recruit Itk and further, lead to the activation of PLC-γ. Therefore, the costimulatory signal of CD28 interacts together with the TCR signaling, causing maximal activation. PIP_3 also activates Akt, which supports the cell's survival [69,70,72].

For proliferation and differentiation of T cells, stimulatory cytokines are necessary. The cytokines IL-2 and IL-12, which are mainly released by $CD4^+$ T cells, induce proliferation of $CD8^+$ T cells (Figure 3). By activating $CD8^+$ T cells, the expression of CD25, which is the α-chain of the IL-2 receptor, on the cell surface is initiated so that IL-2, which has a higher binding affinity can bind [69].

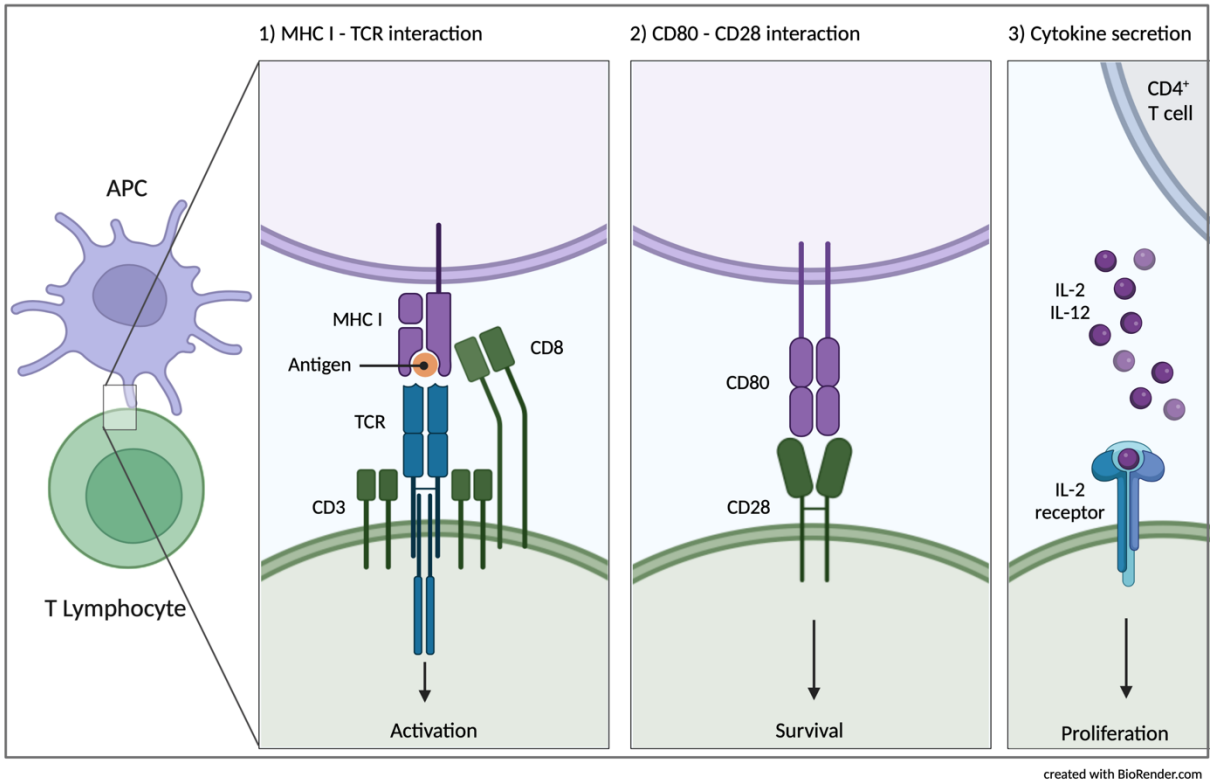

Figure 3: Activation of T lymphocytes. Here, the exemplary activation of a $CD8^+$ T cell is shown. For the activation of T cells, three signals are needed. **1)** Antigen-presenting cells (APCs) process the antigen and present it on the major histocompatibility complex (MHC) I. The T cell receptor (TCR)/CD3 complex as well as the coreceptor CD8 binds to the MHC I. The binding of the TCR to MHC leads to an activation signaling cascade. **2)** A second signal is necessary for survival. Therefore, CD28 on the T cell binds to CD80 on the APC. Costimulatory signals amplify the antigen receptor signals. **3)** Stimulatory cytokines, mainly IL-2 and IL-12, secreted by $CD4^+$ T cells, induce proliferation and differentiation.

Besides, coinhibitory signaling is possible and necessary to prevent autoreactivity and maintain immune homeostasis. CTLA-4 is similar to CD28 and can also bind to CD80 and CD86 but causes inhibition. The binding of CD28 induces the expression of CTLA-4 to maintain homeostasis [72]. Another important coinhibitory signal is the binding of PD-L1 expressed by the APC to PD-1 on the T cell (Figure 4).

Binding to inhibitory receptors leads to dephosphorylation of regulatory proteins such as Lck and ZAP70 disrupting the activation signaling pathway [70].

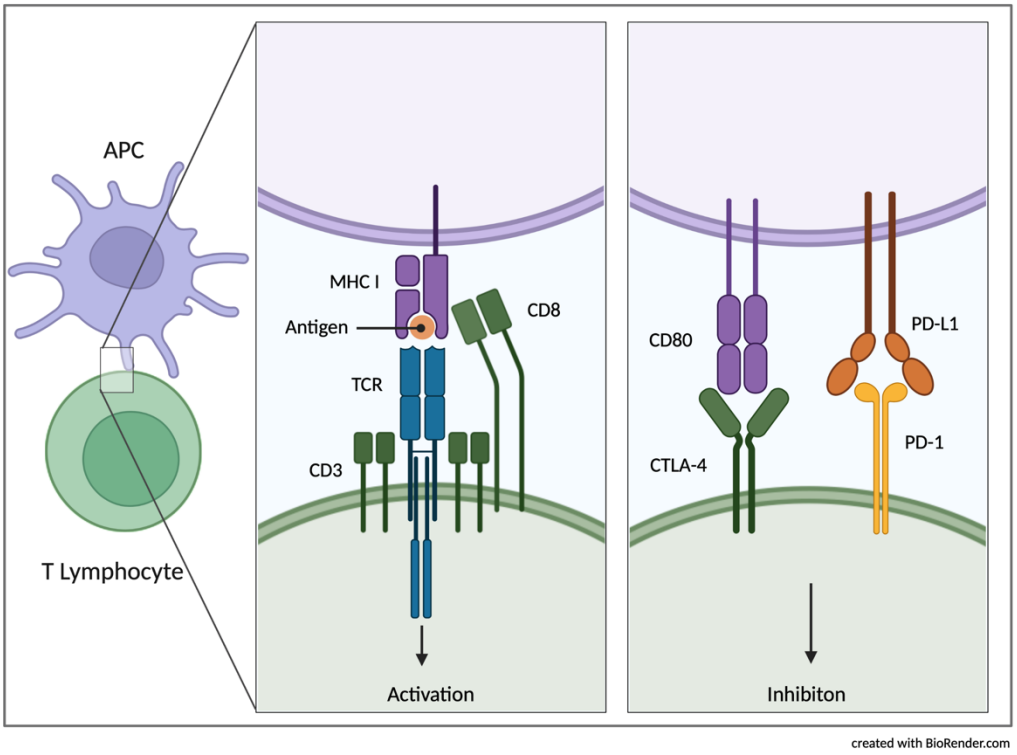

Figure 4: Inhibition of T lymphocytes. Here, the inhibition of a $CD8^+$ T cell is shown exemplarily**.** First, the T cell receptor/CD3 complex as well as the coreceptor CD8 binds to major histocompatibility complex (MHC) I. The binding of the TCR to MHC leads to an activation signaling cascade. However, when cytotoxic T lymphocyte-associated protein-4 (CTLA-4) binds to CD80 or programmed cell death protein-1 (PD-1) to programmed cell death-ligand 1 (PD-L1) a coinhibitory signal follows and the activation signaling cascade is disrupted.

Table 1 shows costimulatory and coinhibitory receptors involved in the co-signaling between APCs and T cells. Some coinhibitory and costimulatory receptors compete for the binding of the same ligand, e.g., binding of CD28 and CTLA-4 to either CD80 or CD86, leading either to activation or inhibition [73]. The binding of CTLA-4 to CD80, e.g., is 20-fold higher compared to CD28.

Table 1: Costimulatory and coinhibitory signals between APCs and T cells.

APC	**T cell**
Costimulatory signal	
CD80 (B7-1)	CD28
CD86 (B7-2)	CD28
CD275 (B7-H2)	CD278 (ICOS) and CD28
CD70	CD27
CD40	CD40L
CD70	CD27
CD48, CD58	CD2

Coinhibitory signal	
CD80 (B7-1)	CD152 (CTLA-4) and CD274 (PD-L1)
CD86 (B7-2)	CD152 (CTLA-4)
CD274 (PD-L1)	CD279 (PD-1) and CD80 (B7-1)
CD273 (PD-L2)	CD279 (PD-1)
Galectin-9	TIM3
CD155, CD112, CD113	TIGIT

After activation and proliferation, T cells enter the blood circulation and infiltrate into the target tissue. If $CD8^+$ T cells are activated and bind to the target cells, they induce apoptosis. For example, $CD8^+$ T cells recognize tumor cells by presenting self-proteins with mutations or overexpression of peptides on the $\alpha1$ and $\alpha2$ domains of MHC I [69].

There are three possible pathways by which $CD8^+$ T cells induce apoptosis in target cells. One is mediated by the release of cytokines, especially IFNγ. Secretion of IFNγ into the surrounding tissue leads to the upregulation of MHC I on the cells, thereby increasing the probability for $CD8^+$ T cells to recognize the target cell. Further, IFNγ differentiates monocytes into M1-phenotype macrophages and stimulates the differentiation of Th0 into Th1 cells [69,74]. The two other mechanisms require cell-cell contact. One mechanism is the binding of FasL (CD95L), which is expressed by $CD8^+$ T cells to Fas (CD95) on the target cell, leading to activation of caspase 8 and apoptosis of the target cell [75]. Moreover, inside $CD8^+$ T cells are cytotoxic granules, containing effector molecules Perforin, Granzymes, and Granulysin, which are released when $CD8^+$ T cells bind to the target cell. Perforin forms pores in the plasma membrane of the target cell, through which Granzyme and Granulysin can enter the cell. Here, Granzyme A damages the mitochondria and Granzyme B activates caspase 3, leading to apoptosis [69].

1.3.2 PD-1 and PD-L1

PD-1, also called CD279, was first identified in 1992 as a mediator of apoptosis [76]. It is a type 1 transmembrane glycoprotein and exhibits some similarities to CTLA-4 and CD28. PD-1 is expressed on T cells, NK cells, B cells, and APCs. On T cells it is especially expressed after activation [77]. PD-1 binds to either PD-L1 (CD274) or PD-L2 (CD273) causing inhibition of T cells. Inhibitory signals are needed to maintain immune homeostasis and prevent autoreactivity.

PD-L1, also known as CD274, was discovered by Chen *et al.* in 1999. It is a type 1 transmembrane protein and expressed on APCs, T cells, B cells, non-hematopoietic cells, epithelial cells, and tumor cells [78]. The pro-inflammatory cytokine IFNγ is a known inducer of PD-L1 expression on the cell surface of tumor cells [79]. Rahn showed that IFNγ is also the strongest inducer of PD-L1 expression in pancreatic ductal epithelial cells (PDECs) and most PDAC cell lines [80].

The binding of PD-1 to PD-L1 leads to phosphorylation of the immunoreceptor tyrosine-based switch motif (ITSM) of the PD-1 receptor and recruitment of the phosphatases SHP1 and SHP2. SHP1 and SHP2 in turn dephosphorylate ZAP70 and PI3-K [69]. This prevents activation of the transcription factors AP-1, NFAT, and NF-κB, which are important for T cell activation, proliferation, and survival [77,81].
Moreover, the binding of PD-1 to its ligand can lead to T cell exhaustion. Importantly, this exhausted state is characterized by elevated expression of inhibitory receptors (PD-1, CTLA-4, and TIM3), reduced production of cytotoxic molecules (Perforin, Granzymes, and Granulysin), decreased production of chemokines (TNFα and IFNγ), and elevated apoptosis of T cells [30,81].

1.4 Metastasis

Metastasis is a multistep process, during which tumor cells of the primary tumor spread to distant organs [82]. Local invasion and metastasis are one hallmark of cancer [83]. Even though the majority of cancer patients (90 %) die due to metastases rather than the primary tumor, the process is still poorly understood and therefore a better understanding of metastasis progression is essential [83,84]. Cancer cells of the primary tumor prefer certain distant organs for metastasis. This was already postulated by Stephan Paget in the year 1889 and was called the “seed and soil” hypothesis. Cancer cells represent the seeds and the microenvironment represents the soil and Stephan Paget concluded that metastases only form if the seed and soil match [85].

1.4.1 The invasion metastasis cascade

The invasion metastasis cascade is briefly described in several steps. The tumor cells leave the primary tumor, enter the blood vessels and circulate, extravasate from the blood vessels, enter the secondary organ, and finally survive in the new microenvironment (Figure 5).
The first step of the cascade is the invasion of tumor cells through the basal membrane and into the surrounding tissue. The transdifferentiation process EMT is an important step to enable tumor cell motility. Tumor cells lose their epithelial-like phenotype and acquire a more mesenchymal-like phenotype by downregulating epithelial proteins, e.g., E-Cadherin and Cytokeratin, and by upregulating mesenchymal proteins, e.g., Vimentin, N-Cadherin, and Fibronectin [86]. Additionally, cell-cell junctions are dissolved [87]. The EMT process is mediated by different transcription factors, e.g., Snail, ZEB, Slug, and Twist. Further, cytokines secreted by cells in the TME, like TGF-β1, TNFα, IL-10, and IL-6 contribute to EMT [53,88]. In turn, TGF-β promotes TAMs, while IL-10 promotes T_{Regs} and inhibits $CD8^+$ T cell activation [89,90]. In breast cancer and non-small cell lung cancer (NSCLC), it was shown that EMT upregulates PD-L1 expression [91,92]. Besides, EMT contributes to chemotherapy

resistance in different PDAC cell lines [93]. During invasion, remodeling of the ECM is achieved by matrix metalloproteinases (MMPs). MMPs are secreted by tumor cells and neutrophils [94,95].

Next, tumor cells must intravasate into the blood vessels and are then called circulating tumor cells (CTCs). This step is promoted by tumor vascularization [96]. Most CTCs circulate as single cells and some in clusters. During circulation, many CTCs get trapped in the small vessels and have to survive the increased shear forces and recognition of immune cells, especially NK cells. Neutrophils within the blood vessels support cluster formation and inhibit the activation of leukocytes. Further, platelets are activated and form a coating shield, protecting CTCs from physical forces and detection by immune cells [84,97]. To inhibit immune cells, especially NK cells, CTCs release TGF-β or PDGF. Afterwards, CTCs extravasate from the blood vessels by transendothelial migration. In the liver, vessels are highly permeable, facilitating extravasation. Furthermore, different cell populations, like monocytes and neutrophils, and the production of proteins, like VEGF and MMPs promote extravasation [94,98].

Finally, disseminated tumor cells (DTCs) enter the parenchyma of the distant organ. Here DTCs must adapt to the new microenvironment to survive, proliferate, and then form clinically relevant metastases. Therefore, the TME of the distant organ is already reshaped into a tumor-promoting pre-metastatic niche during tumor progression [98]. Other studies showed that DTCs in the secondary organ acquire a dormant state, during which they neither proliferate nor die but remain vital [99,100].

The invasion metastasis cascade is a complex process and overall very inefficient as it is predicted that only 0.01 % of CTCs form metastases [101].

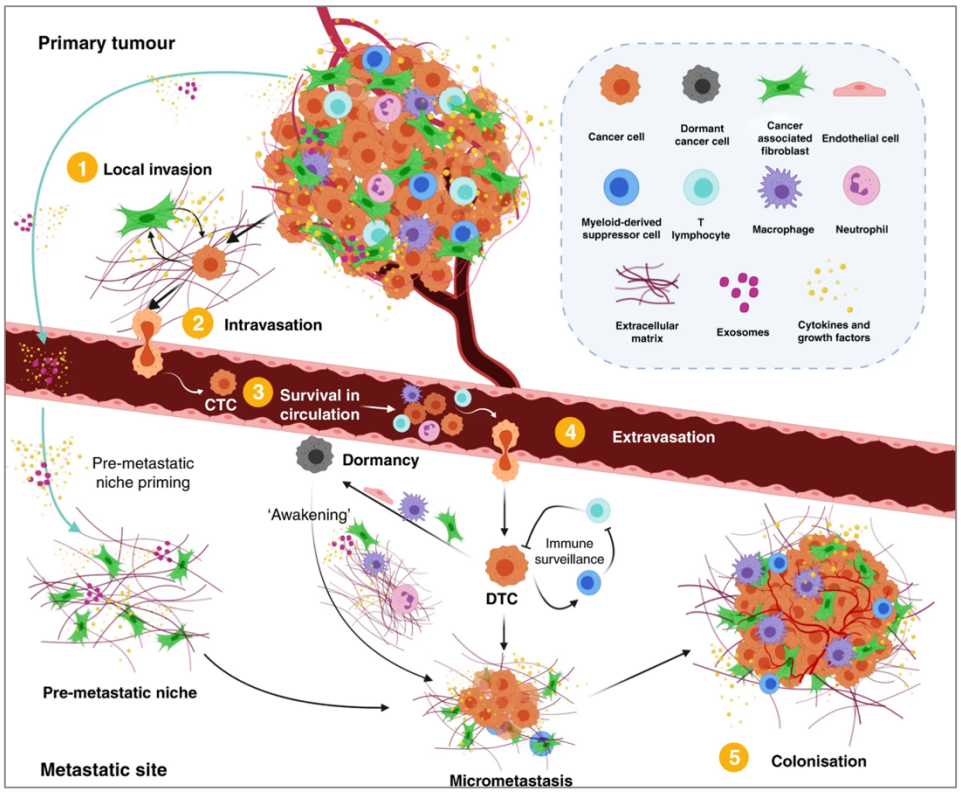

Figure 5: The invasion metastasis cascade: The invasion metastasis cascade is characterized by several steps. (1) The first step of the cascade is the invasion of tumor cells through the basal membrane and into the surrounding tissue. (2) Next, tumor cells must intravasate into the blood vessels and are then called circulating tumor cells (CTCs). (3) Here, the CTCs must survive the high shear forces and recognition by immune cells. (4) Only a few cells survive circulation and extravasate the blood vessels into the secondary site. (5) Finally, disseminated tumor cells (DTCs) enter the parenchyma of the distant organ. Some DTCs go into a dormant state before they start to proliferate and form visible metastases. For colonization, DTCs must adapt to the new microenvironment. Therefore, the tumor microenvironment (TME) of the distant organ is already reshaped into a tumor-promoting pre-metastatic niche during tumor progression. From [102].

1.4.2 Metastasis in PDAC

PDAC patients mostly develop metastases in the lung (~ 50 %), the peritoneum (~ 60 %), and the liver (~ 80 %), the latter representing the main site of metastases [103].

The four "driver" mutations of the genes *kras, p16, p53,* and *SMAD4* contribute to metastatic progression in PDAC. The loss of *p16* and mutation in *kras* (G12D) [104] led to metastases in mice, likewise mutation in *p53* [105] and *SMAD4* depletion in combination with *kras* (G12D) mutation [106] promoted metastasis in PDAC mouse models, concluding that not all four genes need to be mutated. Supporting these findings, patient data showed that not all four "driver" genes need to be mutated to promote metastasis. Patients with metastases only showed 1-2 alterations in these genes, but alterations in 3-4 genes were associated with a higher metastatic burden and shorter median overall

survival [107]. As mutations in “driver” genes were acquired early during progression, it was postulated that metastasis occurs several years after tumor formation (6.8 years). Yachida *et al.* demonstrated genetically that clonal populations in the metastases arise from clones in the primary tumor [108]. However, recent studies provided evidence that metastasis occurs concurrently with primary tumor development. A PDAC mouse model revealed that pre-malignant PDECs undergo EMT and migrate into the liver [109]. Moreover, circulating PDECs could be detected in the blood of patients with pancreatic cystic lesions, supporting the view that metastatic spread is an early event during pancreatic tumorigenesis [110].

1.4.3 The liver as a pre-metastatic niche

During cancer progression, the TME of the primary tumor is reshaped. Moreover, the liver as the secondary organ for metastasis colonization is remodeled as well to ensure that DTCs survive and proliferate.

During the invasion metastasis cascade, tumor cells and neutrophils express metalloproteinases by which they are able to remodel the ECM and to invade the surrounding tissue [94,95]. Grünwald *et al.* showed in a KPC mouse model that tissue inhibitor of metalloproteinases-1 (TIMP-1) is expressed and secreted into the circulation, causing activation of HSC and recruitment of neutrophils. Since in TIMP-1 knock-out mice, the formation of liver metastases was prevented, TIMP-1 seems to contribute to the formation of a pre-metastatic niche [111]. Moreover, it was shown that primary tumor derived exosomes containing proteins contribute to the formation of a pre-metastatic niche. To give one example, exosomes containing the chemokine macrophage migration inhibitory factor are present in the liver and taken up by Kupffer cells, leading to the secretion of TGF-β, activation of HSC, and upregulation of ECM proteins in a PDAC mouse model [112]. Further, the secretion of different chemokines and cytokines recruits different immune cells to the liver to generate an immunosuppressive microenvironment. Giving one example, CCL2 recruits Granulin-producing metastasis-associated macrophages (MAMs) to the liver, leading to the activation of HSC, which produce high amounts of ECM molecules, giving rise to a dense stroma [57,113].

Overall, these findings indicate that already early during PDAC progression, the liver is primed and reshaped for metastasis.

1.4.4 The liver microenvironment

The liver is the main site of metastases in PDAC and is associated with the worst prognosis compared to lung or peritoneum metastases [114]. The liver is important for detoxification and different metabolisms of lipids, proteins, amino acids, and glucose [115]. The liver comprises multiple different cell types, which are either parenchymal or non-parenchymal. Hepatocytes represent ~ 70 % of the

liver cell population and are parenchymal. The rest is composed of non-parenchymal cells. Kupffer cells are the tissue-resident macrophages of the liver and represent around 40 %, while HSC represent 5 - 8 % of the non-parenchymal cells [116]. Kupffer cells phagocytose bacteria thereby protecting the liver from infection [117]. In the physiological liver, HSC perform a variety of tasks to maintain organ homeostasis, e.g., by paracrine secretion of Hepatocyte Growth Factor (HGF) and Epidermal Growth Factor (EGF), and they store ~ 80 % of the body's vitamin A in lipid vacuoles [30]. In response to injury or inflammation, HSC transdifferentiate into HMF [118]. Here, stimuli like TGF-β, PDGF, or IL-6 lead to their activation while, IFNγ inhibits the activation of HSC [119]. HMF are characterized by a high expression of αSMA as well as the secretion of ECM molecules, like collagen I, collagen IV, and fibronectin leading to liver fibrosis. Owing to their ability to release high amounts of ECM proteins and immune regulatory mediators, HMF generate a dense stroma, which acts as a physical barrier for immune cells and drugs [30].

Lenk *et al.* showed that the inflammatory status of the liver microenvironment is an essential driver for the outgrowth of PDAC liver metastases. Here, HMF promoted PDAC cell growth in a VEGF-dependent manner [120]. Moreover, HSC and HMF can impact immune cells in the liver. As mentioned above, the secretion of CCL2 and CCL4 attracts MAMs, in turn activating HSC. *In vitro,* coculture of HSC and monocytes led to the differentiation of monocytes into MDSCs [119], which suppress T cells and induce T_{Regs} [121]. Additionally, PD-L1 is expressed on the cell surface of HSC and even more on HMF, inhibiting T cells [122]. In summary, HSC are only a minor cell population in the liver, but nevertheless, after activation, their inflammatory counterpart (HMF) essentially contributes to the progression of liver metastases in PDAC.

1.5 Cancer Immunity and Immunotherapy

High infiltration of $CD8^+$ T cells is associated with longer overall survival of PDAC patients, indicating that $CD8^+$ T cells exhibit a potent anti-tumorigenic potential in PDAC [123,124].

As shown above, diverse immune cells in the TME promote or suppress tumor progression [30]. CTLs are the key players in the TME for anti-cancer tumor responses. Chen and Mellman postulated the cancer-Immunity cycle, a model to explain stepwise progression for effective killing of tumor cells (Figure 6). First, cancer antigens are released (Figure 6, 1) and presented by APCs (Figure 6, 2), like macrophages DCs. Next, T lymphocytes are activated and primed by APCs in the lymph node (Figure 6, 3). Afterwards, the T cells enter the blood circulation and infiltrate into the tumor (Figure 6, 4+5). Here, the T cells need to recognize the tumor cells (Figure 6, 6) and finally kill them (Figure 6, 7) [125].

However, during tumor progression, tumor cells develop several strategies by which they can evade the immune system, for example, by limiting antigen recognition and inhibiting $CD8^+$ T cells [126]. Evading the immune system is one hallmark of cancer [83].

The complex relation between tumor cells and immune cells is called immunoediting. It is characterized by three phases: Elimination, Equilibrium, and Escape. In the elimination phase, the innate and adaptive immune systems orchestrate together to recognize and eliminate tumor cells. Tumor cells, which have acquired survival strategies and are not eliminated by the immune system, are able to enter the next phase. Here, small lesions develop but its outgrowth is still controlled by the immune system. During the equilibrium phase, tumor cells, which have developed survival strategies, are selected to escape the immune system and progress into the escape phase. Here, the outgrowth and proliferation of tumor cells are not constrained anymore by the immune system and visible tumors develop [127].

Several mechanisms lead to immune evasion. Cancer cells release CXCL12, CCL5, IL-6, IL-10, TGF-β, VEGF, and M-CSF, leading to the recruitment of T_{Regs}, T_H2 cells, MDSCs, and to the differentiation of monocytes into M2-like macrophages [64,128]. These immune cells suppress effector $CD4^+$ and $CD8^+$ T cells, NK cells, and DCs, which are important for antigen presentation [129]. Further, tumor cells downregulate MHC I to impair recognition by $CD8^+$ T cells, which is also seen in PDAC [130,131]. If tumor cells express no MHC I anymore, they are killed by NK cells, however, several factors in the TME suppress these immune cells [30,69]. Moreover, tumor cells express immune checkpoint molecules, like PD-L1 or CTLA-4 to inhibit $CD8^+$ T cells [132]. Blocking these immune checkpoint molecules has emerged as a promising option for cancer therapy [133]. The aim of immune checkpoint inhibitors (ICIs) is to boost cancer-directed immunity by induction of $CD8^+$ T cell-mediated killing of tumor cells. ICI treatment can be successful during priming and activation of $CD8^+$ T cells (3) and during recognition and killing tumor cells (7) in the cancer-immunity cycle.

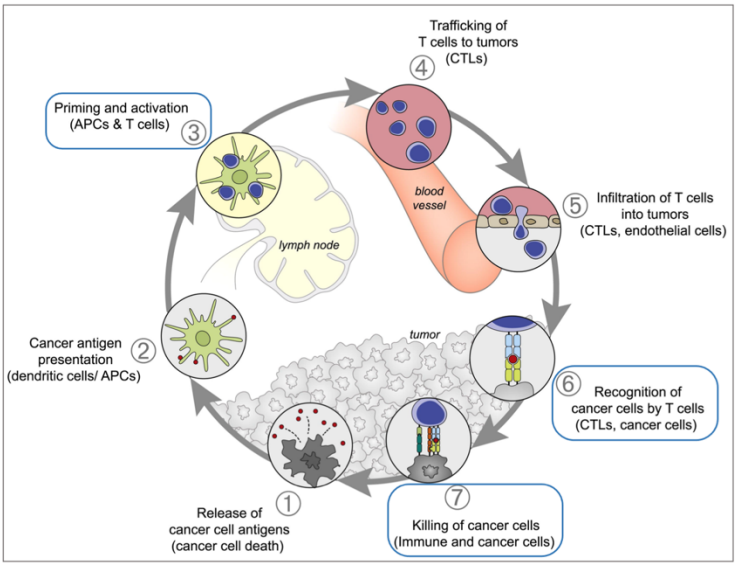

Figure 6: Cancer-immunity cycle. The stepwise progression of effective tumor cell killing. First, (1) cancer cells release antigens (1), which are presented by antigen-presenting (APCs) (2). Next, T cells are primed and activated in the lymph node (3). Afterwards, T cells circulate through the blood vessels (4) to infiltrate into the tumor (5). Here, T cells recognize (6) and finally kill (7) the tumor cells. Immune checkpoint inhibitors can be effective in steps 3, 6, and 7, marked with a blue box. Adapted from [125].

1.5.1 Immune checkpoint blockade in cancer

As mentioned above, tumor cells can evade the immune system by expressing immune checkpoint molecules to inhibit CTLs [132]. Blocking these regulatory/inhibitory proteins with ICIs has broadly impacted and revolutionized cancer therapy [133]. By blocking immune checkpoint molecules, like PD-1 or PD-L1, activation of $CD8^+$ T cells can be increased and in turn, cancer-mediated killing can be induced (Figure 7).

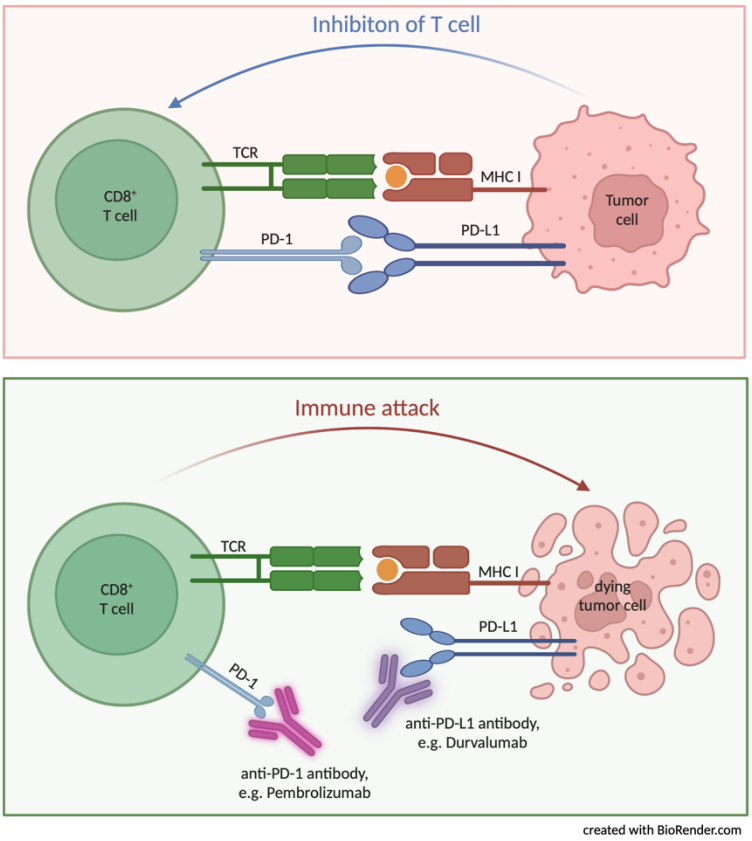

Figure 7: Immune checkpoint inhibitors enhance the activation of CD8⁺ T cells and lead to cancer-mediated killing. Tumor cells can evade the immune system by upregulating cell surface expression of immune checkpoint molecules, like programmed death-ligand 1 (PD-L1). The binding of PD-L1 to programmed death protein-1 (PD-1) on T cells leads to their inhibition so that T cells are not able to kill the tumor cell. If these immune checkpoint molecules are blocked by immune checkpoint inhibitors (ICIs), like Pembrolizumab (binding to PD-1) or Durvalumab (binding to PD-L1), killing ability of CD8⁺ T cells is restored so that they can induce cancer cell death.

Over the recent years, the number of clinical trials testing ICIs increased dramatically [134]. Eight ICIs are approved by the European Medicine Agency (EMA), mainly targeting PD-1 or PD-L1 (Table 2). Tremelimumab (binding to CTLA-4) was just approved in February this year (2023).

Table 2: EMA-approved immune checkpoint inhibitors for cancer treatment.

Immune checkpoint Inhibitors (Tradename)	Target	Isotype	Distributor
Atezolizumab (Tecentriq®)	PD-L1	hIgG1	Roche
Avelumab (Bavencio®)	PD-L1	hIgG1	Merck/Pfizer
Cemiplimab (Libtayo®)	PD-1	hIgG1	Regeneron
Durvalumab (Imfinzi®)	PD-L1	hIgG1	AstraZeneca
Ipilimumab (Yervoy®)	CTLA-4	hIgG1	Bristol-Myers Squibb

Nivolumab (Opdivo®)	PD-1	hIgG1	Bristol-Myers Squibb
Pembrolizumab (Keytruda®)	PD-1	hIgG4	Merck
Tremelimumab (Imjudo®)	CTLA-4	hIgG1	AstraZeneca

Durvalumab and Pembrolizumab targeting PD-L1 and PD-1, respectively, will be described in sections 1.5.1.1 and 1.5.1.2 as they were used in this study to analyze the impact of PD-L1 and PD-1 inhibitors on the effector phenotype of $CD8^+$ T cells in the context of the hepatic microenvironment.

Mostly NSCLC, urothelial carcinoma, melanoma, renal cell carcinoma, triple-negative breast cancer, and colon/rectum carcinoma are treated with ICIs targeting PD-1, PD-L1, or CTLA-4. In some cases, the PD-L1 status of the tumor is determined, by considering PD-L1-positive cancer cells and infiltrating immune cells before applying the drug to the patients [135–138]. In NSCLC, it was shown that Atezolizumab increased overall survival and progression-free survival if more than 50 % of tumor cells and more than 10 % of immune cells are PD-L1 positive [139]. In urothelial carcinoma, the tumor objective response rate was higher in PD-L1 high patients [140]. These studies and the guideline by the EMA underscore that the PD-L1 status in the tumor, including those of cancer and immune cells, might be a good predictor for the efficacy of ICIs.

Recent studies revealed that the combination of different ICIs might be more effective in cancer treatment, however, patients often develop more and stronger side effects. The challenges for effective treatment will be identifying the correct order and time point of application, the best combination, and the appropriate concentration of the drugs. Immune checkpoint therapy can also be combined with radiotherapy, chemotherapy, and strategies targeting the TME [141].

However, ICIs has not yet added any considerable benefit to the treatment of PDAC patients [124,142]. In clinical trials, the combination of Tremelimumab (CTLA-4 inhibitor) with Gemcitabine or the combination of Pembrolizumab (PD-1 inhibitor) and Gemcitabine or Nab-Paclitaxel did not improve the outcome of PDAC patients [143,144].

1.5.1.1 Durvalumab

Durvalumab (Imfinzi®) is a human monoclonal immunoglobulin G1 antibody developed by AstraZeneca. Durvalumab targets PD-L1 expressed by APCs or tumor cells to block the interaction with PD-1 and CD80 on $CD8^+$ T cells. Therefore, the binding affinity of PD-L1 to Durvalumab is higher compared to PD-1 or CD80 [145]. Durvalumab is approved by the EMA and the Committee for Medicinal Products for Human Use (CHMP) for different cancer entities. First, Durvalumab is used for locally advanced and unresectable NSCLC, in which more than 1 % of the tumor cells exhibit PD-L1 expression. The therapy is followed by platinum-based chemoradiation therapy. Further, Durvalumab is used in combination with chemotherapy as a first-line therapy to treat advanced-stage small cell

lung cancer. Last year (2022), Durvalumab was also approved to treat patients with unresectable or metastatic biliary tract cancer in combination with Gemcitabine or Cisplatin. In addition, the combination of Durvalumab and Tremelimumab (blocking CTLA-4) is approved as first-line treatment for patients with metastatic NSCLC in combination with chemotherapy and patients with advanced or unresectable hepatocellular carcinoma [136]. According to the National Library of Medicine, around 600 clinical trials have so far investigated the use of Durvalumab in cancer patients. There are some ongoing clinical trials, investigating Durvalumab therapy, especially in combination with other drugs in PDAC. In a clinal phase II trial, Durvalumab is used in combination with Gemcitabine as a neoadjuvant and adjuvant therapy option [NCT03572400]. In phase I and II, Durvalumab is used in combination with different chemotherapies and with a different ICI (Oleclumab, blocking CD73) [NCT03611556]. Combinational therapy of Tremelimumab and Durvalumab was just approved for NSCLC and hepatocellular carcinoma and is tested in phase II for metastatic PDAC [NCT02558894]. Other combinational therapies target the TME, e.g., in phase I clinical trial, Durvalumab is used in combination with Pexidartinib (anti-CSF1R), to deplete M2-like macrophages [NCT02777710].

1.5.1.2 Pembrolizumab

Pembrolizumab (Keytruda®) is a human monoclonal immunoglobulin G4 antibody developed by Merck. Pembrolizumab targets PD-1 to block the interaction with PD-L1 and PD-L2. The EMA and CHMP approved Pembrolizumab for various cancer entities. Compared to Durvalumab, Pembrolizumab is used as a therapy option in more cancer diseases. Mostly, Pembrolizumab is used for patients with advanced or unresectable tumors, for example, melanoma, NSCLC, urothelial carcinoma, head and neck cancer, renal cell carcinoma, and colorectal cancer. The PD-L1 and PD-1 status must be evaluated in certain cancer entities before the treatment. In melanoma and renal cell carcinoma, Pembrolizumab is used as adjuvant therapy. Besides, Pembrolizumab is often used in combination with chemotherapy and other cancer drugs for esophageal cancer, triple-negative breast cancer, NSCLC, head and neck cancer, and renal cell carcinoma. Compared to Durvalumab Pembrolizumab is already used for more cancer entities as a therapy option [135]. Moreover, according to the National Library of Medicine, around 2,000 clinical trials investigate the use of Pembrolizumab in cancer patients and some clinical trials investigate the efficacy of Pembrolizumab in PDAC. Combinational therapy of Pembrolizumab and different chemotherapies are tested in phase I [NCT04083599] and II [NCT03727880] trials.

1.5.2 PD-L1 expression in PDAC

As mentioned above, the PD-L1 status of a patient might be a good predictor of the efficacy of ICIs. Therefore, it is important to evaluate the PD-L1 expression in PDAC. Rahn *et al.* showed that PD-L1^{+} cells could only be detected in 20 % of the tumors of PDAC patients staged T3N1M0, the most

frequently operated tumor stage. Moreover, poor tumor differentiation was associated with a higher PD-L1 expression [35]. This was also seen by Wang *et al.,* who demonstrated that the amount of PD-L1 expressing cells was significantly higher in TNM stage III compared to I and II [146]. A meta-analysis of 993 PDAC patients showed that an advanced tumor stage is associated with a higher PD-L1 expression [147]. These studies indicate that PD-L1 expression is enhanced during progression in PDAC. Furthermore, the overall survival was lower in patients with high PD-L1 expression [35,147].

Moreover, Rahn *et al.* showed that PD-L1 is rather expressed by stromal cells, especially macrophages, than by tumor cells [35]. Karamitopoulou *et al.* also showed that in 30 % of PDAC patients, PD-L1 is expressed by immune cells [148].

Overall, data on PD-L1 expression in tumor and stromal cells are still rare in PDAC, especially in the metastatic context limiting the understanding of the impact of the PD-L1/PD-1 axis on immune evasion in metastatic PDAC.

1.6 Aim of the study

With a 5-year survival rate of under 5 %, PDAC is one of the most fatal malignancies [2]. In the European Union, PDAC represents the 4th most common cause of cancer-related deaths and it is estimated to become the 3rd leading cause of cancer-related death [3]. Lacking specific symptoms, PDAC is mostly diagnosed at a locally advanced or metastatic stage, with the liver representing the main site of metastases [5,103]. To date, the only curative treatment is an R0 resection of the primary tumor. However, even these patients often relapse and develop metastases shortly after or even during adjuvant therapy [149]. Since PDAC patients with liver metastases have an even worse prognosis, it is of outmost importance to better understand the mechanisms underlying metastatic progression in the liver and to identify effective treatment options [150]. Treatment with ICIs, e.g., PD-L1 or its receptor PD-1, has improved the therapy of many cancers but so far failed in PDAC. Monoclonal antibodies, such as Durvalumab and Pembrolizumab, blocking PD-L1 and PD-1, respectively, aim to boost cancer-directed immunity by induction of CD8$^+$ T cell-mediated killing of tumor cells [124,142]. High infiltration of CD8$^+$ T cells is associated with longer overall survival of PDAC patients, indicating that CD8$^+$ T cells exhibit a potent anti-tumorigenic potential in PDAC [123,124]. Moreover, absent PD-L1 expression and high CD8$^+$ T cell infiltration of PDAC are linked to a better prognosis [151]. Of note, PD-L1 expression in PDAC is very heterogeneous, as some tumors show no PD-L1 expression, while others show high expression [35,151]. In the latter cases, PD-L1 is mostly expressed by stromal cells rather than tumor cells [35]. However, whether and how stromal cell-associated PD-L1 expression impacts immune evasion is still poorly understood, especially in liver metastases, as they are not routinely resected in PDAC patients. Consequently, tissue samples from PDAC metastases are rare and the expression of immune regulatory molecules such as PD-L1 within liver metastases has been rarely characterized.

Therefore, this study aimed to gain further insights into the impact of the liver microenvironment, particularly of HMF, on PDAC cells and CD8$^+$ T cells in the context of immune evasion. For this purpose, metastatic liver tissue sections of PDAC patients were stained to examine the localization of tumor cells, myofibroblasts, CD8$^+$ T cells, and PD-L1 expression comparing small and large metastases in PDAC patients. Further, 2D *in vitro* cocultures were conducted to analyze the impact of PDEC, hepatic stromal cells, and CD8$^+$ T cells on each other, considering the PD-L1 cell surface expression, the activation, and the effector phenotype of CD8$^+$ T cells. Moreover, *in vitro* 3D cocultures using different ratios of PDAC cells and HMF were established to better mimic the complex hepatic tumor stroma interplay in hepatic metastases. Further, CD8$^+$ T cells were added to spheroid cocultures. Here, the efficacy of ICIs (Durvalumab and Pembrolizumab), Gemcitabine, and combinational treatment of Gemcitabine with ICIs was analyzed, regarding the activation, effector phenotype of CD8$^+$ T cells, and the induction of PDAC cell death by CD8$^+$ T cells.

2 Materials

2.1 Chemicals and Reagents

Chemical	Manufacturer
Accutase solution	Pan-Biotech GmbH, Aidenbach, Germany
Acetic acid, 10 %	Carl Roth GmbH, Karlsruhe, Germany
All-trans retinoic acid (ATRA)	Sigma-Aldrich, München, Germany
Bovine pituitary extract (BPE)	ThermoFisher Scientific, Waltham, MA, USA
Bovine serum albumin (BSA)	Biomol, Hamburg, Germany
CellTrace™ Violet Cell Proliferation Kit (CTV)	ThermoFisher Scientific, Waltham, MA, USA
CellTracker™ Green CMFDA Dye (CTG)	ThermoFisher Scientific, Waltham, MA, USA
Dimethyl sulfoxide (DMSO)	Sigma-Aldrich, München, Germany
Ethanol	Merck Millipore, Darmstadt, Germany
Ethylenediaminetetraacetic acid (EDTA)	Carl Roth GmbH, Karlsruhe, Germany
Fetal calf serum (FCS)	Pan-Biotech GmbH, Aidenbach, Germany
4-(2-hydroxyethyl)-1-piperazineethansulfonic acid (HEPES)	Pan-Biotech GmbH, Aidenbach, Germany
Hoechst 33528	ThermoFisher Scientific, Waltham, MA, USA
Human TruStainFcX™ (Fc Receptor Blocking Solution)	BioLegend, San Diego, CA, USA
Keratinocyte serum-free medium	ThermoFisher Scientific, Waltham, MA, USA
L-Glutamine (L-Gln)	Pan-Biotech GmbH, Aidenbach, Germany
LightCycler® 480 SYBR Green I Master	Roche, Basel, Switzerland
Pancoll, 1.077 g/l	Pan-Biotech GmbH, Aidenbach, Germany
Paraformaldehyde (PFA) 4.0 %	ThermoFisher Scientific, Waltham, MA, USA
Penicillin-Streptomycin (Pen/Strep)	ThermoFisher Scientific, Waltham, MA, USA
Phosphate-buffered saline (PBS) Dulbecco	Pan-Biotech GmbH, Aidenbach, Germany
Roswell Park Memorial Institute (RPMI) 1640 medium	Pan-Biotech GmbH, Aidenbach, Germany
RPMI 1640 medium without phenol red	Pan-Biotech GmbH, Aidenbach, Germany
Propidium Iodide (PI)	Sigma-Aldrich®, Saint Louis, MO, USA
Puromycin (10 mg/ml)	Invivo Gen, San Diego, CA, USA
Sodium chloride	Carl Roth GmbH, Karlsruhe, Germany

Sodium pyruvate	Pan-Biotech GmbH, Aidenbach, Germany
Solution 555	Beckmann Coulter GmbH, Krefeld, Germany
Stellate cell medium	Science Cell Research Laboratories, Carlsbad, CA, USA
Trypan blue Stain 0.4 %	ThermoFisher Scientific, Waltham, MA, USA
Trypsin-EDTA	Biowest the serum specialist, Nuaillé, France

2.2 Buffers

Buffer	**Formulation**
Density gradient & counterflow centrifugation	
Elutriation buffer	0.1 % (v/v) FCS 10 mM EDTA in PBS pH 7.4
Erythrocyte lysis buffer	155 mM NH_4Cl 10 mM $KHCO_3$ 0.1 mM EDTA in ddH_2O
Flow Cytometry	
Fixation solution	1 % (v/v) PFA in MACS buffer
MACS buffer	0.5 % (w/v) BSA 2 mM EDTA in PBS pH 7.4 sterile-filtered and vacuum-degassed

2.3 Cell biological material

2.3.1 Cell lines

Cell line	Information/origin
Pre-malignant pancreatic ductal epithelial cells	
H6c7-kras	Ductal epithelial cell line. Cells derived from a human chronically inflamed human pancreas, immortalized with HPV16-E6/E7 genes and additionally transduced with the retroviral vector pBabepuro-K-ras4B^{G12V}. The cells express the oncogene *k-ras* (G12V) and were used as a cell model for pre-malignant cells. H6c7-kras cells were kindly provided by Dr. Tsao (Ontario Cancer Institute, Toronta, Canada) [152].
Malignant pancreatic ductal epithelial cells	
PancTu1	Human PDAC cell line. Cells were isolated from a primary PDAC of a female PDAC patient. Cells show mutations in *k-ras* (G12V) and *p53* (C176S) and a depletion of *p16*. *SMAD4* shows a wildtype status. PancTu1 cells were used as a PDAC cell model. PancTu1 cells were kindly provided by M. v. Bülow (University of Mainz, Germany) [153,154].
Panc89	Human PDAC cell line. Cells were isolated from a lymph node metastasis of a 64-year-old male PDAC patient. Cells show mutations in *p53* (T220C) and depletion of *p16*. The genes *k-ras* and *SMAD4* show a wildtype status. Panc89 cells were used as a cell model for PDAC cells. Panc89 cells were kindly provided by K.Keiichi (Kyto Prefectural University of Medicine, Japan) [153,154].
Panc1	Poorly differentiated human PDAC cell line. Cells were isolated from the primary PDAC of a 56-year-old female PDAC patient. Cells show mutations in *p53* (R273H), *k-ras* (G12D) and depletion of *p16.* The gene *SMAD4* shows a wildtype status. The cells were purchased from the American Type Culture Collection [153–155].

BxPc3	Poorly to moderately differentiated human PDAC cell line. Cells were isolated from a PDAC of a 61-year-old female PDAC patient. Cells show mutations in *p53* (Y220C) and depletion of *p16* and *SMAD4.* The gene *k-ras* is wildtype. BxPc3 cells were purchased from the American Type Culture Collection [42,154–157].
Colo357	Human PDAC cell line. Cells were isolated from a lymph node metastasis of a 77-year-old female PDAC patient. Cells show mutations in *k-ras* (G12V) and a depletion of *SMAD4.* The genes *p16* and *p53* show the wildtype status [153,154,158].
A818-6	Clone of the human PDAC cell line A818. Cells were isolated from ascites of a 75-years old female PDAC patient [159]. A818-6 cells were kindly provided by Prof. Dr. Holger Kalthoff (Kiel, Germany).
PT-45	Human PDAC cell line. Cells were isolated from the primary PDAC. Cells show mutations in *k-ras* (G12A) and *p53* (A280L) and a depletion of *p16* [153,154]. PT-45 cells were kindly provided by Holger Kalthoff (Kiel, Germany).
Hepatic stromal cells	
hHSteC	Human hepatic stellate cells (hHSteC) isolated from the liver of a 3-year-old male infant. Human HSteCs were purchased from Provitro GmbH (Berlin, Germany). To generate hHSteCs with a HSC like phenotype, cells were cultured with 2.5 µM of ATRA. These cells will be called HSC throughout this thesis. HSC were transdifferentiated into hepatic myofibroblasts (HMF) by adding 1 ng/ml TGF-β1 to the culture medium for at least two weeks.

2.3.2 Culture media

Cell line	Culture media
Routine cell culture	
H6c7-kras	50 % (v/v) keratinocyte serum-free medium supplemented with 50 µg/ml BPE 5 ng/ml EGF 4 µg/ml Puromycin 50 % (v/v) RPMI 1640 with 10 % (v/v) FCS 1 % (v/v) L-Gln
PancTu1, Panc89, Panc1, Colo357, BxPc3, A818-6	RPMI 1640 medium supplemented with 10 % (v/v) FCS 1 % (v/v) L-Gln 1 % (v/v) Sodium pyruvate
PT-45	RPMI 1640 medium supplemented with 10 % (v/v) FCS 1 % (v/v) L-Gln
HSC	Stellate Cell Medium supplemented with 2 % (v/v) FCS 1 % (v/v) Pen/Strep 1 % (v/v) Stellate Cell Growth Supplement 2.5 µM ATRA
HMF	Stellate Cell Medium supplemented with 2 % (v/v) FCS 1 % (v/v) Pen/Strep 1 % (v/v) Stellate Cell Growth Supplement 1 ng/ml TGF-β1
T cell activation (TCM)	RPMI 1640 medium supplemented with 10 % (v/v) FCS 20 mM HEPES 1 % (v/v) L-Gln 1 % (v/v) Sodium pyruvate 1 % (v/v) Pen/Strep

Staining medium for CTG labeling	RPMI 1640 medium supplemented with 1 % (v/v) L-Gln 1 % (v/v) Sodium pyruvate
Imaging Medium	RPMI 1640 medium without phenol red supplemented with 1 % (v/v) L-Gln 1 % (v/v) Sodium pyruvate
Coculture	
$CD8^+$ T cells Co H6c7-kras PancTu1	RPMI 1640 medium supplemented with 10 % (v/v) FCS 20 mM HEPES 1 % (v/v) L-Gln 1 % (v/v) Sodium pyruvate 1 % (v/v) Pen/Strep
$CD8^+$ T cells Co HSC HMF	RPMI 1640 medium supplemented with 10 % (v/v) FCS 20 mM HEPES 1 % (v/v) L-Gln 1 % (v/v) Sodium pyruvate 1 % (v/v) Pen/Strep
Spheroids	RPMI 1640 medium supplemented with 10 % (v/v) FCS 20 mM HEPES 1 % (v/v) L-Gln 1 % (v/v) Sodium pyruvate 1 % (v/v) Pen/Strep

2.3.3 Growth factors and cytokines

Compound	Stock concentration (ng/ml)	Manufacturer
EGF, human recombinant	20	ThermoFisher Scientific, Waltham, MA, USA
IFNγ, human recombinant	10	BioLegend, San Diego, CA, USA
IL-2, human recombinant	60	BioLegend, San Diego, CA, USA
IL-6, human recombinant	10	BioLegend, San Diego, CA, USA
IFNγ, human recombinant	10	BioLegend, San Diego, CA, USA
TGF-β1, human recombinant	20	BioLegend, San Diego, CA, USA

2.3.4 Cytostatic drug

Compound	Stock concentration (µg/ml)	Manufacturer
Gemcitabine	1000	Hexal, Holzkirchen, Germany

2.4 Molecular biological material

2.4.1 Primers

Target	5´ - 3´Sequence	Annealing (°C)	Manufacturer
FSP1	fw- AAC TAA AGG AGC TGC TGA CCC rv- TGT TGC TGT CCA AGT TGC TC	60	Biometra GmbH, Jena, Germany
GAPDH	fw- TCC ATG ACA ACT TTG GTA TCG TGG rv- GAC GCC TGC TTC ACC ACC TTC T	58	Eurofins genomics, Ebersberg, Germany
IL-6	fw- ATG CAA TAA CCA CCC CTG AC rv- GAG GTG CCC ATG CTA CAT TT	58	Biomol, Hamburg, Germany
PD-L1	fw- TGA TAC ACA TTT GGA GGA GAC G rv- CCC TCA GGC AATT TGA AAG TAT C	58	Biomol, Hamburg, Germany
TGF-β1	fw- CGT GGA GCT GTA CCA GAA ATA rv- TCC GGT GAC ATC AAA AGA TAA	58	Eurofins genomics, Ebersberg, Germany

2.4.2 Antibodies

AC = T cell activation coculture

CC = Cocultures

FC = Flow Cytometry

IF = Immunofluorescence

IHC = Immunohistochemistry

Specificity (Clone)	Host (Isotype)	Stock in µg/ml (Dilution for application)	Manufacturer
Isotype control			
Isotype (NIP228)	Human (IgG1)	5000	AstraZeneca, Cambridge, UK
Isotype (HP-6025)	Human (IgG4)	1000	Merck, KGaA, Darmstadt, Germany
Isotype-APC (MOPC-21)	Mouse (IgG1)	200	BioLegend, San Diego, CA, USA
Isotype-APC (MOPC-21)	Mouse (IgG2b)	100	BioLegend, San Diego, CA, USA
Isotype-FITC (MOPC-21)	Mouse (IgG1)	500	BioLegend, San Diego, CA, USA
Isotype-PE (MOPC-21)	Mouse (IgG1)	200	BioLegend, San Diego, CA, USA
Isotype-PE-Cy7 (MOPC-21)	Mouse (IgG1)	200	BioLegend, San Diego, CA, USA
Ultra-LEAF™ Isotype (MG1-45)	Mouse (IgG1)	2040	BioLegend, San Diego, CA, USA
Primary Antibodies			
α/βTCR-FITC (IP26)	Mouse (IgG1)	400 (FC: 1:20)	BioLegend, San Diego, CA, USA
αSMA (1A4)	Mouse (IgG2a)	50 (IHC: 1:400)	ThermoFisher Scientific, Waltham, MA, USA

CD3 (UltraLEAF) (OKT3)	Mouse (IgG2a)	1000 (AC: 1:666.7)	BioLegend, San Diego, CA, USA
CD3 (LN10)	Mouse (IgG1)	32 (IHC: 1:100)	Leica Biosystems, Wetzlar, Germany
CD4-APC (RPA-T4)	Mouse (IgG1)	50 (FC: 1:20)	BioLegend, San Diego, CA, USA
CD8 (4B11)	Mouse (IgG2b)	28.5 (IHC: 1:100)	Leica Biosystems, Wetzlar, Germany
CD8a-PE (RPA-T8)	Mouse (IgG1)	50 (FC: 1:20)	BioLegend, San Diego, CA, USA
CD8a-FITC (RPA-T8)	Mouse (IgG1)	200 (FC: 1:20)	BioLegend, San Diego, CA, USA
CD25-APC (BC96)	Mouse (IgG1)	100 (FC: 1:20)	BioLegend, San Diego, CA, USA
CD28 (UltraLEAF) (CD28.2)	Mouse (IgG1)	1000 (AC: 1:1666.7)	BioLegend, San Diego, CA, USA
CD68 (514H12)	Mouse (Ig2a)	37 (IHC: 1:100)	Leica Biosystems, Wetzlar, Germany
CD69-Pe-Cy7 (FN50)	Mouse (IgG1)	100 (FC: 1:20)	BioLegend, San Diego, CA, USA
CD274 Durvalumab	Human (IgG1)	5000 (CC: 1:500)	Kindly provided by AstraZeneca, Cambridge, UK
CD274 (E1L3N)	Rabbit (IgG1)	874 (IF: 1:200 IHC: 1:100)	Cell Signaling, Danvers, MA, USA
CD274-Pe-Cy7 (MIH1)	Mouse (IgG1)	200 (FC: 1:20)	BioLegend, San Diego, CA, USA
CD279 Pembrolizumab	Human (IgG4)	1000 (CC: 1:100)	MSD, Kenilworth, NJ, USA
CD279-PE (EH12.2H7)	Mouse (IgG1)	50 (FC: 1:20)	BioLegend, San Diego, CA, USA
EpCam-APC (9c4)	Mouse (IgG2b)	12 (FC: 1:20)	BioLegend, San Diego, CA, USA

Ki67 (SP6)	Rabbit (IgG1)	30 (IHC: 1:100)	ThermoFisher Scientific, Waltham, MA, USA
Ki67-Alexa Fluor 488 (Ki-67)	Mouse (IgG1)	200 (FC: 1:20)	BioLegend, San Diego, CA, USA
PanCK (AE1/AE3)	Mouse (IgG1)	100 (IHC: 1:200)	ThermoFisher Scientific, Waltham, MA, USA
Ultra-LEAF™ anti IFNγ (B27)	Mouse (IgG1)	2040 (CC: 1:204)	BioLegend, San Diego, CA, USA

2.5 Patient derived material

2.5.1 Ethic statement

Using the liver tissue sections of PDAC patients for research purposes was approved by the ethics committee of the Medical Faculty of Kiel University and the University Hospital Schleswig-Holstein, Campus Kiel (reference number: A110/99). The use of blood donations for research purposes were approved by the ethics committee of the University Hospital Schleswig-Holstein (reference number: A110/99 and D490/17). Written informed consent was obtained from all patients and donors.

2.6 Consumables

Consumable	**Manufacturer**
0.1-10 µl, 10-200 µl, 100-1000 µl pipette tips	Sarstedt, Nümbrecht, Germany
1.25 ml, 5.0 ml Ritips	Ritter, Schwabmünchen, Germany
1.5 ml, 2.0 ml Eppendorf tubes	Sarstedt, Nümbrecht, Germany
12-/24-/96-well flat-bottom plates	Sarstedt, Nümbrecht, Germany
15 ml, 50 ml centrifuge tubes	Sarstedt, Nümbrecht, Germany
5 ml, 10 ml, 25 ml, 50 ml serological pipettes	Sarstedt, Nümbrecht, Germany
75 cm^2 cell culture flasks	Sarstedt, Nümbrecht, Germany
25 cm^2 cell culture flasks	Sarstedt, Nümbrecht, Germany
96-well PCR plates, white	Roche, Basel, Switzerland
96-well V-bottom plates	Greiner Bio-One GmbH, Frickenhausen, Germany
BD Discardit II syringe 5 ml	BD Bioscience, Franklin Lakes, NJ, USA

BD Eclipse Needle 30G x 1/2	BD Bioscience, Franklin Lakes, NJ, USA
BD Plastipak U-40 Insulin 1 ml	BD Bioscience, Franklin Lakes, NJ, USA
BIOFLOAT™ 96-well U-bottom plates - Ultra-low attachment plates (ULA)	faCellitate, Mannheim, Germany
Cell scraper 25 cm	Sarstedt, Nümbrecht, Germany
Coverslip 18 mm diameter	Epredia™, Kalamazoo, MI, USA
CryoPure tube, 1.5 ml, white	Sarstedt, Nümbrecht, Germany
Disposal bag	Sarstedt, Nümbrecht, Germany
Fluoro-Gel (with Tris Buffer)	Electron Microscopy Sciences, Hatfield, PA, USA
LightCycler® 480 Sealing Foil	Roche, Basel, Switzerland
MACS LD Coloumns	Miltenyi Biotec GmbH, Bergisch Gladbach, Germany
Micro-Touch nitrile examination gloves	Ansell GmbH, München, Germany
Parafilm M sealing film	Brand GmbH & Co. KG, Wertheim, Germany
Scalpel	Feather, Osaka, Japan
Starfrost® Slides 76 x 26 mm	Waldemar Knittel Glasbearbeitungs GmbH, Braunschweig, Germany
Transfer pipettes 3.5 ml	Sarstedt, Nümbrecht, Germany

2.7 Kit systems

Consumable	**Manufacturer**
Alexa Fluor™ 488 Tyramide SuperBoost goat, anti-rabbit kit	ThermoFisher Scientific, Waltham, MA, USA
$CD8^+$ T cell isolation kit, human	Miltenyi Biotec GmbH, Bergisch Gladbach, Germany
LEGENDplex™, CD8/NK panel, human	BioLegend, San Diego, CA, USA
LEGENDplex™, CD8/NK Mix and Match panel, human	BioLegend, San Diego, CA, USA
LEGENDplex™, TGF panel, human	BioLegend, San Diego, CA, USA
MycoAlert™ PLUS Mycoplasma Detection Kit	Lonza Group, Basel, Swiss
M30 CytoDeath™ ELISA	VLV bio, Nacka, Sweden
peqGOLD total RNA Kit	VWR International, Radnor, PA; USA
RevertAird First Strand cDNA Synthesis Kit	ThermoFisher Scientific, Waltham, MA, USA

2.8 Laboratory Devices

Device	Manufacturer
Centrifuges	
Heraeus Fresco 17 centrifuge	ThermoFisher Scientific, Waltham, MA, USA
Heraeus Pico 17 centrifuge	ThermoFisher Scientific, Waltham, MA, USA
JE-5.0 Elutriator Rotor	Backmann Coulter GmbH, Krefeld, Germany
Mega Star 1.6	VWR International, Radnor, PA; USA
Mini-Centrifuge	Sustainable Lab Instruments, Mannheim, Germany
Rotina 420 R	Hettich, Tuttlingen, Germany
Incubators/Shaker	
BBD 6220 CO_2 incubator	ThermoFisher Scientific, Waltham, MA, USA
HERA Cell 240 incubator	ThermoFisher Scientific, Waltham, MA, USA
PCMT Thermoshaker	Grant Instruments, Cambridge, UK
PMS-1000i Micorplate shaker	Grant Instruments, Cambridge, UK
Measuring devices	
BD FACSCalibur™ flow cytometer	BD Bioscience, Franklin Lakes, NJ, USA
BD FACSymphony™ A1 flow cytometer	BD Bioscience, Franklin Lakes, NJ, USA
BD FACSverse™ flow cytometer	BD Bioscience, Franklin Lakes, NJ, USA
Infinite 200 PRO Microplate Reader	Tecan Group AG, Männedorf, Switzerland
LightCycler® 480	Roche, Basel, Switzerland
MACSQuant® X flow cytometer	Miltenyi Biotec GmbH, Bergisch Gladbach, Germany
Neubauer counting chamber	Marienfeld Superior GmbH & Co. KG, Lauda-Königshofen, Germany
pH 7110 pH-meter	inoLab, Weilheim, Germany
Microscopes	
AE2000	Motic, Wetzlar, Germany
Evos XL Core Cell Imaging System	AMG, Bothell, USA
Lionheart FX Automated Microscope	BioTek, Bad Friedrichshall, Germany
NYONE® Scientific	Synentec GmbH, Elmshorn, Germany

Other devices	
ARPEGE 110, liquid nitrogen tank	Air Liquide GmbH, Düsseldorf, Germany
BOND-MAX automated IHC/ISH stainer	Leica Biosystems, Wetzlar, Germany
Clamping plate with clamping ring	Hettich, Tuttlingen, Germany
Freezer	Liebherr, Ochsenhausen, Germany
Fridge	Liebherr, Ochsenhausen, Germany
Hamamatsu NanoZoomer S6 digital slide scanner	Hamamatsu Photonics, Shizuoka Prefecture, Japan
HERAfreeze basic freezer (-80°C)	ThermoFisher Scientific, Waltham, MA, USA
Laboport vacuum pump	KNF Neuberger, Freiburg, Germany
MACS MultiStand	Miltenyi Biotec GmbH, Bergisch Gladbach, Germany
Masterflex L/S tubing pump	Cole Parmer Instruments, Novodirect GmbH, Kehl/Rhein, Germany
Mr. Frosty Freezing Container	ThermoFisher Scientific, Waltham, MA, USA
NanoQuant Plate™	Tecan Group AG, Männedorf, Switzerland
VORTEX Genius 3 vortex shaker	IKA-Werke, Staufen, Germany
W12 water bath	Labortechnik medingen, Dresden, Germany
Pipettes	
Finnpipette F1 0.2 – 2 µl	ThermoFisher Scientific, Waltham, MA, USA
Finnpipette F1 1 – 10 µl	ThermoFisher Scientific, Waltham, MA, USA
Finnpipette F1 2 – 20 µl	ThermoFisher Scientific, Waltham, MA, USA
Finnpipette F1 20 – 200 µl	ThermoFisher Scientific, Waltham, MA, USA
Finnpipette F1 100 – 1000 µl	ThermoFisher Scientific, Waltham, MA, USA
Multichannel Finnpipette F1 30 – 300 µl	ThermoFisher Scientific, Waltham, MA, USA
Multichannel Finnpipette F1 5 – 50 µl	ThermoFisher Scientific, Waltham, MA, USA
PIPETBOY acu	Integra Biosciences, Fernwald, Germany
Ripette	Ritter, Schwabmünchen, Germany
Scales	
Precisa BJ 2100D	Precisa Gravimetrics AG, Dietikon, Switzerland
Precisa XB120A	Precisa Gravimetrics AG, Dietikon, Switzerland
Sterile benches	
HERA Safe	ThermoFisher Scientific, Waltham, MA, USA
HERA Safe KS	ThermoFisher Scientific, Waltham, MA, USA

2.9 Software

Software	Manufacturer
BD FACSDiva™ Software	BD Bioscience, Franklin Lakes, NJ, USA
BD CellQuest™ Pro Software	BD Bioscience, Franklin Lakes, NJ, USA
BioRender	Toronto, Ontario, Canada
FlowJo 10.8.1	BD Bioscience, Franklin Lakes, NJ, USA
Gen5 Data Analysis Software	BioTek, Bad Friedrichshall, Germany
GraphPad Prism 9.2	GraphPad Software, San Diego, USA
i-control 2.0 for infinite reader	Tecan Group AG, Männedorf, Switzerland
LEGENDplex Data Analysis software v8	VigeneTech Inc., Carlisle, USA
LightCyclcer® 480 Software	Roche, Basel, Switzerland
MACSQuantifiy™ Software	Miltenyi Biotec GmbH, Bergisch Gladbach, Germany
Mendeley Desktop Version 1.19.8	Elsevier, Amsterdam, Netherlands
Microsoft® 365Version 16.66.1	Microsoft Corporation, Redmond, USA
NDP.view2 software	Hamamatsu Photonics, Shizuoka Prefecture, Japan
YT-SOFTWARE®	Synentec GmbH, Elmshorn, Germany

3 Methods

3.1 Cell biological methods

3.1.1 Thawing cells

Cells were stored in liquid nitrogen at –180 °C for long-term storage. To take cells into cultivation, cells were resuspended with 1 ml prewarmed medium in the cyro tube. The cell suspension was then transferred into a 50 ml tube containing 10 ml of the respective medium. Afterwards, the tube was centrifuged for 5 minutes (min) at 300 xg at room temperature (RT). The supernatant was aspirated, cells were resuspended in 10 ml of their respective medium and transferred into a new 75 cm^2 cell culture flask. On the next day, the medium was removed and fresh prewarmed medium was added.

3.1.2 Cell cultivation

The cultivation of the cells was performed under sterile conditions under a sterile bench. All cell lines were cultivated in a 75 cm^2 cell culture flask with 10 ml of their respective medium (section 2.3.2) at 37 °C, 5 % CO_2, and 86 % humidity. When a confluence of 70 – 90 % was reached, cells were passaged at a ratio between 1:3 and 1:8. For this purpose, medium was discarded, and cells were washed with 5 ml of prewarmed PBS. To detach the cells, 5 ml of either trypsin/EDTA (PDECs) or Accutase (HSteCs) were added to the cell culture flask for 10 – 15 min at 37 °C. To stop the reaction, 5 ml of respective prewarmed medium were added. The cell suspension was transferred into a 50 ml tube and then centrifuged for 5 min at 300 xg at RT. After centrifugation, the supernatant was removed, and the cells were resuspended in 10 ml of their medium. Depending on the cell turnover the respective amount of the cell suspension was transferred to a new cell culture flask and filled up with medium to 10 ml. If needed, additional factors were pipetted into the medium (section 2.3.2.) All cell lines were cultured a maximum of 15 – 20 passages. The cells were regularly examined with a MycoAlert™ PLUS Mycoplasma Detection Kit to assure mycoplasma-free conditions.

3.1.3 Freezing cells

For a longer time periods, cells were stored in liquid nitrogen. Therefore, cells were detached as described in section 3.1.2. After centrifugation, cells were resuspended in prewarmed FCS. Afterwards, 10 % of DMSO were added and the cell suspension was transferred into a cryotube, with a maximum of 1 ml. The cryotubes were placed in a Mr. Frosty freezing container and stored at –80 °C to ensure a slow freezing process. After two days, the cryotubes were transferred into liquid nitrogen.

3.1.4 Counting cells

In order to seed the correct number of cells, cells were counted with the help of a Neubauer counting chamber. For this purpose, the cells were detached, centrifuged, and resuspended as described in section 3.1.2. Ten µl of the cell suspension were filled into the counting chamber. To determine the vital cell number, trypan blue was used at a ratio of 1:10. Trypan blue stains dead cells blue. The following formula determines the number of vital cells per ml:

$$\frac{\text{counted cell number}}{\text{number of counted squares}} \times 10^4 = \frac{\text{cell number}}{\text{ml}}$$

3.1.5 Isolation of peripheral mononuclear blood cells

Peripheral blood mononuclear cells (PBMCs) were isolated from healthy blood donations provided by the Institute of Transfusion Medicine in Kiel. Written informed consents from all donors were obtained. For isolation, a density gradient centrifugation was performed. The leukocyte concentration was transferred into a 75 cm^2 cell culture flask with 20 ml PBS. The leukocyte concentration was diluted with PBS to 70 ml. The suspension was mixed carefully by shaking. Two 50 ml tubes were prepared with 15 ml of Pancoll each. For the next step, 35 ml of the diluted blood suspension were slowly overlaid on top of the Pancoll, forming two phases. Afterwards, samples were centrifuged for 25 min at 350 xg with slow acceleration and no mechanical deceleration. After centrifugation, erythrocytes and granulocytes were located at the bottom and PBMCs in the interphase (Figure 8). To reach the interphase, the supernatant was discarded up to 1 cm above the interphase. The interphase rings containing the PBMCs, were transferred to a new 50 ml tube. The tube was filled up to 50 ml with cold elutriation buffer and centrifuged for 10 min at 300 xg and 4 °C. Afterwards, the cell pellet was resuspended in 10 ml of prewarmed erythrocyte lysis buffer and incubated for 6 min in the dark at RT to remove remaining erythrocytes. After incubation, the tubes were filled up to 50 ml with cold

elutriation buffer and centrifuged for 10 min at 300 xg and 4 °C. In the end, the cell sediment was resuspended in 50 ml cold elutriation buffer and the cell number was determined as described in 3.1.4.

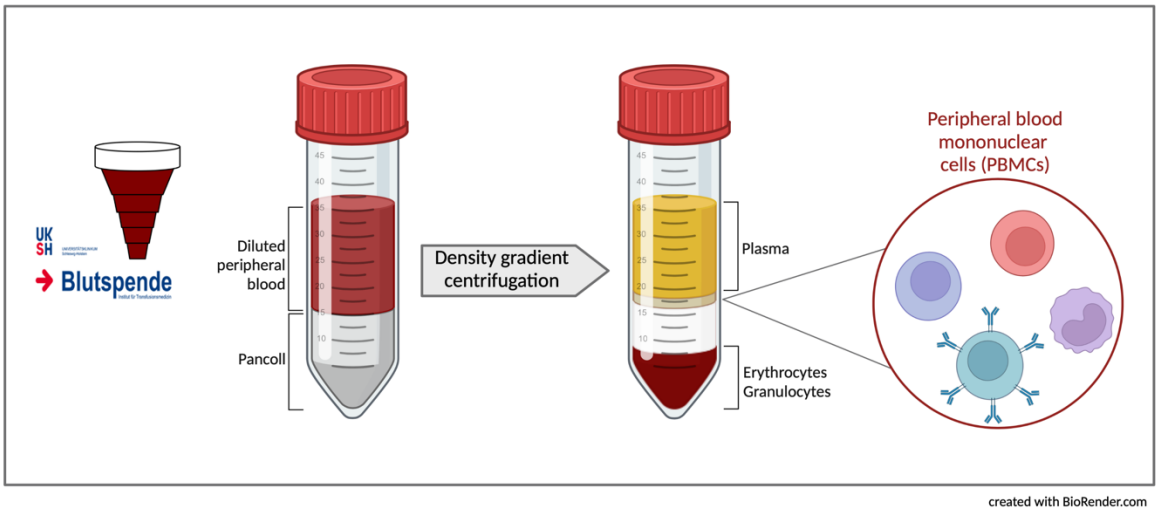

Figure 8: Isolation of peripheral blood mononuclear cells (PBMCs). PBMCs were isolated from healthy blood donations provided by the Institute of Transfusion Medicine in Kiel. The leukocyte concentration was diluted and slowly overlaid on Pancoll. Density gradient centrifugation was performed to separate PBMCs from plasma, erythrocytes, and granulocytes. PBMCs consist of lymphocytes (T cells, B cells, NK cells) and monocytes.

3.1.6 Counterflow centrifugation elutriation

Isolated PBMCs (section 3.1.5) were separated into lymphocytes and monocytes by performing a counterflow centrifugation elutriation (Figure 9). The cell number was adjusted to a maximum of $1.2x10^9$ PBMC/50 ml. First, the tubing system and the elutriation chamber were washed with 70 % ethanol, ddH_2O, and finally with cold elutriation buffer. Afterwards, the PBMC were loaded into the system at 3500 xg, 4°C and a flow rate of 26 ml/min. After loading and washing with 100 ml of elutriation buffer, the different fractions were collected. Fractions 26 A, B, and C were collected with a flow rate of 26 ml/min. For the following fractions, the flow rate was increased in 2 ml/min steps up to 32 ml/min. After fraction 32 (32ml/min), the flow rate was only increased by 1 ml/min steps until a maximum of 42 ml/min. With low flow rates small lymphocytes were pushed out of the elutriation chamber, followed by larger monocytes with increased flow rates. The purity of the fractions was tested by flow cytometry. Monocytes and lymphocytes differ in size and granularity (Supplementary Figure 1). For the assessment of purity, cells were washed once with MACS Buffer and then fixed in fixation solution.

Lymphocyte fractions with a purity higher than 80 % were centrifuged for 10 min at 200 xg and 4 °C to remove dead cells. The cell number was determined (section 3.1.4), followed by centrifugation for 10 min at 300 xg and 4 °C. Afterwards, lymphocytes were resuspended in 900 µl FCS per $30x10^6$ cells

and then 100 µl DMSO were added. The cell suspension was transferred into cryotubes for freezing (section 3.1.3).

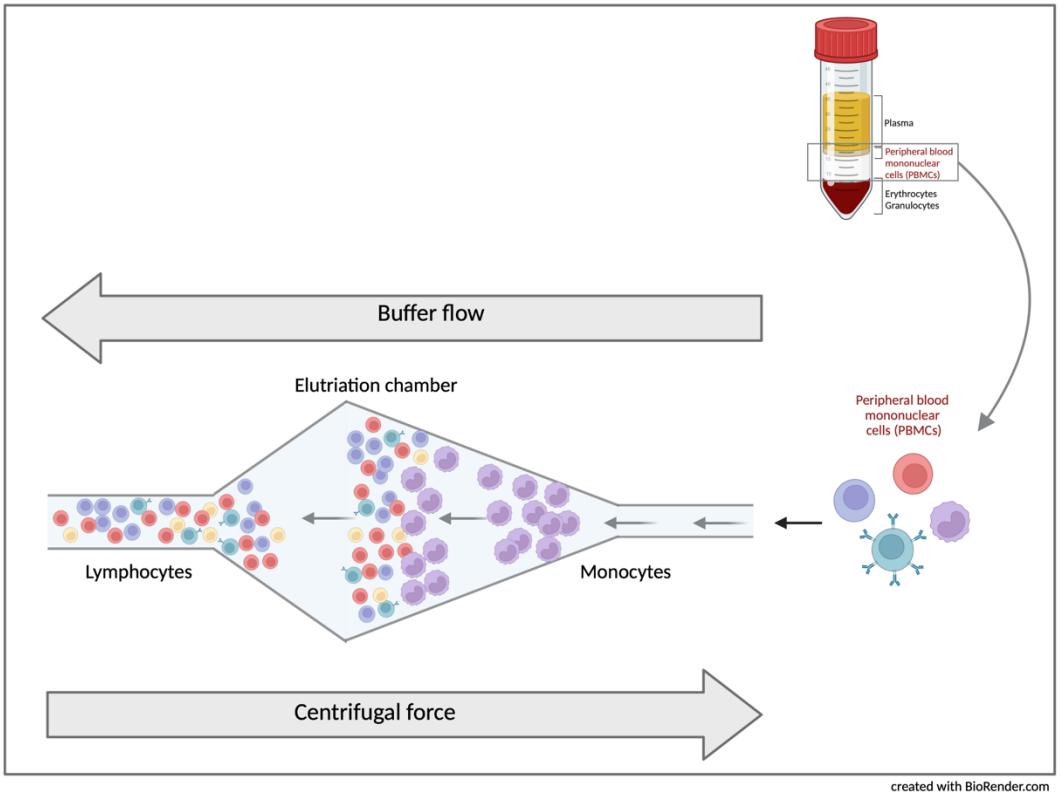

Figure 9: Counterflow centrifugation elutriation. Peripheral blood mononuclear cells (PBMCs) were separated into lymphocytes and monocytes. For this purpose, a counterflow centrifugation elutriation was performed at 3500 xg with an increasing flow rate. Due to the buffer flow, the cells were pushed out of the elutriation chamber. Small cells (lymphocytes) were pushed out at low flow rates, followed by larger cells (monocytes) with increasing flow rates.

3.1.7 Isolation of primary human naïve CD8$^+$ T cells

Naïve CD8$^+$ T cells were isolated from lymphocytes, which were obtained after density gradient centrifugation and counterflow centrifugation (sections 3.1.5 and 3.1.6). The lymphocytes were thawed by adding prewarmed culture medium and the cell suspension was directly diluted in 10 ml prewarmed fresh medium. The cell suspension was centrifuged for 10 min at 300 xg and RT. The cells were resuspended in cold MACS buffer and the total cell number including the dead cells was determined (section 3.1.4). In order to obtain untouched CD8$^+$ T cells, magnetic cell sorting (MACS) using a negative selection strategy with the CD8$^+$ T cell isolation kit from Miltenyi Biotec was performed.

For this purpose, lymphocytes were centrifuged for 10 min at 300 xg and 4 °C and resuspended in 40 µl MACS buffer per 10^7 cells. Afterwards, 5 µl of the biotin-conjugated antibody cocktail per 10^7 cells were added and incubated for 7 min at 4 °C. Here, all non-CD8 positive cells were bound. Then, 30 µl of

MACS buffer and 10 µl of $CD8^+$ T cell MicroBead Cocktail per 10^7 cells were added and resuspended. This was followed by incubation for 15 min at 4 °C. The MicroBeads bind to the biotin-conjugated antibodies. During incubation, MACS LD columns were placed into a magnetic MultiStand and were prepared by rinsing them with 3 ml of MACS buffer. After incubation, the cell suspension was equally distributed onto the LD columns. Per LD column a maximum of 10^8 cells can be added. After the cell suspension ran into the matrix, 3 ml of MACS buffer were added. All non-CD8 positive cells were retained in the column and CD8 positive cells passed through. In the end, all collected unlabeled cells were pooled and the cell number was determined (section 3.1.4). To check the purity of the $CD8^+$ T cells, immunofluorescence staining with antibodies against α/β T cell receptor (TCR), CD4, and CD8a was performed and analyzed by flow cytometry.

3.1.8 Activation and cultivation of primary human naïve $CD8^+$ T cells

To activate primary $CD8^+$ T cells with absence of APC or an antigen, anti-CD3 and anti-CD28 antibodies were used. The TCR complexes on the T cells bind to the CD3 antibodies leading to a first activation signal. For proper activation, a co-stimulatory signal is needed. Normally CD80 or CD86 expressed by APC binds to CD28 on the T cells leading to an activation cascade. Here, anti-CD28 antibodies were used to provide the second activation signal. For T cell proliferation, IL-2 is needed, which is normally secreted by $CD4^+$ T cells [69].

To activate isolated human $CD8^+$ T cells, a 24-well plate was coated with 200 µl anti-CD3 antibody diluted at a concentration of 1.5 µg/ml in PBS per well. The plate was incubated for at least 2 h at 37 °C in the incubator. After the incubation, the plate was washed twice with PBS to remove all unbound antibodies. In the next step, $1.5x10^6$ $CD8^+$ T cells were seeded in 1 ml T cell medium into each well. To each well, 1.5 µg/ml anti-CD28 antibodies were added. Furthermore, $CD8^+$ T cells were stimulated with 60 ng/ml recombinant human IL-2, directly after seeding and again after 72 h.

On day 4 (96 h), $CD8^+$ T cells were collected and seeded in a direct coculture setting with H6c7-kras or PancTu1 cells or either HSC or HMF (sections 3.1.11.2 and 3.1.11.3). For 3D coculture experiments, $CD8^+$ T cells were collected on day 3 (72 h) without a second IL-2 stimulation (section 3.1.11.7).

3.1.9 Dissociation of spheroids

For flow cytometry analysis, cocultured spheroids needed to be dissociated into a single-cell suspension. For this purpose, the supernatant was discarded after 72 h and 100 µl of Accutase were added and incubated for 30 min at 37 C°. Every 10 min, the spheroids were mechanically dissociated with a 30 G needle. After the incubation, 100 µl of TCM were added to stop the reaction. Afterwards, the cells were stained for flow cytometry analysis (section 3.2.1).

3.1.10 Labeling cells with CellTracker Green or CellTrace Violet

For microscopic analysis cells were labeled with CTG or CTV. Therefore, CTG was diluted 1:2000 in staining medium. The cells were resuspended in 1 ml CTG working solution per $5x10^5$ cells and incubated for 30 min at 37 °C. For complete and consistent labeling, cells were gently shaken after 15 min. After incubation, the cells were centrifuged at 300 xg for 5 min and resuspended in their respective medium.

CellTrace Violet was diluted 1:2000 in PBS and then the cells were resuspended in 1 ml CellTrace Violet working solution per $2x10^5$ cells. The cell suspension was gently shaken after 15 min for accurate cell labeling. After another 15 min of incubation, the cell suspension was quenched with 5 ml of TCM. Then, the cells were centrifuged at 300 xg for 5 min and resuspended in their respective medium.

3.1.11 *In vitro* coculture settings

All cocultures were kept in the incubator at 37 °C, 5 % CO_2, and 86 % humidity.

3.1.11.1 Stimulation of PDECs

To examine the PD-L1 expression and the inducibility of PD-L1 expression, H6c7-kras, Panc89, PancTu1, Panc1, Colo357, BxPc3, A818-6, and PT-45 cells were stimulated and PD-L1 expression was analyzed. Therefore, the cells were seeded at a density of $5x10^4$ in 2 ml of the respective medium on day 0. On the next day, the medium was changed to TCM and the cells were either left untreated or were stimulated with 20 ng/ml TGF-β1, 10 ng/ml IL-6, 1 ng/ml Gemcitabine, or 10 ng/ml IFNγ. After 72 h, cells were stained for PD-L1 and analyzed by flow cytometry analysis (section 3.2.1).

3.1.11.2 2D Coculture of PDECs and $CD8^+$ T cells

To determine the influence of $CD8^+$ T cells on H6c7-kras cells and PancTu1 cells, and *vice versa*, a direct coculture in a 12-well plate was conducted. To represent an early stage of progression the pre-malignant cell line H6c7-kras and for later progression, the malignant cell line PancTu1 were used. Further, both cell lines exhibit different cell surface levels of PD-L1.

On day 0, $CD8^+$ T cells were activated (section 3.1.8). On day 3, H6c7-kras and PancTu1 cells were seeded with a density of $5x10^4$ in 2 ml of their respective medium. On the next day (day 4), activated $CD8^+$ T cells (AC: 4 days) were collected by carefully resuspending them in the well of the activation culture and transferring them into warm PBS. Afterwards, the cells were centrifuged at 300 xg for 10 min at RT and then the cells were counted (section 3.1.4). The medium of the PDECs was discarded and 2 ml of TCM were added to the monocultured H6c7-kras and PancTu1 cells. To the other wells containing H6c7-kras and PancTu1 cells, $1x10^6$ $CD8^+$ T cells were added in 2 ml TCM. In parallel, $CD8^+$ T

cells were seeded in monoculture under identical conditions. After 72 h, mono- and cocultures ended (day 7). The experimental setting is depicted in Figure 10.

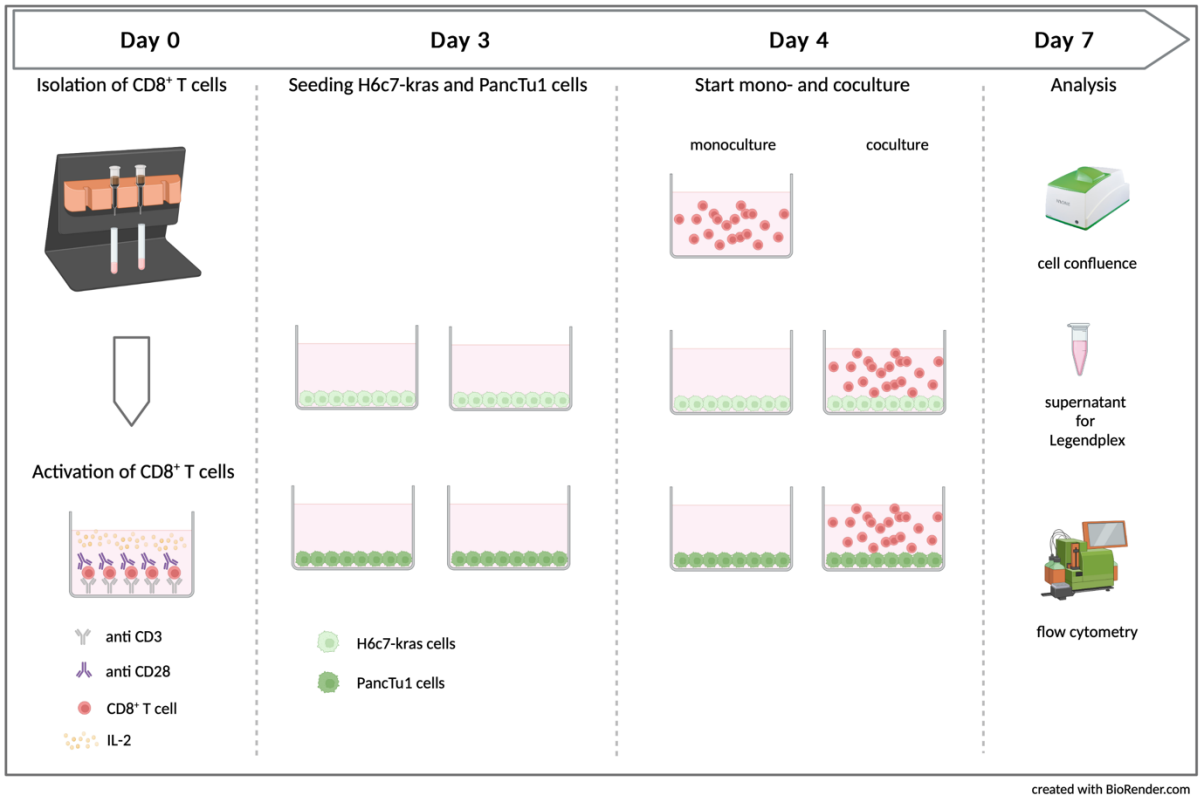

Figure 10: 2D coculture of pancreatic ductal epithelial cells (PDECs) and CD8$^+$ T cells. On day 0, CD8$^+$ T cells were isolated by magnetic cell separation from lymphocytes and then activated with anti-CD3 and anti-CD28 antibodies, as well as IL-2 for 4 days. On day 3, H6c7-kras and PancTu1 cells were seeded with a density of 5x10^4 in 2 ml of their respective medium. On the next day, activated CD8$^+$ T cells were added to the PDECs at a ratio of 1:20 in 2 ml T cell medium (TCM). In parallel, all cells were cultured in monoculture. After 72 h (day 7), mono- and cocultures ended. The supernatants were taken for Legendplex analysis. Further, the confluence of PDECs was measured. Finally, PDECs and CD8$^+$ T cells were analyzed by flow cytometry.

3.1.11.3 2D coculture of human hepatic stromal cells and CD8$^+$ T cells

To determine the influence of the hepatic microenvironment on CD8$^+$ T cells, a direct coculture in a 12-well plate was performed. HSC were used to represent a physiological, uninflamed liver microenvironment and small metastases, while HMF were used representative for an inflamed liver microenvironment and large metastases [160–162].

On day 0, CD8$^+$ T cells were activated (section 3.1.8). On day 3, HSC and HMF were seeded with a density of 3x10^4 in 2 ml of their respective medium. On the next day, the medium of the hepatic stromal cells was discarded and replaced by 2 ml TCM in monocultured HSC and HMF. Further, activated CD8$^+$ T cells (AC: 4 days) were collected as described above and 1x10^6 T cells in 2 ml TCM

were added to HSC and HMF, respectively. In parallel, CD8$^+$ T cells were seeded in monoculture. After 72 h, mono- and cocultures ended (day 7). Figure 11 shows the experimental setting.

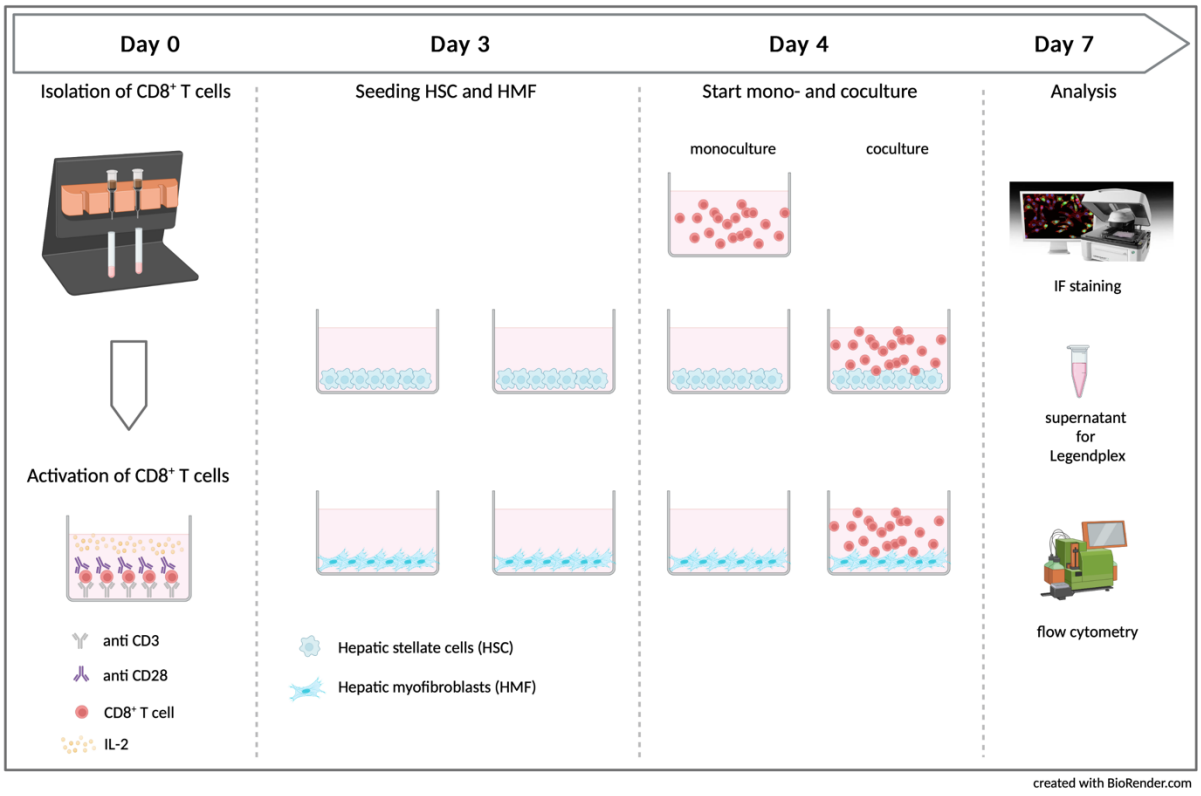

Figure 11: 2D coculture of human hepatic stromal cells and CD8$^+$ T cells. On day 0, CD8$^+$ T cells were isolated by magnetic cell separation from lymphocytes and then activated with anti-CD3 and anti-CD28 antibodies as well as IL-2 for 4 days. On day 3, hepatic stellate cells (HSC) and hepatic myofibroblasts (HMF) were seeded with a density of 3x10^4 in 2 ml of their respective medium. On the next day, activated CD8$^+$ T cells were added to the hepatic stromal cells at a ratio of 1:33 in 2 ml T cell medium (TCM). All cells were also cultured in monoculture. After 72 h (day 7), mono- and cocultures ended. The supernatants were taken for Legendplex analysis. Further, a PD-L1 immunofluorescence staining of hepatic stromal cells was performed. Finally, hepatic stromal cells and CD8$^+$ T cells were analyzed by flow cytometry.

Durvalumab treatment

To investigate the effect of PD-L1 inhibition on the hepatic microenvironment and CD8$^+$ T cells and their interaction, PD-L1 was blocked with Durvalumab.

As described above, CD8$^+$ T cells were activated on day 0 (section 3.1.8). On day 3, HSC and HMF were seeded and one day later, the medium was discarded. Afterwards, 1x10^6 activated CD8$^+$ T cells (AC: 4 days) were added in 2 ml TCM. In parallel, all cells were seeded in monoculture. Further, monocultured and cocultured cells were treated with 10 µg/ml Durvalumab or the respective isotype control (hIgG1). The cultures were maintained for 72 h. The experimental settings are displayed in Figure 12.

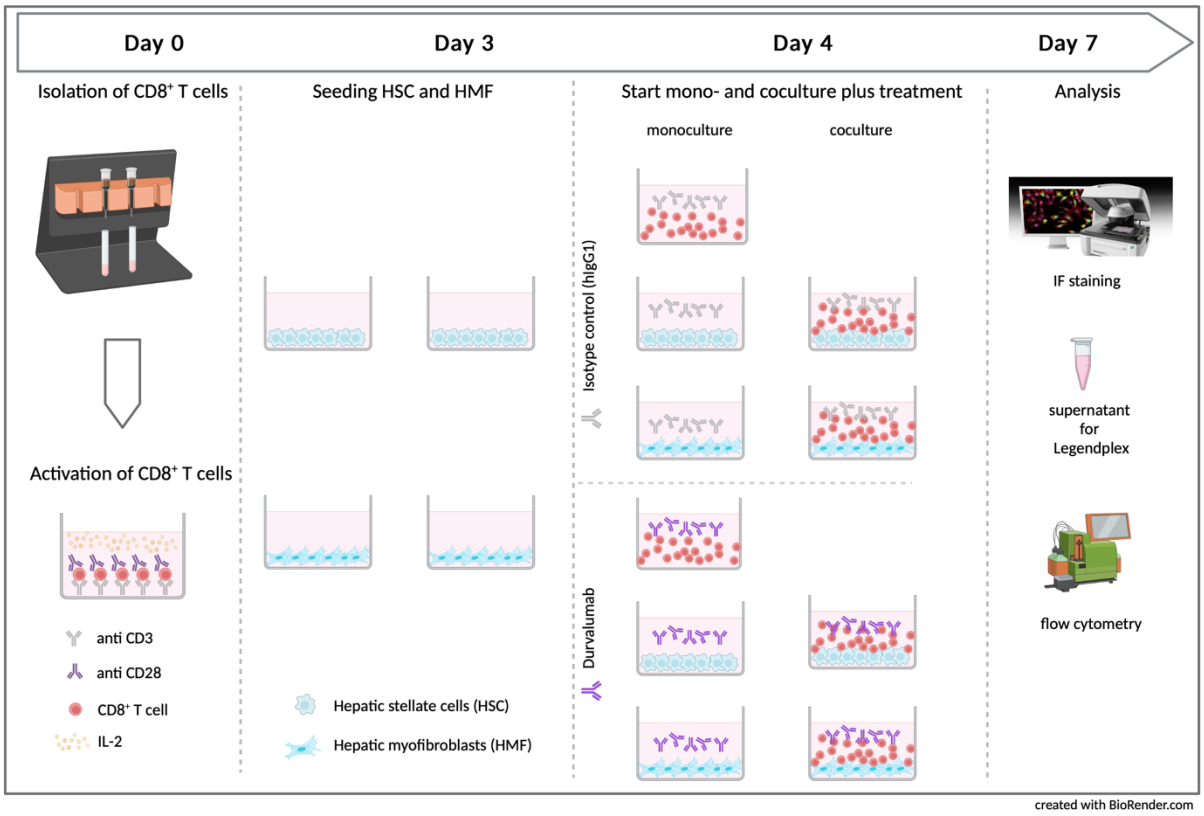

Figure 12: 2D direct coculture of human hepatic stromal cells with CD8⁺ T cells and treatment with Durvalumab. On day 0, CD8⁺ T cells were isolated by magnetic cell separation from lymphocytes and then activated with anti-CD3 anti-CD28 antibodies as well as IL-2 for 4 days. On day 3, hepatic stellate cells (HSC) and hepatic myofibroblasts (HMF) were seeded with a density of $3x10^4$ in 2 ml of their respective medium. On the next day, activated CD8⁺ T cells were added to the hepatic stromal cells at a ratio of 1:33 in 2 ml T cell medium (TCM). All cells were also cultured in monoculture. Further, mono- and cocultured cells were treated with 10 µg/ml Durvalumab or the respective isotype control (hIgG1). After 72 h (day 7), mono- and cocultures ended. The supernatants were taken for Legendplex analysis. Further, a PD-L1 immunofluorescence staining of hepatic stromal cells was performed. Finally, hepatic stromal cells and CD8⁺ T cells were analyzed by flow cytometry.

IFNγ blockade

As described above, on day 0, CD8⁺ T cells were activated (section 3.1.8). On day 3, hepatic stromal cells were seeded. On the next day, the medium of the HSC and HMF was discarded and $1x10^6$ activated CD8⁺ T cells (4 days) were added in 2 ml TCM. In parallel, all cells were cultured in monoculture. To block IFNγ-mediated activities, mono- and cocultured cells were treated with 10 µg/ml ultra-LEAF™ IFNγ antibody or the respective ultra-LEAF™ isotype control. After 72 h, mono- and cocultures ended. Cell surface levels of PD-L1 were analyzed on hepatic stromal cells by immunofluorescence (IF) staining and flow cytometry.

3.1.11.4 2D coculture of PDECs and CD8$^+$ T cells after pre-coculture with hepatic stromal cells

To investigate the influence of the hepatic microenvironment on the killing efficacy of CD8$^+$ T cells, PDEC death was determined after coculture of CD8$^+$ T cells that had been pre-cocultured with hepatic stromal cells. First, H6c7-kras and PancTu1 cells were stained with CTG (section 3.1.10). Afterwards, H6c7-kras and PancTu1 cells were seeded at a density of 5x10^4 in 200 µl of the respective medium in a 96-well plate (day 6). On the next day, CD8$^+$ T cells were collected from the direct coculture with hepatic stromal cells (section 3.1.11.3). CD8$^+$ T cells were either left untreated in coculture with hepatic stromal cells or were treated with Durvalumab or the respective isotype control. The pre-mono- and cocultured CD8$^+$ T cells were added at a ratio of 1:20 (1x10^6) to H6c7-kras and PancTu1 cells in 200 µl TCM (day 7). After 24 h, CD8$^+$ T cells were carefully removed and PDECs were stained with Hoechst 33528 (1:500) in imaging medium. Cell confluence and cell count were measured on the NYONE® Scientific microscope and analyzed with the YT-SOFTWARE®. For cell confluence analysis, the YT-SOFTWARE® only considered the cells with a green-fluorescence signal (CTG) for the cell confluence calculation and for cell count analysis, only cells with a green-fluorescence signal (CTG) and blue-fluorescence signal (Hoechst) were counted, leaving CD8$^+$ T cells out of the calculations.

The experimental setup of the coculture of PDECs and CD8$^+$ T cells after pre-coculture with hepatic stromal cells is shown in Figure 13. Further, the experimental setup of PDECs and CD8$^+$ T cells after pre-mono and coculture combined with Durvalumab treatment is shown in Figure 14.

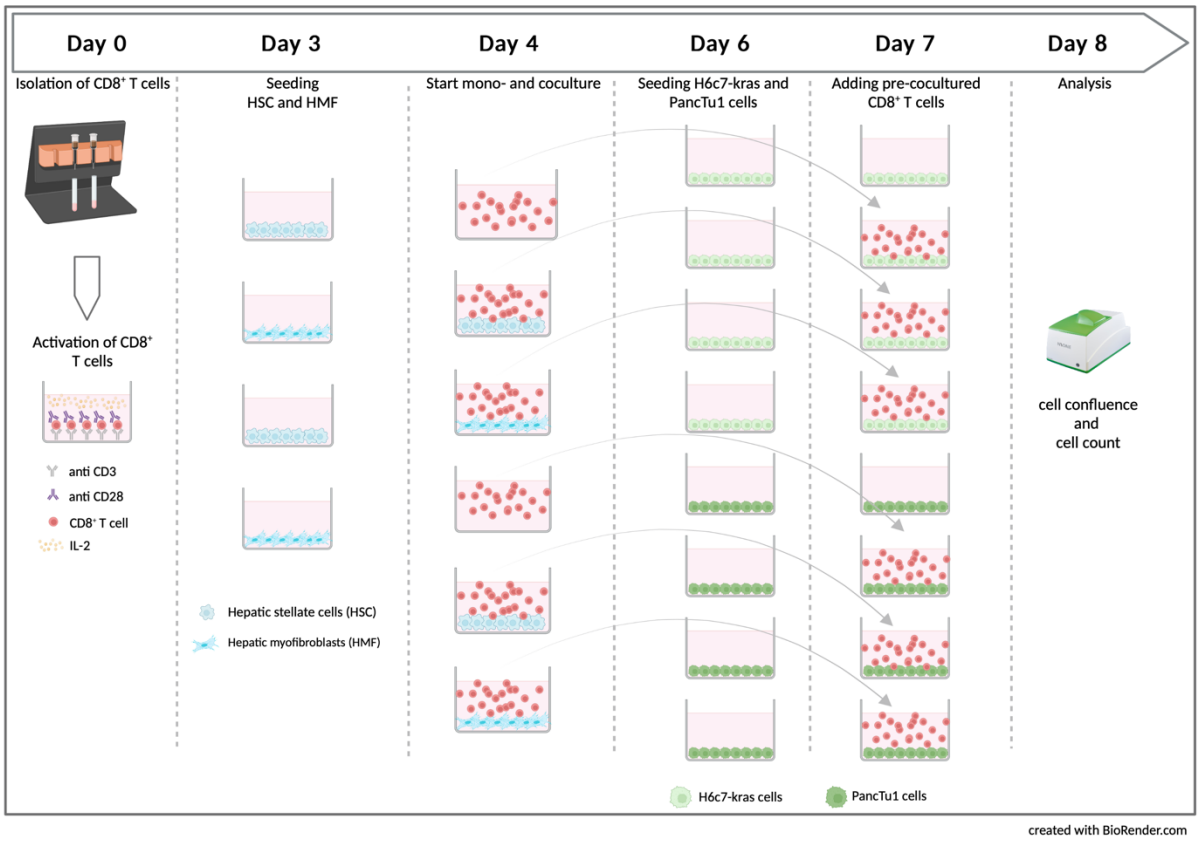

Figure 13: 2D coculture of pancreatic ductal epithelial cells (PDECs) and CD8⁺ T cells after pre-coculture with either hepatic stellate cells (HSC) or hepatic myofibroblasts (HMF). On day 0, CD8⁺ T cells were isolated by magnetic cell separation from lymphocytes and activated with anti-CD3 and anti-CD28 antibodies as well as IL-2 for 4 days. On day 3, HSC and HMF were seeded with a density of $3x10^4$ in 2 ml of their respective medium. On the next day, activated CD8⁺ T cells were added to the hepatic stromal cells at a ratio of 1:33 in 2 ml T cell medium (TCM). On day six, H6c7-kras and PancTu1 cells were labeled with CellTracker Green and were then seeded at a density of $5x10^4$ in 200 µl of their respective medium in a 96-well plate. On the next day, CD8⁺ T cells were collected from the direct coculture with HSC or HMF. CD8⁺ T cells pre-monocultured or pre-cocultured with either HSC or HMF were added to PDECs at a ratio of 1:20 in TCM. After 24 h (day 8), CD8⁺ T cells were removed and the PDECs were stained with Hoechst. The cell confluence and cell number were determined.

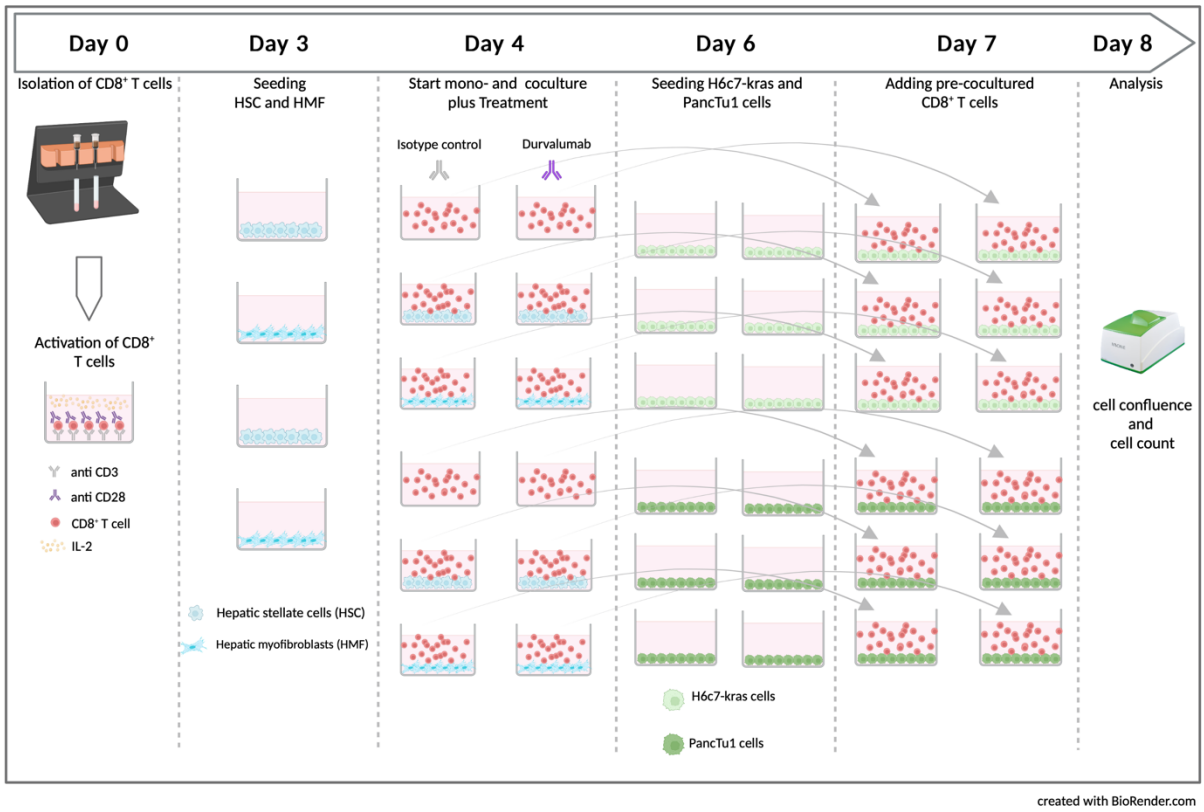

Figure 14: 2D coculture of pancreatic ductal epithelial cells (PDECs) and CD8$^+$ T cells after pre-coculture with hepatic stellate cells (HSC) or hepatic myofibroblasts (HMF) and Durvalumab treatment. On day 0, CD8$^+$ T cells were isolated by magnetic cell separation from lymphocytes and activated with anti-CD3 and anti-CD28 antibodies as well as IL-2 for 4 days. On day 3, HSC and HMF were seeded with a density of 3x10^4 in 2 ml of their respective medium. On the next day, activated CD8$^+$ T cells were added to the hepatic stromal cells at a ratio of 1:33 in 2 ml T cell medium (TCM) and were treated with 10 µg/ml Durvalumab or the respective isotype control. On day six, H6c7-kras and PancTu1 cells were labeled with CellTracker Green and were then seeded at a density of 5x10^4 in 200 µl of their respective medium in a 96-well plate. On the next day, CD8$^+$ T cells were collected from the direct coculture with HSC or HMF. CD8$^+$ T cells pre-monocultured or pre-cocultured with either HSC or HMF were added to PDECs at a ratio of 1:20 in TCM. After 24 h (day 8), CD8$^+$ T cells were removed and the PDECs were stained with Hoechst. The cell confluence and cell number were determined.

3.1.11.5 Spheroid monoculture of human PDECs

In order to determine which PDECs can form spheroids with viable cells, H6c7-kras, PancTu1, Panc89, Panc1, Colo357, BxPc3, A818-6, and PT-45 cells were labeled with CTG (section 3.1.10) seeded at a density of 2x10^4 in 200 µl of TCM in a 96-well ULA plate. After seeding, the plate was centrifuged at 300 xg for 5 min at RT. After 72 h, the spheroids were stained with PI (1:400) for 30 min in imaging medium. The measurement of PDECs was performed on the Lionheart FX Automated microscope.

3.1.11.6 Spheroid coculture of human PDAC cells and human hepatic myofibroblasts

In order to mimic small and large PDAC metastases in the liver, different ratios of PancTu1 or Panc89 cells, and HMF were seeded for spheroid formation. Here, a PDAC cell:HMF ratio of 3:1 mimics a large and a ratio of 5:1 a small metastasis. HMF and either PancTu1 or Panc89 cells were seeded together in different ratios with a total cell number of $2x10^4$ in 150 µl TCM in a 96-well ULA plate. As control, PancTu1 and Panc89 cells were seeded as monoculture spheroids, respectively. After seeding, the plate was centrifuged at 300 xg for 5 min and spheroids were cultured for 72 hours. The different culture settings are shown in Figure 15.

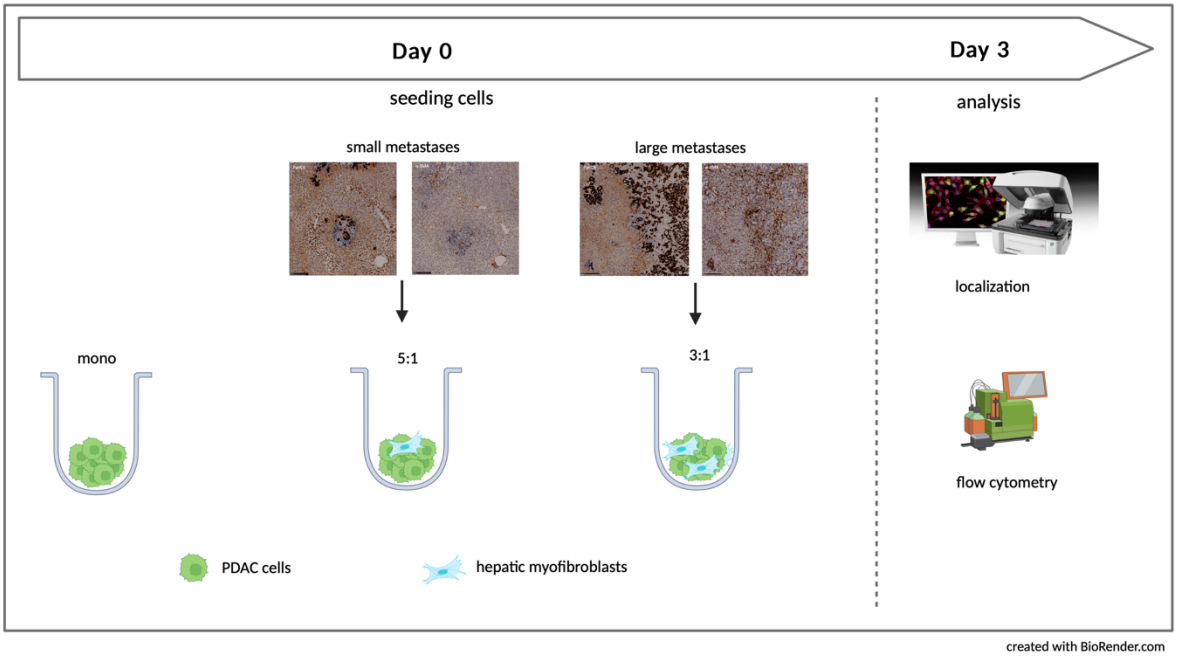

Figure 15: 3D spheroid coculture of human PDAC cells and human hepatic myofibroblasts (HMF). On day 0, HMF and either PancTu1 or Panc89 cells were seeded together at different ratios with a total cell number of $2x10^4$ in 150 µl T cell medium (TCM) in a 96-well ultra-low attachment (ULA) plate. As control, PancTu1 and Panc89 cells were seeded in monoculture. After seeding, the plate was centrifuged at 300 xg for 5 min. On day 3 pictures were taken with the Lionheart FX automated microscope and afterwards the spheroids were dissociated for flow cytometry analysis.

Microscopic analysis

To analyze the distribution of PDAC cells and HMF in the spheroids, PDAC cells were stained with CTG and HMF with CTV (section 3.1.10).

After labeling the cells, they were seeded at different ratios, as mentioned above, in ULA plates. After 72 h, pictures were taken with the Lionheart FX automated microscope.

To determine the size of the spheroids, phase contrast z-stack pictures were taken and the diameter from top to bottom and left to right was measured. Then, the mean of both measurements was calculated. The measurement is shown in Supplementary Figure 2.

3.1.11.7 Culture of CD8⁺ T cells with mono- and coculture PDAC spheroids

To determine the effect of PDAC cells and different amounts of HMF on the activation and cytotoxic phenotype of CD8⁺ T cells, medium from spheroid cultures was removed after 48 h and 20x10^4 activated CD8⁺ T cells (AC: 3 days) (section 3.1.8) were added in 150 µl of TCM/well for further 24 h. A schematic illustration of PDAC mono- and coculture spheroids cultured with CD8⁺ T cells is shown in Figure 16.

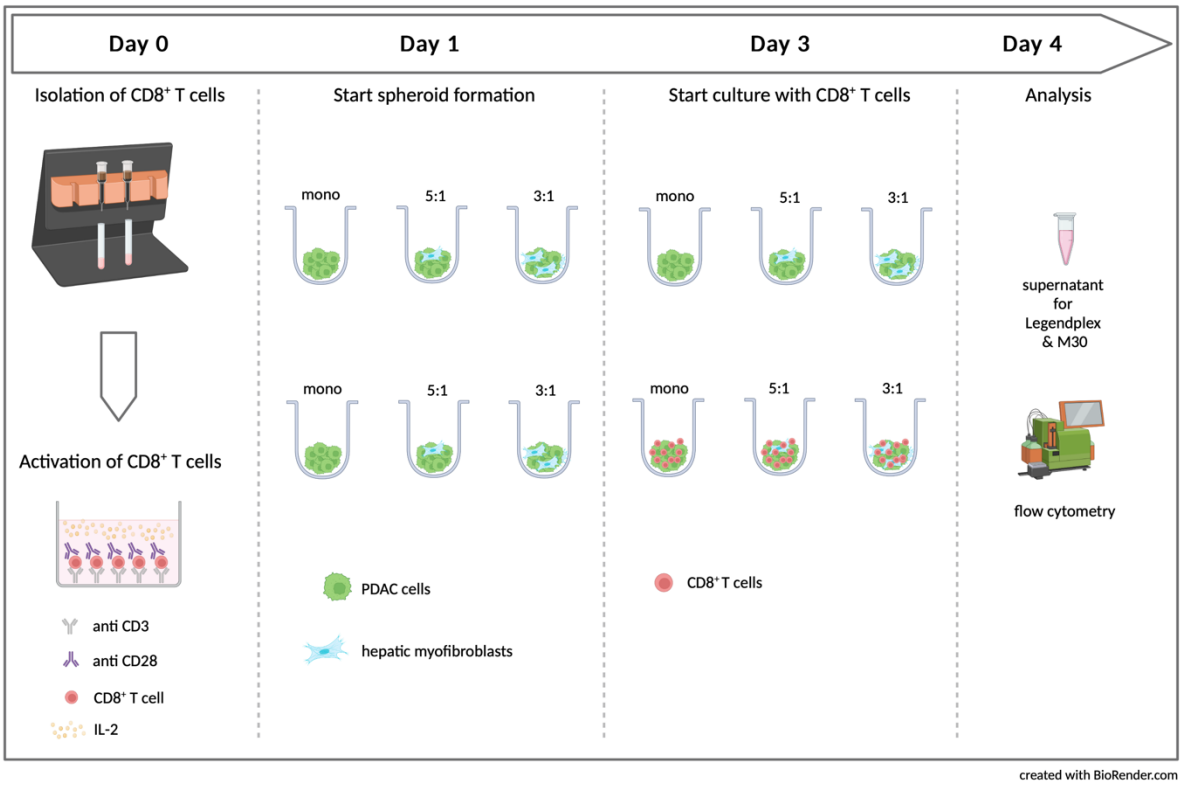

Figure 16: Culture of CD8⁺ T cells with mono- and coculture PDAC spheroids. On day 0, CD8⁺ T cells were isolated by magnetic cell separation from lymphocytes and then activated with anti-CD3 and anti-CD28 antibodies as well as IL-2 for 3 days. On day 1, hepatic myofibroblasts (HMF) and either PancTu1 or Panc89 cells were seeded together in different ratios with a total cell number of 2x10^4 in 150 µl T cell medium (TCM) in a 96-well ultra-low attachment (ULA) plate. As control, PancTu1 and Panc89 cells were seeded in monoculture. After seeding, the plate was centrifuged at 300 xg for 5 min. On day 3, the medium was changed and activated CD8⁺ T cells (20x10^4) were added in 150 µl TCM/well. After 24 h, supernatants were taken for Legendplex and M30 analysis. Further, CD8⁺ T cells were analyzed by flow cytometry.

Durvalumab and Pembrolizumab treatment

To investigate whether ICI treatment enhances the effector phenotype of CD8⁺ T cells along with enhanced PDAC cell death, PD-L1 and PD-1 were blocked by Durvalumab and Pembrolizumab, respectively. For this purpose, activated CD8⁺ T cells were added at a ratio of 1:10 (20x10^4) to the

different spheroid cocultures on day 3 (section 3.1.11.6) and were either treated with 10 µg/ml Durvalumab, 10 µg/ml Pembrolizumab, or their respective isotype control (10 µg/ml hIgG1 or hIgG4) for 24 h. A schematic illustration of PDAC spheroids cultures settings with $CD8^+$ T cells and treatment is shown in Figure 17.

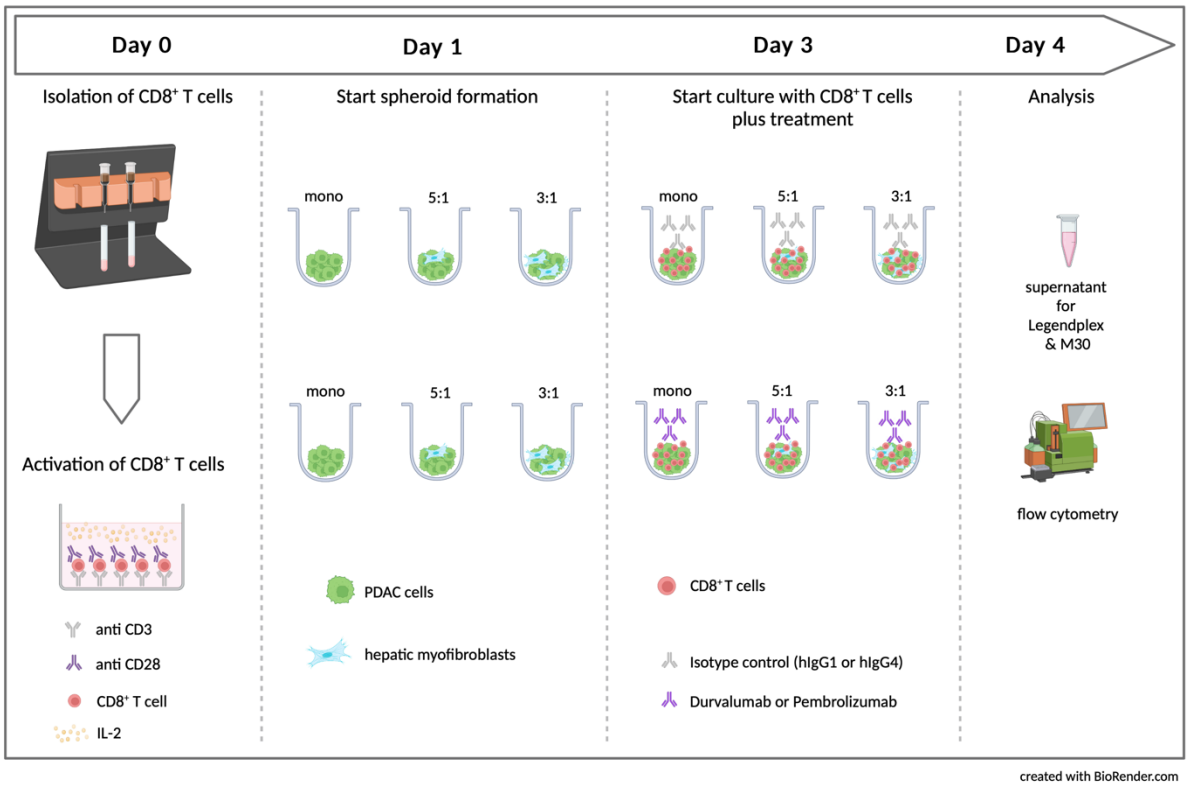

Figure 17: Effect of immune checkpoint inhibition on mono- and coculture PDAC spheroids. On day 0, $CD8^+$ T cells were isolated by magnetic cell separation from lymphocytes and then activated with anti-CD3 and anti-CD28 antibodies as well as IL-2 for 3 days. On day 1, hepatic myofibroblasts (HMF) and either PancTu1 or Panc89 cells were seeded together at different ratios with a total cell number of $2x10^4$ in 150 µl T cell medium (TCM) in a 96-well ultra-low attachment (ULA) plate. As control, PancTu1 and Panc89 cells were seeded in monoculture. After seeding, the plate was centrifuged at 300 xg for 5 min. On day 3, the medium was changed and activated $CD8^+$ T cells ($20x10^4$) were added in 150 µl TCM/well. Further, spheroid cocultures were either treated with 10 µg/ml Durvalumab, 10 µg/ml Pembrolizumab, or their respective isotype control antibodies (hIgG1 or hIgG4). After 24 h, supernatants were taken for Legendplex and M30 analysis. Further, $CD8^+$ T cells were analyzed by flow cytometry.

Gemcitabine treatment

Since treatment with Gemcitabine represents the most frequent first-line therapy of PDAC patients [25], it was investigated whether Gemcitabine impacts PD-L1 and PD-1 expression, as well as the effector phenotype of $CD8^+$ T cells in the context of the PDAC cell-HMF interplay. For this purpose, seeded cocultured spheroids (section 3.1.11.6) were either left untreated or treated with 10 µg/ml

Gemcitabine 24 h after seeding (day 2). On the next day, the medium was removed and activated CD8$^+$ T cells were added for another 24 h (see above). A schematic illustration of Gemcitabine pretreated PDAC spheroids cocultured with CD8$^+$ T cells is shown in Figure 18.

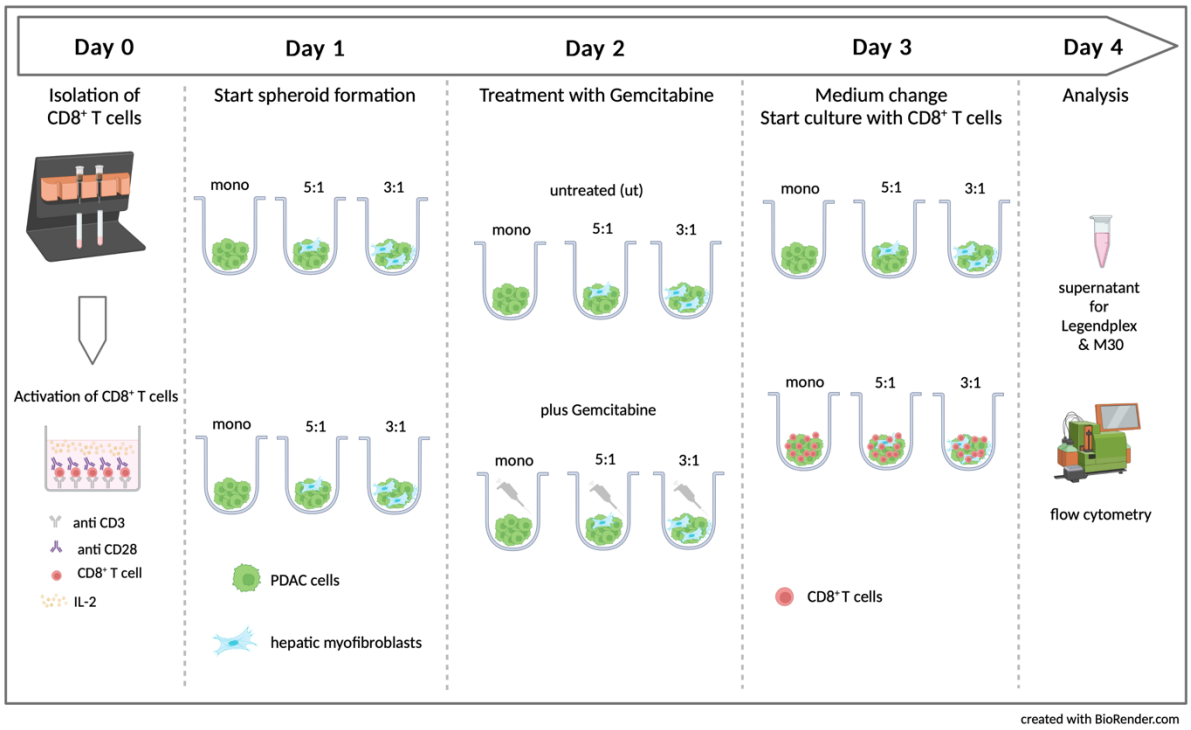

Figure 18: Effect of pretreatment with Gemcitabine of mono- and coculture PDAC spheroids coculture with CD8$^+$ T cells. On day 0, CD8$^+$ T cells were isolated by magnetic cell separation from lymphocytes and then activated with anti-CD3 and anti-CD28 antibodies as well as IL-2 for 3 days. On day 1, hepatic myofibroblasts (HMF) and either PancTu1 or Panc89 cells were seeded together at different ratios with a total cell number of 2x10^4 in 150 µl T cell medium (TCM) in a 96-well ultra-low attachment (ULA) plate. As control, PancTu1 and Panc89 cells were seeded in monoculture. After seeding, the plate was centrifuged at 300 xg for 5 min. On the next day (day 2), spheroids were either left untreated or were treated with 10 µg/ml Gemcitabine. On day 3, the medium was changed and activated CD8$^+$ T cells (20x10^4) were added in 150 µl TCM/well. After 24 h, supernatants were taken for Legendplex and M30 analysis. Further, CD8$^+$ T cells were analyzed by flow cytometry.

Combinational treatment

To evaluate whether a combinational treatment with Gemcitabine and ICIs enhances the effector phenotype of CD8$^+$ T cells and PDAC cell death, seeded spheroids (see above) were treated with 10 µg/ml Gemcitabine 24 h after seeding (day 2). On day 3, the medium was removed, activated CD8$^+$ T cells were added and treated with either 10 µg/ml Durvalumab, or 10 µg/ml Pembrolizumab, or the

respective control antibodies (10 µg/ml hIgG1 or hIgG4), for 24 h. The experimental setup is shown in Figure 19.

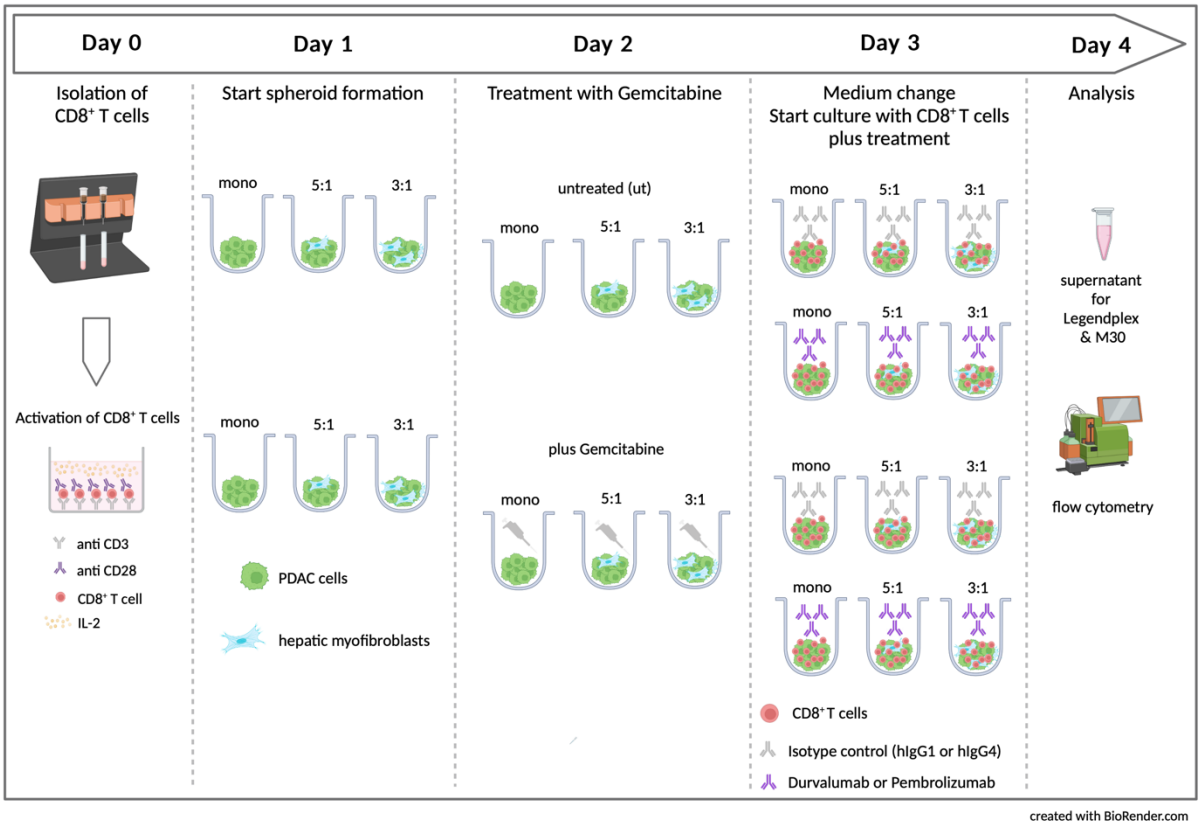

Figure 19: Effect of pretreatment with Gemcitabine on immune checkpoint inhibition of mono- and coculture PDAC spheroids cultured with CD8⁺ T cells. On day 0, CD8⁺ T cells were isolated by magnetic cell separation from lymphocytes and then activated with anti-CD3 and anti-CD28 antibodies as well as IL-2 for 3 days. On day 1, hepatic myofibroblasts (HMF) and either PancTu1 or Panc89 cells were seeded together at different ratios with a total cell number of $2x10^4$ in 150 µl T cell medium (TCM) in a 96-well ultra-low attachment (ULA) plate. As control, PancTu1 and Panc89 cells were seeded in monoculture. After seeding, the plate was centrifuged at 300 xg for 5 min. On the next day, spheroids were either left untreated or were treated with 10 µg/ml Gemcitabine. On day 3, the medium was changed and activated CD8⁺ T cells ($20x10^4$) were added in 150 µl TCM/well. Further, spheroid cocultures were either treated with 10 µg/ml Durvalumab, 10 µg/ml Pembrolizumab, or with 10 µg/ml of their respective isotype control (hIgG1 or hIgG4), After 24 h, supernatants were taken for Legendplex and M30 analysis. Further, CD8⁺ T cells were analyzed by flow cytometry.

3.2 Immunobiological methods

3.2.1 Flow cytometry

To investigate the expression of cell surface proteins on CD8⁺ T cells, PDECs, and hepatic stromal cells, an immunofluorescence staining was performed on ice and the analysis was conducted with a flow cytometer. In 2D cultures, CD8⁺ T cells were first removed by gently pipetting up and down. PDECs and

hepatic stromal cells were detached as described in section 3.1.2. In 3D cultures, first $CD8^+$ T cells were removed from the spheroid cultures, by gently pipetting the medium up and down in the well and then the spheroids were dissociated (section 3.1.9). Afterwards, all cells were counted (section 3.1.4) and $0.5x10^6$ to $1.5x10^6$ cells were resuspended in 100 µl of MACS buffer and 5 µl of human Fc receptor blocking solution, followed by an incubation for 10 min at RT. Afterwards, $2x10^5$ cells per staining were pipetted into a 96-well V-bottom plate. The wells were filled up to 200 µl with MACS buffer. The cell suspension was mixed by resuspension and then centrifuged for 10 min at 300 xg and 4 °C. The supernatant was discarded and the staining was conducted. The respective antibody concentration (section 2.4.2) was mixed in 25 µl MACS buffer. The cells were resuspended in the MACS buffer/antibody solution and incubated for 30 min at 4 °C. Thereafter, the cells were washed twice with 200 µl of cold MACS buffer. Between each washing step, the cells were centrifuged for 10 min at 300 xg and 4 °C. In the end, the cells were resuspended in 150 µl fixation buffer. The plates were sealed with parafilm and aluminum foil for storage at 4 °C. The analysis was performed on a BD FACSCalibur™ or MACSQuant® X flow cytometer. For each measurement between $2x10^4$ and $3x10^4$ cells were measured. The final analysis was done with the FlowJo 10 software. To exclude unspecific binding and autofluorescence, an isotype control staining was performed in parallel for every specific staining. To evaluate the specific cell expression of each protein, the median fluorescence intensity (MFI) ratio was calculated by dividing the MFI of the specific staining by the MFI of the isotype control.

3.2.2 Multiplex analysis of supernatants

The supernatants from mono- and cocultured $CD8^+$ T cells with PDECs or hepatic stromal cells were analyzed to determine concentration of cytokines and effector molecules in cell culture supernatants by using “LEGENDplex™, CD8/NK panel, human”, “LEGENDplex™, CD8/NK Mix and Match panel, human” or “LEGENDplex™, TGFβ panel, human”. The different beads are conjugated with a specific antibody, binding to the particular analyte in the supernatant. The beads differ in size and fluorescence intensities. For this purpose, the supernatants were taken and centrifuged for 10 min at 15,000 xg and at 4 °C to remove all remaining cells. Then, the reagents were prewarmed at RT and were prepared. Afterwards, the 20x wash buffer was diluted with ddH_2O. The standard cocktail was diluted and mixed in 250 µl of assay buffer, yielding the standard with the highest concentration. The top standard concentration differs from analyte to analyte and from kit to kit. Further, 1:4 dilutions were performed to gain 6 standards and a negative control containing only assay buffer. The assay was performed in a 96-well V-bottom plate by pipetting 62.5 µl of the assay buffer in each standard and sample well. Thereafter, 12.5 µl of the standard dilutions and 12.5 µl of the samples (supernatants) were added to the respective well. Then, 12.5 µl of the mixed beads were added. The beads need to be vortexed for 1 min before use. In case of a mix and match panel the amount of the different beads needed to be

mixed and diluted to 1x with assay buffer. The plate was sealed with a plate sealer, covered with aluminum foil to protect it from light, and incubated on a plate shaker (800 rpm) for 2 h at RT. After incubation, the plate was centrifuged at 250 xg for 5 min at RT. Afterwards, the supernatants were dumped by quickly inverting and flicking the plate. The plate was washed with 200 µl of wash buffer. This washing step was repeated twice. Then, 12.5 µl of the detection antibodies were added to each well. The biotinylated detection antibodies then bind to the beads. Again, the plate was sealed with a plate sealer, covered with aluminum foil, and incubated on a plate shaker (800 rpm) for 1 h at RT. Directly after the incubation, 12.5 µl of streptavidin-phycoerythrin were added to each well, which binds to the biotinylated detection antibody, leading to different fluorescence signal intensities depending on the number of analytes. Then, the plate was sealed with a plate sealer, covered with aluminum foil, and incubated on a plate shaker (800 rpm) for 30 min at RT. After incubation, the plate was centrifuged at 250 xg for 5 min at RT. Afterwards, the supernatants were dumped and 200 µl of wash buffer was added to each well. The plate was shaken for 1 min on a plate shaker to resuspend the beads. This washing step was repeated twice. For measuring with the BD FACSverse™ flow cytometer, the standards and samples were resuspended in 300 µl and 150 µl of wash buffer, respectively, and transferred into 1.5 ml Eppendorf tubes. In case the measurement was performed on the BD FACSymphony™ A1 flow cytometer, standards and samples were resuspended in 150 µl and 50 µl of wash buffer, respectively. The evaluation was conducted with the help of the LEGENDplex Data Analysis software.

3.2.3 M30 CytoDeath™ ELISA

To specifically determine the apoptosis induction of PDAC cells in spheroid cocultures, a M30 CytoDeath™ ELISA was performed. Here, the amount of caspase-cleaved keratin 18 (ccK18) was measured in the supernatants. The supernatants were taken and centrifuged for 10 min at 15,000 xg and 4 °C to remove all remaining cells. All reagents were prewarmed at RT and vortexed before use. The wash tablet was dissolved in 500 ml ddH_2O. Further, the M30 CytoDeath HRP conjugate (0.4 ml) was diluted with 9.2 ml of M30 CytoDeath conjugate dilution buffer. First, 25 µl of the standards (zero, low, medium, and high) and the samples were pipetted into the provided 96 well plate, which was coated with mouse monoclonal keratin 18 antibody M6. Directly afterwards, 75 µl of the diluted M30 CytoDeath HRP Conjugate were added. The plate was sealed with a plate sealer and incubated on a plate shaker (600 rpm) for 4 h at RT. Afterwards, the plate was washed 5 times with 250 µl of wash buffer. Then, 200 µl of the TMB substrate were added for 20 min at RT in the dark. Next, 50 µl of the stop solution were added to each well. To mix the TMB substrate with the stop solution, the plate was shaken for a few seconds and incubated for 5 min. In the end, the absorbance was determined at a

wavelength of 450 nm using Infinite 200 PRO Microplate Reader. All samples were normalized to the seeded cell number of PDAC cells.

3.2.4 Immunofluorescence staining of PD-L1 on coverslips

For IF staining of PD-L1, the cells (PDECs and hepatic stromal cells) were seeded onto an 18 mm coverslip. After cultivation (sections 3.1.11.2 and 3.1.11.3), the medium was removed and the cells were washed twice with PBS. Then, the cells were fixed with 4 % PFA for 10 min at RT. Afterwards, the cells were washed three times with PBS. The staining was conducted with the Alexa Fluor™ 488 Tyramide SuperBoost goat, anti-rabbit kit by ThermoFisher Scientific. All incubation steps were performed in a humidified chamber. First, the cells were incubated with 3 % hydrogen peroxidase solution for 60 min. Then, the cells were washed three times with PBS, 2-3 drops of blocking buffer were added, and cells were incubated for 60 min at RT. Then, the cells were incubated with the anti-PD-L1 antibody, diluted 1:200 in 1 % BSA/PBS overnight at 4 °C. On the next day, the cells were washed three times with PBS for 5 min. Next, the cells were incubated with the poly-HRP conjugated secondary antibody for 60 min at RT. Then, the cells were washed twice with PBS and Hoechst 33528, diluted 1:500 in PBS, was added for 30 min. Afterwards, the cells were washed three times with PBS for 5 min. The tyramide working solution was prepared by adding the 100X tyramide stock solution, 100X H_2O_2 solution, and 1X reaction buffer. Then, 100 µl tyramide working solution were added onto the cells for 10 min at RT. To stop the reaction, 100 µl of reaction stop reagent were added. Afterwards, the cells were rinsed three times with PBS and once with H_2O before the coverslips were sealed upside down in a drop of Fluro-Gel onto an object slide with clear nail polish. The slides were stored at 4 °C. The IF staining was evaluated using the Lionheart FX Automated Microscope.

3.3 Molecular biological methods

3.3.1 RNA Isolation

Ribonucleic acid (RNA) was isolated from hepatic stromal cells and $CD8^+$ T cells with the peqGOLD total RNA kit from VWR International. The cells were washed with PBS, lyzed in 300 µl of RNA lysis buffer and transferred into a 1.5 ml tube. With the help of the lysis buffer, all RNAses and other enzymes were inhibited. Lysates were transferred into the DNA removing column, which was stacked in a 2 ml tube. Afterwards, the lysates were centrifuged at 12,000 xg for 2 min. The flow-through was transferred into a new 1.5 ml tube and 300 µl of 70 % ethanol were added and vortexed. The lysates were pipetted onto the membrane of the PrefectBind RNA column and centrifuged at 12,000 xg for 1 min. The PerfectBind RNA column was washed once with 500 µl of RNA wash buffer I and afterwards with 600 µl of RNA wash buffer II. After washing, the columns were centrifuged at 10,000 xg for 2 min,

to dry the membrane. Then, 40 µl of RNAse free water were added onto the membrane and incubated for 2 min. The column was centrifuged at 10,000 xg for 2 min to elute the RNA. The RNA samples were stored at -80 °C. Nucleic acid concentration was measured using the Infinite 200 PRO Microplate Reader with the help of the NanoQuant Plate.

3.3.2 cDNA synthesis

Complementary desoxyribonucleic acid (cDNA) was generated from the isolated RNA (section 3.3.1) using the RevertAid First Strand cDNA Synthesis kit. Between 100 ng and 500 ng RNA were used, mixed with 1 µl oligo dT primer, and filled up to 12.5 µl with nuclease-free water. The solution was incubated at 65 °C for 5 min. Afterwards, the solution was cooled down on ice and spun down. The components written below (Table 3) were added to the solution, mixed, and first incubated at 42 °C for 60 min and then at 70 °C for 5 min to stop the reaction. cDNA was stored at -20 °C.

Table 3: Master Mix composition for cDNA synthesis of RNA

Component	Volume (µl)
5x Reaction buffer	4 µl
RiboLock RNase inhibitor (20 U/µl)	0.5 µl
10 mM dNTP Mix	2 µl
RevertAid M-MuLV Reverse Transcriptase (200 U/µl)	1 µl
Total volume: 7.5 µl	

3.3.3 Quantitative real-time polymerase chain reaction

Quantitative real-time polymerase chain reaction (qPCR) was performed to analyze the gene expression of different markers of hepatic stromal cells and $CD8^+$ T cells. The generated cDNA (section 3.3.2) was diluted at a ratio of 1:3 with nuclease-free water and 2.5 µl were pipetted into a well of a 96-well PCR plate. All samples were pipetted in duplicates. Afterwards, 7.5 µl of the master mix containing the following components (Table 4) were added. The PCR plate was centrifuged at 300 xg at 4 °C for 2 min.

Table 4: Maxter Mix composition per sample for qPCR

Component	Volume (µl) RealTime Primer	Volume (µl) Eurofins Primer	Volume (µl) Biometra Primer
Light Cycler SYBR Green I Master	5	5	5
Forward Primer	-	1	0.0375
Reverse Primer	-	1	0.0375
Forward/Reverse Primer Mix	1	-	-
Nuclease free H_2O	1.5	0.5	2.425

The measurement was performed using a LightCycler® 480 applying the protocol below (Table 5).

Table 5: LightCycler program for qPCR

Step No.	Step	Time	Temperature (°C)
1	Pre-Incubation	5 min	95 °C
2	Denaturation	10 s	95 °C
3	Annealing	20s	Section 2.4.1
4	Elongation	30 s	72 °C
5	Steps 2 - 4 (40 – 50 cycles)		
6	Melting curve		
7	Cooling		40 °C

After each run, a melting curve analysis of the different samples was performed for quality control. The evaluation was performed with the help of the LightCycler480 software and excel. The relative gene expression was determined using the respective Ct value of the housekeeper gene (GAPDH) and by the ΔCt method.

3.4 Microscopic analysis

Formalin-fixed and paraffin embedded (FFPE) biopsy samples or diagnostic resection specimens from liver metastases of 15 PDAC patients were used for immunohistochemical analyses. Thirteen patients were male and two female. The median age at diagnosis was 70 (range: 59-82). The histopathological diagnosis had been confirmed by board certified surgical pathologists.

The serial FFPE sections were stained for PanCK, α-SMA, CD3, CD8, CD68 and PD-L1. The immunohistochemical staining of the sections was carried out on the autostainer BOND™ RX system in the Institute of Pathology at the University Hospital Schleswig-Holstein in Kiel with the kind support of Prof. Dr. med. Christoph Röcken and Sandra Krüger. The respective concentrations of the antibodies are depicted in section 2.4.2.

Afterwards, the sections were scanned on the Hamamatsu NanoZoomer S6 digital slide scanner and analyzed with the NDP.view2 software.

To perform the analysis by two independent investigators, examination of all stainings was conducted in collaboration with Leon Aldag.

3.4.1 Localization of αSMA, CD3, CD8, CD68 and PD-L1 staining in tissue sections with liver metastases from PDAC patients

To explore potential changes of different cell populations and PD-L1 during metastatic outgrowth, metastases were categorized into small (≤ 1500 µm) and large (> 1500 µm). Afterwards, the localization of αSMA, CD3, CD8, CD68, and PD-L1 staining was determined by differentiating between its presence mostly in the tumor center, mostly at the invasion front, evenly distributed between both tumor regions, and absent. This analysis was performed at a magnification of 50- or 100-fold.

3.4.2 The abundance of αSMA, CD8, and PD-L1 staining in tissue sections with liver metastases from PDAC patients

For further analysis of the liver metastases of PDAC patients, the extent of αSMA, CD8, and PD-L1 staining was scored. The extent of αSMA^+ cells was scored, differentiating between low (+), medium (++), or high (+++) abundance considering the whole metastases. For CD8 and PD-L1 staining, a maximum of 10 Fields of View (FoV) were scored at the invasion front of the metastases and in the metastases center at 100-fold magnification, comparing small and large metastases. The number of FoV depended on the size of the metastases and the localization were chosen randomly. For CD8 and PD-L1, the same scoring was applied. Each FoV was scored with a score from 0 to 2. Score 0 was classified as no $CD8^+$ cells were present or no PD-L1 staining was detectable, score 1 as less than or equal 1 % of the present cells were $CD8^+$ or $PD\text{-}L1^+$, and score 2 as more than 1 % of the cells were $CD8^+$ or $PD\text{-}L1^+$. Further, the intensity of PD-L1 staining was analyzed by comparing absent, low, and high for each FoV.

3.5 Statistical analysis

Statistical analysis was performed with the GraphPad Prism 9.2.0 program. First, data were tested for normal distribution and equal variances using Shapiro-Wilk test. Two-tailed t-test was performed for analysis of two normally distributed data sets. Groups of data sets that did not pass the test for normal distribution and equal variances were analyzed using the Mann-Whitney Rank Test. Parametric data sets including more than two groups were analyzed using one-way analysis of variance (one-way ANOVA). For multiple comparisons, the Tukey Test was used. Non-parametric data sets comprising more than two groups were analyzed using Kruskal-Wallis one-way-ANOVA on Ranks and the Dunn's Test intensities of. Grouped data sets were analyzed using two-way ANOVA and for multiple comparison, the Tukey test was used. Normally distributed data were displayed as the mean $\pm$ SD and not normally distributed data were displayed as the median with interquartile range in both directions. Statistical significance was defined at a p-value of < 0.05, according to the Student-Newman-Keuls test for parametric and Dunn method for non-parametric data. The significance is indicated by asterisks as follows: $p < 0.05$ = *, $p < 0.01$ = **, $p < 0.001$ = ***.

4 Results

4.1 *In situ* characterization of the presence of myofibroblasts, $CD3^+$ T cells, $CD8^+$ T cells, macrophages, and the expression of PD-L1 in liver metastases of PDAC patients

Since PDAC patients with liver metastases have an even worse prognosis, it is of outmost importance to better understand the mechanisms underlying metastatic progression in the liver and to identify effective treatment options [150].

Since metastases are not routinely resected in PDAC patients, tissue samples from PDAC metastases are rare and the expression of immune regulatory molecules such as PD-L1 within liver metastases is rarely characterized. Hence, this study intended to elucidate the role of PD-L1 in the interplay of PDAC cells, the hepatic microenvironment, and immune cells, such as macrophages, $CD3^+$ and $CD8^+$ T lymphocytes in order to provide novel insight into the mechanisms contributing to immune escape of PDAC liver metastases. Primary tumor tissues of PDAC patients staged T3N1MO showed PD-L1 expression but only in 20 % of the analyzed tissues [35]. Therefore, it was examined whether PD-L1 is expressed in liver metastases, and how this relates to defined stroma compositions.

For this purpose, serial sections of liver metastases from 15 PDAC patients were stained for PanCK, αSMA, CD68, CD3, CD8, and PD-L1.

Since previous studies reported that stroma composition markedly differs with regard to metastasis size and the number of tumor cells [57], metastases were categorized into small (≤ 1500 µm) and large (> 1500 µm) metastases (Figure 20A). In general, more small (122) than large (19) metastases were detected in the liver sections (Figure 20B).

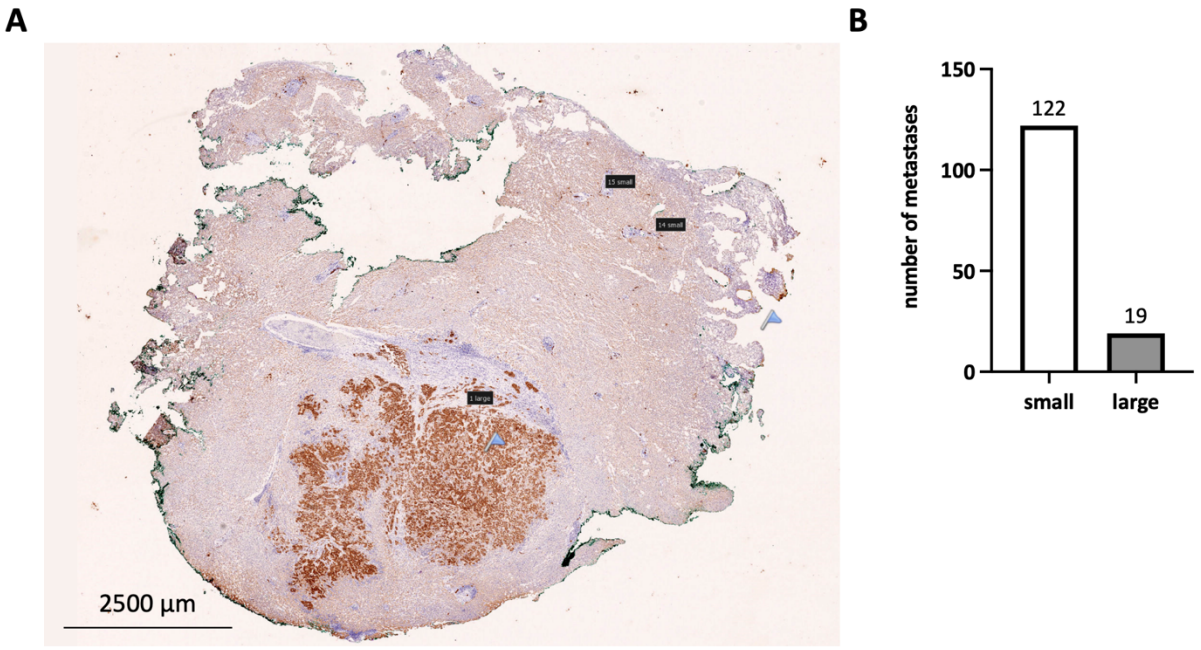

Figure 20: Small and large liver metastases in a liver tissue section of a PDAC patient. (A) Representative image of PanCK and hematoxylin-stained liver tissue sections obtained from a PDAC patient showing small and large metastatic lesions. **(B)** The number of small (white) and large (grey) metastases in the analyzed liver sections. (published in [163]).

4.1.1 Immune cells and PD-L1 expression were mostly present in the tumor center of small metastases and at the invasion front of large metastases

Here, the localization of αSMA, CD68, CD3, CD8, and PD-L1 staining within small and large metastases was scored (section 3.4.1). First, desmoplasia was assessed by evaluating the abundance of myofibroblasts. Small and large metastases clearly differ with respect to the spatial distribution of αSMA^+ myofibroblasts. While in small metastases, αSMA staining was detectable in the tumor center or evenly distributed between the tumor center and the invasion front, αSMA staining was predominantly located inside of large metastases (Figure 21A). In small metastases, CD68 staining was mainly located in the tumor center or was evenly distributed, whole in large metastases CD68 staining was also generally evenly distributed or at the invasion front (Figure 21B). Moreover, also the spatial distribution of $CD3^+$ and $CD8^+$ T cells clearly differed between small and large metastases. CD3 staining was evenly distributed (74 %) in small metastases, whereas in large metastases most $CD3^+$ T cells were found at the invasion front (75 %) (Figure 21C).

While $CD8^+$ T cells were predominantly located inside or evenly distributed in small metastases, in large metastases the majority of $CD8^+$ T cells were almost exclusively found at the invasion front (84 %) (Figure 21D). Finally, histoanatomical localization of PD-L1 staining was analyzed. Here, 35 % of small metastases showed no PD-L1 staining and if present, staining was predominantly observed in the

tumor center. In contrast, PD-L1 staining in large metastases was either evenly distributed or localized predominantly at the invasion front (Figure 21E).

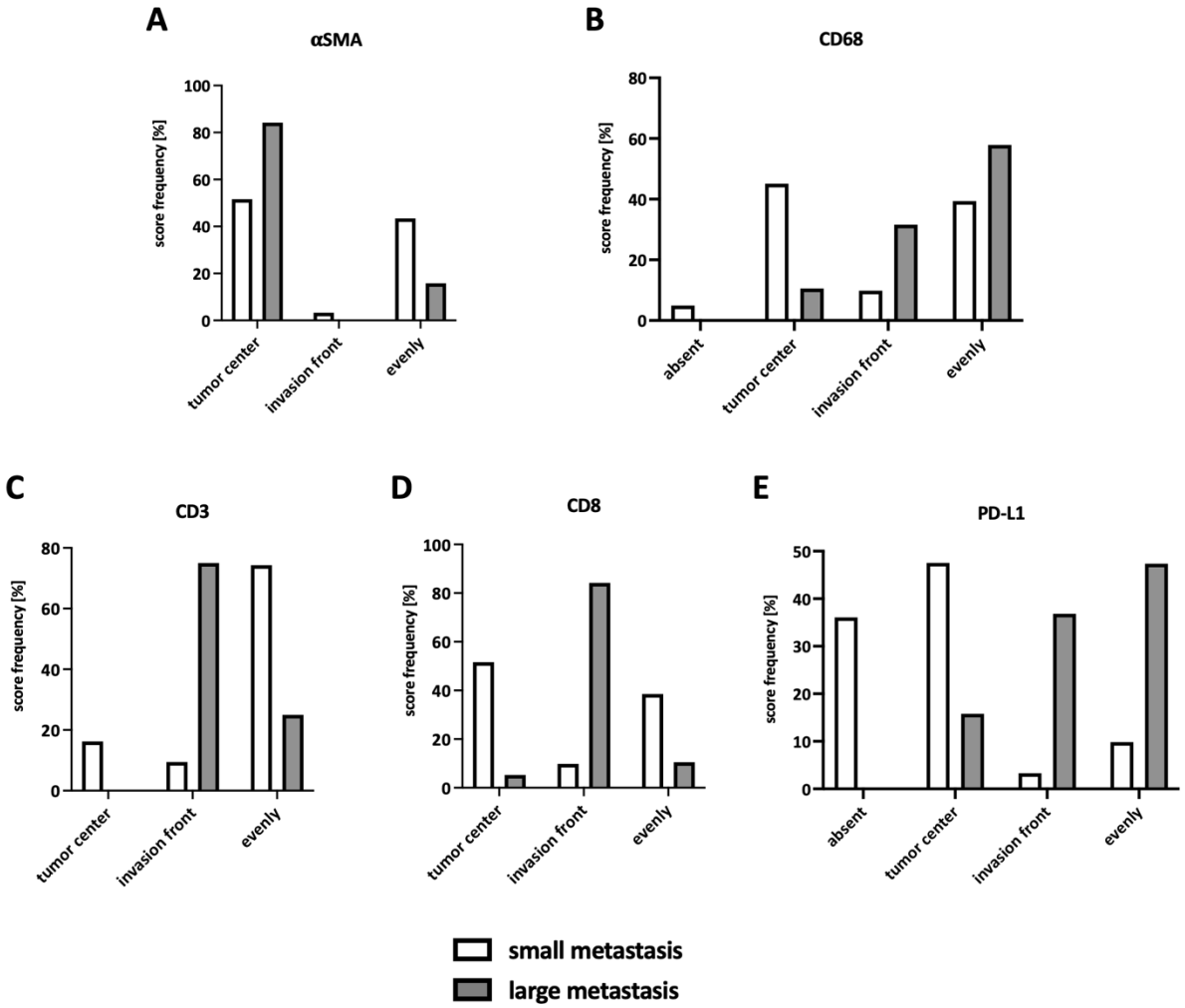

Figure 21: Different spatial distribution of myofibroblasts, macrophages, CD3$^+$ T cells, CD8$^+$ T cells, and PD-L1 expression in small and large liver metastases of PDAC patients. The main localization of **(A)** αSMA, **(B)** CD68, **(C)** CD3, **(D)** CD8, and **(E)** PD-L1 staining was scored by comparing absent staining and staining in the tumor center, at the invasion front or evenly distributed between tumor center and invasion front in small (white) and large (grey) liver metastases. Data represent the mean of 15 independent liver tissue sections of PDAC patients. (partially published in [163]).

Figure 22 shows representative images of the staining of (A) PanCK, (B) αSMA, (C) CD68, (D) CD3, (E) CD8, and (F) PD-L1 at the invasion front and in the tumor center of large and small metastases.

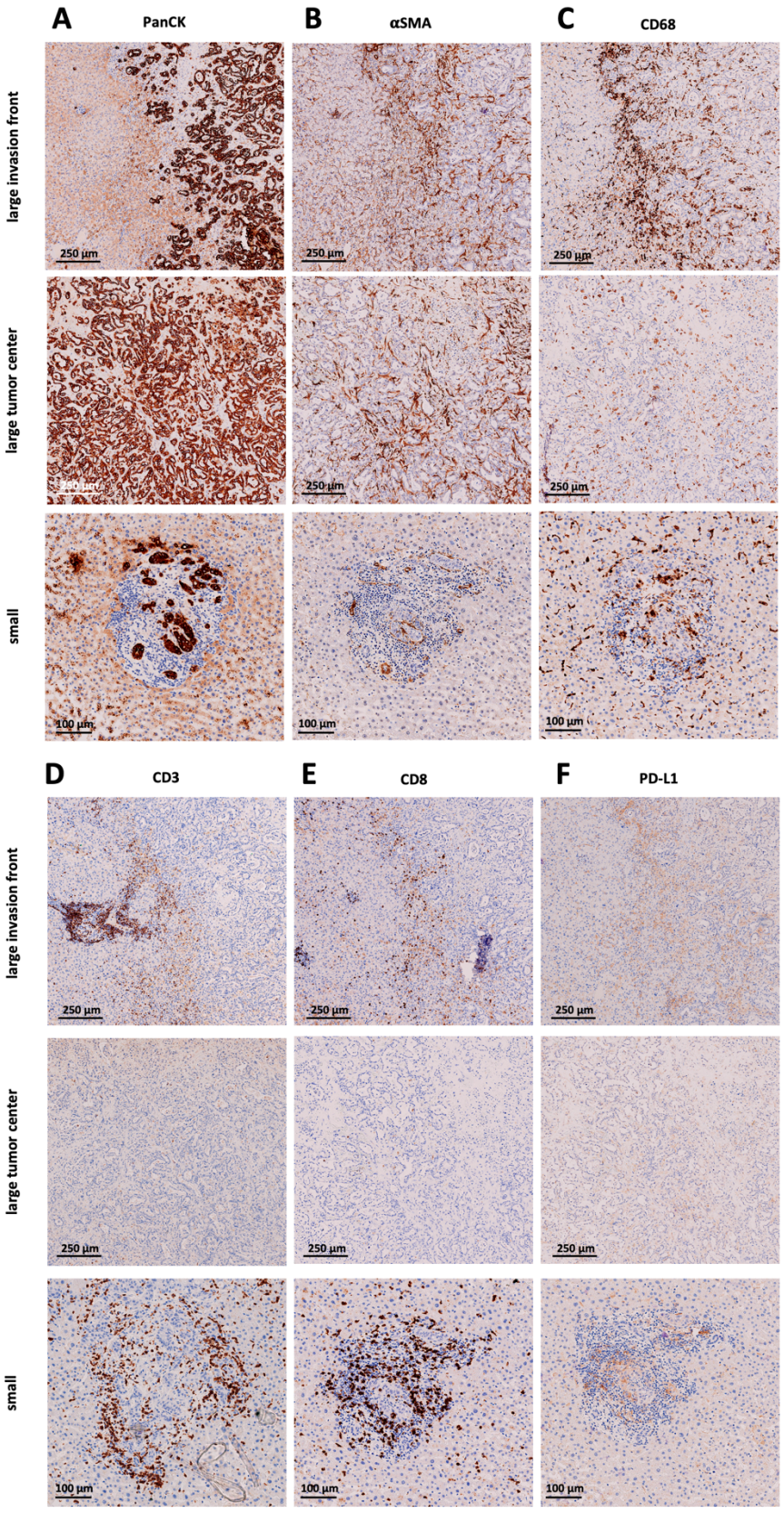

Figure 22: Different spatial distribution of myofibroblasts, macrophages, CD3$^+$ T cells, CD8$^+$ T cells, and PD-L1 staining in small and large liver metastases of PDAC patients. Representative images of the staining of **(A)** PanCK, **(B)** αSMA, **(C)** CD68, **(D)** CD3, **(E)** CD8, and **(F)** PD-L1 at the invasion front or in the tumor center of a large and small liver metastasis of one PDAC patients. (partially published in [163]).

In summary, IHC analyses revealed that immune cells (CD3, CD8, and CD68) were primarily present in the tumor center of small metastases while in large metastases especially $CD3^+$ T cells and $CD8^+$ T cells were predominantly located at the invasion front. In addition, PD-L1 staining was absent or in the tumor center in small metastases, while in large metastases it was mainly found at the invasion front or evenly distributed.

4.1.2 Myofibroblasts were more present in large compared to small metastases

Further, the number of myofibroblasts was rated and compared (+ = low number, ++ = medium number, or +++ = high number of myofibroblasts). Small metastases were mostly characterized by low and medium numbers of myofibroblasts (low: 57 % vs. medium: 42 % vs. high: 0.4 %). In contrast, ~50 % of large metastases exhibited high numbers and only ~15 % low numbers (Figure 23).

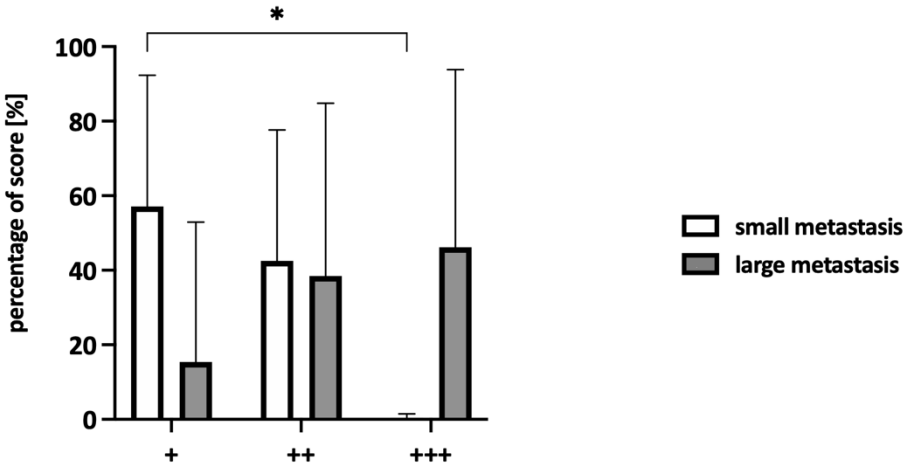

Figure 23: Higher abundance of myofibroblasts were more present in large metastases compared to small metastases of PDAC patients. The abundance of αSMA was rated as low number (+), medium number (++), or high number (+++) of myofibroblasts in small (white) and large (grey) liver metastases. Data represent the mean ± SD. N=11 for small metastases and N=13 for large metastases. * = $p < 0.05$. (published in [163]).

Overall, large metastases showed a higher abundance of myofibroblasts compared to small metastases.

4.1.3 High numbers of $CD8^+$ T cells were present in the tumor center of small metastases and at the invasion front of large metastases

In line with the previous findings showing that $CD8^+$ T cells were predominantly present at the invasion front of large metastases (Figure 21D), 15 % of all examined FoV in large metastases exhibited no $CD8^+$ T cells (Figure 24A). These FoV were only scored in the tumor center (Figure 24B). However, within the majority of FoV more than 1 % of these cells were stained for CD8 in both small and large metastases,

albeit in small metastases over 60 % of FoV contained higher proportions of $CD8^+$ T cells (Figure 24A). FoV containing more than 1 % $CD8^+$ T cells were mainly at the tumor center of small metastases or at the invasion front of large metastases (Figure 24B). Further, only 23 % of FoV with more than 1 % $CD8^+$ T cells were in the tumor center of large metastases, showing again that $CD8^+$ T cells were mainly present at the invasion front of large metastases (Figure 24B).

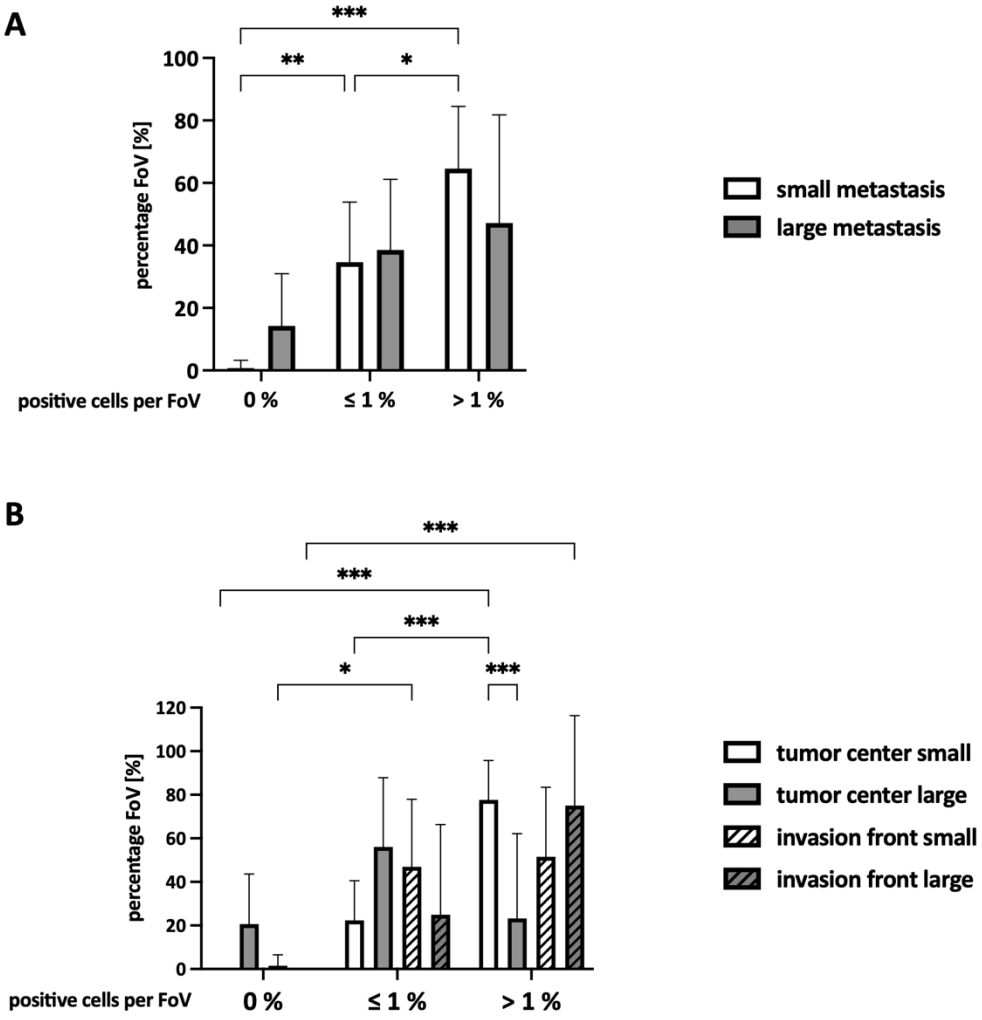

Figure 24: High numbers of $CD8^+$ T cells were present in the tumor center of small metastases and at the invasion front of large metastases of PDAC patients. A maximum of 10 microscopic Fields of View (FoV) in the tumor center and at the invasion front were analyzed and the proportion of $CD8^+$ T cells was determined. The proportion was ranked as 0 %, ≤ 1 %, or > 1 %. **(A)** First, the number of $CD8^+$ T cells was determined in each FoV and further **(B)** their (tumor center or invasion front) localization in small (white) and large (grey) liver metastases was analyzed. Data represent the mean ± SD. N=11 for small metastases and N=13 for large metastases. * = $p < 0.05$, ** = $p < 0.01$, *** = $p < 0.001$. (published in [163]).

In summary, small metastases exhibited more $CD8^+$ T cells, which were mainly located in the tumor center. In contrast to large metastases, where FoV with high numbers of $CD8^+$ T cells were mainly located at the invasion front.

4.1.4 Large metastases exhibit more PD-L1$^+$ cells and stronger PD-L1 staining intensity

Next, the abundance of PD-L1$^+$ cells (Figure 25A+B) and the intensity of PD-L1 staining (Figure 25C+D) were analyzed. In small metastases, 33 % of FoV showed no PD-L1$^+$ cells (Figure 25A). In contrast, only 7 % of FoV in large metastases exhibited no PD-L1$^+$ cells, and these FoV were scored in the tumor center (Figure 25A+B). Of note, FoV in large metastases exhibited significantly more PD-L1$^+$ cells compared to small metastases (small: 16 % vs. large: 53 %) (Figure 25A) and FoV with more than 1 % of PD-L1$^+$ cells were mainly located at the invasion front (Figure 25B).

In small and large metastases PD-L1 staining was mostly scored as low (small: 57 % vs. large: 55 %). Here, no clear trend was observable concerning the main location of these FoV (Figure 25D). In line with the high number of PD-L1$^+$ cells in large metastases compared to small metastases, the staining intensity was also stronger (small: 10 % vs. large: 38 %) (Figure 25C). Interestingly, strong PD-L1 staining was mostly found at the invasion front in large metastases (Figure 25D).

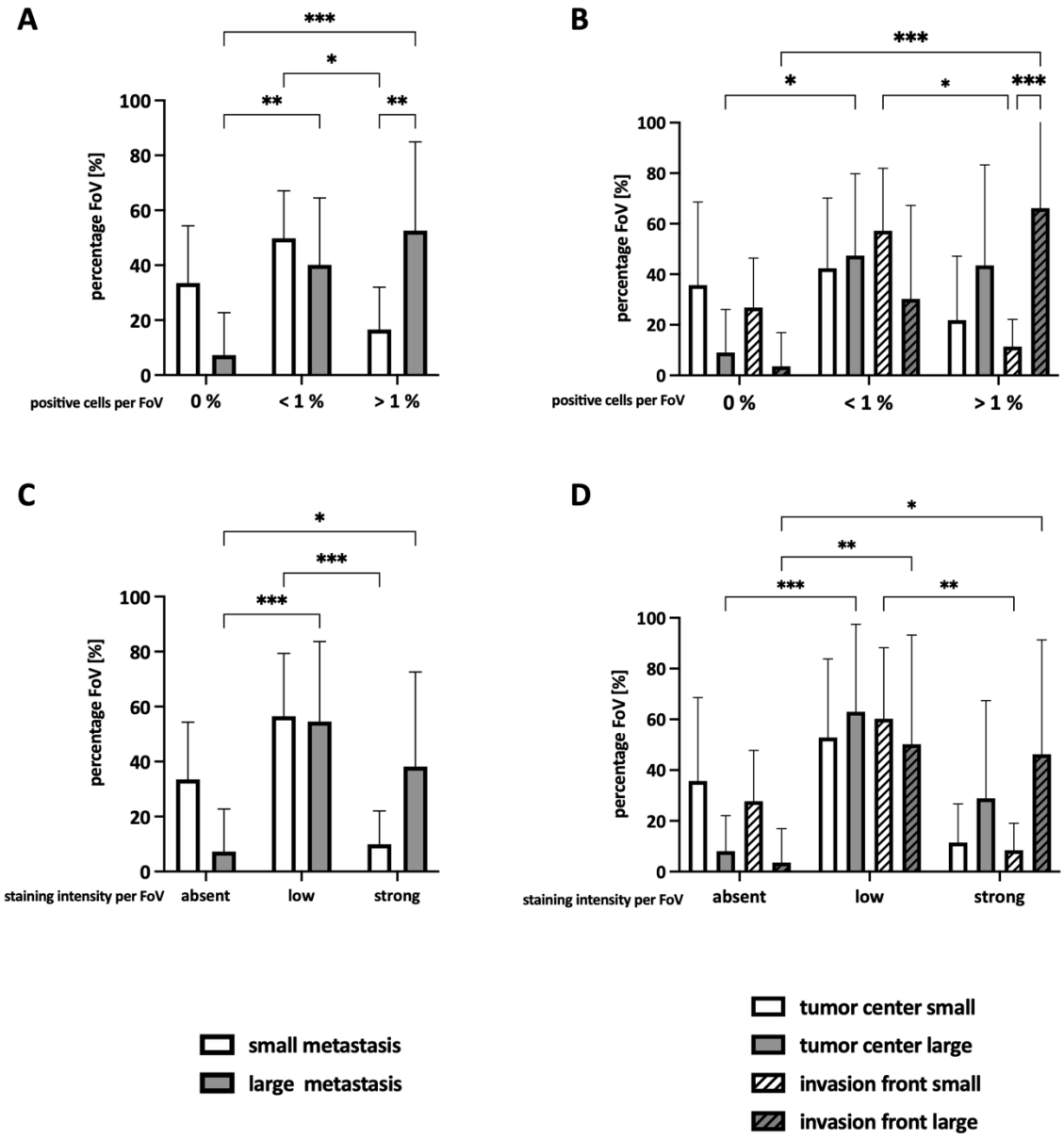

Figure 25: Large metastases exhibit more PD-L1$^+$ cells, which were mainly found at the invasion front and stronger PD-L1 staining intensity. A maximum of 10 microscopic Fields of View (FoV) in the tumor center and at the invasion front in small (white) and large (grey) liver metastases were analyzed and the proportion of PD-L1$^+$ cells was determined. The proportion was ranked as 0 %, <1 %, or >1 %. (**A)** First, the number of PD-L1$^+$ cells was determined in each FoV and further **(B)** the localization was analyzed (tumor center or invasion front). **(C)** Further, intensity of PD-L1 staining was ranked for each FoV, comparing absent, low, or strong and then **(D)** the localization was analyzed (tumor center or invasion front). Data represent the mean ± SD. N=11 for small metastases and N=13 for large metastases. * = $p < 0.05$, ** = $p < 0.01$, *** = $p < 0.001$. (published in [163]).

4.1.5 PD-L1 was rather expressed by stromal cells than tumor cells

The next aim was to analyze which cell populations in the TME mainly express PD-L1. In the primary tumor, it was already shown that PD-L1 is predominantly expressed by stromal cells rather than PDAC cells [35].

Here, comparing the spatial distribution of PD-L1, PanCK, CD68, CD8, and αSMA in serial liver sections demonstrated that PD-L1 staining was mainly colocalized with αSMA staining and CD68 staining and to some extent with CD8 staining rather than PanCK staining, indicating that PD-L1 is mainly expressed by myofibroblasts and macrophages in PDAC liver metastases (Figure 22). Accordingly, IHC double stainings of PanCK/PD-L1, αSMA/PD-L1, and CD68/PD-L1 were performed for validation showing that PD-L1 was expressed more by myofibroblasts and macrophages rather than $PanCK^+$ tumor cells (Figure 26A-C).

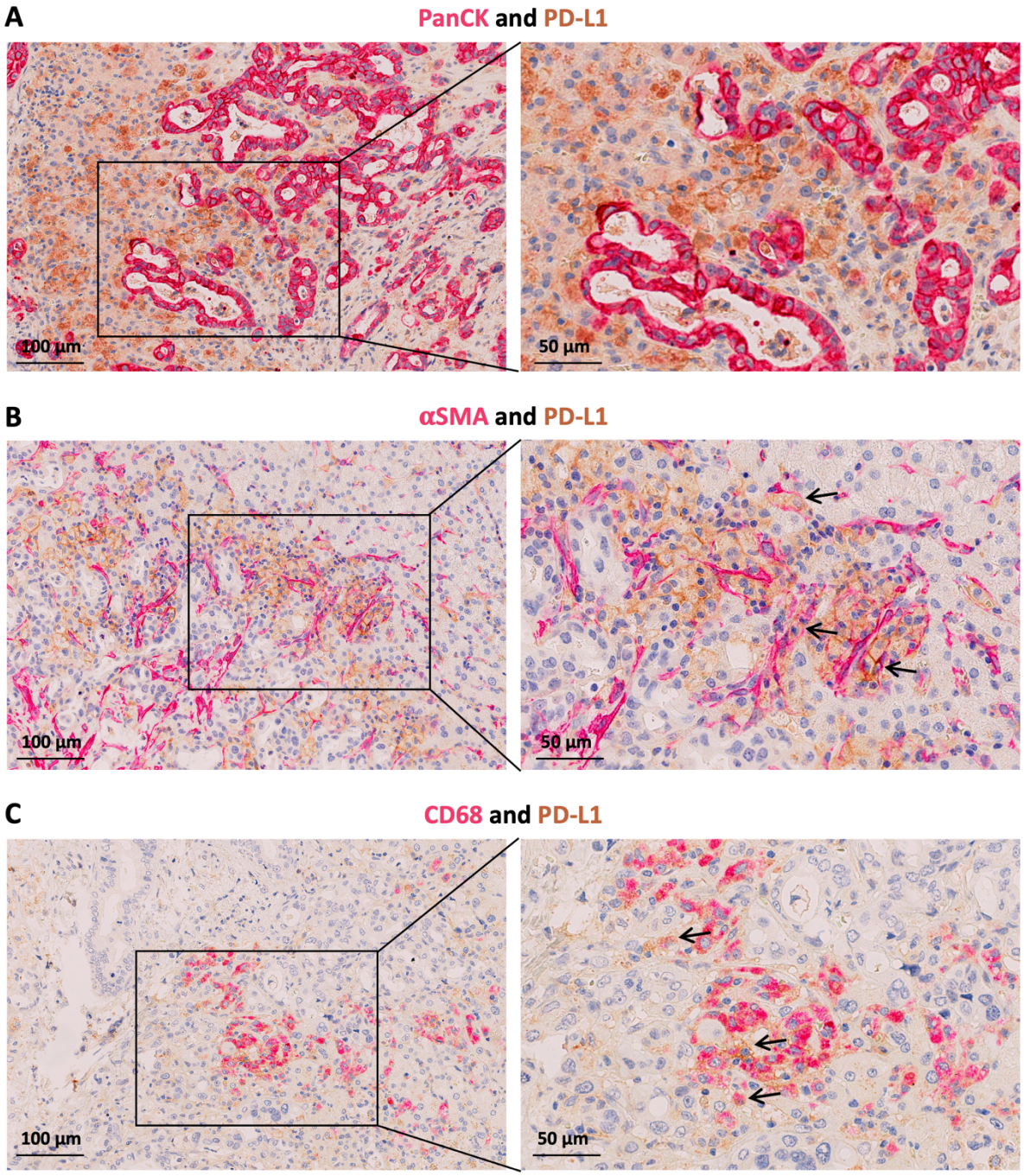

Figure 26: PD-L1 was rather expressed by stromal cells than tumor cells. Representative images of double immunohistochemical staining of **(A)** PanCK/PD-L1, **(B)** αSMA/PD-L1, and **(C)** CD68/PD-L1 in large liver metastases. PanCK, αSMA, and CD68 staining are displayed in red and PD-L1 staining in brown. Arrows indicate respective PD-L1 staining on myofibroblasts or macrophages. (published in [163]).

4.2 2D *in vitro* cocultures of different cell populations in the tumor microenvironment

4.2.1 Characterization of CD8$^+$ T cells before and after activation culture

As revealed by the *in situ* staining, the localization and abundance of CD8$^+$ T cells changed during metastatic outgrowth from small to large liver metastases. In small metastases, CD8$^+$ T cells were present inside while in large metastases, CD8$^+$ T cells were mainly at the margin. To mimic the situation in liver metastases *in vitro*, CD8$^+$ T cells were isolated from blood derived lymphocytes (sections 3.1.5 and 3.1.6) by negative magnetic cell sorting (section 3.1.7). After magnetic cell sorting, the purity of CD8$^+$ T cells was checked by flow cytometry. Therefore, the cells were stained for α/β TCR (FITC), CD8a (PE), and CD4 (APC). In Figure 27, the gating strategy is displayed. First, living cells (here called CD8) were gated (Figure 27A), continuing with the gating of single cells (Figure 27B). Afterwards, all α/β TCR positive cells were determined as the gate was set above the respective isotype control (Figure 27C), showing that around 95 % of the isolated cells were α/β TCR positive. Further, the number of CD8a positive cells and CD4 positive cells was determined (Figure 27D+E), revealing that 96 % of the α/β TCR positive cells were CD8a positive and under 1 % CD4 positive. Overall, 92 % of the isolated cells were α/β TCR and CD8a positive (Figure 27F), indicating a high purity of CD8$^+$ T cells for further cultures.

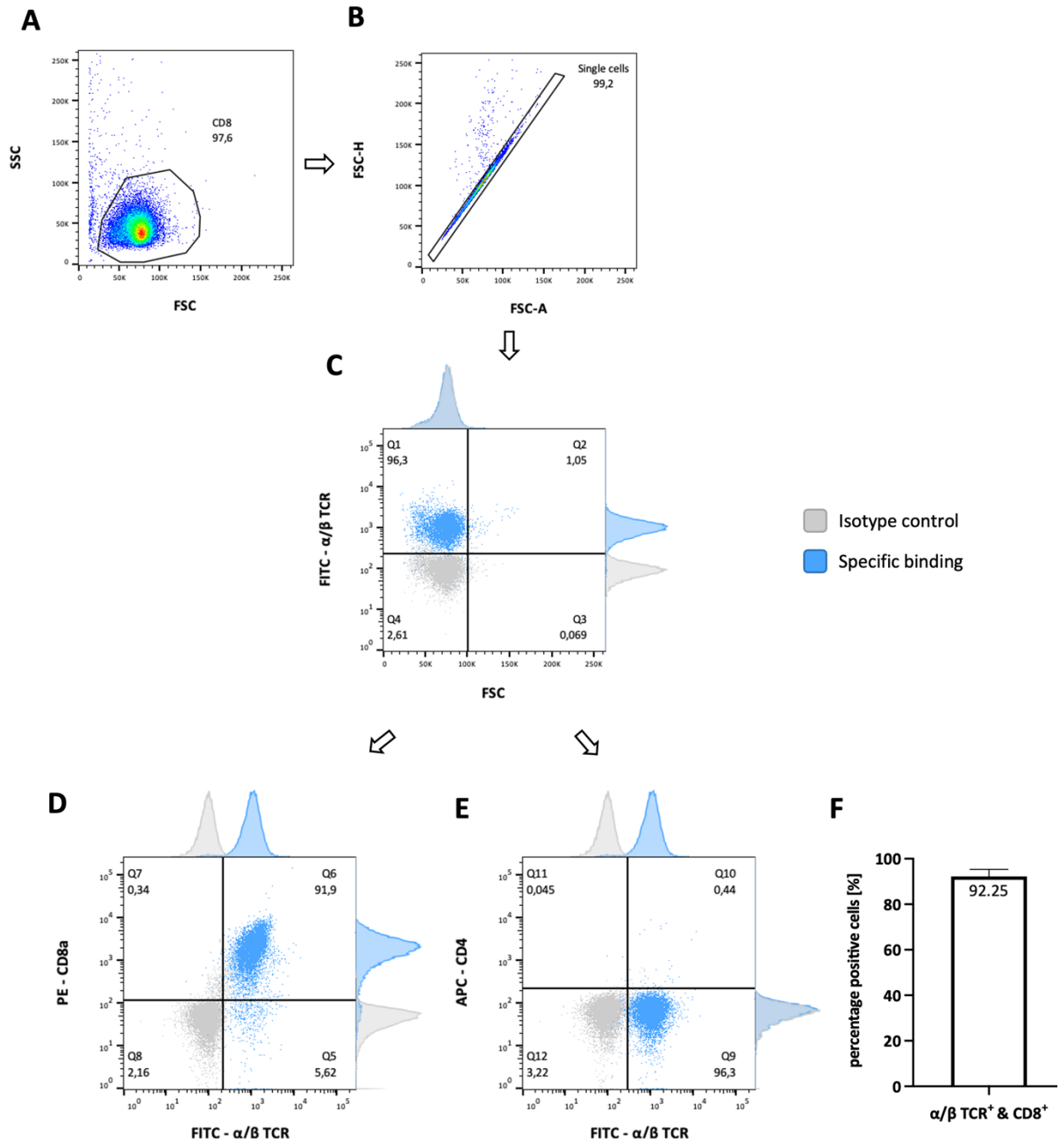

Figure 27: Gating strategy of T lymphocytes and determination of CD8⁺ T cells purity. Lymphocytes were isolated by density gradient centrifugation and by counterflow centrifugation. CD8⁺ T cells were isolated by magnetic cell separation. Gating strategy of T lymphocytes to determine the purity after negative magnetic cell sorting was as follows: **(A)** First, living cells were gated (here called CD8), followed by the gating of **(B)** single cells. **(C)** Afterwards, all α/β TCR positive cells (blue) were determined as the gate was set above the respective isotype control (grey). Among all α/β TCR positive cells, **(D)** CD8a⁺ and **(E)** CD4⁺ cells were gated, always regarding the respective isotype control. **(F)** Percentage of α/β TCR and CD8a positive cells. Data represent the mean ± SD. N=4.

4.2.1.1 Activated CD8⁺ T cells showed elevated PD-1 and PD-L1 cell surface expression levels and an elevated activation phenotype

Next, isolated CD8⁺ T cells were activated for 4 days with anti-CD3 and anti-CD28 antibodies as well as IL-2 (section 3.1.8) and CD8⁺ T cells were characterized directly after isolation (post MACS) on days 3 and 4 of the activation culture.

On days 3 and 4, PD-1 cell surface expression levels on CD8⁺ T cells as well as the number of PD-1 positive cells were elevated compared to post MACS (Figure 28A+B).

The maximum of PD-1 cell surface expression levels on CD8⁺ T cells as well as the number of PD-1 positive cells was on day 4. In addition, the PD-L1 cell surface expression levels became significantly elevated during the activation culture (Figure 28C), in line with a significantly higher number of PD-L1 positive CD8⁺ T cells ($p < 0.001$). However, between 3 and 4 days almost no further increase was observed (Figure 28C+D). Interestingly more CD8⁺ T cells were PD-L1 positive than PD-1 positive (78 % vs. 66 % on day 4).

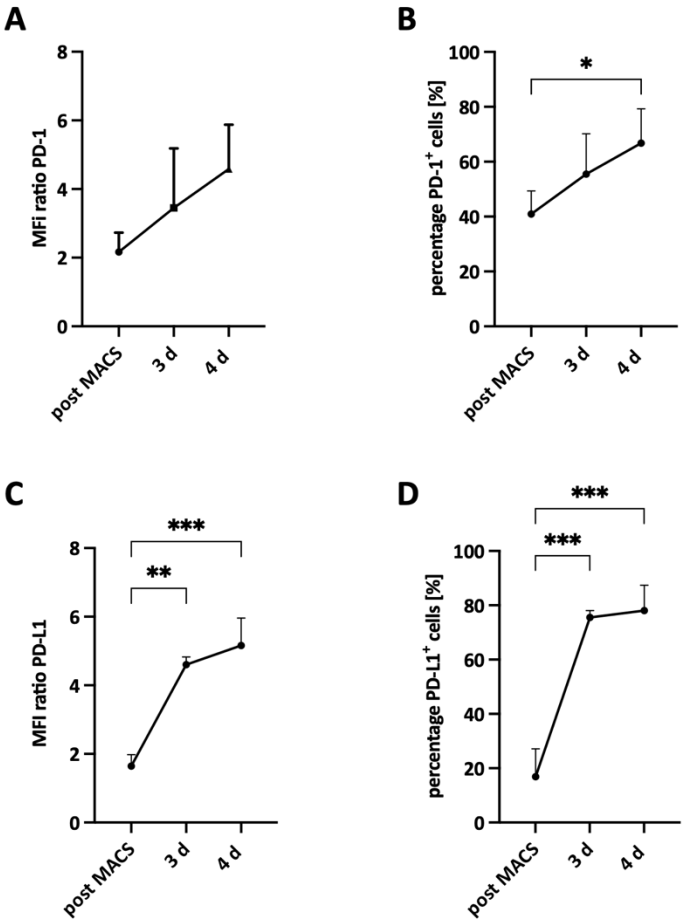

Figure 28: Activated CD8⁺ T cells show elevated PD-1 and PD-L1 cell surface expression levels. CD8⁺ T cells were isolated by magnetic cell separation (MACS) from human blood derived lymphocytes. Cells were characterized directly after isolation (post MACS), as well as on days 3 and 4 of activation culture. Here, CD8⁺ T cells were activated with anti-CD3 and anti-CD28 antibodies, as well as IL-2 for a maximum of 4 days. **(A)** Cell surface

expression levels of PD-1, **(B)** percentage of PD-1 positive CD8⁺ T cells, **(C)** cell surface expression levels of PD-L1, and **(D)** percentage of PD-L1 positive CD8⁺ T cells. Median fluorescence intensity (MFI) ratio was calculated by dividing the MFI of the specific staining by the MFI of the isotype control. Data represent the mean ± SD (normally distributed). N=4. * = $p < 0.05$, ** = $p < 0.01$, *** = $p < 0.001$.

Further, the cell surface expression levels of the early activation marker CD69 increased on CD8⁺ T cells during activation culture, with the difference between post MACS and 4 days being significant ($p < 0.05$) (Figure 29A). In line, the percentage of CD69 positive CD8⁺ T cells increased during activation culture compared to post MACS, with 93 % of the CD8⁺ T cells showing cell surface expression of CD69 on day 4 (Figure 29B). Cell surface expression levels of CD25 were also elevated during activation culture, in line with an increase in the percentage of CD25 positive CD8⁺ T cells comparing 3 and 4 days with post MACS (Figure 29C+D).

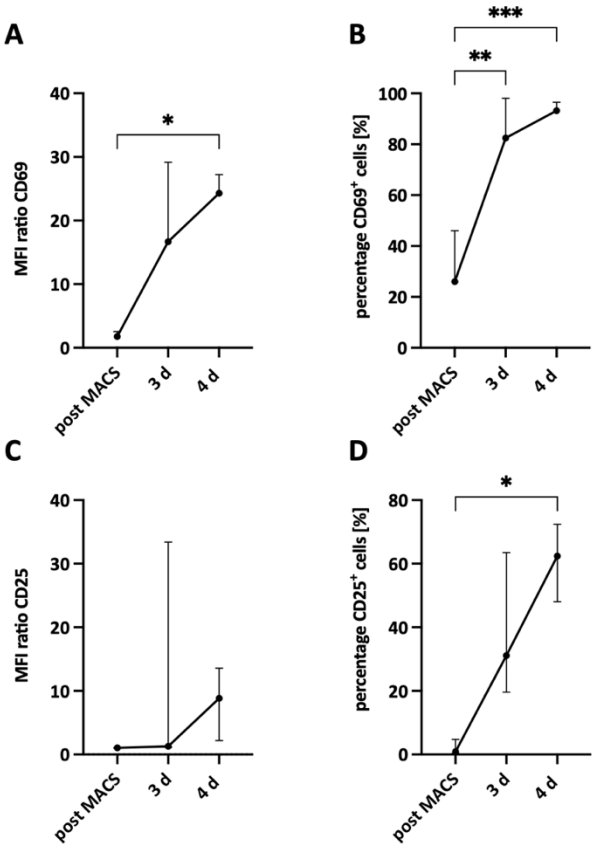

Figure 29: Activated CD8⁺ T cells show elevated CD69 and CD25 cell surface expression levels. CD8⁺ T cells were isolated by magnetic cell separation (MACS) from human blood derived lymphocytes. Cells were characterized directly after isolation (post MACS), as well as on days 3 and 4 of activation culture. Here, CD8⁺ T cells were activated with anti-CD3 and anti-CD28 antibodies, as well as IL-2 for a maximum of 4 days. **(A)** Cell surface expression levels of CD69, **(B)** percentage of CD69 positive CD8⁺ T cells, **(C)** cell surface expression levels of CD25, and **(D)** percentage of CD25 positive CD8⁺ T cells. Median fluorescence intensity (MFI) ratio was calculated by dividing the MFI of the specific staining by the MFI of the isotype control. Data represent the mean ± SD (normally

distributed) or the median with interquartile range (not normally distributed). N=3. * = $p < 0.05$, ** = $p < 0.01$, *** = $p < 0.001$.

In addition, the concentration of different cytokines and effector molecules released in the supernatant of $CD8^+$ T cells was measured on days 3 and 4 of the activation culture using LEGENDplex™. Upon activation, the concentration levels of IL-6, IFNγ, Granzyme A, Perforin, and Granulysin were elevated on day 4 compared to day 3 (Figure 30A-C+E-F). Granzyme B concentrations were almost comparable at both days (Figure 30D).

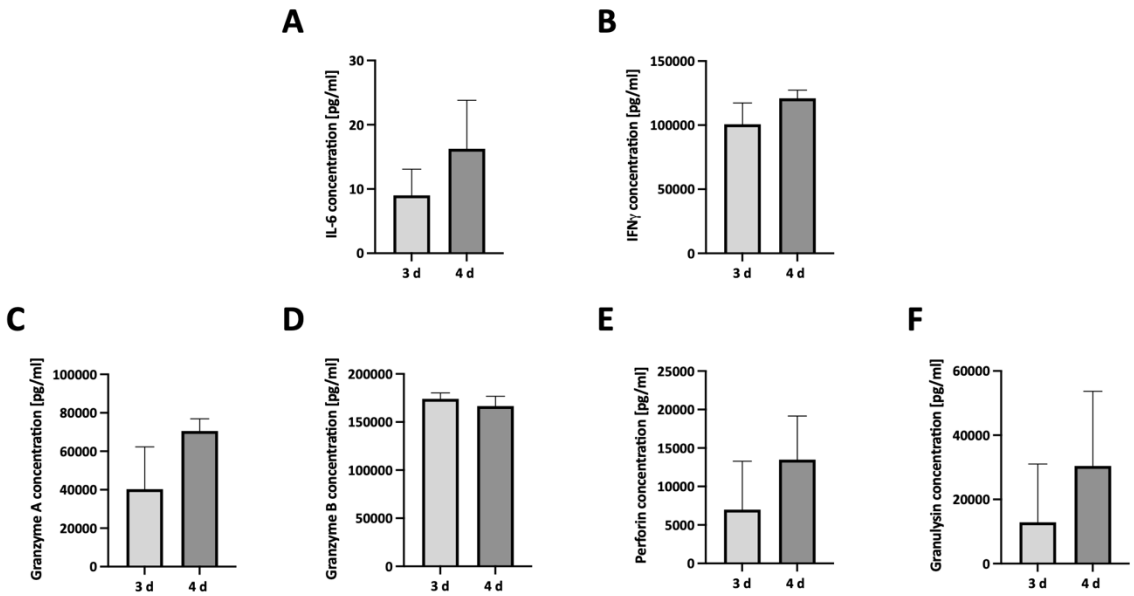

Figure 30: Elevated concentration levels of effector molecules in supernatants of activation culture. $CD8^+$ T cells were isolated by magnetic cell separation (MACS) from human blood derived lymphocytes. Cells were characterized directly after isolation (post MACS), as well as on days 3 and 4 of activation culture. Here, $CD8^+$ T cells were activated with anti-CD3 and anti-CD28 antibodies, as well as IL-2 for a maximum of 4 days. On day 3 (light grey) and day 4 (dark grey) the concentration of **(A)** IL-6, **(B)** IFNγ, **(C)** Granzyme A, **(D)** Granzyme B, **(E)** Perforin, and **(F)** Granulysin were measured in the supernatants of $CD8^+$ T cells. Data represent the mean ± SD (normally distributed). N=3.

Overall, the cell surface expression of PD-1, PD-L1, and the activation markers CD69 and CD25 of $CD8^+$ T cells rose continuously during the activation culture. Further, concentrations of the effector molecules were higher in supernatants of $CD8^+$ T cells on day 4 compared to day 3.

4.2.2 Heterogenous cell surface expression levels of PD-L1 on PDECs and stromal cells

In contrast to primary PDAC [35], IHC of PDAC liver metastases revealed that PD-L1 staining is detectable in each tissue liver section. Of note, PD-L1 staining was mostly found on αSMA$^+$ myofibroblasts and the staining intensity was quite heterogeneous.

For this purpose, cell surface expression levels of PD-L1 were analyzed by flow cytometry on PDECs, hepatic stromal cells, and CD8$^+$ T cells after 72 h in monoculture.

First, PD-L1 was stained on PDECs, comparing H6c7-kras and PancTu1 cells. H6c7-kras cells showed higher cell surface expression levels of PD-L1 compared to PancTu1 cells (MFI ratio: 16.7 vs. 10.8) (Figure 31A). Next, cell surface expression of PD-L1 was compared between HSC and HMF, with HMF showing a slightly higher expression level of PD-L1 (MFI ratio: 1.5 vs. 2.1) (Figure 31B). CD8$^+$ T cells also showed cell surface expression of PD-L1 after 72 h of monoculture (Figure 31C). This level was lower compared to day 4 at the activation culture (Figure 28C).

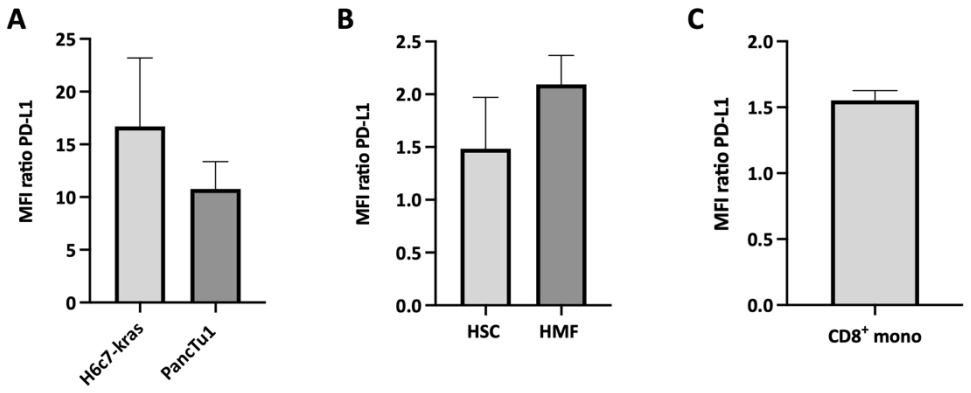

Figure 31: Heterogenous PD-L1 cell surface levels on PDECs, hepatic stromal cells, and CD8$^+$ T cells. H6c7-kras cells, PancTu1 cells, hepatic stellate cells (HSC), hepatic myofibroblasts (HMF), and activated CD8$^+$ T cells were seeded in a 12-well plate in monoculture. After 72 h, PD-L1 was stained and cell surface expression levels were analyzed by flow cytometry on **(A)** H6c7-kras and PancTu1 cells, **(B)** HSC and HMF, and **(C)** CD8$^+$ T cells. Median fluorescence intensity (MFI) ratio was calculated by dividing the MFI of the specific staining by the MFI of the isotype control. Data represent the mean ± SD (normally distributed). N=3.

Overall, different cells of the tumor microenvironment exhibit heterogeneous cell surface levels of PD-L1.

4.2.3 Impact of the interplay of PDECs and CD8$^+$ T cells on PD-L1 expression and the effector phenotype of CD8$^+$ T cells

IHC staining of liver tissue sections showed that the presence of CD8$^+$ T cells changes during metastatic progression. While CD8 staining was only found inside or evenly distributed in small liver metastases, in large metastases CD8 staining was predominantly at the invasion front. Therefore, CD8$^+$ T cells were

closer to PanCK positive cells in small compared to large metastases, raising the question of whether these two cell populations might impact PD-L1 expression on each other. The pre-malignant cell line H6c7-kras and the malignant cell line PancTu1 were used, respectively, to represent early and late stages of progression. Further, both cell lines are used as cell models with different PD-L1 cell surface expression levels (Figure 31A). H6c7-kras and PancTu1 cells were seeded in a 12-well plate and on the next day, activated $CD8^+$ T cells were added for 72 h (section 3.1.11.2).

4.2.3.1 Coculture with PD-L1 expressing PDECs did not significantly impact the effector phenotype of $CD8^+$ T cells

$CD8^+$ T cells were analyzed after coculture with PDECs regarding the cell surface expression levels of PD-1 and PD-L1, the activation status, and the effector phenotype.

Cell surface expression levels of PD-1 were slightly lower on $CD8^+$ T cells after coculture with H6c7-kras and PancTu1 cells compared to monoculture (Figure 32A). Furthermore, the number of PD-1 positive $CD8^+$ T cells was slightly lower after coculture with either PDEC line (Figure 32B). Cell surface levels of PD-L1 were slightly higher after coculture with H6c7-kras and PancTu1 cells (Figure 32C), in line with a slightly increased number of PD-L1 positive cells after coculture with H6c7-kras cells (Figure 32D).

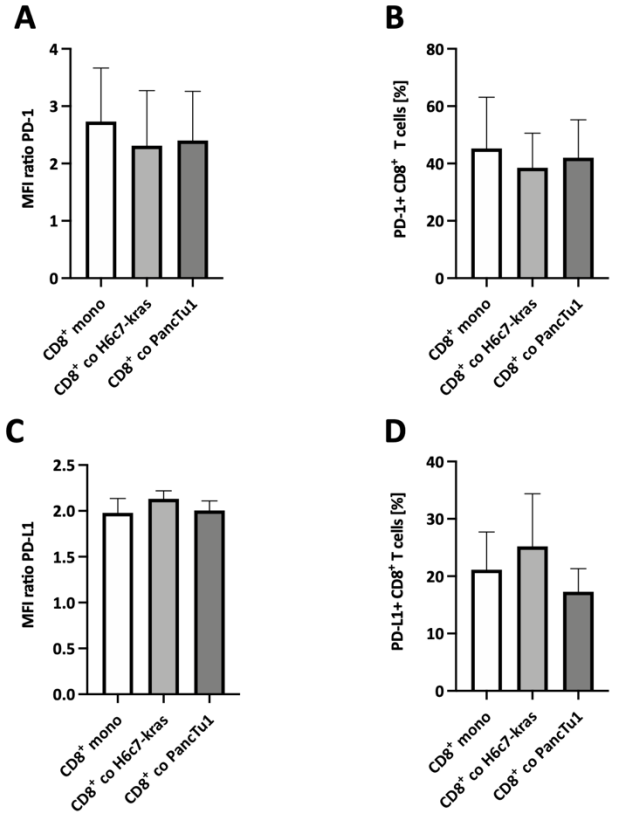

Figure 32: Cell surface levels of PD-1 and PD-L1 were almost unaffected after coculture with PDECs. $CD8^+$ T cells were isolated by magnetic cell separation from human blood derived lymphocytes and then activated with anti-CD3 and anti-CD28 antibodies, as well as IL-2 for 4 days. Afterwards, $CD8^+$ T cells were seeded in mono- (white) or coculture with either H6c7-kras (light grey) or PancTu1 cells (dark grey) for 72 h. Cell surface levels of **(A)** PD-

1 and **(C)** PD-L1 were analyzed by flow cytometry. Further, the percentage of **(B)** PD-1 positive and **(D)** PD-L1 positive $CD8^+$ T cells was determined. Median fluorescence intensity (MFI) ratio was calculated by dividing the MFI of the specific staining by the MFI of the isotype control. Data represent the mean ± SD (normally distributed). N=3.

Further, the activation status of $CD8^+$ T cells was analyzed after 72 h of mono- or coculture with PDECs. The expression of the early activation marker CD69 was not affected by coculture with either PDEC line (Figure 33A) and the number of CD69 positive was also not altered (Figure 33B). After coculture with H6c7-kras cells, CD25 cell surface expression on $CD8^+$ T cells was not altered but slightly decreased after coculture with PancTu1 cells (Figure 33C). Changes in the number of CD25 positive $CD8^+$ T cells were not seen after either coculture (Figure 33D).

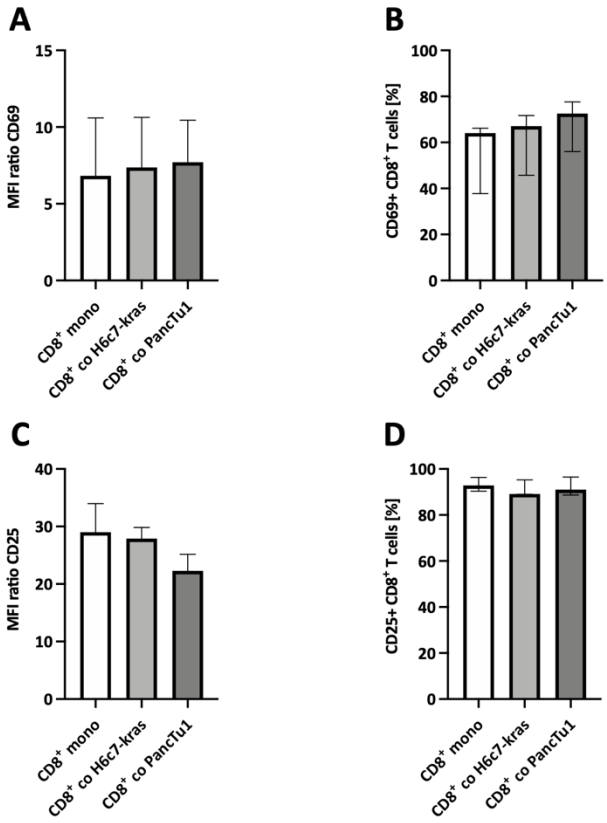

Figure 33: Cell surface levels of the activation markers CD69 and CD25 were almost unaffected after coculture with PDECs. $CD8^+$ T cells were isolated by magnetic cell separation from human blood derived lymphocytes and then activated with anti-CD3 and anti-CD28 antibodies, as well as IL-2 for 4 days. Afterwards, $CD8^+$ T cells were seeded in mono- (white) or coculture with either H6c7-kras (light grey) or PancTu1 cells (dark grey) for 72 h. Cell surface levels of **(A)** CD69 and **(C)** CD25 were analyzed by flow cytometry. Further, the percentage of **(B)** CD69 positive and **(D)** CD25 positive $CD8^+$ T cells was determined. Median fluorescence intensity (MFI) ratio was calculated by dividing the MFI of the specific staining by the MFI of the isotype control. Data represent the mean ± SD (normally distributed) or the median with interquartile range (not normally distributed). N=3.

Next, the secretion of different effector molecules was determined in the supernatants of monocultured and cocultured CD8$^+$ T cells after 72 h. The concentration of IFNγ was not affected by coculture with either H6c7-kras or PancTu1 cells (Figure 34A). CD8$^+$ T cells secreted slightly higher amounts of the effector molecules Granulysin, Granzyme A, Granzyme B, and Perforin when cocultured with H6c7-kras cells (Figure 34B-E). After coculture with PancTu1 cells, levels of effector molecules were not affected (Figure 34B-E).

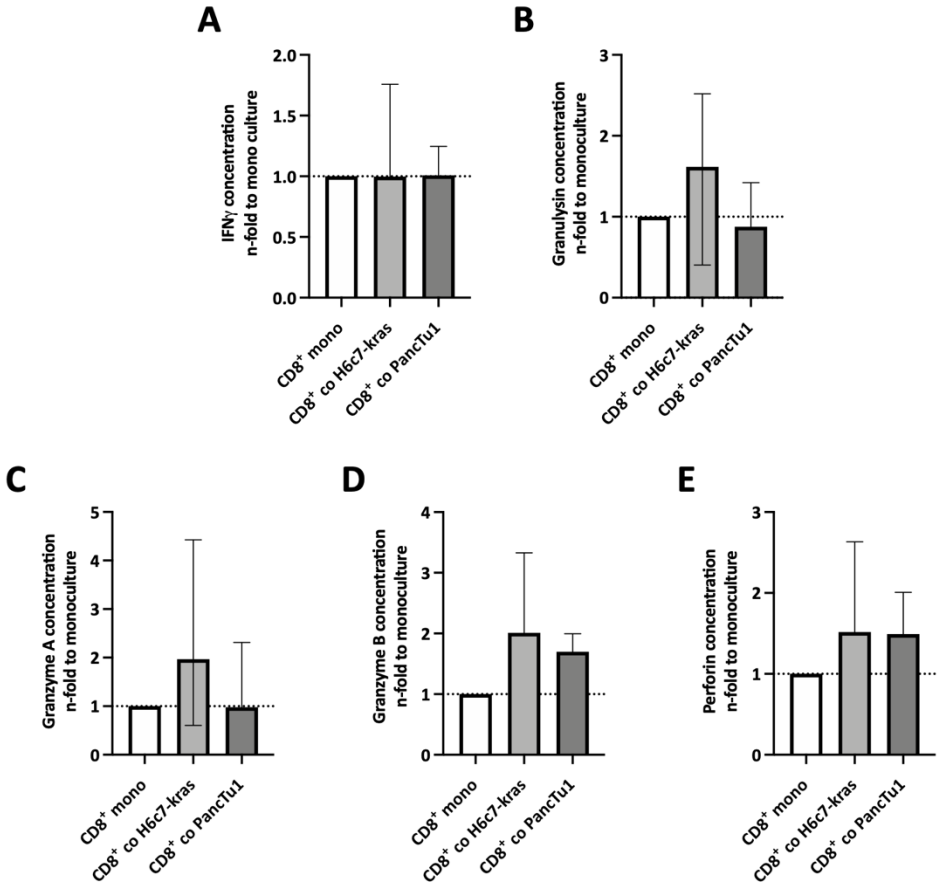

Figure 34: In supernatants of CD8$^+$ T cells concentration levels of effector molecules were slightly higher after coculture with H6c7-kras cells and not affected by coculture with PancTu1 cells. CD8$^+$ T cells were isolated by magnetic cell separation from human blood derived lymphocytes and then activated with anti-CD3 and anti-CD28 antibodies, as well as IL-2 for 4 days. Afterwards, CD8$^+$ T cells were seeded in mono- (white) or coculture with either H6c7-kras (light grey) or PancTu1 cells (dark grey) for 72 h. Concentrations of **(A)** IFNγ, **(B)** Granulysin, **(C)** Granzyme A, **(D)** Granzyme B, and **(E)** Perforin were measured in the supernatant of monocultured and cocultured CD8$^+$ T cells. Data were normalized to the concentrations in monoculture. Data represent the mean ± SD (normally distributed) or the median with interquartile range (not normally distributed). N=3.

Overall, coculture with either H6c7-kras or PancTu1 cells did almost not impact cell surface levels of PD-1, PD-L1, CD69, and CD25. Further, concentrations of effector molecules were not altered in supernatants of $CD8^+$ T cells cocultured with H6c7-kras and PancTu1 cells.

4.2.3.2 Coculture with $CD8^+$ T cells led to enhanced PD-L1 cell surface expression on PDECs and less cell proliferation

Next, H6c7-kras and PancTu1 cells were analyzed after coculture with $CD8^+$ T cells regarding the cell surface expression of PD-L1 and proliferation.

PD-L1 expression was significantly elevated on H6c7-kras cells after coculture with $CD8^+$ T cells (MFI ratio: 6.9 vs. 11.4) (Figure 35A), which was confirmed by IF staining of PD-L1 on H6c7-kras cells after coculture with $CD8^+$ T cells (Figure 35C+D). Likewise, PD-L1 cell surface expression was higher on PancTu1 cells after coculture with $CD8^+$ T cells (MFI ratio: 5.9 vs. 11.6) (Figure 35B), which was also seen in IF staining (Figure 35E+F).

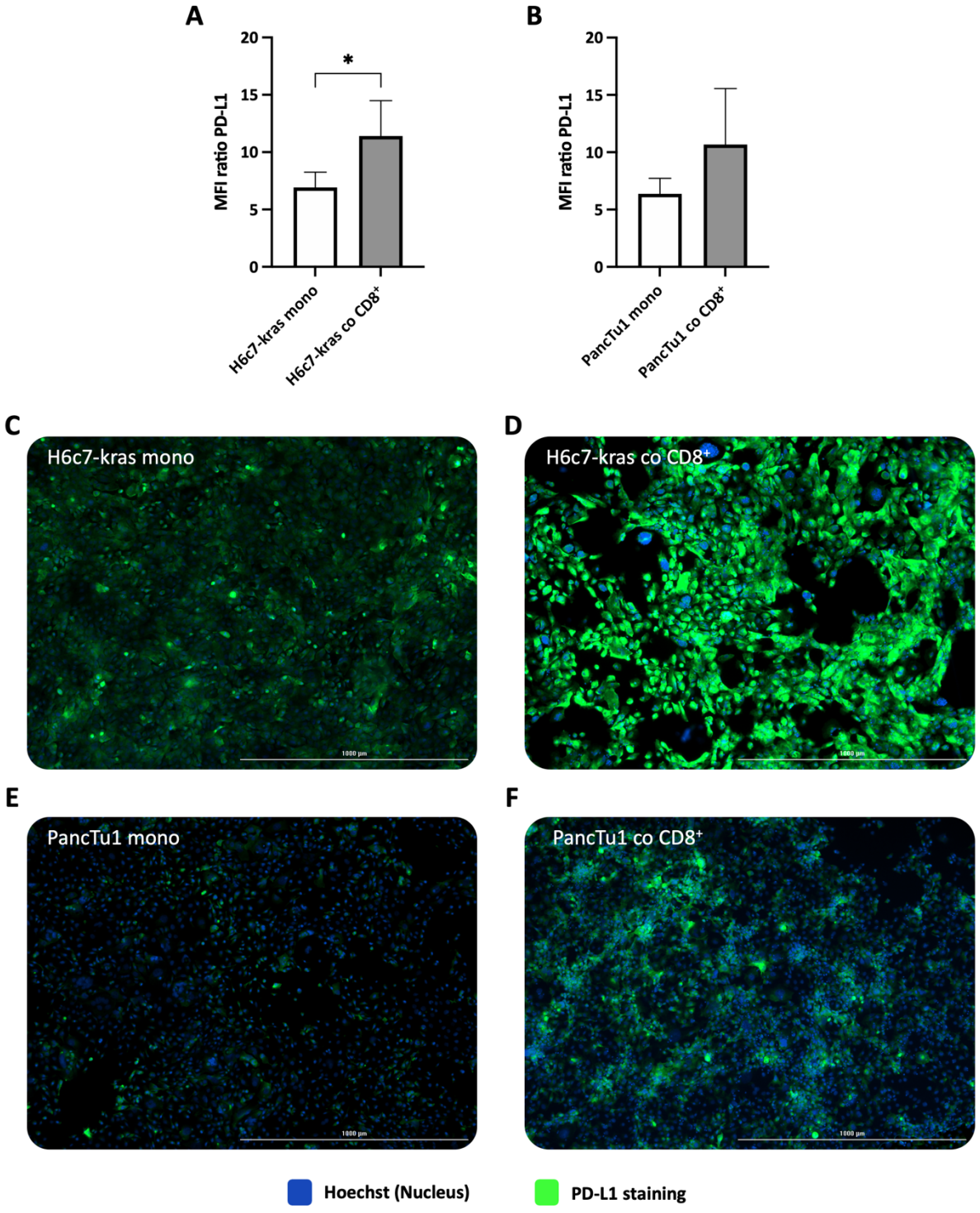

Figure 35: Coculture with CD8⁺ T cells led to enhanced PD-L1 cell surface expression on H6c7-kras and PancTu1 cells. H6c7-kras and PancTu1 cells were seeded either in mono- (white) or coculture with CD8⁺ T cells (grey). After 72 h, cell surface expression of PD-L1 on **(A)** H6c7-kras and **(B)** PancTu1 cells were determined by flow cytometry. Median fluorescence intensity (MFI) ratio was calculated by dividing the MFI of the specific staining by the MFI of the isotype control. Immunofluorescence staining of PD-L1 (green) was performed of **(C)** H6c7-kras in monoculture, **(D)** H6c7-kras cells after coculture with CD8⁺ T cells, **(E)** monocultured PancTu1 cells, and **(F)** PancTu1 cells after CD8⁺ T cell coculture. Nuclei were stained with Hoechst (blue). The scale bar represents

1000 µm. Data represent the mean ± SD (normally distributed). N=4 for H6c7-kras cells and N=3 for PancTu1 cells. * = $p < 0.05$.

Next, it was investigated whether $CD8^+$ T cells impact cell growth and proliferation of PDECs.

First, the cell number, as well as the cell confluence were determined of H6c7-kras and PancTu1 cells after mono- and coculture with $CD8^+$ T cells. Coculture with $CD8^+$ T cells led to a significantly lower vital cell number of H6c7-kras cells compared to monoculture ($p < 0.001$) (Figure 36A). In addition, the cell confluence of H6c7-kras cells was lower due to coculture with $CD8^+$ T cells (Figure 36C). The vital cell number was also lower in PancTu1 cells (Figure 36B), however, the cell confluence was only slightly reduced (Figure 36D).

After coculture with $CD8^+$ T cells, intracellular Ki67 expression was significantly downregulated in H6c7-kras (MFI ratio: 32.2 vs. 14.7) and in PancTu1 cells (MFI ratio: 34.8 vs. 14.9) (Figure 36E+G), indicating less proliferation, in line with lower cell numbers. However, nearly all cells were still Ki67 positive (Figure 36F+H).

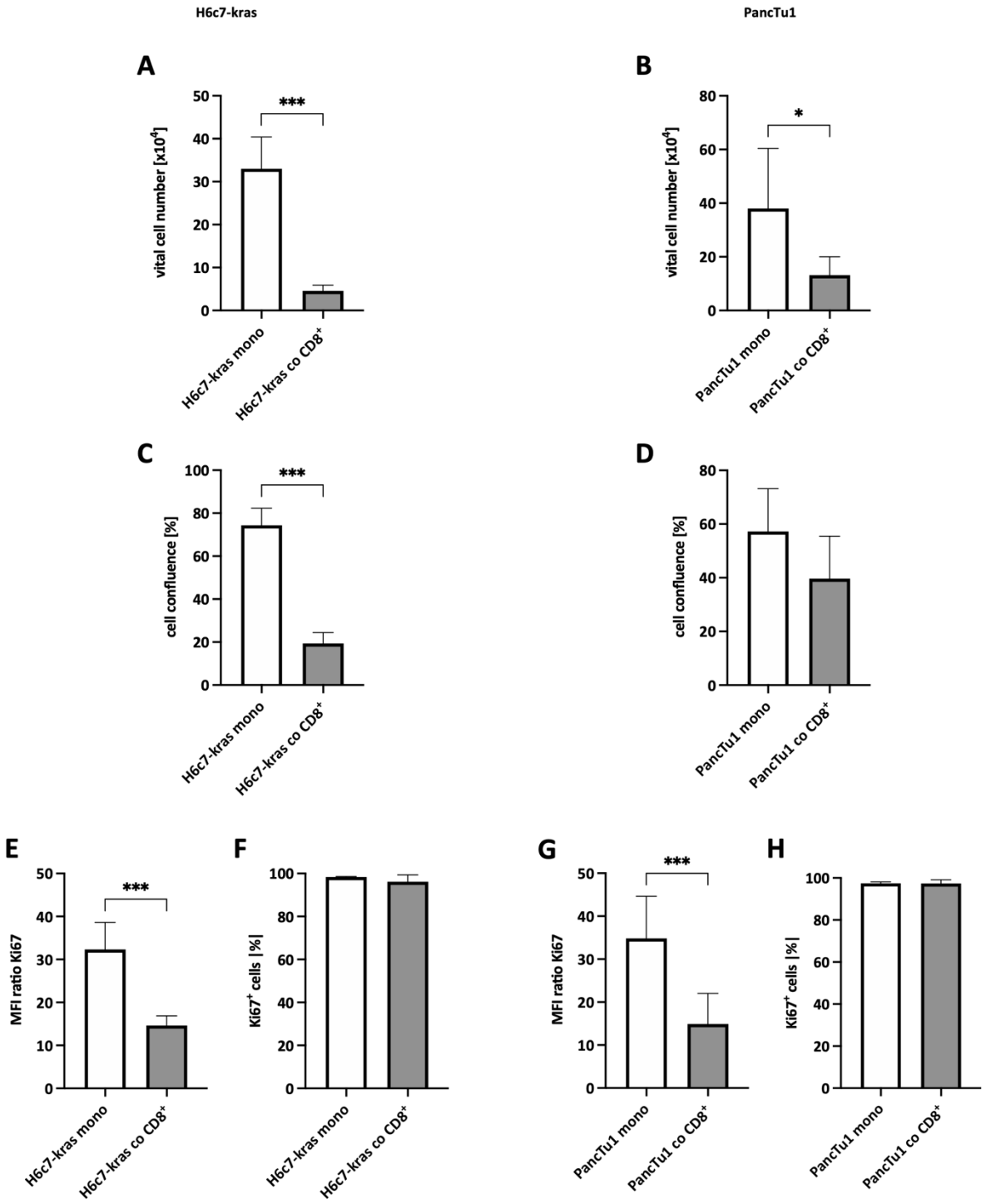

Figure 36: Coculture of CD8⁺ T cells led to a lower number of vital H6c7-kras and PancTu1 cells. H6c7-kras and PancTu1 cells were seeded either in mono- (white) or coculture with CD8⁺ T cells (grey). After 72 h, the vital cell number of **(A)** H6c7-kras and **(B)** PancTu1 cells were counted. The cell confluence was measured of **(C)** H6c7-kras and **(D)** PancTu1 cells on the NYONE Scientific. Further, intracellular Ki67 was measured in **(E)** H6c7-kras and **(G)** PancTu1 cells, and the percentage of Ki67 positive **(F)** H6c7-kras and **(H)** PancTu1 cells was determined. Median fluorescence intensity (MFI) ratio was calculated by dividing the MFI of the specific staining by the MFI of the isotype control. Data represent the mean ± SD (normally distributed). N=5 for vital cell number, N=4 for cell confluence and Ki67 of H6c7-kras cells, and N=3 for cell confluence and Ki67 of PancTu1 cells. * = $p < 0.05$, *** = $p < 0.001$.

Overall, coculture with $CD8^+$ T cells led to enhanced cell surface expression of PD-L1 on both PDEC lines. Furthermore, the presence of $CD8^+$ T cells led to reduced cell growth and proliferation, which is in line with the reduced intracellular expression of Ki67.

4.2.4 Impact of hepatic stromal cells on $CD8^+$ T cells

As shown in Figure 21 and Figure 22, localization of αSMA^+ myofibroblasts and $CD8^+$ T cells along with PD-L1 expression changed during outgrowth of liver metastases. While in small metastases, αSMA staining was detectable in the tumor center or evenly distributed between the tumor center and at the invasion front, αSMA staining was predominantly located inside of large metastases. Further, higher numbers of myofibroblasts were detected in large metastases. $CD8^+$ T cells were predominantly located inside or evenly distributed in small metastases. In contrast in large metastases the majority of $CD8^+$ T cells were almost exclusively found at the invasion front, indicating that immune cells are unable to infiltrate. In addition, more cells were PD-L1 positive in large metastases and showed a stronger PD-L1 staining. To investigate how the liver microenvironment impacts the PD-1/PD-L1 axis and the effector phenotype of $CD8^+$ T cells, a direct coculture with $CD8^+$ T cells and HSC or HMF was performed (section 3.1.11.3). In this context, HSC represent an uninflamed physiological and HMF an inflamed liver microenvironment [160,162].

First, HSC and HMF were characterized to ensure that the cells showed their typical phenotype. While HSC showed a characteristic stellate cell morphology, HMF exhibited a typical spindle shape morphology (Figure 37A+B). In line with this observation, mRNA levels of TGF-β1 and Fibroblast-specific protein 1 (FSP1) were significantly higher in HMF compared to HSC (TGF-β1: 0.0001 vs. 0.0002, $p < 0.05$ and FSP1: 0.00005 vs. 0.0001, $p < 0.05$) (Figure 37C+D). IL-6 mRNA levels were not different in HSC and HMF (Figure 37E). These results confirm the typical phenotype of HMF and HSC.

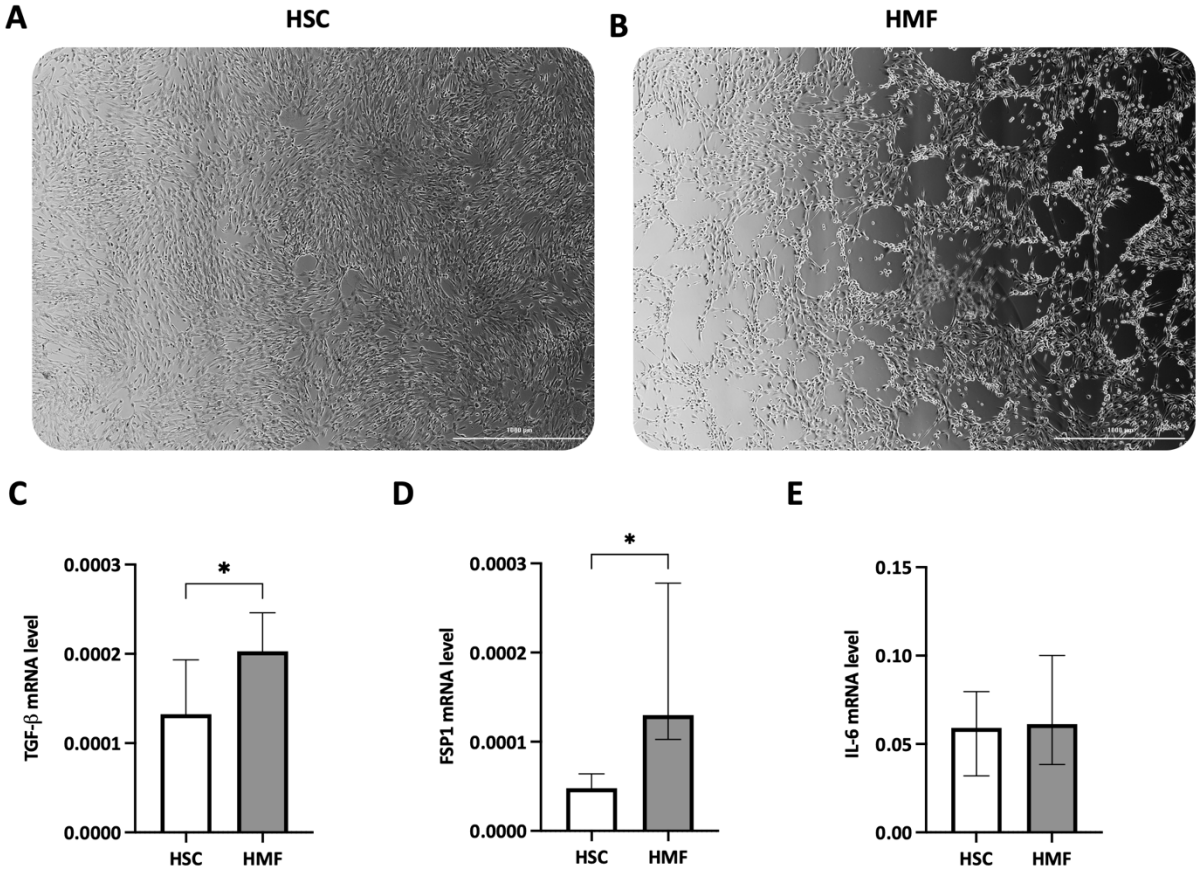

Figure 37: Characterization of hepatic stellate cells (HSC) and hepatic myofibroblasts (HMF). To generate human hepatic stromal cells with an HSC- and HMF-like phenotype, HSteCs were either cultured with 2.5 µm ATRA or 1 ng/ml TGF-β1. Representative images of **(A)** HSC and **(B)** HMF. Cells were characterized by qPCR, analyzing the mRNA levels of **(C)** TGF-β, **(D)** FSP1, and **(E)** IL-6 in HSC (white) and HMF (grey). The mRNA levels were normalized to the housekeeper gene GAPDH. Data represent the mean ± SD (normally distributed) or the median with interquartile range (not normally distributed). N=7 for TGF-β1, N=6 for IL-6, and N=4 for FSP1. * = $p < 0.05$.

4.2.4.1 Coculture with CD8⁺ T cells led to significantly enhanced PD-L1 expression on HSC and HMF

First, the impact of $CD8^+$ T cells on the PD-L1 status of HSC and HMF was analyzed. Higher PD-L1 mRNA levels were detected in monocultured HMF compared to HSC (Figure 38A). After coculture with $CD8^+$ T cells, PD-L1 mRNA expression was significantly elevated in HSC and HMF (Figure 38A). After 72 h of coculture with $CD8^+$ T cells, also cell surface expression levels of PD-L1 were significantly higher on protein level in both HSC and HMF, as revealed by flow cytometry. The MFI ratio was around 4.8 on both hepatic stromal cells compared to 1.4 and 1.8 in monocultured HSC and HMF, respectively ($p < 0.001$) (Figure 38B).

Finally, IF staining of PD-L1 confirmed these results (Figure 38C-F). Here, the heterogenous expression of PD-L1 is seen. HSC expressed less PD-L1 compared to HMF in monoculture (Figure 38C+E). After

coculture with CD8⁺ T cells, more HSC and HMF expressed PD-L1 and further the PD-L1 staining was more intense (Figure 38D+F).

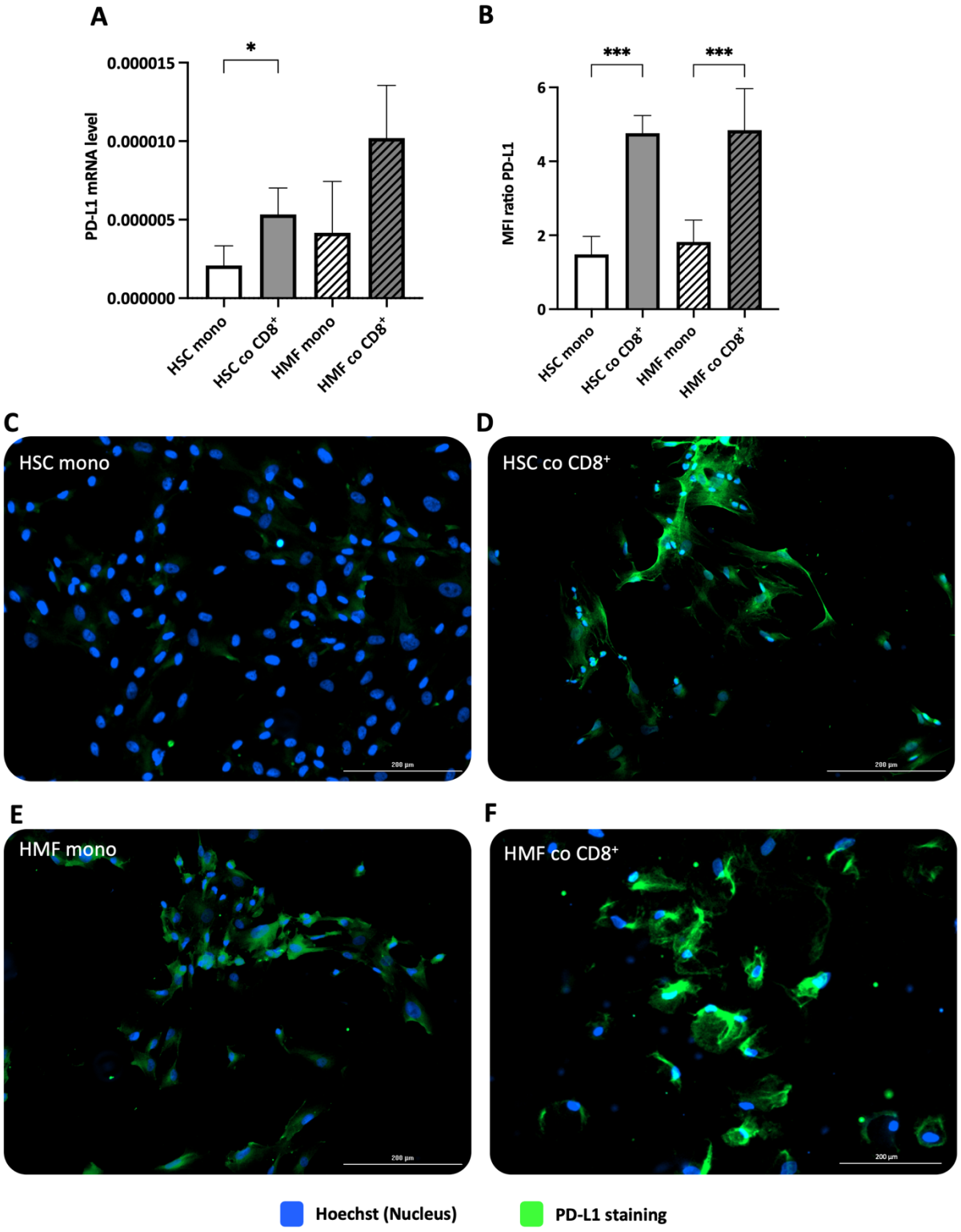

Figure 38: Coculture with CD8⁺ T cells led to significantly enhanced PD-L1 expression on hepatic stellate cells (HSC) and hepatic myofibroblasts (HMF). HSC and HMF were either cultured alone or together with CD8⁺ T cells. After 72 h, **(A)** mRNA levels of PD-L1 were analyzed by qPCR and **(B)** the cell surface expression of PD-L1 by flow cytometry. The mRNA levels were normalized to the housekeeper gene GAPDH. Median fluorescence intensity (MFI) ratio was calculated by dividing the MFI of the specific staining by the MFI of the isotype control. Further,

an immunofluorescence staining of PD-L1 (green) was performed. Nuclei were stained with Hoechst (blue). Representative images of **(C)** monocultured HSC or **(D)** cocultured with $CD8^+$ T cells and **(E)** HMF in monoculture or after **(F)** coculture with $CD8^+$ T cells. The scale bar represents 200 µm. Data represent the mean ± SD (normally distributed). N=4 for flow cytometry analysis and N=3 for qPCR. * = $p < 0.05$, *** = $p < 0.001$.

Overall, these data indicate that coculture with $CD8^+$ T cells enhanced PD-L1 cell surface expressions on HSC and HMF to the same extent.

4.2.4.2 $CD8^+$ T cells enhanced PD-L1 cell surface expression on HSC and HMF by IFNγ

IFNγ is known to be the main inducer of PD-L1 on tumor cells [79] and IFNγ was highly secreted by $CD8^+$ T cells during activation culture (Figure 30B). The question rose whether $CD8^+$ T cells upregulate PD-L1 expression on HSC and HMF by IFNγ. For this purpose, the same culture settings as above were used and cells were treated with 10 µg/ml ultra-LEAF™ IFNγ antibody, to neutralize IFNγ bioactivity, or the respective ultra-LEAF™ isotype control (section 3.1.11.3, IFNγ blockade). After 72, h the cell surface expression of PD-L1 was analyzed by flow cytometry and IF staining.

Here, the cell surface expression of PD-L1 was not affected in monocultured HSC and HMF treated with anti-IFNγ antibody, as the n-fold MFI was around 1.0 (Figure 39A). In contrast, treatment with anti-IFNγ antibody during coculture with $CD8^+$ T cells led to a significantly lower cell surface expression of PD-L1 on HSC and HMF (HSC co $CD8^+$: n-fold 0.35 and HMF co $CD8^+$: n-fold 0.44 (Figure 39A).

This decreased PD-L1 expression upon IFNγ blockade during coculture with $CD8^+$ T cells was also seen in the IF staining, where treatment led to less PD-L1 staining in both hepatic stromal cell populations (Figure 39B-E). These data indicate that $CD8^+$ T cells enhance the cell surface expression of PD-L1 on HSC and HMF by IFNγ.

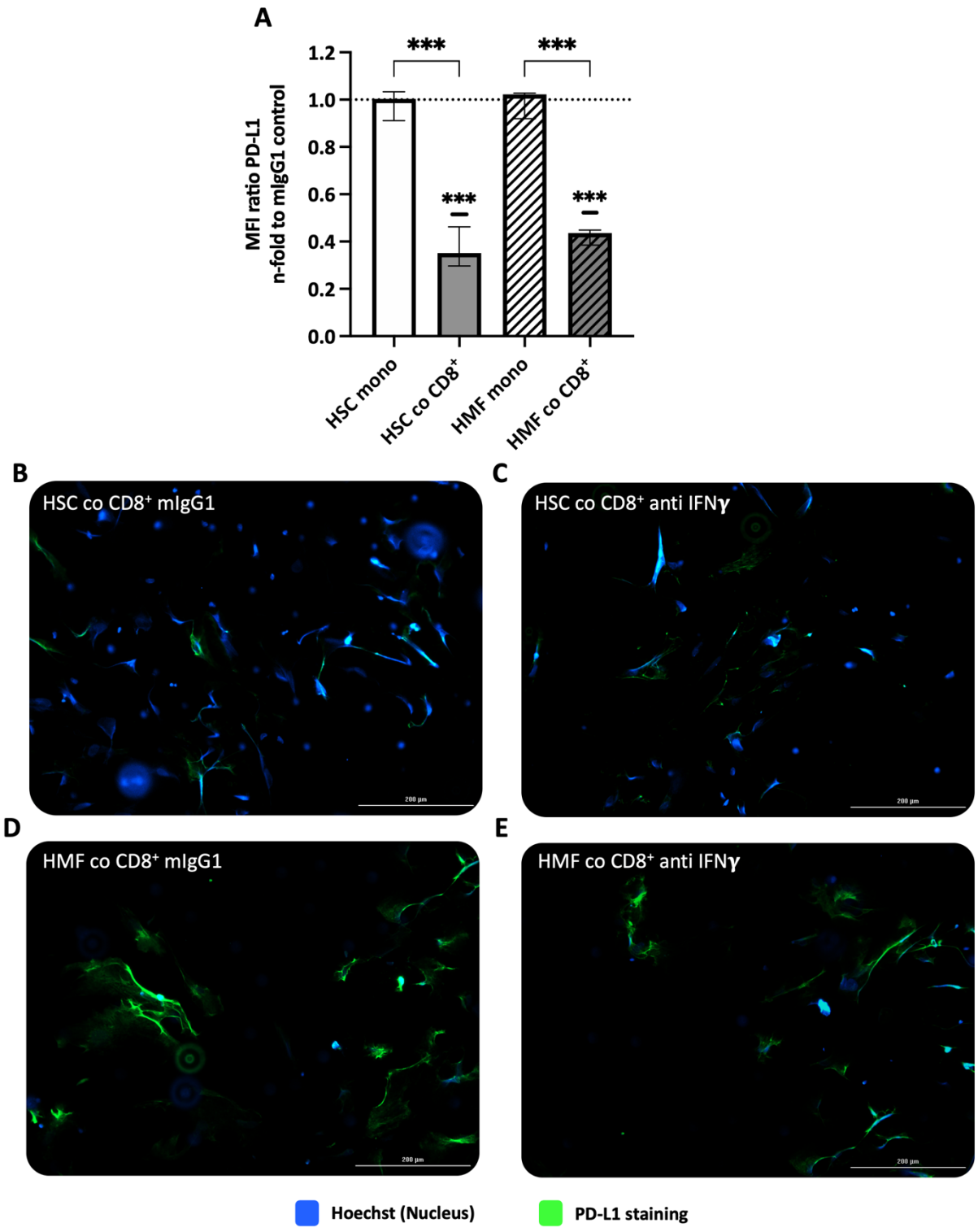

Figure 39: CD8⁺ T cells enhance PD-L1 cell surface expression on hepatic stellate cells (HSC) and hepatic myofibroblasts (HMF) by IFNγ. HSC and HMF were seeded in mono- or coculture with CD8⁺ T cells. Further, the cells were treated with 10 µg/ml ultra-LEAF™ IFNγ antibody to neutralize IFNγ bioactivity or the respective ultra-LEAF™ isotype control (mIgG1). After 72 h, **(A)** the cell surface expression of PD-L1 was analyzed by flow cytometry. Median fluorescence intensity (MFI) ratio was calculated by dividing the MFI of the specific staining by the MFI of the isotype control. Data were normalized to the respective isotype control. Further, an immunofluorescence staining of PD-L1 (green) was performed. Nuclei were stained with Hoechst (blue).

Representative images of **(B)** HSC cocultured with $CD8^+$ T cells treated with **(B)** the isotype control or with **(C)** anti-IFNγ antibody, or HMF cocultured with $CD8^+$ T cells treated with **(D)** the isotype control or with **(E)** anti-IFNγ antibody. The scale bar represents 200 µm. Data represent the median with interquartile range (not normally distributed). N=3. *** = $p < 0.001$.

To summarize, $CD8^+$ T cells enhanced PD-L1 cell surface levels on HSC and HMF by IFNγ.

4.2.4.3 Coculture with HSC and HMF led to a more activated phenotype of $CD8^+$ T cells

Next, the impact of HSC and HMF on $CD8^+$ T cells was analyzed considering the cell surface expression of PD-1 and PD-L1, the activation status, and the effector phenotype.

Cell surface expression levels of PD-1 and PD-L1 were not altered on $CD8^+$ T cells after coculture with HSC or HMF compared to monoculture (Figure 40A+C). The MFI ratio of PD-1 was around 1.9 and of PD-L1 around 1.5. In addition, the number of PD-1 positive and PD-L1 positive $CD8^+$ T cells was not affected by coculture with HSC or HMF (Figure 40B+D).

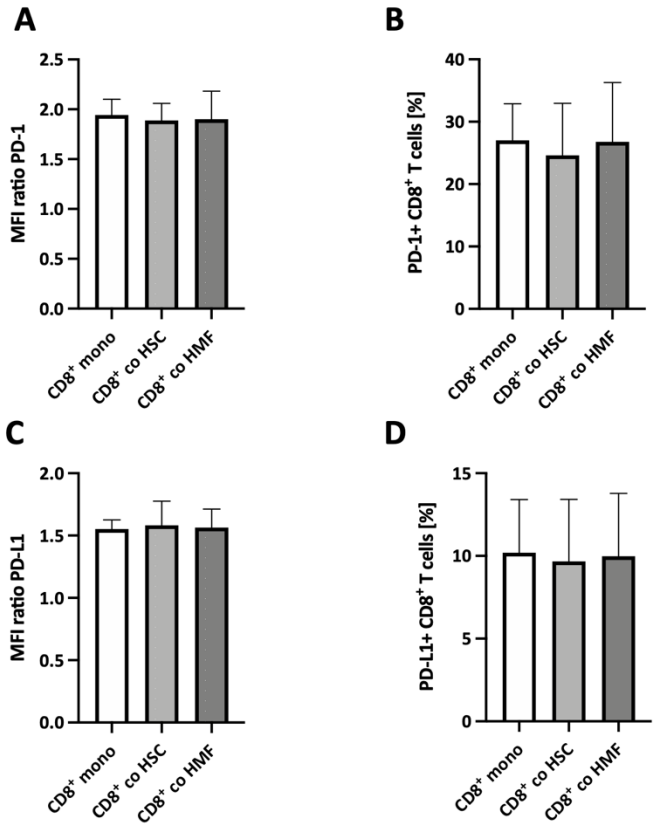

Figure 40: Coculture with hepatic stellate cells (HSC) and hepatic myofibroblasts (HMF) did not affect cell surface expression of PD-1 or PD-L1 on $CD8^+$ T cells. $CD8^+$ T cells were isolated by magnetic cell separation from blood derived lymphocytes and then activated with anti-CD3 and anti-CD28 antibodies, as well as IL-2 for 4 days. Afterwards, they were seeded in mono- (white) or coculture with either HSC (light grey) or HMF (dark grey) for 72 h. Cell surface levels of **(A)** PD-1 and **(C)** PD-L1 were analyzed by flow cytometry. Further, the percentage of **(B)** PD-1 positive and **(D)** PD-L1 positive $CD8^+$ T cells was determined. Median fluorescence intensity (MFI) ratio

was calculated by dividing the MFI of the specific staining by the MFI of the isotype control. Data were normalized to the respective isotype control. Data represent the mean ± SD (normally distributed). N=4.

The levels of the early activation marker CD69 were significantly higher on the cell surface of $CD8^+$ T cells after coculture with HSC and HMF (MFI ratio: mono: 2.3 vs. co HSC: 6.3 vs. co HMF: 6.4). There was no difference of the cell surface expression of CD69 comparing coculture with HSC or HMF (Figure 41A). Moreover, coculture with HSC or HMF led to a significantly higher number of CD69 positive $CD8^+$ T cells ($p < 0.001$) (Figure 41B). The cell surface levels of CD25 were only slightly higher after coculture with HSC and HMF compared to monocultured $CD8^+$ T cells, while the number of CD25 positive $CD8^+$ T cells was almost unaffected (Figure 41D).

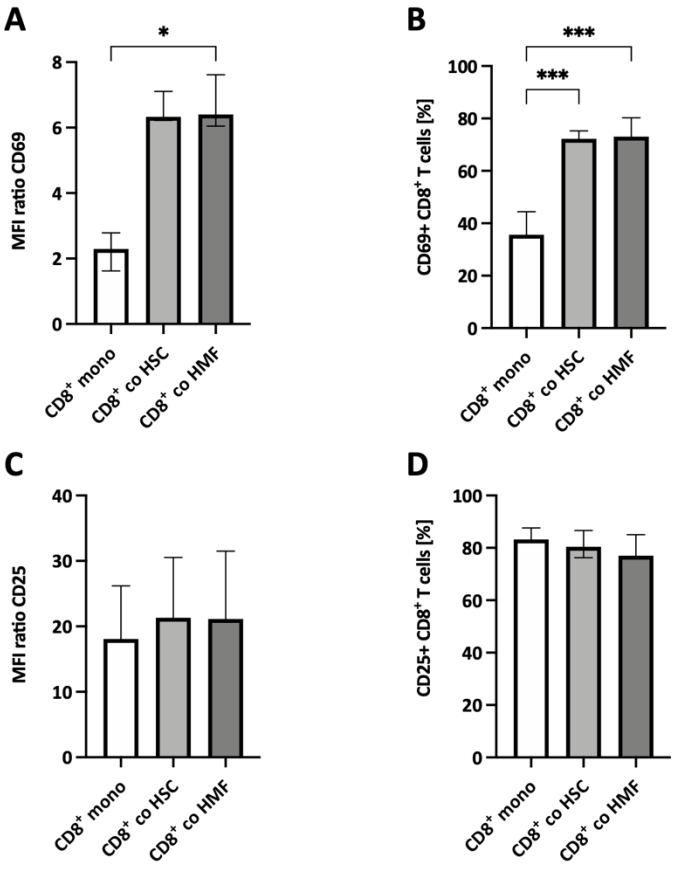

Figure 41: Coculture with hepatic stellate cells (HSC) and hepatic myofibroblasts (HMF) led to a higher cell surface expression of CD69 but not CD25 on $CD8^+$ T cells. $CD8^+$ T cells were isolated by magnetic cell separation from blood derived lymphocytes and then activated with anti-CD3 and anti-CD28 antibodies, as well as IL-2 for 4 days. Afterwards, they were seeded in mono- (white) or coculture with either HSC (light grey) or HMF (dark grey) for 72 h. Cell surface levels of **(A)** CD69 and **(C)** CD25 were analyzed by flow cytometry. Further, the percentage of **(B)** CD69 positive and **(D)** CD25 positive $CD8^+$ T cells was determined. Median fluorescence intensity (MFI) ratio was calculated by dividing the MFI of the specific staining by the MFI of the isotype control. Data represent

the mean ± SD (normally distributed) or the median with interquartile range (not normally distributed). N=4. * = $p < 0.05$, *** = $p < 0.001$.

Next, the release of effector molecules by $CD8^+$ T cells was analyzed after mono- or coculture with either HSC or HMF. The IFNγ concentrations were slightly lower after coculture with HMF which was on the same level after coculture with HSC compared to monoculture (Figure 42A). Coculture with HSC and HMF led to slightly higher concentrations of Granulysin in the supernatants of $CD8^+$ T cells (Figure 42B). After HMF coculture, Granzyme A concentrations were slightly higher and after HSC slightly lower in the supernatant compared to monoculture. In contrast, Granzyme B and Perforin concentration levels were elevated after coculture with HSC or HMF (Figure 42D+E). Here, Granzyme B concentrations were slightly lower comparing HMF and HSC coculture Figure 42D).

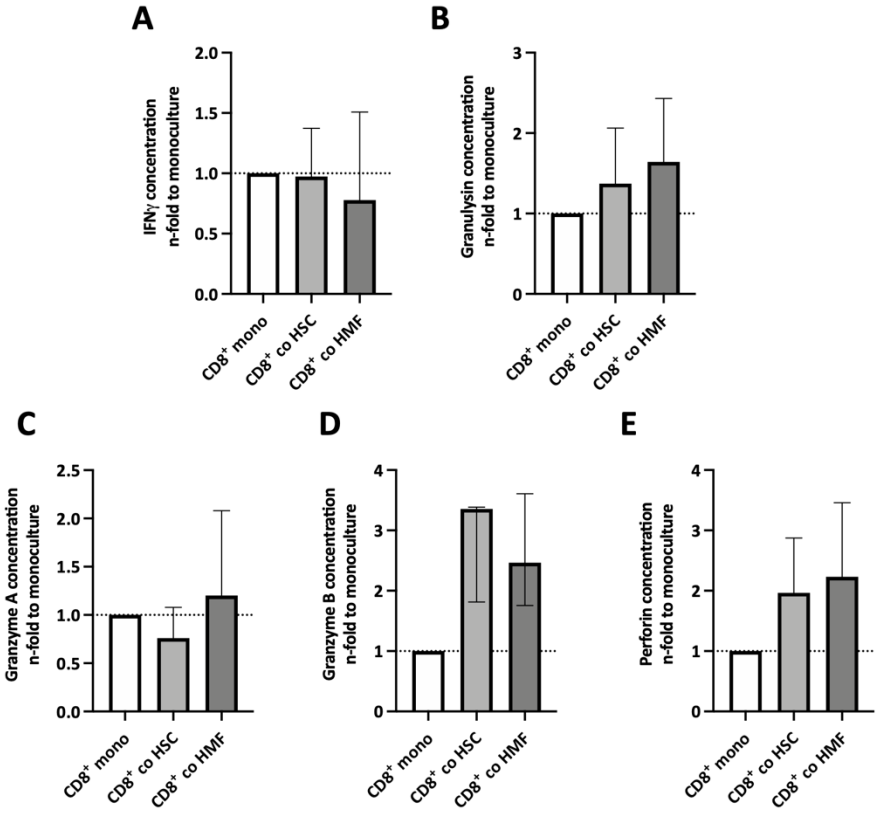

Figure 42: Elevated concentration of $CD8^+$ T cells effector molecules after coculture with hepatic stellate cells (HSC) or hepatic myofibroblasts (HMF). $CD8^+$ T cells were isolated by magnetic cell separation from blood derived lymphocytes and then activated with anti-CD3 and anti-CD28 antibodies, as well as IL-2 for 4 days. Afterwards, they were seeded in mono- (white) or coculture with either HSC (light grey) or HMF (dark grey) for 72 h. Concentrations of **(A)** IFNγ, **(B)** Granulysin, **(C)** Granzyme A, **(D)** Granzyme B, and **(E)** Perforin were measured in the supernatants of mono- and cocultured $CD8^+$ T cells. Data were normalized to the concentrations in monoculture. Data represent the mean ± SD (normally distributed) or the median with interquartile range (not normally distributed). N=3.

Overall, hepatic stromal cells (HSC and HMF) did not impact the cell surface expression of PD-L1 on $CD8^+$ T cells. Further, coculture with HSC and HMF led to a higher activation level, as cell surface expression of CD69 was enhanced on $CD8^+$ T cells. The concentration of the effector molecule Granzyme A was slightly lower and those of Granulysin, Granzyme B, and Perforin were slightly higher after coculture with HSC or HMF.

4.2.4.4 Pre-coculture of $CD8^+$ T cells with HSC or HMF did not enhance the induction of PDECs death

Previous results showed that $CD8^+$ T cells exhibited an enhanced activation phenotype and higher concentrations of some effector molecules, such as Granulysin, Granzyme B, and Perforin after coculture with HSC or HMF. The question rose whether these pre-cocultured $CD8^+$ T cells were more effective to induce cell death in PDECs.

For this purpose, H6c7-kras and PancTu1 cells were labeled with CTG. Twenty-four hours after seeding the labeled PDECs, $CD8^+$ T cells were collected from mono- or coculture with HSC or HMF. Then, $CD8^+$ T cells were added to H6c7-kras and PancTu1 cells at a ratio of 1:20. After 24 h, $CD8^+$ T cells were removed, and the confluence was measured. Further, PDECs were stained with Hoechst and the nuclei count was performed using the NYONE Scientific. The setting is pictured in Figure 13.

The cell confluence of H6c7-kras cells was reduced after coculture with $CD8^+$ T cells, which had been monocultured before (H6c7-kras: n-fold 0.84 vs. H6c7-kras co $CD8^+$ pre-monoculture: n-fold: 0.59) (Figure 43A). If the $CD8^+$ T cells had been pre-cultured with HSC or HMF, the cell confluence of H6c7-kras cells was less reduced compared to pre-monoculture, but still lower than confluence of H6c7-kras cells in monoculture (Figure 43A). Figure 43B+C shows representative images, comparing the cell confluence of H6c7-kras cells in monoculture and coculture with pre-monocultured $CD8^+$ T cells.

Next, the cell number of H6c7-kras cells was determined after cocultures. The cell count was reduced after coculture with pre-monocultured $CD8^+$ T cells (Figure 43D). After coculture with pre-HSC or HMF cocultured $CD8^+$ T cells, the cell count was also lower compared to H6c7-kras cells in monoculture. The reduced cell count was in line with lower cell confluence. Representative images show the reduced number of Hoechst positive cells after coculture with pre-monocultured $CD8^+$ T cells (Figure 43E+F).

Next, the cell confluence of PancTu1 cells after coculture with different pre-cultured $CD8^+$ T cells was analyzed. After coculture with pre-monocultured $CD8^+$ T cells, the cell confluence of PancTu1 cells was reduced (Figure 43G). Pre-HSC or HMF cocultured $CD8^+$ T cells also led to a slightly reduced cell confluence of PancTu1 cells, however, the reduction was not as strong as in coculture with pre-monocultured $CD8^+$ T cells (PancTu1 mono: n-fold 0.87 vs. PancTu1 cells co $CD8^+$ pre-monoculture: 0.68 vs. PancTu1 cells co $CD8^+$ pre-HSC culture: 0.76 vs. PancTu1 cells co $CD8^+$ pre-HMF culture: 0.8) (Figure 43G). Figure 43H+I show representative images, comparing the cell confluence of PancTu1 cells in monoculture and coculture with pre-monocultured $CD8^+$ T cells.

Further, the cell number of PancTu1 cells was not altered after coculture with $CD8^+$ T cells, either pre-monocultured or pre-HSC or HMF cocultured (Figure 43J). Representative images of the cell count are shown in Figure 43K+L.

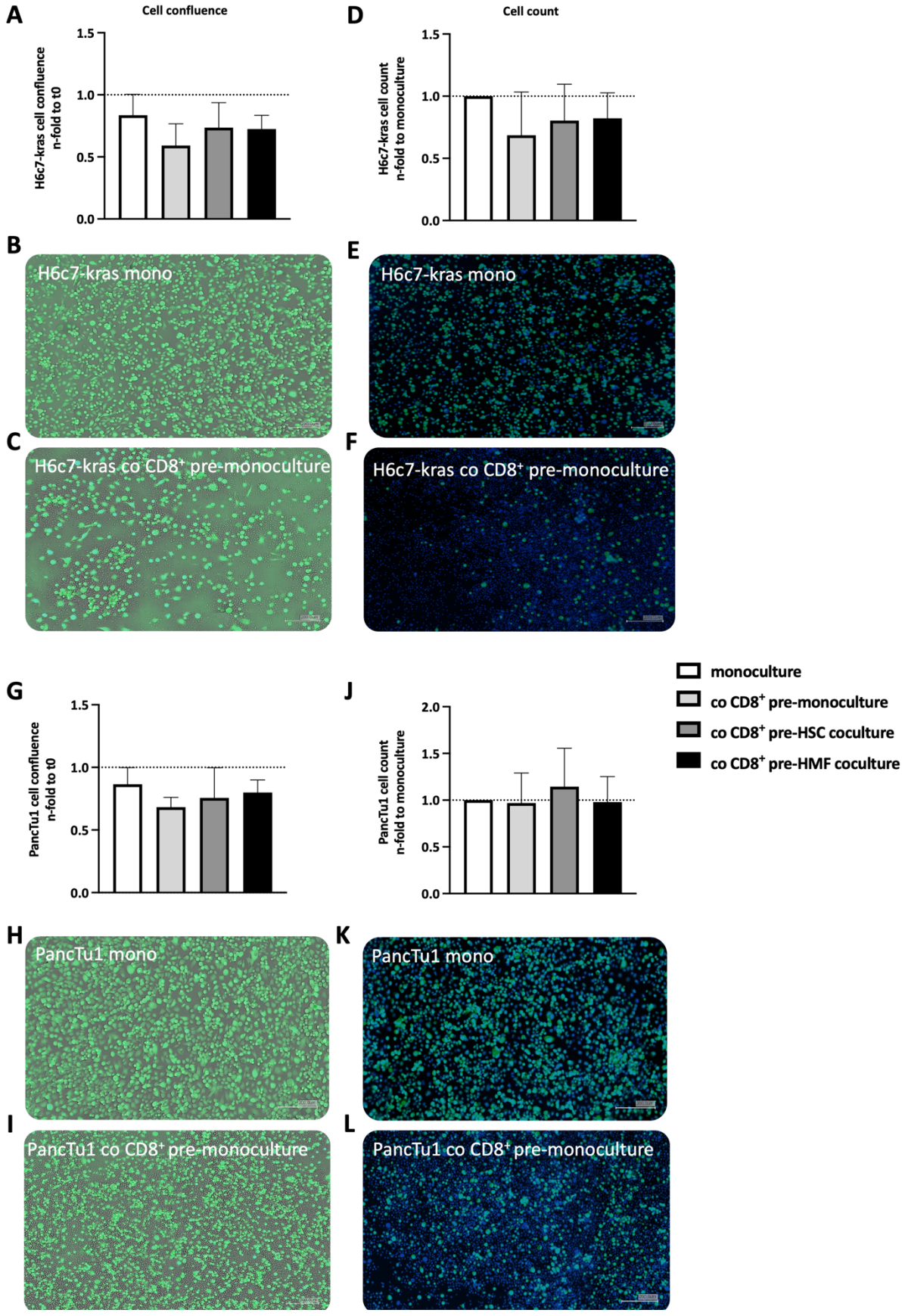

Figure 43: Pre-coculture of CD8⁺ T cells with hepatic stellate cells (HSC) and hepatic myofibroblasts (HMF) did not enhance cell death of H6c7-kras and PancTu1 cells. H6c7-kras and PancTu1 cells were labeled with CellTracker Green (CTG). Twenty-four hours after seeding the labeled H6c7-kras and PancTu1 cells, CD8⁺ T cells

were collected from mono- or coculture with HSC or HMF. Then, $CD8^+$ T cells were added to H6c7-kras and PancTu1 cells at a ratio of 1:20. After 24 h, $CD8^+$ T cells were removed and the cell confluence of **(A)** H6c7-kras and **(G)** PancTu1 cells was measured. Data were normalized to the cell confluence before the coculture with $CD8^+$ T cells (= t0). Representative images of the cell confluence **(B)** H6c7-kras cells in monoculture, **(C)** H6c7-kras cells after coculture with pre-monocultured $CD8^+$ T cells, **(H)** PancTu1 cells in monoculture, and **(I)** PancTu1 cells after coculture with pre-monocultured $CD8^+$ T cells. Further, PDECs were stained with Hoechst (blue) and the cell number was determined of **(D)** H6c7-kras and **(J)** PancTu1 cells. Data were normalized to the cell number of H6c7-kras cells in monoculture. Representative images of the cell count of **(E)** H6c7-kras cells in monoculture, **(F)** H6c7-kras cells after coculture with pre-monocultured $CD8^+$ T cells, **(K)** PancTu1 cells in monoculture, and **(L)** PancTu1 cells after coculture with pre-monocultured $CD8^+$ T cells. The scale bar represents 200 µm. Data represent the mean ± SD (normally distributed). N=5 for cell confluence and N=3 for cell count.

Overall, the cell confluence of H6c7-kras and PancTu1 cells was lower after coculture with pre-monocultured $CD8^+$ T cells. This effect was not enhanced if the $CD8^+$ T cells were pre-cocultured with either HSC or HMF, even though $CD8^+$ T cells were more activated and released higher amounts of Granulysin, Granzyme B, and Perforin.

4.2.5 Impact of hepatic stromal cells on $CD8^+$ T cells under blockade of PD-L1 with Durvalumab

Previous results showed that hepatic stromal cells and $CD8^+$ T cells influence each other. Due to coculture with $CD8^+$ T cells, the cell surface expression of PD-L1 was enhanced on HSC and HMF by IFNγ. Besides, $CD8^+$ T cells were more activated after coculture with HSC and HMF, and additionally, some effector molecules (Granulysin, Granzyme B, and Perforin) were released to a higher extent by $CD8^+$ T cells after coculture with hepatic stromal cells. However, pre-coculture with HSC or HMF did not enhance $CD8^+$ T cell mediated PDEC death. Therefore, the question rose whether the PD-L1/PD-1 axis impairs the effector phenotype of $CD8^+$ T cells and whether blocking of PD-L1 increases PDEC death. For this purpose, a direct coculture with $CD8^+$ T cells and HSC or HMF was performed. As a control, HSC, HMF, and $CD8^+$ T cells were each seeded in monoculture. The cultures were either treated with 10 µg/ml of Durvalumab or 10 µg/ml of the respective isotype control (hIgG1) for 72 h (section 3.1.11.3). After 72 h, pre-mono- or cocultured $CD8^+$ T cells were added to either H6c7-kras or PancTu1 cells.

4.2.5.1 Cell surface expression of PD-L1 was decreased on HSC and HMF after treatment with Durvalumab which was intensified by coculture with CD8$^+$ T cells

First, the impact of Durvalumab treatment on cell surface expression of PD-L1 on HSC and HMF was analyzed.

The cell surface expression of PD-L1 was significantly lower after Durvalumab treatment in monocultured HSC and HMF (HSC and HMF mono + isotype control: n-fold 1.0 vs. HSC mono + Durva: n-fold: 0.3 vs. HMF mono + Durva: n-fold 0.2) (Figure 44A). This observation can be explained by the fact that by binding to PD-L1, Durvalumab prevented the binding of the staining antibody, confirming the successful inhibition of PD-L1 by the treatment antibody. Cell surface expression of PD-L1 was reduced even more on HSC and HMF after coculture with CD8$^+$ T cells and treatment with Durvalumab. This reduction was slightly more pronounced in HMF compared to HSC (HSC co CD8$^+$: n-fold 0.09 vs. HMF co CD8$^+$: n-fold 0.07) (Figure 44A). The decrease of the cell surface expression of PD-L1 comparing HSC and HMF in coculture with CD8$^+$ T cells and treated with Durvalumab was also seen in the IF staining (Figure 44B-E). However, as some cells were still PD-L1 positive the staining antibody seemed to bind to a different binding site compared to Durvalumab.

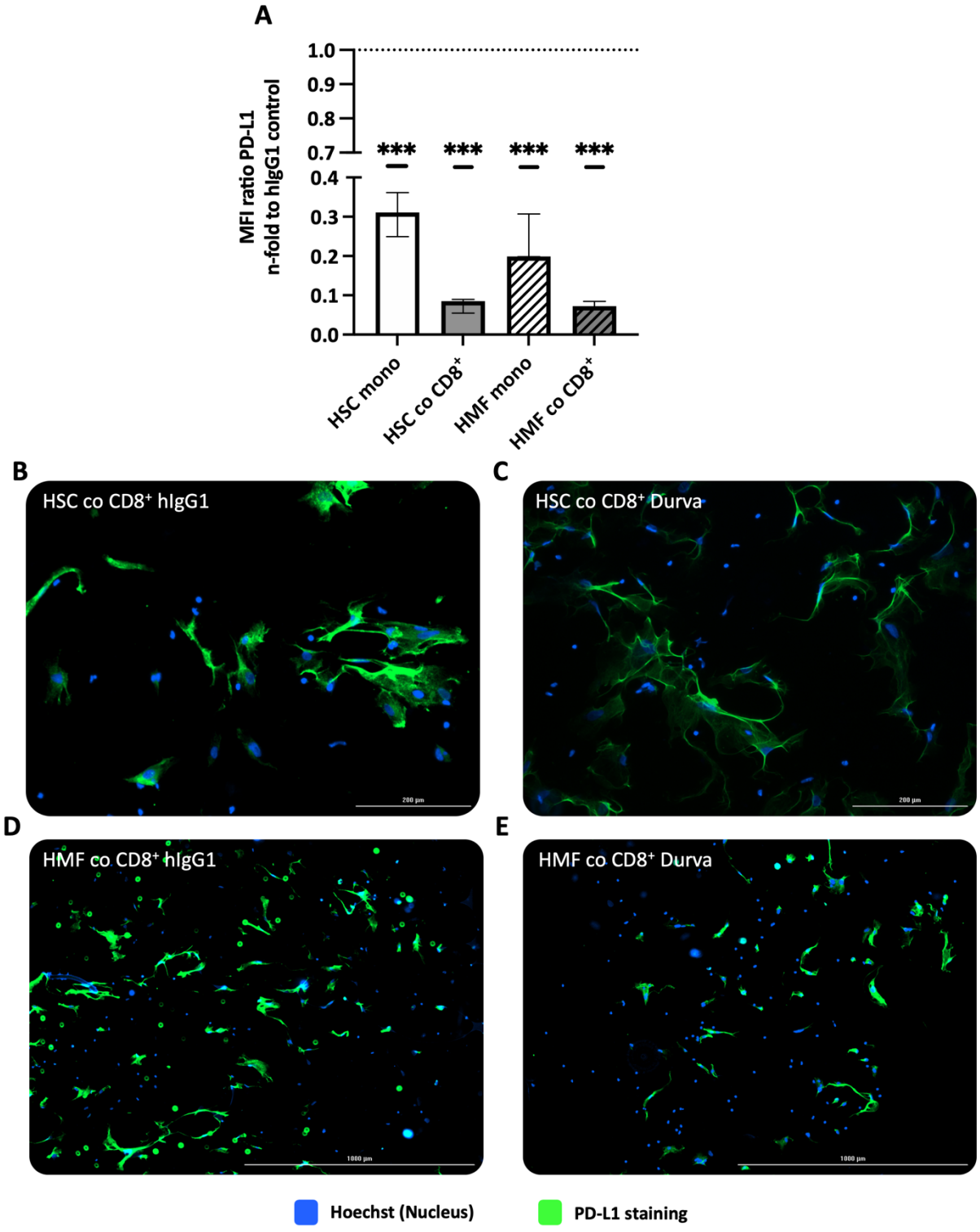

Figure 44: PD-L1 cell surface expression was decreased on hepatic stellate cells (HSC) and hepatic myofibroblasts (HMF) after treatment with Durvalumab and by coculture with CD8⁺ T cells. HSC and HMF were seeded in mono- or coculture with CD8⁺ T cells. Cells were treated with 10 µg/ml Durvalumab (blocking PD-L1) or the respective isotype control (hIgG1). After 72 h, **(A)** the cell surface expression of PD-L1 by flow cytometry was analyzed. Data were normalized to the respective isotype control. Further, an immunofluorescence staining of PD-L1 (green) was performed. Nuclei were stained with Hoechst (blue). Representative images of **(B)** HSC cocultured with CD8⁺ T cells treated with **(B)** the isotype control or **(C)** Durvalumab, and HMF cocultured with

$CD8^+$ T cells treated with **(D)** the isotype control or **(E)** Durvalumab. The scale bar represents 200 µm. Data represent the median with interquartile range (not normally distributed). N=3. *** = $p < 0.001$.

Overall, cell surface expression of PD-L1 was decreased on HSC and HMF after treatment with Durvalumab, which was more pronounced after coculture with $CD8^+$ T cells.

4.2.5.2 Durvalumab hardly impacts activation status and effector phenotype of $CD8^+$ T cells in coculture with HSC or HMF

Next, it was investigated whether Durvalumab treatment impacts the cell surface expression of PD-1 and PD-L1, the activation status, and the effector phenotype of $CD8^+$ T cells in coculture with HSC or HMF.

Durvalumab treatment did not affect cell surface levels of PD-1 and percentage of PD-1 positive $CD8^+$ T cells in monoculture (Figure 45A+B).

In coculture with HSC and HMF, Durvalumab treatment led to a slightly higher cell surface expression of PD-1 on $CD8^+$ T cells, however, the percentage of PD-1 positive $CD8^+$ T cells was not altered (Figure 45A+B). As shown above, Durvalumab prevented binding of the PD-L1 staining antibody, causing a significant reduction of PD-L1 cell surface levels on $CD8^+$ T cells as well as a reduction of PD-L1 positive $CD8^+$ T cells (Figure 45C+D).

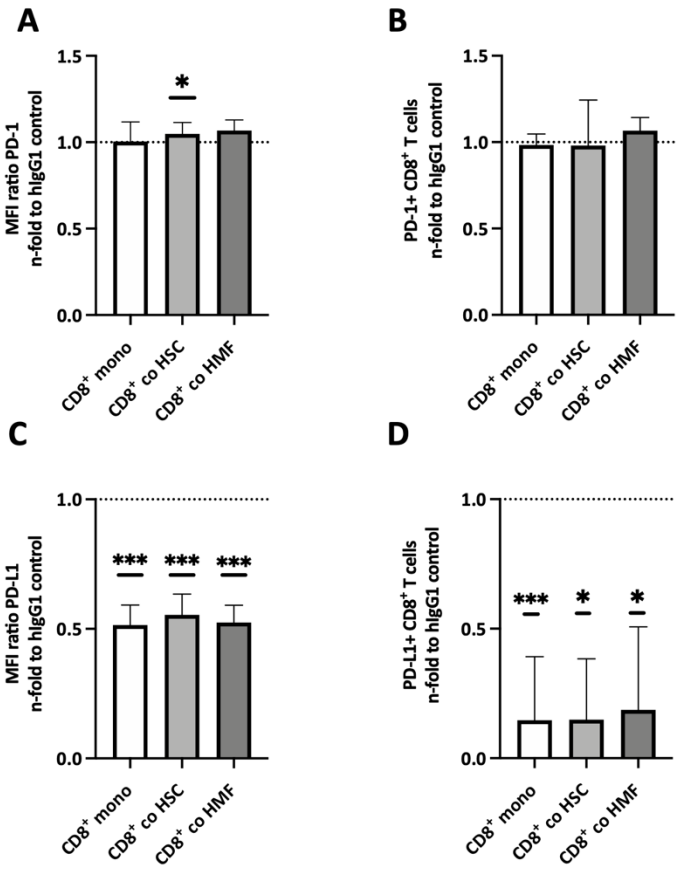

Figure 45: Durvalumab treatment led to a slight enhancement of cell surface expression of PD-1 on CD8$^+$ T cells under hepatic stellate cells (HSC) and hepatic myofibroblasts (HMF) coculture. CD8$^+$ T cells were isolated by magnetic cell separation from human blood derived lymphocytes and then activated with anti-CD3 and anti-CD28 antibodies, as well as IL-2 for 4 days. Afterwards, CD8$^+$ T cells were seeded in mono- (white) or coculture with either HSC (light grey) or HMF (dark grey) for 72 h. Further, the cultures were treated with 10 µg/ml of Durvalumab or 10 µg/ml of the respective isotype control (hIgG1). Cell surface levels of **(A)** PD-1 and **(C)** PD-L1 were analyzed by flow cytometry. Further, the percentage of **(B)** PD-1 positive and **(D)** PD-L1 positive CD8$^+$ T cells was determined. Median fluorescence intensity (MFI) ratio was calculated by dividing the MFI of the specific staining by the MFI of the isotype control. Data were normalized to the hIgG1 isotype control treated sample. Data represent the mean ± SD (normally distributed) or the median with interquartile range (not normally distributed). N=4. * = $p < 0.05$, *** = $p < 0.001$.

Next, the activation status of CD8$^+$ T cells was analyzed. Durvalumab treatment did not alter the cell surface levels of CD69 and the percentage of CD69 positive CD8$^+$ T cells after mono- or coculture with either HSC or HMF (Figure 46A+B). Moreover, cell surface expression of CD25 was not affected by Durvalumab treatment in either culture setting, in line with no change in CD25 positive CD8$^+$ T cells (Figure 46C+D).

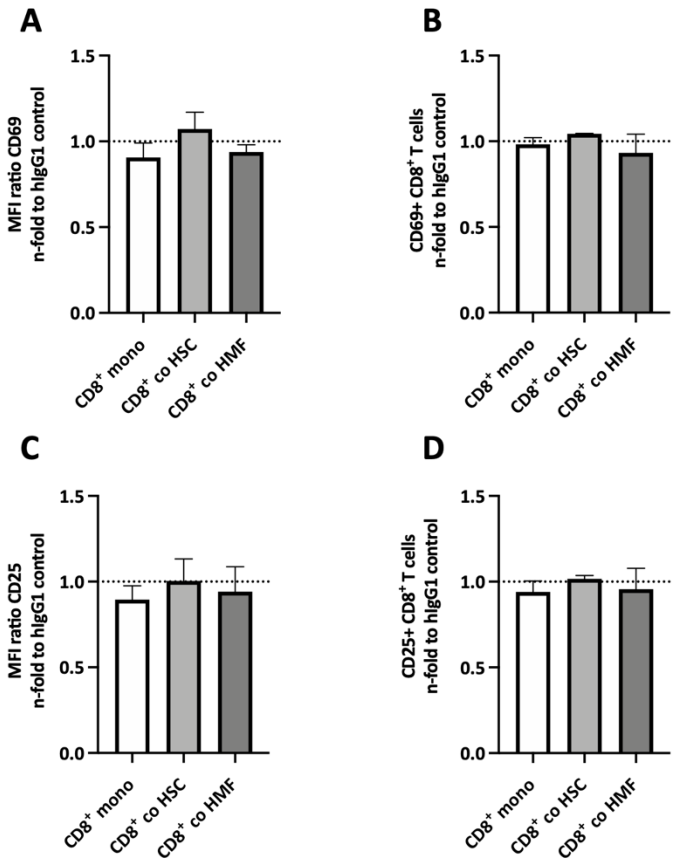

Figure 46: Durvalumab treatment hardly impacted activation of CD8$^+$ T cells in monoculture and coculture with hepatic stellate cells (HSC) and hepatic myofibroblasts (HMF). CD8$^+$ T cells were isolated by magnetic cell separation from human blood derived lymphocytes and then activated with anti-CD3 and anti-CD28 antibodies, as well as IL-2 for 4 days. Afterwards, CD8$^+$ T cells were seeded in mono- (white) or coculture with either hepatic stellate cells (HSC) (light grey) or HMF (dark grey) for 72 h. Further, the cultures were treated with 10 µg/ml of Durvalumab or 10 µg/ml of the respective isotype control (hIgG1). Cell surface levels of **(A)** CD69 and **(C)** CD25 were analyzed by flow cytometry. Further, the percentage of **(B)** CD69 positive and **(D)** CD25 positive CD8$^+$ T cells was determined. Median fluorescence intensity (MFI) ratio was calculated by dividing the MFI of the specific staining by the MFI of the isotype control. Data were normalized to the hIgG1 isotype control treated sample. Data represent the mean ± SD (normally distributed) or the median with interquartile range (not normally distributed). N=3.

Afterwards, the concentrations of effector molecules were analyzed in the supernatants. Durvalumab treatment led to significantly higher concentrations of IFNγ ($p<0.01$), Granulysin ($p<0.01$), and Perforin in supernatants of monocultured CD8$^+$ T cells (Figure 47A+B+E). In addition, concentrations of Granzyme A and Granzyme B were higher in supernatants of monocultured CD8$^+$ T cells and after Durvalumab treatment (Figure 47C+D). While concentrations of IFNγ and Perforin were not affected in supernatants of cocultured CD8$^+$ T cells with HSC after Durvalumab treatment (Figure 47A+E).

However, coculture with HSC and treatment with Durvalumab led to slightly lower concentrations of Granulysin, Granzyme A, and Granzyme B in the supernatants of $CD8^+$ T cells (Figure 47B-D). After coculture with HMF, the concentrations of IFNγ, Granzyme A, Granzyme B, and Perforin were slightly higher after treatment with Durvalumab compared to the isotype control (Figure 47A+C-E).

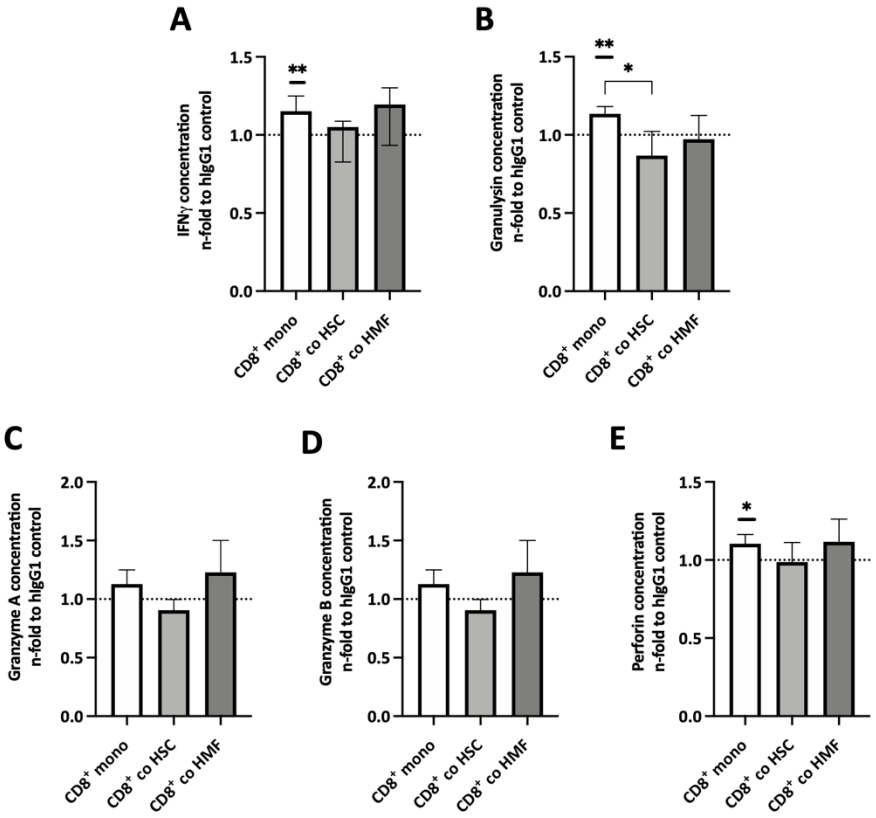

Figure 47: Durvalumab treatment led to higher concentrations of effector molecules in monocultured $CD8^+$ T cells. $CD8^+$ T cells were isolated by magnetic cell separation from human blood derived lymphocytes and then activated with anti-CD3 and anti-CD28 antibodies, as well as IL-2 for 4 days. Afterwards, $CD8^+$ T cells were seeded in monoculture (white) or in coculture with either hepatic stellate cells (HSC) (light grey) or hepatic myofibroblasts (HMF) (dark grey) for 72 h. Further, the cultures were treated with 10 µg/ml of Durvalumab or 10 µg/ml of the respective isotype control (hIgG1). Concentrations of **(A)** IFNγ, **(B)** Granulysin, **(C)** Granzyme A, **(D)** Granzyme B, and **(E)** Perforin were measured in the supernatant of monocultured and cocultured $CD8^+$ T cells. Data were normalized to the concentrations of the hIgG1 isotype control treated sample. Data represent the mean ± SD (normally distributed) or the median with interquartile range (not normally distributed). N=4. * = $p < 0.05$, ** = $p < 0.01$.

Overall, Durvalumab treatment did not affect the cell surface expression of PD-1 on $CD8^+$ T cells. In addition, levels of the activation markers CD69 and CD25 were not affected by Durvalumab treatment

on CD8$^+$ T cells. In contrast, secretion of effector molecules was higher in monocultured and HMF-cocultured CD8$^+$ T cells after Durvalumab treatment.

4.2.5.3 Pre-coculture of CD8$^+$ T cells with HSC or HMF and Durvalumab treatment did not enhance cell death induction of PDECs

Previous results showed that pre-cocultured CD8$^+$ T cells with HSC and HMF did not impact cell death induction of PDECs. After Durvalumab treatment, the concentrations of effector molecules in mono- and cocultured CD8$^+$ T cells were slightly higher. CD8$^+$ T cells in coculture with HSC and HMF were treated with Durvalumab as mentioned above and afterwards cocultured with PDECs to investigate whether this increased induction of cell death of PDECs.

For this purpose, H6c7-kras and PancTu1 cells were labeled with CTG. Twenty-four hours after seeding PDECs, CD8$^+$ T cells were collected from treated mono- or coculture with HSC or HMF. Then, CD8$^+$ T cells were added to H6c7-kras and PancTu1 cells at a ratio of 1:20. After 24 h, CD8$^+$ T cells were removed and the confluence of PDECs was measured. Further, PDECs were stained with Hoechst and the cell number was determined. Both methods were performed on the NYONE Scientific. The setting is pictured in Figure 14.

The cell confluence of H6c7-kras cells was not affected by pre-Durvalumab treated mono- or coculture with either HSC or HMF (Figure 48A). Moreover, the number of counted H6c7-kras cells remained unchanged, if CD8$^+$ T cells were pre-mono- or cocultured with either HSC or HMF and treated with Durvalumab (Figure 48B).

The cell confluence of PancTu1 cells was not altered after coculture with pre-mono and pre-HMF cultured CD8$^+$ T cells and slightly higher after coculture with pre-HSC cocultured CD8$^+$ T cells (Figure 48C). Treatment of CD8$^+$ T cells with Durvalumab in pre-culture did not alter these effects (Figure 48C). This was in line with the counted cell number of PancTu1 cells. The difference in the cell number was minimally lower, if pre-cultured CD8$^+$ T cells were treated with Durvalumab compared to the isotype control (Figure 48D).

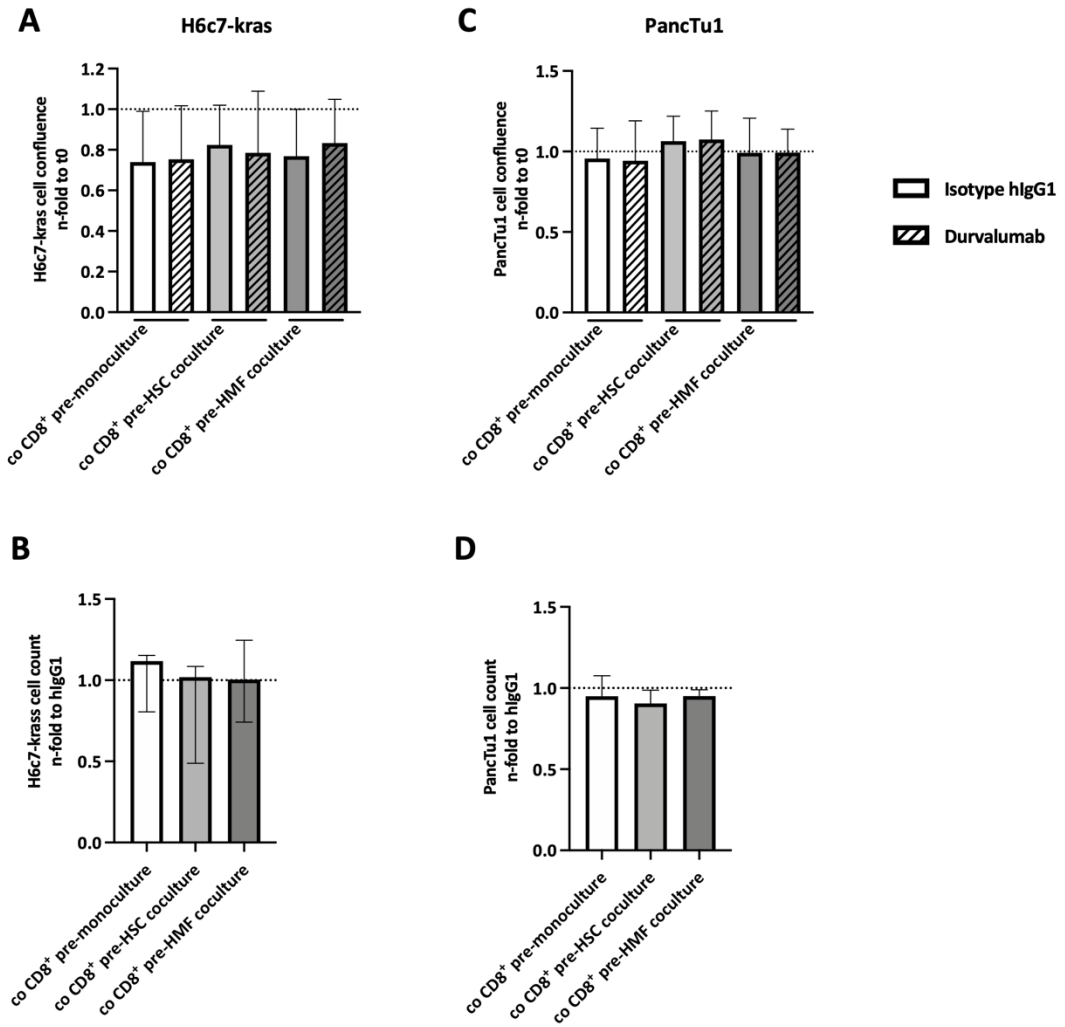

Figure 48: Pre-coculture of CD8$^+$ T cells with hepatic stellate cells (HSC) or hepatic myofibroblasts (HMF) and Durvalumab treatment did not enhance cell death of H6c7-kras and PancTu1 cells. PancTu1 cells were labeled with CellTracker Green (CTG) and were seeded one day before the coculture of CD8$^+$ T cells with HSC and HMF and further isotype or Durvalumab treatment ended. Twenty-four hours after seeding the PDECS, CD8$^+$ T cells were collected from the mono- or coculture with either HSC or HMF. Then CD8$^+$ T cells were added onto the H6c7-kras and PancTu1 cells at a ratio of 1:20. After 24 h, the CD8$^+$ T cells were removed, and the confluence of **(A)** H6c7-kras cells and **(C)** PancTu1 cells was measured. Data were normalized to the cell confluence before the coculture with CD8$^+$ T cells started (=t0). Further, PDAC cells were stained with Hoechst (blue) and the cell number of **(B)** H6c7-kras cells and **(D)** PancTu1 cells was determined. Data were normalized to the cell number of H6c7-kras and PancTu1 cells cocultured with pre-mono or pre-cocultured CD8$^+$ T cells treated with the isotype control (hIgG1). Data represent the mean $\pm$ SD (normally distributed) or the median with interquartile range (not normally distributed). N=3 for coculture with pre-monocultured CD8$^+$ T cells, N=4 for coculture with pre-HSC/HMF cocultured CD8$^+$ T cells.

Overall, these data showed that Durvalumab treatment during pre-mono- or coculture of CD8$^+$ T cells with HSC or HMF did not enhance PDEC death.

4.3 3D *in vitro* cocultures of different cell populations in the tumor microenvironment

Previous experiments were performed using traditional 2D monolayer cell culture models. In order to better mimic the physiological tumor microenvironment and investigate its impact on cytotoxic T cells and their efficacy to induce tumor cell death under different treatments, a stroma enriched 3D spheroid model was established.

4.3.1 Formation of spheroids by different PDEC lines

First of all, it was investigated which PDEC lines are able to form spheroids. For this purpose, H6c7-kras, PancTu1, Panc89, BxPc3, Panc1, Colo357, A818-6, and PT-45 cells were labeled with CTG and seeded in a 96-well ULA plate. After 72 h, the PDEC spheroids were additionally stained with PI to analyze the abundance of dead cells within the spheroid and measured on the Lionheart FX Automated Microscope (section 3.1.11.5).

Panc1 cells did not form an intact spheroid, as the cells were not clustered together (Figure 49A+B). H6c7-kras and PT-45 cells formed the smallest spheroids compared to the other cell lines but did not form compact spheroids as the spheroids were dissociated by only pipetting up and down in the well (Figure 49C+E). Further, PI staining showed a lot of dead cells surrounding the spheroid (Figure 49D+F). This might explain the smaller size of spheroids, as not all of the seeded cells were integrated into the spheroid. It is known that cells with a more mesenchymal phenotype do not form compact spheroids [164]. H6c7-kras cells showed a more mesenchymal phenotype compared to PancTu1 and Panc89 cells (Supplementary Figure 3). BxPc3, A818-6, Colo357, PancTu1, and Panc89 cells formed compact and "round" spheroids (Figure 49G-P). However, in BxPc3 and A818-6 cell spheroids, many cells around the spheroid were PI positive (Figure 49H+J). Further, A818-6 cell spheroids showed a PI signal in the center, which was an indication of a necrotic chore (Figure 49J). In Colo357 cell spheroids, many cells were PI positive throughout the spheroid (Figure 49L). The number of PI positive cells was lower in PancTu1 and Panc89 cell spheroids, compared to the other cell lines (Figure 49N+P). Dissociating the spheroids and counting vital and dead cells with trypan blue revealed that PancTu1 and Panc89 cell spheroids had the lowest vital-to-dead cell ratio (Supplementary Figure 4).

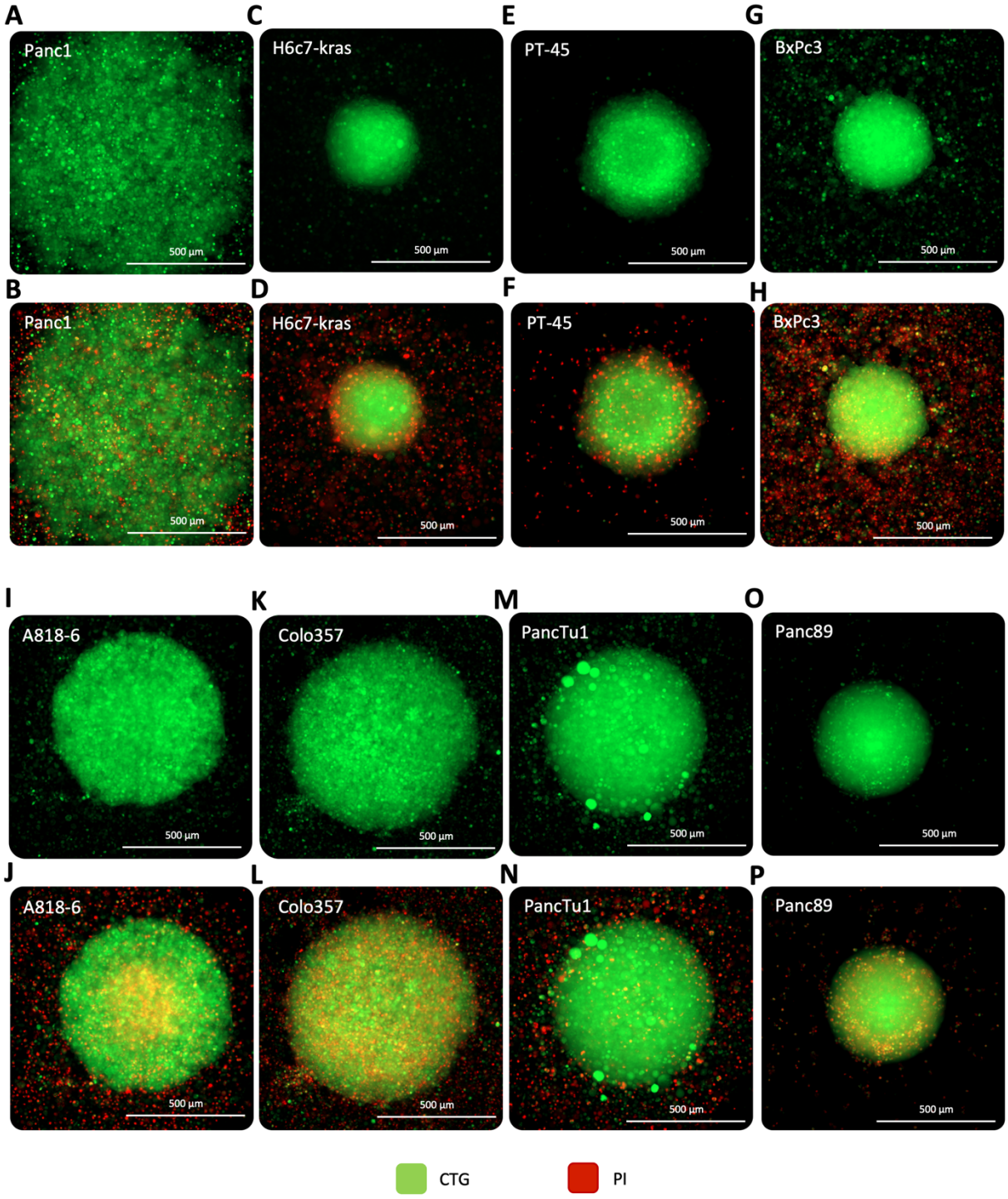

Figure 49: Formation of spheroids by different PDEC lines. H6c7-kras, PancTu1, Panc89, BxPc3, Panc1, Colo357, A818-6, and PT-45 cells were labeled with CellTracker Green (CTG) and seeded in a 96-well ultra-low attachment plate. After 72 h, PDECs were measured on the Lionheart FX Automated Microscope. Representative images of CTG labeled **(A)** Panc1, **(C)** H6c7-Kras, **(E)** PT-45, **(G)** BxPc3, **(I)** A818-6, **(K)** Colo357, **(M)** PancTu1, and **(O)** Panc89 cells. Further, the spheroids were stained with Propidium Iodide (PI) and representative images are shown of **(B)** Panc1, **(D)** H6c7-kras, **(F)** PT-45, **(H)** BxPc3, **(J)** A818-6, **(L)** Colo357, **(N)** PancTu1, and **(P)** Panc89 cells.

These results revealed that the spheroid formation differs between the various PDEC lines. Overall, PancTu1 and Panc89 cells formed compact spheroids with the lowest number of PI positive cells.

4.3.2 Heterogenous cell surface expression levels of PD-L1 on different PDEC lines

For 3D experiments, it was necessary that PDECs exhibit basal cell surface expression of PD-L1, which can be enhanced in order to investigate the impact of stromal cells and immune cells on cell surface expression of PD-L1 on PDECs.

Therefore, H6c7-kras, PancTu1, Panc89, BxPc3, Panc1, Colo357, A818-6, and PT-45 cells were seeded and were either left untreated or treated with TGF-β1 (20 ng/ml), IL-6 (10 ng/ml), Gemcitabine (1 ng/ml), or IFNγ (10 ng/ml). These cytokines were used as they were already described in the literature to induce PD-L1 [165] and in further experiments, spheroids will be treated with the cytostatic drug Gemcitabine. After 72 h, the cell surface expression of PD-L1 was analyzed by flow cytometry (section 3.1.11.1). H6c7-kras and PT-45 cells exhibited the highest cell surface expression of PD-L1 (H6c7-kras: MFI ratio 12 + PT-45: MFI ratio 11.2), followed by PancTu1 cells (MFI ratio 5.5) and A818-6 cells (MFI ratio 5.2). BxPc3 cells showed a moderate cell surface level of PD-L1 (MFI ratio 3.0). Cell surface expression of PD-L1 was low to moderate on Panc89 cells (MFI ratio 1.8) and Colo357 cells (MFI ratio 1.9). Finally, Panc1 cells showed the lowest cell surface expression of PD-L1 (MFI ratio: 1.3). Treatment with IFNγ led to a strong enhancement of cell surface expression of PD-L1 on H6c7-kras, PancTu1, Panc89, BxPc3, Colo357, and A818-6 cells (Figure 50B-E+G-H), while in Panc1 cells, this effect was only minor (Figure 50F) and on PT-45 cells, levels of PD-L1 were not altered compared to untreated cells (Figure 50I). Gemcitabine treatment also increased PD-L1 cell surface expression on H6c7-kras, PancTu1, Panc89, and BxPc3 cells.

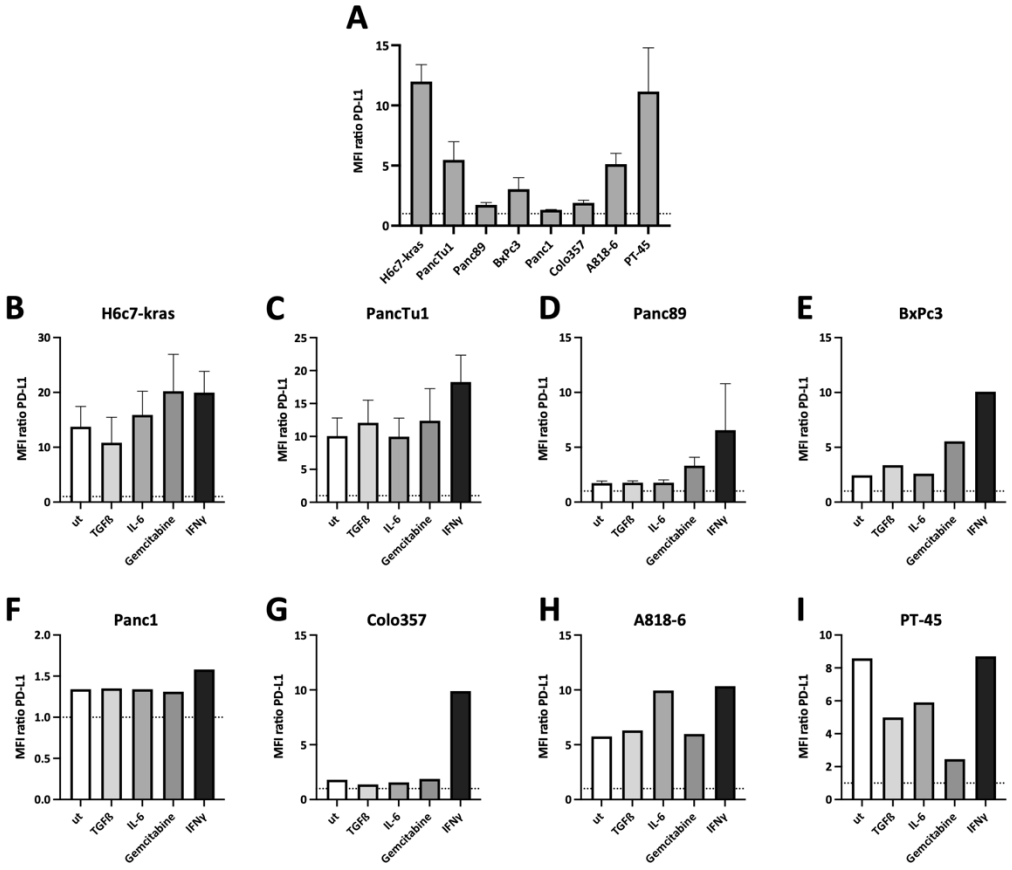

Figure 50: Heterogenous cell surface expressions of PD-L1 on different PDEC lines. (A) H6c7-kras, PancTu1, Panc89, BxPc3, Panc1, Colo357, A818-6, and PT-45 cells were seeded and basal cell surface expression of PD-L1 was analyzed by flow cytometry. Further, **(B)** H6c7-kras, **(C)** PancTu1, **(D)** Panc89, **(E)** BxPc3, **(F)** Panc1, **(G)** Colo357, **(H)** A818-6, and **(I)** PT-45 cells were treated with 20 ng/ml TGF-β1, 10 ng/ml IL-6, 1 ng/ml Gemcitabine, or 10 ng/ml IFNγ for 72 h, and PD-L1 cell surface expression was analyzed by flow cytometry. Median fluorescence intensity (MFI) ratio was calculated by dividing the MFI of the specific staining by the MFI of the isotype control. Data represent the mean ± SD (normally distributed). N=3 for untreated H6c7-kras cells, N=5 for untreated PancTu1, Panc89, and BxPc3 cells, N= 4 for untreated Colo357 cells, N=2 for untreated Panc1, A818-6, and PT-45 cells.

Basal cell surface expression levels of PD-L1 were heterogeneous in analyzed PDEC lines. Besides Panc1 and PT-45 cells, treatment with IFNγ led to an enhanced cell surface expression of PD-L1 in all cell lines.

4.3.3 In 3D cultures, cell surface expression of PD-L1 was lower compared to 2D cultures on PancTu1 and Panc89 cells

As PancTu1 and Panc89 cells were able to form compact spheroids with a low live-to-dead cell ratio and exhibited basal cell surface expression of PD-L1, which differed between both cell lines and could be enhanced by Gemcitabine and IFNγ, these cell lines were chosen for stroma-enriched 3D spheroid cultures.

Next, it was analyzed whether PD-L1 cell surface expression of PancTu1 and Panc89 cells changes when seeded in a 3D culture. Therefore, PancTu1 and Panc89 cells were seeded either in a 12-well plate (2D) or in a 96-well ULA plate (3D). After 72 h, cell surface expression levels of PD-L1 were analyzed. Cell surface expression of PD-L1 was significantly lower on 3D cultured compared to 2D cultured PancTu1 cells (MFI ratio 2D: 12.3 vs. 3D: 4.8) and also slightly decreased on 3D cultured Panc89 cells (MFI ratio 2D: 2.4 vs. 3D: 1.5) (Figure 51A). This was in line with fewer PD-L1 positive PancTu1 and Panc89 cells in 3D culture compared to 2D culture (Figure 51B).

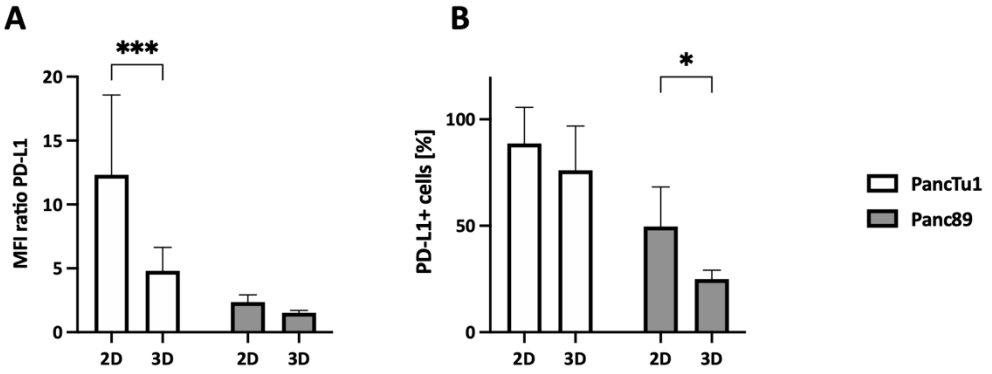

Figure 51: Cell surface expression of PD-L1 was lower in 3D cultured PancTu1 and Panc89 cells compared to 2D culture. PancTu1 (white) and Panc89 (grey) cells were seeded either in a 12-well plate (2D) or in a 96-well ultra-low attachment plate (3D). After 72 h, the cell surface expression of **(A)** PD-L1 and the percentage of **(B)** PD-L1 positive cells were determined by flow cytometry. Median fluorescence intensity (MFI) ratio was calculated by dividing the MFI of the specific staining by the MFI of the isotype control. Data represent the mean ± SD (normally distributed). N=8. * = $p < 0.05$, *** = $p < 0.001$.

Overall, PD-L1 cell surface expression was lower on PancTu1 and Panc89 cells in 3D cultures compared to 2D cultures, however, PancTu1 cells still exhibited higher PD-L1 expression compared to Pan89 cells.

4.3.4 Spheroid coculture of PDAC cells and HMF mimic hepatic PDAC metastases

IHC analysis of PDAC liver metastases revealed differences with respect to PD-L1 staining and number of HMF in small and large metastases. In large metastases, more cells were PD-L1 positive and showed a stronger PD-L1 staining. To investigate whether the PD-1/PD-L1 axis and HMF contribute to immune escape of PDAC liver metastases, a stroma enriched spheroid coculture model was established *in vitro* (section 3.1.11.6). First, it was already shown that PancTu1 and Panc89 cells exhibit different cell surface levels of PD-L1. To mimic small and large hepatic PDAC metastases, PancTu1 or Panc89 cells and HMF were seeded at different ratios (PDAC:HMF 5:1 = small metastases; PDAC:HMF 3:1 = large metastases). As control, PancTu1 and Panc89 cell spheroids were seeded in monoculture.

In line with the *in situ* findings of small and large liver metastases, less HMF were present in the 5:1 ratio (small metastases) compared to the 3:1 ratio (large metastases) in both PDAC cell models after spheroid formation. In addition, it seems that HMF were evenly distributed in the spheroids at a 5:1 ratio and predominantly localized in the center at a 3:1 ratio (Figure 52A). In general, monoculture spheroids of PancTu1 cells were larger (~800 µm) compared to Panc89 cell spheroids (~500 µm) (Figure 52B+C). The diameter of the PancTu1 spheroids was slightly larger after coculture with HMF (Figure 52B). Panc89 cocultured spheroids, independent of the ratio, also showed significantly larger spheroids (mono: 505 µm vs. 5:1: 630 µm vs. 3:1: 640 µm) (Figure 52C).

In line, less cells were PI positive in PancTu1 HMF-enriched spheroids compared to monocultured PancTu1 spheroids (Supplementary Figure 5). In Panc89 spheroids, fewer cells were PI positive when HMF were present at a 3:1 ratio. At a ratio 5:1 more cells were PI positive (Supplementary Figure 5).

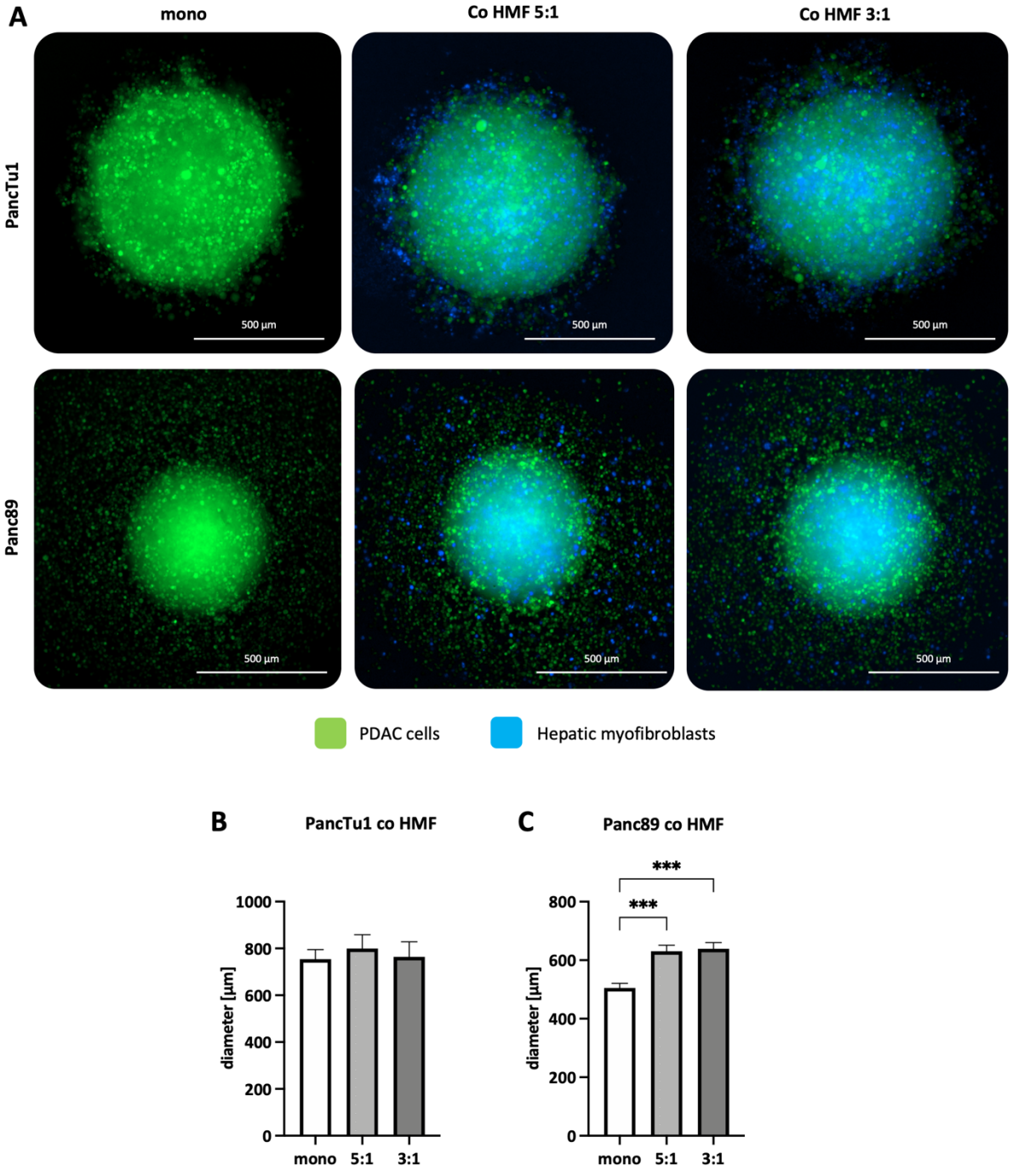

Figure 52: Spheroid coculture of PDAC cells and hepatic myofibroblasts (HMF) mimicked hepatic PDAC metastases. PancTu1 and Panc89 cells were either seeded in mono- or coculture with HMF at different ratios (mono = white, 5:1 = light grey, 3:1 = dark grey) in ultra-low attachment plates for 3 days. **(A)** Representative images of PancTu1 and Panc89 cells in mono- or coculture with HMF after 3 days of forming spheroids. In green (CellTracker green) PDAC cells and in blue (CellTrace violet) HMF. Further, the size of mono- or cocultured **(B)** PancTu1 and **(C)** Panc89 spheroids was determined. Data represent the mean ± SD (normally distributed). N=4. *** = $p < 0.001$. (partially published in [163]).

Next, cell surface levels of PD-L1 on PDAC cells and HMF were analyzed by flow cytometry. To discriminate both cell populations, dissociated single cell suspensions were stained with anti-human CD326 (EpCam), which is only expressed by epithelial cells [166]. The gating strategy is shown in Figure 53. First, living cells were gated, followed by the exclusion of doublets. Afterwards, EpCam positive cells, indicating tumor cells (blue) were determined. EpCam negative cells indicate HMF. Among both cell populations, the percentage of PD-L1 positive cells was determined.

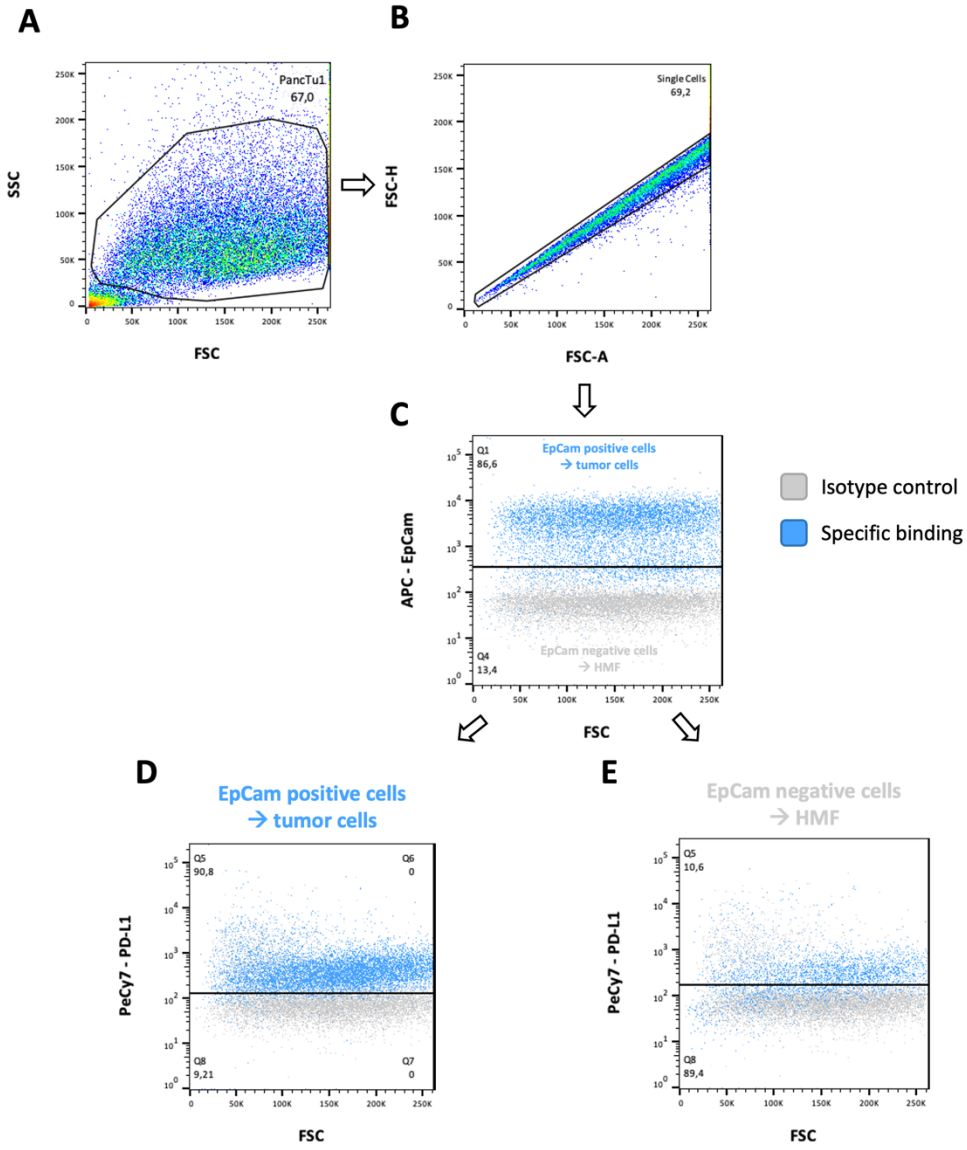

Figure 53: Gating strategy to determine cell surface expression of PD-L1 on tumor cells and hepatic myofibroblasts (HMF). PancTu1 and Panc89 cells were either seeded in mono- or coculture with HMF at different ratios in ultra-low attachment plates. After 3 days, the spheroids were mechanically dissociated for flow cytometry analysis of PD-L1 and EpCam staining. **(A)** First, living cells were gated (here called PancTu1), followed by the gating of **(B)** single cells. **(C)** Afterwards, EpCam positive cells, indicating tumor cells (blue) were determined as the gate was set above the respective isotype control (grey). Here, EpCam negative cells indicate HMF. Among all EpCam positive cells (tumor cells), **(D)** PD-L1 positive cells were gated. Further, among all EpCam negative cells (HMF), **(E)** PD-L1 positive cells were gated.

Monocultured PancTu1 cells exhibited higher PD-L1 cell surface levels compared to Panc89 cells, well reflecting the heterogeneity regarding PD-L1 expression on PDAC cells observed in hepatic PDAC metastases (Figure 22). After coculture, PD-L1 cell surface levels were significantly increased on PancTu1 cells in the presence of HMF independent of the coculture ratio (MFI ratio mono: 3.6 vs. 5:1: 4.7 vs. 3:1: 4.8) (Figure 54A). On Panc89 cells, cell surface expression of PD-L1 was slightly enhanced when cocultured with HMF (Figure 54B). Monocultured HMF exhibited considerable PD-L1 cell surface levels which were slightly downregulated by coculture with PancTu1 cells but slightly upregulated by coculture with Panc89 cells (Figure 54C+D).

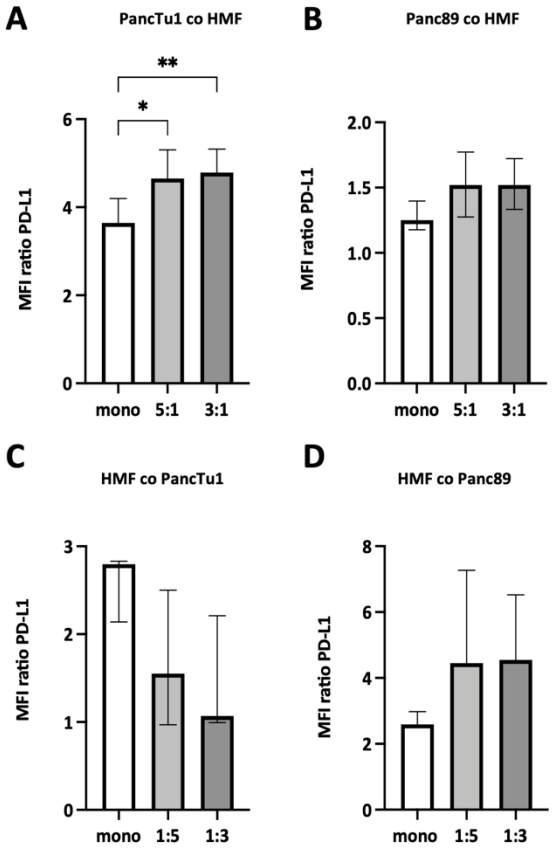

Figure 54: Coculture with hepatic myofibroblasts (HMF) led to elevated cell surface expression levels of PD-L1 on PancTu1 and Panc89 cells. PancTu1 and Panc89 cells were either seeded in mono- or coculture with HMF at different ratios (mono = white, 5:1 = light grey, 3:1 = dark grey) in ultra-low attachment plates for 3 days. For flow cytometry analysis, the spheroids were mechanically dissociated and the MFI ratio of PD-L1 on **(A)** PancTu1, **(B)** Panc89 cells, **(C)** HMF cocultured with PancTu1 cells, and **(D)** HMF cocultured with Panc89 cells was determined. Median fluorescence intensity (MFI) ratio was calculated by dividing the MFI of the specific staining by the MFI of the isotype control. Data represent the mean ± SD (normally distributed) or the median with interquartile range (not normally distributed). N=5. * = $p < 0.05$, ** = $p < 0.01$. (partially published in [163]).

Overall, the spheroid coculture model containing PDAC cells and HMF at different ratios adequately mimicked the proportion and distribution of PDAC cells and HMF as well as their PD-L1 expression observed in small and large hepatic PDAC metastases.

4.3.5 Impact of coculture spheroids on the effector phenotype of $CD8^+$ T cells and the efficacy to induce PDAC cell death

After having established a stroma enriched 3D PDAC cell model, which simulates small and large liver metastases, it was examined whether the effector phenotype of $CD8^+$ T cells is affected by these coculture conditions. For this purpose, $CD8^+$ T cells were pre-activated for 72 h and then seeded in the different spheroid cultures for 24 h (section 3.1.11.7). At this time point, $CD8^+$ T cells exhibited high cell surface expression of CD25 and the early activation marker CD69 along with considerable expression levels of PD-1 (Figure 28+Figure 29).

In order to discriminate $CD8^+$ T cells from tumor cells and HMF after coculture for flow cytometry analysis, the cell suspension was stained for CD8a. The gating strategy is shown in Figure 55. First, living cells were gated, followed by the gating of single cells. Afterwards, all CD8a positive cells were determined and among this population the percentage of PD-1, PD-L1, CD69, and CD25 positive cells was determined.

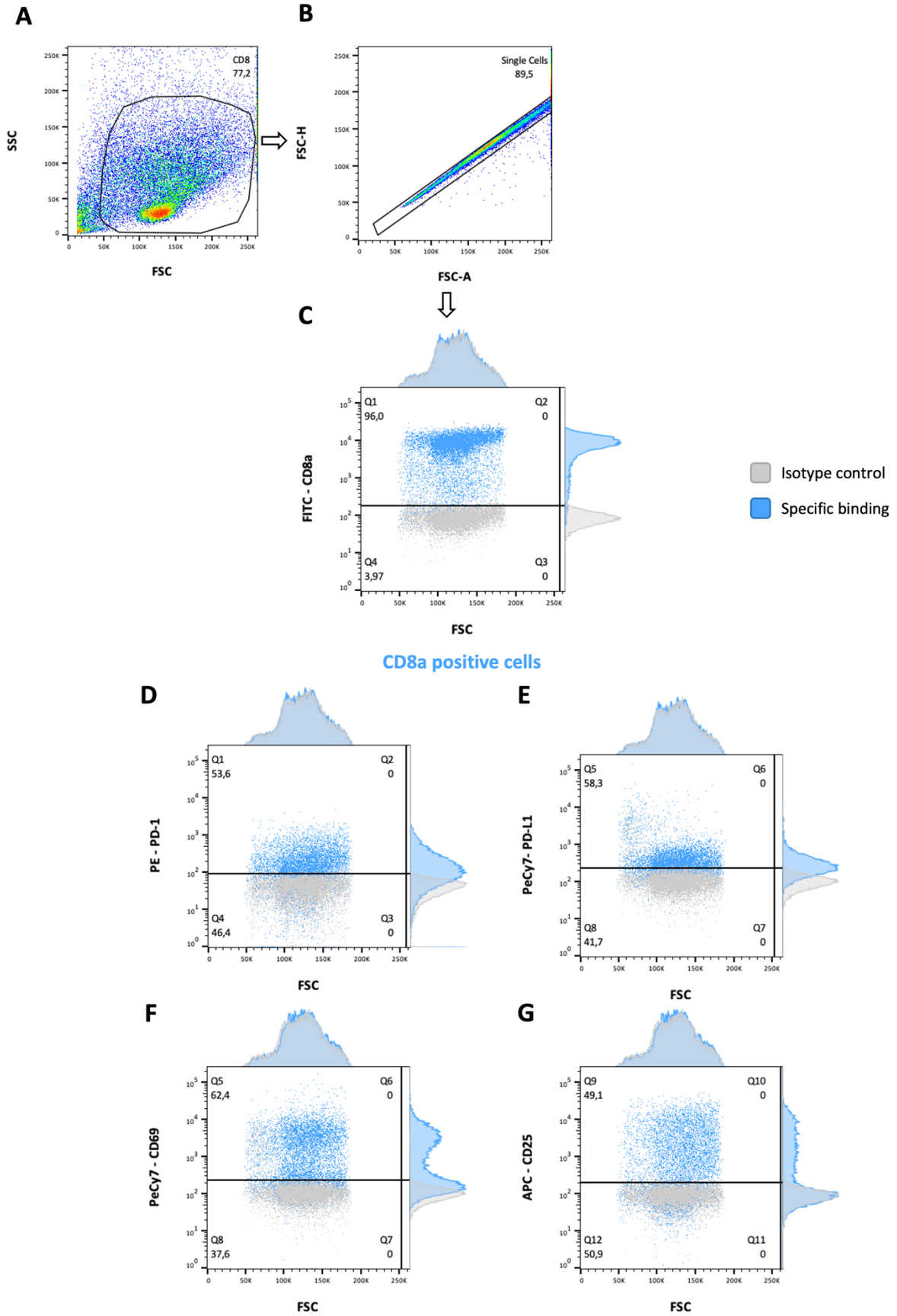

Figure 55: Gating strategy of CD8⁺ T cells to analyze expression of PD-1, PD-L1, and their activation markers after spheroid coculture. CD8⁺ T cells were isolated by magnetic cell separation from human blood derived lymphocytes and then activated with anti-CD3 and anti-CD28 antibodies as well as IL-2 for 3 days. PancTu1 and

Panc89 cells were either seeded in mono- or coculture with hepatic myofibroblasts (HMF) at different ratios in ultra-low attachment plates for 3 days. After 48 h, activated $CD8^+$ T cells were added at a ratio of 1:10. After further 24 h, $CD8^+$ T cells were analyzed by flow cytometry regarding the cell surface levels of PD-1, PD-L1, CD69, and CD25. **(A)** First, living cells were gated (here called CD8), followed by the gating of **(B)** single cells. **(C)** Afterwards, all CD8a positive cells (blue) were determined as the gate was set above the respective isotype control (grey). Among all CD8a positive cells, cells positive for **(D)** PD-1, **(E)** PD-L1, **(F)** CD69, or **(G)** CD25 were gated, always regarding the respective isotype control. Moreover, the median fluorescence intensity of PD-1, PD-L1, CD69, and CD25 was determined within the CD8a positive cell population.

4.3.5.1 Effector phenotype of $CD8^+$ T cells was hardly affected by PancTu1 coculture spheroids and slightly reduced by Panc89 coculture spheroids

Cell surface levels of PD-1, as well as PD-L1 on $CD8^+$ T cells were hardly affected by different PancTu1 spheroid coculture conditions (Figure 56A+C). Independent of the ratio, coculture with Panc89 HMF spheroids slightly decreased cell surface levels of PD-1 and PD-L1 on $CD8^+$ T cells (Figure 56B+D).

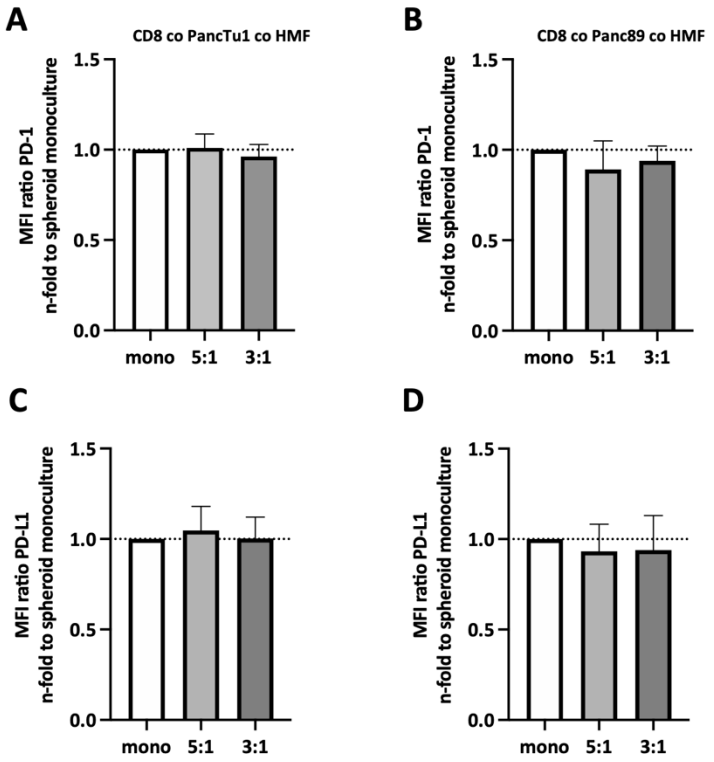

Figure 56: Cell surface levels of PD-1 and PD-L1 were not altered on $CD8^+$ T cells by mono- or coculture PDAC cell spheroids. $CD8^+$ T cells were isolated by magnetic cell separation from human blood derived lymphocytes and then activated with anti-CD3 and anti-CD28 antibodies, as well as IL-2 for 3 days. PancTu1 and Panc89 cells were either seeded in mono- or coculture with hepatic myofibroblasts (HMF) at different ratios (mono = white, 5:1 = light grey, 3:1 = dark grey) in ultra-low attachment plates for 3 days. After 48 h, activated $CD8^+$ T cells were added at a ratio of 1:10. After further24 h, the $CD8^+$ T cells were stained for **(A+B)** PD-1 and **(C+D)** PD-L1 for flow cytometry analysis and the MFI ratio was determined. Median fluorescence intensity (MFI) ratio was calculated

by dividing the MFI of the specific staining by the MFI of the isotype control. Data were normalized to the cell surface expression of $CD8^+$ T cells cultured with monocultured PDAC spheroids. Data represent the mean ± SD (normally distributed). N=4. (partially published data [163])

Next, the activation phenotype of $CD8^+$ T cells was analyzed. Cell surface expression of CD69 was not altered after coculture of PancTu1 HMF spheroids (ratio 5:1) and slightly lower at the 3:1 ratio on $CD8^+$ T cells (Figure 57A). In addition, CD25 levels were slightly lower on $CD8^+$ T cells after coculture with PancTu1 HMF spheroids compared to coculture with monoculture PancTu1 spheroids (Figure 57C). Coculture with Panc89 HMF spheroids also reduced levels of CD69 and CD25 on $CD8^+$ T cells (Figure 57B+D).

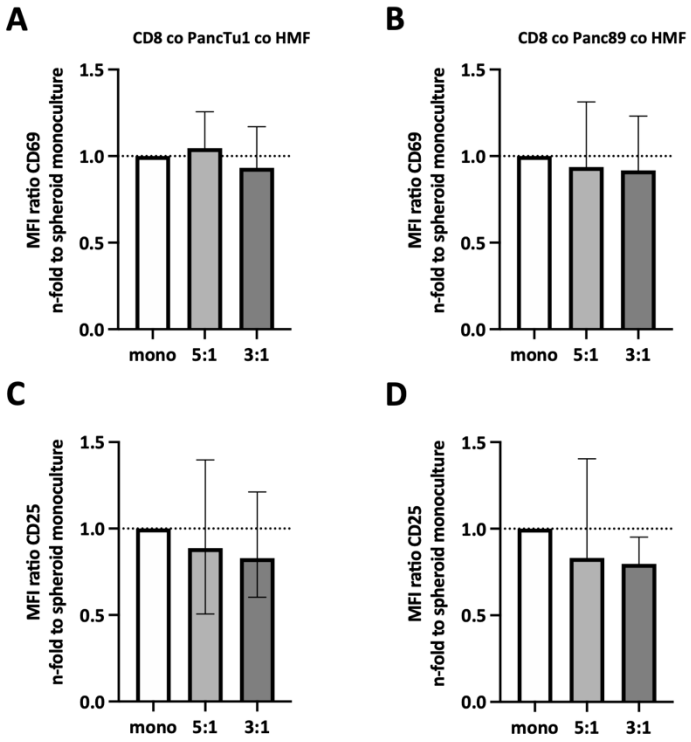

Figure 57: $CD8^+$ T cells were less activated after coculture with Panc89 HMF spheroids. $CD8^+$ T cells were isolated by magnetic cell separation from human blood derived lymphocytes and then activated with anti-CD3 and anti-CD28 antibodies, as well as IL-2 for 3 days. PancTu1 and Panc89 cells were either seeded in mono- or coculture with hepatic myofibroblasts (HMF) at different ratios (mono = white, 5:1 = light grey, 3:1 = dark grey) in ultra-low attachment plates for 3 days. After 48 h, activated $CD8^+$ T cells were added at a ratio of 1:10. After 24 h, cell surface expression of **(A+B)** CD69 and **(C+D)** CD25 was analyzed on $CD8^+$ T cells by flow cytometry. Median fluorescence intensity (MFI) ratio was calculated by dividing the MFI of the specific staining by the MFI of the isotype control. Data were normalized to the cell surface expression of $CD8^+$ T cells cultured with monocultured PDAC spheroids. Data represent the mean ± SD (normally distributed) or the median with interquartile range (not normally distributed). N=4. (published in [163]).

Further, the concentration of effector molecules was determined in supernatants derived from $CD8^+$ T cells cocultured with different PDAC cell spheroids (Figure 58). Levels of Granzyme A and B, Perforin, Granulysin, and IFNγ were not altered in supernatants obtained from $CD8^+$ T cells cultured with HMF-enriched PancTu1 spheroids compared to supernatants from PancTu1 monoculture spheroids (Figure 58A+C+E+G+I). However, levels of Granzyme A, Granulysin, and IFNγ were decreased in supernatants from $CD8^+$ T cells after culture with Panc89 HMF spheroids compared to culture with Panc89 monoculture spheroids being even more reduced in the presence of higher amounts of HMF (PDAC:HMF ratio 3:1) resembling large metastases (Figure 58B+H+J).

Interestingly, concentrations of effector molecules, especially IFNγ, Granulysin, Granzyme A, and Granzyme B were strongly elevated in supernatants of $CD8^+$ T cells cocultured with PancTu1 and Panc89 spheroids compared to $CD8^+$ T cells in monoculture (Supplementary Figure 6).

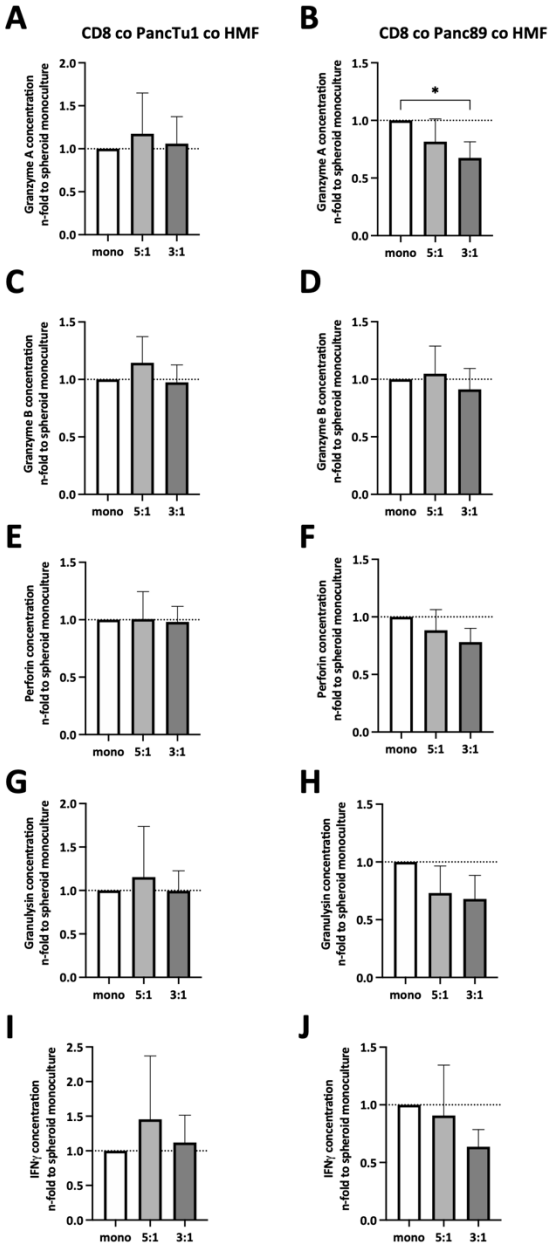

Figure 58: Concentrations of effector molecules were slightly lower in the supernatants derived from CD8⁺ T cells cultured with Panc89 HMF enriched spheroids. CD8⁺ T cells were isolated by magnetic cell separation from human blood derived lymphocytes and then activated with anti-CD3 and anti-CD28 antibodies, as well as IL-2 for 3 days. PancTu1 and Panc89 cells were either seeded in mono- or coculture with hepatic myofibroblasts (HMF) at different ratios (mono = white, 5:1 = light grey, 3:1 = dark grey) in ultra-low attachment plates for 3 days. After 48 h, activated CD8⁺ T cells were added at a ratio of 1:10. The concentrations of **(A+B)** Granzyme A, **(C+D)** Granzyme B, **(E+F)** Perforin, **(G+H)** Granulysin, and **(I+J)** IFNγ were analyzed in the supernatants. Data were normalized to the concentrations in supernatants of CD8⁺ T cells in coculture with monocultured PDAC spheroids. Data represent the mean ± SD (normally distributed). N=4. * = $p < 0.05$. (published in [163]).

To sum up, cell surface expression levels of PD-1 and PD-L1 on CD8⁺ T cells were not altered after culture with either PancTu1 or Panc89 monoculture and HMF-enriched spheroids. However, HMF-

enriched spheroids led to lower levels of CD69 and CD25. Moreover, concentrations of effector molecules were lower, especially in Panc89 HMF-enriched spheroid coculture.

4.3.5.2 Coculture with CD8⁺ T cells led to higher ccK18 levels in both PancTu1 and Panc89 spheroids

Finally, it was analyzed whether the effector phenotype of CD8⁺ T cells correlates with PDAC cell death induction. Therefore, supernatants of mono- and coculture spheroids were analyzed for the presence of ccK18 as an indicator of CD8⁺ T cell-mediated induction of PDAC cell death. As shown in Figure 59, only little ccK18 was detectable in monocultured PancTu1 and Panc89 cells. Significantly higher ccK18 levels were measured in supernatants of both PancTu1 and Panc89 spheroids devoid of HMF but cultured with CD8⁺ T cells (PancTu1 mono without CD8⁺ T cells: 202 U/l vs. PancTu1 mono with CD8⁺ T cells: 832 U/l and Panc89 mono without CD8⁺ T cells: 184 U/l vs. Panc89 mono with CD8⁺ T cells: 342 U7/l) (Figure 59A+B). PDAC cell death was significantly induced by CD8⁺ T cells. Notably, a clear reduction of ccK18 levels was observed in HMF-cocultured spheroids of either PDAC cell line, with the strongest reduction observed in supernatants of spheroids containing higher amounts of HMF (3:1) ($p<0.001$). The ccK18 levels were lower in the Panc89 HMF spheroids compared to PancTu1 spheroids after coculture with CD8⁺ T cells (Figure 59A+B). This was in line with lower concentrations of effector molecules in the supernatant.

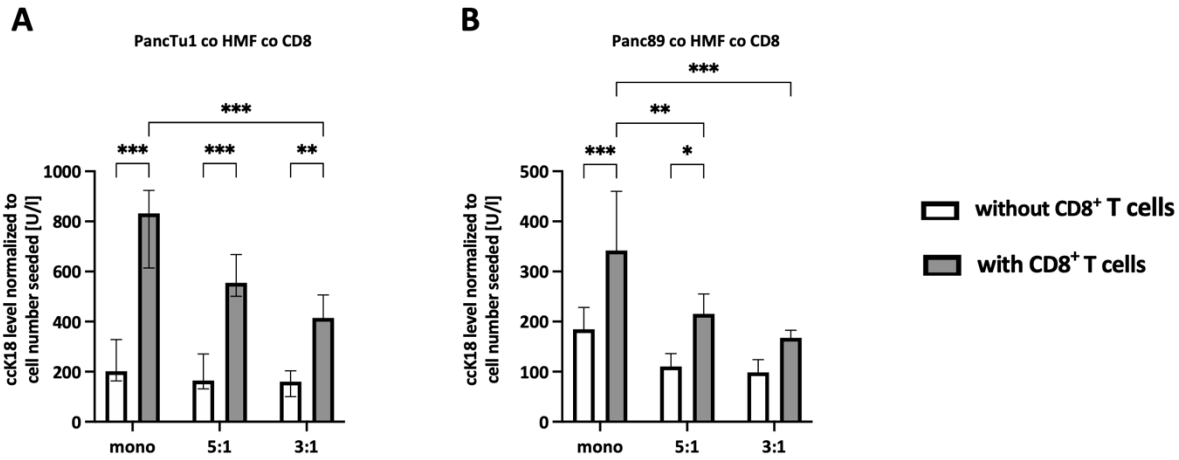

Figure 59: Coculture with CD8⁺ T cells led to higher caspase-cleaved keratin 18 (ccK18) levels in both PancTu1 and Panc89 spheroids. CD8⁺ T cells were isolated by magnetic cell separation from human blood derived lymphocytes and then activated with anti-CD3 and anti-CD28 antibodies, as well as IL-2 for 3 days. PancTu1 and Panc89 cells were either seeded in mono- or coculture with hepatic myofibroblast (HMF) at different ratios (mono = white, 5:1 = light grey, 3:1 = dark grey) in ultra-low attachment plates for 3 days. After 48 h, activated CD8⁺ T cells were added at a ratio of 1:10 for 24 h. The levels of ccK18 were measured in supernatants after coculture with **(A)** PancTu1 and **(B)** Panc89 spheroids. Data were normalized to the seeded PDAC cell number. Data represent the mean ± SD (normally distributed) or the median with interquartile range (not normally distributed). N=5 for PancTu1 spheroids without CD8⁺ T cells and Panc89 spheroids, N=4 for PancTu1 spheroids with CD8⁺ T cells. * = $p < 0.05$, ** = $p < 0.01$, *** = $p < 0.001$. (published in [163]).

Overall, coculture with $CD8^+$ T cells induced cell death in PDAC cell spheroids. This effect was diminished when PDAC cells were cocultured with HMF.

4.3.6 Impact of treatment with Durvalumab and Pembrolizumab on the effector phenotype of $CD8^+$ T cells and the efficacy to induce PDAC cell death in 3D spheroid cultures

After having shown that the PDAC HMF interplay impairs the effector phenotype of $CD8^+$ T cells, it was investigated whether ICI treatment is able to restore the effector phenotype and leads to enhanced induction of PDAC cell death. For this purpose, $CD8^+$ T cells were pre-activated for 72 h and then added to the different spheroid cultures and further PD-L1 or PD-1 were blocked by Durvalumab and Pembrolizumab, respectively for 24 h (section 3.1.11.7, Durvalumab and Pembrolizumab Treatment).

4.3.6.1 Treatment with Pembrolizumab slightly enhanced concentrations of effector molecules in supernatants of $CD8^+$ T cells after spheroid coculture

Successful blocking of cell surface-located PD-L1 and PD-1 by either Durvalumab or Pembrolizumab treatment on each cell population within the coculture setting was validated by flow cytometry. Cell surface levels of PD-1 on $CD8^+$ T cells were significantly lower after Pembrolizumab treatment (Figure 60A+B) and cell surface levels of PD-L1 on $CD8^+$ T cells, PDAC cells, and HMF were also significantly lower after Durvalumab treatment (Figure 60C+D and Supplementary Figure 7). PD-1 cell surface expression was not altered on $CD8^+$ T cells after Durvalumab treatment with negligible differences between the coculture settings (Figure 60A+B). Pembrolizumab treatment did also not affect PD-L1 cell surface levels on $CD8^+$ T cells (Figure 60C+D).

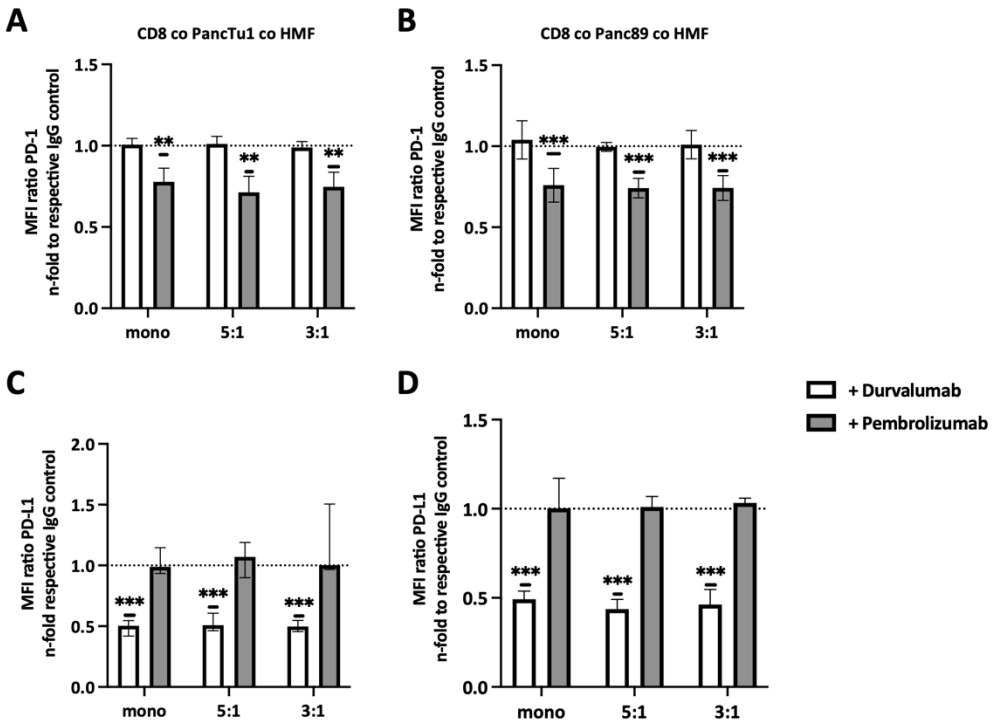

Figure 60: Cell surface levels of PD-1 and PD-L1 were not altered on CD8$^+$ T cells after coculture with PancTu1 or Panc89 spheroids when treated with either Durvalumab or Pembrolizumab. CD8$^+$ T cells were isolated by magnetic cell separation from human blood derived lymphocytes and then activated with anti-CD3 and anti-CD28 antibodies, as well as IL-2 for 3 days. PancTu1 and Panc89 cells were either seeded in mono- or coculture with hepatic myofibroblasts (HMF) at different ratios in ultra-low attachment plates for 3 days. After 48 h, activated CD8$^+$ T cells were added at a ratio of 1:10 and were treated with 10 µg/ml Durvalumab (white) or Pembrolizumab (grey) or with 10 µg/ml of the respective isotype (hIgG1 or hIgG4). After 24 h, the CD8$^+$ T cells were stained for **(A+B)** PD-1 and **(C+D)** PD-L1 for flow cytometry analysis and the MFI ratio was determined. Median fluorescence intensity (MFI) ratio was calculated by dividing the MFI of the specific staining by the MFI of the isotype control. Data were normalized to the respective isotype control. Data represent the mean ± SD (normally distributed) or the median with interquartile range (not normally distributed). N=4. ** = $p < 0.01$, *** = $p < 0.001$. (partially published in [163]).

In order to examine potential effect of Durvalumab and Pembrolizumab treatment on the effector phenotype of CD8$^+$ T cells within the coculture system, cell surface expression levels of T cell activation markers CD25 and CD69 were analyzed after coculture. However, no considerable effects were observed on the cell surface expression levels of CD69 and CD25 on CD8$^+$ T cells by Durvalumab treatment, except for coculture with Panc89 monoculture spheroids, cell surface levels of CD69 were higher (Figure 61A-D). However, treatment with Pembrolizumab led to a slight decrease of the expression of CD25 on CD8$^+$ T cells cultured with PancTu1 coculture spheroids but not with Panc89

coculture spheroids, while the expression of CD69 was only decreased in CD8⁺ T cells when cultured with PancTu1 coculture spheroids at a ratio of 3:1 (Figure 61A-D).

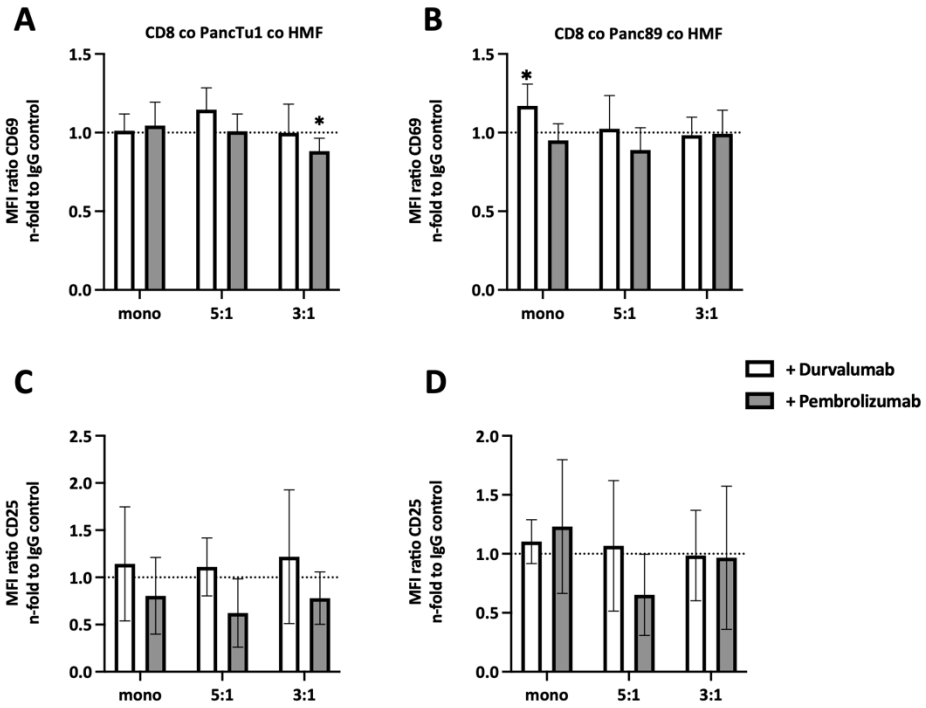

Figure 61: Durvalumab treatment did not affect the activation phenotype and Pembrolizumab slightly reduced the activation phenotype of CD8⁺ T cells. CD8⁺ T cells were isolated by magnetic cell separation from human blood derived lymphocytes and then activated with anti-CD3 and anti-CD28 antibodies, as well as IL-2 for 3 days. PancTu1 and Panc89 cells were either seeded in mono- or coculture with hepatic myofibroblasts (HMF) at different ratios in ultra-low attachment plates for 3 days. After 48 h, activated CD8⁺ T cells were added at a ratio of 1:10 and were treated with 10 µg/ml Durvalumab (white) or Pembrolizumab (grey) or with 10 µg/ml of the respective isotype (hIgG1 or hIgG4). After 24 h, of coculture, the cell surface expression of **(A+B)** CD69 and **(C+D)** CD25 on CD8⁺ T cells was analyzed by flow cytometry. Median fluorescence intensity (MFI) ratio was calculated by dividing the MFI of the specific staining by the MFI of the isotype control. Data were normalized to the respective isotype control. Data represent the mean ± SD (normally distributed) or the median with interquartile range (not normally distributed). N=4. * = $p < 0.05$. (published in [163]).

Next, the concentration of effector molecules in the supernatants of the different cocultures and treatments was analyzed. Durvalumab treatment did almost not affect levels of Granzyme A, Granzyme B, Perforin, Granulysin, and IFNγ in supernatants of CD8⁺ T cells cultured with either PDAC cell spheroids (Figure 62A-J), except Granulysin levels which were diminished after coculture with PancTu1 HMF spheroids (5:1 ratio) (Figure 62G). In contrast, Granzyme B and IFNγ levels were elevated in supernatants from CD8⁺ T cells cultured with Panc89 coculture spheroids but not with Panc89 monoculture spheroids after Durvalumab treatment (Figure 62D+J). Notably, no decrease in Granzyme A, Granulysin, and IFNγ concentration was detectable anymore in supernatants from Panc89 HMF-

enriched spheroids (mainly at 3:1 ratio) (Figure 62B+H+J), indicating a compensation of the HMF mediated inhibitory effect by the PD-L1 inhibitor. Pembrolizumab treatment did almost not affect levels of Granzyme A, Perforin, and Granulysin in supernatants of $CD8^+$ T cells cultured with mono- or coculture spheroids of either PDAC cell line (Figure 62A+B+E+F+G+H), while levels of Granzyme B and IFNγ were enhanced in supernatants of HMF enriched spheroids of PancTu1 and Panc89 cells (Figure 61C+D+I+J).

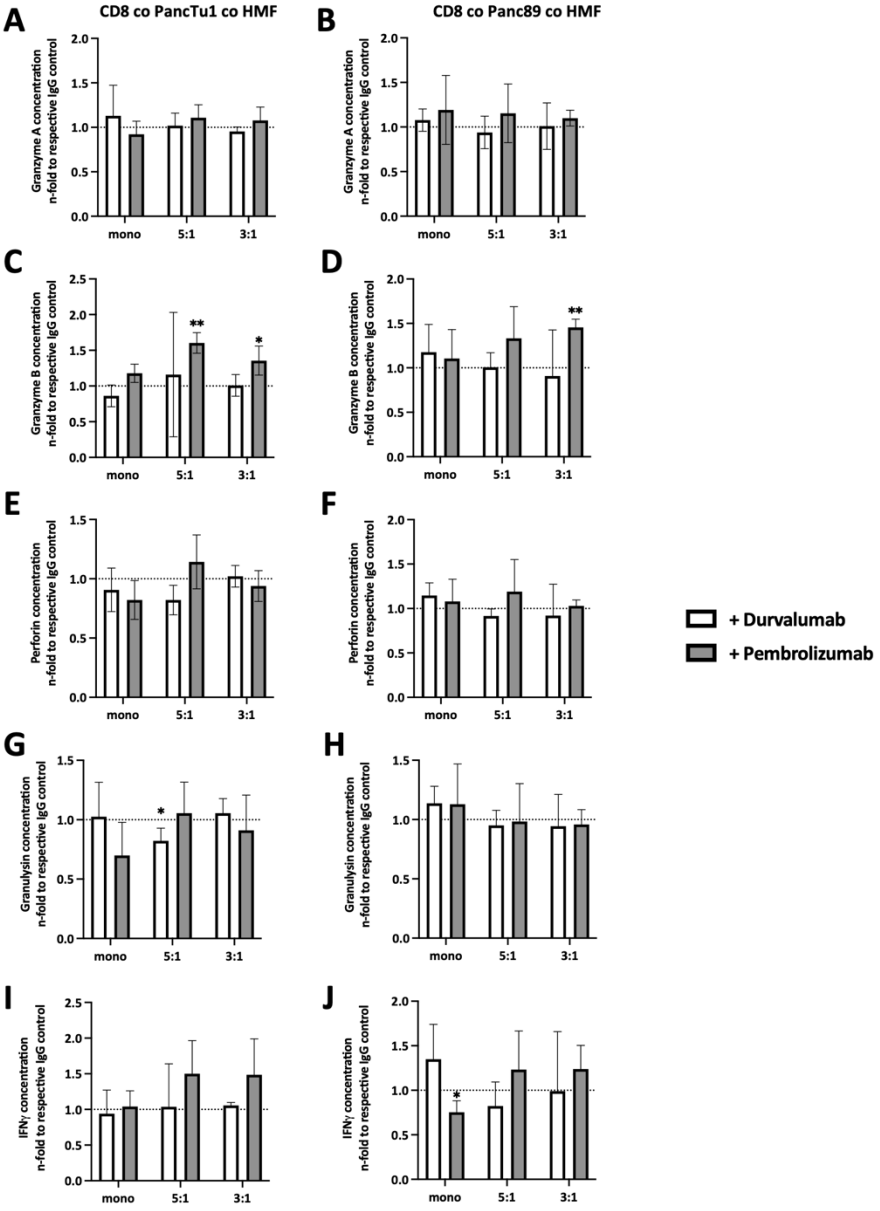

Figure 62: Pembrolizumab treatment slightly enhanced concentrations of effector molecules in supernatants of $CD8^+$ T cells. $CD8^+$ T cells were isolated by magnetic cell separation from human blood derived lymphocytes and then activated with anti-CD3 and anti-CD28 antibodies, as well as IL-2 for 3 days. PancTu1 and Panc89 cells were either seeded in mono- or coculture with hepatic myofibroblasts (HMF) at different ratios in ultra-low attachment plates for 3 days. After 48 h, activated $CD8^+$ T cells were added at a ratio of 1:10 and were treated with 10 µg/ml Durvalumab (white) or Pembrolizumab (grey) or with 10 µg/ml of the respective isotype control

(hIgG1 or hIgG4) for 24 h. The concentrations of **(A+B)** Granzyme A, **(C+D)** Granzyme B, **(E+F)** Perforin, **(G+H)** Granulysin, and **(I+J)** IFNγ was analyzed in the supernatants. Data were normalized to the respective isotype control. Data represent the mean ± SD (normally distributed) or the median with interquartile range (not normally distributed). N=4. * = p < 0.05, ** = < 0.01. (published in [163]).

Overall, treatment of Durvalumab and Pembrolizumab did not affect PD-1 or PD-L1 cell surface levels on $CD8^+$ T cells. Durvalumab treatment did not alter the activation or effector phenotype of $CD8^+$ T cells after coculture with mono- or coculture spheroids. However, Pembrolizumab treatment led to less activation of $CD8^+$ T cells but higher concentrations of effector molecules in the supernatants.

4.3.6.2 Durvalumab and Pembrolizumab treatment hardly impacted PDAC cell death under coculture with $CD8^+$ T cells

Finally, it was analyzed whether ICI treatment increased PDAC cell death by $CD8^+$ T cells under different culture conditions. Overall, no considerable effect of PD-L1 or PD-1 blockade on PDAC cell death was detectable in either spheroid condition (Figure 63A+B) and Durvalumab treatment even led to decreased ccK18 levels in supernatants of $CD8^+$ T cells and HMF-enriched PancTu1 spheroids (at 5:1 ratio, Figure 63A).

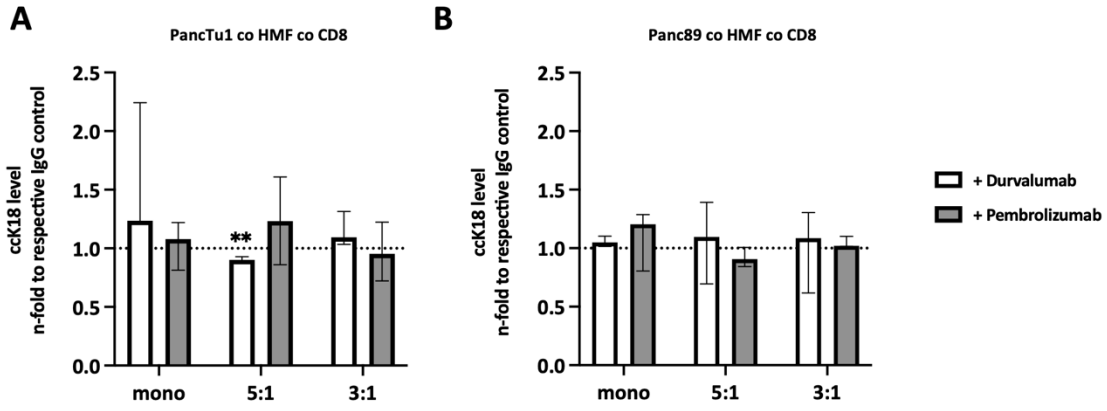

Figure 63: Durvalumab and Pembrolizumab treatment hardly affected PDAC cell death under coculture with $CD8^+$ T cells. $CD8^+$ T cells were isolated by magnetic cell separation from human blood derived lymphocytes and then activated with anti-CD3 and anti-CD28 antibodies, as well as IL-2 for 3 days. PancTu1 and Panc89 cells were either seeded in mono- or coculture with hepatic myofibroblasts (HMF) at different ratios in ultra-low attachment plates for 3 days. After 48 h, activated $CD8^+$ T cells were added at a ratio of 1:10 and were treated with 10 µg/ml Durvalumab (white) or Pembrolizumab (grey) or with 10 µg/ml of the respective isotype control (hIgG1 or hIgG4) for 24 h. The levels of caspase-cleaved keratin18 (ccK18) were measured in supernatants after coculture with **(A)** PancTu1 and **(B)** Panc89 spheroids. Data were normalized to the respective isotype control. Data represent the mean ± SD (normally distributed) or the median with interquartile range (not normally distributed). N=4. ** = p < 0.01. (published in [163]).

Here, ICI treatment did not enhance PDAC cell death by $CD8^+$ T cells.

4.3.7 Impact of coculture spheroids pre-treated with Gemcitabine on the effector phenotype of $CD8^+$ T cells and PDAC cell death

Since treatment with Gemcitabine still represents the most frequent first-line therapy for PDAC patients with reduced general health condition [25], it was investigated whether Gemcitabine impacts PD-L1 and PD-1 expression as well as the effector phenotype of $CD8^+$ T cells in the context of the PDAC cell-HMF interplay. For this purpose, monocultured and HMF-enriched PancTu1 and Panc89 spheroids were either left untreated or treated with Gemcitabine for 24 h, and then cocultured with $CD8^+$ T cells for another 24 h (section 3.1.11.7, Gemcitabine Treatment).

4.3.7.1 The release of effector molecules of $CD8^+$ T cells was lower after coculture with pre-treated Gemcitabine spheroids

Monocultured PancTu1 cells treated with Gemcitabine for 24 h showed slightly higher cell surface levels of PD-L1 than untreated PancTu1 cells, while PD-L1 cell surface expression levels on Panc89 cells and HMF treated with Gemcitabine were not altered (Figure 64).

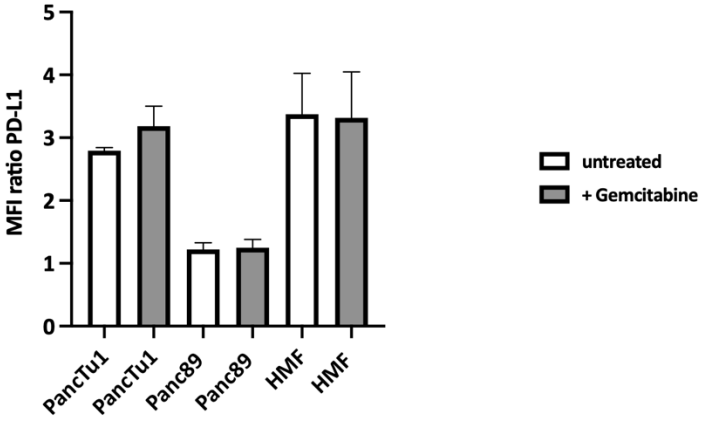

Figure 64: Gemcitabine treatment slightly enhanced cell surface expression of PD-L1 on PancTu1 cells but not on Panc89 cells and hepatic myofibroblasts (HMF). PancTu1 cells, Panc89 cells, and HMF were seeded in monoculture in ultra-low attachment plates. On the next day, cells were left untreated or treated with 10 µg/ml Gemcitabine. After 24 h, the spheroids were dissociated and stained for PD-L1 for flow cytometry analysis. MFI ratio of PD-L1 cell surface expression on PancTu1 cells, Panc89 cells, and HMF. Median fluorescence intensity (MFI) ratio was calculated by dividing the MFI of the specific staining by the MFI of the isotype control. Data represent the mean ± SD (normally distributed). N=3. (published in [163]).

PD-1 cell surface levels were significantly lower on $CD8^+$ T cells derived from any culture with mono- or cocultured PDAC cell spheroids, which were pre-treated with Gemcitabine (Figure 65A+B). Cell

surface levels of PD-L1 on CD8⁺ T cells were slightly higher after coculture with Gemcitabine pre-treated PancTu1 spheroids (Figure 65C). After coculture with mono- or HMF cocultured at a ratio of 3:1 Panc89 spheroids, PD-L1 cell surface expression was slightly enhanced on CD8⁺ T cells if spheroids were pre-treated with Gemcitabine (Figure 65D).

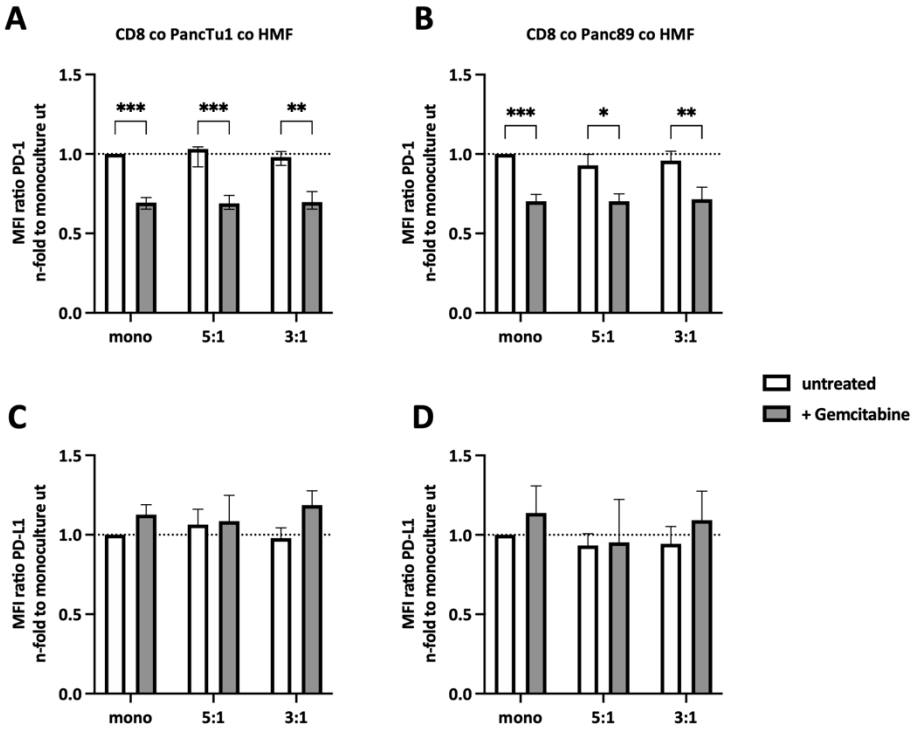

Figure 65: Coculture with Gemcitabine pre-treated PancTu1 and Panc89 spheroids led to lower cell surface expression of PD-1 on CD8⁺ T cells. CD8⁺ T cells were isolated by magnetic cell separation from human blood derived lymphocytes and then activated with anti-CD3 and anti-CD28 antibodies, as well as IL-2 for 3 days. PancTu1 and Panc89 cells were either seeded in mono- or coculture with hepatic myofibroblasts (HMF) at different ratios in ultra-low attachment plates for 3 days. After 24 h, the PancTu1 and Panc89 spheroids were either left untreated (white) or were treated with 10 µg/ml Gemcitabine (grey). On the next day, the medium was changed and activated CD8⁺ T cells were added at a ratio of 1:10. After 24 h, the CD8⁺ T cells were stained for **(A+B)** PD-1 and **(C+D)** PD-L1 for flow cytometry analysis and the MFI ratio was determined. Median fluorescence intensity (MFI) ratio was calculated by dividing the MFI of the specific staining by the MFI of the isotype control. Data were normalized to the coculture of CD8⁺ T cells with monocultured and untreated spheroids. Data represent the mean ± SD (normally distributed) or the median with interquartile range (not normally distributed). N=4. * = $p < 0.05$, ** = $p < 0.01$, *** = $p < 0.001$. (partially published in [163]).

As shown in Figure 66, Gemcitabine pre-treatment led to diminished CD25 cell surface expression levels on CD8⁺ T cells derived from Panc89 mono- and coculture spheroids (Figure 66B), while CD25 cell surface expression on CD8⁺ T cells was not altered after coculture with PancTu1 spheroids (Figure

66C) and cell surface expression of CD69 was almost not altered on CD8⁺ T cells obtained from either PDAC cell spheroid culture (Figure 66A+B).

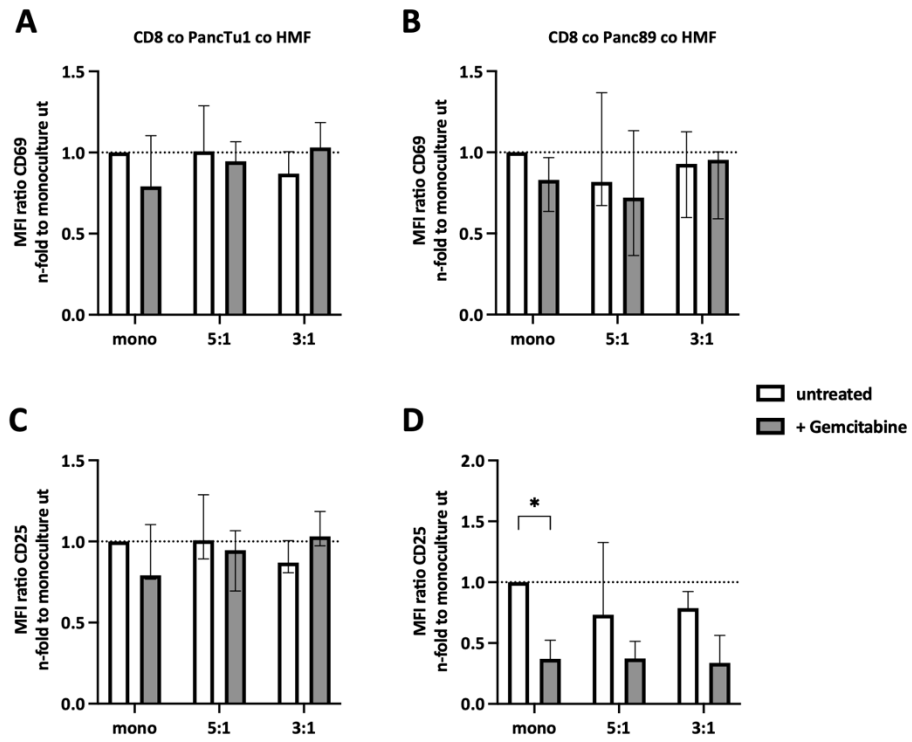

Figure 66: Coculture with Gemcitabine pre-treated PancTu1 and Panc89 spheroids led to lower activation of CD8⁺ T cells. CD8⁺ T cells were isolated by magnetic cell separation from human blood derived lymphocytes and then activated with anti-CD3 and anti-CD28 antibodies, as well as IL-2 for 3 days. PancTu1 and Panc89 cells were either seeded in mono- or coculture with hepatic myofibroblasts (HMF) at different ratios in ultra-low attachment plates for 3 days. After 24 h, the PancTu1 and Panc89 spheroids were either left untreated (white) or were treated with 10 µg/ml Gemcitabine (grey). On the next day, the medium was changed and activated CD8⁺ T cells were added at a ratio of 1:10. After 24 h of coculture, the cell surface expression of **(A+B)** CD69 and **(C+D)** CD25 on CD8⁺ T cells was analyzed by flow cytometry. Median fluorescence intensity (MFI) ratio was calculated by dividing the MFI of the specific staining by the MFI of the isotype control. Data were normalized to the coculture with monocultured and untreated spheroids. Data represent the mean ± SD (normally distributed) or the median with interquartile range (not normally distributed). N=4. * = $p < 0.05$. (published in [163]).

Next, the secretion of effector molecules into the supernatant by CD8⁺ T cells was analyzed.
Levels of Granzyme B and IFNγ coculture supernatants were almost not affected by Gemcitabine pre-treatment in supernatants of CD8⁺ T cells cultivated together with mono- and cocultured PancTu1 and Panc89 spheroids (Figure 67B+G+E+J). Levels of Granzyme A, Granzyme B, Perforin, and Granulysin were reduced – either by trend or significantly - in all supernatants of CD8⁺ T cells and Gemcitabine pre-treated PDAC mono- and coculture spheroids (Figure 67A+F+C+H+D+I).

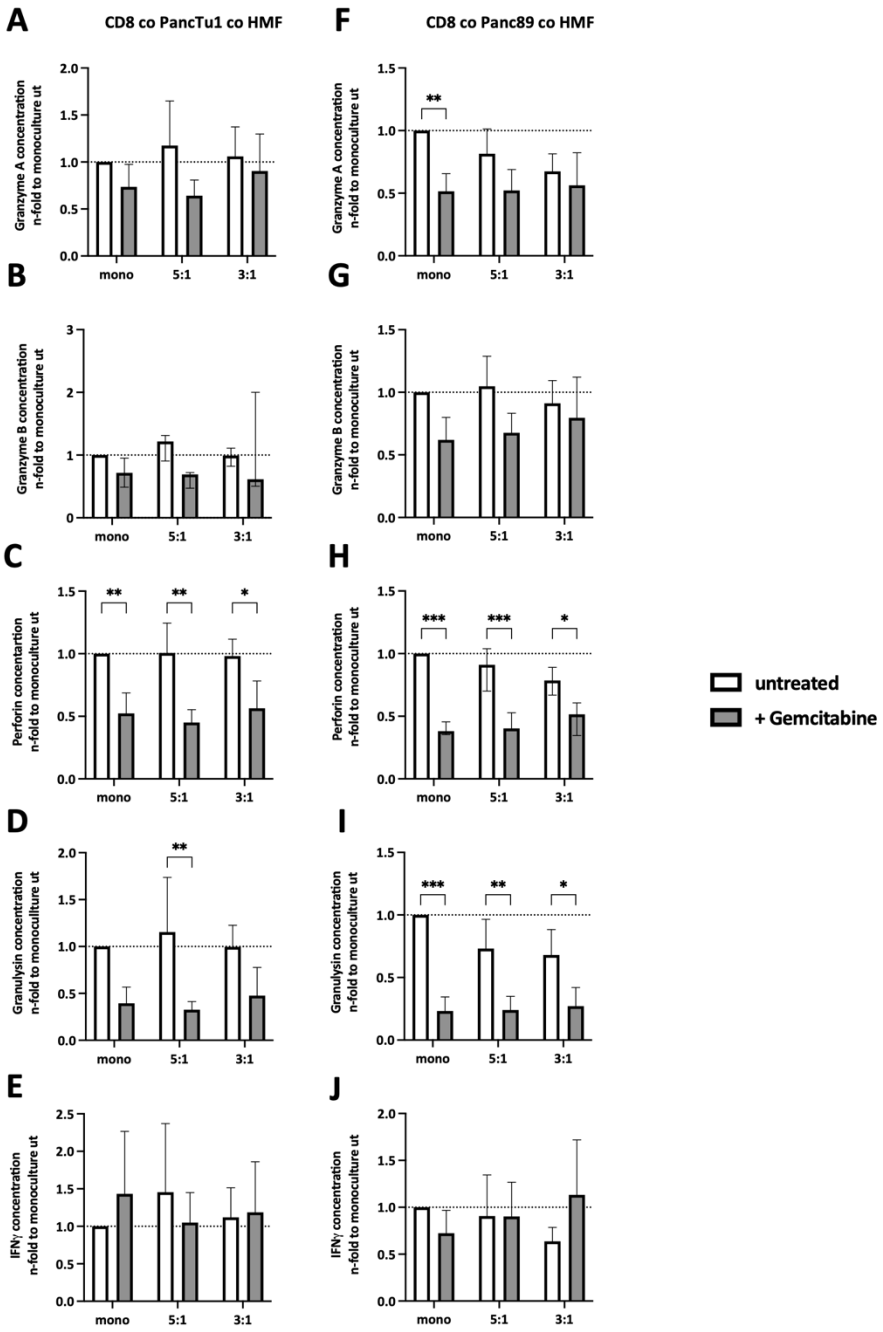

Figure 67: Coculture with Gemcitabine pre-treated PancTu1 and Panc89 spheroids led to lower concentrations of effector molecules in supernatants of CD8⁺ T cells. CD8⁺ T cells were isolated by magnetic cell separation from human blood derived lymphocytes and then activated with anti-CD3 and anti-CD28 antibodies, as well as IL-2 for 3 days. PancTu1 and Panc89 cells were either seeded in mono- or coculture with hepatic myofibroblasts (HMF) at different ratios in ultra-low attachment plates for 3 days. After 24 h, the PancTu1 and Panc89 spheroids were either left untreated (white) or were treated with 10 µg/ml Gemcitabine (grey). After 24 h, the medium was changed and activated CD8⁺ T cells were added at a ratio of 1:10. The concentrations of **(A+B)** Granzyme A, **(C+D)** Granzyme B, **(E+F)** Perforin, **(G+H)** Granulysin, and **(I+J)** IFNγ was analyzed in the supernatants. Data were normalized to the coculture of CD8⁺ T cells with monocultured and untreated spheroids. Data represent the mean ± SD (normally distributed) or the median with interquartile range (not normally distributed). N=4. * = $p < 0.05$, ** = < 0.01, *** = $p < 0.001$. (published in [163]).

Overall, CD8$^+$ T cells cocultured with Gemcitabine pre-treated PancTu1 and Panc89 spheroids showed lower cell surface expression of PD-1 and activation markers. Further, the concentration of effector molecules in the supernatants of CD8$^+$ T cells was reduced.

4.3.7.2 Gemcitabine affects PDAC cell death by CD8$^+$ T cells

Finally, it was analyzed how Gemcitabine affects PDAC cell death in dependence on the presence of HMF and CD8$^+$ T cells. Treatment with Gemcitabine hardly impacted cell death of mono- and cocultured PancTu1 spheroids. Levels of ccK18 were only slightly lower when HMF were present at a ratio of 3:1 (Figure 68A). However, ccK18 levels were markedly lower in supernatants of mono- and cocultured PancTu1 cells together with CD8$^+$ T cells after Gemcitabine treatment compared to respective untreated cultures. This effect was enhanced when more HMF were present in PancTu1 spheroids. Here, ccK18 levels were lower compared to monoculture and 5:1 PancTu1 HMF coculture (mono + CD8$^+$/Gem: 504 U/l vs. 3:1 + CD8$^+$/Gem: 368 U/l vs. 3:1 + CD8$^+$/Gem: 255 U/l) (Figure 68A).

In mono- and cocultured Panc89 spheroid, ccK18 levels were slightly higher when treated with Gemcitabine (Figure 68B). After coculture with CD8$^+$ T cells, elevated ccK18 levels were noted in supernatants of Panc89 mono- and cocultured spheroids, especially after pretreatment with Gemcitabine (Figure 68B).

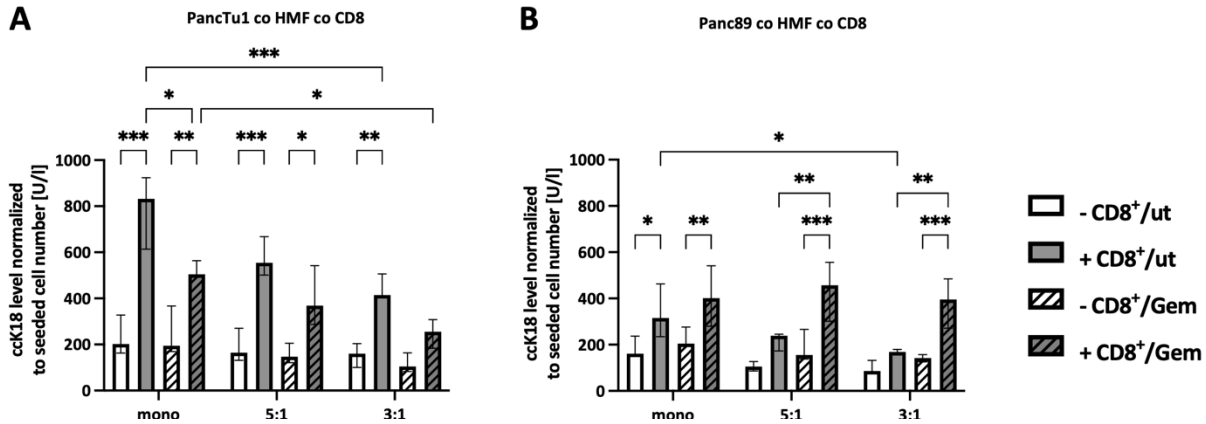

Figure 68: Levels of caspase-cleaved keratin18 (ccK18) were lower in Gemcitabine pre-treated PancTu1 spheroids and higher in Panc89 spheroids after additional coculture with CD8$^+$ T cells. CD8$^+$ T cells were isolated by magnetic cell separation from human blood derived lymphocytes and then activated with anti-CD3 and anti-CD28 antibodies, as well as IL-2 for 3 days. PancTu1 and Panc89 cells were either seeded in mono- or coculture with hepatic myofibroblasts (HMF) at different ratios in ultra-low attachment plates for 3 days. After 24 h, the PancTu1 and Panc89 spheroids were either left untreated (white) or were treated with 10 µg/ml Gemcitabine (grey). On the next day, the medium was changed and activated CD8$^+$ T cells were added at a ratio of 1:10. After 24 h, the levels ccK18 were measured in supernatants after coculture with **(A)** PancTu1 and **(B)** Panc89 spheroids. Data were normalized to the seeded PDAC cell number. Data represent the mean ± SD (normally distributed) or the median with interquartile range (not normally distributed). N=4. * = $p < 0.05$, ** = $p < 0.01$, *** = $p < 0.001$. (published in [163]).

Overall, these data demonstrate that Gemcitabine pre-treatment led to a reduced concentration of T cell effector molecules in the supernatants, especially Granulysin and Perforin but also to a reduced cell surface expression level of PD-1 on $CD8^+$ T cells, in line with lower ccK18 levels in PancTu1 spheroids pretreated with Gemcitabine and cocultured with $CD8^+$ T cells. In the Panc89 cell model pretreated with Gemcitabine and then cocultured with $CD8^+$ T cells, ccK18 levels were higher compared to untreated culture, even though the concentration of effector molecules was lower.

4.3.8 Impact of combinational treatment of Gemcitabine and either Durvalumab or Pembrolizumab on the effector phenotype of $CD8^+$ T cells and PDAC cell death

Previous results showed that pretreatment with Gemcitabine and coculture with $CD8^+$ T cells increased cell death in Panc89 cells. Standard cytostatic drugs including Gemcitabine can increase the cell surface expression of MHC I and expression of tumor-associated antigens, leading to better antigen presentation and more effective recognition by cytotoxic T cells [167]. Thus, combined treatment with cytostatic drugs might be a promising approach to improve immunotherapy [168]. Therefore, monocultured and HMF-enriched PancTu1 and Panc89 spheroids were treated with Gemcitabine for 24 h, before culture with activated $CD8^+$ T cells and treatment with Durvalumab, Pembrolizumab, or the respective isotype control was started (section 3.1.11.7, Combinational Treatment).

4.3.8.1 Combinational treatment with Gemcitabine and ICIs only marginally affected the effector phenotype of $CD8^+$ T cells

As shown before, successful blocking of cell surface located PD-L1 and PD-1 on $CD8^+$ T cells by either Durvalumab or Pembrolizumab treatment was validated by flow cytometry. Cell surface levels of PD-1 on $CD8^+$ T cells were clearly lower after Pembrolizumab treatment in all coculture settings with both PDAC cell lines (Figure 69A+B). Further, cell surface levels of PD-L1 on $CD8^+$ T cells were also significantly lower ($p<0.001$) after Durvalumab treatment in all coculture conditions (Figure 69C+D). PD-1 cell surface levels were not changed after Durvalumab treatment compared to the respective IgG1 control in both PDAC cell lines (Figure 69A+B). Furthermore, PD-L1 cell surface levels were not

altered on CD8+ T cells cocultured with either PDAC spheroids after combined treatment with Gemcitabine and Pembrolizumab (Figure 69C+D).

Figure 69:

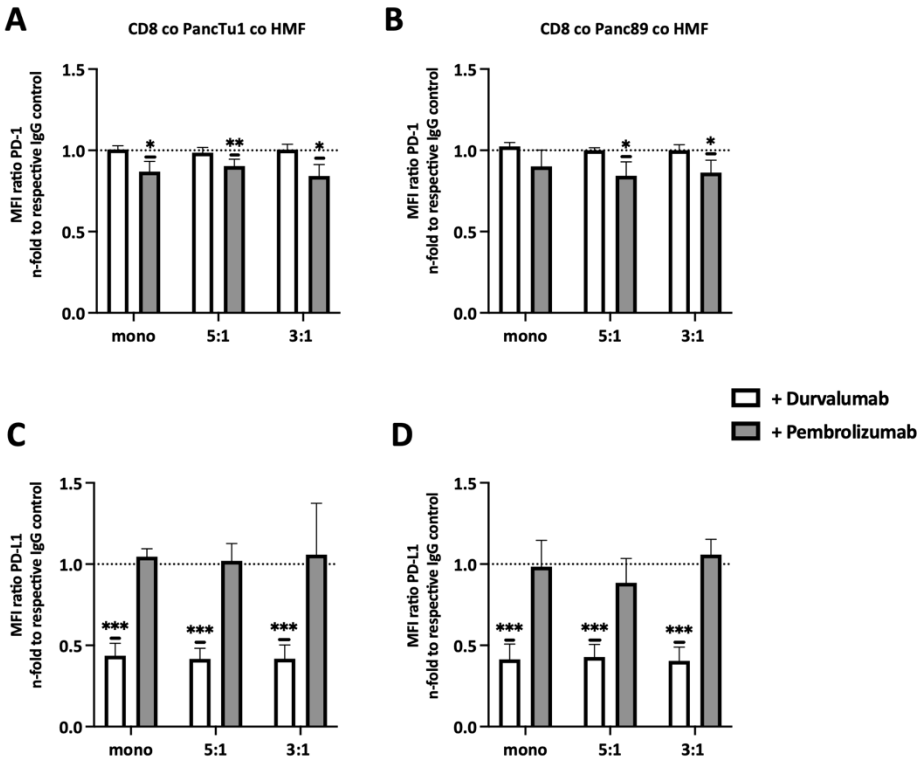

Figure 69: Combined treatment with Gemcitabine and either Durvalumab or Pembrolizumab did not affect cell surface expression of either PD-1 or PD-L1 on CD8+ T cells. CD8+ T cells were isolated by magnetic cell separation from human blood derived lymphocytes and then activated with anti-CD3 and anti-CD28 antibodies, as well as IL-2 for 3 days. PancTu1 and Panc89 cells were either seeded in mono- or coculture with hepatic myofibroblasts (HMF) at different ratios in ultra-low attachment plates for 3 days. After 24 h, the PancTu1 and Panc89 spheroids were treated with 10 µg/ml Gemcitabine. On the next day, the medium was changed and activated CD8+ T cells were added at a ratio of 1:10 and were treated with 10 µg/ml Durvalumab (white) or Pembrolizumab (grey) or with 10 µg/ml of the respective isotype control (hIgG1 or hIgG4). After 24 h, the cell surface expression of **(A+B)** PD-1 and **(C+D)** PD-L1 on CD8+ T cells were analyzed by flow cytometry. Median fluorescence intensity (MFI) ratio was calculated by dividing the MFI of the specific staining by the MFI of the isotype control. Data were normalized to the respective isotype control. Data represent the mean ± SD (normally distributed. N=4. * = $p < 0.05$, ** = $p < 0.01$, *** = $p < 0.001$.

Analyzing activation markers on CD8+ T cells after different cultures with PancTu1 spheroids revealed that combined treatment with Durvalumab hardly affected cell surface expression of CD69 and CD25 (Figure 70A+C), which also applied to culture with the different Panc89 spheroids (Figure 70B+D). Cell surface levels of CD69 and CD5 were not decreased on CD8+ T cells cultured with HMF-enriched Panc89 spheroids (Figure 70B+D). Combined treatment with Pembrolizumab led to slightly higher CD69 cell

surface levels on CD8$^+$ T cells after coculture with mono- and cocultured (3:1 ratio) PancTu1 spheroids (Figure 70A). Levels of CD25 were not changed after combined Pembrolizumab treatment (Figure 70C). Cell surface levels of CD69 and CD25 were slightly decreased on CD8$^+$ T cells cultured with mono- or cocultured (3:1 ratio) Panc89 spheroids after combined Pembrolizumab treatment, which was not the case when fewer HMF were present in the Panc89 spheroids (5:1 ratio), as the levels of CD69 and CD25 were not changed (Figure 70B+D).

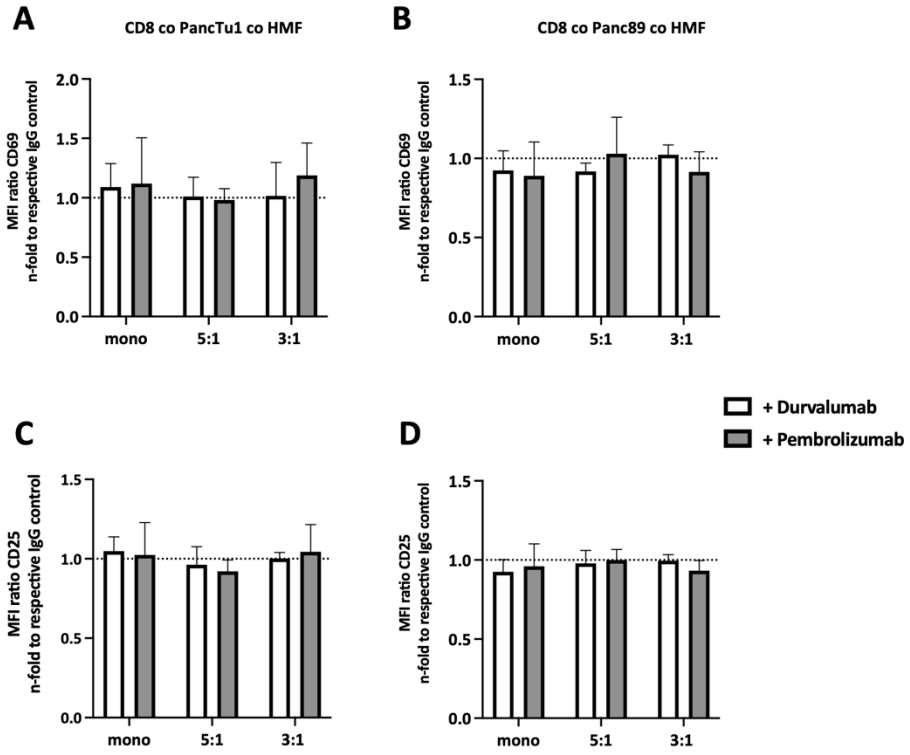

Figure 70: Combined treatment with Gemcitabine and either Durvalumab or Pembrolizumab did not affect activation of CD8$^+$ T cells. CD8$^+$ T cells were isolated by magnetic cell separation from human blood derived lymphocytes and then activated with anti-CD3 and anti-CD28 antibodies, as well as IL-2 for 3 days. PancTu1 and Panc89 cells were either seeded in mono- or coculture with hepatic myofibroblasts (HMF) at different ratios in ultra-low attachment plates for 3 days. After 24 h, PancTu1 and Panc89 spheroids were treated with 10 µg/ml Gemcitabine. After 24 h, the medium was changed and activated CD8$^+$ T cells were added at a ratio of 1:10 and cultures were treated with 10 µg/ml Durvalumab (white) or Pembrolizumab (grey) or with 10 µg/ml of the respective isotype control (hIgG1 or hIgG4). After 24 h, the cell surface expression of **(A+B)** CD69 and **(C+D)** CD25 on CD8$^+$ T cells was analyzed by flow cytometry. Median fluorescence intensity (MFI) ratio was calculated by dividing the MFI of the specific staining by the MFI of the isotype control. Data were normalized to the respective isotype control. Data represent the mean ± SD (normally distributed. N=4.

Next, the concentration of effector molecules in the supernatants of the different cocultures and combinational treatments was analyzed. Combinational therapy of Gemcitabine and Durvalumab did almost not affect the levels of Granzyme A, Granzyme B, Perforin, Granulysin, and IFNγ in supernatants

of CD8+ T cells cocultured with either PDAC cell spheroid (Figure 71A-J). Concentrations of Perforin and Granulysin were also not altered in supernatants of CD8+ T cells after combinational treatment with Gemcitabine and Pembrolizumab, independent of the culture conditions (Figure 71E-H). Combined Pembrolizumab treatment led to higher concentrations of Granzyme A, Granzyme B, and IFNγ after coculture of CD8+ T cells with HMF-enriched PancTu1 and Panc89 spheroids, especially at 3:1 ratio (Figure 71A-D+I-J).

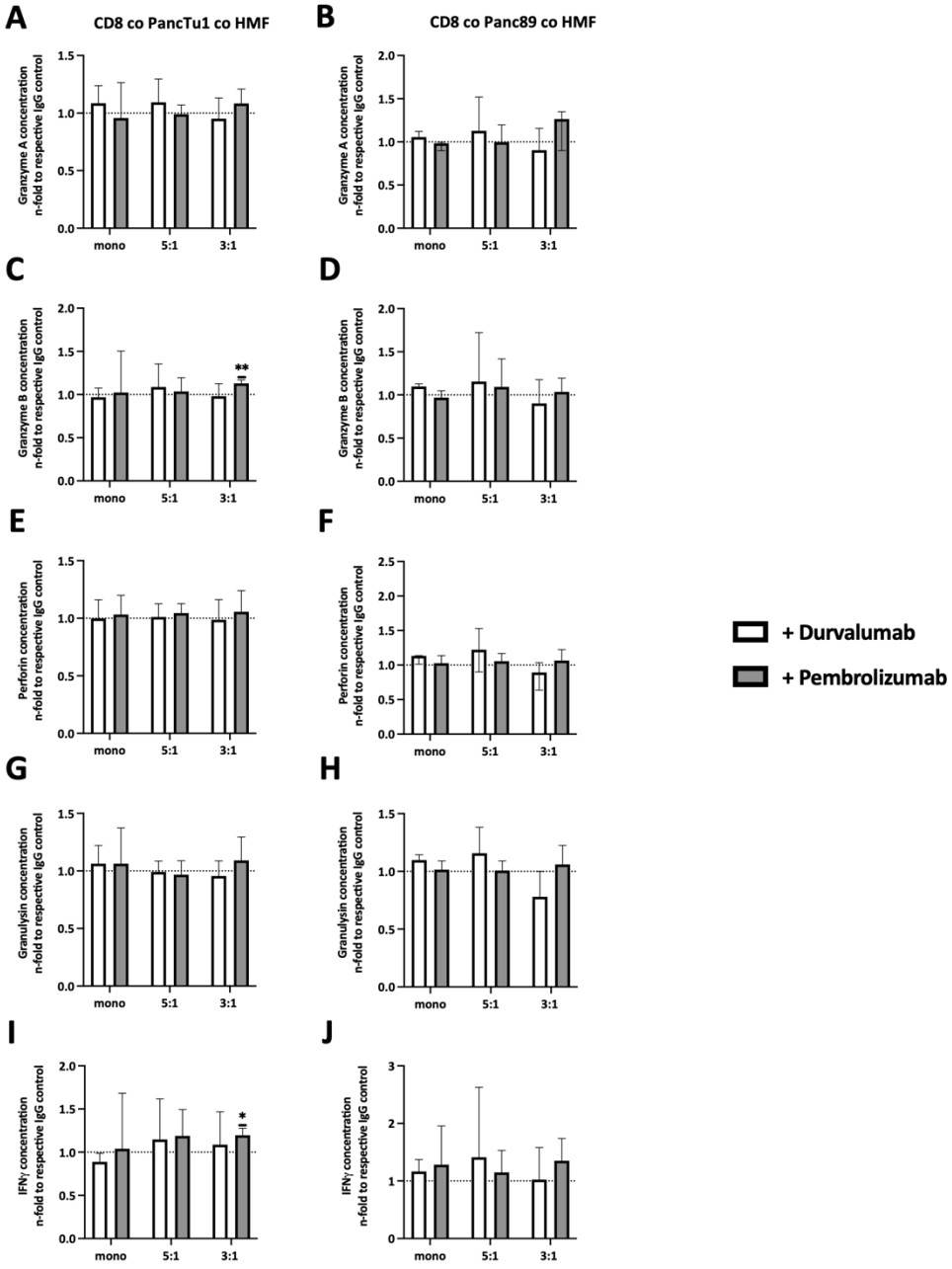

Figure 71: Combined Pembrolizumab treatment led to higher concentrations of effector molecules in the supernatants of CD8+ T cells after coculture with HMF-enriched spheroids. CD8+ T cells were isolated by magnetic cell separation from human blood derived lymphocytes and then activated with anti-CD3 and anti-CD28 antibodies, as well as IL-2 for 3 days. PancTu1 and Panc89 cells were either seeded in mono- or coculture with hepatic myofibroblasts (HMF) at different ratios in ultra-low attachment plates for 3 days. After 24 h,

PancTu1 and Panc89 spheroids were treated with 10 µg/ml Gemcitabine. After 24 h, the medium was changed and activated $CD8^+$ T cells were added at a ratio of 1:10 and cultures were treated with 10 µg/ml Durvalumab (white) or Pembrolizumab (grey) or with 10 µg/ml of the respective isotype control (hIgG1 or hIgG4). The concentrations of **(A+B)** Granzyme A, **(C+D)** Granzyme B, **(E+F)** Perforin, **(G+H)** Granulysin, and **(I+J)** IFNγ were analyzed in the supernatants after 24 h. Data were normalized to the respective isotype control. Data represent the mean ± SD (normally distributed) or the median with interquartile range (not normally distributed). N=4. * = $p < 0.05$, ** = < 0.0.

Overall, combined treatment of Gemcitabine and Durvalumab or Pembrolizumab did not affect the activation phenotype of $CD8^+$ T cells. However, combined Pembrolizumab treatment led to higher concentrations of effector molecules in the supernatants of $CD8^+$ T cells after culture with HMF-enriched spheroids.

4.3.8.2 Combined treatment with Gemcitabine and either Durvalumab or Pembrolizumab did not affect PDAC cell death

Finally, it was analyzed whether the combined treatment of Gemcitabine and ICIs can affect PDAC cell death. Therefore, ccK18 levels were measured in the supernatants after treatment of PDAC spheroids cultured with $CD8^+$ T cells. In supernatants of $CD8^+$ T cells cultured with mono- and cocultured PancTu1 and Panc89 spheroids, ccK18 levels were not altered by combined Durvalumab treatment (Figure 72A+B), while combined Pembrolizumab treatment led to slightly higher levels of ccK18 levels in HMF-enriched PancTu1 spheroids. This was in line with slightly higher concentrations of effector molecules measured in the supernatants of these culture conditions (Figure 71). However, this effect was not seen in HMF-enriched Panc89 spheroids. Here, ccK18 levels were slightly higher in supernatants of $CD8^+$ T cells cultured with monocultured Panc89 spheroids after combined Pembrolizumab treatment (Figure 72B).

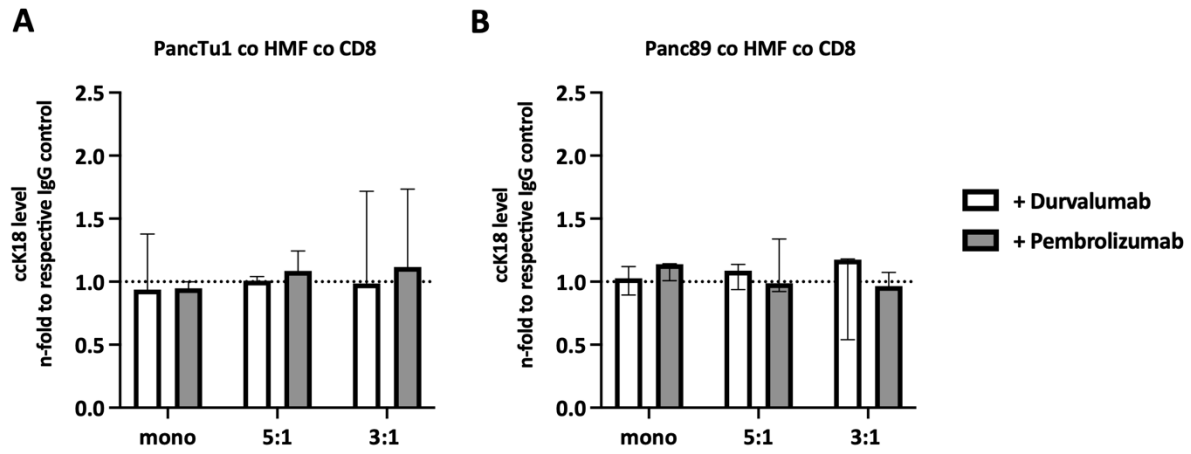

Figure 72: Combined treatment with Gemcitabine and either Durvalumab or Pembrolizumab hardly affected caspase-cleaved keratin18 (ccK18) levels. $CD8^+$ T cells were isolated by magnetic cell separation from human blood derived lymphocytes and then activated with anti-CD3 and anti-CD28 antibodies, as well as IL-2 for 3 days. PancTu1 and Panc89 cells were either seeded in mono- or coculture with hepatic myofibroblasts (HMF) at different ratios in ultra-low attachment plates for 3 days. After 24 h, the PancTu1 and Panc89 spheroids were treated with 10 µg/ml Gemcitabine. After 24 h, the medium was changed and activated $CD8^+$ T cells were added at a ratio of 1:10 and cultures were treated with 10 µg/ml Durvalumab (white) or Pembrolizumab (grey) or with 10 µg/ml of the respective isotype control (hIgG1 or hIgG4). After 24 h, the levels ccK18 were measured in supernatants after culture with mono- and cocultured **(A)** PancTu1 and **(B)** Panc89 spheroids. Data were normalized to the respective isotype control. Data represent the mean ± SD (normally distributed) or the median with interquartile range (not normally distributed). N=4.

Altogether, Gemcitabine pre-treatment of mono- or cocultured PancTu1 and Panc89 spheroids followed by culture with $CD8^+$ T cells and Durvalumab or Pembrolizumab treatment did not enhance PDAC cell death.

5 Discussion

5.1 TME remodeling during the progression of liver metastases

In PDAC patients, 80 % are diagnosed with a locally advanced or metastatic stage [4,5]. To date, the only curative treatment is the R0 resection of the primary tumor. However, even these patients often relapse and develop metastases shortly after or even during adjuvant therapy [149]. Most metastases develop in the lung (~ 50 %), the peritoneum (~ 60 %), and the liver (~ 80 %) [103]. Thus, the liver is the main site of metastases in PDAC and is associated with the worst prognosis compared to lung or peritoneum metastases [114]. Therefore, it is of outmost importance to better understand the mechanisms underlying metastatic progression in the liver to develop effective treatment options [150].

Since metastases are not routinely resected in PDAC patients, tissue samples from PDAC metastases are rare and the expression of immune regulatory molecules such as PD-L1 within liver metastases is rarely characterized. Hence, this study intended to elucidate the role of PD-L1 in the interplay of PDAC cells, the hepatic microenvironment, and immune cells in order to provide novel insight into the mechanisms contributing to the immune escape of PDAC liver metastases.

IHC staining of liver tissue sections revealed that during metastatic progression (from small to large metastases) the TME seems to be remodeled. Staining of αSMA, indicative for myofibroblasts, was less detectable in small metastases compared to large metastases, which is in line with the findings of Quaranta *et al.*, who showed in a PDAC mouse model that αSMA expression was lower in small metastatic lesions compared to large metastatic lesions in the liver [57]. As CAFs enhance tumor cell proliferation, recruit immunosuppressive immune cells, and promote ECM remodeling [30], it is reasonable to conclude that CAFs promote the progression of primary tumors and metastases. Cohen *et al.* and Kawase *et al.* analyzed FAP-expressing CAFs in PDAC patients and showed that a high abundance is associated with a lower survival rate [169,170]. CAF can exhibit different phenotypes and different CAF populations have been discovered in recent years. In the pancreas, major subgroups are myCAF, iCAF and MHCII antigen presenting CAF (apCAF) [30,171]. MyCAF, which are tumor-adjacent and express high levels of αSMA [30,41], suggesting that most CAFs within the metastases are myCAFs. In contrast, iCAF are localized distant from the tumor, express low αSMA levels and exhibit rather tumor-promoting and immunosuppressive properties by secreting inflammatory cytokines, like IL-6, CXCL12, and G-CSF [30,41,171]. As discussed later, it was shown that CXCL12 secreted by CAFs can inhibit the infiltration of T lymphocytes [172]. Huseni et al. investigated that the CTL function is impaired in cancer patients (kidney, bladder, and breast) with high levels of IL-6. Further, they showed *in vitro* that IL-6 directly inhibits CTLs [173], concluding that CAFs present at the invasion front of metastases, especially large metastases might be iCAFs. As discussed later, $CD8^+$ T cells are not able to

infiltrate into the large metastases and are therefore mainly present at the invasion front. In order to identify the different CAF populations in the liver tissue sections of PDAC patients, αSMA and IL-6 should be stained in combination.

Large metastases exhibited higher numbers of myofibroblasts compared to small metastases, in which the number of Ki67$^+$ tumor cells was also higher (Supplementary Figure 8). This was also demonstrated by Lenk and colleagues in a KPC mouse model, where liver metastases with a high HMF to HSC ratio (indicating higher αSMA expression) showed more Ki67$^+$ tumor cells [160].

Myofibroblasts are the main source of ECM molecules such as collagen or fibronectin within the desmoplastic tumor stroma [174]. The ECM is a physical barrier for T cells and has been shown to prevent the penetration of CD8$^+$ T cells into liver metastases [30], particularly in large metastases. Since the proportion of myofibroblasts was higher in large metastases, it can be speculated that myofibroblasts along with the released ECM molecules provide a physical barrier preventing T cell infiltration into metastases. Kobayashi *et al.* showed in a rat model that in hepatic fibrotic tissue the amount of CD4$^+$ and CD8$^+$ T cells was lower and apoptosis of tumor cells was induced [175]. In the IHC study of this thesis, CD3$^+$ and CD8$^+$ T cells, respectively, were mostly found at the invasion front, while in small metastases CD8$^+$ T cells were detected throughout the whole lesions or in the tumor center. To determine a possible role of ECM on T cell exclusion in liver metastases, the sections should be stained for different ECM molecules, like collagen and fibronectin and expression patterns compared between small and large metastases. However, not all types of collagen seem to be a physical barrier for T cells, as Carstens *et al*. showed that collagen type I did not inhibit the infiltration of CD8$^+$ T cells [123]. Moreover, small metastases contained even higher proportions of CD8$^+$ T cells. Quaranta *et al*. demonstrated similar results in liver metastases of PDAC patients. Here, the number of CD8$^+$ T cells was higher and closer to PanCK poor lesions (reflecting small lesions) compared to PanCK rich lesions (reflecting large lesions). Only around 20 % of CD8$^+$ T cells were in the center of the metastases. Such change of CD8$^+$ T cell localization and abundance was also detected in a KPC mouse model. Interestingly, CD8$^+$ T cells were less active and expressed more PD-1 on their cell surface in large metastatic lesions compared to small lesions, pointing to an exhausted phenotype [57].

Similar to the liver metastases a comparable stromal distribution was seen in the corresponding primary tumor, where CD3$^+$ and CD8$^+$ T cells were also mainly located at the invasion front, along with a high number of αSMA$^+$ myofibroblasts were detected (data not shown). Grout *et al.* also showed that in NSCLC tumor infiltration by CD3$^+$ and CD8$^+$ T cells was significantly lower when αSMA$^+$ CAF are present at the invasion front [176].

A KPC PDAC mouse model showed that FAP$^+$ CAFs secrete CXCL12 and thereby inhibit T cell infiltration, as inhibiting chemokine (C-X-C motif) receptor (CXCR) 4, which is the receptor for CXCL12, increased the accumulation of T cells [172]. This was also seen by Lin and colleagues who could further

demonstrate that inhibiting CXCR4 led to higher tumor cell killing [177]. Around 70 % of PDAC patients harbor mutations in the tumor suppressor gene *p53*, Maddalena *et al.* showed that mutations in *p53* are associated with lower infiltration of lymphocytes, presumably due to the higher amount of ECM protein [178].

Comparing the localization of $CD3^+$ T cells and $CD8^+$ T cells, it seems that to some extent $CD3^+$ T cells are more present in the center of large metastases, indicating that these T cells are $CD4^+$ helper cells. In PDAC, the TME mainly promotes the differentiation of T_H2, T_H17, and T_{Reg} cells, which are known to be rather tumor-promoting and immunosuppressive [30]. In order to define these $CD3^+$ T cells, multiplex staining detecting several activation markers, regulatory proteins, and cytokines would be necessary.

Besides, macrophages are a predominant cell population in the TME and therefore the main localization of macrophages was analyzed in this thesis, too. In small metastases, macrophages were in the tumor center or evenly distributed, in contrast in large metastases they were mainly evenly distributed or at the invasion front. Nielsen *et al.* showed that macrophages promote HSC activation into HMF by Granulin in a KPC mouse model. Additionally, Granulin induces the expression of Periostin in myofibroblasts, which in turn enhances cancer cell growth. In line with these findings, granulin is highly expressed in liver metastases of PDAC patients. Overall, this example well illustrates how the TME impacts the progression of liver metastases in PDAC [113].

Localization of CD68 staining was associated with high CD163 staining (data not shown), indicative for M2-like macrophages. The presence of M2-like macrophages might be another factor promoting the exclusion of T cells. Beatty *et al.* showed in a KPC mouse model that $Ly6c^{low}F4/80^+$ macrophages (indicative for M2-like macrophages in mice) regulate the infiltration of T cells [179]. This was also seen in a lung cancer mouse model, in which macrophages inhibited migration and infiltration of $CD8^+$ T cells into the tumor islets [180].

Rahn *et al.* showed that PD-L1 is expressed in primary tumor tissues of PDAC patients staged T3N1M0, however, only in 20 % of the analyzed tissues [35]. As 80 % of PDAC patients are diagnosed at a locally advanced or metastatic stage, with the liver representing the main site of metastases [5,103], it was first to be determined whether PD-L1 is expressed in liver metastases. Here, PD-L1 expression was found in all 15 liver tissue sections of PDAC patients.

Moreover, comparing a small number (n=4) of PDAC primary tumor tissues and their corresponding liver metastases, revealed that all primary tumors and their liver metastases exhibited high PD-L1 expression (data not shown), which is in contrast to the cohort of Rahn *et al*. This might be explained by the fact that poorly differentiated tumors and an advanced tumor stage are associated with a higher PD-L1 expression [35,146,147]. Moreover, the expression of PD-L1 in the primary tumor and matched

liver metastases might indicate that PD-L1 mediated immune evasion operates during tumor progression and metastasis.

However, the abundance and intensity of PD-L1 expression were quite heterogenous within the patients and between small and large metastases. Overall, PD-L1 expression was mainly located at the invasion front or evenly distributed in large metastases, while small metastases either lacked PD-L1 expression or mostly showed weak expression in the center. Of note, small liver metastases with no or low PD-L1 expression comprised more $CD8^+$ T cells in the tumor center, while large metastases exhibiting stronger PD-L1 expression comprised fewer $CD8^+$ T cells being mostly located at the invasion front, indicating inhibition of $CD8^+$ T cells through the PD-1/PD-L1 axis. In metastatic melanoma lesions, it was shown that tumor infiltrating $CD8^+$ lymphocytes exhibit higher cell surface levels of PD-1 compared to T cells in normal tissues. Furthermore, the infiltrating PD-1 positive $CD8^+$ T cells were tumor antigen-specific and showed an exhausted stage [181]. To get such insights into PDAC, staining of PD-1 and in-depth analysis of the $CD8^+$ T cells within the liver metastases would be reasonable.

Since immune cells, such as macrophages and T cells, in the TME can upregulate the expression of PD-L1 through the secretion of cytokines, like TNFα and IFNγ, the increased expression of PD-L1 in large metastases could be explained by the higher abundance of immune cells [165].

Double stainings revealed that PD-L1 is predominantly expressed by stromal cells, especially HMF. Besides HMF also Kupffer cells [182] or metastases-associated macrophages seemed to be an important source of PD-L1 expression in liver metastases, which was also seen in this thesis. The fact that in PDAC stromal cells are the main source of PD-L1 expression rather than the PDAC cells was already demonstrated by Rahn *et al.* in primary tumors of PDAC patients and Karamitopoulou *et al.* also showed that PD-L1 is expressed by immune cells in PDAC patients [35,148]. To gain further information about the PD-L1/PD-1 axis in liver metastases, PD-1 should be also stained, to investigate whether $CD8^+$ T cells express more PD-1 in large metastases compared to small metastases. Overall, multiplex staining of small and large metastases with different markers would be an effective analysis method to characterize stromal remodeling during metastatic progression further.

Overall, the TME changes during metastatic progression and due to the remodeling and expansion of the TME, $CD8^+$ T cells are unable to infiltrate into the tumor center. Here, it seems that the PD-L1/PD-1 axis also contributes to this T cell exclusion.

5.2 Exhaustion of $CD8^+$ T cells in cancer

T cell exhaustion was first described in the context of viral infection [183], where T cells lose their effector function. Meanwhile, T cells have been also often found in an exhausted state in cancer [184].

These T cells, often already activated in the lymph organs become exhausted in the TME. T cell exhaustion is associated with poor survival of patients with different cancer entities [185] and has also been identified as characteristic of PDAC [186]. Exhausted $CD8^+$ T cells often show a high cell surface expression of inhibitory receptors, like PD-1, CTLA-4, and TIM3 [187], which in turn underlines that more checkpoint molecules should be stained in the liver tissue sections to more precisely define the activation status of the $CD8^+$ T cells. T cells often express more than one inhibitory receptor and some expression patterns of different inhibitory molecules are associated with a more pronounced exhausted stage [188,189]. For *in vitro* experiments, $CD8^+$ T cells were activated with anti-CD3 and anti-CD28 antibodies as well as IL-2 to mimic an APC. This activation of $CD8^+$ T cells prior to coculture is reasonable as it better mimics the physiological setting in the TME. During T cell activation, the expression of CD25 on the cell surface is increased, leading to a higher binding affinity of IL-2, thereby promoting proliferation [69]. Thus, cell surface levels of the activation markers CD69 and CD25 became significantly higher during activation culture compared to post MACS (at the beginning of activation culture). Reddy *et al.* already showed that activation of PBMCs with anti-CD3 and anti-CD28 antibodies for 72 h led to higher cell surface levels of CD69 and CD25 compared to non-activated PBMCs [190]. Additionally, cell surface expression of PD-L1 and PD-1 was elevated on T cells upon activation culture, indicating an exhausted phenotype. Diskin *et al.* showed in a KPC mouse model, that PD-L1 cell surface expression was higher in PDAC tumors compared to chronic pancreatitis, and also in liver metastases $CD8^+$ T cells expressed PD-L1. They further demonstrated that PD-L1 on T cells can lead to inhibition of T cells by binding to PD-1 on other T cells in the TME [191]. However, in this thesis, IHC analysis revealed that mostly macrophages and HMF express PD-L1 in liver metastases.

In mice, T cells show elevated PD-1 cell surface expression after activation with anti-CD3 beads [192]. An exhausted stage of T cells is also characterized by less IFNγ and effector molecule production [189]. However, during activation culture, the concentrations of some effector molecules (Granzyme A, Perforin, and Granulysin) were higher on day 4 compared to day 3, despite concentrations of IFNγ and Granzyme B, which were not elevated during activation culture. The exhaustion of $CD8^+$ T cells is described as a stepwise process. First, inhibitory receptors are upregulated, further production of TNFα is lost, and finally, the release of IFNγ and effector molecules is reduced [189]. Interestingly, anti-CD3 antibodies did not enhance the secretion of cytokines, therefore both anti-CD3 and anti-CD28 antibodies are necessary to induce the production of cytokines [193]. Thus, $CD8^+$ T cells obtained from activation culture might be at an early or intermediate stage of exhaustion as cell surface expression of PD-L1 was already enhanced, but the concentrations of some effector molecules were not decreased. The secretion of TNFα, the cell surface level of other inhibitory receptors, like CTLA-4 and TIM3, should be analyzed to gain more insights into the stage of exhaustion of T cells after activation culture.

5.3 PDECs did almost not affect the activation status and effector phenotype of CD8$^+$ T cells

The IHC staining revealed that during metastatic progression the TME remodels, and CD8$^+$ T cells are located closer to PanCK positive tumor cells in small compared to large metastases, raising the question of whether these two cell populations might impact PD-L1 expression on each other. For this purpose, PDECs and CD8$^+$ T cells were mono- and cocultured for 72 h. Cell surface levels of activation markers were almost unaffected on CD8$^+$ T cells after coculture with PDECs. However, PD-L1 cell surface expression was slightly higher on CD8$^+$ T cells after coculture with either PDEC line. PD-L1 expression can be induced by different pro-inflammatory cytokines, like IL-6 or IFNγ [165]. Here, IL-6 was detectable in supernatants of both monocultured PDEC lines (Supplementary Figure 9A). Moreover, IFNγ was highly released by CD8$^+$ T cells, giving two examples of how PD-L1 cell surface expression could be enhanced on PDECs in this coculture setting.

Further, TGF-β1 and IL-10 were also detectable in the supernatants of PDECs in monoculture (Supplementary Figure 9B+C). In B-cell non-Hodgkin's lymphoma and glioblastoma, it was shown that TGF-β and IL-10, respectively, can induce T cell exhaustion [194,195]. However, here it seems as if T cells were not in an exhausted stage, as cell surface expression of PD-1 was not altered, and effector molecules were slightly higher due to coculture with either PDEC line. But TGF-β1 was reported to inhibit T cell proliferation [196,197]. In line with that, the cell number of CD8$^+$ T cells was reduced after coculture with PDECs (Supplementary Figure 10), especially after coculture with H6c7-kras cells, which also released more TGF-β1 into supernatants. In addition, H6c7-kras cells express higher cell surface levels of PD-L1, which can bind to PD-1 on T cells and lead to their inhibition [132]. To evaluate whether the PD-L1/PD-1 axis contributes to the lower number of CD8$^+$ T cells in the PDEC coculture setting, PD-L1 should be blocked with Durvalumab. Comparing both PDEC cell lines, H6c7-kras cells showed a higher PD-L1 expression, while PancTu1 cells exhibited only a weak to moderate expression underscoring the high heterogeneity regarding tumor cell-associated PD-L1 expression observed in primary PDAC [35] and in liver metastases. The heterogenous PD-L1 expression was also observed by Rahn *et al.* and Principe *et al.*, demonstrating varying levels of PD-L1 on PDEC cell lines [80,198]. IFNγ is a strong inducer of PD-L1 through the transcription factor STAT1 [199]. CD8$^+$ T cells enhanced cell surface expression of PD-L1 on H6c7-kras and PancTu1 cells and released high amounts of IFNγ into the supernatants, explaining the induction of PD-L1 on PDECs. Even though, both PDEC lines expressed PD-L1 on their cell surface, which was further enhanced by CD8$^+$ T cells, CD8$^+$ T cells significantly reduced PDEC proliferation as less Ki67 was expressed by PDECs, in line with lower cell numbers and less cell confluence of H6c7-kras and PancTu1 cells, which could be associated with PDEC death. The reduced cell number and cell confluence were stronger in H6c7-kras cells than in PancTu1 cells. The

concentrations of some effector molecules (Granulysin, Granzyme B, and Perforin) and of sFasL (CD95L) (data not shown) were slightly elevated after coculture with PancTu1 and especially with H6c7-kras cells, giving one explanation for the induction of cell death. The binding of CD95L to CD95 induces apoptosis and CTLs express CD95L to kill cancer and virus-infected cells [75]. However, sFas (CD95) was not detectable in supernatants of both PDEC cell lines (data not shown). This might be due to the fact that soluble Fas was measured and Rashied *et al.* and Trauzold *et al.* showed that membrane bound CD95 is highly expressed by different PDAC cell lines, also PancTu1 cells [200,201]. However, Trauzold *et al.* demonstrated that PancTu1 cells are resistant towards CD95-mediated apoptosis induction. The response towards CD95-mediated apoptosis was quite heterogenous comparing different PDAC cell lines [201], maybe explaining the stronger induction of cell death in H6c7-kras cells compared to PancTu1 cells.

Nevertheless, as the coculture was maintained for 72 h, the induction of cell death is most likely induced by an allogeneic T cell reaction and therefore not specific.

Additionally, H6c7-kras cells were established by immortalizing HPDE cells with HPV16-E6/E7 genes and further transduced with the retroviral vector pBabepuro-K-ras4B^{G12V}. Therefore H6c7-kras cells express the viral proteins E6/E7 [202], as T cells are able to recognize presented proteins on forgein MHC as well [203], this might be one more explanation for the enhanced H6c7-kras cell death.

5.4 Hepatic myofibroblasts enhance the activation status and the effector phenotype of CD8$^+$ T cells

The *in situ* analysis of liver tissue section from PDAC patients revealed that the localization of αSMA$^+$ myofibroblasts and CD8$^+$ T cells along with PD-L1 expression changed during outgrowth of liver metastases. While in small metastases, αSMA staining was detectable in the tumor center or evenly distributed between the tumor center and the invasion front, αSMA staining was predominantly located inside large metastases. Further, higher numbers of myofibroblasts were detected in large metastases. CD8$^+$ T cells were predominantly located inside or evenly distributed in small metastases, while in large metastases the majority of CD8$^+$ T cells were almost exclusively found at the invasion front, indicating that immune cells are unable to infiltrate large metastases. In addition, more cells were PD-L1 positive and showed a stronger PD-L1 staining in large metastases. To investigate how hepatic stromal cells impact the PD-1/PD-L1 axis and the effector phenotype of CD8$^+$ T cells (representing the most important cell population in the TME for tumor killing), a direct coculture with CD8$^+$ T cells and HSC or HMF was performed.

The vital cell number of CD8$^+$ T cells was lower after coculture with HSC or HMF compared to monoculture, in line with a higher percentage of trypan blue positive cells, indicating that CD8$^+$ T cells

die in the presence of HSC and HMF, respectively (Supplementary Figure 11). Zhao *et al.* demonstrated in a hepatocellular carcinoma model that activated HSC enhanced T cell apoptosis and further inhibited T cell-mediated lysis of tumor cells [204]. Several other studies also showed the inhibition of HSC or activated HSC on T cells [175,205,206]. Charles *et al.* demonstrated that direct cell-cell contact is necessary for the inhibition of T cells by activated HSC and that by blocking PD-L1 this inhibitory effect is reversed [205]. This was also confirmed by Yu and colleagues [206]. In this thesis, HSC and HMF exhibited cell surface expression of PD-L1. Although, the expression was slightly higher on HMF, though, the percentage of dead $CD8^+$ T cells was higher after HSC coculture. Further, blocking of PD-L1 with Durvalumab did not enhance the number of vital $CD8^+$ T cells (Supplementary Figure 12), suggesting that other mechanisms inhibit T cells.

However, cell surface expression of PD-L1 was significantly enhanced on HSC and HMF after coculture with $CD8^+$ T cells. As mentioned before in section 5.3, different cytokines are known to induce the gene expression of PD-L1, especially IFNγ [199]. Yu *et al.* and Charles *et al.* showed that cell surface expression of PD-L1 increased during stimulation with IFNγ on HSC [175,205]. However, Charles *et al.* also showed that IFNγ concentrations were lower in supernatants of T cells after coculture with HSC [205]. In line with these findings concentrations of IFNγ were slightly lower in the supernatants of $CD8^+$ T cells after coculture with HSC or HMF compared to monocultured $CD8^+$ T cells. To confirm that cell surface expression of PD-L1 on HSC and HMF is mediated by IFNγ by $CD8^+$ T cells, IFNγ bioactivity was blocked in the coculture of $CD8^+$ T cells with either HSC or HMF, which led to significantly lower levels of PD-L1 on HSC and HMF after coculture with $CD8^+$ T cells. These data support the view that $CD8^+$ T cells induce PD-L1 expression on HSC and HMF by IFNγ and are in line with the *in situ* findings, where $CD8^+$ T cells are close to areas with PD-$L1^+$ cells, including HMF.

As mentioned above, blocking PD-L1 with Durvalumab did not reverse the inhibition of $CD8^+$ T cells, suggesting that HSC and HMF inhibit $CD8^+$ T cells by other mechanisms. IL-6 and TGF-β1 secreted by myofibroblasts can inhibit $CD8^+$ T cells [196,197,207]. Both cytokines were detectable in the supernatants of mono- and cocultured cell populations (Supplementary Figure 13 A+B). Concentrations of IL-6 were higher after coculture with $CD8^+$ T cells compared to HSC and HMF in monoculture (Supplementary Figure 13B), giving one more explanation for the inhibition of $CD8^+$ T cells after coculture with both hepatic stromal cell populations, as IL-6 was detected only at low levels in the supernatant of monocultured $CD8^+$ T cells and during the activation culture.

In esophageal cancer, it was shown that IL-6 secreted by CAFs negatively regulates the infiltration of $CD8^+$ T cells [208], suggesting that IL-6 may also contribute to the impaired accumulation of $CD8^+$ T cells inside large liver metastases.

As mentioned above in section 5.3, IL-6 is also known to induce cell surface expression of PD-L1 [165]. However, cell surface expression of PD-L1 was not altered on $CD8^+$ T cells after coculture with either

HSC or HMF. Also, cell surface expression of PD-1 on $CD8^+$ T cells was not affected by coculture with HSC or HMF, while cell surface expression of CD80 was lower after coculture with both hepatic stromal cells (data not shown). CD80 can bind in cis to PD-L1, preventing the binding of PD-1 to PD-L1 and CTLA-4 to CD80, nevertheless, CD28 can still bind to CD80, resulting in activation and not inhibition of $CD8^+$ T cells [209,210]. Therefore, lower cell surface levels of CD80 support the binding of PD-L1 to PD-1, thereby exerting an inhibition effect on $CD8^+$ T cells. However, here activation markers of $CD8^+$ T cells, especially CD69 were higher. Blocking of PD-L1 by Durvalumab did not alter the activation status of $CD8^+$ T cells, suggesting that the PD-L1/PD-1 axis does not contribute to the higher activation of $CD8^+$ T cells after coculture with either HSC or HMF.

Thomas *et al.* and Trapani *et al.* showed that TGF-β inhibits the expression of genes encoding for cytotoxic effector molecules [207,211]. However, here concentrations of some effector molecules were slightly higher in supernatants of $CD8^+$ T cells after coculture with HSC and HMF and the TGF-β1 concentration was lower in supernatants of hepatic stromal cells after coculture with $CD8^+$ T cells (Supplementary Figure 13A), explaining the slight enhancement of effector molecule secretion by $CD8^+$ T cells under coculture with HSC or HMF.

After coculture with HSC and HMF, not only concentrations of some effector molecules but also the concentration of sFasL (CD95L) were higher in supernatants of $CD8^+$ T cells (Supplementary Figure 14), indicating a higher cytotoxic potential of $CD8^+$ T cells. Even though the activation status and the effector phenotype of $CD8^+$ T cells were enhanced after coculture with HSC or HMF, this was not associated with enhanced PDEC death. To prevent the allogenic T cell reaction, coculture with pre-cultured $CD8^+$ T cells and PDECs was only conducted for 24 h. However, this time frame of 24 h might be already too long, as the allogenic reaction also depends on the donor. The induction of cell death was higher in H6c7-kras cells compared to PancTu1 cells, suggesting as mentioned above the expression of the viral protein E6/E7 contributes to the higher apoptosis induction [202]. Further, PancTu1 cells might inhibit $CD8^+$ T cells more compared to H6c7-kras cells, but probably not by PD-L1 as H6c7-kras cells exhibit higher cell surface levels of PD-L1 and PD-1 cell surface levels were not altered on $CD8^+$ T cells after coculture with HSC or HMF. Moreover, PancTu1 cells exhibit a high resistance towards death ligand induced apoptosis, which will be discussed in more detail in section 5.7.

Blocking of PD-L1 with Durvalumab during pre-culture with HSC or HMF prior coculture with H6c7-kras and PancTu1 cells did not lead to enhanced PDEC death.

Overall, HSC and HMF inhibited T cell growth, however, the activation status and the effector phenotype were enhanced by both hepatic stromal cells. Nevertheless, pre-coculture with HSC or HMF did not enhance induction of PDEC death.

5.5 The formation of spheroids differs between different PDEC lines

Previous experiments were performed using traditional 2D monolayer cell culture models. However, 2D cultures exhibit some limitations, e.g., the cells grow in monolayers in cell culture plates, which does not reflect the physiological conditions and microenvironment of a tumor. In order to better mimic the TME, the use of 3D tumor models has increased within the last years [212]. 3D tumor models offer several advantages: First, in contrast to 2D, where the cells are forced to grow flat and in single layers, 3D cultured cells are able to form multiple cell layers and show their natural shape [213], consequentially leading to more cell junctions, allowing cell-cell communications, and well-differentiated cells [214]. Further, nutrients in the medium are not distributed equally within 3D cultured cells, leading to a necrotic core, which is also often seen in tumors [212]. Different methods for 3D cultures have been established, e.g., spheroid formation in ULA plates, hanging drop, patient-derived organoids, scaffold-based, or magnetic levitation. All models have their advantages but also limitations. In this thesis, 3D spheroid cultures were generated using ULA plates. The advantages of using ULA plates for spheroid formation are increased cell-cell communication, nutrient and oxygen gradient, easy drug screening, and low costs [215,216].

First, it was tested which PDEC lines are able to form spheroids. Therefore, 8 different cell lines were seeded in ULA plates for 72 h. The formation of spheroids was quite heterogenous comparing the different PDEC lines. For further experiments in this thesis, PancTu1 and Panc89 cells were chosen for spheroid cocultures, as both cell lines formed compact spheroids and exhibited a low live-to-dead cell ratio. In contrast, Gaviraghi *et al.* described PancTu1 cells as a non-forming spheroid cell line. However, a different method was used for spheroid formation [217]. Shichi *et al.* demonstrated that cell lines with a mesenchymal phenotype form looser spheroids compared to an epithelial phenotype [164]. Panc1 cells are described as mesenchymal and Colo357 as a quasi-mesenchymal cell line, explaining the loose clustering of cells [164]. Here, Panc1 cells were only loosely clustered, which was also seen by Longati and colleagues [218], which can be explained by the pronounced mesenchymal phenotype. H6c7-kras exhibit higher levels of mesenchymal marker, like Vimentin compared to PancTu1 and Panc89 cells, giving one explanation for different spheroid formations (Supplementary Figure 3). Longati *et al.* also showed that BxPC3 cells formed compact spheroids with a well-defined contour [218], which was also seen in this study. This was also confirmed by several other studies. However, most studies focused on Panc1, BxPc3, MIA PaCa-2, Capan-1, and AsPC-1 cells [164,218–220], all showing that the formation of spheroids differs from cell line to cell line. However, the number of dead cells within or around the spheroids was not analyzed in these studies and especially BxPc3 cells showed high numbers of dead cells around the spheroid in this thesis.

Furthermore, the cell lines needed to express PD-L1 on their cell surface, which should be inducible to investigate the impact of stromal cells and immune cells on PD-L1 expression on tumor cells. Flow

cytometry analysis revealed that cell surface expression of PD-L1 is quite heterogeneous on different PDEC lines, which was already discussed in section 5.3. PancTu1 cells exhibited a moderate to high and Panc89 cells a low PD-L1 cell surface expression, which could be enhanced by IFNγ and Gemcitabine. Of note, cell surface levels of PD-L1 were significantly lower on both cell lines in 3D cultures compared to 2D cultures. Moreover, the percentage of PD-L1$^+$ PDAC cells was reduced in 3D cultures, maybe reflecting the situation in the liver metastases better as PD-L1 is rather expressed by stromal cells than tumor cells. Moreover, PD-L1 might be only expressed by the tumor cells on the edge of the spheroid, in order to evade the immune system, explaining the lower number of PD-L1$^+$ tumor cells in 3D compared to 2D culture. Spheroids should be embedded and stained for PanCK and PD-L1 to confirm this theory.

5.6 3D in vitro cocultures well mimic small and large metastases

The differences between small and large metastases detected by IHC staining of the liver tissue sections of PDAC patients were experimentally well mimicked in the established 3D cocultures *in vitro* by using different tumor cell to HMF ratios (3:1 ratio = large and 5:1 ratio = small metastases). The fact that the diameter of the spheroids was larger after coculture with HMF along with a higher number of PDAC cells indicates that HMF support tumor cell growth, which is in line with previous findings from other *in vivo* and *in vitro* studies [120,221]. Kpeglo *et al.* also showed that the size of the spheroids was larger when Panc1 cells were cocultured with PSC in ULA plates and Norberg *et al.* showed that Panc1 cells proliferate more in 3D coculture with PSC [222,223]. These data indicate that CAFs are an essential cell population for tumor growth in the primary tumor and liver metastases. Here, only the size of spheroids was determined but to analyze the proliferation of PancTu1 and Panc89 cells in spheroid HMF culture, the amount of Ki67$^+$ cells, indicative for cell proliferation, should be determined by flow cytometry.

In spheroids larger than 300 µm oxygen, nutrients, and other soluble factors are not equally distributed and a gradient is formed, as is also seen in tumors [224]. Further, in spheroids larger than 500 µm, cells within the spheroid often undergo apoptosis and a necrotic core develops due to a gradient of nutrients and oxygen [224], explaining the slightly higher ccK18 levels in monocultured PancTu1 spheroids compared to monocultured Panc89 spheroids, as PancTu1 spheroids were larger.

As observed in the liver metastases, HMF exhibited higher PD-L1 expression compared to PDAC cells. Moreover, PD-L1 cell surface levels on HMF were altered in the presence of PDAC cells, and HMF were able to increase PD-L1 expression on PDAC cell lines. In line with these findings, Inoue *et al.* reported that patients with lung adenocarcinoma classified with a high expression of αSMA were PD-L1 positive suggesting a correlation between a high abundance of myofibroblasts and elevated PD-L1 expression.

Furthermore, CAFs have been shown to increase PD-L1 expression on different lung adenocarcinoma cell lines via CXCL2 secretion and signaling [225]. CXCL2 can activate the JAK-STAT signaling pathway, resulting in the upregulation of transcriptional factors that enhance the expression of PD-L1 [226]. Therefore, strong PD-L1 expression and high local abundance of myofibroblasts might be also mechanistically linked to hepatic PDAC metastases. In order to analyze the localization of PD-L1 within the spheroids, further studies should aim to embed spheroids and stain them for PD-L1, αSMA, and PanCK. Gorchs *et al*. also showed that CAFs isolated from tumor tissues of PDAC patients enhance the expression of immune checkpoint molecules, like PD-1 and CTLA-4, on $CD8^+$ and $CD4^+$ T cells [227]. However, here and in 2D cocultures the cell surface expression of PD-1 on $CD8^+$ T cells was neither affected by HSC nor HMF. In a PDAC mouse model, $CD8^+$ T cells that were located around large liver metastases showed higher PD-1 expression compared to those located around small metastases [57], further pointing to a role of the PD-L1/PD-1 axis in immune evasion of PDAC. Indeed, ccK18 levels were lower in supernatants of $CD8^+$ T cells cultured with PDAC coculture spheroids, particularly when a high amount of HMF was present in the spheroids, indicating a reduced PDAC cell death induction the more HMF are abundant. Majety *et al.* and Kuen *et al.* showed that coculture with fibroblasts enhanced the cell survival of PDAC cells, especially of PancTu1 cells, which was further enhanced in 3D culture [228,229]. This might also explain the reduced cell death, especially in HMF-enriched PancTu1 spheroids in this thesis. Moreover, as discussed earlier (section 5.4), hepatic stromal cells exhibited cell surface expression of PD-L1 and by binding to PD-1 on $CD8^+$ T cells, they are able to inhibit their killing abilities, explaining the reduced PDAC cell death under HMF coculture. However, blocking PD-L1 or PD-1 with Durvalumab or Pembrolizumab did not alter this. The effect of treatment with Durvalumab and Pembrolizumab will be discussed in section 5.7. Mollica and colleagues demonstrated in a 3D pancreatic tumor model that the infiltration of activated T cells was lower when cancer cells were cocultured with PSC compared to monoculture [230], giving another explanation for the reduced cell death in HMF-enriched spheroids.

Different PDAC cell lines express ECM proteins like collagen IV, collagen I, or fibronectin [231] and this expression was enhanced in 3D culture, with the peak on day 4 [218]. Kpeglo *et al.* showed that collagen I production was higher by PSC cocultured tumor cells, which was further enhanced by TGF-β1 stimulation [222]. The enhanced presence of collagen in the coculture of tumor cells and PSC was also seen by Ware *et al.* [219]. In this thesis, TGF-β1 concentration was higher in the supernatants of HMF-enriched PancTu1 cells (Supplementary Figure 15), compared to monocultured PancTu1 cells indicating that the amount of ECM might be higher in HMF-enriched spheroids, especially in those with PancTu1 cells, which in turn acts as a physical barrier for T cells. Therefore, the production of different ECM proteins should be analyzed in this model along with a more precise analysis of T cell infiltration within the spheroids.

All these mentioned factors may contribute to the reduced PDAC cell death in HMF-enriched spheroids under the presence of $CD8^+$ T cells.

Overall, 3D cultures and especially cocultures with different cell populations of the TME better reflect the situation in the primary tumor and liver metastases. However, 3D coculture settings with tumor cells, HMF, macrophages and PBMCs of the same patient would reflect the TME of the primary tumor and liver metastases even better. Accordingly, patient-derived cells should be used, especially analyzing different treatment options.

5.7 Treatment with Durvalumab or Pembrolizumab did not enhance the effector phenotype of $CD8^+$ T cells and did not induce higher tumor cell death in 3D cocultures

To investigate whether the PD-1/PD-L1 inhibitory axis is involved in the HMF-mediated impairment of $CD8^+$ T cells in the stroma-enriched PDAC spheroid models, treatment with the clinically validated PD-L1 and PD-1 inhibitors Durvalumab and Pembrolizumab, respectively, was performed. In line with results from recent clinical trials that tested the benefit of ICIs for the treatment of PDAC patients [232–234], neither Durvalumab nor Pembrolizumab treatment improved the effector phenotype of $CD8^+$ T cells and increased PDAC cell death in human stroma enriched 3D PDAC model. Thus, these findings support the view that the PD-1/PD-L1 axis is not a major regulator of T cell-mediated immunity in liver metastases of PDAC and rather indicate that other mechanisms are more relevant.

However, Lee and colleagues pointed out that the size of monoclonal antibodies targeting PD-1/PD-L1 is too large to penetrate the tumor tissue [145]. As discussed in section 5.6, spheroids are compact and therefore, Durvalumab and Pembrolizumab might not be able to penetrate. The inability to infiltrate the tumor tissue might be also a problem in the clinic and therefore Lee and colleagues suggested that developing smaller antibodies is necessary [145]. In this study, the successful blocking of PD-L1 and PD-1 on PancTu1 and Panc89 cells, HMF, and $CD8^+$ T cells by Durvalumab and Pembrolizumab, respectively, was confirmed in the 3D culture model. However, the question rises where PD-L1 is mainly expressed in the spheroid and if the successful blocking might be explained by the localization of PD-L1 on the border of the spheroids.

As mentioned above, ICI treatment with Durvalumab or Pembrolizumab did not enhance the effector phenotype of $CD8^+$ T cells and PDAC cell death was not increased. However, IHC staining revealed that PD-L1 is expressed in liver metastases of PDAC patients. Therefore, the question rises, which mechanisms might impact the resistance towards ICIs.

In NSCLC, it was shown that mutations in the *k-ras* gene were associated with higher resistance to ICIs [235]. PancTu1 cells show a mutation in the *k-ras* gene and even more relevant nearly all PDAC patients

show a mutation [24,153,154], which might explain that Durvalumab and Pembrolizumab treatment *in vitro* did not enhance PDAC cell death and further support the view of ICI resistance in PDAC patients. Furthermore, it has been shown that signaling via the tumor suppressor protein *p53* can upregulate expression of CD80 on tumor cells, which in turn causes T cell suppression via CTLA-4 signaling [236]. In around 70 % of PDAC patients, *p53* is mutated [20] and also both cell lines, used in this 3D culture model (PancTu1 and Panc89 cells) show mutations in the *p53* gene [153,154]. Further, Yazdanifar *et al*. showed that pancreatic cancer cells express Galectin-9, which can inhibit $CD8^+$ T cells by binding to TIM3 [237]. The expression of different mucins, like MUC1, MUC4, and MUC16, which are upregulated during cancer progression, may also inhibit apoptosis of tumor cells [238]. The membrane bound enzyme CD73 is expressed in many solid tumors, including PDAC, and it is known that CD73 can suppress T cells by generating adenosine [239–241]. Other reported mechanisms that enforce the resistance towards ICIs might be: downregulation of the MHCI complex resulting in less antigen recognition, loss of IFNγ sensitivity due to IFNγ receptor mutations or deletions, an immunosuppressive TME or upregulation of other immune checkpoint regulators (TIM3, LAG3, CTLA-4) [242]. Thus, the cell surface expression of other immune inhibitory receptors than PD-L1 should be analyzed on tumor cells, HMF, and $CD8^+$ T cells in this stroma enriched PDAC cell model. Another mediator of ICI resistance might be a hypoxic microenvironment. PDAC is a hypoxic tumor [243] and in other cancer entities tumor hypoxia has been identified as a physical and molecular driver of resistance towards PD-1 blockade [244,245]. Furthermore, Thomas *et al.* and Trapani *et al.* showed that TGF-β secreted by myofibroblasts inhibits $CD8^+$ T cells, especially the expression of genes encoding for cytotoxic effector molecules [207,211]. In our spheroid models, TGF-β1 level in supernatants of PancTu1 coculture spheroids was slightly elevated compared to the respective monoculture, especially in coculture spheroids containing the highest proportion of HMF, fitting together with the mostly reduced PDAC cell death under these conditions (Supplementary Figure 15). However, TGF-β1 levels were not altered in supernatants of Panc89 coculture spheroids, suggesting that also other mechanisms contribute to the impairment of the T cell effector phenotype. Besides Granzyme A/B, Perforin, Granulysin, and IFNγ, $CD8^+$ T cells secrete various other effector molecules by which they are able to induce cell death in their target cells. One of these mediators is FasL (CD95L), which binds to its membrane-bound receptor Fas (CD95) and, thereby, initiates caspase-mediated apoptosis. As mentioned in section 5.4 in 2D cocultures of $CD8^+$ T cells with HMF, FasL levels were slightly elevated in comparison to respective monocultured $CD8^+$ T cells, indicating that effector molecules like FasL might also play a role in our spheroid culture system. Rashid *et al*. showed that PDAC cell lines exhibit different cell surface levels of Fas, which can be altered by Gemcitabine [200]. However as discussed above, many PDAC cell lines show a high resistance toward CD95-induced apoptosis, including PancTu1 and Panc89 cells [201]. This

resistance can be linked to the expression of Fas-associated phosphatase 1 [246,247]. Moreover, PDAC cell lines like PancTu1 and Panc89 cells are also resistant towards TRAIL-induced apoptosis [201,248]. To summarize, there are several factors that may promote the inability of $CD8^+$ T cells to induce tumor cell death and which cannot be overcome by immune checkpoint blockade.

5.8 HMF-enriched spheroids are more resistant towards Gemcitabine

Since treatment with Gemcitabine still represents a frequent first-line therapy for PDAC patients with reduced general health status [25] and as more than half of the patients are diagnosed at over 70 years old [8], it was investigated how Gemcitabine impacts PD-L1 and PD-1 expression as well as the effector phenotype of $CD8^+$ T cells in the context of the PDAC cell-HMF interplay.

First, treatment with Gemcitabine for 24 h led to slightly higher cell surface levels of PD-L1 on PancTu1 spheroids but not on Panc89 spheroids and HMF. However, treatment with Gemcitabine in 2D led to higher elevated cell surface expression of PD-L1 on Panc89 and PancTu1 cells, pointing out that Gemcitabine cannot perfuse the spheroids, especially Panc89 spheroids, in line with the findings of Ware *et al.* showing that drug perfusion is reduced in spheroids, especially when cocultured with PSC [219].

However, although Gemcitabine is one of the first-line therapies for PDAC patients, it only slightly prolongs the overall survival [249]. One important reason for this is the often intrinsic or acquired resistance of PDAC cells which can be also seen in PDAC cell lines [250]. Accordingly, PancTu1 cells have been described as chemoresistant, as apoptosis could not or only slightly be induced by Gemcitabine [251].

This is in line with the findings in this study, in which treatment with Gemcitabine led to lower ccK18 levels in supernatants from PancTu1 spheroids compared to Panc89 spheroids. However, it has been shown that the inhibitory concentration of 50 % needs to be much higher for Gemcitabine in 3D cultures spheroids compared to 2D cultures, pointing out that the penetration is reduced in 3D culture [164,218,252], suggesting that the dense stroma in the primary and secondary site might also be a barrier for cytostatic drugs in PDAC patients.

Furthermore, sensitivity towards Gemcitabine treatment was reduced in both PancTu1 and Panc89 spheroids cocultured with HMF, underscoring the impact of myofibroblasts on the mediation of drug resistance in PDAC [253,254]. Firuzi *et al.* demonstrated that the response towards Gemcitabine was reduced when tumor cells were cocultured with PSC in a 3D culture model [255], which was also confirmed by Kpeglo *et al.,* where the cell viability of Panc1 cells was more reduced in monoculture compared to coculture with PSC after Gemcitabine treatment [222]. Moreover, Sasaki *et al.* pointed out that ATP-binding cassette subfamily G member 2 (ABCG2), which is a transporter involved in drug

excretion, is higher expressed in 3D compared to 2D culture and is associated with a higher resistance towards different cytostatic drugs. By additionally treating the cells with Verapamil, inhibiting transporters, cell viability was strongly reduced [256]. In another study, expression levels of other transporters, like ABCB1 or ABCC1 were increased in 3D cultures of PDAC cells [164].

Of note, pretreatment of Panc89 spheroids with Gemcitabine reversed the HMF-reduced PDAC cell death in the presence of $CD8^+$ T cells, although activation markers and release of cytotoxic molecules were decreased. Interestingly, the secretion of TGF-β1 was reduced in Panc89 spheroids pretreated with Gemcitabine compared to untreated spheroids, providing an explanation for the observed elevated PDAC cell death induction under these conditions (Supplementary Figure 16).

The reduced activation of $CD8^+$ T cells by Gemcitabine treatment was also seen by Smith *et al.* [257]. Of note, Gemcitabine treatment affected PD-L1 expression on PDAC cells and HMF in 3D culture only a little, but significantly diminished PD-1 surface levels on $CD8^+$ T cells. Considering this finding, Gemcitabine treatment might also affect the therapeutic efficiency of ICI treatment in PDAC patients, as $CD8^+$ T cells might be less inhibited by the binding of PD-L1 on PD-1, suggesting a combinational therapy.

5.9 Combinational treatment to overcome therapeutic resistance in PDAC

Immunotherapy has broadly impacted and revolutionized cancer treatment of several cancers [133]. However, ICIs have not yet added any considerable benefit to the treatment of PDAC patients [124,142], which was also seen *in vitro* in this study.

As outlined above, HMF showed high expression of PD-L1 and clearly exerted immunosuppressive effects on $CD8^+$ T cells, but this seemed to be independent of or at least not exclusively dependent on the PD-L1/PD-1 axis. Therefore, combinational therapeutic strategies simultaneously targeting different immune checkpoints or different tumor-promoting stromal cells or in combination with a cytostatic drug might be a more effective approach to overcome immunosuppression leading to tumor elimination of PDAC. Previous results showed that some tumor cells within the spheroid underwent apoptosis due to Gemcitabine treatment (data not shown) and the hypothesis was that combining Gemcitabine and ICIs might enhance tumor cell death by blocking PD-1 or PD-L1 to increase the activation of $CD8^+$ T cells.

However, in this thesis, combinational therapy of pre-treatment with Gemcitabine followed by treatment with Durvalumab or Pembrolizumab did not enhance the activation or effector phenotype of $CD8^+$ T cells and did not lead to enhanced PDAC cell death.

In an immunocompetent PDAC mouse model, Ho *et al.* showed that a combination of Gemcitabine treatment and anti-PD-1 antibody significantly reduced tumor sizes and enhanced infiltration of $CD8^+$

and $CD4^+$ T cells, leading to a longer survival of mice [258]. Principe *et al.* also showed in a transgenic PDAC mouse model that combinational treatment of Gemcitabine and anti-PD-1 antibody enhanced $CD8^+$ T cell response and prolonged the overall survival [259].

However, the combination of Pembrolizumab and Gemcitabine led to disease progression in all patients suffering from PDAC in a clinical phase I/II study [NCT02331251]. The response could be improved by combining Pembrolizumab with Gemcitabine and Nab-paclitaxel [NCT02331251] [144,260]. If PDAC patients are in good health condition, they receive FLORINOX, a combination of four different agents, which increased disease-free survival compared to Gemcitabine mono treatment [26], suggesting that a pre-treatment with a combination of different cytostatic drugs might be an option to enhance PDAC cell death

As already mentioned, the TME makes up 80-90 % of the whole tumor mass in PDAC [29]. Moreover, the TME is highly immunosuppressive and therefore many treatment options still fail in PDAC. On this account, it might be reasonable to target the TME. In a clinical phase I study, the combination of Nivolumab (blocking PD-1) and Mogamulizumab (T_{Reg} depleting CCR4 antibody) showed antitumor activity [NCT02476123] [261]. CAFs inhibit T cell infiltration by secretion of CXCL12 [172]. Bockorny and colleagues investigated the response towards the combinational treatment of Pembrolizumab and BL-8040 (antagonist of CXCR4) and most patients showed stable disease. Moreover, the TME changed due to the combinational treatment: more $CD8^+$ T cells infiltrated into the tumor, while less MDSCs and T_{Regs} were present [NCT02826486] [262]. TGF-β also plays a pivotal role in PDAC, including the suppression of immune cells, activation of HSC, and promoting therapy resistance, therefore blocking TGF-β1 in combination with ICIs might be an option [263]. In unresectable PDAC patients, combined treatment with a TGF-β blocking agent (Galunisertib) and Gemcitabine led to a better survival compared to Gemcitabine alone [264], however, the combination of Galunisertib with Durvalumab still led to a disease progression in most patients [NCT02734160] [265]. Interestingly, treatment with a TGF-β1 receptor inhibitor (LY364947) and an anti-PD-L1 antibody led to higher $CD8^+$ T cell infiltration and longer overall survival in a mouse model of colon adenocarcinoma, however, this effect was not seen in a KPC PDAC model [266].

Besides the PD-L1/PD-1 axis also other mechanisms might impair $CD8^+$ T cell-mediated tumor efficacy and the infiltration into the tumor. Infiltrating $CD8^+$ T cells express high levels of inhibitory receptors, like TIGIT, CTLA-4, PD-1, and TIM3 [184], suggesting that blocking other inhibitory receptors or a dual blocking might be a more effective option. Freed-Pastor *et al.* showed that the CD155/TIGIT axis promotes and maintains immune evasion in a PDAC mouse model and combinational therapy of targeting TIGIT, PD-1, and CD40a led to enhanced activation and higher infiltration of $CD8^+$ T cells [267]. This was also confirmed by Pearce *et al.*, who demonstrated that dual blocking of PD-1 and TIGIT led to a higher proliferation of T cells and enhanced secretion of IFNγ [268]. Both studies showed that

CD155 (ligand of TIGIT) is highly expressed in PDAC tumors, especially on tumor cells [267,268]. Based on their findings it is reasonable to investigate which regulatory molecules play a role in immune evasion of liver metastases in PDAC using multiplex staining.

6 Conclusion

This thesis revealed that the TME is remodeled during the progression of PDAC liver metastases. The localization and abundance of HMF, $CD8^+$ T cells and PD-L1 expression changed comparing small and large metastases. Moreover, PD-L1 is rather expressed by stromal cells, especially HMF and macrophages than tumor cells. The highly expression of PD-L1 in liver metastases, might indicate that PD-L1 mediated immune evasion operates during tumor progression and metastasis.

An established 3D culture spheroid model using two PDAC cell lines with different PD-L1 cell surface expressions and different ratios of HMF mimicked the proportion and distribution of PDAC cells and HMF as well as their PD-L1 expression observed in small and large hepatic PDAC metastases. HMF show high expression of PD-L1, which is in line with the *in situ* findings, and clearly exert immunosuppressive effects on $CD8^+$ T cells, but this seemed to be independent of or at least not exclusively dependent on the PD-L1/PD-1 axis, suggesting that immune evasion of PDAC liver metastases relies on other immunosuppressive mechanisms.

Therefore, combinational therapeutic strategies simultaneously targeting different immune checkpoints or different tumor promoting stromal cells, might be a more effective approach to overcome immunosuppression leading to tumor elimination of PDAC, as recently demonstrated in PDAC mouse models [269,270].

7 References

1. Sung H, Ferlay J, Siegel RL, Laversanne M, Soerjomataram I, Jemal A, Bray F. Global Cancer Statistics 2020: GLOBOCAN Estimates of Incidence and Mortality Worldwide for 36 Cancers in 185 Countries. CA Cancer J Clin. 2021 May 1;71(3):209–49. DOI: 10.3322/CAAC.21660
2. Bengtsson A, Andersson R, Ansari D. The actual 5-year survivors of pancreatic ductal adenocarcinoma based on real-world data. Sci Reports 2020 101. 2020 Oct 2;10(1):1–9. DOI: 10.1038/s41598-020-73525-y
3. Dalmartello M, La Vecchia C, Bertuccio P, Boffetta P, Levi F, Negri E, Malvezzi M. European cancer mortality predictions for the year 2022 with focus on ovarian cancer. Ann Oncol. 2022 Mar 1;33(3):330–9. DOI: 10.1016/J.ANNONC.2021.12.007
4. Becker AE, Hernandez YG, Frucht H, Lucas AL. Pancreatic ductal adenocarcinoma: Risk factors, screening, and early detection. World J Gastroenterol. 2014 Aug 8;20(32):11182. DOI: 10.3748/WJG.V20.I32.11182
5. Houg DS, Bijlsma MF. The hepatic pre-metastatic niche in pancreatic ductal adenocarcinoma [Internet]. Vol. 17, Molecular Cancer. BioMed Central Ltd.; 2018. p. 1–18. DOI: 10.1186/s12943-018-0842-9
6. Åkerberg D, Ansari D, Andersson R, Tingstedt B, Åkerberg D, Ansari D, Andersson R, Tingstedt B. The Effects of Surgical Exploration on Survival of Unresectable Pancreatic Carcinoma: A Retrospective Case-Control Study. J Biomed Sci Eng. 2017 Jan 19;10(1):1–9. DOI: 10.4236/JBISE.2017.101001
7. Tong J, Wu S, Lu C, Yang Y, Mao S, Lu C. Risk Factors of Early Liver Metastasis for Pancreatic Ductal Adenocarcinoma after Radical Resection. Gastroenterol Res Pract. 2022;2022. DOI: 10.1155/2022/8061879
8. Ilic M, Ilic I. Epidemiology of pancreatic cancer. World J Gastroenterol. 2016 Nov 11;22(44):9694. DOI: 10.3748/WJG.V22.I44.9694
9. Klein AP, Brune KA, Petersen GM, Goggins M, Tersmette AC, Offerhaus GJA, Griffin C, Cameron JL, Yeo CJ, Kern S, Hruban RH. Prospective risk of pancreatic cancer in familial pancreatic cancer kindreds. Cancer Res. 2004 Apr 1;64(7):2634–8. DOI: 10.1158/0008-5472.CAN-03-3823
10. J I, A R, J L, HT L, P M, P G, WD F, S A, A E, SL N, L S, CF S, P A, C KS, N T, E F, M L, S P, SA N. The incidence of pancreatic cancer in BRCA1 and BRCA2 mutation carriers. Br J Cancer. 2012;107(12). DOI: 10.1038/BJC.2012.483
11. Giardiello FM, Brensinger JD, Tersmette AC, Goodman SN, Petersen GM, Booker S V., Cruz-Correa M, Offerhaus JA. Very high risk of cancer in familial Peutz-Jeghers syndrome.

Gastroenterology. 2000 Dec 1;119(6):1447–53. DOI: 10.1053/gast.2000.20228

12. Singh RR, Klein AP, Sharma NR, O'Reilly EM. Does acute pancreatitis herald pancreatic ductal adenocarcinoma? A multicenter electronic health research network study. Cancer Med. 2023 Feb 1;12(3):2505–13. DOI: 10.1002/CAM4.5094
13. Gandhi S, De La Fuente J, Murad MH, Majumder S. Chronic Pancreatitis Is a Risk Factor for Pancreatic Cancer, and Incidence Increases With Duration of Disease: A Systematic Review and Meta-analysis. 2022; DOI: 10.14309/ctg.0000000000000463
14. Larsson SC, Orsini N, Wolk A. Body mass index and pancreatic cancer risk: A meta-analysis of prospective studies. Int J cancer. 2007 May 1;120(9):1993–8. DOI: 10.1002/IJC.22535
15. Bosetti C, Lucenteforte E, Silverman DT, Petersen G, Bracci PM, Ji BT, Negri E, Li D, Risch HA, Olson SH, Gallinger S, Miller AB, Bueno-de-Mesquita HB, Talamini R, Polesel J, Ghadirian P, Baghurst PA, Zatonski W, Fontham E, Bamlet WR, Holly EA, Bertuccio P, Gao YT, Hassan M, Yu H, Kurtz RC, Cotterchio M, Su J, Maisonneuve P, Duell EJ, Boffetta P, La Vecchia C. Cigarette smoking and pancreatic cancer: an analysis from the International Pancreatic Cancer Case-Control Consortium (Panc4). Ann Oncol. 2012;23(7):1880. DOI: 10.1093/ANNONC/MDR541
16. Hezel AF, Kimmelman AC, Stanger BZ, Bardeesy N, DePinho RA. Genetics and biology of pancreatic ductal adenocarcinoma. Genes Dev. 2006 May 15;20(10):1218–49. DOI: 10.1101/GAD.1415606
17. Collisson EA, Bailey P, Chang DK, Biankin A V. Molecular subtypes of pancreatic cancer. Nat Rev Gastroenterol Hepatol. 2019 Apr 1;16(4):207–20. DOI: 10.1038/S41575-019-0109-Y
18. Distler M, Aust D, Weitz J, Pilarsky C, Grützmann R. Precursor Lesions for Sporadic Pancreatic Cancer: PanIN, IPMN, and MCN. Biomed Res Int. 2014;2014. DOI: 10.1155/2014/474905
19. Hruban RH, Adsay NV, Albores-Saavedra J, Compton C, Garrett ES, Goodman SN, Kern SE, Klimstra DS, Klöppel G, Longnecker DS, Lüttges J, Offerhaus GJA. Pancreatic intraepithelial neoplasia: a new nomenclature and classification system for pancreatic duct lesions. Am J Surg Pathol. 2001;25(5):579–86. DOI: 10.1097/00000478-200105000-00003
20. Koorstra JBM, Feldmann G, Habbe N, Maitra A. Morphogenesis of pancreatic cancer: role of pancreatic intraepithelial neoplasia (PanINs). Langenbecks Arch Surg. 2008 Jul;393(4):561. DOI: 10.1007/S00423-008-0282-X
21. Hingorani SR, Petricoin EF, Maitra A, Rajapakse V, King C, Jacobetz MA, Ross S, Conrads TP, Veenstra TD, Hitt BA, Kawaguchi Y, Johann D, Liotta LA, Crawford HC, Putt ME, Jacks T, Wright CVE, Hruban RH, Lowy AM, Tuveson DA. Preinvasive and invasive ductal pancreatic cancer and its early detection in the mouse. Cancer Cell. 2003 Dec 1;4(6):437–50. DOI: 10.1016/S1535-6108(03)00309-X
22. Day JD, Digiuseppe JA, Yeo C, Lai-Goldman M, Anderson SM, Goodman SN, Kern SE, Hruban RH.

Immunohistochemical evaluation of HER-2/neu expression in pancreatic adenocarcinoma and pancreatic intraepithelial neoplasms. Hum Pathol. 1996;27(2):119–24. DOI: 10.1016/S0046-8177(96)90364-0

23. Shibata W, Kinoshita H, Hikiba Y, Sato T, Ishii Y, Sue S, Sugimori M, Suzuki N, Sakitani K, Ijichi H, Mori R, Endo I, Maeda S. Overexpression of HER2 in the pancreas promotes development of intraductal papillary mucinous neoplasms in mice. Sci Reports 2018 81. 2018 Apr 18;8(1):1–10. DOI: 10.1038/s41598-018-24375-2
24. Koorstra JBM, Hustinx SR, Offerhaus GJA, Maitra A. Pancreatic Carcinogenesis. Pancreatology. 2008;8(2):110. DOI: 10.1159/000123838
25. Principe DR, Underwood PW, Korc M, Trevino JG, Munshi HG, Rana A. The Current Treatment Paradigm for Pancreatic Ductal Adenocarcinoma and Barriers to Therapeutic Efficacy. Front Oncol. 2021 Jul 15;11:2773. DOI: 10.3389/FONC.2021.688377/BIBTEX
26. Conroy T, Hammel P, Hebbar M, Ben Abdelghani M, Wei AC, Raoul JL, Choné L, Francois E, Artru P, Biagi JJ, Lecomte T, Assenat E, Faroux R, Ychou M, Volet J, Sauvanet A, Breysacher G, Di Fiore F, Cripps C, Kavan P, Texereau P, Bouhier-Leporrier K, Khemissa-Akouz F, Legoux JL, Juzyna B, Gourgou S, O'Callaghan CJ, Jouffroy-Zeller C, Rat P, Malka D, Castan F, Bachet JB. FOLFIRINOX or Gemcitabine as Adjuvant Therapy for Pancreatic Cancer. N Engl J Med. 2018 Dec 20;379(25):2395–406. DOI: 10.1056/NEJMOA1809775/SUPPL_FILE/NEJMOA1809775_DATA-SHARING.PDF
27. Glimelius B, Hoffman K, Sjödén PO, Jacobsson G, Sellström H, Enander LK, Linné T, Svensson C. Chemotherapy improves survival and quality of life in advanced pancreatic and biliary cancer. Ann Oncol Off J Eur Soc Med Oncol. 1996;7(6):593–600. DOI: 10.1093/OXFORDJOURNALS.ANNONC.A010676
28. Heinemann V. Role of Gemcitabine in the Treatment of Advanced and Metastatic Breast Cancer. Oncology. 2003;64:191–206. DOI: 10.1159/000069315
29. Amrutkar M, Gladhaug IP. Pancreatic Cancer Chemoresistance to Gemcitabine. Cancers (Basel). 2017 Nov 16;9(11). DOI: 10.3390/CANCERS9110157
30. Aldag L, Beckinger S, Daunke T, Philipp LM, Surrow A, Yesilyurt UU, Wandmacher AM, Mehdorn AS, Sebens S. The Heterogeneity of the Tumor Microenvironment as Essential Determinant of Development, Progression and Therapy Response of Pancreatic Cancer. Cancers (Basel). 2021 Oct 1;13(19):4932. DOI: 10.3390/CANCERS13194932
31. Belgiovine C, Digifico E, Anfray C, Ummarino A, Andón FT. Targeting Tumor-Associated Macrophages in Anti-Cancer Therapies: Convincing the Traitors to Do the Right Thing. J Clin Med. 2020 Oct 1;9(10):1–24. DOI: 10.3390/JCM9103226
32. Helm O, Mennrich R, Petrick D, Goebel L, Freitag-Wolf S, Röder C, Kalthoff H, Röcken C, Sipos B,

Kabelitz D, Schäfer H, Oberg HH, Wesch D, Sebens S. Comparative Characterization of Stroma Cells and Ductal Epithelium in Chronic Pancreatitis and Pancreatic Ductal Adenocarcinoma. PLoS One. 2014 May 5;9(5):94357. DOI: 10.1371/JOURNAL.PONE.0094357

33. Lankadasari MB, Mukhopadhyay P, Mohammed S, Harikumar KB. TAMing pancreatic cancer: combat with a double edged sword. Mol Cancer. 2019 Mar 30;18(1). DOI: 10.1186/S12943-019-0966-6
34. Mills CD. M1 and M2 Macrophages: Oracles of Health and Disease. Crit Rev Immunol. 2012;32(6):463–88. DOI: 10.1615/CRITREVIMMUNOL.V32.I6.10
35. Rahn S, Krüger S, Mennrich R, Goebel L, Wesch D, Oberg HH, Vogel I, Ebsen M, Röcken C, Helm O, Sebens S. POLE Score: A comprehensive profiling of programmed death 1 ligand 1 expression in pancreatic ductal adenocarcinoma. Oncotarget. 2019 Feb 1;10(16):1572–88. DOI: 10.18632/oncotarget.26705
36. Hu H, Hang JJ, Han T, Zhuo M, Jiao F, Wang LW. The M2 phenotype of tumor-associated macrophages in the stroma confers a poor prognosis in pancreatic cancer. Tumor Biol. 2016 Jul 1;37(7):8657–64. DOI: 10.1007/S13277-015-4741-Z/TABLES/4
37. Sun Q, Zhang B, Hu Q, Qin Y, Xu W, Liu W, Yu X, Xu J. The impact of cancer-associated fibroblasts on major hallmarks of pancreatic cancer. Theranostics. 2018;8(18):5072. DOI: 10.7150/THNO.26546
38. Baum J, Duffy HS. Fibroblasts and Myofibroblasts: What are we talking about? J Cardiovasc Pharmacol. 2011 Apr;57(4):376. DOI: 10.1097/FJC.0B013E3182116E39
39. Wang D, Li Y, Ge H, Ghadban T, Reeh M, Güngör C. The Extracellular Matrix: A Key Accomplice of Cancer Stem Cell Migration, Metastasis Formation, and Drug Resistance in PDAC. Cancers (Basel). 2022 Aug 1;14(16). DOI: 10.3390/CANCERS14163998
40. Sperb N, Tsesmelis M, Wirth T. Crosstalk between Tumor and Stromal Cells in Pancreatic Ductal Adenocarcinoma. Int J Mol Sci. 2020 Aug 1;21(15):1–23. DOI: 10.3390/IJMS21155486
41. Öhlund D, Handly-Santana A, Biffi G, Elyada E, Almeida AS, Ponz-Sarvise M, Corbo V, Oni TE, Hearn SA, Lee EJ, Chio IIC, Hwang C Il, Tiriac H, Baker LA, Engle DD, Feig C, Kultti A, Egeblad M, Fearon DT, Crawford JM, Clevers H, Park Y, Tuveson DA. Distinct populations of inflammatory fibroblasts and myofibroblasts in pancreatic cancer. J Exp Med. 2017 Mar;214(3):579–96. DOI: 10.1084/jem.20162024
42. Öhlund D, Franklin O, Lundberg E, Lundin C, Sund M. Type IV collagen stimulates pancreatic cancer cell proliferation, migration, and inhibits apoptosis through an autocrine loop. BMC Cancer. 2013 Mar 26;13. DOI: 10.1186/1471-2407-13-154
43. Pickup MW, Mouw JK, Weaver VM. The extracellular matrix modulates the hallmarks of cancer. EMBO Rep. 2014 Dec;15(12):1243–53. DOI: 10.15252/EMBR.201439246

44. Ene-Obong A, Clear AJ, Watt J, Wang J, Fatah R, Riches JC, Marshall JF, Chin-Aleong J, Chelala C, Gribben JG, Ramsay AG, Kocher HM. Activated Pancreatic Stellate Cells Sequester CD8+ T-Cells to Reduce Their Infiltration of the Juxtatumoral Compartment of Pancreatic Ductal Adenocarcinoma. Gastroenterology. 2013;145(5):1121. DOI: 10.1053/J.GASTRO.2013.07.025

45. Gorchs L, Moro CF, Bankhead P, Kern KP, Sadeak I, Meng Q, Rangelova E, Kaipe H. Human pancreatic carcinoma-associated fibroblasts promote expression of co-inhibitory markers on CD4+ and CD8+ T-cells. Front Immunol. 2019;10(APR):847. DOI: 10.3389/FIMMU.2019.00847/FULL

46. Lakins MA, Ghorani E, Munir H, Martins CP, Shields JD. Cancer-associated fibroblasts induce antigen-specific deletion of CD8+ T Cells to protect tumour cells. Nat Commun. 2018 Dec 1;9(1). DOI: 10.1038/S41467-018-03347-0

47. Gok Yavuz B, Gunaydin G, Gedik ME, Kosemehmetoglu K, Karakoc D, Ozgur F, Guc D. Cancer associated fibroblasts sculpt tumour microenvironment by recruiting monocytes and inducing immunosuppressive PD-1 + TAMs. Sci Rep. 2019 Dec;9(1):1–15. DOI: 10.1038/s41598-019-39553-z

48. Yang X, Lin Y, Shi Y, Li B, Liu W, Yin W, Dang Y, Chu Y, Fan J, He R. FAP Promotes Immunosuppression by Cancer-Associated Fibroblasts in the Tumor Microenvironment via STAT3-CCL2 Signaling. Cancer Res. 2016 Jul 15;76(14):4124–35. DOI: 10.1158/0008-5472.CAN-15-2973

49. Zhang A, Qian Y, Ye Z, Chen H, Xie H, Zhou L, Shen Y, Zheng S. Cancer-associated fibroblasts promote M2 polarization of macrophages in pancreatic ductal adenocarcinoma. Cancer Med. 2017 Feb;6(2):463–70. DOI: 10.1002/cam4.993

50. Orimo A, Weinberg RA. Stromal fibroblasts in cancer: A novel tumor-promoting cell type. Vol. 5, Cell Cycle. Taylor and Francis Inc.; 2006. p. 1597–601. DOI: 10.4161/cc.5.15.3112

51. Guleng B, Tateishi K, Ohta M, Kanai F, Jazag A, Ijichi H, Tanaka Y, Washida M, Morikane K, Fukushima Y, Yamori T, Tsuruo T, Kawabe T, Miyagishi M, Taira K, Sata M, Omata M. Blockade of the stromal cell-derived factor-1/CXCR4 axis attenuates in vivo tumor growth by inhibiting angiogenesis in a vascular endothelial growth factor-independent manner. Cancer Res. 2005 Jul 1;65(13):5864–71. DOI: 10.1158/0008-5472.CAN-04-3833

52. Müerköster SS, Werbing V, Koch D, Sipos B, Ammerpohl O, Kalthoff H, Tsao MS, Fölsch UR, Schäfer H. Role of myofibroblasts in innate chemoresistance of pancreatic carcinoma--epigenetic downregulation of caspases. Int J cancer. 2008 Oct 15;123(8):1751–60. DOI: 10.1002/IJC.23703

53. Geismann C, Morscheck M, Koch D, Bergmann F, Ungefroren H, Arlt A, Tsao MS, Bachem MG, Altevogt P, Sipos B, Fölsch UR, Schäfer H, Müerköster SS. Up-regulation of L1CAM in pancreatic

duct cells is transforming growth factor beta1- and slug-dependent: role in malignant transformation of pancreatic cancer. Cancer Res. 2009 May 15;69(10):4517–26. DOI: 10.1158/0008-5472.CAN-08-3493

54. Schäfer H, Geismann C, Heneweer C, Egberts JH, Korniienko O, Kiefel H, Moldenhauer G, Bachem MG, Kalthoff H, Altevogt P, Sebens S. Myofibroblast-induced tumorigenicity of pancreatic ductal epithelial cells is L1CAM dependent. Carcinogenesis. 2012 Jan 1;33(1):84–93. DOI: 10.1093/CARCIN/BGR262
55. Kallies A, Zehn D, Utzschneider DT. Precursor exhausted T cells: key to successful immunotherapy? Nat Rev Immunol. 2020 Feb 1;20(2):128–36. DOI: 10.1038/S41577-019-0223-7
56. Daley D, Zambirinis CP, Seifert L, Akkad N, Mohan N, Werba G, Barilla R, Torres-Hernandez A, Hundeyin M, Mani VRK, Avanzi A, Tippens D, Narayanan R, Jang JE, Newman E, Pillarisetty VG, Dustin ML, Bar-Sagi D, Hajdu C, Miller G. γδ T Cells Support Pancreatic Oncogenesis by Restraining αβ T Cell Activation. Cell. 2016 Sep 9;166(6):1485. DOI: 10.1016/J.CELL.2016.07.046
57. Quaranta V, Rainer C, Nielsen SR, Raymant ML, Ahmed MS, Engle DD, Taylor A, Murray T, Campbell F, Palmer DH, Tuveson DA, Mielgo A, Schmid MC. Macrophage-derived granulin drives resistance to immune checkpoint inhibition in metastatic pancreatic cancer. Cancer Res. 2018 Aug 1;78(15):4253–69. DOI: 10.1158/0008-5472.CAN-17-3876
58. Geginat J, Paroni M, Maglie S, Alfen JS, Kastirr I, Gruarin P, de Simone M, Pagani M, Abrignani S. Plasticity of human CD4 T cell subsets. Front Immunol. 2014 Dec 16;5(DEC):630. DOI: 10.3389/FIMMU.2014.00630/BIBTEX
59. Bellone G, Turletti A, Artusio E, Mareschi K, Carbone A, Tibaudi D, Robecchi A, Emanuelli G, Rodeck U. Tumor-Associated Transforming Growth Factor-β andInterleukin-10 Contribute to a Systemic Th2 Immune Phenotype inPancreatic Carcinoma Patients. Am J Pathol. 1999;155(2):537. DOI: 10.1016/S0002-9440(10)65149-8
60. Romagnani S. T-cell subsets (Th1 versus Th2). Ann Allergy Asthma Immunol. 2000;85(1):9–18. DOI: 10.1016/S1081-1206(10)62426-X
61. Piro G, Simionato F, Carbone C, Frizziero M, Malleo G, Zanini S, Casolino R, Santoro R, Mina MM, Zecchetto C, Merz V, Scarpa A, Bassi C, Tortora G, Melisi D. A circulating TH2 cytokines profile predicts survival in patients with resectable pancreatic adenocarcinoma. Oncoimmunology. 2017 Sep 2;6(9). DOI: 10.1080/2162402X.2017.1322242
62. Tang Y, Xu X, Guo S, Zhang C, Tang Y, Tian Y, Ni B, Lu B, Wang H. An Increased Abundance of Tumor-Infiltrating Regulatory T Cells Is Correlated with the Progression and Prognosis of Pancreatic Ductal Adenocarcinoma. PLoS One. 2014 Mar 17;9(3). DOI: 10.1371/JOURNAL.PONE.0091551

63. Hiraoka N, Onozato K, Kosuge T, Hirohashi S. Prevalence of FOXP3+ regulatory T cells increases during the progression of pancreatic ductal adenocarcinoma and its premalignant lesions. Clin Cancer Res. 2006 Sep 15;12(18):5423–34. DOI: 10.1158/1078-0432.CCR-06-0369

64. Wang X, Lang M, Zhao T, Feng X, Zheng C, Huang C, Hao J, Dong J, Luo L, Li X, Lan C, Yu W, Yu M, Yang S, Ren H. Cancer-FOXP3 directly activated CCL5 to recruit FOXP3+Treg cells in pancreatic ductal adenocarcinoma. Oncogene. 2017 May 5;36(21):3048. DOI: 10.1038/ONC.2016.458

65. Shen T, Jia S, Ding G, Ping D, Zhou L, Zhou S, Cao L. BxPC-3-Derived Small Extracellular Vesicles Induce FOXP3+ Treg through ATM-AMPK-Sirtuins-Mediated FOXOs Nuclear Translocations. iScience. 2020 Aug 8;23(8). DOI: 10.1016/J.ISCI.2020.101431

66. Upadhrasta S, Zheng L. Strategies in Developing Immunotherapy for Pancreatic Cancer: Recognizing and Correcting Multiple Immune “Defects” in the Tumor Microenvironment. J Clin Med. 2019 Sep 16;8(9):1472. DOI: 10.3390/jcm8091472

67. Karamitopoulou E. The tumor microenvironment of pancreatic cancer [Internet]. Vol. 12, Cancers. MDPI AG; 2020. p. 1–4. DOI: 10.3390/cancers12103076

68. Germain RN. T-cell development and the CD4–CD8 lineage decision. Nat Rev Immunol 2002 25. 2002;2(5):309–22. DOI: 10.1038/nri798

69. Murphy K, Weaver C. Janeway Immunologie. 9th ed. Janeway Immunologie. Springer Berlin Heidelberg; 2018. DOI: 10.1007/978-3-662-56004-4

70. Hwang JR, Byeon Y, Kim D, Park SG. Recent insights of T cell receptor-mediated signaling pathways for T cell activation and development. Exp Mol Med 2020 525. 2020 May 21;52(5):750–61. DOI: 10.1038/s12276-020-0435-8

71. Rohrs JA, Wang P, Finley SD. Understanding the Dynamics of T-Cell Activation in Health and Disease Through the Lens of Computational Modeling. JCO Clin Cancer Informatics. 2019 Dec 28;(3):1–8. DOI: 10.1200/cci.18.00057

72. Chandler NJ, Call MJ, Call ME. T Cell Activation Machinery: Form and Function in Natural and Engineered Immune Receptors. Int J Mol Sci 2020, Vol 21, Page 7424. 2020 Oct 8;21(19):7424. DOI: 10.3390/IJMS21197424

73. Chen L, Flies DB. Molecular mechanisms of T cell co-stimulation and co-inhibition. Nat Rev Immunol. 2013 Apr;13(4):227. DOI: 10.1038/NRI3405

74. Jorgovanovic D, Song M, Wang L, Zhang Y. Roles of IFN-γ in tumor progression and regression: a review. Biomark Res 2020 81. 2020 Sep 29;8(1):1–16. DOI: 10.1186/S40364-020-00228-X

75. Peter ME, Hadji A, Murmann AE, Brockway S, Putzbach W, Pattanayak A, Ceppi P. The role of CD95 and CD95 ligand in cancer. Cell Death Differ 2015 224. 2015 Feb 6;22(4):549–59. DOI: 10.1038/cdd.2015.3

76. Ishida Y, Agata Y, Shibahara K, Honjo T. Induced expression of PD-1, a novel member of the immunoglobulin gene superfamily, upon programmed cell death. EMBO J. 1992;11(11):3887–95. DOI: 10.1002/J.1460-2075.1992.TB05481.X

77. Waldman AD, Fritz JM, Lenardo MJ. A guide to cancer immunotherapy: from T cell basic science to clinical practice. Nat Rev Immunol 2020 2011. 2020 May 20;20(11):651–68. DOI: 10.1038/s41577-020-0306-5

78. Akinleye A, Rasool Z. Immune checkpoint inhibitors of PD-L1 as cancer therapeutics. J Hematol Oncol. 2019 Sep 5;12(1):1–13. DOI: 10.1186/S13045-019-0779-5/TABLES/3

79. Dong H, Strome SE, Salomao DR, Tamura H, Hirano F, Flies DB, Roche PC, Lu J, Zhu G, Tamada K, Lennon VA, Cells E, Chen L. Tumor-associated B7-H1 promotes T-cell apoptosis: a potential mechanism of immune evasion. Nat Med. 2002;8(8):793–800. DOI: 10.1038/NM730

80. Rahn S. Characterization of programmed death ligand 1 expression and analyses of its immune-regulatory role in pancreatic ductal adenocarcinoma _____ Dissertation. 2019.

81. Sharpe AH, Pauken KE. The diverse functions of the PD1 inhibitory pathway. Nat Rev Immunol 2017 183. 2017 Nov 13;18(3):153–67. DOI: 10.1038/nri.2017.108

82. Talmadge JE, Fidler IJ. AACR Centennial Series: The Biology of Cancer Metastasis: Historical Perspective. Cancer Res. 2010 Jul 7;70(14):5649. DOI: 10.1158/0008-5472.CAN-10-1040

83. Hanahan D, Weinberg RA. Hallmarks of Cancer: The Next Generation. Cell. 2011;57(1):E41–6. DOI: 10.1016/j.cell.2011.02.013

84. Fares J, Fares MY, Khachfe HH, Salhab HA, Fares Y. Molecular principles of metastasis: a hallmark of cancer revisited. Signal Transduct Target Ther 2020 51. 2020 Mar 12;5(1):1–17. DOI: 10.1038/s41392-020-0134-x

85. Fidler IJ. The pathogenesis of cancer metastasis: the “seed and soil” hypothesis revisited. Nat Rev Cancer 2003 36. 2003 Jun;3(6):453–8. DOI: 10.1038/nrc1098

86. Kalluri R, Weinberg RA. The basics of epithelial-mesenchymal transition. J Clin Invest. 2009 Jun 6;119(6):1420. DOI: 10.1172/JCI39104

87. Le Bras GF, Taubenslag KJ, Andl CD. The regulation of cell-cell adhesion during epithelial-mesenchymal transition, motility and tumor progression. Cell Adh Migr. 2012 Jul 7;6(4):365. DOI: 10.4161/CAM.21326

88. Jing Y, Han Z, Zhang S, Liu Y, Wei L. Epithelial-Mesenchymal Transition in tumor microenvironment. Cell Biosci. 2011 Aug 31;1(1):29. DOI: 10.1186/2045-3701-1-29

89. Taki M, Abiko K, Ukita M, Murakami R, Yamanoi K, Yamaguchi K, Hamanishi J, Baba T, Matsumura N, Mandai M. Tumor immune microenvironment during epithelial- mesenchymal transition. Clin Cancer Res. 2021 Sep 1;27(17):4669–79. DOI: 10.1158/1078-0432.CCR-20-

4459/672159/AM/TUMOR-IMMUNE-MICROENVIRONMENT-DURING-EPITHELIAL

90. Smith LK, Boukhaled GM, Condotta SA, Mazouz S, Guthmiller JJ, Vijay R, Butler NS, Bruneau J, Shoukry NH, Krawczyk CM, Richer MJ. INTERLEUKIN-10 DIRECTLY INHIBITS CD8+ T CELL FUNCTION BY ENHANCING N-GLYCAN BRANCHING TO DECREASE ANTIGEN SENSITIVITY. Immunity. 2018 Feb 2;48(2):299. DOI: 10.1016/J.IMMUNI.2018.01.006
91. Alsuliman A, Colak D, Al-Harazi O, Fitwi H, Tulbah A, Al-Tweigeri T, Al-Alwan M, Ghebeh H. Bidirectional crosstalk between PD-L1 expression and epithelial to mesenchymal transition: Significance in claudin-low breast cancer cells. Mol Cancer. 2015 Aug 7;14(1):1–13. DOI: 10.1186/S12943-015-0421-2/FIGURES/5
92. Lou Y, Diao L, Cuentas ERP, Denning WL, Chen L, Fan YH, Byers LA, Wang J, Papadimitrakopoulou VA, Behrens C, Rodriguez JC, Hwu P, Wistuba II, Heymach J V., Gibbons DL. Epithelial-mesenchymal transition is associated with a distinct tumor microenvironment including elevation of inflammatory signals and multiple immune checkpoints in lung adenocarcinoma. Clin Cancer Res. 2016 Jul 15;22(14):3630–42. DOI: 10.1158/1078-0432.CCR-15-1434/268058/AM/EPITHELIAL-MESENCHYMAL-TRANSITION-IS-ASSOCIATED
93. Arumugam T, Ramachandran V, Fournier KF, Wang H, Marquis L, Abbruzzese JL, Gallick GE, Logsdon CD, McConkey DJ, Choi W. Epithelial to mesenchymal transition contributes to drug resistance in pancreatic cancer. Cancer Res. 2009 Jul 15;69(14):5820–8. DOI: 10.1158/0008-5472.CAN-08-2819
94. Leach J, Morton JP, Sansom OJ. Neutrophils: Homing in on the myeloid mechanisms of metastasis. Mol Immunol. 2019 Jun 1;110:69. DOI: 10.1016/J.MOLIMM.2017.12.013
95. Benson DD, Meng X, Fullerton DA, Moore EE, Lee JH, Ao L, Silliman CC, Barnett CC. Activation state of stromal inflammatory cells in murine metastatic pancreatic adenocarcinoma. Am J Physiol - Regul Integr Comp Physiol. 2012 May 5;302(9):R1067. DOI: 10.1152/AJPREGU.00320.2011
96. Valastyan S, Weinberg RA. Tumor Metastasis: Molecular Insights and Evolving Paradigms. Cell. 2011 Oct 10;147(2):275. DOI: 10.1016/J.CELL.2011.09.024
97. Strilic B, Offermanns S. Intravascular Survival and Extravasation of Tumor Cells. Cancer Cell. 2017 Sep 11;32(3):282–93. DOI: 10.1016/J.CCELL.2017.07.001
98. Lambert AW, Pattabiraman DR, Weinberg RA. Emerging Biological Principles of Metastasis. Cell. 2017 Feb 9;168(4):670–91. DOI: 10.1016/J.CELL.2016.11.037
99. Gomis RR, Gawrzak S. Tumor cell dormancy. Mol Oncol. 2017 Jul 6;11(1):62. DOI: 10.1016/J.MOLONC.2016.09.009
100. Giancotti FG. Mechanisms governing metastatic dormancy and reactivation. Cell. 2013 Nov 7;155(4):750. DOI: 10.1016/J.CELL.2013.10.029

101. Luzzi KJ, MacDonald IC, Schmidt EE, Kerkvliet N, Morris VL, Chambers AF, Groom AC. Multistep nature of metastatic inefficiency: dormancy of solitary cells after successful extravasation and limited survival of early micrometastases. Am J Pathol. 1998;153(3):865–73. DOI: 10.1016/S0002-9440(10)65628-3

102. Boulter L, Bullock E, Mabruk Z, Brunton VG. The fibrotic and immune microenvironments as targetable drivers of metastasis. Br J Cancer 2020 1241. 2020 Nov 26;124(1):27–36. DOI: 10.1038/s41416-020-01172-1

103. Yachida S, White CM, Naito Y, Zhong Y, Brosnan JA, Macgregor-Das AM, Morgan RA, Saunders T, Laheru DA, Herman JM, Hruban RH, Klein AP, Jones S, Velculescu V, Wolfgang CL, Iacobuzio-Donahue CA. Clinical significance of the genetic landscape of pancreatic cancer and implications for identification of potential long-term survivors. Clin Cancer Res. 2012 Nov 15;18(22):6339–47. DOI: 10.1158/1078-0432.CCR-12-1215

104. Qiu W, Sahin F, Iacobuzio-Donahue CA, Garcia-Carracedo D, Wang WM, Kuo CY, Chen D, Arking DE, Lowy AM, Hruban RH, Remotti HE, Su GH. Disruption of p16 and activation of Kras in pancreas increase ductal adenocarcinoma formation and metastasis in vivo. Oncotarget. 2011;2(11):862–73. DOI: 10.18632/ONCOTARGET.357

105. Muller PAJ, Caswell PT, Doyle B, Iwanicki MP, Tan EH, Karim S, Lukashchuk N, Gillespie DA, Ludwig RL, Gosselin P, Cromer A, Brugge JS, Sansom OJ, Norman JC, Vousden KH. Mutant p53 Drives Invasion by Promoting Integrin Recycling. Cell. 2009 Dec 24;139(7):1327–41. DOI: 10.1016/j.cell.2009.11.026

106. Bardeesy N, Cheng KH, Berger JH, Chu GC, Pahler J, Olson P, Hezel AF, Horner J, Lauwers GY, Hanahan D, DePinho RA. Smad4 is dispensable for normal pancreas development yet critical in progression and tumor biology of pancreas cancer. Genes Dev. 2006 Nov 15;20(22):3130–46. DOI: 10.1101/GAD.1478706

107. Yachida S, White CM, Naito Y, Zhong Y, Brosnan JA, Macgregor-Das AM, Morgan RA, Saunders T, Laheru DA, Herman JM, Hruban RH, Klein AP, Jones S, Velculescu V, Wolfgang CL, Iacobuzio-Donahue CA. Clinical Significance of the Genetic Landscape of Pancreatic Cancer and Implications for Identification of Potential Long Term Survivors. Clin Cancer Res. 2012 Nov 11;18(22):6339. DOI: 10.1158/1078-0432.CCR-12-1215

108. Yachida S, Jones S, Bozic I, Antal T, Leary R, Fu B, Kamiyama M, Hruban RH, Eshleman JR, Nowak MA, Velculescu VE, Kinzler KW, Vogelstein B, Iacobuzio-Donahue CA. Distant metastasis occurs late during the genetic evolution of pancreatic cancer. Nat 2010 4677319. 2010 Oct 27;467(7319):1114–7. DOI: 10.1038/nature09515

109. Rhim AD, Mirek ET, Aiello NM, Maitra A, Bailey JM, McAllister F, Reichert M, Beatty GL, Rustgi AK, Vonderheide RH, Leach SD, Stanger BZ. EMT and dissemination precede pancreatic tumor

formation. Cell. 2012 Jan 1;148(1–2):349. DOI: 10.1016/J.CELL.2011.11.025

110. Rhim AD, Thege FI, Santana SM, Lannin TB, Saha TN, Tsai S, Maggs LR, Kochman ML, Ginsberg GG, Lieb JG, Chandrasekhara V, Drebin JA, Ahmad N, Yang YX, Kirby BJ, Stanger BZ. Detection of Circulating Pancreas Epithelial Cells in Patients with Pancreatic Cystic Lesions. Gastroenterology. 2014;146(3):647. DOI: 10.1053/J.GASTRO.2013.12.007
111. Grünwald B, Harant V, Schaten S, Frühschütz M, Spallek R, Höchst B, Stutzer K, Berchtold S, Erkan M, Prokopchuk O, Martignoni M, Esposito I, Heikenwalder M, Gupta A, Siveke J, Saftig P, Knolle P, Wohlleber D, Krüger A. Pancreatic Premalignant Lesions Secrete Tissue Inhibitor of Metalloproteinases-1, Which Activates Hepatic Stellate Cells Via CD63 Signaling to Create a Premetastatic Niche in the Liver. Gastroenterology. 2016 Nov;151(5):1011-1024.e7. DOI: 10.1053/j.gastro.2016.07.043
112. Costa-Silva B, Aiello NM, Ocean AJ, Singh S, Zhang H, Thakur BK, Becker A, Hoshino A, Mark MT, Molina H, Xiang J, Zhang T, Theilen TM, García-Santos G, Williams C, Ararso Y, Huang Y, Rodrigues G, Shen TL, Labori KJ, Lothe IMB, Kure EH, Hernandez J, Doussot A, Ebbesen SH, Grandgenett PM, Hollingsworth MA, Jain M, Mallya K, Batra SK, Jarnagin WR, Schwartz RE, Matei I, Peinado H, Stanger BZ, Bromberg J, Lyden D. Pancreatic cancer exosomes initiate pre-metastatic niche formation in the liver. Nat Cell Biol. 2015 Jun 1;17(6):816. DOI: 10.1038/NCB3169
113. Nielsen SR, Quaranta V, Linford A, Emeagi P, Rainer C, Santos A, Ireland L, Sakai T, Sakai K, Kim YS, Engle D, Campbell F, Palmer D, Ko JH, Tuveson DA, Hirsch E, Mielgo A, Schmid MC. Macrophage-secreted granulin supports pancreatic cancer metastasis by inducing liver fibrosis. Nat Cell Biol. 2016 May 1;18(5):549–60. DOI: 10.1038/ncb3340
114. Groot VP, Gemenetzis G, Blair AB, Ding D, Javed AA, Burkhart RA, Yu J, Borel Rinkes IH, Molenaar IQ, Cameron JL, Fishman EK, Hruban RH, Weiss MJ, Wolfgang CL, He J. Implications of the Pattern of Disease Recurrence on Survival Following Pancreatectomy for Pancreatic Ductal Adenocarcinoma. Ann Surg Oncol. 2018 Aug 1;25(8):2475. DOI: 10.1245/S10434-018-6558-7
115. Trefts E, Gannon M, Wasserman DH. The liver. Curr Biol. 2017 Nov 11;27(21):R1147. DOI: 10.1016/J.CUB.2017.09.019
116. Ding C, Li Y, Guo F, Jiang Y, Ying W, Li D, Yang D, Xia X, Liu W, Zhao Y, He Y, Li X, Sun W, Liu Q, Song L, Zhen B, Zhang P, Qian X, Qin J, He F. A Cell-type-resolved Liver Proteome. Mol Cell Proteomics. 2016 Oct 1;15(10):3190. DOI: 10.1074/MCP.M116.060145
117. Nguyen-Lefebvre AT, Horuzsko A. Kupffer Cell Metabolism and Function. J Enzymol Metab. 2015;1(1).
118. Zhang CY, Yuan WG, He P, Lei JH, Wang CX. Liver fibrosis and hepatic stellate cells: Etiology, pathological hallmarks and therapeutic targets. World J Gastroenterol. 2016 Dec

12;22(48):10512. DOI: 10.3748/WJG.V22.I48.10512

119. Höchst B, Schildberg FA, Sauerborn P, Gäbel YA, Gevensleben H, Goltz D, Heukamp LC, Türler A, Ballmaier M, Gieseke F, Müller I, Kalff J, Kurts C, Knolle PA, Diehl L. Activated human hepatic stellate cells induce myeloid derived suppressor cells from peripheral blood monocytes in a CD44-dependent fashion. J Hepatol. 2013 Sep;59(3):528–35. DOI: 10.1016/J.JHEP.2013.04.033
120. Lenk L, Pein M, Will O, Gomez B, Viol F, Hauser C, Egberts JH, Gundlach JP, Helm O, Tiwari S, Weiskirchen R, Rose-John S, Röcken C, Mikulits W, Wenzel P, Schneider G, Saur D, Schäfer H, Sebens S. The hepatic microenvironment essentially determines tumor cell dormancy and metastatic outgrowth of pancreatic ductal adenocarcinoma. Oncoimmunology. 2018 Jan 2;7(1). DOI: 10.1080/2162402X.2017.1368603
121. Gabrilovich DI, Nagaraj S. Myeloid-derived suppressor cells as regulators of the immune system. Nat Rev Immunol 2009 93. 2009 Mar;9(3):162–74. DOI: 10.1038/nri2506
122. Weiskirchen R, Tacke F. Cellular and molecular functions of hepatic stellate cells in inflammatory responses and liver immunology. Hepatobiliary Surg Nutr. 2014;3(6):344. DOI: 10.3978/J.ISSN.2304-3881.2014.11.03
123. Carstens JL, De Sampaio PC, Yang D, Barua S, Wang H, Rao A, Allison JP, Le Bleu VS, Kalluri R. Spatial computation of intratumoral T cells correlates with survival of patients with pancreatic cancer. Nat Commun. 2017;8. DOI: 10.1038/NCOMMS15095
124. Brahmer JR, Tykodi SS, Chow LQM, Hwu WJ, Topalian SL, Hwu P, Drake CG, Camacho LH, Kauh J, Odunsi K, Pitot HC, Hamid O, Bhatia S, Martins R, Eaton K, Chen S, Salay TM, Alaparthy S, Grosso JF, Korman AJ, Parker SM, Agrawal S, Goldberg SM, Pardoll DM, Gupta A, Wigginton JM. Safety and Activity of Anti–PD-L1 Antibody in Patients with Advanced Cancer. N Engl J Med. 2012 Jun 6;366(26):2455. DOI: 10.1056/NEJMOA1200694
125. Chen DS, Mellman I. Oncology Meets Immunology: The Cancer-Immunity Cycle. Immunity. 2013 Jul 25;39(1):1–10. DOI: 10.1016/J.IMMUNI.2013.07.012
126. Kim SK, Cho SW. The Evasion Mechanisms of Cancer Immunity and Drug Intervention in the Tumor Microenvironment. Front Pharmacol. 2022 May 24;13. DOI: 10.3389/FPHAR.2022.868695
127. O'Donnell JS, Teng MWL, Smyth MJ. Cancer immunoediting and resistance to T cell-based immunotherapy. Nat Rev Clin Oncol 2018 163. 2018 Dec 6;16(3):151–67. DOI: 10.1038/s41571-018-0142-8
128. Gong R, Ren H. Targeting chemokines/chemokine receptors: a promising strategy for enhancing the immunotherapy of pancreatic ductal adenocarcinoma. Signal Transduct Target Ther. 2020 Dec 1;5(1). DOI: 10.1038/S41392-020-00267-8
129. Timmer FEF, Geboers B, Nieuwenhuizen S, Dijkstra M, Schouten EAC, Puijk RS, de Vries JJJ,

Petrousjka van den Tol M, Bruynzeel AME, Streppel MM, Wilmink JW, van der Vliet HJ, Meijerink MR, Scheffer HJ, de Gruijl TD. Pancreatic Cancer and Immunotherapy: A Clinical Overview. Cancers (Basel). 2021 Aug 2;13(16). DOI: 10.3390/CANCERS13164138

130. Pandha H, Rigg A, John J, Lemoine N. Loss of expression of antigen-presenting molecules in human pancreatic cancer and pancreatic cancer cell lines. Clin Exp Immunol. 2007 Apr;148(1):127. DOI: 10.1111/J.1365-2249.2006.03289.X
131. Yamamoto K, Venida A, Yano J, Biancur DE, Kakiuchi M, Gupta S, Sohn ASW, Mukhopadhyay S, Lin EY, Parker SJ, Banh RS, Paulo JA, Wen KW, Debnath J, Kim GE, Mancias JD, Fearon DT, Perera RM, Kimmelman AC. Autophagy promotes immune evasion of pancreatic cancer by degrading MHC-I. Nature. 2020 May 7;581(7806):100. DOI: 10.1038/S41586-020-2229-5
132. Saka D, Gökalp M, Piyade B, Cevik NC, Sever EA, Unutmaz D, Ceyhan GO, Demir IE, Asimgil H. Mechanisms of T-Cell Exhaustion in Pancreatic Cancer. Cancers (Basel). 2020 Aug 1;12(8):1–27. DOI: 10.3390/CANCERS12082274
133. Robert C. A decade of immune-checkpoint inhibitors in cancer therapy. Nat Commun 2020 111. 2020 Jul 30;11(1):1–3. DOI: 10.1038/s41467-020-17670-y
134. Upadhaya S, Neftelinov ST, Hodge J, Campbell J. Challenges and opportunities in the PD1/PDL1 inhibitor clinical trial landscape. Nat Rev Drug Discov. 2022 Jul 1;21(7):482–3. DOI: 10.1038/D41573-022-00030-4
135. Keytruda | European Medicines Agency [Internet].
136. CHMP. Imfinzi, INN-durvalumab.
137. Opdivo | European Medicines Agency [Internet].
138. Tecentriq | European Medicines Agency [Internet].
139. Rittmeyer A, Barlesi F, Waterkamp D, Park K, Ciardiello F, von Pawel J, Gadgeel SM, Hida T, Kowalski DM, Dols MC, Cortinovis DL, Leach J, Polikoff J, Barrios C, Kabbinavar F, Frontera OA, De Marinis F, Turna H, Lee JS, Ballinger M, Kowanetz M, He P, Chen DS, Sandler A, Gandara DR. Atezolizumab versus docetaxel in patients with previously treated non-small-cell lung cancer (OAK): a phase 3, open-label, multicentre randomised controlled trial. Lancet (London, England). 2017 Jan 1;389(10066):255. DOI: 10.1016/S0140-6736(16)32517-X
140. Powles T, O'Donnell PH, Massard C, Arkenau HT, Friedlander TW, Hoimes CJ, Lee JL, Ong M, Sridhar SS, Vogelzang NJ, Fishman MN, Zhang J, Srinivas S, Parikh J, Antal J, Jin X, Gupta AK, Ben Y, Hahn NM. Efficacy and Safety of Durvalumab in Locally Advanced or Metastatic Urothelial Carcinoma: Updated Results From a Phase 1/2 Open-label Study. JAMA Oncol. 2017 Sep 1;3(9). DOI: 10.1001/JAMAONCOL.2017.2411
141. Emens LA, Ascierto PA, Darcy PK, Demaria S, Eggermont AMM, Redmond WL, Seliger B, Marincola FM. Cancer immunotherapy: Opportunities and challenges in the rapidly evolving

clinical landscape. Eur J Cancer. 2017 Aug 1;81:116–29. DOI: 10.1016/J.EJCA.2017.01.035

142. Patnaik A, Kang SP, Rasco D, Papadopoulos KP, Elassaiss-Schaap J, Beeram M, Drengler R, Chen C, Smith L, Espino G, Gergich K, Delgado L, Daud A, Lindia JA, Nicole Li X, Pierce RH, Yearley JH, Wu D, Laterza O, Lehnert M, Iannone R, Tolcher AW. Phase I Study of Pembrolizumab (MK-3475; Anti-PD-1 Monoclonal Antibody) in Patients with Advanced Solid Tumors. Clin Cancer Res. 2015 Oct 1;21(19):4286–93. DOI: 10.1158/1078-0432.CCR-14-2607
143. Aglietta M, Barone C, Sawyer MB, Moore MJ, Miller WH, Bagalà C, Colombi F, Cagnazzo C, Gioeni L, Wang E, Huang B, Fly KD, Leone F. A phase I dose escalation trial of tremelimumab (CP-675,206) in combination with gemcitabine in chemotherapy-naive patients with metastatic pancreatic cancer. Ann Oncol Off J Eur Soc Med Oncol. 2014;25(9):1750–5. DOI: 10.1093/ANNONC/MDU205
144. Weiss GJ, Blaydorn L, Beck J, Bornemann-Kolatzki K, Urnovitz H, Schütz E, Khemka V. Phase Ib/II study of gemcitabine, nab-paclitaxel, and pembrolizumab in metastatic pancreatic adenocarcinoma. Invest New Drugs. 2018 Feb 1;36(1):96–102. DOI: 10.1007/S10637-017-0525-1
145. Lee HT, Lee JY, Lim H, Lee SH, Moon YJ, Pyo HJ, Ryu SE, Shin W, Heo YS. Molecular mechanism of PD-1/PD-L1 blockade via anti-PD-L1 antibodies atezolizumab and durvalumab. Sci Reports 2017 71. 2017 Jul 17;7(1):1–12. DOI: 10.1038/s41598-017-06002-8
146. Wang L, Ma Q, Chen X, Guo K, Li J, Zhang M. Clinical significance of B7-H1 and B7-1 expressions in pancreatic carcinoma. World J Surg. 2010 May 10;34(5):1059–65. DOI: 10.1007/S00268-010-0448-X/FIGURES/3
147. Hu Y, Chen W, Yan Z, Ma J, Zhu F, Huo J. Prognostic value of PD-L1 expression in patients with pancreatic cancer: A PRISMA-compliant meta-analysis. Medicine (Baltimore). 2019;98(3). DOI: 10.1097/MD.0000000000014006
148. Karamitopoulou E, Andreou A, de Mortanges AP, Tinguely M, Gloor B, Perren A. PD-1/PD-L1-Associated Immunoarchitectural Patterns Stratify Pancreatic Cancer Patients into Prognostic/Predictive Subgroups. Cancer Immunol Res. 2021 Dec 1;9(12):1439–50. DOI: 10.1158/2326-6066.CIR-21-0144/665773/AM/PD-1-PD-L1-ASSOCIATED-IMMUNOARCHITECTURAL-PATTERNS
149. Guillén-Ponce C, Blázquez J, González I, de-Madaria E, Montáns J, Carrato A. Diagnosis and staging of pancreatic ductal adenocarcinoma. Clin Transl Oncol. 2017 Oct 1;19(10):1205–16. DOI: 10.1007/S12094-017-1681-7
150. Ghaneh P, Costello E, Neoptolemos JP. Biology and management of pancreatic cancer. Postgrad Med J. 2008 Sep 1;84(995):478–97. DOI: 10.1136/GUT.2006.103333
151. Danilova L, Ho WJ, Zhu Q, Vithayathil T, De Jesus-Acosta A, Azad NS, Laheru DA, Fertig EJ, Anders

R, Jaffee EM, Yarchoan M. Programmed cell death ligand-1 (PD-L1) and CD8 expression profiling identify an immunologic subtype of pancreatic ductal adenocarcinomas with favorable survival. Cancer Immunol Res. 2019 Jun 1;7(6):886. DOI: 10.1158/2326-6066.CIR-18-0822

152. Qian J, Niu J, Li M, Chiao PJ, Tsao MS. In vitro modeling of human pancreatic duct epithelial cell transformation defines gene expression changes induced by K-ras oncogenic activation in pancreatic carcinogenesis. Cancer Res. 2005 Jun 15;65(12):5045–53. DOI: 10.1158/0008-5472.CAN-04-3208
153. Moore PS, Sipos B, Orlandini S, Sorio C, Real FX, Lemoine NR, Gress T, Bassi C, Klöppel G, Kalthoff H, Ungefroren H, Löhr M, Scarpa A. Genetic profile of 22 pancreatic carcinoma cell lines. Analysis of K-ras, p53, p16 and DPC4/Smad4. Virchows Arch. 2001;439(6):798–802. DOI: 10.1007/S004280100474
154. Sipos B, Möser S, Kalthoff H, Török V, Löhr M, Klöppel G. A comprehensive characterization of pancreatic ductal carcinoma cell lines: towards the establishment of an in vitro research platform. Virchows Arch. 2003 May 1;442(5):444–52. DOI: 10.1007/S00428-003-0784-4
155. Deer EL, González-Hernández J, Coursen JD, Shea JE, Ngatia J, Scaife CL, Firpo MA, Mulvihill SJ. Phenotype and Genotype of Pancreatic Cancer Cell Lines. Pancreas. 2010;39(4):425. DOI: 10.1097/MPA.0B013E3181C15963
156. Tan MH, Nowak NJ, Loor R, Ochi H, Sandberg AA, Lopez C, Pickren JW, Berjian R, Douglass HO, Chu TM. Characterization of a new primary human pancreatic tumor line. Cancer Invest. 1986;4(1):15–23. DOI: 10.3109/07357908609039823
157. Sun C, Yamato T, Furukawa T, Ohnishi Y, Kijima H, Horii A. Characterization of the mutations of the K-ras, p53, p16, and SMAD4 genes in 15 human pancreatic cancer cell lines. Oncol Rep. 2001;8(1):89–92. DOI: 10.3892/OR.8.1.89
158. Morgan RT, Woods LK, Moore GE, Quinn LA, McGavran L, Gordon SG. Human cell line (COLO 357) of metastatic pancreatic adenocarcinoma. Int J cancer. 1980;25(5):591–8. DOI: 10.1002/IJC.2910250507
159. Tawfik D, Zaccagnino A, Bernt A, Szczepanowski M, Klapper W, Schwab A, Kalthoff H, Trauzold A. The A818-6 system as an in-vitro model for studying the role of the transportome in pancreatic cancer. BMC Cancer. 2020 Mar 30;20(1):1–17. DOI: 10.1186/S12885-020-06773-W/TABLES/3
160. Lenk L, Pein M, Will O, Gomez B, Viol F, Hauser C, Egberts JH, Gundlach JP, Helm O, Tiwari S, Weiskirchen R, Rose-John S, Röcken C, Mikulits W, Wenzel P, Schneider G, Saur D, Schäfer H, Sebens S. The hepatic microenvironment essentially determines tumor cell dormancy and metastatic outgrowth of pancreatic ductal adenocarcinoma. Oncoimmunology. 2017 Jan 2;7(1). DOI: 10.1080/2162402X.2017.1368603

161. Sebens S, Miarka L, Hauser C, Helm O, Holdhof D, Beckinger S, Egberts JH, Gundlach JP, Lenk L, Rahn S, Mikulits W, Trauzold A. The hepatic microenvironment and trail-r2 impact outgrowth of liver metastases in pancreatic cancer after surgical resection. Cancers (Basel). 2019 Jun 1;11(6). DOI: 10.3390/cancers11060745

162. Fabian A, Stegner S, Miarka L, Zimmermann J, Lenk L, Rahn S, Buttlar J, Viol F, Knaack H, Esser D, Schäuble S, Großmann P, Marinos G, Häsler R, Mikulits W, Saur D, Kaleta C, Schäfer H, Sebens S. Metastasis of pancreatic cancer: An uninflamed liver micromilieu controls cell growth and cancer stem cell properties by oxidative phosphorylation in pancreatic ductal epithelial cells. Cancer Lett. 2019 Jul 1;453:95–106. DOI: 10.1016/J.CANLET.2019.03.039

163. Beckinger S, Daunke T, Aldag L, Krüger S, Heckl S, Wesch D, Schäfer H, Röcken C, Rahn S, Sebens S. Hepatic myofibroblasts exert immunosuppressive effects independent of the immune checkpoint regulator PD-L1 in liver metastasis of pancreatic ductal adenocarcinoma. Front Oncol. 2023 May 3;13. DOI: 10.3389/FONC.2023.1160824

164. Shichi Y, Gomi F, Sasaki N, Nonaka K, Arai T, Ishiwata T. Epithelial and Mesenchymal Features of Pancreatic Ductal Adenocarcinoma Cell Lines in Two- and Three-Dimensional Cultures. J Pers Med. 2022 May 1;12(5). DOI: 10.3390/JPM12050746/S1

165. Cha JH, Chan LC, Li CW, Hsu JL, Hung MC. Molecular Cell Review Mechanisms Controlling PD-L1 Expression in Cancer. Mol Cell. 2019;76:359–70. DOI: 10.1016/j.molcel.2019.09.030

166. Munz M, Baeuerle PA, Gires O. The emerging role of EpCAM in cancer and stem cell signaling. Cancer Res. 2009 Jul 15;69(14):5627–9. DOI: 10.1158/0008-5472.CAN-09-0654

167. Zitvogel L, Galluzzi L, Smyth MJ, Kroemer G. Mechanism of Action of Conventional and Targeted Anticancer Therapies: Reinstating Immunosurveillance. Immunity. 2013 Jul 25;39(1):74–88. DOI: 10.1016/J.IMMUNI.2013.06.014

168. Gotwals P, Cameron S, Cipolletta D, Cremasco V, Crystal A, Hewes B, Mueller B, Quaratino S, Sabatos-Peyton C, Petruzzelli L, Engelman JA, Dranoff G. Prospects for combining targeted and conventional cancer therapy with immunotherapy. Nat Rev Cancer 2017 175. 2017 Mar 24;17(5):286–301. DOI: 10.1038/nrc.2017.17

169. Cohen SJ, Alpaugh RK, Palazzo I, Meropol NJ, Rogatko A, Xu Z, Hoffman JP, Weiner LM, Cheng JD. Fibroblast activation protein and its relationship to clinical outcome in pancreatic adenocarcinoma. Pancreas. 2008 Aug;37(2):154–8. DOI: 10.1097/MPA.0B013E31816618CE

170. Kawase T, Yasui Y, Nishina S, Hara Y, Yanatori I, Tomiyama Y, Nakashima Y, Yoshida K, Kishi F, Nakamura M, Hino K. Fibroblast activation protein-aα-expressing fibroblasts promote the progression of pancreatic ductal adenocarcinoma. BMC Gastroenterol. 2015 Sep 2;15(1):1–9. DOI: 10.1186/S12876-015-0340-0/FIGURES/4

171. Biffi G, Tuveson DA. Diversity and Biology of Cancer-Associated Fibroblasts. Physiol Rev. 2021

Jan 1;101(1):147–76. DOI: 10.1152/physrev.00048.2019

172. Feig C, Jones JO, Kraman M, Wells RJB, Deonarine A, Chan DS, Connell CM, Roberts EW, Zhao Q, Caballero OL, Teichmann SA, Janowitz T, Jodrell DI, Tuveson DA, Fearon DT. Targeting CXCL12 from FAP-expressing carcinoma-associated fibroblasts synergizes with anti-PD-L1 immunotherapy in pancreatic cancer. Proc Natl Acad Sci U S A. 2013 Dec;110(50):20212–7. DOI: 10.1073/pnas.1320318110
173. Huseni MA, Wang L, Klementowicz JE, Yuen K, Breart B, Orr C, Liu LF, Li Y, Gupta V, Li C, Rishipathak D, Peng J, Xenbabaoğlu YS, Modrusan Z, Keerthivasan S, Madireddi S, Chen YJ, Fraser EJ, Leng N, Hamidi H, Koeppen H, Ziai J, Hashimoto K, Fassò M, Williams P, Mcdermott DF, Rosenberg JE, Powles T, Emens LA, Hegde PS, Mellman I, Turley SJ, Wilson MS, Mariathasan S, Molinero L, Merchant M, West NR. CD8 + T cell-intrinsic IL-6 signaling promotes resistance to anti-PD-L1 immunotherapy ll CD8 + T cell-intrinsic IL-6 signaling promotes resistance to anti-PD-L1 immunotherapy. Cell Reports Med. 2023;4:100878. DOI: 10.1016/j.xcrm.2022.100878
174. Pickup MW, Mouw JK, Weaver VM. The extracellular matrix modulates the hallmarks of cancer. EMBO Rep. 2014 Dec;15(12):1243–53. DOI: 10.15252/embr.201439246
175. Kobayashi S, Seki S, Kawada N, Morikawa H, Nakatani K, Uyama N, Ikeda K, Nakajima Y, Arakawa T, Kaneda K. Apoptosis of T cells in the hepatic fibrotic tissue of the rat: A possible inducing role of hepatic myofibroblast-like cells. Cell Tissue Res. 2003 Mar 1;311(3):353–64. DOI: 10.1007/S00441-002-0670-4/FIGURES/11
176. Grout JA, Sirven P, Leader AM, Maskey S, Hector E, Puisieux I, Steffan F, Cheng E, Tung N, Maurin M, Vaineau R, Karpf L, Plaud M, Begue AL, Ganesh K, Mesple J, Casanova-Acebes M, Tabachnikova A, Keerthivasan S, Lansky A, Le Berichel J, Walker L, Rahman AH, Gnjatic S, Girard N, Lefevre M, Damotte D, Adam J, Martin JC, Wolf A, Flores RM, Beasley MB, Pradhan R, Muller S, Marron TU, Turley SJ, Merad M, Kenigsberg E, Salmon H. Spatial Positioning and Matrix Programs of Cancer-Associated Fibroblasts Promote T-cell Exclusion in Human Lung Tumors. Cancer Discov. 2022 Nov 1;12(11):2606–25. DOI: 10.1158/2159-8290.CD-21-1714
177. Lin YN, Schmidt MO, Sharif GM, Vietsch EE, Kiliti AJ, Barefoot ME, Riegel AT, Wellstein A. Impaired CXCL12 signaling contributes to resistance of pancreatic cancer subpopulations to T cell-mediated cytotoxicity. Oncoimmunology. 2022;11(1). DOI: 10.1080/2162402X.2022.2027136
178. Maddalena M, Mallel G, Nataraj NB, Shreberk-Shaked M, Hassin O, Mukherjee S, Arandkar S, Rotkopf R, Kapsack A, Lambiase G, Pellegrino B, Ben-Isaac E, Golani O, Addadi Y, Hajaj E, Eilam R, Straussman R, Yarden Y, Lotem M, Oren M. TP53 missense mutations in PDAC are associated with enhanced fibrosis and an immunosuppressive microenvironment. Proc Natl Acad Sci U S A. 2021 Apr 29;118(23). DOI: 10.1073/PNAS.2025631118/-/DCSUPPLEMENTAL

179. Beatty GL, Winograd R, Evans RA, Long KB, Luque SL, Lee JW, Clendenin C, Gladney WL, Knoblock DM, Guirnalda PD, Vonderheide RH. Exclusion of T Cells From Pancreatic Carcinomas in Mice is Regulated by Ly6Clow F4/80+ Extra-tumor Macrophages. Gastroenterology. 2015 Jul 1;149(1):201. DOI: 10.1053/J.GASTRO.2015.04.010

180. Peranzoni E, Lemoine J, Vimeux L, Feuillet V, Barrin S, Kantari-Mimoun C, Bercovici N, Guérin M, Biton J, Ouakrim H, Régnier F, Lupo A, Alifano M, Damotte D, Donnadieu E. Macrophages impede CD8 T cells from reaching tumor cells and limit the efficacy of anti–PD-1 treatment. Proc Natl Acad Sci U S A. 2018 Apr 24;115(17):E4041–50. DOI: 10.1073/PNAS.1720948115/SUPPL_FILE/PNAS.1720948115.SM08.AVI

181. Ahmadzadeh M, Johnson LA, Heemskerk B, Wunderlich JR, Dudley ME, White DE, Rosenberg SA. Tumor antigen–specific CD8 T cells infiltrating the tumor express high levels of PD-1 and are functionally impaired. Blood. 2009 Aug 8;114(8):1537. DOI: 10.1182/BLOOD-2008-12-195792

182. Iwai Y, Terawaki S, Ikegawa M, Okazaki T, Honjo T. PD-1 Inhibits Antiviral Immunity at the Effector Phase in the Liver. J Exp Med. 2003 Jul 7;198(1):39. DOI: 10.1084/JEM.20022235

183. Zajac AJ, Blattman JN, Murali-Krishna K, Sourdive DJD, Suresh M, Altman JD, Ahmed R. Viral Immune Evasion Due to Persistence of Activated T Cells Without Effector Function. J Exp Med. 1998 Dec 21;188(12):2205–13. DOI: 10.1084/JEM.188.12.2205

184. Steele NG, Carpenter ES, Kemp SB, Sirihorachai VR, The S, Delrosario L, Lazarus J, Amir E ad D, Gunchick V, Espinoza C, Bell S, Harris L, Lima F, Irizarry-Negron V, Paglia D, Macchia J, Chu AKY, Schofield H, Wamsteker EJ, Kwon R, Schulman A, Prabhu A, Law R, Sondhi A, Yu J, Patel A, Donahue K, Nathan H, Cho C, Anderson MA, Sahai V, Lyssiotis CA, Zou W, Allen BL, Rao A, Crawford HC, Bednar F, Frankel TL, Pasca di Magliano M. Multimodal Mapping of the Tumor and Peripheral Blood Immune Landscape in Human Pancreatic Cancer. Nat cancer. 2020 Nov 1;1(11):1097. DOI: 10.1038/S43018-020-00121-4

185. Chow A, Perica K, Klebanoff CA, Wolchok JD. Clinical implications of T cell exhaustion for cancer immunotherapy. Nat Rev Clin Oncol 2022 1912. 2022 Oct 10;19(12):775–90. DOI: 10.1038/s41571-022-00689-z

186. Saka D, Gökalp M, Piyade B, Cevik NC, Sever EA, Unutmaz D, Ceyhan GO, Demir IE, Asimgil H. Mechanisms of t-cell exhaustion in pancreatic cancer [Internet]. Vol. 12, Cancers. MDPI AG; 2020. p. 1–27. DOI: 10.3390/cancers12082274

187. Fourcade J, Sun Z, Pagliano O, Guillaume P, Luescher IF, Sander C, Kirkwood JM, Olive D, Kuchroo V, Zarour HM. CD8 + T cells specific for tumor antigens can be rendered dysfunctional by the tumor microenvironment through upregulation of the inhibitory receptors BTLA and PD-1. Cancer Res. 2012 Feb 15;72(4):887–96. DOI: 10.1158/0008-5472.CAN-11-2637/650035/AM/CD8-T-CELLS-SPECIFIC-FOR-TUMOR-ANTIGENS-CAN-BE

188. Zhang Z, Liu S, Zhang B, Qiao L, Zhang Y, Zhang Y. T Cell Dysfunction and Exhaustion in Cancer. Front Cell Dev Biol. 2020 Feb 11;8:17. DOI: 10.3389/FCELL.2020.00017

189. Jiang Y, Li Y, Zhu B. T-cell exhaustion in the tumor microenvironment. Cell Death Dis 2015 66. 2015 Jun 18;6(6):e1792–e1792. DOI: 10.1038/cddis.2015.162

190. Reddy M, Eirikis E, Davis C, Davis HM, Prabhakar U. Comparative analysis of lymphocyte activation marker expression and cytokine secretion profile in stimulated human peripheral blood mononuclear cell cultures: an in vitro model to monitor cellular immune function. J Immunol Methods. 2004 Oct 1;293(1–2):127–42. DOI: 10.1016/J.JIM.2004.07.006

191. Diskin B, Adam S, Cassini MF, Sanchez G, Liria M, Aykut B, Buttar C, Li E, Sundberg B, Salas RD, Chen R, Wang J, Kim M, Farooq MS, Nguy S, Fedele C, Tang KH, Chen T, Wang W, Hundeyin M, Rossi JAK, Kurz E, Haq MIU, Karlen J, Kruger E, Sekendiz Z, Wu D, Shadaloey SAA, Baptiste G, Werba G, Selvaraj S, Loomis C, Wong KK, Leinwand J, Miller G. PD-L1 engagement on T cells promotes self-tolerance and suppression of neighboring macrophages and effector T cells in cancer. Nat Immunol 2020 214. 2020 Mar 9;21(4):442–54. DOI: 10.1038/s41590-020-0620-x

192. Carter LL, Fouser LA, Jussif J, Fitz L, Deng B, Wood CR, Collins M, Honjo T, Freeman GJ, Carreno BM. PD-1:PD-L inhibitory pathway affects both CD4 + and CD8 + T cells and is overcome by IL-2. DOI: 10.1002/1521-4141

193. Thompson CB, Lindsten T, Ledbetter JA, Kunkel SL, Young HA, Emerson SG, Leiden JM, June CH. CD28 activation pathway regulates the production of multiple T-cell-derived lymphokines/cytokines. Proc Natl Acad Sci U S A. 1989;86(4):1333–7. DOI: 10.1073/PNAS.86.4.1333

194. Yang ZZ, Grote DM, Xiu B, Ziesmer SC, Price-Troska TL, Hodge LS, Yates DM, Novak AJ, Ansell SM. TGF-β upregulates CD70 expression and induces exhaustion of effector memory T cells in B-cell non-Hodgkin's lymphoma. Leukemia. 2014;28(9):1872. DOI: 10.1038/LEU.2014.84

195. Ravi VM, Neidert N, Will P, Joseph K, Maier JP, Kückelhaus J, Vollmer L, Goeldner JM, Behringer SP, Scherer F, Boerries M, Follo M, Weiss T, Delev D, Kernbach J, Franco P, Schallner N, Dierks C, Carro MS, Hofmann UG, Fung C, Sankowski R, Prinz M, Beck J, Salié H, Bengsch B, Schnell O, Heiland DH. T-cell dysfunction in the glioblastoma microenvironment is mediated by myeloid cells releasing interleukin-10. Nat Commun. 2022 Dec 1;13(1). DOI: 10.1038/S41467-022-28523-1

196. Wolfraim LA, Walz TM, James Z, Fernandez T, Letterio JJ. p21Cip1 and p27Kip1 act in synergy to alter the sensitivity of naive T cells to TGF-beta-mediated G1 arrest through modulation of IL-2 responsiveness. J Immunol. 2004 Sep 1;173(5):3093–102. DOI: 10.4049/JIMMUNOL.173.5.3093

197. Dahmani A, Delisle JS. TGF-β in T Cell Biology: Implications for Cancer Immunotherapy. Cancers

(Basel). 2018 Jun 11;10(6). DOI: 10.3390/CANCERS10060194

198. Principe DR, Underwood PW, Kumar S, Timbers KE, Koch RM, Trevino JG, Munshi HG, Rana A. Loss of SMAD4 Is Associated With Poor Tumor Immunogenicity and Reduced PD-L1 Expression in Pancreatic Cancer. Front Oncol. 2022 Jan 28;12:1. DOI: 10.3389/FONC.2022.806963/FULL
199. Chen S, Crabill GA, Pritchard TS, McMiller TL, Wei P, Pardoll DM, Pan F, Topalian SL. Mechanisms regulating PD-L1 expression on tumor and immune cells. J Immunother Cancer. 2019 Nov 15;7(1). DOI: 10.1186/s40425-019-0770-2
200. Rashid K, Röder C, Goumas F, Egberts JH, Kalthoff H. CD95L inhibition impacts gemcitabine-mediated effects and non-apoptotic signaling of tnf-α and trail in pancreatic tumor cells. Cancers (Basel). 2021 Nov 1;13(21):5458. DOI: 10.3390/CANCERS13215458/S1
201. Trauzold A, Schmiedel S, Röder C, Tams C, Christgen M, Oestern S, Arlt A, Westphal S, Kapischke M, Ungefroren H, Kalthoff H. Multiple and synergistic deregulations of apoptosis-controlling genes in pancreatic carcinoma cells. Br J Cancer. 2003 Nov 11;89(9):1714. DOI: 10.1038/SJ.BJC.6601330
202. Ouyang H, Mou LJ, Luk C, Liu N, Karaskova J, Squire J, Tsao MS. Immortal Human Pancreatic Duct Epithelial Cell Lines with Near Normal Genotype and Phenotype. Am J Pathol. 2000;157(5):1623. DOI: 10.1016/S0002-9440(10)64800-6
203. Marino J, Paster J, Benichou G. Allorecognition by T lymphocytes and allograft rejection. Front Immunol. 2016 Dec 14;7(DEC):582. DOI: 10.3389/FIMMU.2016.00582/BIBTEX
204. Zhao W, Su W, Kuang P, Zhang L, Liu J, Yin Z, Wang X. The role of hepatic stellate cells in the regulation of T-cell function and the promotion of hepatocellular carcinoma. Int J Oncol. 2012 Aug;41(2):457. DOI: 10.3892/IJO.2012.1497
205. Charles R, Chou HS, Wang L, Fung JJ, Lu L, Qian S. Human Hepatic Stellate Cells Inhibit T cell Response through B7-H1 Pathway. Transplantation. 2013 Jul 7;96(1):17. DOI: 10.1097/TP.0B013E318294CAAE
206. Yu MC, Chen CH, Liang X, Wang L, Gandhi CR, Fung JJ, Lu L, Qian S. Inhibition of T-cell responses by hepatic stellate cells via B7-H1-mediated T-cell apoptosis in mice. Hepatology. 2004 Dec;40(6):1312–21. DOI: 10.1002/HEP.20488
207. Thomas DA, Massagué J. TGF-beta directly targets cytotoxic T cell functions during tumor evasion of immune surveillance. Cancer Cell. 2005;8(5):369–80. DOI: 10.1016/J.CCR.2005.10.012
208. Kato T, Noma K, Ohara T, Kashima H, Katsura Y, Sato H, Komoto S, Katsube R, Ninomiya T, Tazawa H, Shirakawa Y, Fujiwara T. Cancer-associated fibroblasts affect intratumoral CD8þ and Foxp3þ T cells via IL6 in the tumor microenvironment. Clin Cancer Res. 2018 Oct 1;24(19):4820–33. DOI: 10.1158/1078-0432.CCR-18-0205/72949/AM/CANCER-ASSOCIATED-FIBROBLASTS-

AFFECT-INTRATUMORAL

209. Zhao Y, Lee CK, Lin CH, Gassen RB, Xu X, Huang Z, Xiao C, Bonorino C, Lu LF, Bui JD, Hui E. PD-L1:CD80 Cis-Heterodimer Triggers the Co-stimulatory Receptor CD28 While Repressing the Inhibitory PD-1 and CTLA-4 Pathways. Immunity. 2019 Dec 12;51(6):1059. DOI: 10.1016/J.IMMUNI.2019.11.003
210. Sugiura D, Maruhashi T, Okazaki IM, Shimizu K, Maeda TK, Takemoto T, Okazaki T. Restriction of PD-1 function by cis-PD-L1/CD80 interactions is required for optimal T cell responses. Science. 2019;364(6440):558–66. DOI: 10.1126/SCIENCE.AAV7062
211. Trapani JA. The dual adverse effects of TGF-beta secretion on tumor progression. Cancer Cell. 2005;8(5):349–50. DOI: 10.1016/J.CCR.2005.10.018
212. Jensen C, Teng Y. Is It Time to Start Transitioning From 2D to 3D Cell Culture? Front Mol Biosci. 2020 Mar 6;7:33. DOI: 10.3389/FMOLB.2020.00033/BIBTEX
213. Anton D, Burckel H, Josset E, Noel G. Three-Dimensional Cell Culture: A Breakthrough in Vivo. Int J Mol Sci. 2015 Mar 11;16(3):5517. DOI: 10.3390/IJMS16035517
214. Habanjar O, Diab-Assaf M, Caldefie-Chezet F, Delort L. 3D Cell Culture Systems: Tumor Application, Advantages, and Disadvantages. Int J Mol Sci. 2021 Nov 1;22(22). DOI: 10.3390/IJMS222212200
215. Langhans SA. Three-Dimensional in Vitro Cell Culture Models in Drug Discovery and Drug Repositioning. Front Pharmacol. 2018 Jan 23;9(JAN):6. DOI: 10.3389/FPHAR.2018.00006
216. Guzzeloni V, Veschini L, Pedica F, Ferrero E, Ferrarini M. 3D Models as a Tool to Assess the Anti-Tumor Efficacy of Therapeutic Antibodies: Advantages and Limitations. Antibodies. 2022 Sep 1;11(3). DOI: 10.3390/ANTIB11030046
217. Gaviraghi M, Tunici P, Valensin S, Rossi M, Giordano C, Magnoni L, Dandrea M, Montagna L, Ritelli R, Scarpa A, Bakker A. Pancreatic cancer spheres are more than just aggregates of stem marker-positive cells. Biosci Rep. 2011 Feb 1;31(1):45–55. DOI: 10.1042/BSR20100018
218. Longati P, Jia X, Eimer J, Wagman A, Witt MR, Rehnmark S, Verbeke C, Toftgård R, Löhr M, Heuchel RL. 3D pancreatic carcinoma spheroids induce a matrix-rich, chemoresistant phenotype offering a better model for drug testing. BMC Cancer. 2013 Feb 27;13:95. DOI: 10.1186/1471-2407-13-95
219. Ware MJ, Keshishian V, Law JJ, Ho JC, Favela CA, Rees P, Smith B, Mohammad S, Hwang RF, Rajapakshe K, Coarfa C, Huang S, Edwards DP, Corr SJ, Godin B, Curley SA. Generation of an in vitro 3D PDAC stroma rich spheroid model. Biomaterials. 2016 Nov 1;108:129. DOI: 10.1016/J.BIOMATERIALS.2016.08.041
220. Zeeberg K, Cardone RA, Greco MR, Saccomano M, Nøhr-Nielsen A, Alves F, Pedersen SF, Reshkin SJ. Assessment of different 3D culture systems to study tumor phenotype and chemosensitivity

in pancreatic ductal adenocarcinoma. Int J Oncol. 2016 Jul 1;49(1):243–52. DOI: 10.3892/IJO.2016.3513/HTML

221. Sun Q, Zhang B, Hu Q, Qin Y, Xu W, Liu W, Yu X, Xu J. The impact of cancer-associated fibroblasts on major hallmarks of pancreatic cancer. Theranostics. 2018;8(18):5072. DOI: 10.7150/THNO.26546
222. Kpeglo D, Hughes MDG, Dougan L, Haddrick M, Knowles MA, Evans SD, Peyman SA. Modeling the mechanical stiffness of pancreatic ductal adenocarcinoma. Matrix Biol Plus. 2022 Jun 1;14. DOI: 10.1016/J.MBPLUS.2022.100109
223. Norberg KJ, Liu X, Fernández Moro C, Strell C, Nania S, Blümel M, Balboni A, Bozóky B, Heuchel RL, Löhr JM. A novel pancreatic tumour and stellate cell 3D co-culture spheroid model. BMC Cancer. 2020 May 27;20(1):1–13. DOI: 10.1186/S12885-020-06867-5/FIGURES/7
224. Narayanan S, Vicent S, Ponz-Sarvisé M. PDAC as an Immune Evasive Disease: Can 3D Model Systems Aid to Tackle This Clinical Problem? Front Cell Dev Biol. 2021 Dec 10;9. DOI: 10.3389/FCELL.2021.787249
225. Inoue C, Miki Y, Saito R, Hata S, Abe J, Sato I, Okada Y, Sasano H. PD-L1 Induction by Cancer-Associated Fibroblast-Derived Factors in Lung Adenocarcinoma Cells. Cancers (Basel). 2019 Sep 1;11(9). DOI: 10.3390/CANCERS11091257
226. Lee SJ, Jang BC, Lee SW, Yang Y Il, Suh S Il, Park YM, Oh S, Shin JG, Yao S, Chen L, Choi IH. Interferon regulatory factor-1 is prerequisite to the constitutive expression and IFN-gamma-induced upregulation of B7-H1 (CD274). FEBS Lett. 2006 Feb 6;580(3):755–62. DOI: 10.1016/J.FEBSLET.2005.12.093
227. Gorchs L, Moro CF, Bankhead P, Kern KP, Sadeak I, Meng Q, Rangelova E, Kaipe H. Human pancreatic carcinoma-associated fibroblasts promote expression of co-inhibitory markers on CD4+ and CD8+ T-cells. Front Immunol. 2019;10(APR). DOI: 10.3389/fimmu.2019.00847
228. Majety M, Pradel LP, Gies M, Ries CH. Fibroblasts Influence Survival and Therapeutic Response in a 3D Co-Culture Model. PLoS One. 2015 Jun 8;10(6). DOI: 10.1371/JOURNAL.PONE.0127948
229. Kuen J, Darowski D, Kluge T, Majety M. Pancreatic cancer cell/fibroblast co-culture induces M2 like macrophages that influence therapeutic response in a 3D model. PLoS One. 2017 Jul 1;12(7). DOI: 10.1371/JOURNAL.PONE.0182039
230. Mollica H, Teo YJ, Tan ASM, Tan DZM, Decuzzi P, Pavesi A, Adriani G. A 3D pancreatic tumor model to study T cell infiltration. Biomater Sci. 2021 Nov 9;9(22):7420–31. DOI: 10.1039/D1BM00210D
231. Lohrl M, Trautmann B, Gottlerl M, Peters S, Zauner I, Maillet B, Kloppel G. Human ductal adenocarcinomas of the pancreas express extracellular matrix proteins. Br J Cancer. 1994;69(1):144–51. DOI: 10.1038/BJC.1994.24

232. Mukherji R, Debnath D, Hartley ML, Noel MS. The Role of Immunotherapy in Pancreatic Cancer. Curr Oncol. 2022 Oct 1;29(10):6864. DOI: 10.3390/CURRONCOL29100541

233. Brahmer JR, Tykodi SS, Chow LQM, Hwu WJ, Topalian SL, Hwu P, Drake CG, Camacho LH, Kauh J, Odunsi K, Pitot HC, Hamid O, Bhatia S, Martins R, Eaton K, Chen S, Salay TM, Alaparthy S, Grosso JF, Korman AJ, Parker SM, Agrawal S, Goldberg SM, Pardoll DM, Gupta A, Wigginton JM. Safety and Activity of Anti–PD-L1 Antibody in Patients with Advanced Cancer. N Engl J Med. 2012 Jun 28;366(26):2455–65. DOI: 10.1056/NEJMOA1200694/SUPPL_FILE/NEJMOA1200694_DISCLOSURES.PDF

234. Royal RE, Levy C, Turner K, Mathur A, Hughes M, Kammula US, Sherry RM, Topalian SL, Yang JC, Lowy I, Rosenberg SA. Phase 2 trial of single agent ipilimumab (Anti-CTLA-4) for locally advanced or metastatic pancreatic adenocarcinoma. J Immunother. 2010 Oct;33(8):828–33. DOI: 10.1097/CJI.0B013E3181EEC14C

235. Li Y, Hu L, Peng X, Xu H, Tang B, Xu C. Resistance to immune checkpoint inhibitors in KRAS-mutant non-small cell lung cancer. Cancer drug Resist (Alhambra, Calif). 2022;5(1):129–46. DOI: 10.20517/CDR.2021.102

236. Scarpa M, Marchiori C, Scarpa M, Castagliuolo I. CD80 expression is upregulated by TP53 activation in human cancer epithelial cells. Oncoimmunology. 2021;10(1). DOI: 10.1080/2162402X.2021.1907912

237. Yazdanifar M, Zhou R, Grover P, Williams C, Bose M, Moore LJ, Wu ST, Maher J, Dreau D, Mukherjee P. Overcoming Immunological Resistance Enhances the Efficacy of a Novel Anti-tMUC1-CAR T Cell Treatment against Pancreatic Ductal Adenocarcinoma. Cells. 2019 Sep 1;8(9). DOI: 10.3390/CELLS8091070

238. Suh H, Pillai K, Morris DL. Mucins in pancreatic cancer: biological role, implications in carcinogenesis and applications in diagnosis and therapy. Am J Cancer Res. 2017;7(6):1372.

239. Jin D, Fan J, Wang L, Thompson LF, Liu A, Daniel BJ, Shin T, Curiel TJ, Zhang B. CD73 on tumor cells impairs anti-tumor T cell responses: a novel mechanism of tumor-induced immune suppression. Cancer Res. 2010 Mar 3;70(6):2245. DOI: 10.1158/0008-5472.CAN-09-3109

240. Faraoni EY, Singh K, Chandra V, Le Roux O, Dai Y, Sahin I, O'Brien BJ, Strickland LN, Li L, Vucic E, Warner AN, Pruski M, Clark T, Van Buren G, Thosani NC, Bynon JS, Wray CJ, Bar-Sagi D, Poulsen KL, Vornik LA, Savage MI, Sei S, Mohammed A, Zhao Z, Brown PH, Mills T, Eltzschig HK, McAllister F, Bailey-Lundberg JM. CD73-dependent adenosine signaling through Adora2b drives immunosuppression in ductal pancreatic cancer. Cancer Res. 2023 Mar 27; DOI: 10.1158/0008-5472.CAN-22-2553

241. King RJ, Shukla SK, He C, Vernucci E, Thakur R, Attri KS, Dasgupta A, Chaika N V., Mulder SE, Abrego J, Murthy D, Gunda V, Pacheco CG, Grandgenett PM, Lazenby AJ, Hollingsworth MA, Yu

F, Mehla K, Singh PK. CD73 induces GM-CSF/MDSC-mediated suppression of T cells to accelerate pancreatic cancer pathogenesis. Oncogene 2021 417. 2022 Jan 10;41(7):971–82. DOI: 10.1038/s41388-021-02132-6

242. Schoenfeld AJ, Hellmann MD. Acquired Resistance to Immune Checkpoint Inhibitors. Cancer Cell. 2020 Apr 4;37(4):443. DOI: 10.1016/J.CCELL.2020.03.017
243. Koong AC, Mehta VK, Le QT, Fisher GA, Terris DJ, Brown JM, Bastidas AJ, Vierra M. Pancreatic tumors show high levels of hypoxia. Int J Radiat Oncol Biol Phys. 2000 Nov 1;48(4):919–22. DOI: 10.1016/S0360-3016(00)00803-8
244. Zandberg DP, Menk A V., Velez M, Normolle D, Depeaux K, Liu A, Ferris RL, Delgoffe GM. Tumor hypoxia is associated with resistance to PD-1 blockade in squamous cell carcinoma of the head and neck. J Immunother cancer. 2021 May 13;9(5). DOI: 10.1136/JITC-2020-002088
245. Najjar YG, Menk A V., Sander C, Rao U, Karunamurthy A, Bhatia R, Zhai S, Kirkwood JM, Delgoffe GM. Tumor cell oxidative metabolism as a barrier to PD-1 blockade immunotherapy in melanoma. JCI insight. 2019 Mar 7;4(5). DOI: 10.1172/JCI.INSIGHT.124989
246. Ungefroren H, Voss M, Bernstorff W V., Schmid A, Kremer B, Kalthoff H. Immunological escape mechanisms in pancreatic carcinoma. Ann N Y Acad Sci. 1999;880:243–51. DOI: 10.1111/J.1749-6632.1999.TB09529.X
247. Sato T, Irie S, Kitada S, Reed JC. FAP-1: a protein tyrosine phosphatase that associates with Fas. Science. 1995;268(5209):411–5. DOI: 10.1126/SCIENCE.7536343
248. Hinz S, Trauzold A, Boenicke L, Sandberg C, Beckmann S, Bayer E, Walczak H, Kalthoff H, Ungefroren H. Bcl-XL protects pancreatic adenocarcinoma cells against CD95- and TRAIL-receptor-mediated apoptosis. Oncogene. 2000 Nov 16;19(48):5477–86. DOI: 10.1038/SJ.ONC.1203936
249. Burris HA, Moore MJ, Andersen J, Green MR, Rothenberg ML, Modiano MR, Cripps MC, Portenoy RK, Storniolo AM, Tarassoff P, Nelson R, Dorr FA, Stephens CD, Von Hoff DD. Improvements in survival and clinical benefit with gemcitabine as first-line therapy for patients with advanced pancreas cancer: a randomized trial. J Clin Oncol. 1997;15(6):2403–13. DOI: 10.1200/JCO.1997.15.6.2403
250. Liu K, Geng Y, Wang L, Xu H, Zou M, Li Y, Zhao Z, Chen T, Xu F, Sun L, Wu S, Gu Y. Systematic exploration of the underlying mechanism of gemcitabine resistance in pancreatic adenocarcinoma. Mol Oncol. 2022 Aug 1;16(16):3034–51. DOI: 10.1002/1878-0261.13279
251. Arlt A, Gehrz A, Müerköster S, Vorndamm J, Kruse ML, Fölsch UR, Schäfer H. Role of NF-κB and Akt/PI3K in the resistance of pancreatic carcinoma cell lines against gemcitabine-induced cell death. Oncogene 2003 2221. 2003 May 22;22(21):3243–51. DOI: 10.1038/sj.onc.1206390
252. Xie B, Hänsel J, Mundorf V, Betz J, Reimche I, Erkan M, Büdeyri I, Gesell A, Kerr RG, Ariantari NP,

Yu H, Proksch P, Teusch N, Mrsny RJ. Pseudopterosin and O-Methyltylophorinidine Suppress Cell Growth in a 3D Spheroid Co-Culture Model of Pancreatic Ductal Adenocarcinoma. Bioengineering. 2020 Jun 1;7(2):1–20. DOI: 10.3390/BIOENGINEERING7020057

253. Müerköster S, Wegehenkel K, Arlt A, Witt M, Sipos B, Kruse ML, Sebens T, Klöppel G, Kalthoff H, Fölsch UR, Schäfer H. Tumor Stroma Interactions Induce Chemoresistance in Pancreatic Ductal Carcinoma Cells Involving Increased Secretion and Paracrine Effects of Nitric Oxide and Interleukin-1β. Cancer Res. 2004;64(4):1331–7. DOI: 10.1158/0008-5472.CAN-03-1860
254. Neumann CCM, von Hörschelmann E, Reutzel-Selke A, Seidel E, Sauer IM, Pratschke J, Bahra M, Schmuck RB. Tumor–stromal cross-talk modulating the therapeutic response in pancreatic cancer. Hepatobiliary Pancreat Dis Int. 2018 Oct 1;17(5):461–72. DOI: 10.1016/j.hbpd.2018.09.004
255. Firuzi O, Che PP, El Hassouni B, Buijs M, Coppola S, Löhr M, Funel N, Heuchel R, Carnevale I, Schmidt T, Mantini G, Avan A, Saso L, Peters GJ, Giovannetti E. Role of c-MET Inhibitors in Overcoming Drug Resistance in Spheroid Models of Primary Human Pancreatic Cancer and Stellate Cells. Cancers (Basel). 2019 May 1;11(5):638. DOI: 10.3390/CANCERS11050638
256. Sasaki N, Ishiwata T, Hasegawa F, Michishita M, Kawai H, Matsuda Y, Arai T, Ishikawa N, Aida J, Takubo K, Toyoda M. Stemness and anti-cancer drug resistance in ATP-binding cassette subfamily G member 2 highly expressed pancreatic cancer is induced in 3D culture conditions. Cancer Sci. 2018 Apr 1;109(4):1135. DOI: 10.1111/CAS.13533
257. Smith PL, Yogaratnam Y, Samad M, Kasow S, Dalgleish AG. Effect of Gemcitabine based chemotherapy on the immunogenicity of pancreatic tumour cells and T-cells. Clin Transl Oncol. 2021 Jan 1;23(1):110. DOI: 10.1007/S12094-020-02429-0
258. Ho TTB, Nasti A, Seki A, Komura T, Inui H, Kozaka T, Kitamura Y, Shiba K, Yamashita T, Yamashita T, Mizukoshi E, Kawaguchi K, Wada T, Honda M, Kaneko S, Sakai Y. Combination of gemcitabine and anti-PD-1 antibody enhances the anticancer effect of M1 macrophages and the Th1 response in a murine model of pancreatic cancer liver metastasis. J Immunother Cancer. 2020 Nov 13;8(2). DOI: 10.1136/jitc-2020-001367
259. Principe DR, Narbutis M, Kumar S, Park A, Viswakarma N, Dorman MJ, Kamath SD, Grippo PJ, Fishel ML, Hwang RF, Thummuri D, Underwood PW, Munshi HG, Trevino JG, Rana A. Long-Term Gemcitabine Treatment Reshapes the Pancreatic Tumor Microenvironment and Sensitizes Murine Carcinoma to Combination Immunotherapy. Cancer Res. 2020 Aug 8;80(15):3101. DOI: 10.1158/0008-5472.CAN-19-2959
260. Weiss GJ, Waypa J, Blaydorn L, Coats J, Mcgahey K, Sangal A, Niu J, Lynch CA, Farley JH, Khemka V. A phase Ib study of pembrolizumab plus chemotherapy in patients with advanced cancer (PembroPlus). Br J Cancer. 2017 Jun 6;117(1):33. DOI: 10.1038/BJC.2017.145

261. Doi T, Muro K, Ishii H, Kato T, Tsushima T, Takenoyama M, Oizumi S, Gemmoto K, Suna H, Enokitani K, Kawakami T, Nishikawa H, Yamamoto N. A Phase I Study of the Anti-CC Chemokine Receptor 4 Antibody, Mogamulizumab, in Combination with Nivolumab in Patients with Advanced or Metastatic Solid Tumors. Clin Cancer Res. 2019 Nov 15;25(22):6614–22. DOI: 10.1158/1078-0432.CCR-19-1090

262. Bockorny B, Semenisty V, Macarulla T, Borazanci E, Wolpin BM, Stemmer SM, Golan T, Geva R, Borad MJ, Pedersen KS, Park JO, Ramirez RA, Abad DG, Feliu J, Muñoz A, Ponz-Sarvise M, Peled A, Lustig TM, Bohana-Kashtan O, Shaw SM, Sorani E, Chaney M, Kadosh S, Vainstein Haras A, Von Hoff DD, Hidalgo M. BL-8040, a CXCR4 antagonist, in combination with pembrolizumab and chemotherapy for pancreatic cancer: the COMBAT trial. Nat Med 2020 266. 2020 May 25;26(6):878–85. DOI: 10.1038/s41591-020-0880-x

263. Gulley JL, Schlom J, Barcellos-Hoff MH, Wang XJ, Seoane J, Audhuy F, Lan Y, Dussault I, Moustakas A. Dual inhibition of TGF-β and PD-L1: a novel approach to cancer treatment. Mol Oncol. 2022 Jun 1;16(11):2117. DOI: 10.1002/1878-0261.13146

264. Melisi D, Garcia-Carbonero R, Macarulla T, Pezet D, Deplanque G, Fuchs M, Trojan J, Oettle H, Kozloff M, Cleverly A, Smith C, Estrem ST, Gueorguieva I, Lahn MMF, Blunt A, Benhadji KA, Tabernero J. Galunisertib plus gemcitabine vs. gemcitabine for first-line treatment of patients with unresectable pancreatic cancer. Br J Cancer. 2018 Nov 13;119(10):1208–14. DOI: 10.1038/S41416-018-0246-Z

265. Melisi D, Oh DY, Hollebecque A, Calvo E, Varghese A, Borazanci E, Macarulla T, Merz V, Zecchetto C, Zhao Y, Gueorguieva I, Man M, Gandhi L, Estrem ST, Benhadji KA, Lanasa MC, Avsar E, Guba SC, Garcia-Carbonero R. Safety and activity of the TGFβ receptor I kinase inhibitor galunisertib plus the anti-PD-L1 antibody durvalumab in metastatic pancreatic cancer. J Immunother cancer. 2021 Mar 9;9(3). DOI: 10.1136/JITC-2020-002068

266. Sow HS, Ren J, Camps M, Ossendorp F, Ten Dijke P. Combined Inhibition of TGF-β Signaling and the PD-L1 Immune Checkpoint Is Differentially Effective in Tumor Models. Cells. 2019 Apr 1;8(4). DOI: 10.3390/CELLS8040320

267. Freed-Pastor WA, Lambert LJ, Ely ZA, Pattada NB, Bhutkar A, Eng G, Mercer KL, Garcia AP, Lin L, Rideout WM, Hwang WL, Schenkel JM, Jaeger AM, Bronson RT, Westcott PMK, Hether TD, Divakar P, Reeves JW, Deshpande V, Delorey T, Phillips D, Yilmaz OH, Regev A, Jacks T. The CD155/TIGIT axis promotes and maintains immune evasion inneoantigen-expressing pancreatic cancer. Cancer Cell. 2021 Oct 10;39(10):1342. DOI: 10.1016/J.CCELL.2021.07.007

268. Pearce H, Croft W, Nicol SM, Margielewska-Davies S, Powell R, Cornall R, Davis SJ, Marcon F, Pugh MR, Fennell É, Powell-Brett S, Mahon BS, Brown RM, Middleton G, Roberts K, Moss P. Tissue-Resident Memory T Cells in Pancreatic Ductal Adenocarcinoma Coexpress PD-1 and TIGIT

and Functional Inhibition Is Reversible by Dual Antibody Blockade. Cancer Immunol Res. 2023 Apr 4;11(4):435. DOI: 10.1158/2326-6066.CIR-22-0121

269. Kim DK, Jeong J, Lee DS, Hyeon DY, Park GW, Jeon S, Lee KB, Jang JY, Hwang D, Kim HM, Jung K. PD-L1-directed PlGF/VEGF blockade synergizes with chemotherapy by targeting CD141+ cancer-associated fibroblasts in pancreatic cancer. Nat Commun 2022 131. 2022 Oct 22;13(1):1–19. DOI: 10.1038/s41467-022-33991-6

270. Gulhati P, Schalck A, Jiang S, Shang X, Wu CJ, Hou P, Ruiz SH, Soto LS, Parra E, Ying H, Han J, Dey P, Li J, Deng P, Sei E, Maeda DY, Zebala JA, Spring DJ, Kim M, Wang H, Maitra A, Moore D, Clise-Dwyer K, Wang YA, Navin NE, DePinho RA. Targeting T cell checkpoints 41BB and LAG3 and myeloid cell CXCR1/CXCR2 results in antitumor immunity and durable response in pancreatic cancer. Nat Cancer 2022. 2022 Dec 30;1–19. DOI: 10.1038/s43018-022-00500-z

8 List of Figures

9 List of Tables

Supplementary

Supplementary Figures

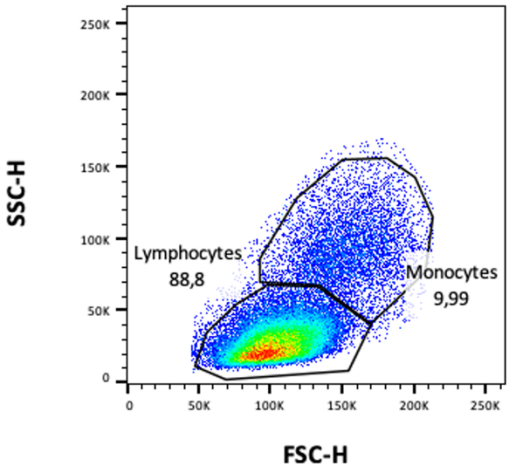

Supplementary Figure 1: Flow cytometry analysis of peripheral blood mononuclear cells (PBMCs). Isolated PBMCs were separated into lymphocytes and monocytes by performing a counterflow centrifugation elutriation. Afterwards, the purity of the fractions was tested by flow cytometry. Monocytes and lymphocytes differ in size (FSC-H) and granularity (SSC-H). Lymphocytes are smaller and show less granularity compared to monocytes.

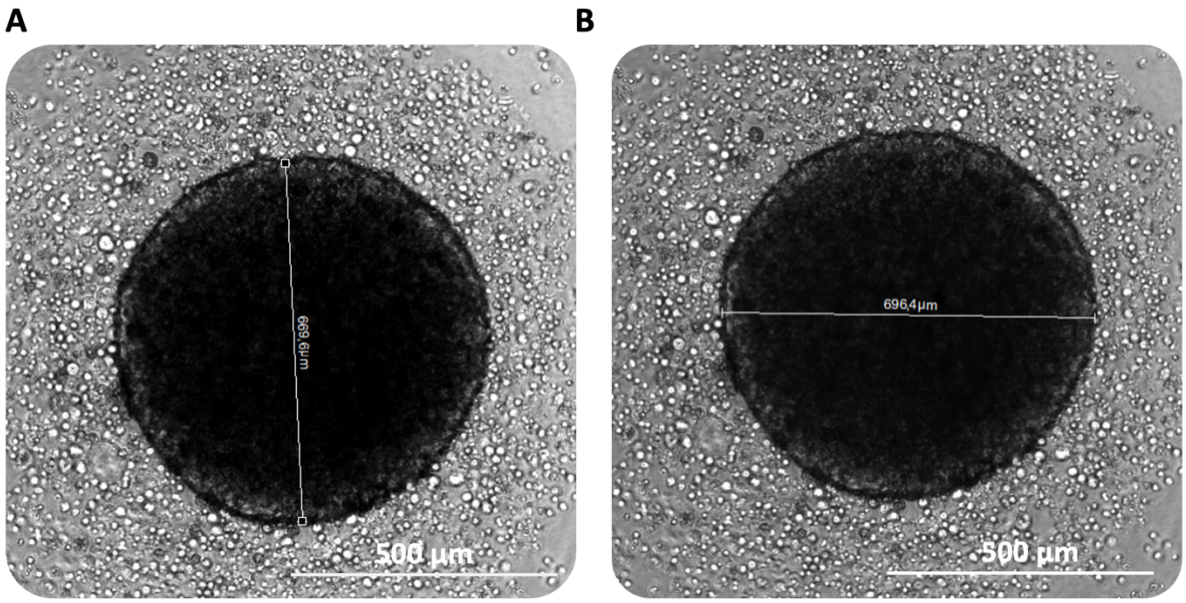

C

$$\text{Diameter (µm)} = \frac{Diameter\ top\ to\ bottom + diameter\ left\ to\ right}{2}$$

$$683\ \mu m = \frac{669.6\ \mu m + 696.4\ \mu m}{2}$$

Supplementary Figure 2: Measurement of the size of spheroids. To determine the spheroid size, phase contrast z-stack pictures were taken using the Lionheart FX automated microscope and the diameter from **(A)** top to bottom and **(B)** left to right was measured with the help of the measurement tool of the Gen5 Data Analysis Software. **(C)** Then, the mean of both measurements was calculated according to the given formula. The scale bar represents 500 µm.

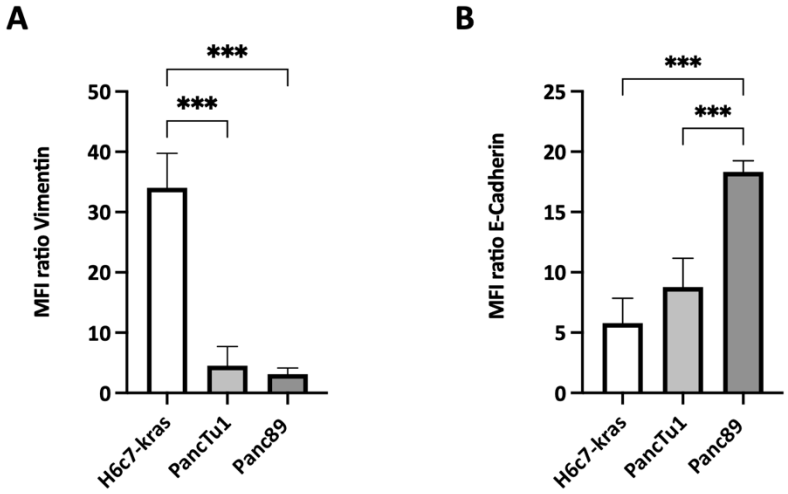

Supplementary Figure 3: H6c7-kras cells show a more mesenchymal phenotype and PancTu1 and Panc89 cells a more epithelial phenotype. H6c7-kras, PancTu1, and Panc89 cells were seeded for in T cell medium. After 72 h,

the expression of **(A)** Vimentin and **(B)** E-Cadherin was analyzed by flow cytometry. Median fluorescence intensity (MFI) ratio was calculated by dividing the MFI of the specific staining by the MFI of the isotype control. Data represent the mean ± SD (normally distributed). N=5. *** = $p < 0.001$.

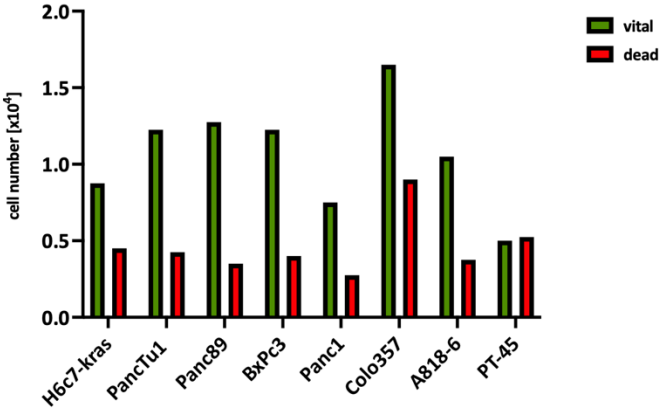

Supplementary Figure 4: Vital and dead cell count of PDEC spheroids. H6c7-kras, PancTu1, Panc89, Panc1, Colo357, BxPc3, A818-6, and PT-45 cells were seeded at a density of $2x10^4$ in 200 µl of T cell medium in a 96-well ultra-low attachment plate. After seeding, the plate was centrifuged at 300 xg for 5 min at RT. After 72 h, the spheroids were mechanically dissociated. The cell suspension was stained with trypan blue to determine the vital (green) and dead (red) cell number. N=2.

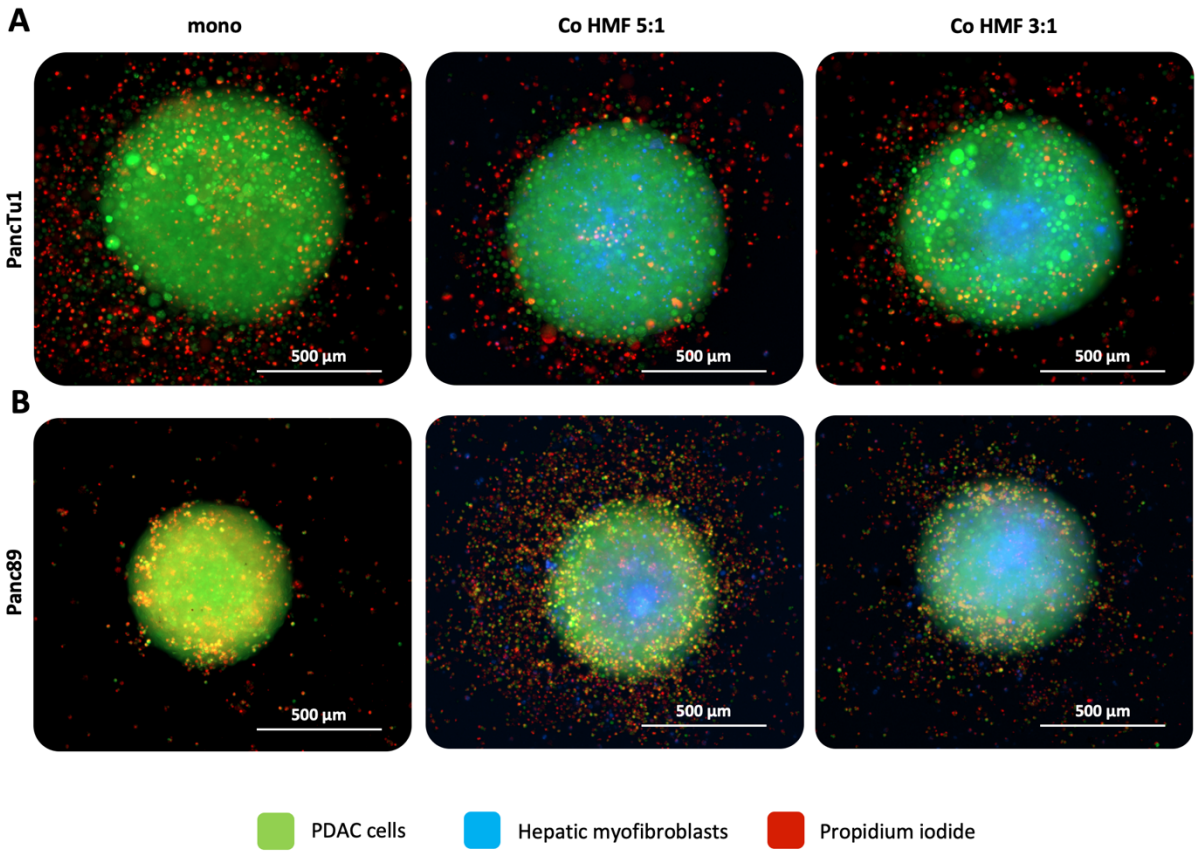

Supplementary Figure 5: HMF-enriched PancTu1 and Panc89 spheroids contain less propidium iodide positive cells. PancTu1 and Panc89 cells were either seeded in mono- or coculture with hepatic myofibroblasts (HMF) at different ratios in ultra-low attachment plates. After 72 h, the spheroids were stained with propidium iodide (red). Representative images of **(A)** PancTu1 and **(B)** Panc89 cells in mono- or coculture with HMF after 3 days. In green (CellTracker Green) PDAC cells and in blue (CellTrace Violet) HMF.

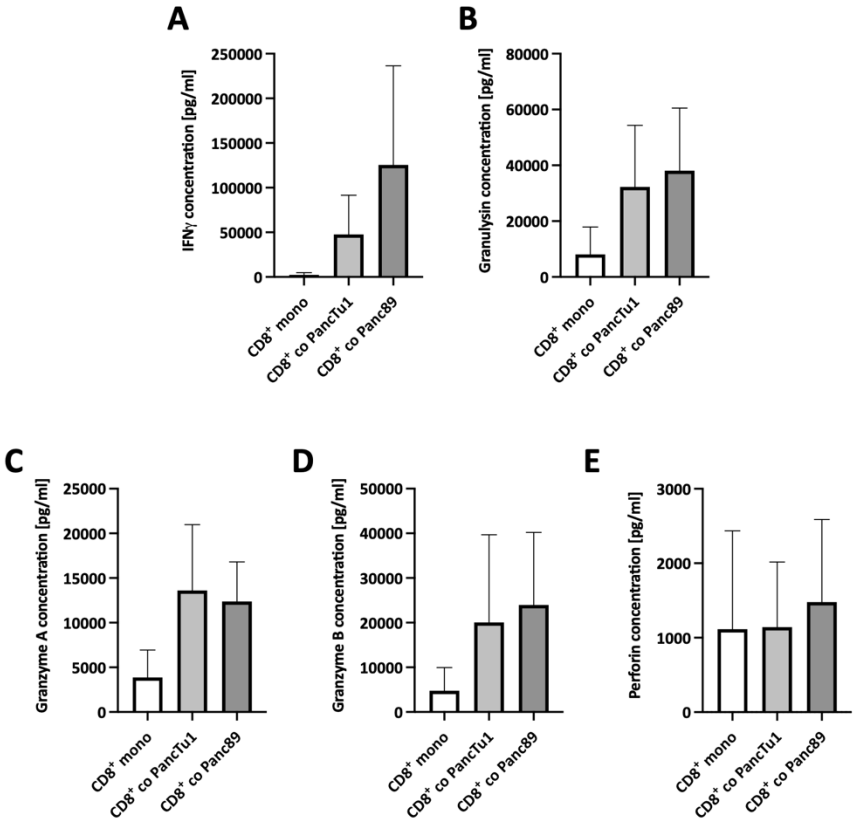

Supplementary Figure 6: Concentrations of effector molecules were higher in the supernatants derived from CD8⁺ T cells cultured with PancTu1 and Panc89 spheroids. PancTu1 and Panc89 cells were seeded in monoculture in ultra-low attachment plates for 3 days. After 48 h, activated CD8⁺ T cells were added at a ratio of 1:10. As control, CD8⁺ T cells were seeded in monoculture. The concentrations of **(A)** IFNγ, **(B)** Granulysin, **(C)** Granzyme A, **(D)** Granzyme B, and **(E)** Perforin were analyzed in culture supernatants. Data represent the mean ± SD (normally distributed). N=4.

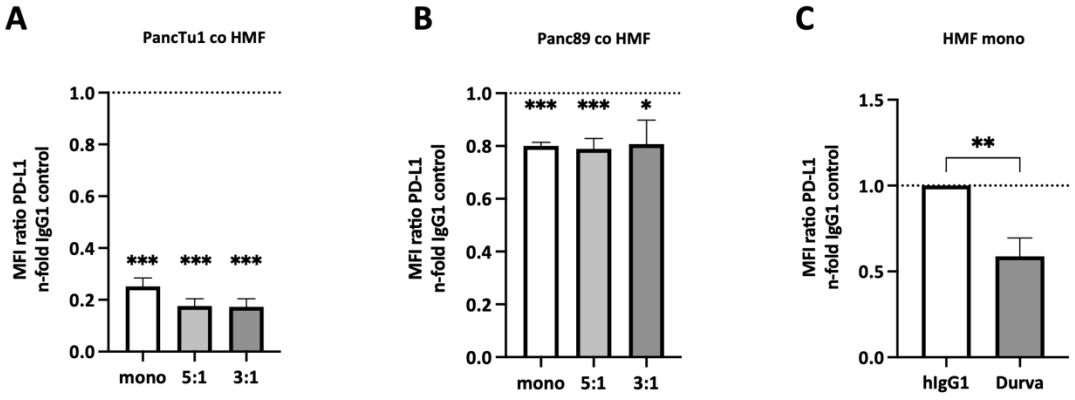

Supplementary Figure 7: Durvalumab binds to PD-L1 on PDAC cells and HMF. PancTu1 and Panc89 cells were seeded in mono- or coculture with hepatic myofibroblasts (HMF) at different ratios in ultra-low attachment plates. After 48 h, either 10 µg/ml isotype control or 10 ug/ml Durvalumab were added for 24 h. Afterwards, **(A)** PancTu1, **(B)** Panc89 cells, and **(C)** HMF were stained for cell surface localized PD-L1, and the MFI ratio for PD-L1

staining was determined via flow cytometry. Median fluorescence intensity (MFI) ratio was calculated by dividing the MFI of the specific staining by the MFI of the isotype control. Data were normalized to the hIgG1 isotype control. Data represent the mean ± SD (normally distributed). N=3. * = p < 0.05, ** = p < 0.01, *** = p < 0.001. (published in [163]).

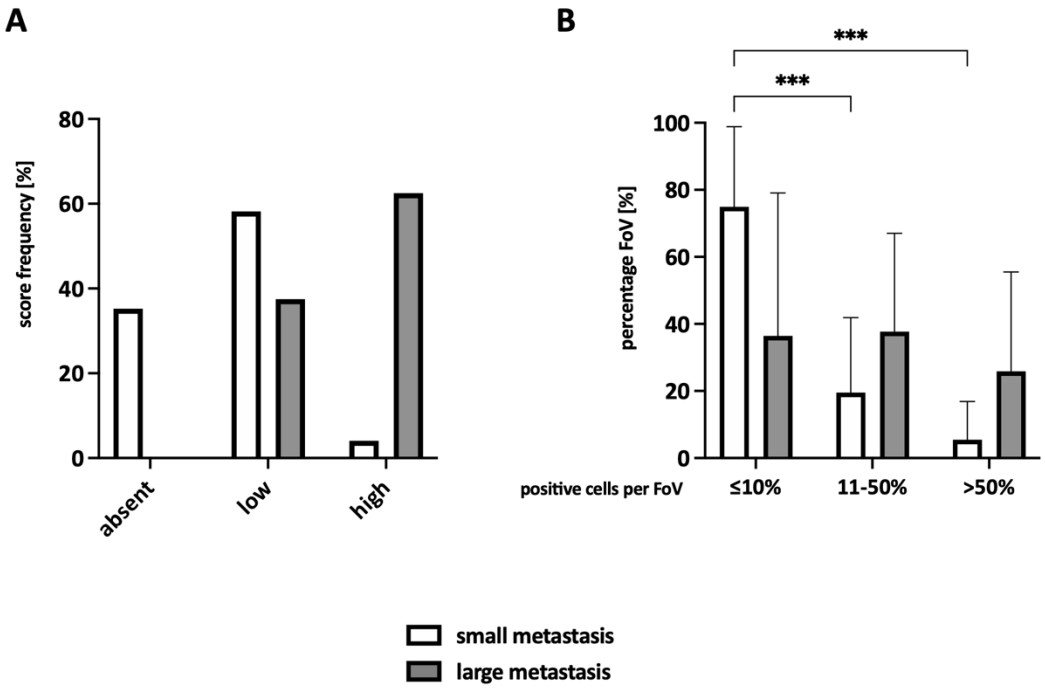

Supplementary Figure 8: Different spatial distribution of Ki67 staining in small and large liver metastases of PDAC patients. (A) The abundance of Ki67 staining was rated as absent, low expression or high expression comparing small and large liver metastases. **(B)** Furthermore, a maximum of 10 microscopic Fields of View (FoV) in the tumor center and at the invasion front were analyzed and the proportion of $Ki67^+$ tumor cells was determined. The proportion was ranked as ≤10 %, 11-50 %, or >50 %. Data represent the mean ± SD (normally distributed). N=11 for small metastases and N=13 for large metastases. *** = p < 0.001.

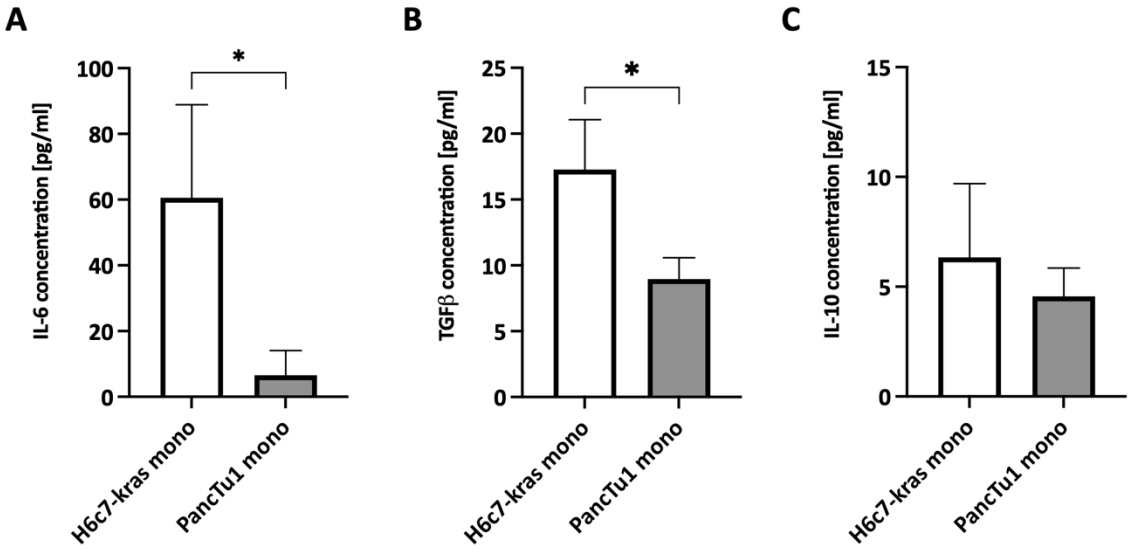

Supplementary Figure 9: Monocultured PDECs release IL-6, TGF-β1, and IL-10 in monoculture into the supernatants. H6c7-kras (white) and PancTu1 cells (grey) were seeded in a 12-well plate and after 24 h, the medium was replaced with T cell medium. After 72 h in monoculture, the concentrations of **(A)** IL-6, **(B)** TGF-β1, and **(C)** IL-10 were measured. Data represents the mean ± SD (normally distributed). N=3. * = $p < 0.05$.

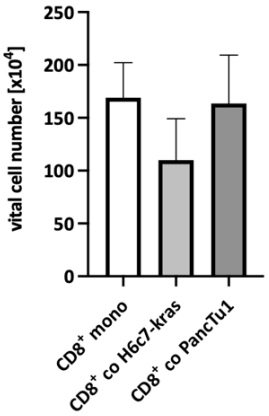

Supplementary Figure 10: Vital cell number of CD8⁺ T cells was reduced after coculture with H6c7-kras cells. CD8⁺ T cells were isolated by magnetic cell separation from human blood derived lymphocytes and then activated with anti-CD3 and anti-CD28 antibodies as well as IL-2 for 4 days. Afterwards, CD8⁺ T cells were seeded in monoculture (white) or in coculture with either H6c7-kras (light grey) or PancTu1 cells (dark grey) for 72 h. The vital cell number was determined. Data represent the mean ± SD (normally distributed). N=6.

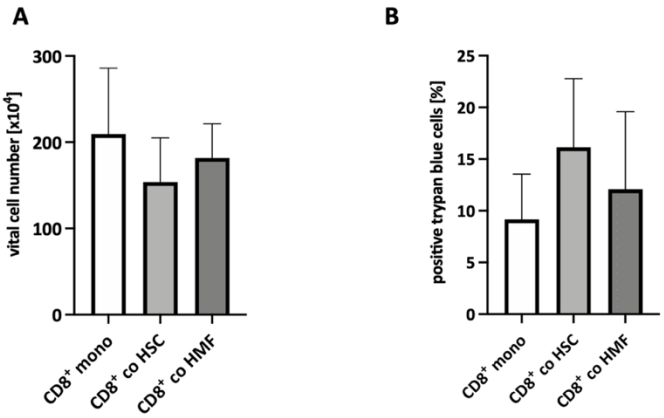

Supplementary Figure 11: Vital cell number of CD8⁺ T cells was reduced after coculture with HSC or HMF. CD8⁺ T cells were isolated by magnetic cell separation from human blood derived lymphocytes and then activated with anti-CD3 and anti-CD28 antibodies, as well as IL-2 for 4 days. Afterwards, CD8⁺ T cells were seeded in mono- (white) or coculture with either HSC (light grey) or HMF (dark grey) for 72 h. **(A)** The vital cell number and **(B)** the percentage of trypan blue positive CD8⁺ T cells was determined. Data represent the mean ± SD (normally distributed). N=4.

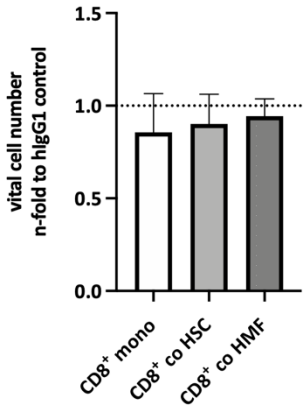

Supplementary Figure 12: Durvalumab treatment did not affect the vital cell number of CD8⁺ T cells in mono- or coculture with HSC or HMF. CD8⁺ T cells were isolated by magnetic cell separation from human blood derived lymphocytes and then activated with anti-CD3 and anti-CD28 antibodies, as well as IL-2 for 4 days. Afterwards, CD8⁺ T cells were seeded in mono- (white) or coculture with either HSC (light grey) or HMF (dark grey) for 72 h. Further, the cultures were treated with 10 µg/ml of Durvalumab or 10 µg/ml of the respective isotype control (hIgG1). After 72 h, the vital cell number was determined. Data were normalized on the hIgG1 isotype control treated sample. Data represent the mean ± SD (normally distributed). N=4.

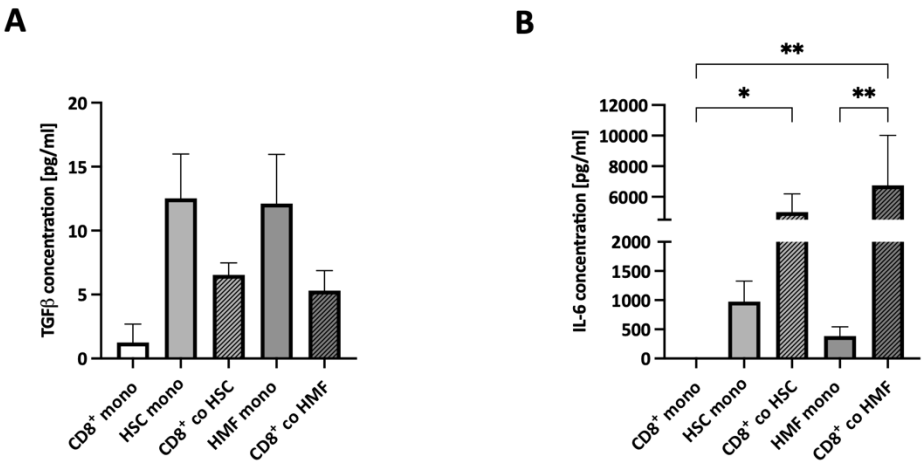

Supplementary Figure 13: TGF-β1 and IL-6 concentrations in supernatants of CD8⁺ T cells and hepatic stromal cells. CD8⁺ T cells were isolated by magnetic cell separation from human blood derived lymphocytes and then activated with anti-CD3 and anti-CD28 antibodies, as well as IL-2 for 4 days. Hepatic stellate (HSC) cells and hepatic myofibroblasts (HMF) were seeded and on the next day, activated CD8⁺ T cells were added. As control CD8⁺ T cells, HSC, and HMF were seeded in monoculture. After 72 h, concentrations of TGF-β1 and IL-6 were measured in the supernatants. Data represent the mean ± SD (normally distributed). N=4 for TGF-β1 and N=3 for IL-6. * = $p < 0.05$, ** = $p < 0.01$.

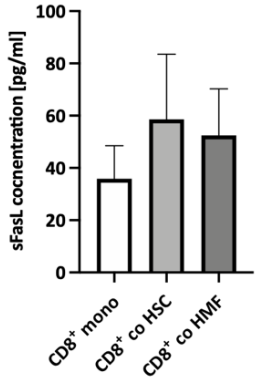

Supplementary Figure 14: Concentrations of sFasL (CD95L) were higher in supernatants of CD8⁺ T cells after coculture with hepatic stellated cells (HSC) or hepatic myofibroblasts (HMF). CD8⁺ T cells were isolated by magnetic cell separation from human blood derived lymphocytes and then activated with anti-CD3 and anti-CD28 antibodies as well as IL-2 for 4 days. Afterwards, activated CD8⁺ T cells were seeded in monoculture (white) or in coculture with either HSC (light grey) or HMF (dark grey). After 72 h, the concentration of sFasL was determined in the supernatants. Data represent the mean ± SD (normally distributed). N=3.

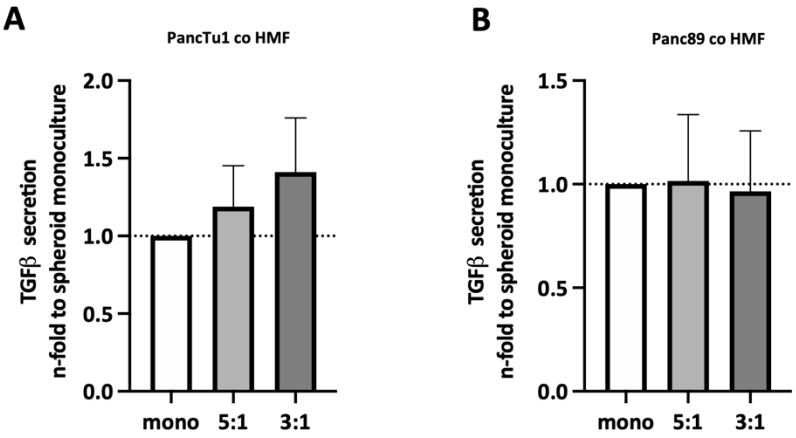

Supplementary Figure 15: TGF-β1 concentration was elevated in PancTu1 HMF-enriched spheroids. PancTu1 and Panc89 cells were either seeded in mono- or coculture with hepatic myofibroblasts (HMF) at different ratios (mono = white, 5:1 = light grey, 3:1 = dark grey) in ultra-low attachment plates for 3 days. The concentration of TGF-β1 was measured in the supernatants of **(A)** PancTu1 spheroids and **(B)** Panc89 spheroids after 72 h of mono- or coculture. Data were normalized on the concentration of TGF-ß in monocultured spheroids. Data represent the mean ± SD (normally distributed). N=4. (published in [163]).

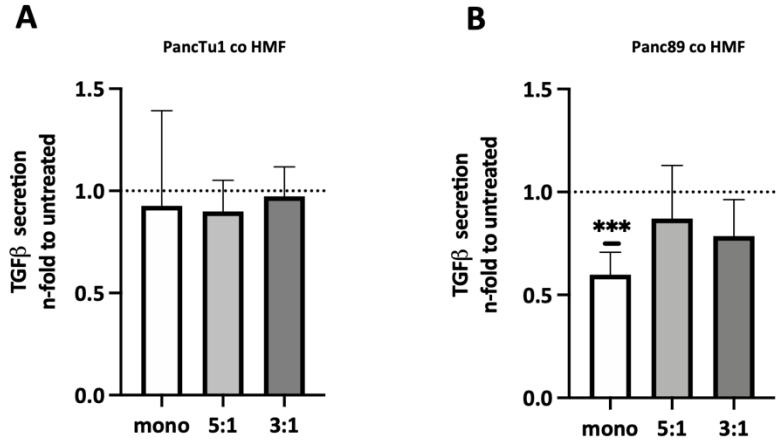

Supplementary Figure 16: TGF-β1 concentration was decreased in Panc89 spheroids after Gemcitabine treatment. PancTu1 and Panc89 cells were either seeded in mono- or coculture with hepatic myofibroblasts (HMF) at different ratios (mono = white, 5:1 = light grey, 3:1 = dark grey) in ultra-low attachment plates. On the next day, the spheroids were treated with 10 µg/ml Gemcitabine for 24 h. The concentration of TGF-β1 was measured in the supernatants of **(A)** PancTu1 spheroids and **(B)** Panc89 spheroids after 72 h of mono- or coculture. Data were normalized to the TGF-ß concentration in untreated spheroids. Data represent the mean ± SD (normally distributed). N=4. *** = $p < 0.001$. (published in [163]).

Declaration of Authorship

Hiermit erkläre ich, Silje Victoria Beckinger (geboren am 05.03.1995 in Berlin), dass die vorliegende Dissertation mit dem Titel *„The impact of the liver microenvironment on the immune checkpoint regulator PD-L1 in liver metastasis of pancreatic cancer“* unter Einhaltung der Regeln guter wissenschaftlicher Praxis der Deutschen Forschungsgemeinschaft verfasst wurde und ich keine anderen als die angegebenen Hilfsmittel und Quellen benutzt habe. Ich versichere weiterhin, dass ich außer der wissenschaftlichen Beratung durch meine Doktormutter Prof. Dr. Susanne Sebens keine Hilfe in Anspruch genommen habe. Weder wurde diese Arbeit bisher im Rahmen eines Prüfungsverfahrens vorgelegt, noch wurde ein akademischer Grad entzogen. Teile dieser Dissertation wurden bereits veröffentlicht.

Ort, Datum	Silje Victoria Beckinger

Acknowledgment

Zuallererst möchte ich mich bei meiner Doktormutter Prof. Dr. Susanne Sebens bedanken, da sie mir ermöglicht hat, meine Masterarbeit und nun die Doktorarbeit in ihrer Arbeitsgruppe zu absolvieren. Ich bedanke mich für die gute Betreuung, immer ein offenes Ohr, die motivierenden Diskussionen und die weiterführenden Ideen für dieses Projekt.

Des Weiteren möchte ich mich bei Herrn Prof. Dr. Hinrich Schulenburg und Herrn Prof. Dr. Thomas Roeder bedanken, dass Beide das Zweitgutachten anfertigten würden.

Ein weiterer Dank geht an Herrn Prof. Dr. Christoph Röcken und Sandra Krüger. Ohne die Beiden wäre die Analyse der histologischen Leberschnitte nicht möglich gewesen.

Ein ganz großer Dank geht an die Kolleginnen und Kollegen in der Arbeitsgruppe Inflammatorische Karzinogenese und am Institut für Experimentelle Tumorforschung. Vor allem die Mittagspausen, der freaky friday und die Betriebsausflüge werden immer in guter Erinnerung bleiben. Besonders hervorheben möchte ich Dagmar Leisner, Sandra Ussat, Sascha Rahn, Anna Willms, Lisa-Marie Philipp, Leon Aldag, Arne Surrow, Luisa Hattingen, Anna-Maxi Wandmacher, Charlotte Kayser und natürlich Tina Daunke. Ich danke euch von Herzen für eure Unterstützung in den vergangenen Jahren.

Tina Daunke, Dir möchte ich ganz besonders danken, denn durch dich hat die Arbeit im Labor und vor allem die abendlichen Sessions noch mehr Freude und Spaß gebracht. Unsere Diskussionen haben meine Arbeit vorangetrieben. Auch privat bist du immer für mich da. Ich bin froh, dass wir uns in der AG kennen gelernt haben, denn du bist inzwischen ein ganz wichtiger Mensch in meinem Leben geworden. Ich freue mich auf viele weitere Erlebnisse mit dir! Ein weiterer großer Dank geht an Florian Kraus. Danke, dass du mich die ganze Zeit unterstützt und immer für mich da bist. Ich bin sehr froh, dass du an meiner Seite bist.

Ich danke meinen Freunden, die immer für mich da sind und mich unterstützen.

Ein ganz großer Dank geht an meine Familie, vor allem an meine Eltern Rositha und Thomas Beckinger. Sie haben mich immer tatkräftig unterstützt und mir den Rücken gestärkt.

Danke!

Publications

Beckinger S*, Daunke T*, Aldag L, Krüger S, Heckl S, Wesch D, Schäfer H, Röcken C, Rahn S, Sebens S. Hepatic myofibroblasts exert immunosuppressive effects independent of the immune checkpoint regulator PD-L1 in liver metastasis of pancreatic ductal adenocarcinoma. Front Oncol. 2023 May 3;13. doi:10.3389/FONC.2023.1160824
*These authors share first authorship.

Daunke T*, **Beckinger S***, Rahn S, Krüger S, Heckl S, Schäfer H, Wesch D, Pilarsky C, Eckstein M, Hartmann A, Röcken C, Wandmacher AM, Sebens S. Analysis of the immune checkpoint regulator PD-L1 in the tumor-stroma interplay in pancreatic ductal adenocarcinoma. Front Immunol. 2023 Jun 28;14:1157397. doi: 10.3389/fimmu.2023.1157397
*These authors share first authorship.

Group Young Researchers In Inflammatory Carcinogenesis*, Wandmacher AM, Mehdorn AS, Sebens S. The Heterogeneity of the Tumor Microenvironment as Essential Determinant of Development, Progression and Therapy Response of Pancreatic Cancer. *Cancers (Basel)*. 2021;13(19):4932. Published 2021 Sep 30. doi:10.3390/cancers13194932
*Group members (in alphabetical order) share first authorship: Aldag L, **Beckinger S**, Daunke T, Philipp LM, Surrow A, Yesilyurt UU

Hellmold D, Kubelt C, Daunke T, **Beckinger S**, Ottmar J, Hauck M, Schütt F, Adelung R, Lucius R, Haag J, Sebens S, Synowitz M, Held-Feindt J. Sequential treatment with Temozolomide plus naturally-derived AT101 as an alternative therapeutic strategy: Insights into chemoresistance mechanisms of surviving glioblastoma cells. Int. J. Mol. Sci. 2023 May, 22. doi:10.3390/ijms24109075

Mehdorn AS, Gemoll T, Busch H, Kern K, **Beckinger S**, Daunke T, Kahlert C, Uzunoglu FG, Hendricks A, Buertin F, Wittel UA, Sunami Y, Röcken C, Becker T, Sebens S. Biomarkers in Liquid Biopsies for Prediction of Early Liver Metastases in Pancreatic Cancer. Cancers (Basel). 2022 Sep 22;14(19):4605. doi: 10.3390/cancers14194605. PMID: 36230528; PMCID: PMC9562670.

Walter F, Winter E, Rahn S, Heidland J, Meier S, Struzek AM, Lettau M, Philipp LM, **Beckinger S**, Otto L, Möller JL, Helm O, Wesch D, Scherließ R, Sebens S. Chitosan nanoparticles as antigen vehicles to induce

effective tumor specific T cell responses. PLoS One. 2020 Sep 30;15(9):e0239369. doi: 10.1371/journal.pone.0239369. PMID: 32997691; PMCID: PMC7526875.

Heckl SM, Mau F, Senftleben A, Daunke T, **Beckinger S**, Abdullazade S, Schreiber S, Röcken C, Sebens S, Schäfer H. Programmed Death-Ligand 1 (PD-L1) Expression Is Induced by Insulin in Pancreatic Ductal Adenocarcinoma Cells Pointing to Its Role in Immune Checkpoint Control. Med Sci (Basel). 2021 Jun 25;9(3):48. doi: 10.3390/medsci9030048. PMID: 34202040; PMCID: PMC8293454.

Miarka L, Hauser C, Helm O, Holdhof D, **Beckinger S**, Egberts JH, Gundlach JP, Lenk L, Rahn S, Mikulits W, Trauzold A, Sebens S. The Hepatic Microenvironment and TRAIL-R2 Impact Outgrowth of Liver Metastases in Pancreatic Cancer after Surgical Resection. Cancers (Basel). 2019 May 29;11(6):745. doi: 10.3390/cancers11060745. PMID: 31146405; PMCID: PMC6627672.

Congress Presentations

Beckinger S, Aldag L., Krüger S, Röcken C, Sebens S (2022). Role of the immune checkpoint regulator PD-L1 in liver metastasis of pancreatic cancer. German Pancreas Club, Lübeck (online)

Beckinger S, Aldag L., Daunke T, Krüger S, Rahn S, Heckl S, Wesch D, Röcken C, Sebens S (2022). The impact of the liver microenvironment on the immune checkpoint regulator PD-L1 in liver metastasis of pancreatic cancer. Signal Transduction Society, Weimar

Beckinger S, Aldag L., Daunke T, Krüger S, Rahn S, Heckl S, Wesch D, Röcken C, Sebens S (2022). The impact of immune checkpoint inhibitors on $CD8^+$ T cells in liver metastasis of pancreatic cancer. New Developments in Immunology, Inflammation and Infection, Borstel

Daunke T, **Beckinger S**, Rahn S, Krüger S, Wesch D, Röcken C, Sebens S (2022). Analysis of immune checkpoint regulator PD-L1 on tumor and stroma cells in pancreatic cancer. German Pancreas Club, Lübeck (online)

Daunke T, **Beckinger S**, Rahn S, Krüger S, Wesch D, Röcken C, Sebens S (2022). *In situ* and *in vitro* analysis of immune checkpoint regulator PD-L1 in the tumor-stroma interplay of pancreatic ductal adenocarcinoma. Signal Transduction Society, Weimar

Daunke T, **Beckinger S**, Rahn S, Krüger S, Wesch D, Röcken C, Sebens S (2022). Analysis of immune checkpoint regulator PD-L1 in the tumor-stroma interplay in pancreatic ductal adenocarcinoma. New Developments in Immunology, Inflammation and Infection, Borstel

Aldag L, **Beckinger S**, Heckl S, Krüger S, Daunke T, Röcken C, Wesch D, Sebens S (2022). Influence of the liver microenvironment on tumor cell growth and immune evasion in liver metastasis of pancreatic cancer. European Pancreatic Club, Kiev (online)

Hellmold D, Kubelt C, Daunke T, **Beckinger S**, Janssen O, Hauck M, Schütt F, Adelung R, Sebens S, Synowitz M, Held-Feindet J (2022). Insights into the influence of the tumor microenvironment on the response of residual tumor cells to chemotherapy after GBM resection. Brain Tumor Meeting 2022, Berlin

Hellmold D, Kubelt C, Daunke T, **Beckinger S**, Janssen O, Hauck M, Schütt F, Adelung R, Sebens S, Synowitz M, Held-Feindet J (2022). Influence of the tumor microenvironment on the therapeutic response of residual tumor cells after GBM resection. Jahrestagung der Deutschen Gesellschaft für Neurochirugie, Köln

Veil C, Meschke E, Sebens S, Ussat S, **Beckinger S**, Daunke T, Schrappe M, Klein M, Ankermann T, Knecht C, Bergholz R (2023). Leucine-rich a-2-glycoprotein 1 im Urin zur Differentialdiagnostik der Appendizitis - vorläufige Ergebnisse. Deutscher Chirurgie Kongress, München

Meschke E, Veil C, **Beckinger S**, Daunke T, Ussat S, Sebens S, Longardt A C, Schrappe M, Ankermann T, Knecht C, Bergholz R (2023). Leucine-rich α-2-glycoprotein 1 im Urin zur Diagnostik der Nekrotisierenden Enterokolitis – vorläufige Ergebnisse. Deutscher Chirurgie Kongress, München

Appendix

First Publication

frontiers | Frontiers in Oncology

TYPE Original Research
PUBLISHED 03 May 2023
DOI 10.3389/fonc.2023.1160824

OPEN ACCESS

EDITED BY
Jinhui Liu,
Nanjing Medical University, China

REVIEWED BY
Sen Yang,
Peking Union Medical College Hospital (CAMS), China
Longlong Gong,
GeneCast Biotechnology Co., Ltd., China

*CORRESPONDENCE
Susanne Sebens
susanne.sebens@email.uni-kiel.de

†These authors have contributed equally to this work and share first authorship

‡These authors contributed equally to this work and share last authorship

RECEIVED 07 February 2023
ACCEPTED 17 April 2023
PUBLISHED 03 May 2023

CITATION
Beckinger S, Daunke T, Aldag L, Krüger S, Heckl S, Wesch D, Schäfer H, Röcken C, Rahn S and Sebens S (2023) Hepatic myofibroblasts exert immunosuppressive effects independent of the immune checkpoint regulator PD-L1 in liver metastasis of pancreatic ductal adenocarcinoma.
Front. Oncol. 13:1160824.
doi: 10.3389/fonc.2023.1160824

Hepatic myofibroblasts exert immunosuppressive effects independent of the immune checkpoint regulator PD-L1 in liver metastasis of pancreatic ductal adenocarcinoma

Silje Beckinger[1†], Tina Daunke[1†], Leon Aldag[1], Sandra Krüger[2], Steffen Heckl[2,3], Daniela Wesch[4], Heiner Schäfer[1], Christoph Röcken[3], Sascha Rahn[5‡] and Susanne Sebens[1*‡]

[1]Institute for Experimental Cancer Research, Kiel University and University Hospital Schleswig-Holstein Campus Kiel, Kiel, Germany, [2]Department of Pathology, University Hospital Schleswig-Holstein Campus Kiel, Kiel, Germany, [3]Department of Internal Medicine II, University Hospital Schleswig-Holstein Campus Kiel, Kiel, Germany, [4]Institute of Immunology, Kiel University and University Hospital Schleswig-Holstein Campus Kiel, Kiel, Germany, [5]Institute of Biochemistry, Kiel University, Kiel, Germany

Introduction: Pancreatic ductal adenocarcinoma (PDAC) represents the 4th most common cause of cancer-related deaths in Western countries. Most patients are diagnosed at advanced stages, often already with metastases. The main site of metastasis is the liver and hepatic myofibroblasts (HMF) play a pivotal role in metastatic outgrowth. Immune checkpoint inhibitors (ICI) targeting programmed death ligand 1 (PD-L1) or programmed cell death protein 1 (PD-1) improved treatment of several cancers but not of PDAC. Therefore, this study aimed to better understand the impact of HMF on PD-L1 expression and immune evasion of PDAC cells during liver metastasis.

Methods: Formalin-fixed and paraffin embedded biopsy samples or diagnostic resection specimens from liver metastases of 15 PDAC patients were used for immunohistochemical analyses. Serial sections were stained with antibodies directed against Pan-Cytokeratin, αSMA, CD8, and PD-L1. To investigate whether the PD-1/PD-L1 axis and HMF contribute to immune escape of PDAC liver metastases, a stroma enriched 3D spheroid coculture model was established *in vitro*, using two different PDAC cell lines, HMF, and CD8$^+$ T cells. Here, functional and flow cytometry analyses were conducted.

Results: Immunohistochemical analysis of liver tissue sections of PDAC patients revealed that HMF represent an abundant stroma population in liver metastases, with clear differences in the spatial distribution in small (1500 µm) and large (> 1500 µm) metastases. In the latter, PD-L1 expression was mainly located at the invasion front or evenly distributed, while small metastases either lacked PD-L1 expression or showed mostly weak expression in the center. Double stainings revealed that PD-L1 is predominantly expressed by stromal cells, especially HMF. Small liver metastases with no or low PD-L1 expression comprised more CD8$^+$ T

10.3389/fonc.2023.1160824

cells in the tumor center, while large metastases exhibiting stronger PD-L1 expression comprised less $CD8^+$ T cells being mostly located at the invasion front. HMF-enriched spheroid cocultures with different ratios of PDAC cells and HMF well mimicking conditions of hepatic metastases *in situ*. Here, HMF impaired the release of effector molecules by $CD8^+$ T cells and the induction of PDAC cell death, an effect that was dependent on the amount of HMF but also of PDAC cells. ICI treatment led to elevated secretion of distinct $CD8^+$ T cell effector molecules but did not increase PDAC cell death under either spheroid condition.

Conclusion: Our findings indicate a spatial reorganization of HMF, $CD8^+$ T cells, and PD-L1 expression during progression of PDAC liver metastases. Furthermore, HMF potently impair the effector phenotype of $CD8^+$ T cells but the PD-L1/PD-1 axis apparently plays a minor role in this scenario suggesting that immune evasion of PDAC liver metastases relies on other immunosuppressive mechanisms.

KEYWORDS

pancreatic cancer, immune evasion, 3D coculture, hepatic metastasis, programmed death ligand 1, tumor microenvironment

1 Introduction

Pancreatic ductal adenocarcinoma (PDAC) is the 4th most common cause of cancer-related deaths in Western countries with a 5-year survival rate of less than 10% (1). Lacking specific symptoms, PDAC is lately (80%) diagnosed at a locally advanced or metastatic stage, with the liver representing the main site of metastases (2). To date, the only curative treatment is the R0 resection of the primary tumor. However, even these patients often relapse and develop metastases shortly after or even during adjuvant therapy (3). Since PDAC patients with liver metastases have an even worse prognosis, it is of outmost importance to better understand the mechanisms underlying metastatic progression in the liver and to identify effective treatment options (4). Treatment with immune checkpoint inhibitors (ICI), e.g. targeting programmed death ligand 1 (PD-L1) or its receptor programmed cell death protein 1 (PD-1), have improved the therapy of many cancers but failed in PDAC yet. Monoclonal antibodies such as Durvalumab and Pembrolizumab blocking PD-L1 and PD-1, respectively, aim to boost cancer-directed immunity by induction of $CD8^+$ T cell-mediated killing of tumor cells. However, so far ICI did not add any considerable benefit to the treatment of PDAC patients (5, 6). Nevertheless, a high infiltration of $CD8^+$ T cells is associated with longer overall survival of PDAC patients indicating that $CD8^+$ T cells exhibit a potent anti-tumorigenic potential in PDAC (5, 7). Moreover, absent PD-L1 expression and high $CD8^+$ T cell infiltration of PDAC are even linked to a better prognosis (8). Of note, PD-L1 expression in PDAC is very heterogeneous, as some tumors show no PD-L1 expression while others show high expression (8, 9). In the latter cases, PD-L1 is mostly expressed by stromal cells rather than tumor cells (9). However, whether and how stromal cell-associated PD-L1 expression impacts immune evasion is still poorly understood.

Desmoplasia, the tumor-associated excessive formation of connective tissue formed by fibroblasts, stellate cells, and their activated counterparts, the myofibroblasts, represents a hallmark of PDAC (10). Desmoplasia is an integral component of the stroma of primary PDAC as well as its liver metastases. Hepatic stellate cells (HSC) make up to 5% of all liver cells and are important to maintain liver homeostasis. In the presence of Transforming Growth Factor-beta 1 (TGF-β1), Platelet-derived Growth Factor (PDGF), or Interleukin-6 (IL-6) HSC transdifferentiate into hepatic myofibroblasts (HMF). HMF are characterized by a high expression of alpha-smooth muscle actin (αSMA) as well as the secretion of various inflammatory mediators and ECM molecules, that have been

Abbreviations: αSMA, alpha-Smooth Muscle actin; ccK18, caspase-cleaved Keratin 18; CAF, cancer-associated fibroblasts; CD, Cluster of Differentiation; CTLA-4, Cytotoxic T-Lymphocyte-associated Protein 4; CXCL, chemokine C-X-C motif ligand; ECM, extracellular matrix; FFPE, formalin-fixed and paraffin-embedded; FoV, Fields of View; G-CSF, Granulocyte Colony-stimulating Factor; HMF, hepatic myofibroblasts; HSC, hepatic stellate cells; ICI, immune checkpoint inhibitors; IFNγ, Interferon-gamma; IHC, immunohistochemical; IL, Interleukin; LAG3, Lymphocyte-Activation Gene 3; M-CSF, Macrophage Colony-stimulating Factor; MHC, Major Histocompatibility Complex; NSCLC, Non-small cell lung cancer; PanCK, Pan-Cytokeratin; PBMC, peripheral blood mononuclear cells; PDAC, Pancreatic ductal adenocarcinoma; PDGF, Platelet-derived Growth Factor; PD-1, Programmed cell death protein 1; PD-L1, Programmed cell death protein 1-ligand 1; TCM, T cell medium; TGF-β1, Transforming Growth Factor-beta 1; TIM3, T cell immunoglobulin and mucin domain-containing protein 3; TME, tumor microenvironment; VEGF, Vascular Endothelial Growth Factor.

10.3389/fonc.2023.1160824

reported to support tumor growth (11, 12). Furthermore, cancer-associated fibroblasts (CAF) can impact the immune response by secreting cytokines, like IL-6, Granulocyte Colony-stimulating Factor (G-CSF), and Macrophage Colony-stimulating Factor (M-CSF), or inhibiting $CD8^+$ T cells by either expressing PD-L1 or promoting expression of PD-1 and cytotoxic T-lymphocyte-associated protein 4 (CTLA-4) on $CD8^+$ T cells (13). Lenk et al. showed that the inflammatory status of the liver microenvironment is an essential driver for the outgrowth of liver metastases. Here, HMF promoted PDAC cell growth in a Vascular Endothelial Growth Factor (VEGF) dependent manner (14). Owing to their ability to release high amounts of ECM proteins and immune regulatory mediators, HMF generate a dense stroma, which acts as a physical barrier for immune cells and drugs (12). Although several studies have already demonstrated that myofibroblasts essentially contribute to drug resistance and immune evasion in PDAC (15–17), their impact on immune evasion of PDAC liver metastases is still poorly understood. Since metastases are not routinely resected in PDAC patients, tissue samples from PDAC metastases are rare and the expression of immune regulatory molecules such as PD-L1 within liver metastases is rarely characterized. Hence, this study intended to elucidate the role of PD-L1 in the interplay of PDAC cells, the hepatic microenvironment, and $CD8^+$ T lymphocytes in order to provide novel insight into the mechanisms contributing to immune escape of PDAC liver metastases.

2 Material and methods

2.1 Immunohistochemical analysis of liver tissues with PDAC metastases

Formalin-fixed and paraffin embedded (FFPE) biopsy samples or diagnostic resection specimens from liver metastases of 15 PDAC patients were used for immunohistochemical (IHC) analyses. The study was approved by the ethics committee of the Medical Faculty of Kiel University (reference number: A110/99). Written informed consent was obtained from all patients. Thirteen patients were male and two were female. The median age at diagnosis was 70 (range: 59-82). The histopathological diagnosis was confirmed by board certified surgical pathologists. From one patient a histopathological assessment was also performed from the primary tumor, from all other patients only from the liver biopsies. One patient suffered from metastasized PDAC with liver metastases and peritoneal carcinosis. Liver tissues for sectioning were mostly obtained from liver biopsies. Serial sections were used throughout this study and stained with antibodies directed against Pan-Cytokeratin (PanCK) (dilution 1:200, clone AE1/AE3, NeoMarkers *via* ThermoFisher Scientific, Waltham, MA, USA), αSMA (dilution 1:400, clone 1A4, NeoMarkers *via* ThermoFisher Scientific, Waltham, MA, USA), CD8 (dilution 1:100, clone C8144B, Leica Biosystems GmbH, Wetzlar, Germany), and PD-L1 (dilution 1:100, clone: E1L3N, Cell Signaling Technology, Danvers, MA, USA).

Furthermore, IHC double staining of liver metastases was performed. The first step involved the staining of PD-L1 (dilution 1:100, clone E1L3N; Cell Signaling Technology, Danvers, MA, USA). Antigen retrieval was achieved with ER2 (EDTA-buffer Bond pH 9.0; 20 minutes). The antigen retrieval step was modified for the PD-L1 staining of those slides, which were to be combined with αSMA staining in the second step. In those cases, PD-L1 visualization was enhanced in relation to the naturally intense αSMA signal by prolonging ER2 antigen retrieval to 30 minutes. The immunoreaction was visualized with the Bond™ Polymer Refine Detection Kit (DS 9800; brown labeling; Novocastra; Leica Biosystems GmbH, Wetzlar, Germany) resulting in a brown color. The second step involved the staining of either αSMA (dilution 1:400, clone: 1A4, NeoMarkers *via* Thermo Fisher Scientific, Waltham, MA, USA), or CD68 (dilution 1:100, clone: 514H12, Leica Biosystems GmbH, Wetzlar, Germany), or PanCK (dilution 1:200, clone AE1/AE3, NeoMarkers *via* ThermoFisher Scientific, Waltham, MA, USA). Antigen retrieval was carried out with ER1 (citrate buffer Bond pH 6.0; 20 minutes for αSMA), or ER2 (EDTA-buffer Bond pH 9.0; 20 minutes for CD68). The immunoreaction was visualized with the BOND™ Polymer Refine Red Detection Kit (DS9390; red labeling; Leica Biosystems GmbH, Wetzlar, Germany) resulting in a red color.

The IHC stainings were carried out on the autostainer BOND™ RX system (Leica Biosystems GmbH, Wetzlar, Germany). The stained tissue sections were scanned on the Hamamatsu NanoZoomer 2.0 RS digital slide scanner (Hamamatsu Photonics, Shizuoka Prefecture, Japan). Scanned tissue sections were analyzed with NDP.view2 software (Hamamatsu Photonics, Shizuoka Prefecture, Japan).

First, PanCK staining of the liver sections were used to categorize metastases into small (≤ 1500 µm) and large (> 1500 µm) metastases. Afterwards, the predominant localization of CD8, αSMA, and PD-L1 staining was rated as followed i) mostly in the tumor center, ii) mostly at the invasion front, or iii) evenly distributed between both regions. The analysis was performed at a magnification of 5-fold or 10 fold depending on the size of the respective metastasis. Further, the proportion of cells stained for CD8 and PD-L1 was analyzed in 10 representative fields of view (FoV) both at the invasion front of the metastases and in the tumor center at 100-fold magnification. The scoring was graded as i) 0% (negative), ii) ≤ 1%, or iii) > 1%. Additionally, PD-L1 staining intensity was scored as absent, low, or high. Finally, the percentages of the proportion of each score were calculated. All stainings were evaluated independently by two examiners (SB and LA).

2.2 Cell lines and cell culture

Human PDAC cell lines PancTu1 and Panc89 were cultured in PDAC cell medium (RPMI 1640 medium supplemented with 10% FCS, 1% L-Glutamine, and 1% sodium pyruvate (PAN-Biotech GmbH, Aidenbach, Germany)). PancTu1 cells were isolated from a primary tumor of a female PDAC patient and were used as a PDAC cell line with moderate PD-L1 cell surface expression. PancTu1 cells exhibit mutations in *k-ras* (G12V) and *p53* (C176S) and a depletion of *p16*, while *SMAD4* shows a wildtype status (18, 19). Panc89 cells were isolated of a lymph node metastasis of a 64-year-old male PDAC patient and were used as a PDAC cell line with low PD-L1 surface expression. Panc89 cells exhibit a mutation in *p53* (T220C) and depletion of *p16*, while the genes *k-ras* and *SMAD4* show a wildtype status (18, 19). Human myofibroblasts (Provitro GmbH, Berlin, Germany) were cultured in stellate cell medium

supplemented with 2% FCS, 1% stellate cell growth supplement, and 1% Penicillin and Streptomycin (Science Cell Research Laboratories, Carlsbad, CA, USA). One ng/ml of recombinant human TGF-β1 (BioLegend, San Diego, CA, USA) was added to maintain the myofibroblastic phenotype. All cell lines were cultivated in a 75 cm^2 cell culture flask at 37°C, 5% CO_2, and 86% relative humidity. The cells were regularly examined with a MycoAlert™ PLUS Mycoplasma Detection Kit (Lonza Group, Basel, Switzerland) to assure mycoplasma-free conditions.

2.3 Isolation of primary human $CD8^+$ T cells

Peripheral blood mononuclear cells (PBMC) were isolated from blood donations by healthy donors provided by the Institute of Transfusion Medicine, UKSH Campus Kiel. The research was approved by the ethics committee of the Medical Faculty of Kiel University and the University Hospital Schleswig-Holstein, Campus Kiel (reference number: A110/99 and D490/17). Written informed consent from all donors was obtained. For PBMC isolation, a Pancoll (PAN-Biotech GmbH, Aidenbach, Germany) density gradient centrifugation (350 xg, 25 min, 4°C) was performed. Afterwards, $125x10^6$ isolated PBMCs suspended in 10 ml RPMI 1640 medium supplemented with 1% FCS were transferred into a 75 cm^2 cell culture flask. After 45 minutes, the supernatant was carefully removed to obtain only the lymphocytes. Only lymphocyte purities of over 80% were used for isolation of $CD8^+$ T cells, which were verified by flow cytometry. In order to obtain untouched $CD8^+$ T cells, magnetic cell sorting was performed using a negative selection strategy with the $CD8^+$ T cell isolation kit from Miltenyi Biotec, according to the manufacturer's instructions (Miltenyi Biotec GmbH, Bergisch Gladbach, Germany).

2.4 Activation of $CD8^+$ T cells

Activation of primary naïve $CD8^+$ T cells was performed by stimulation with anti-CD3 and anti-CD28 antibodies which were used to mimic antigen-presenting cells. For this purpose, a 24-well plate was coated with 1.5 µg/ml anti-CD3 antibody (clone: OKT3, BioLegend, San Diego, CA, USA) diluted in 200 µl sterile PBS for 2 h at 37°C. Afterwards, the plate was washed twice with PBS to remove all unbound antibodies. Then, 1.5 $x10^6$ $CD8^+$ T cells per well were seeded in 1 ml PDAC cell medium further supplemented with 2% HEPES and 1% Penicillin and Streptomycin (TCM). Finally, 1.5 µg/ml anti-CD28 antibody (clone: CD28.2, BioLegend, San Diego, CA, USA), and 60 ng/ml recombinant human IL-2 (BioLegend, San Diego, CA, USA) were added. After 72 h, $CD8^+$ T cells were collected and used for subsequent coculture experiments.

2.5 Spheroid cultures of PDAC cells and HMF

In order to mimic the tumor cell to HMF ratio in small and large PDAC liver metastases, different ratios of PancTu1 or Panc89 cells and HMF were seeded for spheroid formation. Here, a PDAC cell to HMF ratio of 3:1 was seeded to mimic large metastases. A PDAC cell to HMF ratio of 5:1 was seeded to mimic small metastases. HMF and either PancTu1 or Panc89 cells were seeded together at the respective ratios at a total cell number of $2x10^4$ in 150 µl TCM in 96-well ultra-low attachment plates (faCellitate, Mannheim, Germany). As control, PancTu1 and Panc89 cells, respectively, were seeded as monoculture spheroids. After seeding, plates were centrifuged at 300 xg for 5 min and spheroids were cultured for 72 h, at 37°C, 5% CO2, and 86% relative humidity.

2.6 Spheroid cultures with $CD8^+$ T cells

In order to investigate the effect of PDAC cells and different amounts of HMF on the effector phenotype of $CD8^+$ T cells, medium from spheroid cultures was removed after 48 h and $2x10^5$ activated $CD8^+$ T cells were added in 150 µl of TCM/well for further 24 h.

2.7 Treatments of spheroid cultures

For ICI treatment medium of spheroid cultures was discarded after 48 h. Then, $2x10^5$ activated $CD8^+$ T cells were added and spheroid cocultures were treated with either 10 µg/ml of the respective isotype control antibody [hIgG1 (AstraZeneca, Cambridge, UK)/hIgG4 (Merck, KGaA, Darmstadt, Germany)], 10 µg/ml Durvalumab (AstraZeneca, Cambridge, UK), or 10 µg/ml Pembrolizumab (MSD, Kenilworth, NJ, USA) for 24 h.

Treatment with 10 µg/ml Gemcitabine (Hexal, Holzkirchen, Germany) was conducted 24 h after seeding of the spheroids. Respective controls were left untreated. After 24 h of treatment, the medium was discarded and $2x10^5$ activated $CD8^+$ T cells were added for further 24 h.

2.8 Flow cytometry

The expression of cell surface proteins on PDAC, HMF, and $CD8^+$ T cells was examined by immunofluorescence staining and subsequent flow cytometric analysis. For staining, supernatants containing $CD8^+$ T cells were collected from spheroid cultures and spheroids were mechanically dissociated with a 30G cannula to generate a single-cell suspension. Staining was performed according to the protocol of BioLegend. PancTu1, Panc89 cells, and HMF were stained with anti-PD-L1-PeCy7 antibody (clone: MIH3, #374506). PDAC cells were also stained with anti-EpCAM-APC antibody (clone: 9c4, #324208 (all from BioLegend, San Diego, CA, USA). $CD8^+$ T cells were stained with anti-CD8-FITC (clone: RPA-T8, #301006), anti-PD-1-PE (clone: EH12.2H7, #621608), anti-CD69-PeCy7 (clone: FN50, #310912), and anti-CD25-APC antibodies (clone: BC96, #302610) (all from BioLegend, San Diego, CA, USA). Staining specificity was verified by staining with respective isotype control antibodies: mIgG1-PeCy7 (clone: MOPC-21, #400126), mIgG2b-APC (clone: MPC-11, #400321), mIgG1-FITC (clone: MOPC-21, #400108), mIgG1-PE (clone: MOPC-21, #400112), and mIgG1-PAC (clone: MOPC-21, #400122), (all from

10.3389/fonc.2023.1160824

BioLegend, San Diego, CA, USA)). For relative quantification of cell surface expression levels, median fluorescence intensity (MFI) ratio was calculated by dividing the MFI detected for the specific staining by the MFI detected for the staining with the respective isotype controls. For the assessment of the lymphocyte purity prior to isolation of $CD8^+$ T cells (see section Isolation of primary human $CD8^+$ T cells) cells were washed once with MACS Buffer (PBS (PAN-Biotech GmbH, Aidenbach, Germany) supplemented with 0.5% BSA (Biomol, Hamburg, Germany) and 2 mM EDTA (Carl Roth GmbH, Karlsruhe, Germany)) and then fixed in MACS Buffer supplemented with 1% PFA (ThermoFisher Scientific, Waltham, MA, USA). Data acquisition was performed with a MACS Quant X (Miltenyi Biotec GmbH, Bergisch Gladbach, Germany) and evaluation was conducted using the FlowJo program v10.8.1 (BD Bioscience, Franklin Lakes, New Jersey, USA).

2.9 LEGENDplex™

LEGENDplex™ Human CD8/NK Mix and Match Subpanel and LEGENDplex™ Human total TGF-β1 (BioLegend, San Diego, CA, USA) were used according to the manufacturer's instructions for quantification of Interferon-gamma (IFN-γ), Granzyme A, Granzyme B, Perforin, Granulysin, and TGFβ-1 concentrations in cell culture supernatants. Measurement was performed on the BD FACSymphony™ A1 flow cytometer (BD Bioscience, Franklin Lakes, New Jersey, USA). The evaluation was conducted using the LEGENDplex™ data analysis software (BioLegend, San Diego, CA, USA).

2.10 M30 CytoDeath™ ELISA

Cell death induction in PDAC cells in the different spheroid cultures was assessed with the M30 CytoDeath ELISA kit following the manufacturer's instructions (Diapharma Group Inc., West Chester, OH, USA). The assay detects caspase-cleaved Keratin 18 (ccK18) which is generated exclusively by PDAC cells undergoing apoptotic cell death in the used spheroid cultures. Measurement of ccK18 in supernatants of spheroid cultures was performed on the Infinite 200 PRO microplate reader (Tecan, Crailsheim, Germany).

2.11 Statistical analysis

Statistical analyses were performed with GraphPad Prism 9.2.0 (GraphPad Software, San Diego, CA, USA). First, data was tested for normal distribution and equal variances using Shapiro-Wilk test. Two tailed t-test was performed for analysis of two normally distributed data sets. Groups of data sets that did not pass the test for normal distribution and equal variances were analyzed by the Mann-Whitney Rank Test. Parametric data sets of including more than two groups were analyzed with the one-way-analysis of variance (one-way-ANOVA). For multiple comparison the Tukey Test was used. Non-parametric data sets comprising more than two groups were analyzed using Kruskal-Wallis one-way-ANOVA on Ranks and for multiple comparison the Dunn's Test was performed. Statistical significance was considered for p-values of < 0.05, according to Student-Newman-Keuls test for parametric and Dunn method for non-parametric data. The significance levels are indicated by asterisks: $p < 0.05$ = *, $p < 0.01$ = **, $p < 0.001$ = ***.

3 Results

3.1 Different spatial distribution of myofibroblasts, $CD8^+$ T cells, and PD-L1 expression in small and large liver metastases of PDAC patients

To better understand whether PD-L1 might play a role in immune evasion of PDAC cells in liver metastasis, it was examined whether PD-L1 is expressed in liver metastasis, and how this relates to defined stroma compositions. For this purpose, serial sections of liver metastases from 15 PDAC patients were stained for PanCK, αSMA, CD8, and PD-L1 (Figure 1A). Since previous studies reported that stroma composition markedly differs with regard to metastasis size (20), metastases were categorized into small (≤ 1500 µm) and large (> 1500 µm) metastases (Supplementary Figure 1A). In general, more small than large metastases were detected in the liver sections (Supplementary Figure 1B). First, desmoplasia was assessed by evaluating the abundance of myofibroblasts. Small and large metastases clearly differ with respect to aSMA+ the spatial distribution (Figure 1B) and extent (Figure 1C) of αSMA+ myofibroblasts. While in small metastases αSMA-expression was detectable in the tumor center or evenly distributed between tumor center and the invasion front, αSMA staining was predominantly located inside of large metastases (Figure 1B). Further, the number of myofibroblasts was rated and compared (+ = low number, ++ = medium number, or +++ = high number of myofibroblasts). While small metastases were mostly characterized by low numbers of myofibroblasts, 50% of large metastases exhibited high numbers (Figure 1C). Moreover, also spatial distribution of $CD8^+$ T cells clearly differed between small and large metastases. While $CD8^+$ T cells were predominantly located inside or evenly distributed in small metastases, in large metastases the majority of $CD8^+$ T cells were almost exclusively found at the invasion front (Figure 1D). In line with these findings, 15% of all FoV examined in the tumor center of large metastases exhibited no $CD8^+$ T cells. These FoV were only scored in the tumor centers (Supplementary Figure 1C). However, within the majority of FoV more than 1% of these cells were stained for CD8 in both small and large metastases, albeit in small metastases over 60% of FoV contained even higher proportions of $CD8^+$ T cells (Figure 1E). Finally, histoanatomical localization and intensity of PD-L1 staining were analyzed. Here, 35% of small metastases showed no PD-L1 staining and if present, staining was predominantly observed in the tumor center. In contrast, PD-L1 staining in large metastases was either evenly distributed or localized predominantly at the invasion front (Figure 1F). Of note, FoV in large metastases exhibited significantly more $PD\text{-}L1^+$ cells compared to small metastases (Figure 1G) which were associated with significantly more FoV with strong PD-L1 staining. Interestingly, strong PD-L1

10.3389/fonc.2023.1160824

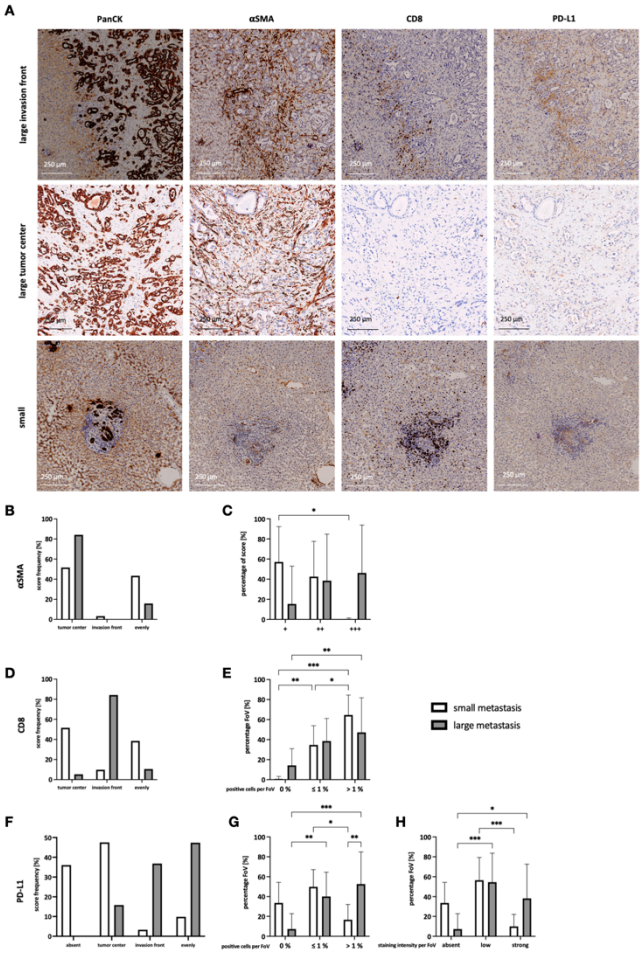

FIGURE 1
Different spatial distribution of myofibroblasts, CD8$^+$ T cells, and PD-L1 expression in small and large liver metastases of PDAC patients. **(A)** Representative images of the staining of PanCK, αSMA, CD8 and PD-L1 in large and small liver metastases of PDAC patients. The main localization of **(B)** αSMA, **(D)** CD8 T cells, and **(F)** PD-L1 expression were scored comparing absent expression and expression in the tumor center, at the invasion front, or evenly distributed between tumor center and invasion front in small and large liver metastases. **(C)** The abundance of αSMA was rated as low number (+), medium number (++), or higher number (+++) of myofibroblasts in each metastasis. Furthermore, a maximum of 10 microscopic Fields of View (FoV) in the tumor center and at the invasion front were analyzed and the proportion of **(E)** CD8$^+$ T cells and **(G)** PD-L1$^+$ cells was determined. The proportion was ranked as 0%, ≤ 1%, or > 1% for CD8 and PD-L1, respectively. **(H)** Intensity of PD-L1 staining was ranked for each FoV, comparing absent, low, or strong expression. Data represents the mean ± SD of 15 independent liver tissue sections. * = $p < 0.05$, ** = $p < 0.01$, ***$p < 0.001$.

staining was mostly found at the invasion front (Figure 1H, Supplementary Figure 1E). In contrast, PD-L1$^+$ cells were detected only in 33% of all FoV in small metastases. Comparing the spatial distribution of PD-L1, PanCK, and αSMA in serial liver sections demonstrated that PD-L1 staining was mainly colocalized with αSMA staining rather than PanCK staining, indicating that PD-L1 is mainly expressed by myofibroblasts in PDAC liver metastases (Figure 1A). For validation, IHC double stainings of PanCK/PD-L1, αSMA/PD-L1, and CD68/PD-L1 were performed showing that PD-L1 was more expressed by myofibroblasts and also macrophages rather than tumor cells (Supplementary Figures 2A-C).

In summary, our IHC analyses revealed that small liver metastases comprise more CD8$^+$ T cells in their tumor center with no or low PD-L1 expression, while large metastases exhibit stronger PD-L1 expression and less CD8$^+$ T cells being mostly located at the invasion front. Furthermore, HMF represent an

10.3389/fonc.2023.1160824

abundant stroma population in liver metastases of PDAC, with clear differences in the spatial distribution in small and large metastases and being a main source of PD-L1 expression. Overall, these findings support the hypothesis that outgrowth of hepatic PDAC metastases is accompanied by stroma remodeling involving considerable alterations in the localization and number of $CD8^+$ T cells, myofibroblasts as well as PD-L1 expression.

3.2 Spheroid coculture of PDAC cells and HMF mimic hepatic PDAC metastases

The IHC analysis of PDAC liver metastases revealed clear differences with respect to PD-L1 expression and number of HMF in small and large metastases. To investigate whether the PD-1/PD-L1 axis and HMF contribute to immune escape of PDAC liver metastases, a stroma enriched 3D spheroid coculture model was established *in vitro*. To mimic small and large hepatic PDAC metastases, PancTu1 or Panc89 PDAC cells and HMF were seeded at different ratios (PDAC : HMF 5:1 = 83,3% vs. 16.7%, representative for small metastases; PDAC : HMF 3:1 = 75% vs. 25%, representative for large metastases). As control, PancTu1 and Panc89 cell monoculture spheroids were seeded (Figure 2A). In general, mono- and coculture spheroids of PancTu1 cells were larger (~800 µm) compared to Panc89 cell spheroids (~500 µm). In line with the *in situ* findings of small and large liver metastases, less HMF were present at the 5:1 ratio (small metastases) compared to the 3:1 ratio (large metastases) in both PDAC cell models after

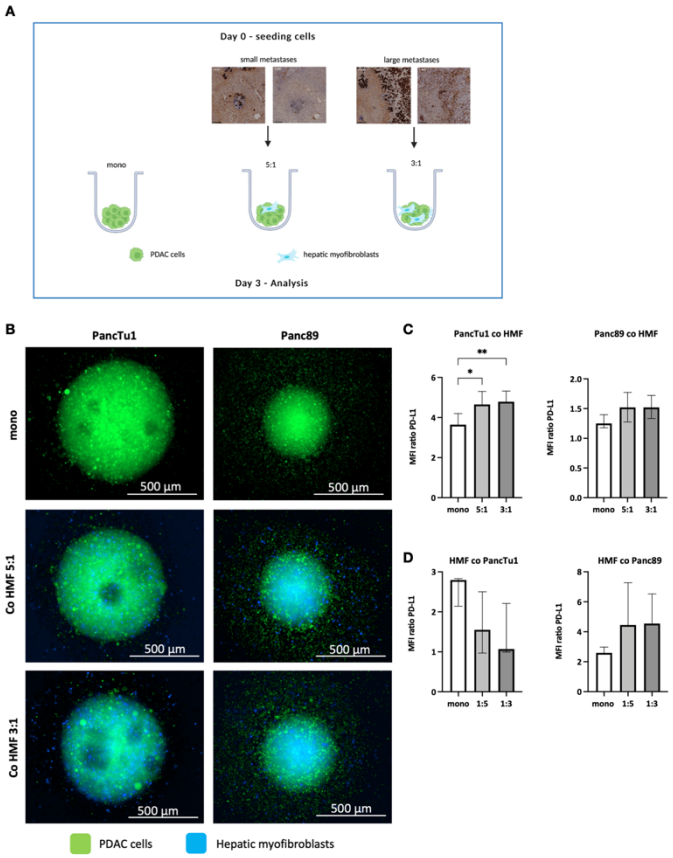

FIGURE 2
Spheroid coculture of PDAC cells and HMF mimic hepatic PDAC metastases. **(A)** Schematic illustration of the PDAC spheroids cultures: PancTu1 and Panc89 cells were either seeded in mono- or coculture with hepatic myofibroblasts (HMF) at different ratios (5:1 or 3:1) in ultra-low attachment plates for 3 days. Figure was created with BioRender.com. **(B)** Representative images of PancTu1 and Panc89 spheroids in mono- and coculture with HMF after 3 days. In green (cell tracker green) PDAC cells and in blue (cell trace violet) HMF. For flow cytometry analysis, spheroids were mechanically dissociated and the median fluorescence intensity (MFI) ratio of PD-L1 on **(C)** PancTu1 cells, Panc89 cells, and **(D)** HMF after mono- or coculture was determined. Data represents the mean ± SD (normally distributed) or the median with interquartile range (not normally distributed). N=5. * = $p < 0.05$, ** = $p < 0.01$.

10.3389/fonc.2023.1160824

spheroid formation. In addition, HMF appeared to be evenly distributed in the spheroids at a 5:1 ratio and more inside at a 3:1 ratio (Figure 2B). Moreover, monocultured PancTu1 cells exhibited higher PD-L1 cell surface levels compared to Panc89 cells, which well mimics the expression heterogeneity in tumor cells observed in hepatic PDAC metastases. After coculture, PD-L1 cell surface levels were slightly increased in both PDAC cell lines in the presence of HMF independent of the coculture condition (Figure 2C). In line with the *in situ* findings, monocultured HMF exhibited higher PD-L1 cell surface levels compared to those on PDAC cells which were slightly downregulated by coculture with PancTu1 cells and slightly upregulated by coculture with Panc89 cells (Figure 2D).

Overall, our stroma enriched spheroid coculture model containing PDAC cells and HMF at different ratios well mimicked the proportion and distribution of PDAC cells and HMF as well as their PD-L1 expression detected in small and large hepatic PDAC metastases.

3.3 The effector phenotype of CD8$^+$ T cells and induction of PDAC cell death are impaired by HMF in PDAC coculture spheroids

Having provided evidence that our *in vitro* model well simulates the contextual situation identified in PDAC liver metastases *in situ*, we next examined whether the effector phenotype of CD8$^+$ T cells is impacted by the different stroma conditions. For this purpose, CD8$^+$ T cells were pre-activated for 72 hours and then seeded in the different spheroid cultures (Figure 3A). At this time point, CD8$^+$ T cells exhibited high cell surface expression of CD25 and the early activation marker CD69 along with considerable expression levels of PD-1 (data not shown). As seen in Figure 3B, cell surface levels of CD25 and CD69 as well as PD-1 in CD8$^+$ T cells were hardly affected by different spheroid coculture conditions in both PDAC cell models. Next, supernatants derived from CD8$^+$ T cells cultured with mono- and coculture PDAC cell spheroids were analyzed for the presence of cytotoxic effector molecules (Figure 3C). Levels of Granzyme A and B, Perforin, Granulysin, and IFNγ were not altered in supernatants obtained from CD8$^+$ T cells cultured with HMF-enriched PancTu1 spheroids compared to supernatants from PancTu1 monoculture spheroids. However, levels of Granzyme A, Granulysin, and IFNγ were decreased in supernatants from CD8$^+$ T cells after culture with Panc89 HMF spheroids compared to culture with Panc89 monoculture spheroids being even more reduced in the presence of higher amounts of HMF (PDAC : HMF ratio 3:1) resembling large metastases (Figure 3C). Finally, we analyzed whether the effector phenotype of CD8$^+$ T cells correlates with the induction of PDAC cell death. For this purpose, supernatants of CD8$^+$ T cells cultured with PDAC mono- and coculture spheroids were analyzed for the presence of ccK18 indicative for induction of PDAC cell death. As shown in Figure 3D, ccK18 levels were detectable at low levels and comparable between mono- and coculture PancTu1 and Panc89 spheroids in the absence of CD8$^+$ T cells. In the presence of CD8$^+$ T cells, significantly elevated ccK18 levels were measured in both PancTu1 and Panc89 spheroids devoid of HMF. However, a clear reduction of ccK18 levels was observed in supernatants of coculture spheroids of either PDAC cell line in the presence of CD8$^+$ T cells, with the strongest reduction observed in supernatants of spheroids containing higher amounts of HMF (3:1). This effect was more pronounced in the Panc89 HMF spheroids being in line with more pronounced reduction of CD8$^+$ T cell effector molecules in supernatants from HMF enriched Panc89 coculture spheroids (Figure 3D).

Overall, these data suggest that HMF impair the release of effector molecules by CD8$^+$ T cells and the induction of PDAC cell death, an effect that is dependent on the amount of HMF but not on the PDAC cells.

3.4 ICI treatment leads to elevated secretion of distinct CD8$^+$ T cell effector molecules but does not increase PDAC cell death

After having shown that the PDAC-HMF interplay impairs the effector phenotype of CD8$^+$ T cells, it was investigated whether ICI treatment is able to restore the effector phenotype and leads to enhanced induction of PDAC cell death. PD-L1 and PD-1 were blocked by Durvalumab and Pembrolizumab, respectively, for 24 hours under the distinct spheroid conditions cultured with CD8$^+$ T cells (Figure 4A). Successful blocking of cell surface associated PD-L1 and PD-1 by either Durvalumab or Pembrolizumab treatment on each cell population was validated by flow cytometry. Cell surface levels of PD-1 on CD8$^+$ T cells were significantly lower after Pembrolizumab treatment (Figure 4B) and cell surface levels of PD-L1 on PDAC cells and HMF were also significantly lower after Durvalumab treatment compared to treatment with respective the control antibody (Supplementary Figures 3A-C). In order to examine the effect of Durvalumab and Pembrolizumab treatment on the respective effector phenotype of CD8$^+$ T cells, we first analyzed cell surface expression levels of T cell activation markers CD25 and CD69. No considerable effects on the cell surface expression levels of CD69 and CD25 on CD8$^+$ T cells by Durvalumab treatment after culture with either spheroid condition was observed (Figure 4B). However, treatment with Pembrolizumab led to a slight decrease of the expression of CD25 in CD8$^+$ T cells cultured with PancTu1 coculture spheroids but not with Panc89 coculture spheroids, while the expression of CD69 was only decreased on CD8$^+$ T cells when cultured with PancTu1 coculture spheroids at a ratio of 3:1 (Figure 4B). Next, the concentration of CD8$^+$ T cell effector molecules in supernatants of the different spheroid cultures was analyzed. Durvalumab did almost not affect levels of Granzyme A, Granzyme B, Perforin, Granulysin, and IFNγ in supernatants of CD8$^+$ T cells cultured with either PDAC cell spheroids (Figure 4C, light grey), except Granulysin levels which were diminished after coculture with PancTu1:HMF spheroids (5:1 ratio). In contrast, levels of Granzyme B and IFNγ were elevated in supernatants from CD8$^+$ T cells cultured with Panc89 coculture spheroids but not with Panc89 monoculture spheroids after Durvalumab treatment. Notably, no decrease in Granzyme A, Granulysin, and IFNγ concentration was detectable

10.3389/fonc.2023.1160824

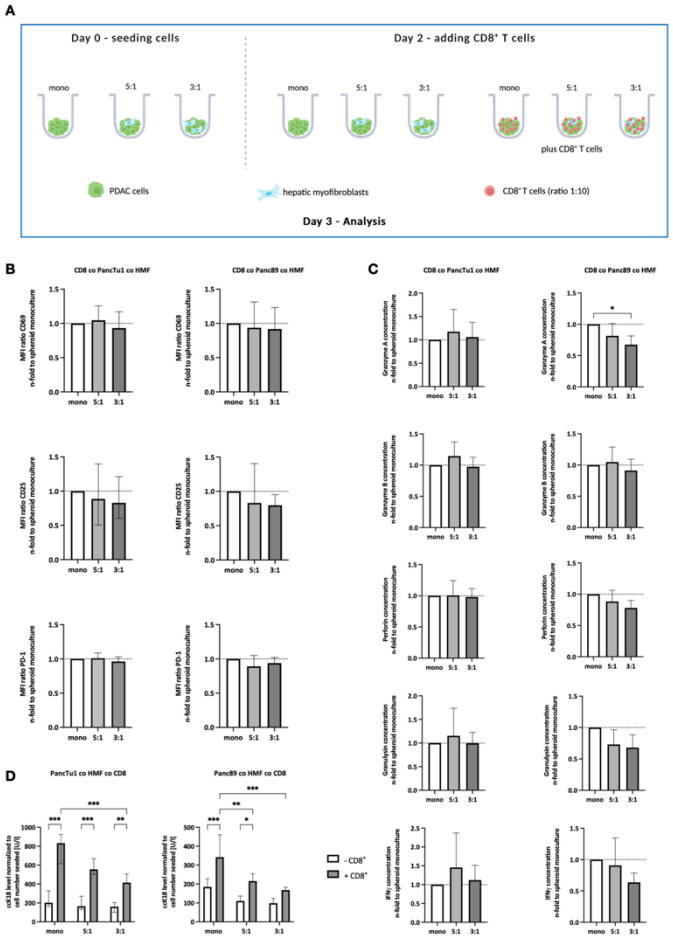

FIGURE 3
The effector phenotype of CD8$^+$ T cells and induction of PDAC cell death are impaired by HMF in PDAC coculture spheroids. **(A)** Schematic illustration of the PDAC spheroids cultures in the absence or presence of CD8$^+$ T cells. PancTu1 and Panc89 cells were either seeded in mono- or coculture with hepatic myofibroblasts (HMF) at different ratios (5:1 or 3:1) in ultra-low attachment plates. After 48 h, activated CD8$^+$ T cells were added at a ratio of 1:10 in one half of the cultures for further 24 h. Figure was created with BioRender.com. **(B)** CD8$^+$ T cells obtained from different spheroid cultures were stained for CD69, CD25, and PD-1 analyzed by flow cytometry analysis and the median fluorescence intensity (MFI) ratio of each specific staining was determined. **(C)** The concentration of Granzyme A, Granzyme B, Perforin, Granulysin, and IFNγ was analyzed in the supernatants of differentially cultured spheroids. Data was normalized on the expression and the concentration in supernatants of CD8$^+$ T cells in culture with mono-culture spheroids. **(D)** Levels of caspase-cleaved cytokeratin 18 (ccK18) were measured in supernatants of mono- and coculture spheroids in the absence or presence of CD8$^+$ T cells and normalized to the seeded PDAC cell number. Data represents the mean ± SD (normally distributed) or the median with interquartile range (not normally distributed). N=4. * = $p < 0.05$, ** = $p < 0.01$, ***$p < 0.001$.

anymore in supernatants from Panc89 cell spheroids enriched with HMF (mainly at 3:1 ratio, Figure 4B, light grey), indicating a compensation of the HMF mediated inhibitory effect by the PD-L1 inhibitor. Pembrolizumab treatment did almost not affect levels of Granzyme A, Perforin, and Granulysin in supernatants of CD8$^+$ T cells cultured with mono- or coculture spheroids of either PDAC cell line (Figure 4C, dark grey), while levels of Granzyme B and IFNγ were enhanced in supernatants of HMF enriched spheroids of PancTu1 and Panc89 cells. Finally, it was analyzed whether ICI treatment increased PDAC cell death under the different culture conditions. Overall, no considerable effect of PD-L1 or PD-1 blockade on PDAC cell death was detectable in either spheroid condition and Durvalumab treatment led even to decreased ccK18 levels in supernatants of CD8$^+$ T cells and HMF-enriched PancTu1 spheroids (at 5:1 ratio, Figure 4D, light grey).

Overall, these data indicate that although either ICI treatment led to slight elevation of distinct CD8$^+$ T cell cytotoxic effector molecules

10.3389/fonc.2023.1160824

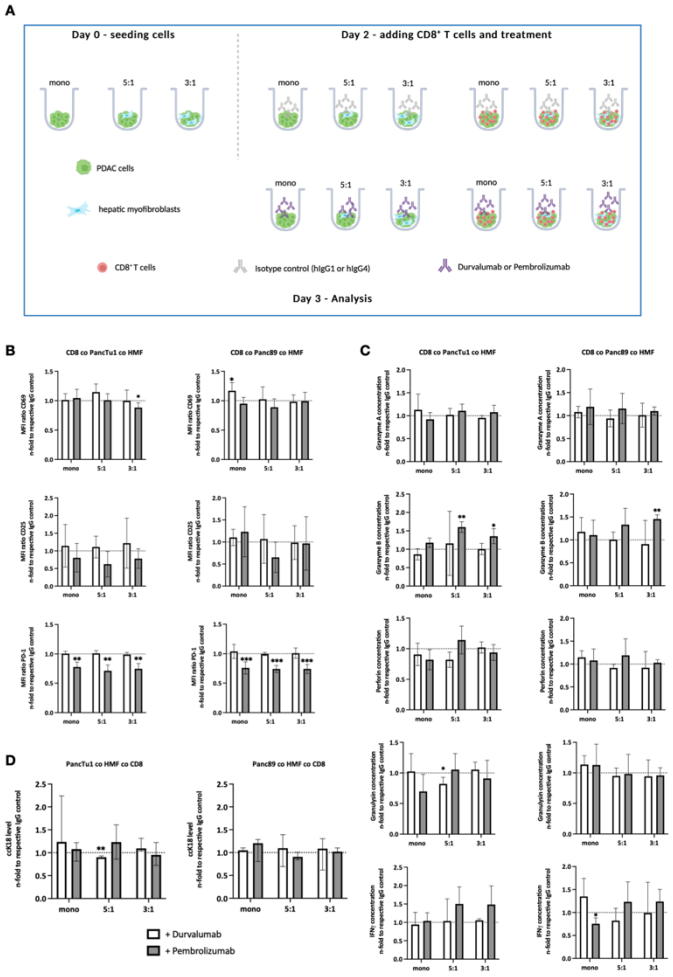

FIGURE 4
ICI treatment leads to elevated secretion of distinct CD8$^+$ T cell effector molecules but does not increase PDAC cell death. **(A)** Schematic illustration of the PDAC spheroids cultures before adding CD8$^+$ T cells. PancTu1 and Panc89 cells were either seeded in mono- or coculture with hepatic myofibroblasts (HMF) at different ratios (5:1 or 3:1) in ultra-low attachment plates. After 48 h, the medium was discarded and activated CD8$^+$ T cells were added at a ratio of 1:10 in one half of the cultures and either 10 µg/ml of the respective isotype control, Durvalumab or Pembrolizumab were applied for 24 h. Figure was created with BioRender.com. **(B)** CD8$^+$ T cells obtained from different spheroid cultures were stained for CD69, CD25, and PD-1 by flow cytometry analysis where the median fluorescence intensity (MFI) ratio of each specific staining was determined. **(C)** The concentration of Granzyme A, Granzyme B, Perforin, Granulysin, and IFNγ was analyzed in the supernatants of differentially treated culture spheroids. Data was normalized on the expression and on the concentration in supernatants of the respective IgG control treated spheroid cultures. **(D)** Levels of caspase-cleaved cytokeratin 18 (ccK18) were measured in supernatants of CD8$^+$ T cells with mono- and coculture spheroids after ICI treatment. Data was normalized to the isotype control of the respective spheroid culture setting. Data represents the mean ± SD (normally distributed) or the median with interquartile range (not normally distributed). N=4. * = $p < 0.05$, ** = $p < 0.01$, ***$p < 0.001$.

10.3389/fonc.2023.1160824

which seemed to be dependent on the presence of HMF and PDAC cells, this did not result in enhanced induction of PDAC cell death.

3.5 Gemcitabine affects the effector phenotype of CD8$^+$ T cells and PDAC cell death induction in dependence on PDAC cells

Since treatment with Gemcitabine represents the most frequent first-line therapy of PDAC patients, it was investigated whether Gemcitabine impacts PD-L1 and PD-1 expression as well as the effector phenotype of CD8$^+$ T cells in the context of the PDAC-HMF interplay. For this purpose, monocultured and HMF-enriched PancTu1 and Panc89 spheroids were either left untreated or treated with Gemcitabine for 24 hours and then cultured with CD8$^+$ T cells (Figure 5A). As shown in Figure 5B, Gemcitabine treatment led to diminished CD25 cell surface expression levels on CD8$^+$ T cells derived from Panc89 mono- and coculture spheroids, while CD69 cell surface expression was almost not altered on CD8$^+$ T cells obtained from either PDAC cell spheroid culture (Figure 5B). PD-1 cell surface levels were significantly lower on CD8$^+$ T cells derived from any culture with PDAC mono- or coculture spheroids, which were pretreated with Gemcitabine (Figure 5B). In contrast, Gemcitabine hardly altered PD-L1 cell surface expression on monocultured PDAC cells as well as HMF (Supplementary Figure 4). Moreover, levels of Granzyme A, Granzyme B, Perforin, and Granulysin were reduced – either by trend or significantly - in all supernatants of CD8$^+$ T cells and Gemcitabine treated PDAC mono- and coculture spheroids, while IFNγ was almost not altered in supernatants of Gemcitabine treated cultures (Figure 5C). Finally, it was analyzed whether Gemcitabine affects induction of PDAC cell death in dependence on the presence of HMF and CD8$^+$ T cells. While treatment with Gemcitabine hardly impacted cell death of either PDAC cell line in mono- and coculture spheroids in the absence of CD8$^+$ T cells, clear differences were observed in their presence (Figure 5D). While ccK18 levels were markedly lower in supernatants of CD8$^+$ T cells cultured with Gemcitabine treated PancTu1 mono- and coculture spheroids, elevated ccK18 levels were noted in supernatants from any Panc89 cell spheroids cultured with CD8$^+$ T cells (Figure 5D).

Overall, these data demonstrate that Gemcitabine treatment diminishes the release of CD8$^+$ T cell effector molecules and reduces cell surface expression level of PD-1 on CD8$^+$ T cells. Since cell death induction was reduced in PancTu1 spheroids but enhanced in Panc89 spheroids cultured with CD8$^+$ T cells after Gemcitabine treatment, these effects seem to be dependent on the PDAC cells.

4 Discussion

In many cancer entities, ICI treatment has emerged as a successful therapeutic option even at advanced disease stages prolonging the overall survival of the patients (21–23). However, PDAC patients have not shown significant treatment responses yet (24, 25). Still, the mechanisms of ICI resistance of PDAC are poorly understood, particularly regarding the metastatic setting. Besides expression of PD-L1 and PD-1 by tumor and stromal cells, a high mutational tumor burden and high infiltration and presence of CD8$^+$ T cells are known prognostic parameters for the prediction of an ICI response (26–30). PDAC is characterized by a low mutational burden and regarded as a so called “cold” or “excluded” tumor with a general low T cell infiltration into the tumor (30). In addition, CD8$^+$ T cells are often defined as exhausted and show a higher resistance towards ICI treatment (31, 32). Altogether, these findings provide an explanation for ICI resistance of this tumor (33). However, these parameters have been described for primary PDAC and still knowledge about expression of PD-L1 and stromal composition in PDAC metastases is rare and whether immune evasion of metastatic PDAC relies on the PD-L1/PD-1 axis.

Rahn et al. showed that PD-L1 is expressed in primary tumor tissues of PDAC patients staged T3N1M0, however, only in 20% of the analyzed tissues (9). As 80% of PDAC patients are diagnosed at a locally advanced or metastatic stage, with the liver representing the main site of metastases (2, 34), it was first to be determined whether PD-L1 is expressed in liver metastases of PDAC patients and how this relates to the abundance and spatial distribution of CD8$^+$ T cells. In this study, IHC stainings of liver tissue sections revealed that during metastatic progression (from small to large metastases) the tumor microenvironment (TME) seems to be remodeled. Staining of αSMA, indicative for myofibroblasts, was less detectable in small metastases compared to large metastases which is in line with the findings of Quaranta et al., who showed in a PDAC mouse model that αSMA expression was lower in small metastatic lesions compared to large liver metastases (20). Myofibroblasts are the main source of ECM molecules such as collagen or fibronectin within the desmoplastic tumor stroma (11). The ECM is a physical barrier for T cells and has been shown to prevent the penetration of CD8$^+$ T cells into the liver metastases (12). The inability of CD3$^+$ and CD8$^+$ T cells to infiltrate into metastases was also observed in our cohort, particularly in large metastases. Here, CD3$^+$ T cells and CD8$^+$ T cells, respectively were mostly found at the invasion front, while in small metastases CD8$^+$ T cells were detected throughout the whole lesions or in the tumor center. Since the proportion of myofibroblasts was higher in large metastases, it can be speculated that myofibroblasts along with the released ECM molecules provide a physical barrier preventing T cell infiltration into metastases. Quaranta et al. demonstrated similar results in liver metastases of PDAC patients. Here, the number of CD8$^+$ T cells was higher and closer to PanCK poor lesions (reflecting small lesions) compared to PanCK rich lesions (reflecting large lesions) (20). Grout et al. also showed that in non-small-cell lung cancer (NSCLC) tumor infiltration by CD3$^+$ and CD8$^+$ T cells was significantly lower when αSMA$^+$ CAF are present at the invasion front (35). Finally, PD-L1 expression was mainly located at the invasion front or evenly distributed in large metastases, while small metastases either lacked PD-L1 expression or showed mostly weak expression in the center. Double staining revealed that PD-L1 is predominantly expressed by stromal cells, especially HMF. Besides HMF also Kupffer cells (36) or other metastases-associated macrophages seemed to be an important source of tumoral PD-L1 expression. The fact that in PDAC stromal cells appear to be the main source of PD-L1 expression rather than

10.3389/fonc.2023.1160824

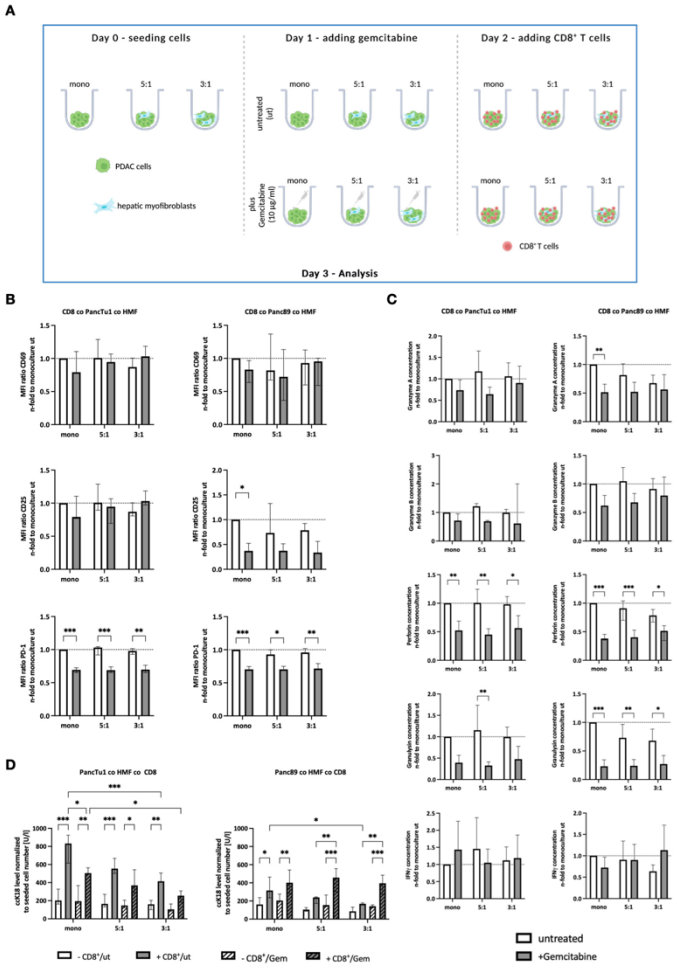

FIGURE 5
Gemcitabine affects the effector phenotype of CD8$^+$ T cells and PDAC cell death induction in dependence on PDAC cells. **(A)** Schematic illustration of Gemcitabine treatment of PDAC spheroids cultures before adding CD8$^+$ T cells. PancTu1 and Panc89 cells were either seeded in mono- or coculture with hepatic myofibroblasts (HMF) at different ratios (5:1 or 3:1) in ultra-low attachment plates for 24 h. Then, spheroids were either left untreated or treated with 10 µg/ml Gemcitabine. After 24 h, the medium was changed and activated CD8$^+$ T cells were added at a ratio of 1:10 in one half of the cultures. **(B)** CD8$^+$ T cells obtained from different spheroid cultures were stained for CD69, CD25, and PD-1 by flow cytometry analysis and the median fluorescence intensity (MFI) ratio of each specific staining was determined. **(C)** The concentration of Granzyme A, Granzyme B, Perforin, Granulysin, and IFNγ was analyzed in supernatants of differentially and treated culture spheroids. Data was normalized on the expression and on the concentration in supernatants of CD8$^+$ T cells in culture with untreated mono-cultured spheroids. **(D)** Levels of caspase-cleaved cytokeratin 18 (ccK18) were measured in supernatants of CD8$^+$ T cells with untreated or Gemcitabine treated mono- and coculture spheroids. The ccK18 levels were normalized to seeded cell number of PDAC cells. Data represents the mean ± SD (normally distributed) or the median with interquartile range (not normally distributed). N=4. * = $p < 0.05$, ** = $p < 0.01$, ***$p < 0.001$.

the PDAC cells has been already demonstrated by Rahn et al. in primary tumors of PDAC patients (9). Of note, small liver metastases with no or low PD-L1 expression comprised more CD8$^+$ T cells in the tumor center, while large metastases exhibiting stronger PD-L1 expression comprised less CD8$^+$ T cells being mostly located at the invasion front. Overall, these findings led to the conclusion that HMF associated PD-L1 expression might contribute to immune evasion of PDAC cells.

These differences between small and large metastases were experimentally well mimicked in 3D cocultures *in vitro* by using

different tumor cell to HMF ratios (3:1 ratio = large and 5:1 ratio = small metastases). The fact that the diameter of the spheroids was larger after coculture with HMF along with a higher number of PDAC cells (data not shown) indicates that HMF support tumor cell growth, which is in line with previous findings from other *in vivo* and *in vitro* studies (14, 37). As observed in the liver metastases, HMF exhibited higher PD-L1 expression compared to PDAC cells. Moreover, PD-L1 cell surface levels on HMF were altered in the presence of PDAC cells, and HMF were able to increase PD-L1 expression on PDAC cell lines. In line with these findings, Inoue et al. reported that patients with lung adenocarcinoma classified with a high expression of αSMA were PD-L1 positive suggesting a correlation between a high abundance of myofibroblasts and elevated PD-L1 expression. Furthermore, CAF have been shown to increase PD-L1 expression on different lung adenocarcinoma cell lines *via* CXCL2 secretion and signaling (32). CXCL2 can activate the JAK-STAT signaling pathway, resulting in the upregulation of transcriptional factors that control the expression of PD-L1 (38). Therefore, strong PD-L1 expression and high local abundance of myofibroblasts might be also mechanistically linked in hepatic PDAC metastases. Gorchs et al. also showed that CAF isolated from tumor tissues of PDAC patients enhance the expression of immune checkpoint molecules, like PD-1 and CTLA-4, on $CD8^+$ and $CD4^+$ T cells (13). In PDAC tissues, most $CD8^+$ T cells are exhausted and show a high expression of PD-1 (39). Likewise, $CD8^+$ T cells used in our 3D cultures were characterized by high PD-1 expression. In a PDAC mouse model, it was shown that $CD8^+$ T cells around large liver metastases showed higher PD-1 expression compared to those located around small metastases (20) further pointing to a role of the PD-L1/PD-1 axis in immune evasion of PDAC. Indeed, ccK18 levels were lower in supernatants of $CD8^+$ T cells cultured with PDAC coculture spheroids, particularly when a high amount of HMF was present in the spheroids, indicating a reduced PDAC cell death induction the more HMF are abundant. This finding is in line with the lower cell surface expression levels of activation markers on $CD8^+$ T cells as well as lower levels of cytotoxic T cell associated effector molecules in the supernatants, particularly of culture with Panc89 HMF spheroids.

In order to investigate whether the PD-1/PD-L1 inhibitory axis is involved in the HMF mediated impairment of $CD8^+$ T cells in our stroma enriched PDAC spheroid models, treatment with the clinically validated PD-L1 and PD-1 inhibitors Durvalumab and Pembrolizumab, respectively, was performed. In line with results from recent clinical trials that tested the benefit of ICI for the treatment of PDAC patients (5, 31, 40), neither Durvalumab nor Pembrolizumab treatment improved the effector phenotype of $CD8^+$ T cells and increased PDAC cell death in our human stroma enriched 3D PDAC model. In this context, it has to be critically noted that based on our current imaging modalities, no reliable conclusion can be made whether $CD8^+$ T cells infiltrate differentially into HMF enriched spheroids compared to monoculture PDAC spheroids and whether this is impacted by ICI. For obtaining clear information regarding the spatial distribution of $CD8^+$ T cells and the other cell components in our spheroids, ongoing studies have been started to fix the spheroids in formalin and embed them in paraffin for sectioning and immunohistochemical stainings as performed with the liver metastases. Nevertheless, overall these findings support the view that PD-1/PD-L1 axis may not be the major regulator of T cell mediated immunity in liver metastases of PDAC and rather indicate that other mechanisms are more relevant.

In this context, it has been shown that signaling *via* the tumor suppressor protein p53 can upregulate expression of CD80 on tumor cells, which in turn causes T cell suppression *via* CTLA-4 signaling (41). Further, Yazdanifar et al. showed that pancreatic cancer cells express Galectin-9, which can inhibit $CD8^+$ T cells by binding to T cell immunoglobulin and mucin domain-containing protein 3 (TIM3) (42). The expression of different mucins, like MUC1, MUC4, and MUC16, which are upregulated during cancer progression, may also inhibit apoptosis of tumor cells (43). Other reported mechanisms that affect the resistance towards ICI might be: downregulation of the major histocompatibility complex I (MHCI), resulting in less antigen recognition, loss of IFNγ sensitivity due to IFNγ receptor mutations or deletions, an immunosuppressive TME or upregulation of other immune checkpoint regulators (TIM3, LAG3, CTLA-4) (44). Another mediator of ICI resistance might be a hypoxic microenvironment. PDAC is a hypoxic tumor (45) and in other cancer entities tumor hypoxia has been identified as a physical and molecular driver of resistance towards PD-1 blockade (32, 46). Furthermore, Thomas et al. and Trapani et al. showed that TGF-β secreted by myofibroblasts inhibits $CD8^+$ T cells, especially the expression of genes encoding for cytotoxic effector molecules (47, 48). In our spheroid models, TGF-β1 levels in supernatants of PancTu1 coculture spheroids were slightly elevated compared to the respective monoculture, especially in coculture spheroids containing the highest proportion of HMF, fitting together with the reduced PDAC cell death under these conditions (Supplementary Figure 5A). However, in supernatants of Panc89 coculture spheroids TGF-β1 levels were not altered, suggesting that also other mechanisms contribute to the impairment of the T cell effector phenotype (Supplementary Figure 5B). Besides Granzyme A/B, Perforin, Granulysin, and IFNγ, $CD8^+$ T cells secrete various other effector molecules by which they are able to induce cell death in their target cells. One of these mediators is FasL (CD95), which binds to its membrane-bound receptor Fas (CD95) and, thereby, initiates caspase-mediated apoptosis. In 2D cocultures of $CD8^+$ T cells with HMF, we observed lower FasL levels in comparison to respective monocultured $CD8^+$ T cells (data not shown), indicating that effector molecules like FasL might also play a role in our spheroid culture system. Rashid et al. showed that PDAC cell lines exhibit different cell surface levels of Fas, which can be altered by Gemcitabine (49).

Of note, pretreatment of Panc89 spheroids with Gemcitabine reversed the HMF reduced PDAC cell death in the presence of $CD8^+$ T cells, although activation markers and release of cytotoxic molecules were decreased. Interestingly, the secretion of TGF-β1 was reduced in Panc89 spheroids pretreated with Gemcitabine compared to untreated spheroids, providing an explanation for the observed elevated PDAC cell death induction under these conditions (Supplementary Figure 5D). However, although Gemcitabine is one of the first-line therapies for PDAC patients, it only slightly prolongs the overall survival (50). One important reason for this is the often intrinsic or acquired resistance of PDAC

cells which can be also seen in PDAC cell lines (51). Accordingly, PancTu1 cells have been described as chemoresistant, as apoptosis could not or only slightly be induced by Gemcitabine (52). This is in line with the findings of our study, in which treatment with Gemcitabine led to slightly lower ccK18 levels in supernatants from PancTu1 spheroids compared to Panc89 spheroids. Furthermore, sensitivity towards Gemcitabine treatment was reduced in both PancTu1 and Panc89 spheroids cocultured with HMF, underscoring the impact of myofibroblasts on the mediation of drug resistance in PDAC (53, 54). Of note, Gemcitabine treatment did not alter PD-L1 expression on PDAC cells and HMF but significantly diminished PD-1 surface levels on $CD8^+$ T cells. Considering this finding, Gemcitabine treatment might also impair therapeutic efficiency of ICI treatment in PDAC patients

As outlined above, HMF show high expression of PD-L1 and clearly exert immunosuppressive effects on $CD8^+$ T cells, but this seemed to be independent of or at least not exclusively dependent on the PD-L1/PD-1 axis. Therefore, combinational therapeutic strategies simultaneously targeting different immune checkpoints or different tumor promoting stromal cells, might be a more effective approach to overcome immunosuppression leading to tumor elimination of PDAC, as recently demonstrated in PDAC mouse models (55, 56).

Data availability statement

The original contributions presented in the study are included in the article/Supplementary Material. Further inquiries can be directed to the corresponding author.

Ethics statement

The studies involving human participants were reviewed and approved by the ethics committee of the Medical Faculty of Kiel University (reference number: A110/99 and D490/17). The patients/participants provided their written informed consent to participate in this study.

Author contributions

Conceptualization: SB, TD, and SS. Methodology: SB, TD, LA, SR, SK, and SH. Investigation: SB, TD, and LA. Resources: SS, SR, HS, DW, and CR. Visualization: SB. Funding acquisition: SS. Writing—original draft preparation: SB, TD, and SS. Writing—review and editing: all authors. All authors contributed to the article and approved the submitted version.

Funding

This research was funded by the Deutsche Krebshilfe (AZ 70112935, SS). We acknowledge financial support by DFG within the funding program Open Access-Publikationskosten. The work was also supported by the DFG under Germany`s Excellence Strategy -EXC22167-390884018.

Acknowledgments

We thank Sandra Ussat for her excellent technical support. We thank the TRIBanK biobank (formerly BMB-CCC) for providing tissue samples and clinical data for this study. TRIBanK is a member of the PopGen 2.0 Biobanking Network (P2N) Kiel and was funded by the German Federal Ministry of Education and Research (BMBF grant 01EY1103).

Conflict of interest

The authors declare that the research was conducted in the absence of any commercial or financial relationships that could be construed as a potential conflict of interest.

Durvalumab was kindly provided by AstraZeneca. AstraZeneca had no role in the design of the study, in the collection, analyses, or interpretation of data; in the writing of the manuscript, or in the decision to publish the results.

Publisher's note

Supplementary material

The Supplementary Material for this article can be found online at: https://www.frontiersin.org/articles/10.3389/fonc.2023.1160824/full#supplementary-material

SUPPLEMENTARY FIGURE 1
Analysis of small and large PDAC metastases in liver tissue sections.**(A)** Representative image of PanCK stained liver tissue sections obtained from a PDAC patient showing small and large metastatic lesions. **(B)** Number of small and large metastases in all analyzed liver sections of PDAC patients. Proportion and localization (discriminated into tumor center and invasion front) of **(C)** $CD8^+$ and **(D)** $PD\text{-}L1^+$ cells as well as **(E)** intensity of PD-L1 staining in small and large metastases. Data represents the mean ± SD of 15 independent liver tissue sections. * = $p < 0.05$, ** = $p < 0.01$, *** $p < 0.001$.

SUPPLEMENTARY FIGURE 2
αSMA^+ myofibroblasts and $CD68^+$ macrophages are the main PD-L1 expressing cells in liver metastases of PDAC patients. Representative images of double immunohistochemical staining of **(A)** PanCK/PD-L1, **(B)** αSMA/PD-L1, and **(C)** CD68/PD-L1 in a large liver metastasis of a PDAC

patient at 200 x (left images) and 400 x magnification (right images). Arrows indicate PD-L1 staining in αSMA^+ myofibroblasts or $CD68^+$ macrophages.

SUPPLEMENTARY FIGURE 3
Durvalumab binds to PD-L1 on PDAC cells and hepatic myofibroblasts. PancTu1 and Panc89 cells were either seeded in mono- or in coculture with hepatic myofibroblasts (HMF) at different ratios in ultra-low attachment plates. After 48 h, either 10 µg/mlisotype control or Durvalumab were added to spheroid cultures for 24 h. Afterwards **(A)** PancTu1 cells, **(B)** Panc89 cells, and **(C)** HMF were stained for cell surface localized PD-L1 and analyzed via flow cytometry. Data were normalized on the respective isotype control. MFI ratio for specific PD-L1 staining was determined. Data represents the mean ± SD (normally distributed). N=3. * = p < 0.05, ** = p < 0.01, *** = p < 0.001

SUPPLEMENTARY FIGURE 4
PD-L1 expression on PancTu1, Panc89 cells, and hepatic myofibroblasts after Gemcitabine treatment. PancTu1, Panc89 cells, and hepatic myofibroblasts (HMF) were seeded in monoculture in ultra-low attachment plates for 24 h. Then, cells were either left untreated or treated with 10 µg/ml Gemcitabine. After 24 h, spheroids were dissociated and stained for PD-L1 by flow cytometry analysis. MFI ratio of PD-L1 cell surface expression on PancTu1 cells, Panc89 cells, and HMF. Data represents the mean ± SD (normally distributed). N=3.

SUPPLEMENTARY FIGURE 5
TGF-β1 concentration in supernatants of PDAC mono- and coculture spheroids. PancTu1 and Panc89 cells were either seeded in mono- or coculture with hepatic myofibroblasts (HMF) at different ratios in ultra-low attachment plates. Concentration of TGF-β1 was measured in the supernatants of **(A)** PancTu1 spheroids and **(B)** Panc89 spheroids after 72 h of mono- or coculture. Data were normalized on the coculture with monocultured spheroids. Concentration of TGF-β1 was measured after a total duration of 72 h insupernatants of mono- or coculture **(C)** PancTu1 spheroids and **(D)** Panc89 spheroids, stimulated with 10 µg/ml Gemcitabine for 24 h. Data were normalized on the coculture with untreated spheroids. Data represents the mean ± SD (normally distributed). N=4. *** = p < 0.001

References

1. Siegel RL, Miller KD, Fuchs HE, Jemal A. Cancer statistics, 2021. *CA Cancer J Clin* (2021) 71(1):7–33. doi: 10.3322/CAAC.21654

2. Houg DS, Bijlsma MF. The hepatic pre-metastatic niche in pancreatic ductal adenocarcinoma. *Mol Cancer BioMed Cent Ltd* (2018) 17:1–18. doi: 10.1186/s12943-018-0842-9

3. Guillén-Ponce C, Blázquez J, González I, de-Madaria E, Montáns J, Carrato A. Diagnosis and staging of pancreatic ductal adenocarcinoma. *Clin Transl Oncol* (2017) 19(10):1205–16. doi: 10.1007/S12094-017-1681-7

4. Ghaneh P, Costello E, Neoptolemos JP. Biology and management of pancreatic cancer. *Postgrad Med J* (2008) 84(995):478–97. doi: 10.1136/GUT.2006.103333

5. Brahmer JR, Tykodi SS, Chow LQM, Hwu WJ, Topalian SL, Hwu P, et al. Safety and activity of anti–PD-L1 antibody in patients with advanced cancer. *N Engl J Med* (2012) 366(26):2455. doi: 10.1056/NEJMOA1200694

6. Patnaik A, Kang SP, Rasco D, Papadopoulos KP, Elassaiss-Schaap J, Beeram M, et al. Phase I study of pembrolizumab (MK-3475; anti-PD-1 monoclonal antibody) in patients with advanced solid tumors. *Clin Cancer Res* (2015) 21(19):4286–93. doi: 10.1158/1078-0432.CCR-14-2607

7. Carstens JL, De Sampaio PC, Yang D, Barua S, Wang H, Rao A, et al. Spatial computation of intratumoral T cells correlates with survival of patients with pancreatic cancer. *Nat Commun* (2017) 8. doi: 10.1038/NCOMMS15095

8. Danilova L, Ho WJ, Zhu Q, Vithayathil T, De Jesus-Acosta A, Azad NS, et al. Programmed cell death ligand-1 (PD-L1) and CD8 expression profiling identify an immunologic subtype of pancreatic ductal adenocarcinomas with favorable survival. *Cancer Immunol Res* (2019) 7(6):886. doi: 10.1158/2326-6066.CIR-18-0822

9. Rahn S, Krüger S, Mennrich R, Goebel L, Wesch D, Oberg HH, et al. POLE score: a comprehensive profiling of programmed death 1 ligand 1 expression in pancreatic ductal adenocarcinoma. *Oncotarget* (2019) 10(16):1572–88. doi: 10.18632/oncotarget.26705

10. Rasheed ZA, Matsui W, Maitra A. Pathology of pancreatic stroma in PDAC. In: *Pancreat cancer tumor microenviron*. Trivandrum (India): Transworld Research Network (2012).

11. Pickup MW, Mouw JK, Weaver VM. The extracellular matrix modulates the hallmarks of cancer. *EMBO Rep* (2014) 15(12):1243–53. doi: 10.15252/EMBR.201439246

12. Aldag L, Beckinger S, Daunke T, Philipp LM, Surrow A, Yesilyurt UU, et al. The heterogeneity of the tumor microenvironment as essential determinant of development, progression and therapy response of pancreatic cancer. *Cancers (Basel)* (2021) 13(19):4932. doi: 10.3390/CANCERS13194932

13. Gorchs L, Moro CF, Bankhead P, Kern KP, Sadeak I, Meng Q, et al. Human pancreatic carcinoma-associated fibroblasts promote expression of co-inhibitory markers on CD4+ and CD8+ T-cells. *Front Immunol* (2019) 10:847(APR). doi: 10.3389/fimmu.2019.00847

14. Lenk L, Pein M, Will O, Gomez B, Viol F, Hauser C, et al. The hepatic microenvironment essentially determines tumor cell dormancy and metastatic outgrowth of pancreatic ductal adenocarcinoma. *Oncoimmunology* (2018) 7(1). doi: 10.1080/2162402X.2017.1368603

15. Skorupan N, Palestino Dominguez M, Ricci SL, Alewine C. Clinical strategies targeting the tumor microenvironment of pancreatic ductal adenocarcinoma. *Cancers (Basel)* (2022) 14(17). doi: 10.3390/CANCERS14174209

16. Carvalho TMA, Di Molfetta D, Greco MR, Koltai T, Alfarouk KO, Reshkin SJ, et al. Tumor microenvironment features and chemoresistance in pancreatic ductal adenocarcinoma: insights into targeting physicochemical barriers and metabolism as therapeutic approaches. *Cancers (Basel)* (2021) 13(23):6135. doi: 10.3390/CANCERS13236135

17. Shields MA, Dangi-Garimella S, Redig AJ, Munshi HG. Biochemical role of the collagen-rich tumour microenvironment in pancreatic cancer progression. *Biochem J* (2012) 441(2):541. doi: 10.1042/BJ20111240

18. Moore PS, Sipos B, Orlandini S, Sorio C, Real FX, Lemoine NR, et al. Genetic profile of 22 pancreatic carcinoma cell lines. *Anal K-ras p53 p16 DPC4/Smad4 Virchows Arch* (2001) 439(6):798–802. doi: 10.1007/S004280100474

19. Sipos B, Möser S, Kalthoff H, Török V, Löhr M, Klöppel G. A comprehensive characterization of pancreatic ductal carcinoma cell lines: towards the establishment of an *in vitro* research platform. *Virchows Arch* (2003) 442(5):444–52. doi: 10.1007/S00428-003-0784-4

20. Quaranta V, Rainer C, Nielsen SR, Raymant ML, Ahmed MS, Engle DD, et al. Macrophage-derived granulin drives resistance to immune checkpoint inhibition in metastatic pancreatic cancer. *Cancer Res* (2018) 78(15):4253–69. doi: 10.1158/0008-5472.CAN-17-3876

21. Xu L, Yan X, Ding W. Meta-analysis of efficacy from CTLA-4 and PD-1/PD-L1 inhibitors in cancer patients. *Front Oncol* (2022) 12:1460. doi: 10.3389/fonc.2022.876098

22. Xu Y, Wang Q, Xie J, Chen M, Liu H, Zhan P, et al. The predictive value of clinical and molecular characteristics or immunotherapy in non-small cell lung cancer: a meta-analysis of randomized controlled trials. *Front Oncol* (2021) :11:3605. doi: 10.3389/fonc.2021.732214

23. Zou Y, Zou X, Zheng S, Tang H, Zhang L, Liu P, et al. Efficacy and predictive factors of immune checkpoint inhibitors in metastatic breast cancer: a systematic review and meta-analysis. *Ther Adv Med Oncol* (2020) 12. doi: 10.1177/1758835920940928

24. Kabacaoglu D, Ciecielski KJ, Ruess DA, Algül H. Immune checkpoint inhibition for pancreatic ductal adenocarcinoma: current limitations and future options. *Front Immunol* (2018) 9:1878(AUG). doi: 10.3389/FIMMU.2018.01878

25. Wandmacher AM, Letsch A, Sebens S. Challenges and future perspectives of immunotherapy in pancreatic cancer. *Cancers (Basel)* (2021) 13(16). doi: 10.3390/CANCERS13164235

26. Patel SP, Kurzrock R. PD-L1 expression as a predictive biomarker in cancer immunotherapy. *Mol Cancer Ther* (2015) 14(4):847–56. doi: 10.1158/1535-7163.MCT-14-0983/86482/AM/PD-L1-EXPRESSION-AS-A-PREDICTIVE-BIOMARKER-IN

27. Noguchi T, Ward JP, Gubin MM, Arthur CD, Lee SH, Hundal J, et al. Temporally distinct PD-L1 expression by tumor and host cells contributes to immune escape. *Cancer Immunol Res* (2017) 5(2):106–17. doi: 10.1158/2326-6066.CIR-16-0391

28. Lau J, Cheung J, Navarro A, Lianoglou S, Haley B, Totpal K, et al. Tumour and host cell PD-L1 is required to mediate suppression of anti-tumour immunity in mice. *Nat Commun* (2017) 8. doi: 10.1038/NCOMMS14572

29. Strickler JH, Hanks BA, Khasraw M. Tumor mutational burden as a predictor of immunotherapy response: is more always better? *Clin Cancer Res* (2021) 27(5):1236–41. doi: 10.1158/1078-0432.CCR-20-3054

30. Zhou X, Ni Y, Liang X, Lin Y, An B, He X, et al. Mechanisms of tumor resistance to immune checkpoint blockade and combination strategies to overcome resistance. *Front Immunol* (2022) 13:915094. doi: 10.3389/FIMMU.2022.915094

31. Mukherji R, Debnath D, Hartley ML, Noel MS. The role of immunotherapy in pancreatic cancer. *Curr Oncol* (2022) 29(10):6864. doi: 10.3390/CURRONCOL29100541

32. Zandberg DP, Menk AV, Velez M, Normolle D, Depeaux K, Liu A, et al. Tumor hypoxia is associated with resistance to PD-1 blockade in squamous cell carcinoma of the head and neck. *J Immunother Cancer* (2021) 9(5). doi: 10.1136/JITC-2020-002088

33. Lawlor RT, Mattiolo P, Mafficini A, Hong SM, Piredda ML, Taormina SV, et al. Tumor mutational burden as a potential biomarker for immunotherapy in pancreatic cancer: systematic review and still-open questions. *Cancers (Basel)* (2021) 13(13):3119. doi: 10.3390/CANCERS13133119/S1

34. Yachida S, White CM, Naito Y, Zhong Y, Brosnan JA, Macgregor-Das AM, et al. Clinical significance of the genetic landscape of pancreatic cancer and implications for identification of potential long-term survivors. *Clin Cancer Res* (2012) 18(22):6339–47. doi: 10.1158/1078-0432.CCR-12-1215

35. Grout JA, Sirven P, Leader AM, Maskey S, Hector E, Puisieux I, et al. Spatial positioning and matrix programs of cancer-associated fibroblasts promote T-cell exclusion in human lung tumors. *Cancer Discovery* (2022) 12(11):2606–25. doi: 10.1158/2159-8290.CD-21-1714

36. Iwai Y, Terawaki S, Ikegawa M, Okazaki T, Honjo T. PD-1 inhibits antiviral immunity at the effector phase in the liver. *J Exp Med* (2003) 198(1):39. doi: 10.1084/JEM.20022235

37. Sun Q, Zhang B, Hu Q, Qin Y, Xu W, Liu W, et al. The impact of cancer-associated fibroblasts on major hallmarks of pancreatic cancer. *Theranostics* (2018) 8 (18):5072. doi: 10.7150/THNO.26546

38. Lee SJ, Jang BC, Lee SW, Yang Y, Suh SII, Park YM, et al. Interferon regulatory factor-1 is prerequisite to the constitutive expression and IFN-gamma-induced upregulation of B7-H1 (CD274). *FEBS Lett* (2006) 580(3):755–62. doi: 10.1016/J.FEBSLET.2005.12.093

39. Saka D, Gökalp M, Piyade B, Cevik NC, Sever EA, Unutmaz D, et al. Mechanisms of t-cell exhaustion in pancreatic cancer. *Cancers MDPI AG;* (2020) 12:1–27. doi: 10.3390/cancers12082274

40. Royal RE, Levy C, Turner K, Mathur A, Hughes M, Kammula US, et al. Phase 2 trial of single agent ipilimumab (Anti-CTLA-4) for locally advanced or metastatic pancreatic adenocarcinoma. *J Immunother* (2010) 33(8):828–33. doi: 10.1097/CJI.0B013E3181EEC14C

41. Scarpa M, Marchiori C, Scarpa M, Castagliuolo I. CD80 expression is upregulated by TP53 activation in human cancer epithelial cells. *Oncoimmunology* (2021) 10(1). doi: 10.1080/2162402X.2021.1907912

42. Yazdanifar M, Zhou R, Grover P, Williams C, Bose M, Moore LJ, et al. Overcoming immunological resistance enhances the efficacy of a novel anti-tMUC1-CAR T cell treatment against pancreatic ductal adenocarcinoma. *Cells* (2019) 8(9). doi: 10.3390/CELLS8091070

43. Suh H, Pillai K, Morris DL. Mucins in pancreatic cancer: biological role, implications in carcinogenesis and applications in diagnosis and therapy. *Am J Cancer Res* (2017) 7(6):1372.

44. Schoenfeld AJ, Hellmann MD. Acquired resistance to immune checkpoint inhibitors. *Cancer Cell* (2020) 37(4):443. doi: 10.1016/J.CCELL.2020.03.017

45. Koong AC, Mehta VK, Le QT, Fisher GA, Terris DJ, Brown JM, et al. Pancreatic tumors show high levels of hypoxia. *Int J Radiat Oncol Biol Phys* (2000) 48(4):919–22. doi: 10.1016/S0360-3016(00)00803-8

46. Najjar YG, Menk AV, Sander C, Rao U, Karunamurthy A, Bhatia R, et al. Tumor cell oxidative metabolism as a barrier to PD-1 blockade immunotherapy in melanoma. *JCI Insight* (2019) 4(5). doi: 10.1172/JCI.INSIGHT.124989

47. Trapani JA. The dual adverse effects of TGF-beta secretion on tumor progression. *Cancer Cell* (2005) 8(5):349–50. doi: 10.1016/J.CCR.2005.10.018

48. Thomas DA, Massagué J. TGF-beta directly targets cytotoxic T cell functions during tumor evasion of immune surveillance. *Cancer Cell* (2005) 8(5):369–80. doi: 10.1016/J.CCR.2005.10.012

49. Rashid K, Röder C, Goumas F, Egberts JH, Kalthoff H. CD95L inhibition impacts gemcitabine-mediated effects and non-apoptotic signaling of tnf-α and trail in pancreatic tumor cells. *Cancers (Basel)* (2021) 13(21):5458. doi: 10.3390/CANCERS13215458/S1

50. Burris HA, Moore MJ, Andersen J, Green MR, Rothenberg ML, Modiano MR, et al. Improvements in survival and clinical benefit with gemcitabine as first-line therapy for patients with advanced pancreas cancer: a randomized trial. *J Clin Oncol* (1997) 15(6):2403–13. doi: 10.1200/JCO.1997.15.6.2403

51. Liu K, Geng Y, Wang L, Xu H, Zou M, Li Y, et al. Systematic exploration of the underlying mechanism of gemcitabine resistance in pancreatic adenocarcinoma. *Mol Oncol* (2022) 16(16):3034–51. doi: 10.1002/1878-0261.13279

52. Arlt A, Gehrz A, Müerköster S, Vorndamm J, Kruse ML, Fölsch UR, et al. Role of NF-κB and Akt/PI3K in the resistance of pancreatic carcinoma cell lines against gemcitabine-induced cell death. *Oncogene* (2003) 22(21):3243–51. doi: 10.1038/sj.onc.1206390

53. Müerköster S, Wegehenkel K, Arlt A, Witt M, Sipos B, Kruse ML, et al. Tumor stroma interactions induce chemoresistance in pancreatic ductal carcinoma cells involving increased secretion and paracrine effects of nitric oxide and interleukin-1β. *Cancer Res* (2004) 64(4):1331–7. doi: 10.1002/1878-0261.13279

54. Neumann CCM, von Hörschelmann E, Reutzel-Selke A, Seidel E, Sauer IM, Pratschke J, et al. Tumor–stromal cross-talk modulating the therapeutic response in pancreatic cancer. *Hepatobiliary Pancreat Dis Int* (2018) 17(5):461–72. doi: 10.1016/j.hbpd.2018.09.004

55. Kim DK, Jeong J, Lee DS, Hyeon DY, Park GW, Jeon S, et al. PD-L1-directed PlGF/VEGF blockade synergizes with chemotherapy by targeting CD141+ cancer-associated fibroblasts in pancreatic cancer. *Nat Commun* (2022) 13(1):1–19. doi: 10.1038/s41467-022-33991-6

56. Gulhati P, Schalck A, Jiang S, Shang X, Wu CJ, Hou P, et al. Targeting T cell checkpoints 41BB and LAG3 and myeloid cell CXCR1/CXCR2 results in antitumor immunity and durable response in pancreatic cancer. *Nat Cancer* (2022) 2022:1–19. doi: 10.1038/s43018-022-00500-z

Second Publication

cancers

MDPI

Review

The Heterogeneity of the Tumor Microenvironment as Essential Determinant of Development, Progression and Therapy Response of Pancreatic Cancer

Group Young Researchers in Inflammatory Carcinogenesis [1,†], Anna Maxi Wandmacher [2], Anne-Sophie Mehdorn [3,‡] and Susanne Sebens [1,*,‡]

[1] Institute for Experimental Cancer Research, Kiel University and University Hospital Schleswig-Holstein Campus Kiel, Arnold-Heller-Str. 3, Building U30 Entrance 1, 24105 Kiel, Germany; stu208555@mail.uni-kiel.de (L.A.); silje.beckinger@email.uni-kiel.de (S.B.); tina.daunke@email.uni-kiel.de (T.D.); lisa.philipp@email.uni-kiel.de (L.-M.P.); stu207555@mail.uni-kiel.de (A.S.); stu212154@mail.uni-kiel.de (U.-U.Y.)
[2] Department of Internal Medicine II, University Hospital Schleswig-Holstein Campus Kiel, Arnold-Heller-Str. 3, 24105 Kiel, Germany; annamaxi.wandmacher@uksh.de
[3] Department of General, Visceral, Thoracic, Transplantation and Pediatric Surgery, University Hospital Schleswig-Holstein Campus Kiel, Arnold-Heller-Str. 3, Building C, 24105 Kiel, Germany; Anne-Sophie.Mehdorn@uksh.de
* Correspondence: susanne.sebens@email.uni-kiel.de
† Group members (in alphabetical order): Leon Aldag, Silje Beckinger, Tina Daunke, Lisa-Marie Philipp, Arne Surrow, Umut-Ulas Yesilyurt.
‡ These authors share last authorship and contributed equally to this work.

check for updates

Citation: Group Young Researchers in Inflammatory Carcinogenesis; Wandmacher, A.M.; Mehdorn, A.-S.; Sebens, S. The Heterogeneity of the Tumor Microenvironment as Essential Determinant of Development, Progression and Therapy Response of Pancreatic Cancer. *Cancers* **2021**, *13*, 4932. https://doi.org/10.3390/cancers13194932

Academic Editor: Eva Diamantis Karamitopoulou

Received: 26 August 2021
Accepted: 14 September 2021
Published: 30 September 2021

Publisher's Note: MDPI stays neutral with regard to jurisdictional claims in published maps and institutional affiliations.

Simple Summary: Pancreatic ductal adenocarcinoma (PDAC) is still one of the deadliest cancers in western countries. It is commonly diagnosed at advanced stages and most anti-cancer therapies have failed to substantially improve prognosis of PDAC patients. PDAC is characterized by a profound inflammatory tumor microenvironment (TME) comprising various non-neoplastic cells e.g., myofibroblasts, macrophages, T cells and endothelial cells which can exhibit different functional phenotypes. Furthermore, the microbiome is altered in the tumor and other body compartments of PDAC patients adding to the great TME heterogeneity and its impact on PDAC development, progression and therapy responses. This review summarizes the recent knowledge on the diverse phenotypes of these different stromal components. A better understanding of tumor cells as well as TME heterogeneity and considering tumor-suppressing and tumor-promoting phenotypes might provide an important step towards a more effective treatment for this highly malignant tumor.

Abstract: Pancreatic ductal adenocarcinoma (PDAC) is commonly diagnosed at advanced stages and most anti-cancer therapies have failed to substantially improve prognosis of PDAC patients. As a result, PDAC is still one of the deadliest tumors. Tumor heterogeneity, manifesting at multiple levels, provides a conclusive explanation for divergent survival times and therapy responses of PDAC patients. Besides tumor cell heterogeneity, PDAC is characterized by a pronounced inflammatory stroma comprising various non-neoplastic cells such as myofibroblasts, endothelial cells and different leukocyte populations which enrich in the tumor microenvironment (TME) during pancreatic tumorigenesis. Thus, the stromal compartment also displays a high temporal and spatial heterogeneity accounting for diverse effects on the development, progression and therapy responses of PDAC. Adding to this heterogeneity and the impact of the TME, the microbiome of PDAC patients is considerably altered. Understanding this multi-level heterogeneity and considering it for the development of novel therapeutic concepts might finally improve the dismal situation of PDAC patients. Here, we outline the current knowledge on PDAC cell heterogeneity focusing on different stromal cell populations and outline their impact on PDAC progression and therapy resistance. Based on this information, we propose some novel concepts for treatment of PDAC patients.

Keywords: PDAC; tumor stroma; immune cells; endothelial cells; CAFs; myofibroblasts; microbiome; macrophages; personalized medicine

1. Clinical Situation and Challenges

Pancreatic ductal adenocarcinoma (PDAC) is the 4th most frequent cause of cancer related deaths in western countries [1]. Since 80% of PDAC are diagnosed at advanced tumor stages, curative treatment options are limited. Accordingly, the overall 5-year survival rate is still less than 10% [1]. Besides late diagnosis, an early metastatic dissemination as well as a profound therapy resistance contribute to the clinical challenges in the treatment of PDAC and thereby to the patient's dismal situation [2,3].

Originating from pancreatic ductal epithelial cells (PDEC) or pancreatic acinar cells, PDAC can develop via different precursor lesions, such as pancreatic intraepithelial neoplasia (PanIN), intraductal papillary mucinous neoplasm (IPMN), mucinous cystic neoplasm, or other lesions [4], to an invasive carcinoma with the liver being the main site of metastasis [5,6]. During this multi-step progression various epi-/genetic alterations are acquired e.g., mutations in the oncogene *KRAS* which is one of the earliest genetic alterations and found in 99% of even early low-grade PanIN [7,8]. Besides genetic and epigenetic changes in PDEC and later on PDAC cells, the adjacent microenvironment also undergoes considerable alterations. These involve enrichment of different leukocyte cell populations (e.g., monocytes, lymphocytes), activation and modification of tissue resident cells (e.g., fibroblasts/stellate cells, endothelial cells), remodeling of the extracellular matrix (ECM) and changes of the microbiome [9–11]. Accordingly, composition and proportion of the microenvironment in close vicinity to precursor/PDAC cells are highly variable as they evolve concomitantly with PDAC progression. Furthermore, the TME is mutually dependent on both environmental factors (e.g., aging, exposure to lifestyle factors) and the (epi-)genetic make-up of PDEC and PDAC cells, respectively [12]. This indicates a dynamic co-evolution of neoplastic and non-neoplastic cells during pancreatic tumorigenesis being characterized and driven by a high heterogeneity of both different tumor cell clones and stromal cell populations. PDAC is characterized by a pronounced inflammatory tumor microenvironment (TME), which often accounts for the major tumor mass. Therefore, it is not surprising that therapies targeting genetically related alterations (e.g., altered signaling by mutant *KRAS* or sustained Epidermal Growth Factor Receptor (EGFR)-signaling caused by *EGFR* overexpression) have failed to improve treatment of PDAC patients as the blocked signaling pathways are bypassed by the stroma-mediated signaling which further sustains the cellular processes in the transformed cells [13,14]. Similarly, chemotherapeutic regimens have largely failed to improve the prognosis of PDAC patients because PDAC cells exhibit multiple strategies by which they evade the effect of cytostatic drugs. Importantly, these strategies are promoted by the stromal cells and additionally, the TME itself impairs the drug efficacy of PDAC (e.g., by metabolization of cytostatic drugs) [15–18]. In this context, the microbiome seems to play an important role, too. Several studies have already shown that the gut and tumor microbiome are altered in PDAC patients, promoting tumor progression and reducing treatment responses of PDAC cells, thereby substantially impairing survival of PDAC patients [11,19,20].

Finally, immune checkpoint inhibitors have revolutionized the treatment of various solid tumors even at advanced stages such as non-small cell lung carcinoma but have failed in the treatment of PDAC patients [21–23]. Besides a heterogeneous expression pattern of the immune checkpoint regulator programmed cell death 1 ligand 1 (PD-L1) on PDAC cells [24], another reason might be the high heterogeneity of the stromal compartment not only with respect to PD-L1 expression, but also regarding the cellular composition (inflamed versus non-inflamed tumors) [25,26].

Thus, experimental and clinical data strongly support the view that the failure of current therapeutic strategies is due to an insufficient consideration of the heterogeneity of

PDAC cells but also stromal cells. In order to improve our understanding of this heterogeneity, we herein outline the recent knowledge on TME diversity and its impact on PDAC development, progression and therapy resistance. Being aware of the numerous publications in this field in recent years, we apologize for only citing a selection. Furthermore, considering this knowledge we propose some concepts for novel therapeutic strategies to improve prognosis of PDAC patients.

2. Heterogeneity of the Tumor Cell Compartment in PDAC

Comprehensive (single cell) omics analyses revealed a high diversity of tumors at multiple levels, namely interpatient, intertumor and intratumor heterogeneity altogether providing an explanation for the noticeable differences in therapy responses and survival of cancer patients [27]. In stroma-rich PDAC, those analyses were combined with microdissection allowing a distinct investigation of tumor and stromal cells. In recent years, mainly three studies revealed substantial insights into interpatient heterogeneity. Collisson et al. classified PDAC into "classical", "quasi-mesenchymal" and "exocrine-like" subtypes. Besides differences in the expression profile, the classical phenotype was an independent prognostic factor for longer overall survival of resected PDAC patients and classical PDAC lines were more resistant towards Gemcitabine treatment than cell lines with a quasi-mesenchymal phenotype [28].

Moffitt et al. identified two tumor cell subtypes ("basal-like" and "classical", the latter one overlapping with those identified by Collisson et al.) but additionally two stromal subtypes ("normal" and "activated"). Here, patients with a tumor of the "basal-like" subtype or exhibiting an activated stroma had a worse prognosis compared to either corresponding subgroup. However, basal-like tumors seemed to show better responses towards adjuvant therapy. Importantly, the normal stroma signature was associated with high expression of genes typical for pancreatic stellate cells (PSC), while an activated stroma signature was characterized by high expression of genes related to macrophages and myofibroblasts, both being abundant in the PDAC stroma [29].

Finally, Bailey et al. identified four subtypes, namely "squamous", "pancreatic progenitor", "immunogenic" and "aberrantly differentiated endocrine exocrine (ADEX)". These subtypes clearly differed with respect to genetic and epigenetic alterations as well as transcription profiles. Additionally, the "immunogenic" subtype was characterized by an enrichment of different immune cell subsets and enhanced immune evasion pathways e.g., mediated by the immune checkpoint regulators Cytotoxic T-Lymphocyte-Associated Protein 4 (CTLA-4) and Programmed cell death protein 1 (PD-1) [30].

Extending these findings, Birnbaum et al. compared the tumor subtypes identified by Collisson, Moffitt and Bailey and confirmed the independent prognostic value of the classification from the latter two studies [31]. Additionally, Rashid et al. provided evidence that a tumor classification into two subtypes (basal-like and classical) according to Moffitt et al. exhibits the highest robustness and clinical relevance by demonstrating that basal-like tumors showed a strong resistance to FOLFIRINOX compared to classical tumors [32]. Although all studies revealed important insights into interpatient tumor heterogeneity, prospective trails are still needed to validate the clinical utility of this tumoral subtyping in particular with respect to optimized treatment.

With respect to intratumor heterogeneity, it is assumed that phenotypic and genotypic diversity of tumor cell clones within (primary and secondary) tumors originate from clonal expansions and differentiation hierarchies according to the current model of cancer stem cells (CSC) [33,34]. Thus, intratumor heterogeneity can occur and manifest on multiple levels based on the expansion of tumor cell clones with different genetic (driver as well as passenger mutations) and epigenetic alterations (hypermethylated DNA regions, histone modifications) as well as divergent differentiation stages (CSC versus non-CSC stage). These alterations in turn essentially contribute to different metabolic requirements (dependence on glucose, lactate or glutamine) as well as phenotypic diversity within the tumor mass resulting in e.g., proliferating versus resting, sessile versus motile/invasive

or therapy responsive or resistant tumor cell clones [35,36]. Important to note, expansion and evolution of certain tumor cell clones are highly dependent on the adjacent stroma which co-evolves with the different tumor cell clones during pancreatic tumorigenesis, applying to the primary as well as to the secondary context [37,38]. Although it can be speculated whether the metastatic tumor stroma induces the above-mentioned epigenetic, metabolic and thereby phenotypic alterations or selects for those clones that have acquired these alterations before leaving the primary tumor, a fundamental role of the stromal compartment in this heterogeneity determining process is meanwhile indisputable.

Thus, it is necessary to unravel all levels of tumor diversity and in particular stromal cell heterogeneity (Figure 1) to gain a complete picture of PDAC complexity which has to be considered for optimized treatment strategies.

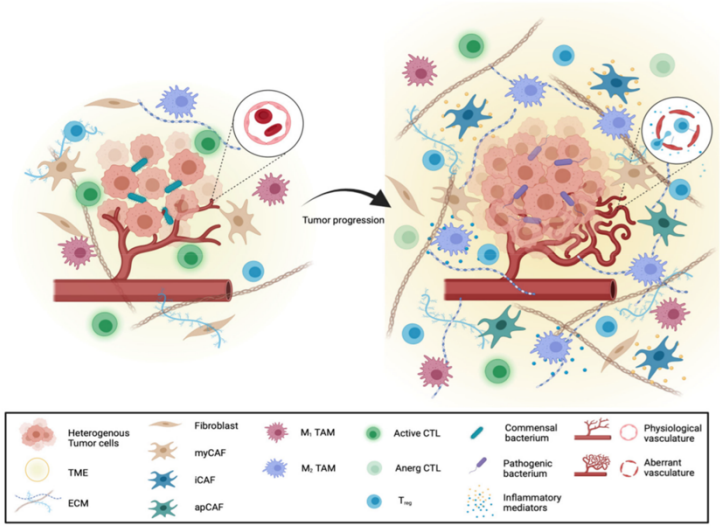

Figure 1. Pancreatic cancer is characterized by a high tumor and stroma heterogeneity. During pancreatic tumorigenesis, tumor cells acquire multiple alterations resulting in a heterogeneous pool of tumor cell clones. Along with the evolution of these divergent tumor cell clones, the tumor microenvironment (TME) also undergoes fundamental alterations involving, (i) activation of fibroblasts and transdifferentiation into carcinoma associated fibroblasts (CAFs) with different phenotypes (myCAF, iCAF, apCAF), (ii) alteration of the extent and composition of the extracellular matrix (ECM), (iii) enrichment of immunosuppressive and tumor-promoting immune cells e.g., tumor-associated macrophages with different phenotypes (M1 TAM versus M2 TAM), anergy cytotoxic T cells (CTL) and regulatory T cells (Treg), (iv) enrichment of pathological bacteria and extrusion of commensal bacteria, (v) elevation of inflammatory mediators and (vi) formation of new and modified blood vessels. Overall, this TME heterogeneity is an essential driver of PDAC development and progression. Figure created with BioRender.com.

3. Heterogeneity of the Stromal Compartment in PDAC

3.1. Heterogeneity of Carcinoma Associated Fibroblasts

The most abundant inflammatory stroma cells in PDAC are myofibroblasts, also termed carcinoma associated fibroblasts (CAF). CAF are abundant in primary PDAC as well as in metastases e.g., in the liver. During cancer development, several cell types can transdifferentiate into CAF. Besides PSC, adipocytes, monocytes, bone marrow-derived mesenchymal stem cells and endothelial cells (EC) can give rise to CAF in the pancreas [39–43]. In the liver, the main

source of CAF is hepatic stellate cells (HSC), with CAF also originating from hepatic sinusoidal endothelial cells or portal mesenchymal cells [44–50].

Under physiological conditions, most pancreatic fibroblasts are a heterogeneous group of desmin+ PSC which produce and maintain physiological levels of ECM proteins such as collagen IV, laminin, fibronectin and glycosaminoglycans. Thereby, these cells essentially contribute to the physiological pancreas homeostasis [51–56]. PSC are located at the base of the acini and contain high amounts of vitamin A vesicles [51]. Upon activation PSC lose these lipid vesicles and transdifferentiate into myofibroblasts, thereby increasing their proliferative and migratory potential, suppressing pro-apoptotic gene expression and secreting cell cycle promoting proteins [57–59]. Furthermore, myofibroblasts produce elevated amounts of ECM proteins at an altered composition, resulting in fibrosis. This fibrotic ECM is composed of less elastin and more fibronectin as well as crosslinked collagen type I and III [60]. Baron et al. distinguished two groups of pancreatic myofibroblasts: The first phenotype is characterized by production of ECM, and the second phenotype, called immune-activated PSC, exhibits and releases high expression levels of immunomodulating cytokines, interleukins and chemokines (e.g., chemokine (C-X-C motif) ligand 3 (CXCL3), Interleukin-33 (IL-33), IL-2) [61]. Exposure to stressful conditions including exogenous toxins, surgical intervention, inflammatory injury or mediators released by immune cells [56,62,63] promotes proliferation and activation of PSC into myofibroblasts leading to increased alpha-smooth muscle actin (α-SMA) expression. Stimuli leading to the transdifferentiation and activation of myofibroblasts/CAF are Transforming Growth Factor-beta (TGF-β), Platelet-derived Growth Factor (PDGF) and IL-6 [64–67]. Meanwhile, it is well known that CAF can exhibit different phenotypes and different CAF populations have been discovered in recent years. In the pancreas, major subgroups are myofibroblastic CAF (myCAF), inflammatory CAF (iCAF) and major histocompatibility complex II (MHCII) antigen presenting CAF (apCAF) [68]. MyCAF, which are tumor-adjacent and express high levels of α-SMA, are activated in a TGF-β dependent manner [69,70]. In contrast, iCAF are localized distant from the tumor, express low α-SMA levels and exhibit rather tumor-promoting and immunosuppressive properties by secreting inflammatory cytokines, like IL-6, CXCL12 and Granulocyte-Colony stimulating Factor (G-CSF). In contrast to myCAF, iCAF differentiation is stimulated by cancer-secreted IL-1 via the Januskinase-Signal Transducer and Activator of Transcription (JAK-STAT) pathway and antagonized by TGF-β. In vitro, PSC can differentiate into either myCAF or iCAF and even after this differentiation, iCAF can transdifferentiate into tumor-suppressive myCAF [68,69]. These findings strongly support the existence of different (functional) CAF phenotypes which seem to be interchangeable and highly context dependent. In both murine and human tissues, Hutton et al. recently identified two further functionally distinct pancreatic fibroblast populations by cluster of differentiation 105 (CD105) expression. While CD105+ fibroblasts did hardly impact tumor growth in vivo, CD105- fibroblasts promoted anti-tumor immunity and suppressed tumor growth. Characteristics of the established myCAF and iCAF populations were found in either lineage, whereas all apCAF were CD105-. In contrast to myCAF and iCAF populations, CD105+ and CD105- pancreatic fibroblasts seemed not to be interconvertible [71].

As outlined above, CAF are the major source of ECM in the TME. Cross-linked and oriented collagens cause a stiffened matrix, which stimulates accelerated cell cycle progression in adjacent tumor cells and thus fuels tumor growth [72]. Besides, the dense stroma acts as a physical barrier for drugs and immune cells [69]. Neumann et al. showed that the response to chemotherapeutic treatment (e.g., Gemcitabine, Nab-paclitaxel) is reduced when tumor cells are directly cocultured with human CAF compared to monocultured tumor cells [73]. Furthermore, T cells are unable to infiltrate into the dense matrix, which might be one reason for the limited clinical success of immunotherapy in PDAC patients [74]. By compressing blood and lymphatic vessels, perfusion is impaired and the interstitial fluid pressure increased, which induces hypoxia mediated progression and promotes cancer invasiveness, respectively [75–78]. Hypoxia in turn selects the most malignant

cancer cells and through hypoxia-inducible factor 1 (HIF-1) suppresses tumor suppressor genes while promoting the metastatic cascade [79–82]. By promoting M2-like polarization in macrophages and increasing PD-L1 expression in cancer cells, tumor-associated macrophages (TAM) and dendritic cells (DC), HIF-1 supports immunosuppression in the TME [83–87].

Besides the ECM-mediated effects, CAF exert several direct effects on the tumor. Thus, CAF promote an immunosuppressive TME by selecting tumor-promoting immune cells and inhibiting tumor-suppressive ones. Hence, in a KPC mouse model, increased PD-L1 and PD-L2 expression was demonstrated on CAF compared to fibroblasts [88]. Multiple murine and human studies showed their capability of excluding cytotoxic T cells (CTL) from tumor islands and inhibiting T cell activity in multifaceted ways [88–91]. In a mouse model, Feig et al. found CAF-derived CXCL12 to coat PDAC cells and protect them from CD8+ T cell invasion [90]. Lakins et al. showed murine CAF to cross-present tumor-derived antigens on MHC I and upon contact with CTL, induce cell death via PD-1/PD-L2 and Fas/FasL interaction [91]. While preventing CTL functions, CAF recruit immunosuppressive immune cells, such as myeloid derived suppressor cells (MDSCs) and monocytes, and promote monocyte differentiation into M2-like macrophages via Macrophage-Colony Stimulating Factor (M-CSF) [92–96]. MDSC-promoting factors secreted by CAF include IL-6, Vascular Endothelial Growth Factor (VEGF) and M-CSF [97]. In PDAC, iCAF have been identified to be the major source of these immunomodulating ligands, which might explain their above-mentioned localization at the edge of the tumor [24,70,98–100]. Another CAF subpopulation found in murine and human PDAC and breast cancer are apCAF [101], which are characterized by expression of MHC II molecules and their capability to present antigens to CD4+ T cells. However, apCAF lack costimulatory molecules required to promote T cell proliferation. Thus, MHC II molecules on apCAF were hypothesized to act as decoy receptors and exert immunosuppression via induction of anergy in T cells or transdifferentiation into regulatory T cells (Tregs) [100]. Furthermore, CAF can enhance cell growth [102], induce Epithelial-Mesenchymal-Transition (EMT) thereby facilitating PDAC cell dissemination and metastasis and promote an apoptosis and drug resistant phenotype in PDAC as well as precursor cells in a paracrine manner [17,18,103,104].

The mechanisms of myofibroblasts/CAF generation and their functional impact on tumorigenesis apply also to HSC and the derived hepatic myofibroblasts (HMF) [105–107]. HSC make up 5% of all liver cells and share many properties with PSC [108,109]. In the physiological liver, HSC perform a variety of tasks to maintain organ homeostasis by paracrine secretion of hepatocyte mitogens such as Hepatocyte Growth Factor (HGF) and Epidermal Growth Factor (EGF), and they store 50–80% of all retinoids in the body [110–115]. In contrast in the inflamed liver, HMF essentially impact immune responses inducing infiltration of neutrophils and lymphocytes or by acting as professional antigen presenting cells (APC), while also inhibiting T cells via the expression of PD-L1 [116–120]. In a KPC mouse model, Costa-Silva et al. [105] demonstrated that PDAC-derived circulating exosomes are taken up by Kupffer cells inducing TGF-β expression in these liver resident macrophages. TGF-β in turn activates HSC to HMF leading to an increased production of fibronectin and collagen I and III. This pre-metastatic niche was shown to be crucial for the onset of PDAC metastases [105,121–124]. Recently, Bhattacharjee et al. also identified different CAF populations in murine and human liver tissues based on subpopulations previously characterized in pancreatic and breast cancer. Thus, most liver CAF exhibit a myCAF-like expression profile with high collagen and α-SMA levels, while a smaller subpopulation expresses less α-SMA, but more growth factors and cytokines, and is therefore defined as iCAF [125]. Besides the role in immunomodulation and ECM remodeling, HSC and HMF differentially impact cell growth of PDAC cells, thereby controlling outgrowth of liver metastases. Accordingly, Lenk et al. showed that both murine and human HSC inhibit PDEC and promote a dormant phenotype in an IL-8 dependent manner, while HMF promote reawakening of the dormant stage and enhance proliferation in a VEGF dependent fashion [106].

3.2. Approaches for Targeted Therapy of Carcinoma Associated Fibroblasts

In light of the broad impact of CAF on PDAC progression, immune modulation and drug response, targeting CAF, CAF-derived factors or factors leading to their generation have emerged as attractive targets for PDAC therapy (Table 1).

TGF-β, produced by CAF and being their main activator, enhances tumor progression and dampens the immune and therapy responses [126,127]. Thus, it represents a promising target to interfere with CAF function [128]. However, an early phase clinical trial testing the therapeutic efficacy of pharmacological TGF-blockade with the small molecule inhibitor Galunisertib in combination with chemotherapy for the treatment of unresectable PDAC did not reveal convincing results [129]. Additionally, data from a phase Ib clinical trial investigating Galunisertib in combination with the anti-PD-L1 antibody Durvalumab did not yield clinical improvements for patients with metastatic PDAC [130]. Of note, Özdemir et al. showed in a PDAC mouse model that complete depletion of α-SMA+ myofibroblasts led to enhanced tumor growth, decreased immune cell infiltration and increased number of Treg in the TME. These findings indicate that complete depletion of CAF is not a reasonable treatment strategy, as tumor-restraining CAF populations are eliminated, too. However, concomitant depletion of CAF and blocking of CTLA-4 decreased tumor growth and prolonged survival of PDAC bearing mice [131].

Furthermore, it has been shown that tumor derived ligands of the Sonic Hedgehog (Shh) signaling system leads to activation of stellate cells into CAF [132]. Based on this finding, Shh inhibitors were tested in preclinical and clinical trials to improve PDAC treatment. However, depletion or pharmacological inhibition of Shh reduced stroma formation but accelerated tumor growth of tumor bearing KPC mice [133]. In line with this finding, combined treatment of metastatic PDAC patients with Gemcitabine and Shh inhibitors, targeting the signal transducing component Smoothened (SMO), showed no superior effect compared to Gemcitabine monotherapy [134]. Another clinical trial investigated the efficacy of the SMO inhibitor Saridegib (IPI-926) in combination with FOLFIRINOX for treatment of patients with advanced PDAC demonstrating an antitumor activity along with acceptable safety [135]. However, since a study demonstrated that patients being treated with IPI-926 in combination with Gemcitabine showed even shorter survival times than patients treated with Gemcitabine alone, this study was terminated prematurely (see Infinity Pharmaceuticals company website) and other trials investigating the therapeutic efficacy of Hh inhibitors were withdrawn or stopped.

Due to the tumor boosting effect, achieved by depleting the entire CAF population, recent research has rather focused on stromal reprogramming than on stroma depletion by e.g., reversal of CAF activation or shifting the CAF populations. Since activated myofibroblasts can be reversed into a quiescent phenotype by retinoic acid [136], all-trans retinoic acid (ATRA) has been used for myofibroblast reversal. Thus, ATRA treatment of tumor bearing KPC mice resulted in an enhanced CTL infiltration in the tumor tissue, which was explained by reduced secretion of the chemokine CXCL12 by reverted stellate cells [88]. Another strategy aiming at a stromal (CAF) reprogramming is the treatment with Calcipotriol, which is a derivative of vitamin D. The vitamin D receptor itself is a transcriptional factor suppressing the activation of PSC. Treatment with Calcipotriol led to stroma remodeling and combined treatment with Gemcitabine reduced tumor growth and increased overall survival of PDAC bearing mice [137]. Recently, Biffi et al. demonstrated a phenotypic shift from tumor-promoting iCAF to tumor suppressive myCAF by JAK inhibition, which was associated with reduced tumor growth and increased collagen deposition in tumor bearing KPC mice, further impairing drug penetration into the tumor stroma [70]. This was also seen in clinical trials where the combination of a JAK inhibitor and chemotherapy did not prolong the overall survival [138].

Taken together, CAF represent a heterogeneous cell population in the TME of PDAC at the primary site as well as in metastases exerting diverse functions on other stromal cells (immune cells, EC) and PDAC cells. Importantly, CAF and their quiescent/non-activated counterpart, the stellate cells may exert tumor-restraining functions, which have been

taken into consideration for the development of stroma-targeted therapeutic strategies to improve PDAC treatment.

Table 1. Overview of the cited therapeutic approaches targeting carcinoma associated fibroblasts (CAF).

Study System	Targeting Strategy	Reference
Preclinical studies		
PKT mouse model	Myofibroblast depletion by Ganciclovir	[131]
PKT mouse model	Myofibroblast depletion by Ganciclovir + anti-CTLA-4 antibody	[131]
KPC mouse model	Depletion or pharmacological inhibition of Shh	[133]
KPC mouse model	Myofibroblast reversal by ATRA	[88]
KPC mouse model	Vitamin D derivative Calcipotriol + Gemcitabine	[137]
KPC mouse model	Phenotype shift by JAK inhibitor (AZD1480)	[70]
Clinical trials		
Phase 1b/2 clinical trial	TGF-β blockade by Galusertinib + Gemcitabine	[129]
Phase 1b clinical trial	TGF-β blockade by Galusertinib + PD-L1 antibody Durvalumab	[130]
Phase 1b/2 clinical trial	Shh blockade by Vismodegib + Gemcitabine	[134]
Phase 1 clinical trial	SMO inhibition by Saridegib (IPI-926) + FOLFIRINOX	[135]
Phase 3 clinical trial	JAK1/JAK2 inhibition by Ruxolitinib + Capecitabine	[138]

3.3. Heterogeneity of Macrophages

Besides CAF, macrophages are also found in high numbers in many tumor entities representing the most abundant leucocyte population in the TME [139], also applying to PDAC [140]. Other, but less abundant, myeloid cell populations in PDAC are DC and MDSC. Tjomsland et al. showed that increased numbers of DC in the peripheral blood are associated with a better survival in PDAC patients [141]. However, most human PDAC specimens are characterized by low numbers of DC [142] and even if DC are present, they are mostly located at the tumor margins [142], a finding which could be similarly found in a modified KPC mouse model [143]. DC comprise a variety of subtypes including conventional and plasmacytoid DC exhibiting distinct phenotypes [144]. Of note, DC are key APC for the activation of T cells. Accordingly, these cells essentially determine the efficacy of anti-tumor immunosurveillance and immunotherapeutic treatment strategies, such as immune checkpoint inhibition and vaccinations. As described for other stromal cell populations, also MDSC can exhibit different phenotypes. In humans, three major MDSC subsets were identified: polymorphonuclear (PMN)-MDSCs, monocytic (M)-MDSCs and "early-stage MDSCs" (e-MDSC) [145]. Trovato et al. demonstrated that the MDSC frequency in PDAC was significantly correlated with overall survival and metastatic disease in PDAC patients, but only in some patients the immunosuppressive activity of purified MSDC was detectable. However, this finding was ascribed only to the monocytic subset [146]. One reason for the activity and expansion of MDSC in PDAC seems to be CD200, a regulator of myeloid cell activity, which is expressed in the PDAC TME. Choueiry et al. showed that MDSC isolated from human PDAC tissues express elevated levels of the CD200 receptor, by which CD200 can activate MDSC. Additionally, they found in a mouse model that the CD200 blockade impaired tumor progression and enhanced the efficacy of PD-1 immune checkpoint inhibition [147] supporting the immunosuppressive nature of these cells. Besides, it was shown that MDSC decrease T cell proliferation and lead to an enhanced apoptosis of activated T cells [148]. However, the exact mechanisms by which

MDSC exert their immunosuppressive functions are still not fully elucidated and we refer to other excellent reviews on this cell type [149].

Owing to their prominent abundance in PDAC, we will focus in the following text mainly on the recent knowledge on TAM. TAM mainly originate from tissue resident macrophages or from blood derived monocytes which infiltrate into the injured tissue (e.g., due to cell infection or otherwise induced cell damage). Ontogeny studies in a murine PDAC model revealed that monocyte-derived TAM acquire functions such as antigen presentation, whereas embryonically-derived TAM show a more pro-fibrotic transcriptional profile indicating their role in ECM production and relating the origin of TAM to distinct functional phenotypes [150]. Importantly, in dependence on the environmental factors, monocytes/macrophages acquire different phenotypes exerting distinct functional effects. According to a simplified model, macrophages can differentiate into M1- and M2-macrophages. While interferon-gamma (IFN-γ) and bacterial lipopolysaccharide (LPS) promote polarization of pro-inflammatory M1-macrophages, IL-4, IL-13, IL-10 and TGF-β foster an anti-inflammatory M2-phenotype in humans [151–153]. Thus, the composition of the TME (e.g., oxygen level, amount and type of other stromal or tumor cells) impacts phenotype and effector function of macrophages and promotes the switch from one type to another, a process which also occurs under physiological conditions [154]. As outlined above, CAF promote an immunosuppressive environment e.g., via CXCL12 and M-CSF secretion thereby recruiting monocytes and promoting the accumulation of M2-polarized macrophages [90,155,156]. Moreover, a hypoxic TME provokes an M2-polarization, while an oxygen enriched microenvironment drives M1-polarization [83]. In a murine PDAC model, PDAC cell derived small extracellular vesicles (sEV) covered with Ezrin were shown to foster a polarization towards an M2-phenotype and supporting metastasis formation in the liver [157]. Studies in another PDAC mouse model showed that uptake of PDAC-derived exosomes by Kupffer cells contributes to formation of a pre-metastatic niche in the liver involving the recruitment of bone marrow-derived macrophages [105]. Granulin, expressed by circulating monocytes and hepatic metastasis-associated macrophages, leads to activation of HSC into HMF thereby promoting liver metastasis formation [158]. Thus, CAF and TAM maintain a vicious stimulatory cycle that sustains and further fuels itself, contributing to a tumor-promoting TME.

M1-macrophages secrete different pro-inflammatory cytokines such as IL-12, IL-23 and express elevated levels of B7 family members (B7-1, B7-2) and MHC II for appropriate activation of a TH1 response by which these cells foster anti-tumor effects [159]. In contrast, M2-macrophages secrete anti-inflammatory cytokines such as IL-10, TGF-β and others to prevent T cells from effectively exerting their anti-tumor functions [160].

Although the frequency and phenotype of macrophages are subject to high dynamic variation of the pancreatic microenvironment during tumorigenesis [140], TAM in PDAC predominantly exhibit M2-characteristics. These are associated with diverse pro-tumoral effects including promotion of tumorigenesis, immunosuppression, metastasis acceleration and chemotherapeutic resistance [159]. In primary PDAC, a high infiltration of macrophages, particularly CD163+ macrophages, is observed [24,140,161–163], indicating an M2-type which has been associated with a poor prognosis and decreased survival [162–165]. Additionally, the number of TAM is inversely associated with the maturity of the tumor stroma, as an immature (highly cellular and collagen poor) stroma correlates with an increased the number of TAM [163]. As M2-macrophages secrete a plethora of growth factors, cytokines and chemokines (e.g., IL-10, IL-6, Tumor Necrosis Factor-alpha (TNF-α), TGF-β, chemokine (C-C motif) ligand 20 (CCL20)), they are potent inducers of the EMT [161,166]. Furthermore, PDAC tumor growth and metastasis formation are dependent on phosphatidylinositol 3-kinases (PI3Kγ) expression in macrophages [167]. Of note, TAM can co-exist as M1- or M2-macrophages or also intermediate forms in the TME which are associated with anti- or pro-tumoral functions [168]. Accordingly, Helm et al. could demonstrate that human PDAC-derived TAM can exhibit both M1- and M2-properties and that also M1-macrophages are able to increase migratory and invasive abilities of PDAC cells [161,168]. In line with these findings, Chen et al. showed that M2-

polarized macrophages cause inflammation via IL-1β release. This increased IL-1β release in turn promotes EMT induction and thereby formation of metastases in an orthotropic PDAC mouse model [169].

Macrophages also contribute to apoptosis and therapy resistance of PDAC. Buchholz et al. showed that murine and human macrophages can rapidly metabolize and inactivate the chemotherapeutic drug Gemcitabine resulting in profound therapy resistance [15]. Another study could show that murine bone marrow derived macrophages when exposed to PDAC cells release pyrimidine species, among others deoxycytidine, which inhibits gemcitabine through molecular competition representing another mechanism of macrophage mediated chemoresistance [170]. Liu et al. suggest that macrophages contribute to immunosuppression and failure of immunotherapies by demonstrating an accumulation of MDSC and M2-polarized TAM in tumoral lesions of different PDAC mouse models which is accompanied by a reduction of CTL and T helper cells. Besides, the number of M2-macrophages increased after application of Gemcitabine in this model system, which could be another mechanism for drug resistance [171]. Weizman et al. identified in humans another TAM-mediated mechanism of chemoresistance via upregulation of cytidine deaminase (CDA) which leads to reduction of Gemcitabine-induced apoptosis. CDA is the enzyme which transports chemotherapeutics into cells and is responsible for their metabolization [172]. Using a genetic mouse model, Binenbaum et al. revealed that TAM communicate with cancer cells via so called macrophage-derived exosomes which are internalized by cancer cells leading to reduced Gemcitabine concentrations by upregulation of CDA in the PDAC cells [173]. Moreover, tumor-derived exosomes can be taken up by human and murine macrophages, thereby increasing expression of the immune checkpoint molecule PD-L1 on these cells and promoting macrophage-mediated immune suppression. Uptake of tumor-derived exosomes also alters the cytokine secretion (IL-6, IL-1β, IL-10 and TNFα) of macrophages thereby facilitating several pro-tumoral functions [174].

3.4. Approaches for Targeted Therapy of Macrophages

As macrophages exert diverse pro-tumoral effects e.g., promoting an immunosuppressive TME and drug resistance, these stromal cells have been qualified as a reasonable target for cancer therapy (Table 2). Accordingly, several preclinical and clinical trials targeting macrophages have been conducted. One approach to simultaneously harness multiple immune cell types including macrophages against cancer cells is the treatment with CD40 agonists [175]. CD40 is a cell surface receptor primarily expressed by B cells, DC and myeloid cells including macrophages. Through interaction with its ligand CD40L (expressed on CD4+ T cells), CD40 is activated. This activation results in various physiological effects including increased expression of MHC II and T cell costimulatory receptors on its target cells [175,176]. Consequently, antigen presentation and CTL activation are promoted. Moreover, in the KPC mouse model, CD40 agonist treatment resulted in macrophage activation with increased expression of matrix metalloproteinases. Via this mechanism, macrophages reduced the pronounced PDAC-associated desmoplasia [177]. Recently, macrophage-mediated stroma depletion and reprogramming towards an M2-phenotype were confirmed for human PDAC by translational data obtained from a clinical trial that assessed the CD40 agonist Selicrelumab [178]. Moreover, in a PDAC mouse model, CD40 agonists synergized with checkpoint inhibitors [179]. Whilst early clinical trials suggested a positive clinical effect of CD40 agonist monotherapy or combination with Nivolumab [177,180], this could not be confirmed in phase II clinical trials [181]. However, multiple clinical trials evaluating CD40 agonists for the treatment of PDAC in combination with chemotherapeutic or targeted agents are ongoing (NCT03214250; NCT04536077; NCT04807972; NCT04888312) and may yield more promising results. Furthermore, the combination of an anti-PD-1 antibody with Gemcitabine showed a beneficial effect in a murine PDAC liver metastasis model, which was explained by an increase of M1-macrophages and a TH1 response [182].

Table 2. Overview of the cited therapeutic approaches targeting macrophages.

Study System	Targeting Strategy	Reference
Preclinical studies		
KPC mice	CD40 agonist treatment by CP-870,893	[177]
KPC mice	CD11b agonist treatment by ADH-503	[183]
C57BL/6 mice including Batf3 KO, CD40 KO, MyD88 KO, STING KO and IFNAR KO	CD40 agonist treatment by FGK45 combined with anti-PD-1 by RMP1-14 and/or anti-CTLA-4 by 9H10	[179]
Clinical studies		
Phase1 clinical trial	CD40 agonist treatment by Selicrelumab	[178]
Phase 1b clinical trial	CD40 agonist treatment by Sotigalimab in monotherapy or in combination with PD-1 blockade by Nivolumab	[180]
Phase 2 clinical trial	CD40 agonist treatment by Sotigalimab in monotherapy or in combination with PD-1 blockade by Nivolumab	[181]
Phase 1b/2 clinical trial	CD40 agonist treatment by Sotigalimab in combination with PD-1 blockade (Nivolumab) + Gemcitabine + Nab-Paclitaxel, or Sotigalimab + Gemcitabine + Nab-Paclitaxel.	NCT03214250
Phase 2 clinical trial	Addition of recombinant fms-like tyrosine kinase 3 (Flt-3) ligand (CDX-301) to the CD40 agonistic antibody (CDX-1140)	NCT04536077
Phase 2 clinical trial	modified FOLFIRINOX (mFFX) combined with ABBV-927 with or without Budigalimab	NCT04807972
Phase 1b/2 clinical trial	CD40 agonist Mitazalimab in combination with modified FOLFIRINOX	NCT04888312

Since specific targeting of macrophages spares other immunosuppressive monocytic cell populations which may impair the therapeutic efficacy, targeting of the integrin CD11b/CD18 which highly expressed on several myeloid cell subsets has been suggested as a promising strategy for PDAC treatment. Using the CD11b small-molecule agonist (ADH-503) in KPC mice, a partial activation of CD11b along with TAM repolarization was observed. In addition, increased numbers of immunosuppressive myeloid cells in tumor tissues were observed as well as enhanced dendritic cell activity. Thus, this strategy targeting multiple immunosuppressive myeloid cells led to an improved antitumor T cell response which might be even more effective in combination with immune checkpoint inhibitors [183].

However, to date no convincing strategies targeting macrophages have been elaborated and implemented in treatment of PDAC patients. One explanation might be that as demonstrated for CAF, macrophages represent a heterogeneous cell population exerting highly context-dependent pro- and anti-tumoral effects. Thus, this dynamic phenotype

switching, which also seemed to be influenced by the different therapeutic strategies, have to be considered in an effective and sustainable anti-tumor therapy of PDAC patients.

3.5. Heterogeneity of T Cells

Although we focus on T lymphocytes in this article, we want to briefly mention the other group of lymphocytes, namely the B cells. The role of B cells in PDAC is still controversially discussed but in general, B cells are described to be rather tumor promoting. Thus, Pylayeva-Gupta et al. showed that B cells secrete IL-35, which promotes the proliferation of tumor cells [184]. Furthermore, coculture of B cells isolated from PDAC patients enhanced the production of collagen by fibroblasts, resulting in ECM remodeling [185]. In a mouse model, it was shown that B cells are recruited by the B cell chemoattractant CXCL13 already during PanIN formation. Similarly, accumulation of B cells was also observed in PanIN lesions in PDAC patients [184,185]. Overall, there are not a lot of studies focusing on B cells in PDAC but it might be useful to investigate further on B cells in order to understand the complex microenvironment better.

Besides diverse CAF and macrophage phenotypes, different T cell populations can be found in the TME of the primary tumor and metastases in PDAC patients. Owing to their different effector phenotypes, T cells essentially impact the process of tumor and metastases formation in several ways. In general, an increase of immunosuppressive (T) cells can be observed during PDAC development, while tumor directed immune functions are impaired and/or even lost [140,186,187]. Key players of the immune response against tumor cells are CD8+ CTL. Accordingly, several studies showed that a high tumor infiltration of CD8+ CTL is associated with a longer overall survival of PDAC patients [188–191].

Rahn et al. showed in human PDAC tissues that CTL are predominantly present in the TME and less in close proximity to PDAC cells [24]. One reason for this can be seen in the desmoplastic stroma containing the ECM which acts as a physical barrier for immune cells and in particular CTL [69,192]. Similar findings were reported on liver metastases. Accordingly, in a KPC mouse model small metastatic lesions in the liver show a high CD8+ T cell infiltration compared to large metastatic lesions. Furthermore, in small lesions CD8+ T cells express CD69 and no PD-1, indicating that these CTL still exhibit their effector phenotype, while in large metastatic lesions CTL express PD-1 but no CD69, indicating T cell exhaustion [193]. Importantly, this exhausted state is characterized by elevated expression of inhibitory receptors (PD-1, CTLA-4 and T cell immunoglobulin domain and mucin domain-3 (TIM-3)), decreased production of cytotoxic molecules (perforin, granzyme A/B and granulysin), decreased production of chemokines (TNF-α and IFN-γ) and higher CTL apoptosis [194,195]. For optimal CTL survival and effector function, CD4+ T helper cells are pivotal. In line with this finding, a high tumor infiltration of CD8+ CTL together with CD4+ T cells correlate with a better prognosis for PDAC patients [188,189]. CD4+ T cells are another very heterogeneous T cell population, as they can differentiate into divergent subsets (TH1, TH2, TH17 and Treg). The differentiation of TH0 helper cells into different subsets is dependent on cytokines (IL-12, IL-4, TGFβ, IL-6 and IL-2) in the microenvironment [196]. The different subsets are characterized by expression of distinct cytokines and therefore show divergent impacts on all cells in the TME. Similar to CAF and macrophages, the effects can be either tumor-promoting or tumor-suppressing.

TH1 cells are regarded as tumor-suppressing as they exert various immune response activating functions e.g., they release IFNγ, which promotes recruitment of CTL, M1-macrophages and Natural Killer (NK) cells, and IL-2 which activates CTL [197,198]. On the other hand, IFNγ also induces PD-L1 expression on tumor cells, T cells, myofibroblasts and macrophages, thereby supporting CTL inhibition and immune escape in PDAC [199].

However, PDAC cells and the TME rather promote differentiation of TH2 cells which are regarded as immune-suppressing and thereby tumor-promoting [200], mainly because of the release of cytokines like IL-4, IL-5, IL-6, IL-10 and IL-13 [187]. IL-4 and IL-10 foster the differentiation of monocytes into M2-macrophages [201], IL-4 and IL-13 trigger the collagen synthesis in myofibroblasts thereby contributing to ECM remodeling [202] and

IL-13 has been shown to enhance growth of PDAC cells [203]. Accordingly, elevated levels of TH2 cytokines can be detected in plasma samples [187] and the TME of PDAC patients comprises higher numbers of TH2 cells compared to TH1 cells [204]. Moreover, high plasma levels of TH2 cytokines in patients with resectable PDAC are associated with a shorter survival [205].

Furthermore, human PDAC tissues contain higher numbers of TH17 cells compared to normal pancreatic tissue, which is associated with a shorter median survival of PDAC patients [206]. TH17 cells are regarded mainly as tumor-promoting because this T cell subset is characterized by elevated release of IL-17, IL-21 and IL-22 [197]. Importantly, IL-17 has been shown to enhance initiation and progression of PanIN in a murine PanIN model, thus being a trigger in early pancreatic tumorigenesis [207].

Another important immunosuppressive cell population in PDAC tissues are Treg. Especially in human PDAC, Tregs are mostly located in the stroma and only rarely in the epithelial layer of pancreatic ducts. Furthermore, Hiraoka et al. demonstrated a significant increase in the number of Treg during progression from low grade PanIN to an invasive PDAC. Additionally, a high prevalence of Treg in PDAC is significantly correlated with distant metastases, advanced tumor stage and high tumor grade as well as poorer prognosis [208,209]. The mechanisms by which Treg enrich in human and murine PDAC can be diverse e.g., tumor associated Treg can derive from peripheral Treg recruitment, expansion of tissue resident Treg, differentiation from local naïve T cells or conversion of conventional T cells [210]. Here, tumor- or CAF derived TGF-β can induce conversion of CD4+ CD25- T cells into Treg [211,212]. It was also shown that Forkhead box protein 3 (FoxP3) expressing tumor cells recruit Treg by directly trans-activating CCL5 [213]. Yang et al. observed a correlation of highly expressed secreted frizzled-related protein 4 (SFRP4) and Treg infiltration in tumors of KPC mice and PDAC patients [214]. Shen et al. speculated that PDAC cell-derived sEVs induce an enrichment of human FoxP3+ Treg and further an overexpression of immune checkpoint molecules PD-1, PD-L1, CTLA-4 and TIM-3 as well as an enrichment of FoxP3+ Treg [215]. Finally, L1 cell adhesion molecule (L1CAM) expression in the pancreatic ductal epithelium was shown to promote enrichment of human Treg in PDAC by e.g., enhancing migration of Treg, decreasing proliferation of CD4+ effector T cells and promoting conversion into a CD4+CD25-CD69+ regulatory T cell phenotype [216]. Moreover, these CD4+CD25-CD69+ Treg are detectable at high numbers in human PDAC tissues and correlate with nodal invasion and higher grading in PDAC patients [216]. One mechanism by which Treg suppress the anti-tumor response is by interaction of CTLA-4 with CD80/CD86 on DC leading to a reduced expression of MHC class II, CD40 and CD86 molecules, all being important for Treg maturation and activation. Besides, tumor-associated DC express Indolamine-pyrrole 2,3-dioxygenase (IDO), which suppress T cell responses and promote immune tolerance [217]. Moreover, Treg crosstalk with and are dependent on MDSCs as in a PDAC mouse model, depletion of MDSC led to a reduced recruitment and/or induction of Treg in pancreatic tumors and development/expansion of Treg seems to require a direct cell–cell interaction with MDSC [148]. Furthermore, TGF-β is not only a trigger for Treg development but also production of reactive oxygen species (ROS) by these cells contributing to oxidative stress in the TME [218].

Finally, γδ T cells represent a promising tumor-suppressive T cell population because of their ability to recognize antigens in an MHC-independent manner, to present antigens to CD3+ αβ T cells as well as their phagocytic properties. γδ T cells have a prevalence of 1–10% in the blood [219]. In human PDAC tissues, γδ T cells are mainly found in the tumor stroma or adjacent to or within ductal epithelium [220]. γδ T cell infiltration can be promoted by CAF derived CXCL12 [221,222]. However, the presence of γδ T cells is not sufficient to exert potent anti-tumor responses, because it has been shown that Galectin-3 which is expressed on PDAC cells but also αβ- and γδ T cells, inhibits T cell proliferation and is thus regarded as an intrinsic tumor escape mechanism [223,224]. Furthermore, kynurenine, a downstream metabolite of IDO, was identified as an inhibitor of γδ T cell

cytotoxicity and proliferation in PDAC [225]. However, Daley et al. showed that γδ T cells can inhibit αβ T cell activation via checkpoint receptor ligation leading to suppression of CD4+ and CD8+ T cells and acquisition of an activated CD44+CD62L- phenotype. Additionally, γδ T cells were shown to decrease TNF-α expression of αβ T cells in vitro. Importantly, these processes can be reversed by PD-L1 blockade suggesting that γδ T cells are important modulators of a checkpoint receptor-dependent immunosuppression and pinpoint also to a tumor-suppressing role of these cells in PDAC [226].

First attempts have been undertaken to consider this T cell heterogeneity to provide a rationale for patient stratification and optimized treatment choice. Depending on the number of infiltrating lymphocytes, tumors have been categorized into immunological subtypes: T cell inflamed ("hot tumors") or non-T cell inflamed ("cold tumors"). Owing to the low T cell infiltration especially of CD8+ CTL, PDAC is mostly characterized as a cold tumor [227]. Importantly, immunotherapies are often not effective in "cold" tumors explaining their common failure in PDAC [25,228].

3.6. Approaches for Targeted Therapy of T Cells

Since single agent immunotherapy with cancer vaccines or immune checkpoint inhibitors has failed so far in clinical trials [21,22,229,230], multi-agent combinations and combinations with radiotherapy have been evaluated as treatment option for PDAC. In order to boost T cell responses against cancer cells, combinations of two checkpoint inhibitors (Durvalumab and Tremelimumab) targeting the CTLA-4 and PD-1/PDL-1 axes have been evaluated [231,232]. Moreover, clinical trials were designed to assess combinations of cancer vaccines (e.g., GVAX and CRS-207) and checkpoint inhibitors or checkpoint inhibitors with oncolytic viruses (Pelareorep) or chemokine receptor inhibitors (BL-8040) based on promising preclinical data [233–236]. To date these approaches have not yielded relevant clinical improvements for PDAC patients. However, a high number of clinical trials investigating innovative immune checkpoint inhibitor-based combinations (e.g., with IL-6 antagonists (NCT04258150), agonists of stimulator of interferon genes (NCT03010176) and kinase inhibitors (NCT04820179) are underway.

As outlined above, γδ T cells represent an attractive effector T cell population for cancer therapy as they recognize antigens and kill target cells MHC independently. Thus, bispecific Abs binding CD3 or Vγ9 on γδ T cells and HER2/neu on PDAC cells enhanced the cytotoxicity of γδ T cells via granzyme B and perforin release and led to a reduced tumor growth in a subcutaneous PDAC Xenograft model [219]. Furthermore, the tribody [(HER2)2xCD16] activated human γδ T cells and NK cells to lyse HER2 expressing PDAC cells via granzyme B release [237]. Additionally, monitoring of γδ T cells subpopulations in PDAC patient's blood and determination of their cytotoxicity can also help to optimize γδ T cell-based immunotherapy [238].

Depleting Treg could also be an option to improve PDAC therapy. As Treg express CCR5, a current phase1/2 clinical trial investigates the therapeutic efficacy of CCR2 and CCR5 inhibitors in advanced PDAC with the aim to reduce Treg, MDSC and M2-polarized TAM and to increase anti-tumor immunity [209]. The bispecific antibody ATOR-1015 [CTLA-4xOX40] induced CD8+ T cell activation and Treg depletion in several syngeneic tumor models including a PDAC model, thereby resulting in a tumor-specific and long-term immunological memory. Furthermore, ATOR-1015 enhanced the response to PD-1 blockade, thus providing a reasonable combination with PD-L1 inhibitors [239]. However, depletion of the entire Treg population might bear the risk for the development of autoimmunity. Additionally, preclinical studies in a PDAC mouse model demonstrated that Treg depletion does not lead to diminished immunosuppressive activity and accelerates tumor growth. Since Tregs release high amounts TGF-β, Treg depletion resulted in a reduced TGF-β levels by which in turn tumor-restraining α-SMA+ CAF were reprogramed into iCAFs. Furthermore, increased numbers of myeloid cells were observed in the tumors indicating that specific targeting of this particular T cell population essentially alters the

stroma cell dynamics in the TME by which unexpected tumor promoting effects might be induced [240].

In summary, PDAC-associated T cells are characterized by a great diversity exemplified by their abundance (high versus low numbers), spatial localization (in close proximity to tumor cells versus located in the TME) and effector phenotype (activated versus anergy/exhausted). Adding to this huge complexity, distinct T cell populations exert both tumor-promoting and tumor-suppressing functions. Importantly, the immunological TME composition and overall immunity in a tumor and patient, respectively, seem to be highly dependent on a variety of host intrinsic (e.g., genetics) and extrinsic factors (e.g., exposure to pathogens or environmental factors) [241] defining the above-mentioned parameters which have to be considered for an effective anti-PDAC therapy.

3.7. Heterogeneity of Endothelial Cells

In general, human PDAC tissues exhibit a high microvascular density and poorly perfused blood vessels, the latter showing a heterogeneous distribution pattern in PDAC subtypes [242,243]. Moreover, a high microvascular density along with a diminished integrity of these microvessels is associated with disease progression and poorer survival in PDAC patients [244]. This immature vasculature and the high intratumoral pressure in PDAC due to the pronounced desmoplastic stroma results in an irregular as well as disorganized tubular architecture. Murine and human studies revealed that this in turn impairs drug delivery, suppresses lymphocyte infiltration and increases hypoxia within the tumor mass [133,245–247]. In general, blood vessels support tumor growth by enabling influx of nutrients and oxygen. In addition, EC also affect tumor cells, stromal cells in the TME and therapy responses [248–250].

Tumor angiogenesis is induced by proangiogenic factors such as VEGF released by tumor and stromal cells [251]. Upon this "endothelial cell activation", changes in the gene expression profile and phenotypes of EC occur by which these cells exert their pleiotropic effects in the tumor [252,253]. Thus, increased expression levels of Vascular Endothelial Growth Factor Receptor (VEGF-R), EGF-R and diverse cell adhesion molecules (e.g., Intercellular Adhesion Molecule (ICAM), Vascular Cell Adhesion Molecule (VCAM), E-selectin) as well as an increased secretion of cytokines (e.g., IL-8) are observed in activated EC or tumor associated endothelial cells (TEC). These alterations essentially contribute to tumor inflammation and immune evasion in human as well as in murine tumors [254–260]. Thus, human derived material as well as murine xenografts revealed that TEC are not only morphologically distinct from their physiological counterparts, but also exhibit diverse genetic and phenotypic alterations by which these cells impact tumor development and progression as well as therapy responses. Furthermore, TEC can undergo Endothelial-Mesenchymal-Transition thereby giving rise to CAF and contributing to CAF enrichment in PDAC. In humans, this process seems to be mediated by inflammatory factors such as TNF-α [261–263].

Furthermore, Issa et al. demonstrated that upregulation of L1CAM expression on human PDAC-derived TEC increase adhesion and transmigration of PDAC cells to and through the PDAC-derived endothelium, thereby facilitating PDAC metastasis [264]. Sano et al. described that elevated expression of VCAM-1 on TEC promotes progression of PDAC as well as PanIN in a genetically engineered mouse model, but also increases the incidence of cancer-associated thrombosis in mice and patients, which is known as a poor prognostic factor in PDAC. Moreover, this is accompanied by an increased infiltration of immunosuppressive leucocytes into the tumor tissues. Blocking VCAM-1 reduces the number of thrombotic/thromboembolic events as well as infiltration of TAM and tumor-associated neutrophils and prolonged overall survival of treated mice [265]. In line with these findings, PDAC-derived TEC exhibit an enhanced expression of distinct adhesion molecules (e.g., E-selectin, ICAM-1, VCAM-1, Mucosal vascular address in cell adhesion molecule 1 (MAdCAM-1)) compared to EC from healthy pancreas. These PDAC-derived EC promote transendothelial migration of Treg thereby contributing to the immunosuppressive

TME in human as well as murine PDAC [266]. In contrast, downregulation of these adhesion molecules (e.g., ICAM-1/2, VCAM-1, MAdCAM-1, E-selectin) on TEC leads to a decreased infiltration of putative tumor-directed lymphocytes into the TME [209,267].

3.8. Approaches for Targeted Therapy of Endothelial Cells/Angiogenesis

Overall, these data indicate that TEC can exhibit different phenotypes and functions compared to their physiological counterpart, which is dependent on the tumor entity and TME composition e.g., the amount of macrophages which are a main source of VEGF. Importantly, the aberrant morphology of TEC and their altered expression profile of adhesion molecules are essential determinants for various malignancy-associated processes, such as immune evasion and drug resistance in PDAC patients [268]. Accordingly, TEC and angiogenesis, the latter being a hallmark of cancer, have been identified as promising targets for cancer therapy and many anti-angiogenic strategies have meanwhile been approved for the treatment of a variety of cancer entities. Demonstrated in preclinical and clinical studies, those strategies primarily aim at the inhibition of angiogenesis, thereby reducing nutrient supply and deactivating EC on the one hand [269–272] and normalizing the vasculature to improve drug delivery and immune cell access into the TME on the other hand [273–276]. Two commonly used anti-angiogenic drugs are Bevacizumab and Aflibercept, both binding to VEGF, and Aflibercept additionally binding to Placenta-derived Growth Factor (PGF). In addition, tyrosine kinase inhibitors (such as Sunitinib, Sorafenib, Pazopanib) that target VEGF-R2 e.g., expressed by TEC [277] are also FDA approved for anti-angiogenic cancer therapy. However, the above-mentioned strategies still fail to significantly improve overall or progression free survival of PDAC patients [278,279].

Accordingly, intensive research efforts are ongoing to identify predictive markers that allow for rational patient stratification in order to select the optimal therapeutic strategy to specifically target the aberrant vasculature in PDAC [280]. Considering the pleiotropic effects of TEC in PDAC, TEC targeting may be more effective in combination with e.g., immune checkpoint inhibitors or modified drugs (e.g., encapsulated forms) to optimize treatment strategies. Furthermore, more studies are required investigating the optimal timing for anti-angiogenetic therapies (particularly in combination with other therapies) in order to exert the maximum effect.

3.9. Heterogeneity of the Microbiome

In recent years compelling evidence has emerged that not only the TME but also the microbiome is altered in PDAC patients—in the tumor as well as in other body compartments. Experimental data support the view that the altered microbiome is not just a surrogate of the disease but rather essentially impacts development, progression and therapy responses of PDAC [11,19,20]. Miller et al. also identified an influence of the microbiome on the TME, thereby promoting PDAC development and explaining reduced therapeutic efficacy of several agents. Hence, ablation of the microbiome was shown to prevent PDAC in preclinical studies [281].

It is still not fully understood how bacteria, detectable in PDAC tissues, enter the pancreas. Potential mechanisms include the oral route or translocation from the lower gastrointestinal tract through the portal circulation or mesenteric lymph nodes [282]. Thus, it has been shown that human cystic pancreatic precursor lesions contain Fusobacterium nucleatum and Granulicatella adiacens, both bacterial populations commonly found in the oral cavity [283,284]. In line with this finding, increased amounts of Fusobacterium species were detected in PDAC tissues and correlated with a worse prognosis of PDAC patients [285]. Another study demonstrated that Gammaproteobacteria are the predominant bacterial species in human PDAC tissues, most of them being members of Enterobacteriaceae and Pseudomonadacea families [19].

It has been shown in patient suffering from malignant melanoma and lung cancer that the gut microbiome impacts the response to immunotherapy and chemotherapy. This finding suggests that the composition of the gut microbiome impacts activation of

the immune system [286–288] and thereby promotes cancer-associated inflammation, a mechanism which might also be relevant in PDAC. Of note, chronic pancreatitis (CP), being a risk factor for PDAC development, can be caused by microbial infections [289].

As outlined above, an inflammatory and desmoplastic environment supports various malignancy-associated processes, such as immune evasion and metastasis and impacts therapy responses [290–292], all processes related to EMT [293]. Importantly, a tumor-associated microbiome was shown to promote EMT, thereby leading to epithelial barrier alterations and tumor-promoting inflammation. In detail, it could be shown that infections by Fusebacterium nucleatum lead to the loss of membranous E-cadherin [294], a key step in EMT [11,295–297]. Owing to the fact that high levels of Fusebacterium are found in human pancreatic precursor lesions and PDAC tissues, it is reasonable that this might be one mechanism by which early EMT is induced in pancreatic tissues. Of note, EMT-associated alterations are already found in PDEC in human CP tissues [296] and lead to early PDEC dissemination prior to tumor formation in the pancreas in a murine mouse model [297]. Zhang et al. postulated that each microbial pathogen conquering the pancreatic tissue has the potential to induce EMT-related pathological changes [11]. Since EMT induction has been also linked to the acquisition of CSC properties and drug resistance [2,6,10], EMT/CSC induction might represent another mechanism by which the altered microbiome contributes to the pronounced therapy resistance in PDAC.

In this context, Geller et al. reported not only the presence of Gammaproteobacteria in human PDAC tissues but also that these bacteria, expressing the long form of the enzyme CDA, are able to metabolize the cytostatic drug Gemcitabine into its inactive form. These findings suggest that the presence of Gammaproteobacteria in PDAC tissues may contribute to Gemcitabine resistance in these patients [19].

Moreover, Riquelme et al. discriminated long-term survivor (LTS) PDAC patients showing a high bacterial alpha diversity from short-time survivor (STS) PDAC patients with a lower alpha diversity. They also demonstrated that the microbiome composition in PDAC tissues differs from that in normal tissues and that the gut microbiome accounts for 25% of the tumor microbiome, supporting translocation of bacteria from the gut into pancreatic tissues as one mechanism for bacterial PDAC tissue colonization [20]. Additionally, they determined greater numbers of CD3+ T cells, CD8+ T cells and granzyme B+ cells in LTS compared to STS PDAC patients, thus correlating a higher CTL infiltration with a higher microbiome diversity. These data indicate that the tumor microbiome composition influences both the extent of immune infiltration and the degree of CD8+ T cell activation in PDAC tissues [20]. It also suggests that alterations of the microbiome directly in the tumor but also in other body compartments (e.g., the gut) essentially contribute to shaping the patient's immune response. In line with these findings, it was shown in different tumor mouse models that the efficacy of the CTLA-4 inhibitor Ipilimumab depends on the presence of distinct commensal gut *Bacteroides* species (spp.) which apparently trigger TH1 immune responses, being important for the anti-tumor effects. Hence, administration of antibiotics decreased the therapeutic effect of Ipilimumab [298]. Moreover, this study also demonstrated that fecal microbiota transplantation (FMT) of human *Bacteroides* spp.-rich feces significantly increases the overall outcome of tumor bearing animals by markedly increasing the response to CTLA-4 blockade. Supporting these data, Tanoue et al. detected an 11-strain consortium of bacteria isolated from gut microbiota of human healthy control donors (HC) which can induce IFN-g+ CD8+ T cells to enhance the efficacy of immune checkpoint inhibitors in tumor-bearing mice [299]. Underscoring the therapeutic potential of FMT, a significant reduction in tumor growth was observed in PDAC bearing mice after FMT from PDAC LTS donors with no evidence of disease (LTS-NED) compared to mice obtaining FMT from STS patients or HC [20]. Moreover, tumors from mice treated with FMT of STS PDAC patients were larger than those from mice who received FMT of HC. Finally, short-term antibiotic treatment of tumor bearing mice which had received FMT from LTS-NED donors led to even larger tumors than those of untreated mice. These data suggest that certain PDAC-associated bacteria exert a tumor-promoting effect on the one

hand and that bacterial ablation by antibiotic treatment decreases the anti-tumoral efficacy of distinct bacterial species e.g., found LTS PDAC patients on the other hand.

3.10. Approaches for Microbiome Modulating Therapies

As already mentioned above, studies provide evidence that the response of cancer patients to blockade of the immune checkpoints PD-1/PD-L1 or CTLA-4 is influenced by the gut microbiome [298,299]. Tumor mouse models revealed that different microbiome compositions cause significant differences in response to treatment with PD-1/PD-L1 inhibitors [298] so that probiotics have been suggested as part of the anti-cancer therapy. Accordingly, Sivan et al. demonstrated reduced tumor growth and a beneficial response to anti-PD-1 therapy in melanoma bearing mice after oral administration of Bifidobacterium spp. containing probiotics. Furthermore, the superior anti-tumor effect from mice with a favorable microbiome composition could be transferred to other mice by FMT or co-housing [298,300]. In summary, these findings strongly support the therapeutic potential of FMT or certain diets/probiotics with the aim to restore the commensal (tumor-suppressing) microbiome and to displace the tumor-promoting microbiome. Combining such strategies with chemo- or immunotherapy might help to overcome therapy resistances and to improve PDAC patient prognosis.

4. Therapeutic Implications and Challenges of TME Targeting

The study by Rashid et al. revealed that consideration of different molecular subtypes e.g., those identified by [28–30], might be reasonable for stratifying PDAC patients for chemotherapy, as they provided evidence for efficacy prediction towards FOLFIRINOX treatment according to molecular tumor subtypes [32]. Adding to the multiple levels of tumor heterogeneity, stromal cell populations as well as the microbiome have been characterized by a high heterogeneity, too, implying both tumor-promoting and tumor-restraining functions. As outlined in the sections above, multiple therapeutic approaches have been developed and tested to target distinct TME components in order to improve treatment outcome of PDAC patients. However, many of these studies revealed unexpected results (e.g., by depleting the entire CAF population leading to even more aggressive tumors [131] or promising preclinical findings could not be confirmed in clinical trials [134]. Thus, until today, less than 5% PDAC patients receive a targeted therapy and significant improvements of survival are still missing [301]. Current clinical trials such as the "Precision-Panc" (NCT04161417) and the "Precision Promise" studies (NCT04229004) are ongoing with the aim to validate the therapeutic efficacy of novel individualized therapies in PDAC patients [302,303]. However, results from these trials are still pending.

The clinical failure of these strategies might also be explained by the use of inadequate preclinical models and/or an insufficient consideration of the stromal cell heterogeneity, to clearly discriminate which stromal phenotype is "friend or foe" [192,304,305]. For any kind of targeted and personalized therapy in cancer patients, pre-therapeutic samples and biopsies, respectively, are of pivotal importance and a critical determinant to assess inter- and intratumoral characteristics as well as changes during treatment courses. These allow identification of the most effective therapy and to eventually select therapies according to the profile identified [32]. In this context, surgically resected specimens provide the largest number of cells, reflect best tumor heterogeneity and enable pathologists to perform comprehensive analyses [306]. In cases of patients with an advanced disease, not being suitable for surgical resection or with recurrent tumors, fine needle aspirated (FNA) samples have been proven to be useful for identification of targets for targeted therapies. However, FNA samples only reflect a small portion of the tumor bearing the risk of not fully representing tumor and stroma heterogeneity [32,301,303]. Nonetheless, FNA-obtained samples are in certain cases the only option to obtain information on tumor and TME characteristics and help to provide individualized therapy to patients with metastatic disease whose tumor is not resectable. Liquid biopsies and analysis of cell free nucleic acids, circulating tumor cells or extracellular vesicles are additional methods to obtain information on tumor cell

characteristics. Repeated blood draws (or collection of other body fluids) are more feasible than repeated biopsy sampling and may therefore complement tissue-based analysis for longitudinal monitoring of PDAC dynamics and therapy response [307]. However, important players of PDAC biology, i.e., the TME and the microbiome are not considered in these approaches.

Of note, Birnbaum et al. already suggested to consider not only the PDAC tumor subtypes but also the stromal subtypes classified by Collisson et al., Moffitt et al. and Bailey et al. for targeted therapy in PDAC patients [28–31]. Even though targeting the TME based on stromal subtypes might be a more efficient therapeutic approach, a challenge will be to fully consider differences in distribution and extent of the TME at different sites (primary tumor versus metastases) which might be associated with divergent functional effects on PDAC development. Furthermore, the TME might be further differentially modified by chemotherapy [303,308]. Additionally, Torphy et al. identified a high stroma content as a factor for a favorable outcome in patients suffering from metastatic PDAC [309], further underscoring that the TME heterogeneity is a critical determinant for targeted stromal therapy.

The current knowledge gained from comprehensive preclinical and clinical trials demonstrating a rather limited efficacy of tumor and TME targeted therapies in PDAC patients, leads us to the following assumptions: (i) due to its extraordinary complexity and peculiarity, the TME in PDAC easily compensates pathways, interactions and effects that are modulated by mono-targeted therapies resulting in limited therapeutic efficiency, (ii) targeted therapies applied so far have impaired both tumor-promoting and tumor-restraining TME populations, thereby counteracting the beneficial therapeutic effects albeit it was intended to solely target the tumor-promoting cell populations, (iii) the functional impact of certain host-derived factors on PDAC development and on shaping therapy responses are still insufficiently understood and considered (e.g., the host microbiome) and (iv) the usage of reliable biomarker (not only in tumor tissue but also other compartments) for therapy decision making has still to be improved for treatment of this tumor entity.

Accordingly, concepts aiming at restoration and normalization of a physiological, tumor-restraining microenvironment, respectively, rather than at precisely targeting distinct TME components might be more effective strategies [180,310]. For example, Kocher et al. focused on the stroma in patients with locally advanced or metastatic PDAC and replenished the Gemcitabine-Nab-Paclitaxel chemotherapy with ATRA in a phase I clinical trial. Clinical safe and tolerable efficiency and successful reprogramming of the TME was detectable [311] which was also observed in other preclinical studies [137]. Another "normalization" or "reprogramming" strategy might be the modulation of the patient's microbiome. As outlined above, the microbiome substantially influences the efficacy of chemotherapeutic drugs in PDAC-patients [11,19,20] as well as the response to immune checkpoint inhibition [298]. Additionally, restoration of a tumor-restraining microbiome by application of distinct microbiome species, e.g., such as FMT, may not only overcome drug resistances, but also help to boost the patient's immune system to induce a long-term control of the tumor burden [11,20].

Overall, the above-mentioned studies and continuously elaborated novel concepts have essentially broadened our understanding of this challenging disease. However, additional studies are needed to further dissect the dynamics and heterogeneity of the TME regarding the tumor-promoting and tumor-restraining functions in order to translate this knowledge into personalized therapeutic concepts to improve the prognosis of PDAC patients. Consideration of this heterogeneity and its impact on PDAC development and therapy responses is enabled by collecting and comprehensively analyzing tumor, stroma and the patient's microbiome to generate an integrated tumor subtype. This identified subtype allows stratification of each patient for the individualized and most effective therapy (Figure 2).

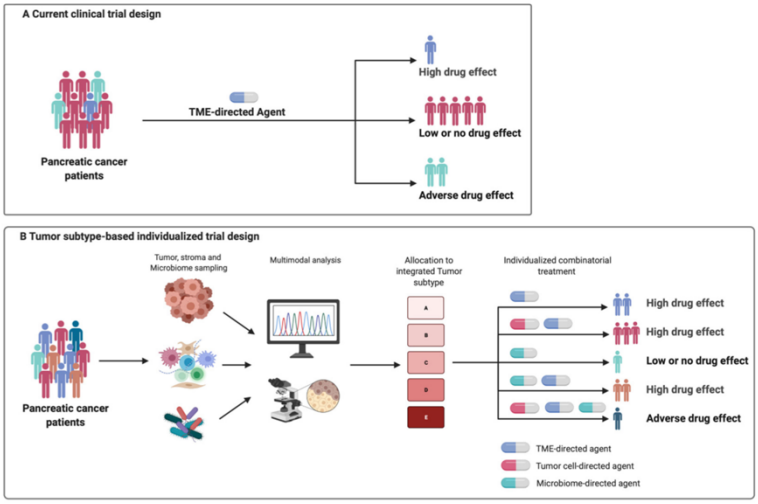

Figure 2. Current and future therapeutic concepts for the treatment of pancreatic cancer patients. (**A**) In current clinical trials, pancreatic cancer patients are not stratified according to distinct tumor and stroma characteristics. Accordingly, the given therapy exerts an anti-tumor effect only in few patients. However, in the majority of patients this strategy fails or has even adverse effects. (**B**) A tumor subtype-based individualized trial design implies sampling of the patient's tumor, stroma and microbiome prior to treatment and multimodal analysis of these samples will generate an integrated tumor subtype for each patient. Considering these tumor, stroma and microbiome characteristics, the identified subtype allows stratification of pancreatic cancer patients for the treatment strategy with the best predicted outcome. Figure created with BioRender.com.

5. Conclusions

Extensive preclinical and clinical evaluation of PDAC has resulted in detailed characterization of its complexity on multiple levels. In this article, we summarized how PDAC biology is determined by a plethora of cell types and microbiota shaping the TME and their context-dependent pro- or anti-tumorigenic characteristics. This challenging level of complexity is further increased by countless interactions between the involved cell types. In the future, increased efforts will be needed to translate these insights into TME heterogeneity into clinically meaningful benefits for PDAC patients. To this end, we propose comprehensive analysis of patient material (tumor, tumor stroma and microbiome) and the development of integrated tumor subtypes based on this data base. Respective integrated tumor subtypes may then serve for informed patient stratification in clinical trials and truly individualized therapeutic decisions.

Author Contributions: Conceptualization, S.S.; Supervision, A.-S.M. and S.S.; Visualization, A.M.W.; Writing—original draft, L.A., S.B., T.D., L.-M.P., A.S., U.-U.Y., A.-S.M. and S.S.; Writing—review and editing, all authors. All authors have read and agreed to the published version of the manuscript.

Funding: Funding by the Research and Training Group 2501 on Translational Evolutionary Research (RTG 2501 TransEvo, DFG for S.S.), by Deutsche Forschungsgemeinschaft (DFG, German Research Foundation)—Projektnummer 413490537 (for A.M.W.) and the Deutsche Krebshilfe (AZ 70112935 for S.S.) is acknowledged. The authors also acknowledge financial support by DFG within the funding program Open Access Publizieren.

Conflicts of Interest: All authors declare no conflict of interest. The funders had no role in the writing of the manuscript.

Abbreviations

ADEX: aberrantly differentiated endocrine exocrine; α-SMA: Alpha-smooth muscle actin; APC: Antigen presenting cells; apCAF: antigen presenting carcinoma associated fibroblasts; ATRA: All-trans retinoic acid; CCL: Chemokine (C-C motif) ligand; CAF: Carcinoma associated fibroblasts; CD: Cluster of differentiation; CDA: Cytidine deaminase; CP: Chronic pancreatitis; CSC: Cancer stem cells; CTLA-4: Cytotoxic T-Lymphocyte-Associated Protein 4; CXCL: chemokine (C-X-C motif) ligand; CTL: Cytotoxic T cells; DC: Dendritic cells; EC: endothelial cells; ECM: Extracellular matrix; EGF: Epidermal Growth Factor; EGFR: Epidermal Growth Factor-Receptor EMT: Epithelial-Mesenchymal-Transition; FNA: Fine needle aspirated; FMT: Fecal microbiota transplantation; FoxP3: Forkhead box protein 3; G-CSF: Granulocyte-Colony Stimulating Factor; HC: Healthy control donor; HGF: Hepatocyte Growth Factor, HIF-1: Hypoxia-inducible factor-1; HSC: Hepatic stellate cells; HMF: Hepatic myofibroblasts; iCAF: inflammatory CAF; ICAM: Intracellular Cell Adhesion Protein; IDO: Indoleamine-pyrrole 2,3-dioxygenase; IL: Interleukin; IFN-γ: Interferon-gamma; IPMN: Intraductal papillary mucinous neoplasm; JAK: Januskinase; L1CAM: L1 cell adhesion molecule; LPS: Lipopolysaccharide; LTS: Long-term survivor; PanIN: Pancreatic Intraepithelial Neoplasia; MAdCAM-1: Mucosal vascular addressin cell adhesion molecule 1; M-CSF: Macrophage-Colony Stimulating Factor MDSC: Myeloid-derived suppressor cell; MHC: Major histocompatibility complex; myCAF: myofibroblastic CAF; NED: No evidence of disease; NK: Natural killer; PDAC: Pancreatic ductal adenocarcinoma; PDEC: Pancreatic ductal epithelial cells; PD-1: Programmed cell death protein 1; PDGF: Platelet-Derived Growth Factor; PD-L1: Programmed cell death 1 ligand 1; PI3K: Phosphatidylinositol 3-kinase; PGF: Placenta-derived Growth Factor; PMN: polymorphonuclear; PSC: Pancreatic stellate cells; ROS: Reactive oxygen species; sEV: small extracellular vesicle; SFRP4: secreted frizzled-related protein 4; Shh: Sonic hedgehog; SMO: Single transducing component smoothened; STAT: Signal transducer and activator of transcription protein; STS: Short-term survivor; TGF-β: Transforming Growth Factor-beta; TAM: Tumor-associated macrophages; TEC: Tumor associated Endothelial Cells, TIM-3: T cell immunoglobulin domain and mucin domain-3; TME: Tumor microenvironment; TNF-α: Tumor Necrosis Factor-alpha; Treg: Regulatory T cells; VCAM: Vascular Cell Adhesion Molecule; VEGF: Vascular Endothelial Growth Factor, VEGF-R: Vascular Endothelial Growth Factor-Receptor.

References

1. Siegel, R.L.; Miller, K.D.; Fuchs, H.E.; Jemal, A. Cancer Statistics, 2021. *CA Cancer J. Clin.* **2021**, *71*, 7–33. [CrossRef]
2. Neesse, A.; Bauer, C.A.; Öhlund, D.; Lauth, M.; Buchholz, M.; Michl, P.; Tuveson, D.A.; Gress, T. Stromal biology and therapy in pancreatic cancer: Ready for clinical translation? *Gut* **2019**, *68*, 159–171. [CrossRef] [PubMed]
3. Michl, P.; Gress, T. Current concepts and novel targets in advanced pancreatic cancer. *Gut* **2013**, *62*, 317–326. [CrossRef] [PubMed]
4. Basturk, O.; Hong, S.-M.; Wood, L.D.; Adsay, V.; Albores-Saavedra, J.; Biankin, A.; Brosens, L.A.; Fukushima, N.; Goggins, M.; Hruban, R.H.; et al. A Revised Classification System and Recommendations From the Baltimore Consensus Meeting for Neoplastic Precursor Lesions in the Pancreas. *Am. J. Surg. Pathol.* **2015**, *39*, 1730–1741. [CrossRef]
5. Tuveson, D.A.; Neoptolemos, J.P. Understanding Metastasis in Pancreatic Cancer: A Call for New Clinical Approaches. *Cell* **2012**, *148*, 21–23. [CrossRef]
6. Neuzillet, C.; Tijeras-Raballand, A.; Bourget, P.; Cros, J.; Couvelard, A.; Sauvanet, A.; Vullierme, M.-P.; Tournigand, C.; Hammel, P. State of the art and future directions of pancreatic ductal adenocarcinoma therapy. *Pharmacol. Ther.* **2015**, *155*, 80–104. [CrossRef]
7. Kanda, M.; Matthaei, H.; Vogelstein, B.; Goggins, M.; Wu, J.; Hong, S.M.; Yu, J.; Borges, M.; Hruban, R.H.; Maitra, A.; et al. Presence of Somatic Mutations in Most Early-Stage Pancreatic Intraepithelial Neoplasia. *Gastroenterology* **2012**, *142*, 730–733.e9. [CrossRef] [PubMed]
8. Hruban, R.H.; Goggins, M.; Parsons, J.; Kern, S.E. Progression model for pancreatic cancer. *Clin. Cancer Res.* **2000**, *6*, 2969–2972.
9. Hessmann, E.; Buchholz, S.M.; Demir, I.E.; Singh, S.K.; Gress, T.M.; Ellenrieder, V.; Neesse, A. Microenvironmental Determinants of Pancreatic Cancer. *Physiol. Rev.* **2020**, *100*, 1707–1751. [CrossRef] [PubMed]
10. Neesse, A.; Algül, H.; Tuveson, D.A.; Gress, T. Stromal biology and therapy in pancreatic cancer: A changing paradigm. *Gut* **2015**, *64*, 1476–1484. [CrossRef]
11. Zhang, W.; Zhang, K.; Zhang, P.; Zheng, J.; Min, C.; Li, X. Research Progress of Pancreas-Related Microorganisms and Pancreatic Cancer. *Front. Oncol.* **2021**, *10*, 1–12. [CrossRef]
12. Murphy, K.; Chambers, C.; Herrmann, D.; Timpson, P.; Pereira, B. Dynamic Stromal Alterations Influence Tumor-Stroma Crosstalk to Promote Pancreatic Cancer and Treatment Resistance. *Cancers* **2021**, *13*, 3481. [CrossRef] [PubMed]

13. Indini, A.; Rijavec, E.; Ghidini, M.; Cortellini, A.; Grossi, F. Targeting KRAS in Solid Tumors: Current Challenges and Future Opportunities of Novel KRAS Inhibitors. *Pharmaceutics* **2021**, *13*, 653. [CrossRef]
14. Verma, H.K.; Kampalli, P.K.; Lakkakula, S.; Chalikonda, G.; Bhaskar, L.V.; Pattnaik, S. A Retrospective Look at Anti-EGFR Agents in Pancreatic Cancer Therapy. *Curr. Drug Metab.* **2020**, *20*, 958–966. [CrossRef]
15. Buchholz, S.M.; Goetze, R.G.; Singh, S.K.; Ammer-Herrmenau, C.; Richards, F.M.; Jodrell, D.I.; Buchholz, M.; Michl, P.; Ellenrieder, V.; Hessmann, E.; et al. Depletion of Macrophages Improves Therapeutic Response to Gemcitabine in Murine Pancreas Cancer. *Cancers* **2020**, *12*, 1978. [CrossRef]
16. Patzak, M.S.; Kari, V.; Patil, S.; Hamdan, F.; Goetze, R.G.; Brunner, M.; Gaedcke, J.; Kitz, J.; Jodrell, D.I.; Richards, F.M.; et al. Cytosolic 5′-nucleotidase 1A is overexpressed in pancreatic cancer and mediates gemcitabine resistance by reducing intracellular gemcitabine metabolites. *EBioMedicine* **2019**, *40*, 394–405. [CrossRef]
17. Müerköster, S.S.; Werbing, V.; Koch, D.; Sipos, B.; Ammerpohl, O.; Kalthoff, H.; Tsao, M.-S.; Fölsch, U.R.; Schäfer, H. Role of myofibroblasts in innate chemoresistance of pancreatic carcinoma-Epigenetic downregulation of caspases. *Int. J. Cancer* **2008**, *123*, 1751–1760. [CrossRef] [PubMed]
18. Müerköster, S.; Wegehenkel, K.; Arlt, A.; Witt, M.; Sipos, B.; Kruse, M.-L.; Sebens, T.; Klöppel, G.; Kalthoff, H.; Fölsch, U.R.; et al. Tumor Stroma Interactions Induce Chemoresistance in Pancreatic Ductal Carcinoma Cells Involving Increased Secretion and Paracrine Effects of Nitric Oxide and Interleukin-1β. *Cancer Res.* **2004**, *64*, 1331–1337. [CrossRef] [PubMed]
19. Geller, L.T.; Barzily-Rokni, M.; Danino, T.; Jonas, O.H.; Shental, N.; Nejman, D.; Gavert, N.; Zwang, Y.; Cooper, Z.A.; Shee, K.; et al. Potential role of intratumor bacteria in mediating tumor resistance to the chemotherapeutic drug gemcitabine. *Science* **2017**, *357*, 1156–1160. [CrossRef] [PubMed]
20. Riquelme, E.; Zhang, Y.; Zhang, L.; Montiel, M.; Zoltan, M.; Dong, W.; Quesada, P.; Sahin, I.; Chandra, V.; Lucas, A.S.; et al. Tumor Microbiome Diversity and Composition Influence Pancreatic Cancer Outcomes. *Cell* **2019**, *178*, 795–806.e12. [CrossRef]
21. Brahmer, J.R.; Tykodi, S.S.; Chow, L.Q.M.; Hwu, W.-J.; Topalian, S.L.; Hwu, P.; Drake, C.G.; Camacho, L.H.; Kauh, J.; Odunsi, K.; et al. Safety and Activity of Anti–PD-L1 Antibody in Patients with Advanced Cancer. *New Engl. J. Med.* **2012**, *366*, 2455–2465. [CrossRef]
22. Royal, R.E.; Levy, C.; Turner, K.; Mathur, A.; Hughes, M.; Kammula, U.S.; Sherry, R.M.; Topalian, S.L.; Yang, J.C.; Lowy, I.; et al. Phase 2 Trial of Single Agent Ipilimumab (Anti-CTLA-4) for Locally Advanced or Metastatic Pancreatic Adenocarcinoma. *J. Immunother.* **2010**, *33*, 828–833. [CrossRef]
23. Patnaik, A.; Kang, S.P.; Rasco, D.; Papadopoulos, K.P.; Elassaiss-Schaap, J.; Beeram, M.; Drengler, R.; Chen, C.; Smith, L.; Espino, G.; et al. Phase I Study of Pembrolizumab (MK-3475; Anti–PD-1 Monoclonal Antibody) in Patients with Advanced Solid Tumors. *Clin. Cancer Res.* **2015**, *21*, 4286–4293. [CrossRef]
24. Rahn, S.; Krüger, S.; Mennrich, R.; Goebel, L.; Wesch, D.; Oberg, H.-H.; Vogel, I.; Ebsen, M.; Röcken, C.; Helm, O.; et al. POLE Score: A comprehensive profiling of programmed death 1 ligand 1 expression in pancreatic ductal adenocarcinoma. *Oncotarget* **2019**, *10*, 1572–1588. [CrossRef]
25. Bonaventura, P.; Shekarian, T.; Alcazer, V.; Valladeau-Guilemond, J.; Valsesia-Wittmann, S.; Amigorena, S.; Caux, C.; Depil, S. Cold Tumors: A Therapeutic Challenge for Immunotherapy. *Front. Immunol.* **2019**, *10*, 168. [CrossRef] [PubMed]
26. De Guillebon, E.; Dardenne, A.; Saldmann, A.; Séguier, S.; Tran, T.; Paolini, L.; Lebbe, C.; Tartour, E. Beyond the concept of cold and hot tumors for the development of novel predictive biomarkers and the rational design of immunotherapy combination. *Int. J. Cancer* **2020**, *147*, 1509–1518. [CrossRef] [PubMed]
27. Grzywa, T.M.; Paskal, W.; Włodarski, P.K. Intratumor and Intertumor Heterogeneity in Melanoma. *Transl. Oncol.* **2017**, *10*, 956–975. [CrossRef]
28. Collisson, E.A.; Sadanandam, A.; Olson, P.; Gibb, W.J.; Truitt, M.; Gu, S.; Cooc, J.; Weinkle, J.; Kim, G.E.; Jakkula, L.; et al. Subtypes of pancreatic ductal adenocarcinoma and their differing responses to therapy. *Nat. Med.* **2011**, *17*, 500–503. [CrossRef] [PubMed]
29. Moffitt, R.A.; Marayati, R.; Flate, E.L.; Volmar, K.E.; Loeza, S.G.H.; Hoadley, K.A.; Rashid, N.U.; Williams, L.A.; Eaton, S.C.; Chung, A.H.; et al. Virtual microdissection identifies distinct tumor- and stroma-specific subtypes of pancreatic ductal adenocarcinoma. *Nat. Genet.* **2015**, *47*, 1168–1178. [CrossRef]
30. Bailey, P.; Chang, D.K.; Nones, K.; Johns, A.L.; Patch, A.-M.; Gingras, M.-C.; Miller, D.K.; Christ, A.N.; Bruxner, T.J.C.; Quinn, M.C.; et al. Genomic analyses identify molecular subtypes of pancreatic cancer. *Nature* **2016**, *531*, 47–52. [CrossRef]
31. Birnbaum, D.J.; Finetti, P.; Birnbaum, D.; Mamessier, E.; Bertucci, F. Validation and comparison of the molecular classifications of pancreatic carcinomas. *Mol. Cancer* **2017**, *16*, 168. [CrossRef] [PubMed]
32. Rashid, N.U.; Peng, X.L.; Jin, C.; Moffitt, R.A.; Volmar, K.E.; Belt, B.A.; Panni, R.Z.; Nywening, T.M.; Herrera, S.G.; Moore, K.J.; et al. Purity Independent Subtyping of Tumors (PurIST), A Clinically Robust, Single-sample Classifier for Tumor Subtyping in Pancreatic Cancer. *Clin. Cancer Res.* **2019**, *26*, 82–92. [CrossRef]
33. Fulawka, L.; Donizy, P.; Halon, A. Cancer stem cells—The current status of an old concept: Literature review and clinical approaches. *Biol. Res.* **2014**, *47*, 66. [CrossRef]
34. Oskarsson, T.; Batlle, E.; Massagué, J. Metastatic Stem Cells: Sources, Niches, and Vital Pathways. *Cell Stem Cell* **2014**, *14*, 306–321. [CrossRef]
35. Hass, R.; Von Der Ohe, J.; Ungefroren, H. Impact of the Tumor Microenvironment on Tumor Heterogeneity and Consequences for Cancer Cell Plasticity and Stemness. *Cancers* **2020**, *12*, 3716. [CrossRef] [PubMed]

36. Hernández-Camarero, P.; López-Ruiz, E.; Marchal, J.A.; Perán, M. Cancer: A mirrored room between tumor bulk and tumor microenvironment. *J. Exp. Clin. Cancer Res.* **2021**, *40*, 217. [CrossRef]
37. Zhan, H.-X.; Xu, J.-W.; Wu, D.; Zhang, T.-P.; Hu, S.-Y. Pancreatic cancer stem cells: New insight into a stubborn disease. *Cancer Lett.* **2015**, *357*, 429–437. [CrossRef] [PubMed]
38. Hermann, P.C.; Sainz, B. Pancreatic cancer stem cells: A state or an entity? *Semin. Cancer Biol.* **2018**, *53*, 223–231. [CrossRef]
39. Arina, A.; Idel, C.; Hyjek, E.M.; Alegre, M.-L.; Wang, Y.; Bindokas, V.P.; Weichselbaum, R.R.; Schreiber, H. Tumor-associated fibroblasts predominantly come from local and not circulating precursors. *Proc. Natl. Acad. Sci. USA* **2016**, *113*, 7551. [CrossRef]
40. Apte, M.V.; Haber, P.S.; Darby, S.J.; Rodgers, S.C.; Mccaughan, G.W.; Korsten, M.A.; Pirola, R.C.; Wilson, J.S. Pancreatic stellate cells are activated by proinflammatory cytokines: Implications for pancreatic fibrogenesis. *Gut* **1999**, *44*, 534–541. [CrossRef]
41. Bochet, L.; Lehuédé, C.; Dauvillier, S.; Wang, Y.Y.; Dirat, B.; Laurent, V.; Dray, C.; Guiet, R.; Maridonneau-Parini, I.; Le Gonidec, S.; et al. Adipocyte-derived fibroblasts promote tumor progression and contribute to the desmoplastic reaction in breast cancer. *Cancer Res.* **2013**, *73*, 5657–5668. [CrossRef] [PubMed]
42. Kidd, S.; Spaeth, E.; Watson, K.; Burks, J.; Lu, H.; Klopp, A.; Andreeff, M.; Marini, F.C. Origins of the Tumor Microenvironment: Quantitative Assessment of Adipose-Derived and Bone Marrow–Derived Stroma. *PLoS ONE* **2012**, *7*, e30563. [CrossRef]
43. Zeisberg, E.M.; Potenta, S.; Xie, L.; Zeisberg, M.; Kalluri, R. Discovery of Endothelial to Mesenchymal Transition as a Source for Carcinoma-Associated Fibroblasts. *Cancer Res.* **2007**, *67*, 10123–10128. [CrossRef] [PubMed]
44. Mederacke, I.; Hsu, C.C.; Troeger, J.S.; Huebener, P.; Mu, X.; Dapito, D.H.; Pradère, J.-P.; Schwabe, R.F. Fate tracing reveals hepatic stellate cells as dominant contributors to liver fibrosis independent of its aetiology. *Nat. Commun.* **2013**, *4*, 2823. [CrossRef]
45. Puche, J.E.; Lee, Y.A.; Jiao, J.; Aloman, C.; Fiel, M.I.; Muñoz, U.; Kraus, T.; Lee, T.; Yee, H.F.; Friedman, S.L. A novel murine model to deplete hepatic stellate cells uncovers their role in amplifying liver damage in mice. *Hepatology* **2013**, *57*, 339–350. [CrossRef]
46. Bhattacharya, S.D.; Mi, Z.; Talbot, L.J.; Guo, H.; Kuo, P.C. Human mesenchymal stem cell and epithelial hepatic carcinoma cell lines in admixture: Concurrent stimulation of cancer-associated fibroblasts and epithelial-to-mesenchymal transition markers. *Surgery* **2012**, *152*, 449–454. [CrossRef]
47. Dufton, N.; Peghaire, C.R.; Osuna-Almagro, L.; Raimondi, C.; Kalna, V.; Chauhan, A.; Webb, G.; Yang, Y.; Birdsey, G.M.; Lalor, P.; et al. Dynamic regulation of canonical TGFβ signalling by endothelial transcription factor ERG protects from liver fibrogenesis. *Nat. Commun.* **2017**, *8*, 1–14. [CrossRef] [PubMed]
48. Ribera, J.; Pauta, M.; Melgar-Lesmes, P.; Córdoba, B.; Bosch, A.; Calvo, M.; Rodrigo-Torres, D.; Sancho-Bru, P.; Mira, A.; Jiménez, W.; et al. A small population of liver endothelial cells undergoes endothelial-to-mesenchymal transition in response to chronic liver injury. *Am. J. Physiol. Liver Physiol.* **2017**, *313*, G492–G504. [CrossRef]
49. Koyama, Y.; Wang, P.; Brenner, D.A.; Kisseleva, T. Stellate Cells, Por-tal Myofibroblasts, and Epithelial-to-Mesenchymal Transition. In *Stellate Cells in Health and Disease*; Chapter 6; Elsevier: Amsterdam, The Netherlands, 2015; pp. 87–106. ISBN 9780128005446.
50. Cassiman, D.; Libbrecht, L.; Desmet, V.; Denef, C.; Roskams, T. Hepatic stellate cell/myofibroblast subpopulations in fibrotic human and rat livers. *J. Hepatol.* **2002**, *36*, 200–209. [CrossRef]
51. Apte, M.; Haber, P.S.; Applegate, T.; Norton, I.D.; Mccaughan, G.; Korsten, M.A.; Pirola, R.C.; Wilson, J. Periacinar stellate shaped cells in rat pancreas: Identification, isolation, and culture. *Gut* **1998**, *43*, 128–133. [CrossRef]
52. Omary, M.B.; Lugea, A.; Lowe, A.W.; Pandol, S.J. The pancreatic stellate cell: A star on the rise in pancreatic diseases. *J. Clin. Investig.* **2007**, *117*, 50–59. [CrossRef] [PubMed]
53. Apte, M.V.; Wilson, J. Dangerous liaisons: Pancreatic stellate cells and pancreatic cancer cells. *J. Gastroenterol. Hepatol.* **2012**, *27*, 69–74. [CrossRef]
54. Frantz, C.; Stewart, K.M.; Weaver, V.M. The extracellular matrix at a glance. *J. Cell Sci.* **2010**, *123 Pt 24*, 4195–4200. [CrossRef] [PubMed]
55. Apte, M.V.; Yang, L.; Phillips, P.; Xu, Z.; Kaplan, W.; Cowley, M.; Pirola, R.C.; Wilson, J.S. Extracellular matrix composition significantly influences pancreatic stellate cell gene expression pattern: Role of transgelin in PSC function. *Am. J. Physiol. Liver Physiol.* **2013**, *305*, G408–G417. [CrossRef] [PubMed]
56. Garcia, P.E.; Scales, M.K.; Allen, B.L.; Di Magliano, M.P. Pancreatic Fibroblast Heterogeneity: From Development to Cancer. *Cells* **2020**, *9*, 2464. [CrossRef]
57. Buchholz, M.; Krebshilfe, F.T.G.P.C.N.O.T.D.; Braun, M.; Heidenblut, A.; Kestler, H.; Klöppel, G.; Schmiegel, W.; Hahn, S.; Lüttges, J.; Gress, T. Transcriptome analysis of microdissected pancreatic intraepithelial neoplastic lesions. *Oncogene* **2005**, *24*, 6626–6636. [CrossRef]
58. Apte, M.V.; Wilson, J.S. Stellate Cell Activation in Alcoholic Pancreatitis. *Pancreas* **2003**, *27*, 316–320. [CrossRef]
59. Marzoq, A.J.; Mustafa, S.A.; Heidrich, L.; Hoheisel, J.D.; Alhamdani, M.S.S. Impact of the secretome of activated pancreatic stellate cells on growth and differentiation of pancreatic tumour cells. *Sci. Rep.* **2019**, *9*, 1–16. [CrossRef]
60. Ryschich, E.; Khamidjanov, A.; Kerkadze, V.; Büchler, M.W.; Zöller, M.; Schmidt, J. Promotion of Tumor Cell Migration by Extracellular Matrix Proteins in Human Pancreatic Cancer. *Pancreas* **2009**, *38*, 804–810. [CrossRef]
61. Baron, M.; Veres, A.; Wolock, S.; Faust, A.L.; Gaujoux, R.; Vetere, A.; Ryu, J.H.; Wagner, B.K.; Shen-Orr, S.S.; Klein, A.M.; et al. A Single-Cell Transcriptomic Map of the Human and Mouse Pancreas Reveals Inter- and Intra-cell Population Structure. *Cell Syst.* **2016**, *3*, 346–360.e4. [CrossRef]
62. Whittle, M.C.; Hingorani, S.R. Fibroblasts in Pancreatic Ductal Adenocarcinoma: Biological Mechanisms and Therapeutic Targets. *Gastroenterology* **2019**, *156*, 2085–2096. [CrossRef]

63. Bolm, L.; Cigolla, S.; Wittel, U.A.; Hopt, U.T.; Keck, T.; Rades, D.; Bronsert, P.; Wellner, U.F. The Role of Fibroblasts in Pancreatic Cancer: Extracellular Matrix Versus Paracrine Factors. *Transl. Oncol.* **2017**, *10*, 578–588. [CrossRef]
64. Shao, Z.-M.; Nguyen, M.; Barsky, S.H. Human breast carcinoma desmoplasia is PDGF initiated. *Oncogene* **2000**, *19*, 4337–4345. [CrossRef]
65. Giannoni, E.; Bianchini, F.; Masieri, L.; Serni, S.; Torre, E.; Calorini, L.; Chiarugi, P. Reciprocal Activation of Prostate Cancer Cells and Cancer-Associated Fibroblasts Stimulates Epithelial-Mesenchymal Transition and Cancer Stemness. *Cancer Res.* **2010**, *70*, 6945–6956. [CrossRef] [PubMed]
66. Ronnov-Jessen, L.; Petersen, O.W. Induction of α-Smooth Muscle Actin by Trans-forming Growth Factor-B1 in Quiescent Human Breast Gland Fibroblasts. *Lab. Investig.* **1993**, *68*, 696–707. [PubMed]
67. Bachem, M.G.; Schünemann, M.; Ramadani, M.; Siech, M.; Beger, H.; Buck, A.; Zhou, S.; Schmid-Kotsas, A.; Adler, G. Pancreatic carcinoma cells induce fibrosis by stimulating proliferation and matrix synthesis of stellate cells. *Gastroenterology* **2005**, *128*, 907–921. [CrossRef]
68. Biffi, G.; Tuveson, D.A. Diversity and Biology of Cancer-Associated Fibroblasts. *Physiol. Rev.* **2021**, *101*, 147–176. [CrossRef]
69. Öhlund, D.; Handly-Santana, A.; Biffi, G.; Elyada, E.; Almeida, A.S.; Ponz-Sarvise, M.; Corbo, V.; Oni, T.E.; Hearn, S.A.; Lee, E.J.; et al. Distinct populations of inflammatory fibroblasts and myofibroblasts in pancreatic cancer. *J. Exp. Med.* **2017**, *214*, 579–596. [CrossRef] [PubMed]
70. Biffi, G.; Oni, T.E.; Spielman, B.; Hao, Y.; Elyada, E.; Park, Y.; Preall, J.; Tuveson, D.A. IL1-Induced JAK/STAT Signaling Is Antagonized by TGFβ to Shape CAF Heterogeneity in Pancreatic Ductal Adenocarcinoma. *Cancer Discov.* **2019**, *9*, 282–301. [CrossRef] [PubMed]
71. Hutton, C.; Heider, F.; Blanco-Gomez, A.; Banyard, A.; Kononov, A.; Zhang, X.; Karim, S.; Paulus-Hock, V.; Watt, D.; Steele, N.; et al. Single-cell analysis defines a pancreatic fibroblast lineage that supports anti-tumor immunity. *Cancer Cell* **2021**, *14*, 1535. [CrossRef]
72. Pickup, M.W.; Mouw, J.K.; Weaver, V.M. The extracellular matrix modulates the hallmarks of cancer. *EMBO Rep.* **2014**, *15*, 1243–1253. [CrossRef]
73. Neumann, C.C.; Von Hörschelmann, E.; Reutzel-Selke, A.; Seidel, E.; Sauer, I.; Pratschke, J.; Bahra, M.; Schmuck, R.B. Tumor–stromal cross-talk modulating the therapeutic response in pancreatic cancer. *Hepatobiliary Pancreat. Dis. Int.* **2018**, *17*, 461–472. [CrossRef]
74. Hartmann, N.; Giese, N.A.; Giese, T.; Poschke, I.; Offringa, R.; Werner, J.; Ryschich, E. Prevailing Role of Contact Guidance in Intrastromal T-cell Trapping in Human Pancreatic Cancer. *Clin. Cancer Res.* **2014**, *20*, 3422–3433. [CrossRef]
75. Tse, J.M.; Cheng, G.; Tyrrell, J.A.; Wilcox-Adelman, S.A.; Boucher, Y.; Jain, R.K.; Munn, L.L. Mechanical compression drives cancer cells toward invasive phenotype. *Proc. Natl. Acad. Sci.* **2012**, *109*, 911–916. [CrossRef]
76. Sanchez, M.E.F.; Barbier, S.; Whitehead, J.; Béalle, G.; Michel, A.; Latorre-Ossa, H.; Rey, C.; Fouassier, L.; Claperon, A.; Brullé, L.; et al. Mechanical induction of the tumorigenic β-catenin pathway by tumour growth pressure. *Nat. Cell Biol.* **2015**, *523*, 92–95. [CrossRef]
77. Martin, J.; Seano, G.; Jain, R.K. Normalizing Function of Tumor Vessels: Progress, Opportunities, and Challenges. *Annu. Rev. Physiol.* **2019**, *81*, 505–534. [CrossRef]
78. Jain, R.K. Normalizing Tumor Microenvironment to Treat Cancer: Bench to Bedside to Biomarkers. *J. Clin. Oncol.* **2013**, *31*, 2205–2218. [CrossRef] [PubMed]
79. Wilson, W.R.; Hay, M. Targeting hypoxia in cancer therapy. *Nat. Rev. Cancer* **2011**, *11*, 393–410. [CrossRef] [PubMed]
80. Carmeliet, P.; Dor, Y.; Herbert, J.-M.; Fukumura, D.; Brusselmans, K.; Dewerchin, M.; Neeman, M.; Bono, F.; Abramovitch, R.; Maxwell, P.; et al. Role of HIF-1α in hypoxia-mediated apoptosis, cell proliferation and tumour angiogenesis. *Nat. Cell Biol.* **1998**, *394*, 485–490. [CrossRef]
81. Thienpont, B.; Steinbacher, J.; Zhao, H.; D'Anna, F.; Kuchnio, A.; Ploumakis, A.; Ghesquière, B.; Van Dyck, L.; Boeckx, B.; Schoonjans, L.; et al. Tumour hypoxia causes DNA hypermethylation by reducing TET activity. *Nat. Cell Biol.* **2016**, *537*, 63–68. [CrossRef]
82. Schito, L.; Semenza, G.L. Hypoxia-Inducible Factors: Master Regulators of Cancer Progression. *Trends Cancer* **2016**, *2*, 758–770. [CrossRef]
83. Ke, X.; Chen, C.; Song, Y.; Cai, Q.; Li, J.; Tang, Y.; Han, X.; Qu, W.; Chen, A.; Wang, H.; et al. Hypoxia modifies the polarization of macrophages and their inflammatory microenvironment, and inhibits malignant behavior in cancer cells. *Oncol. Lett.* **2019**, *18*, 5871–5878. [CrossRef] [PubMed]
84. Noman, M.Z.; Desantis, G.; Janji, B.; Hasmim, M.; Karray, S.; Dessen, P.; Bronte, V.; Chouaib, S. PD-L1 is a novel direct target of HIF-1α, and its blockade under hypoxia enhanced MDSC-mediated T cell activation. *J. Exp. Med.* **2014**, *211*, 781–790. [CrossRef]
85. Jiang, X.; Wang, J.; Deng, X.; Xiong, F.; Ge, J.; Xiang, B.; Wu, X.; Ma, J.; Zhou, M.; Li, X.; et al. Role of the tumor microenvironment in PD-L1/PD-1-mediated tumor immune escape. *Mol. Cancer* **2019**, *18*, 1–17. [CrossRef]
86. Barsoum, I.B.; Smallwood, C.A.; Siemens, D.R.; Graham, C.H. A Mechanism of Hypoxia-Mediated Escape from Adaptive Immunity in Cancer Cells. *Cancer Res.* **2014**, *74*, 665–674. [CrossRef] [PubMed]
87. Engblom, C.; Pfirschke, C.; Pittet, C.E.C.P.M.J. The role of myeloid cells in cancer therapies. *Nat. Rev. Cancer* **2016**, *16*, 447–462. [CrossRef] [PubMed]

88. Ene–Obong, A.; Clear, A.J.; Watt, J.; Wang, J.; Fatah, R.; Riches, J.C.; Marshall, J.F.; Chin–Aleong, J.; Chelala, C.; Gribben, J.G.; et al. Activated Pancreatic Stellate Cells Sequester CD8+ T Cells to Reduce Their Infiltration of the Juxtatumoral Compartment of Pancreatic Ductal Adenocarcinoma. *Gastroenterology* **2013**, *145*, 1121–1132. [CrossRef]
89. Gorchs, L.; Moro, C.F.; Bankhead, P.; Kern, K.P.; Sadeak, I.; Meng, Q.; Rangelova, E.; Kaipe, H. Human Pancreatic Carcinoma-Associated Fibroblasts Promote Expression of Co-inhibitory Markers on CD4+ and CD8+ T-Cells. *Front. Immunol.* **2019**, *10*, 847. [CrossRef]
90. Feig, C.; Jones, J.O.; Kraman, M.; Wells, R.J.; Deonarine, A.; Chan, D.S.; Connell, C.M.; Roberts, E.W.; Zhao, Q.; Caballero, O.L.; et al. Targeting CXCL12 from FAP-expressing carcinoma-associated fibroblasts synergizes with anti-PD-L1 immunotherapy in pancreatic cancer. *Proc. Natl. Acad. Sci. USA* **2013**, *110*, 20212–20217. [CrossRef]
91. Lakins, M.A.; Ghorani, E.; Munir, H.; Martins, C.P.; Shields, J.D. Cancer-associated fibroblasts induce antigen-specific deletion of CD8 + T Cells to protect tumour cells. *Nat. Commun.* **2018**, *9*, 948. [CrossRef]
92. Yavuz, B.G.; Gunaydin, G.; Gedik, M.E.; Kosemehmetoglu, K.; Karakoc, D.; Ozgür, F.F.; Guc, D. Cancer associated fibroblasts sculpt tumour microenvironment by recruiting monocytes and inducing immunosuppressive PD-1+ TAMs. *Sci. Rep.* **2019**, *9*, 1–15. [CrossRef]
93. Yang, X.; Lin, Y.; Shi, Y.; Li, B.; Liu, W.; Ying-Hong, S.; Dang, Y.; Chu, Y.; Fan, J.; He, R. FAP Promotes Immunosuppression by Cancer-Associated Fibroblasts in the Tumor Microenvironment via STAT3–CCL2 Signaling. *Cancer Res.* **2016**, *76*, 4124–4135. [CrossRef] [PubMed]
94. Comito, G.; Giannoni, E.; Segura, C.P.; Barcellos-De-Souza, P.; Raspollini, M.R.; Baroni, G.; Lanciotti, M.; Serni, S.; Chiarugi, P. Cancer-associated fibroblasts and M2-polarized macrophages synergize during prostate carcinoma progression. *Oncogene* **2013**, *33*, 2423–2431. [CrossRef] [PubMed]
95. Mathew, E.; Brannon, A.L.; Del Vecchio, A.; Garcia, P.E.; Penny, M.K.; Kane, K.T.; Vinta, A.; Buckanovich, R.J.; di Magliano, M.P. Mesenchymal Stem Cells Promote Pancreatic Tumor Growth by Inducing Alternative Polarization of Macrophages. *Neoplasia* **2016**, *18*, 142–151. [CrossRef]
96. Zhang, A.; Qian, Y.; Ye, Z.; Chen, H.; Xie, H.; Zhou, L.; Shen, Y.; Zheng, S. Cancer-associated fibroblasts promote M2 polarization of macrophages in pancreatic ductal adenocarcinoma. *Cancer Med.* **2017**, *6*, 463–470. [CrossRef]
97. Mace, T.A.; Ameen, Z.; Collins, A.; Wojcik, S.; Mair, M.; Young, G.S.; Fuchs, J.R.; Eubank, T.D.; Frankel, W.L.; Bekaii-Saab, T.; et al. Pancreatic Cancer-Associated Stellate Cells Promote Differentiation of Myeloid-Derived Suppressor Cells in a STAT3-Dependent Manner. *Cancer Res.* **2013**, *73*, 3007–3018. [CrossRef]
98. Li, J.; Byrne, K.T.; Yan, F.; Yamazoe, T.; Chen, Z.; Baslan, T.; Richman, L.P.; Lin, J.H.; Sun, Y.H.; Rech, A.J.; et al. Tumor Cell-Intrinsic Factors Underlie Heterogeneity of Immune Cell Infiltration and Response to Immunotherapy. *Immunity* **2018**, *49*, 178–193.e7. [CrossRef]
99. Flint, T.R.; Janowitz, T.; Connell, C.M.; Roberts, E.; Denton, A.; Coll, A.P.; Jodrell, D.I.; Fearon, D.T. Tumor-Induced IL-6 Reprograms Host Metabolism to Suppress Anti-tumor Immunity. *Cell Metab.* **2016**, *24*, 672–684. [CrossRef]
100. Elyada, E.; Bolisetty, M.; Laise, P.; Flynn, W.F.; Courtois, E.T.; Burkhart, R.A.; Teinor, J.A.; Belleau, P.; Biffi, G.; Lucito, M.S.; et al. Cross-Species Single-Cell Analysis of Pancreatic Ductal Adenocarcinoma Reveals Antigen-Presenting Cancer-Associated Fibroblasts. *Cancer Discov.* **2019**, *9*, 1102–1123. [CrossRef] [PubMed]
101. Friedman, G.; Levi-Galibov, O.; David, E.; Bornstein, C.; Giladi, A.; Dadiani, M.; Mayo, A.; Halperin, C.; Pevsner-Fischer, M.; Lavon, H.; et al. Cancer-Associated Fibro-blast Compositions Change with Breast-Cancer Progression Linking S100A4 and PDPN Ratios with Clinical Outcome. *bioRxiv* **2020**. [CrossRef]
102. Orimo, A.; Weinberg, R.A. Stromal Fibroblasts in Cancer: A Novel Tumor-Promoting Cell Type. *Cell Cycle* **2006**, *5*, 1597–1601. [CrossRef]
103. Schäfer, H.; Geismann, C.; Heneweer, C.; Egberts, J.-H.; Korniienko, O.; Kiefel, H.; Moldenhauer, G.; Bachem, M.G.; Kalthoff, H.; Altevogt, P.; et al. Myofibroblast-induced tumorigenicity of pancreatic ductal epithelial cells is L1CAM dependent. *Carcinogenesis* **2011**, *33*, 84–93. [CrossRef] [PubMed]
104. Geismann, C.; Morscheck, M.; Koch, D.; Bergmann, F.; Ungefroren, H.; Arlt, A.; Tsao, M.; Bachem, M.G.; Altevogt, P.; Sipos, B.; et al. Up-regulation of L1CAM in Pancreatic Duct Cells Is Transforming Growth Factor β1– and Slug-Dependent: Role in Malignant Transformation of Pancreatic Cancer. *Cancer Res.* **2009**, *69*, 4517–4526. [CrossRef] [PubMed]
105. Costa-Silva, B.; Aiello, N.M.; Ocean, A.J.; Singh, S.; Zhang, H.; Thakur, B.K.; Becker, A.; Hoshino, A.; Mark, M.T.; Molina, H.; et al. Pancreatic cancer exosomes initiate pre-metastatic niche formation in the liver. *Nat. Cell Biol.* **2015**, *17*, 816–826. [CrossRef]
106. Lenk, L.; Pein, M.; Will, O.; Gomez, B.; Viol, F.; Hauser, C.; Egberts, J.-H.; Gundlach, J.-P.; Helm, O.; Tiwari, S.; et al. The hepatic microenvironment essentially determines tumor cell dormancy and metastatic outgrowth of pancreatic ductal adenocarcinoma. *OncoImmunology* **2017**, *7*, e1368603. [CrossRef] [PubMed]
107. Miarka, L.; Hauser, C.; Helm, O.; Holdhof, D.; Beckinger, S.; Egberts, J.-H.; Gundlach, J.-P.; Lenk, L.; Rahn, S.; Mikulits, W.; et al. The Hepatic Microenvironment and TRAIL-R2 Impact Outgrowth of Liver Metastases in Pancreatic Cancer after Surgical Resection. *Cancers* **2019**, *11*, 745. [CrossRef] [PubMed]
108. Häberle, L.; Steiger, K.; Schlitter, A.M.; Safi, S.A.; Knoefel, W.T.; Erkan, M.; Esposito, I. Stromal heterogeneity in pancreatic cancer and chronic pancreatitis. *Pancreatology* **2018**, *18*, 536–549. [CrossRef]
109. Ding, C.; Li, Y.; Guo, F.; Jiang, Y.; Ying, W.; Li, D.; Yang, D.; Xia, X.; Liu, W.; Zhao, Y.; et al. A Cell-type-resolved Liver Proteome. *Mol. Cell. Proteom.* **2016**, *15*, 3190–3202. [CrossRef]

110. Libbrecht, L.; Cassiman, D.; Desmet, V.; Roskams, T. The correlation between portal myofibroblasts and development of intrahepatic bile ducts and arterial branches in human liver. *Liver Int.* **2002**, *22*, 252–258. [CrossRef] [PubMed]
111. Passino, M.A.; Adams, R.A.; Sikorski, S.L.; Akassoglou, K. Regulation of Hepatic Stellate Cell Differentiation by the Neurotrophin Receptor p75NTR. *Science* **2007**, *315*, 1853–1856. [CrossRef]
112. Schirmacher, P.; Geerts, A.; Pietrangelo, A.; Dienes, H.P.; Rogler, C.E. Hepatocyte growth factor/hepatopoietin A is expressed in fat-storing cells from rat liver but not myofibroblast-like cells derived from fat-storing cells. *Hepatology* **1992**, *15*, 5–11. [CrossRef]
113. Kitto, L.J.; Henderson, N.C. Hepatic Stellate Cell Regulation of Liver Regeneration and Repair. *Hepatol. Commun.* **2021**, *5*, 358–370. [CrossRef] [PubMed]
114. Hendriks, H.F.J.; Blaner, W.S.; Wennekers, H.M.; Piantedosi, R.; Brouwer, A.; Leeuw, A.M.; Goodman, D.S.; Knook, D.L. Distributions of retinoids, retinoid-binding proteins and related parameters in different types of liver cells isolated from young and old rats. *JBIC J. Biol. Inorg. Chem.* **1988**, *171*, 237–244. [CrossRef]
115. Haaker, M.W.; Vaandrager, A.B.; Helms, J.B. Retinoids in health and disease: A role for hepatic stellate cells in affecting retinoid levels. *Biochim. Biophys. Acta BBA Mol. Cell Biol. Lipids* **2020**, *1865*, 158674. [CrossRef]
116. Bigorgne, A.E.; John, B.; Ebrahimkhani, M.R.; Shimizu-Albergine, M.; Campbell, J.S.; Crispe, I.N. TLR4-Dependent Secretion by Hepatic Stellate Cells of the Neutrophil-Chemoattractant CXCL1 Mediates Liver Response to Gut Microbiota. *PLoS ONE* **2016**, *11*, e0151063. [CrossRef]
117. Viñas, O. Human hepatic stellate cells show features of antigen-presenting cells and stimulate lymphocyte proliferation. *Hepatology* **2003**, *38*, 919–929. [CrossRef]
118. Mehrfeld, C.; Zenner, S.; Kornek, M.; Lukacs-Kornek, V. The Contribution of Non-Professional Antigen-Presenting Cells to Immunity and Tolerance in the Liver. *Front. Immunol.* **2018**, *9*, 635. [CrossRef]
119. Kobayashi, S.; Seki, S.; Kawada, N.; Morikawa, H.; Nakatani, K.; Uyama, N.; Ikeda, K.; Nakajima, Y.; Arakawa, T.; Kaneda, K. Apoptosis of T cells in the hepatic fibrotic tissue of the rat: A possible inducing role of hepatic myofibroblast-like cells. *Cell Tissue Res.* **2003**, *311*, 353–364. [CrossRef] [PubMed]
120. Yu, M.-C.; Chen, C.-H.; Liang, X.; Wang, L.; Gandhi, C.R.; Fung, J.J.; Lu, L.; Qian, S. Inhibition of T-cell responses by hepatic stellate cells via B7-H1-mediated T-cell apoptosis in mice. *Hepatology* **2004**, *40*, 1312–1321. [CrossRef] [PubMed]
121. Seubert, B.; Grünwald, B.; Kobuch, J.; Cui, H.; Schelter, F.; Schaten, S.; Siveke, J.T.; Lim, N.H.; Nagase, H.; Simonavicius, N.; et al. Tissue inhibitor of metalloproteinases (TIMP)-1 creates a premetastatic niche in the liver through SDF-1/CXCR4-dependent neutrophil recruitment in mice. *Hepatology* **2015**, *61*, 238–248. [CrossRef]
122. Grünwald, B.; Harant, V.; Schaten, S.; Frühschütz, M.; Spallek, R.; Höchst, B.; Stutzer, K.; Berchtold, S.; Erkan, M.; Prokopchuk, O.; et al. Pancreatic Premalignant Lesions Secrete Tissue Inhibitor of Metalloproteinases-1, Which Activates Hepatic Stellate Cells Via CD63 Signaling to Create a Premetastatic Niche in the Liver. *Gastroenterology* **2016**, *151*, 1011–1024.e7. [CrossRef] [PubMed]
123. Lee, J.; Stone, M.L.; Porrett, P.M.; Thomas, S.; Komar, C.A.; Li, J.; Delman, D.; Graham, K.; Gladney, W.L.; Hua, X.; et al. Hepatocytes direct the formation of a pro-metastatic niche in the liver. *Nat. Cell Biol.* **2019**, *567*, 249–252. [CrossRef] [PubMed]
124. Houg, D.S.; Bijlsma, M.F. The hepatic pre-metastatic niche in pancreatic ductal adenocarcinoma. *Mol. Cancer* **2018**, *17*, 95. [CrossRef] [PubMed]
125. Bhattacharjee, S.; Hamberger, F.; Ravichandra, A.; Miller, M.; Nair, A.; Affo, S.; Filliol, A.; Chin, L.; Savage, T.M.; Yin, D.; et al. Tumor restriction by type I collagen opposes tumor-promoting effects of cancer-associated fibroblasts. *J. Clin. Investig.* **2021**, *131*. [CrossRef]
126. Gorelik, L.; Flavell, R.A. Transforming growth factor-β in T-cell biology. *Nat. Rev. Immunol.* **2002**, *2*, 46–53. [CrossRef]
127. Sperb, N.; Tsesmelis, M.; Wirth, T. Crosstalk between Tumor and Stromal Cells in Pancreatic Ductal Adenocarcinoma. *Int. J. Mol. Sci.* **2020**, *21*, 5486. [CrossRef]
128. Liu, S.; Ren, J.; Dijke, P.T. Targeting TGFβ signal transduction for cancer therapy. *Signal Transduct. Target. Ther.* **2021**, *6*, 1–20. [CrossRef] [PubMed]
129. Melisi, D.; Garcia-Carbonero, R.; Macarulla, T.; Pezet, D.; Deplanque, G.; Fuchs, M.; Trojan, J.; Oettle, H.; Kozloff, M.; Cleverly, A.; et al. Galunisertib plus gemcitabine vs. gemcitabine for first-line treatment of patients with unresectable pancreatic cancer. *Br. J. Cancer* **2018**, *119*, 1208–1214. [CrossRef]
130. Melisi, D.; Oh, D.-Y.; Hollebecque, A.; Calvo, E.; Varghese, A.; Borazanci, E.; Macarulla, T.; Merz, V.; Zecchetto, C.; Zhao, Y.; et al. Safety and activity of the TGFβ receptor I kinase inhibitor galunisertib plus the anti-PD-L1 antibody durvalumab in metastatic pancreatic cancer. *J. Immunother. Cancer* **2021**, *9*, e002068. [CrossRef] [PubMed]
131. Özdemir, B.C.; Pentcheva-Hoang, T.; Carstens, J.L.; Zheng, X.; Wu, C.-C.; Simpson, T.R.; Laklai, H.; Sugimoto, H.; Kahlert, C.; Novitskiy, S.V.; et al. Depletion of Carcinoma-Associated Fibroblasts and Fibrosis Induces Immunosuppression and Accelerates Pancreas Cancer with Reduced Survival. *Cancer Cell* **2014**, *25*, 719–734. [CrossRef]
132. Bailey, J.M.; Swanson, B.J.; Hamada, T.; Eggers, J.P.; Singh, P.K.; Caffery, T.; Ouellette, M.M.; Hollingsworth, M.A. Sonic Hedgehog Promotes Desmoplasia in Pancreatic Cancer. *Clin. Cancer Res.* **2008**, *14*, 5995–6004. [CrossRef] [PubMed]
133. Rhim, A.D.; Oberstein, P.E.; Thomas, D.H.; Mirek, E.T.; Palermo, C.F.; Sastra, S.A.; Dekleva, E.N.; Saunders, T.; Becerra, C.P.; Tattersall, I.; et al. Stromal Elements Act to Restrain, Rather Than Support, Pancreatic Ductal Adenocarcinoma. *Cancer Cell* **2014**, *25*, 735–747. [CrossRef]

134. Catenacci, D.V.T.; Junttila, M.R.; Karrison, T.; Bahary, N.; Horiba, M.N.; Nattam, S.R.; Marsh, R.; Wallace, J.; Kozloff, M.; Rajdev, L.; et al. Randomized Phase Ib/II Study of Gemcitabine Plus Placebo or Vismodegib, a Hedgehog Pathway Inhibitor, in Patients With Metastatic Pancreatic Cancer. *J. Clin. Oncol.* **2015**, *33*, 4284–4292. [CrossRef] [PubMed]
135. Ko, A.H.; LoConte, N.; Tempero, M.A.; Walker, E.J.; Kelley, R.K.; Lewis, S.; Chang, W.-C.; Kantoff, E.; Vannier, M.W.; Catenacci, D.V.; et al. A Phase I Study of FOLFIRINOX Plus IPI-926, a Hedgehog Pathway Inhibitor, for Advanced Pancreatic Adenocarcinoma. *Pancreas* **2016**, *45*, 370–375. [CrossRef]
136. Froeling, F.E.; Feig, C.; Chelala, C.; Dobson, R.; Mein, C.E.; Tuveson, D.; Clevers, H.; Hart, I.R.; Kocher, H.M. Retinoic Acid–Induced Pancreatic Stellate Cell Quiescence Reduces Paracrine Wnt–β-Catenin Signaling to Slow Tumor Progression. *Gastroenterology* **2011**, *141*, 1486–1497.e14. [CrossRef]
137. Sherman, M.H.; Yu, R.T.; Engle, D.D.; Ding, N.; Atkins, A.R.; Tiriac, H.; Collisson, E.A.; Connor, F.; Van Dyke, T.; Kozlov, S.; et al. Vitamin D Receptor-Mediated Stromal Reprogramming Suppresses Pancreatitis and Enhances Pancreatic Cancer Therapy. *Cell* **2014**, *159*, 80–93. [CrossRef]
138. Hurwitz, H.; Van Cutsem, E.; Bendell, J.; Hidalgo, M.; Li, C.-P.; Salvo, M.G.; Macarulla, T.; Sahai, V.; Sama, A.; Greeno, E.; et al. Ruxolitinib + capecitabine in advanced/metastatic pancreatic cancer after disease progression/intolerance to first-line therapy: JANUS 1 and 2 randomized phase III studies. *Investig. New Drugs* **2018**, *36*, 683–695. [CrossRef]
139. Belgiovine, C.; Digifico, E.; Anfray, C.; Ummarino, A.; Andón, F.T. Targeting Tumor-Associated Macrophages in Anti-Cancer Therapies: Convincing the Traitors to Do the Right Thing. *J. Clin. Med.* **2020**, *9*, 3226. [CrossRef]
140. Helm, O.; Mennrich, R.; Petrick, D.; Goebel, L.; Freitag-Wolf, S.; Röder, C.; Kalthoff, H.; Röcken, C.; Sipos, B.; Kabelitz, D.; et al. Comparative Characterization of Stroma Cells and Ductal Epithelium in Chronic Pancreatitis and Pancreatic Ductal Adenocarcinoma. *PLoS ONE* **2014**, *9*, e94357. [CrossRef]
141. Tjomsland, V.; Sandström, P.; Spångeus, A.; Messmer, D.; Emilsson, J.; Falkmer, U.; Falkmer, S.; Magnusson, K.-E.; Borch, K.; Larsson, M. Pancreatic adenocarcinoma exerts systemic effects on the peripheral blood myeloid and plasmacytoid dendritic cells: An indicator of disease severity? *BMC Cancer* **2010**, *10*, 87. [CrossRef] [PubMed]
142. Dallal, R.M.; Christakos, P.; Lee, K.; Egawa, S.; Son, Y.-I.; Lotze, M.T. Paucity of dendritic cells in pancreatic cancer. *Surgery* **2002**, *131*, 135–138. [CrossRef]
143. Hegde, S.; Krisnawan, V.; Herzog, B.H.; Zuo, C.; Breden, M.A.; Knolhoff, B.L.; Hogg, G.D.; Tang, J.P.; Baer, J.M.; Mpoy, C.; et al. Dendritic Cell Paucity Leads to Dysfunctional Immune Surveillance in Pancreatic Cancer. *Cancer Cell* **2020**, *37*, 289–307.e9. [CrossRef]
144. Murphy, T.L.; Murphy, K.M. Dendritic cells in cancer immunology. *Cell. Mol. Immunol.* **2021**, 1–11. [CrossRef]
145. Bronte, V.; Brandau, S.; Chen, S.-H.; Colombo, M.P.; Frey, A.B.; Greten, T.F.; Mandruzzato, S.; Murray, P.J.; Ochoa, A.; Ostrand-Rosenberg, S.; et al. Recommendations for myeloid-derived suppressor cell nomenclature and characterization standards. *Nat. Commun.* **2016**, *7*, 12150. [CrossRef]
146. Trovato, R.; Fiore, A.; Sartori, S.; Canè, S.; Giugno, R.; Cascione, L.; Paiella, S.; Salvia, R.; De Sanctis, F.; Poffe, O.; et al. Immunosuppression by monocytic myeloid-derived suppressor cells in patients with pancreatic ductal carcinoma is orchestrated by STAT3. *J. Immunother. Cancer* **2019**, *7*, 255. [CrossRef] [PubMed]
147. Choueiry, F.; Torok, M.; Shakya, R.; Agrawal, K.; Deems, A.; Benner, B.; Hinton, A.; Shaffer, J.; Blaser, B.W.; Noonan, A.M.; et al. CD200 promotes immunosuppression in the pancreatic tumor microenvironment. *J. Immunother. Cancer* **2020**, *8*, e000189. [CrossRef]
148. Siret, C.; Collignon, A.; Silvy, F.; Robert, S.; Cheyrol, T.; André, P.; Rigot, V.; Iovanna, J.; van de Pavert, S.; Lombardo, D.; et al. Deciphering the Crosstalk Between Myeloid-Derived Suppressor Cells and Regulatory T Cells in Pancreatic Ductal Adenocarcinoma. *Front. Immunol.* **2020**, *10*, 3070. [CrossRef]
149. Fujimura, T.; Mahnke, K.; Enk, A.H. Myeloid derived suppressor cells and their role in tolerance induction in cancer. *J. Dermatol. Sci.* **2010**, *59*, 1–6. [CrossRef]
150. Zhu, Y.; Herndon, J.M.; Sojka, D.K.; Kim, K.-W.; Knolhoff, B.L.; Zuo, C.; Cullinan, D.R.; Luo, J.; Bearden, A.R.; Lavine, K.J.; et al. Tissue-Resident Macrophages in Pancreatic Ductal Adenocarcinoma Originate from Embryonic Hematopoiesis and Promote Tumor Progression. *Immunity* **2017**, *47*, 323–338.e6. [CrossRef] [PubMed]
151. Lankadasari, M.B.; Mukhopadhyay, P.; Mohammed, S.; Harikumar, K.B. TAMing pancreatic cancer: Combat with a double edged sword. *Mol. Cancer* **2019**, *18*, 1–13. [CrossRef]
152. Mills, C.D. M1 and M2 Macrophages: Oracles of Health and Disease. *Crit. Rev. Immunol.* **2012**, *32*, 463–488. [CrossRef]
153. Mills, C.D.; Kincaid, K.; Alt, J.M.; Heilman, M.J.; Hill, A.M. M-1/M-2 Macrophages and the Th1/Th2 Paradigm. *J. Immunol.* **2000**, *164*, 6166–6173. [CrossRef]
154. Horwood, N.J. Macrophage Polarization and Bone Formation: A review. *Clin. Rev. Allergy Immunol.* **2016**, *51*, 79–86. [CrossRef] [PubMed]
155. Takahashi, H.; Sakakura, K.; Kudo, T.; Toyoda, M.; Kaira, K.; Oyama, T.; Chikamatsu, K. Cancer-associated fibroblasts promote an immunosuppressive microenvironment through the induction and accumulation of protumoral macrophages. *Oncotarget* **2016**, *8*, 8633–8647. [CrossRef] [PubMed]
156. Li, C.; Cui, L.; Yang, L.; Wang, B.; Zhuo, Y.; Zhang, L.; Wang, X.; Zhang, Q.; Zhang, S. Pancreatic Stellate Cells Promote Tumor Progression by Promoting an Immunosuppressive Microenvironment in Murine Models of Pancreatic Cancer. *Pancreas* **2020**, *49*, 120–127. [CrossRef] [PubMed]

157. Chang, Y.-T.; Peng, H.-Y.; Hu, C.-M.; Huang, S.-C.; Tien, S.-C.; Jeng, Y.-M. Pancre-atic Cancer-Derived Small Extracellular Vesical Ezrin Regulates Macrophage Polari-zation and Promotes Metastasis. *Am. J. Cancer Res.* **2020**, *10*, 12–37. [PubMed]
158. Nielsen, S.R.; Quaranta, V.; Linford, A.; Emeagi, P.; Rainer, C.; Santos, A.; Ireland, L.; Sakai, T.; Sakai, K.; Kim, Y.-S.; et al. Macrophage-secreted granulin supports pancreatic cancer metastasis by inducing liver fibrosis. *Nat. Cell Biol.* **2016**, *18*, 549–560. [CrossRef] [PubMed]
159. Yang, S.; Liu, Q.; Liao, Q. Tumor-Associated Macrophages in Pancreatic Ductal Adenocarcinoma: Origin, Polarization, Function, and Reprogramming. *Front. Cell Dev. Biol.* **2021**, *8*, 1–24. [CrossRef]
160. Mira, E.; Carmona-Rodríguez, L.; Tardáguila, M.; Azcoitia, I.; Gonzalez-Martin, A.; Almonacid, L.; Casas, J.; Fabrias, G.; Mañes, S. A lovastatin-elicited genetic program inhibits M2 macrophage polarization and enhances T cell infiltration into spontaneous mouse mammary tumors. *Oncotarget* **2013**, *4*, 2288–2301. [CrossRef]
161. Helm, O.; Held-Feindt, J.; Grage-Griebenow, E.; Reiling, N.; Ungefroren, H.; Vogel, I.; Krüger, U.; Becker, T.; Ebsen, M.; Röcken, C.; et al. Tumor-associated macrophages exhibit pro- and anti-inflammatory properties by which they impact on pancreatic tumorigenesis. *Int. J. Cancer* **2014**, *135*, 843–861. [CrossRef] [PubMed]
162. Hu, H.; Hang, J.-J.; Han, T.; Zhuo, M.; Jiao, F.; Wang, L.-W. The M2 phenotype of tumor-associated macrophages in the stroma confers a poor prognosis in pancreatic cancer. *Tumor Biol.* **2016**, *37*, 8657–8664. [CrossRef]
163. Knudsen, E.S.; Vail, P.; Balaji, U.; Ngo, H.; Botros, I.W.; Makarov, V.; Riaz, N.; Balachandran, V.; Leach, S.; Thompson, D.M.; et al. Stratification of Pancreatic Ductal Adenocarcinoma: Combinatorial Genetic, Stromal, and Immunologic Markers. *Clin. Cancer Res.* **2017**, *23*, 4429–4440. [CrossRef]
164. Kurahara, H.; Takao, S.; Maemura, K.; Mataki, Y.; Kuwahata, T.; Maeda, K.; Sakoda, M.; Iino, S.; Ishigami, S.; Ueno, S.; et al. M2-Polarized Tumor-Associated Macrophage Infiltration of Regional Lymph Nodes Is Associated With Nodal Lymphangiogenesis and Occult Nodal Involvement in pN0 Pancreatic Cancer. *Pancreas* **2013**, *42*, 155–159. [CrossRef]
165. Kurahara, H.; Shinchi, H.; Mataki, Y.; Maemura, K.; Noma, H.; Kubo, F.; Sakoda, M.; Ueno, S.; Natsugoe, S.; Takao, S. Significance of M2-Polarized Tumor-Associated Macrophage in Pancreatic Cancer. *J. Surg. Res.* **2011**, *167*, e211–e219. [CrossRef]
166. Bulle, A.; Lim, K.-H. Beyond just a tight fortress: Contribution of stroma to epithelial-mesenchymal transition in pancreatic cancer. *Signal Transduct. Target. Ther.* **2020**, *5*, 1–12. [CrossRef] [PubMed]
167. Kaneda, M.M.; Cappello, P.; Nguyen, A.V.; Ralainirina, N.; Hardamon, C.R.; Foubert, P.; Schmid, M.C.; Sun, P.; Mose, E.; Bouvet, M.; et al. Macrophage PI3Kγ Drives Pancreatic Ductal Adenocarcinoma Progression. *Cancer Discov.* **2016**, *6*, 870–885. [CrossRef] [PubMed]
168. Helm, O.; Held-Feindt, J.; Schäfer, H.; Sebens, S. M1 and M2: There is no "good" and "bad"—How macrophages promote malignancy-associated features in tumorigenesis. *OncoImmunology* **2014**, *3*, e946818. [CrossRef] [PubMed]
169. Chen, Q.; Wang, J.; Zhang, Q.; Zhang, J.; Lou, Y.; Yang, J.; Chen, Y.; Wei, T.; Zhang, J.; Fu, Q.; et al. Tumour cell-derived debris and IgG synergistically promote metastasis of pancreatic cancer by inducing inflammation via tumour-associated macrophages. *Br. J. Cancer* **2019**, *121*, 786–795. [CrossRef] [PubMed]
170. Halbrook, C.J.; Pontious, C.; Kovalenko, I.; Lapienyte, L.; Dreyer, S.; Lee, H.-J.; Thurston, G.; Zhang, Y.; Lazarus, J.; Sajjakulnukit, P.; et al. Macrophage-Released Pyrimidines Inhibit Gemcitabine Therapy in Pancreatic Cancer. *Cell Metab.* **2019**, *29*, 1390–1399.e6. [CrossRef] [PubMed]
171. Liu, Q.; Li, Y.; Niu, Z.; Zong, Y.; Wang, M.; Yao, L.; Lu, Z.; Liao, Q.; Zhao, Y. Atorvastatin (Lipitor) attenuates the effects of aspirin on pancreatic cancerogenesis and the chemotherapeutic efficacy of gemcitabine on pancreatic cancer by promoting M2 polarized tumor associated macrophages. *J. Exp. Clin. Cancer Res.* **2016**, *35*, 1–16. [CrossRef]
172. Weizman, N.; Krelin, Y.; Shabtayorbach, A.; Amit, M.; Binenbaum, Y.; Wong, R.J.; Gil, Z. Macrophages mediate gemcitabine resistance of pancreatic adenocarcinoma by upregulating cytidine deaminase. *Oncogene* **2013**, *33*, 3812–3819. [CrossRef] [PubMed]
173. Binenbaum, Y.; Fridman, E.; Yaari, Z.; Milman, N.; Schroeder, A.; Ben David, G.; Shlomi, T.; Gil, Z. Transfer of miRNA in Macrophage-Derived Exosomes Induces Drug Resistance in Pancreatic Adenocarcinoma. *Cancer Res.* **2018**, *78*, 5287–5299. [CrossRef] [PubMed]
174. Cheng, L.; Liu, J.; Liu, Q.; Liu, Y.; Fan, L.; Wang, F.; Yu, H.; Li, Y.; Bu, L.; Li, X.; et al. Exosomes from Melatonin Treated Hepatocellularcarcinoma Cells Alter the Immunosupression Status through STAT3 Pathway in Macrophages. *Int. J. Biol. Sci.* **2017**, *13*, 723–734. [CrossRef] [PubMed]
175. Deronic, A.; Nilsson, A.; Thagesson, M.; Werchau, D.; Smith, K.E.; Ellmark, P. The human anti-CD40 agonist antibody mitazalimab (ADC-1013; JNJ-64457107) activates antigen-presenting cells, improves expansion of antigen-specific T cells, and enhances anti-tumor efficacy of a model cancer vaccine in vivo. *Cancer Immunol. Immunother.* **2021**, 1–14. [CrossRef]
176. Vonderheide, R.H. CD40 Agonist Antibodies in Cancer Immunotherapy. *Annu. Rev. Med.* **2020**, *71*, 47–58. [CrossRef]
177. Beatty, G.; Chiorean, E.G.; Fishman, M.P.; Saboury, B.; Teitelbaum, U.R.; Sun, W.; Huhn, R.D.; Song, W.; Li, D.; Sharp, L.L.; et al. CD40 Agonists Alter Tumor Stroma and Show Efficacy Against Pancreatic Carcinoma in Mice and Humans. *Science* **2011**, *331*, 1612–1616. [CrossRef] [PubMed]
178. Byrne, K.T.; Betts, C.B.; Mick, R.; Sivagnanam, S.; Bajor, D.L.; Laheru, D.A.; Chiorean, E.G.; O'Hara, M.H.; Liudahl, S.M.; Newcomb, C.W.; et al. Neoadjuvant selicrelumab, an agonist CD40 antibody, induces changes in the tumor microenvironment in patients with resectable pancreatic cancer. *Clin. Cancer Res.* **2021**, *27*, 4574–4586. [CrossRef]
179. Morrison, A.H.; Diamond, M.S.; Hay, C.A.; Byrne, K.T.; Vonderheide, R.H. Sufficiency of CD40 activation and immune checkpoint blockade for T cell priming and tumor immunity. *Proc. Natl. Acad. Sci.* **2020**, *117*, 8022–8031. [CrossRef]

180. O'Hara, M.H.; O'Reilly, E.M.; Varadhachary, G.; Wolff, R.A.; Wainberg, Z.A.; Ko, A.H.; Fisher, G.; Rahma, O.; Lyman, J.P.; Cabanski, C.R.; et al. CD40 agonistic monoclonal antibody APX005M (sotigalimab) and chemotherapy, with or without nivolumab, for the treatment of metastatic pancreatic adenocarcinoma: An open-label, multicentre, phase 1b study. *Lancet Oncol.* **2021**, *22*, 118–131. [CrossRef]
181. O'Hara, M.H.; O'Reilly, E.M.; Wolff, R.A.; Wainberg, Z.A.; Ko, A.H.; Rahma, O.E.; Fisher, G.A.; Lyman, J.P.; Cabanski, C.R.; Karakunnel, J.J.; et al. Gemcitabine (Gem) and nab-paclitaxel (NP) ± nivolumab (nivo) ± CD40 agonistic monoclonal antibody APX005M (sotigalimab), in patients (Pts) with untreated metastatic pancreatic adenocarcinoma (mPDAC): Phase (Ph) 2 final results. *J. Clin. Oncol.* **2021**, *39*, 4019. [CrossRef]
182. Ho, T.T.B.; Nasti, A.; Seki, A.; Komura, T.; Inui, H.; Kozaka, T.; Kitamura, Y.; Shiba, K.; Yamashita, T.; Yamashita, T.; et al. Combination of gemcitabine and anti-PD-1 antibody enhances the anticancer effect of M1 macrophages and the Th1 response in a murine model of pancreatic cancer liver metastasis. *J. Immunother. Cancer* **2020**, *8*, e001367. [CrossRef]
183. Panni, R.Z.; Herndon, J.M.; Zuo, C.; Hegde, S.; Hogg, G.D.; Knolhoff, B.L.; Breden, M.A.; Li, X.; Krisnawan, V.E.; Khan, S.Q.; et al. Agonism of CD11b reprograms innate immunity to sensitize pancreatic cancer to immunotherapies. *Sci. Transl. Med.* **2019**, *11*, eaau9240. [CrossRef] [PubMed]
184. Pylayeva-Gupta, Y.; Das, S.; Handler, J.; Hajdu, C.H.; Coffre, M.; Koralov, S.; Bar-Sagi, D. IL35-Producing B Cells Promote the Development of Pancreatic Neoplasia. *Cancer Discov.* **2016**, *6*, 247–255. [CrossRef]
185. Minici, C.; Rigamonti, E.; Lanzillotta, M.; Monno, A.; Rovati, L.; Maehara, T.; Kaneko, N.; Deshpande, V.; Protti, M.P.; De Monte, L.; et al. B lymphocytes contribute to stromal reaction in pancreatic ductal adenocarcinoma. *OncoImmunology* **2020**, *9*, 1794359. [CrossRef] [PubMed]
186. Zheng, L.; Xue, J.; Jaffee, E.; Habtezion, A. Role of Immune Cells and Immune-Based Therapies in Pancreatitis and Pancreatic Ductal Adenocarcinoma. *Gastroenterology* **2013**, *144*, 1230–1240. [CrossRef]
187. Wörmann, S.M.; Diakopoulos, K.N.; Lesina, M.; Algül, H. The immune network in pancreatic cancer development and progression. *Oncogene* **2014**, *33*, 2956–2967. [CrossRef]
188. Ino, Y.; Yamazaki-Itoh, R.; Shimada, K.; Iwasaki, M.; Kosuge, T.; Kanai, Y.; Hiraoka, N. Immune cell infiltration as an indicator of the immune microenvironment of pancreatic cancer. *Br. J. Cancer* **2013**, *108*, 914–923. [CrossRef]
189. Fukunaga, A.; Miyamoto, M.; Cho, Y.; Murakami, S.; Kawarada, Y.; Oshikiri, T.; Kato, K.; Kurokawa, T.; Suzuoki, M.; Nakakubo, Y.; et al. CD8+ Tumor-Infiltrating Lymphocytes Together with CD4+ Tumor-Infiltrating Lymphocytes and Dendritic Cells Improve the Prognosis of Patients with Pancreatic Adenocarcinoma. *Pancreas* **2004**, *28*, e26–e31. [CrossRef]
190. Tewari, N.; Zaitoun, A.M.; Arora, A.; Madhusudan, S.; Ilyas, M.; Lobo, D.N. The presence of tumour-associated lymphocytes confers a good prognosis in pancreatic ductal adenocarcinoma: An immunohistochemical study of tissue microarrays. *BMC Cancer* **2013**, *13*, 436. [CrossRef]
191. Carstens, J.L.; de Sampaio, P.C.; Yang, D.; Barua, S.; Wang, H.; Rao, A.; Allison, J.; LeBleu, V.S.; Kalluri, R. Spatial computation of intratumoral T cells correlates with survival of patients with pancreatic cancer. *Nat. Commun.* **2017**, *8*, 15095. [CrossRef] [PubMed]
192. Hosein, A.N.; Brekken, R.A.; Maitra, A. Pancreatic cancer stroma: An update on therapeutic targeting strategies. *Nat. Rev. Gastroenterol. Hepatol.* **2020**, *17*, 487–505. [CrossRef]
193. Quaranta, V.; Rainer, C.; Nielsen, S.R.; Raymant, M.L.; Ahmed, M.S.; Engle, D.D.; Taylor, A.; Murray, T.; Campbell, F.; Palmer, D.H.; et al. Macrophage-Derived Granulin Drives Resistance to Immune Checkpoint Inhibition in Metastatic Pancreatic Cancer. *Cancer Res.* **2018**, *78*, 4253–4269. [CrossRef] [PubMed]
194. Saka, D.; Gökalp, M.; Piyade, B.; Cevik, N.C.; Sever, E.A.; Unutmaz, D.; Ceyhan, G.O.; Demir, I.E.; Asimgil, H. Mechanisms of T-Cell Exhaustion in Pancreatic Cancer. *Cancers* **2020**, *12*, 2274. [CrossRef]
195. Wherry, E.J.; Kurachi, M. Molecular and cellular insights into T cell exhaustion. *Nat. Rev. Immunol.* **2015**, *15*, 486–499. [CrossRef]
196. Russ, B.E.; Prier, J.; Rao, S.; Turner, S.J. T cell immunity as a tool for studying epigenetic regulation of cellular differentiation. *Front. Genet.* **2013**, *4*, 218. [CrossRef] [PubMed]
197. Huber, M.; Brehm, C.U.; Gress, T.M.; Buchholz, M.; Alhamwe, B.A.; Von Strandmann, E.P.; Slater, E.P.; Bartsch, J.W.; Bauer, C.; Lauth, M. The Immune Microenvironment in Pancreatic Cancer. *Int. J. Mol. Sci.* **2020**, *21*, 7307. [CrossRef] [PubMed]
198. Liao, W.; Lin, J.-X.; Leonard, W.J. Interleukin-2 at the Crossroads of Effector Responses, Tolerance, and Immunotherapy. *Immunity* **2013**, *38*, 13–25. [CrossRef]
199. Chen, S.; Crabill, G.A.; Pritchard, T.S.; McMiller, T.L.; Wei, P.; Pardoll, D.M.; Pan, F.; Topalian, S.L. Mechanisms regulating PD-L1 expression on tumor and immune cells. *J. Immunother. Cancer* **2019**, *7*, 1–12. [CrossRef]
200. De Monte, L.; Reni, M.; Tassi, E.; Clavenna, D.; Papa, I.; Recalde, H.; Braga, M.; Di Carlo, V.; Doglioni, C.; Protti, M.P. Intratumor T helper type 2 cell infiltrate correlates with cancer-associated fibroblast thymic stromal lymphopoietin production and reduced survival in pancreatic cancer. *J. Exp. Med.* **2011**, *208*, 469–478. [CrossRef]
201. Sica, A.; Schioppa, T.; Mantovani, A.; Allavena, P. Tumour-associated macrophages are a distinct M2 polarised population promoting tumour progression: Potential targets of anti-cancer therapy. *Eur. J. Cancer* **2006**, *42*, 717–727. [CrossRef]
202. Wynn, T.A. Fibrotic disease and the TH1/TH2 paradigm. *Nat. Rev. Immunol.* **2004**, *4*, 583–594. [CrossRef]
203. Formentini, A.; Prokopchuk, O.; Sträter, J.; Kleeff, J.; Grochola, L.F.; Leder, G.; Henne-Bruns, D.; Korc, M.; Kornmann, M. Interleukin-13 exerts autocrine growth-promoting effects on human pancreatic cancer, and its expression correlates with a propensity for lymph node metastases. *Int. J. Color. Dis.* **2008**, *24*, 57–67. [CrossRef] [PubMed]

204. Tassi, E.; Gavazzi, F.; Albarello, L.; Senyukov, V.; Longhi, R.; Dellabona, P.; Doglioni, C.; Braga, M.; Di Carlo, V.; Protti, M.P. Carcinoembryonic Antigen-Specific but Not Antiviral CD4+ T Cell Immunity Is Impaired in Pancreatic Carcinoma Patients. *J. Immunol.* **2008**, *181*, 6595–6603. [CrossRef]
205. Piro, G.; Simionato, F.; Carbone, C.; Frizziero, M.; Malleo, G.; Zanini, S.; Casolino, R.; Santoro, R.; Mina, M.M.; Zecchetto, C.; et al. A circulating TH2 cytokines profile predicts survival in patients with resectable pancreatic adenocarcinoma. *OncoImmunology* **2017**, *6*, e1322242. [CrossRef] [PubMed]
206. He, S.; Fei, M.; Wu, Y.; Zheng, D.; Wan, D.; Wang, L.; Li, D. Distribution and Clinical Significance of Th17 Cells in the Tumor Microenvironment and Peripheral Blood of Pancreatic Cancer Patients. *Int. J. Mol. Sci.* **2011**, *12*, 7424–7437. [CrossRef] [PubMed]
207. McAllister, F.; Bailey, J.M.; Alsina, J.; Nirschl, C.; Sharma, R.; Fan, H.; Rattigan, Y.; Roeser, J.C.; Lankapalli, R.H.; Zhang, H.; et al. Oncogenic Kras Activates a Hematopoietic-to-Epithelial IL-17 Signaling Axis in Preinvasive Pancreatic Neoplasia. *Cancer Cell* **2014**, *25*, 621–637. [CrossRef] [PubMed]
208. Hiraoka, N.; Onozato, K.; Kosuge, T.; Hirohashi, S. Prevalence of FOXP3+ Regulatory T Cells Increases During the Progression of Pancreatic Ductal Adenocarcinoma and Its Premalignant Lesions. *Clin. Cancer Res.* **2006**, *12*, 5423–5434. [CrossRef]
209. Tang, Y.; Xu, X.; Guo, S.; Zhang, C.; Tang, Y.; Tian, Y.; Ni, B.; Lu, B.; Wang, H. An Increased Abundance of Tumor-Infiltrating Regulatory T Cells Is Correlated with the Progression and Prognosis of Pancreatic Ductal Adenocarcinoma. *PLoS ONE* **2014**, *9*, e91551. [CrossRef]
210. Cinier, J.; Hubert, M.; Besson, L.; Di Roio, A.; Rodriguez, C.; Lombardi, V.; Caux, C.; Ménétrier-Caux, C. Recruitment and Expansion of Tregs Cells in the Tumor Environment—How to Target Them? *Cancers* **2021**, *13*, 1850. [CrossRef]
211. Lohr, J.; Knoechel, B.; Abbas, A.K. Regulatory T cells in the periphery. *Immunol. Rev.* **2006**, *212*, 149–162. [CrossRef]
212. Fu, S.; Zhang, N.; Yopp, A.C.; Chen, D.; Mao, M.; Chen, D.; Zhang, H.; Ding, Y.; Bromberg, J.S. TGF-beta Induces Foxp3 + T-Regulatory Cells from CD4 + CD25—Precursors. *Arab. Archaeol. Epigr.* **2004**, *4*, 1614–1627. [CrossRef] [PubMed]
213. Wang, X.; Lang, M.; Zhao, T.; Feng, X.; Zheng, C.; Huang, C.; Hao, J.; Dong, J.; Luo, L.; Li, X.; et al. Cancer-FOXP3 directly activated CCL5 to recruit FOXP3+Treg cells in pancreatic ductal adenocarcinoma. *Oncogene* **2017**, *36*, 3048–3058. [CrossRef] [PubMed]
214. Yang, M.-W.; Tao, L.-Y.; Yang, J.-Y.; Jiang, Y.-S.; Fu, X.-L.; Liu, W.; Huo, Y.-M.; Li, J.; Zhang, J.-F.; Hua, R.; et al. SFRP4 is a prognostic marker and correlated with Treg cell infiltration in pancreatic ductal adenocarcinoma. *Am. J. Cancer Res.* **2019**, *9*, 363–377. [PubMed]
215. Shen, T.; Jia, S.; Ding, G.; Ping, D.; Zhou, L.; Zhou, S.; Cao, L. BxPC-3-Derived Small Extracellular Vesicles Induce FOXP3+ Treg through ATM-AMPK-Sirtuins-Mediated FOXOs Nuclear Translocations. *iScience* **2020**, *23*, 101431. [CrossRef] [PubMed]
216. Grage-Griebenow, E.; Jerg, E.; Gorys, A.; Wicklein, D.; Wesch, D.; Freitag-Wolf, S.; Goebel, L.; Vogel, I.; Becker, T.; Ebsen, M.; et al. L1CAM promotes enrichment of immunosuppressive T cells in human pancreatic cancer correlating with malignant progression. *Mol. Oncol.* **2014**, *8*, 982–997. [CrossRef] [PubMed]
217. Jang, J.-E.; Hajdu, C.H.; Liot, C.; Miller, G.; Dustin, M.L.; Bar-Sagi, D. Crosstalk between Regulatory T Cells and Tumor-Associated Dendritic Cells Negates Anti-tumor Immunity in Pancreatic Cancer. *Cell Rep.* **2017**, *20*, 558–571. [CrossRef]
218. Chang, C.-H.; Pauklin, S. ROS and TGFβ: From pancreatic tumour growth to metastasis. *J. Exp. Clin. Cancer Res.* **2021**, *40*, 1–11. [CrossRef] [PubMed]
219. Himoudi, N.; Morgenstern, D.A.; Yan, M.; Vernay, B.; Saraiva, L.; Wu, Y.; Cohen, C.J.; Gustafsson, K.; Anderson, J. Human γδ T Lymphocytes Are Licensed for Professional Antigen Presentation by Interaction with Opsonized Target Cells. *J. Immunol.* **2012**, *188*, 1708–1716. [CrossRef]
220. Oberg, H.-H.; Peipp, M.; Kellner, C.; Sebens, S.; Krause, S.; Petrick, D.; Adam-Klages, S.; Röcken, C.; Becker, T.; Vogel, I.; et al. Novel Bispecific Antibodies Increase γδ T-Cell Cytotoxicity against Pancreatic Cancer Cells. *Cancer Res.* **2014**, *74*, 1349–1360. [CrossRef]
221. Viey, E.; Lucas, C.; Romagne, F.; Escudier, B.; Chouaib, S.; Caignard, A. Chemokine Receptors Expression and Migration Potential of Tumor-infiltrating and Peripheral-expanded Vγ9Vδ2 T Cells From Renal Cell Carcinoma Patients. *J. Immunother.* **2008**, *31*, 313–323. [CrossRef]
222. Matsuo, Y.; Ochi, N.; Sawai, H.; Yasuda, A.; Takahashi, H.; Funahashi, H.; Takeyama, H.; Tong, Z.; Guha, S. CXCL8/IL-8 and CXCL12/SDF-1α co-operatively promote invasiveness and angiogenesis in pancreatic cancer. *Int. J. Cancer* **2009**, *124*, 853–861. [CrossRef] [PubMed]
223. Gonnermann, D.; Oberg, H.-H.; Lettau, M.; Peipp, M.; Bauerschlag, D.; Sebens, S.; Kabelitz, D.; Wesch, D. Galectin-3 Released by Pancreatic Ductal Adenocarcinoma Suppresses γδ T Cell Proliferation but Not Their Cytotoxicity. *Front. Immunol.* **2020**, *11*, 1328. [CrossRef]
224. Song, S.; Ji, B.; Ramachandran, V.; Wang, H.; Hafley, M.; Logsdon, C.; Bresalier, R. Overexpressed Galectin-3 in Pancreatic Cancer Induces Cell Proliferation and Invasion by Binding Ras and Activating Ras Signaling. *PLoS ONE* **2012**, *7*, e42699. [CrossRef]
225. Jonescheit, H.; Oberg, H.-H.; Gonnermann, D.; Hermes, M.; Sulaj, V.; Peters, C.; Kabelitz, D.; Wesch, D. Influence of Indoleamine-2,3-Dioxygenase and Its Metabolite Kynurenine on γδ T Cell Cytotoxicity against Ductal Pancreatic Adenocarcinoma Cells. *Cells* **2020**, *9*, 1140. [CrossRef]
226. Daley, D.; Zambirinis, C.P.; Seifert, L.; Akkad, N.; Mohan, N.; Werba, G.; Barilla, R.; Torres-Hernandez, A.; Hundeyin, M.; Mani, V.R.; et al. γδ T Cells Support Pancreatic Oncogenesis by Restraining αβ T Cell Activation. *Cell* **2016**, *166*, 1485–1499.e15. [CrossRef]

227. Upadhrasta, S.; Zheng, L. Strategies in Developing Immunotherapy for Pancreatic Cancer: Recognizing and Correcting Multiple Immune "Defects" in the Tumor Microenvironment. *J. Clin. Med.* **2019**, *8*, 1472. [CrossRef]
228. Karamitopoulou, E. The Tumor Microenvironment of Pancreatic Cancer. *Cancers* **2020**, *12*, 3076. [CrossRef] [PubMed]
229. Hewitt, D.B.; Nissen, N.; Hatoum, H.; Musher, B.; Seng, J.; Coveler, A.L.; Al-Rajabi, R.; Yeo, C.J.; Leiby, B.; Banks, J.; et al. A Phase 3 Randomized Clinical Trial of Chemotherapy With or Without Algenpantucel-L (HyperAcute-Pancreas) Immunotherapy in Subjects with Borderline Resectable or Locally Advanced Unresectable Pancreatic Cancer. *Ann. Surg.* Publish Ah. **2020**. [CrossRef]
230. Middleton, G.; Silcocks, P.; Cox, T.; Valle, J.; Wadsley, J.; Propper, D.; Coxon, F.; Ross, P.; Madhusudan, S.; Roques, T.; et al. Gemcitabine and capecitabine with or without telomerase peptide vaccine GV1001 in patients with locally advanced or metastatic pancreatic cancer (TeloVac): An open-label, randomised, phase 3 trial. *Lancet Oncol.* **2014**, *15*, 829–840. [CrossRef]
231. Xie, C.; Duffy, A.G.; Brar, G.; Fioravanti, S.; Mabry-Hrones, D.; Walker, M.; Bonilla, C.M.; Wood, B.J.; Citrin, D.E.; Gil Ramirez, E.M.; et al. Immune Checkpoint Blockade in Combination with Stereotactic Body Radiotherapy in Patients with Metastatic Pancreatic Ductal Adenocarcinoma. *Clin. Cancer Res.* **2020**, *26*, 2318–2326. [CrossRef] [PubMed]
232. O'Reilly, E.M.; Oh, D.-Y.; Dhani, N.; Renouf, D.J.; Lee, M.A.; Sun, W.; Fisher, G.; Hezel, A.; Chang, S.-C.; Vlahovic, G.; et al. Durvalumab With or Without Tremelimumab for Patients With Metastatic Pancreatic Ductal Adenocarcinoma: A Phase 2 Randomized Clinical Trial. *JAMA Oncol.* **2019**, *5*, 1431–1438. [CrossRef]
233. Mahalingam, D.; Goel, S.; Aparo, S.; Arora, S.P.; Noronha, N.; Tran, H.; Chakrabarty, R.; Selvaggi, G.; Gutierrez, A.; Coffey, M.; et al. A Phase II Study of Pelareorep (REOLYSIN®) in Combination with Gemcitabine for Patients with Advanced Pancreatic Adenocarcinoma. *Cancers* **2018**, *10*, 160. [CrossRef]
234. Bockorny, B.; Semenisty, V.; Macarulla, T.; Borazanci, E.; Wolpin, B.M.; Stemmer, S.M.; Golan, T.; Geva, R.; Borad, M.J.; Pedersen, K.S.; et al. BL-8040, a CXCR4 antagonist, in combination with pembrolizumab and chemotherapy for pancreatic cancer: The COMBAT trial. *Nat. Med.* **2020**, *26*, 878–885. [CrossRef] [PubMed]
235. Tsujikawa, T.; Crocenzi, T.; Durham, J.N.; Sugar, E.A.; Wu, A.A.; Onners, B.; Nauroth, J.M.; Anders, R.A.; Fertig, E.J.; Laheru, D.A.; et al. Evaluation of Cyclophosphamide/GVAX Pancreas Followed by Listeria-Mesothelin (CRS-207) with or without Nivolumab in Patients with Pancreatic Cancer. *Clin. Cancer Res.* **2020**, *26*, 3578–3588. [CrossRef] [PubMed]
236. Wu, A.A.; Bever, K.M.; Ho, W.J.; Fertig, E.J.; Niu, N.; Zheng, L.; Parkinson, R.M.; Durham, J.N.; Onners, B.L.; Ferguson, A.K.; et al. A Phase II Study of Allogeneic GM-CSF–Transfected Pancreatic Tumor Vaccine (GVAX) with Ipilimumab as Maintenance Treatment for Metastatic Pancreatic Cancer. *Clin. Cancer Res.* **2020**, *26*, 5129–5139. [CrossRef] [PubMed]
237. Oberg, H.-H.; Kellner, C.; Gonnermann, D.; Sebens, S.; Bauerschlag, D.; Gramatzki, M.; Kabelitz, D.; Peipp, M.; Wesch, D. Tribody [(HER2)2xCD16] Is More Effective Than Trastuzumab in Enhancing γδ T Cell and Natural Killer Cell Cytotoxicity Against HER2-Expressing Cancer Cells. *Front. Immunol.* **2018**, *9*, 814. [CrossRef]
238. Oberg, H.-H.; Kellner, C.; Peipp, M.; Sebens, S.; Adam-Klages, S.; Gramatzki, M.; Kabelitz, D.; Wesch, D. Monitoring Circulating γδ T Cells in Cancer Patients to Optimize γδ T Cell-Based Immunotherapy. *Front. Immunol.* **2014**, *5*, 643. [CrossRef]
239. Kvarnhammar, A.M.; Veitonmäki, N.; Hägerbrand, K.; Dahlman, A.; Smith, K.E.; Fritzell, S.; Von Schantz, L.; Thagesson, M.; Werchau, D.; Smedenfors, K.; et al. The CTLA-4 x OX40 bispecific antibody ATOR-1015 induces anti-tumor effects through tumor-directed immune activation. *J. Immunother. Cancer* **2019**, *7*, 103. [CrossRef]
240. Zhang, Y.; Lazarus, J.; Steele, N.G.; Yan, W.; Lee, H.-J.; Nwosu, Z.C.; Halbrook, C.J.; Menjivar, R.; Kemp, S.B.; Sirihorachai, V.R.; et al. Regulatory T-cell Depletion Alters the Tumor Microenvironment and Accelerates Pancreatic Carcinogenesis. *Cancer Discov.* **2020**, *10*, 422–439. [CrossRef]
241. Chen, D.S.; Mellman, I. Elements of cancer immunity and the cancer–immune set point. *Nature* **2017**, *541*, 321–330. [CrossRef]
242. Barău, A.; Ruiz-Sauri, A.; Valencia, G.; Gómez-Mateo, M.D.C.; Sabater, L.; Ferrández, A.; Llombart-Bosch, A. High microvessel density in pancreatic ductal adenocarcinoma is associated with high grade. *Virchows Archiv.* **2013**, *462*, 541–546. [CrossRef]
243. Van Der Zee, J.A.; Van Eijck, C.H.; Hop, W.C.; Van Dekken, H.; Dicheva, B.M.; Seynhaeve, A.L.; Koning, G.A.; Eggermont, A.M.; Hagen, T.L.T. Angiogenesis: A prognostic determinant in pancreatic cancer? *Eur. J. Cancer* **2011**, *47*, 2576–2584. [CrossRef]
244. Wang, W.-Q.; Liu, L.; Xu, H.-X.; Luo, G.; Chen, T.; Wu, C.-T.; Xu, Y.-F.; Xu, J.; Liu, C.; Zhang, B.; et al. Intratumoral α-SMA Enhances the Prognostic Potency of CD34 Associated with Maintenance of Microvessel Integrity in Hepatocellular Carcinoma and Pancreatic Cancer. *PLoS ONE* **2013**, *8*, e71189. [CrossRef]
245. Yamakawa, M.; Liu, L.X.; Date, T.; Belanger, A.J.; Vincent, K.A.; Akita, G.Y.; Kuriyama, T.; Cheng, S.H.; Gregory, R.J.; Jiang, C. Hypoxia-Inducible Factor-1 Mediates Activation of Cultured Vascular Endothelial Cells by Inducing Multiple Angiogenic Factors. *Circ. Res.* **2003**, *93*, 664–673. [CrossRef]
246. Masamune, A.; Kikuta, K.; Watanabe, T.; Satoh, K.; Hirota, M.; Shimosegawa, T. Hypoxia stimulates pancreatic stellate cells to induce fibrosis and angiogenesis in pancreatic cancer. *Am. J. Physiol. Liver Physiol.* **2008**, *295*, G709–G717. [CrossRef]
247. Li, S.; Xu, H.-X.; Wu, C.-T.; Wang, W.-Q.; Jin, W.; Gao, H.-L.; Li, H.; Zhang, S.-R.; Xu, J.-Z.; Qi, Z.-H.; et al. Angiogenesis in pancreatic cancer: Current research status and clinical implications. *Angiogenesis* **2019**, *22*, 15–36. [CrossRef]
248. Carmeliet, P.; Jain, R.K. Angiogenesis in cancer and other diseases. *Nature* **2000**, *407*, 249–257. [CrossRef] [PubMed]
249. Dudley, A.C. Tumor Endothelial Cells. *Cold Spring Harb. Perspect. Med.* **2011**, *2*, a006536. [CrossRef] [PubMed]
250. Lugano, R.; Ramachandran, M.; Dimberg, A. Tumor angiogenesis: Causes, consequences, challenges and opportunities. *Cell. Mol. Life Sci.* **2019**, *77*, 1745–1770. [CrossRef] [PubMed]

251. Hida, K.; Maishi, N.; Annan, D.A.; Hida, Y. Contribution of Tumor Endothelial Cells in Cancer Progression. *Int. J. Mol. Sci.* **2018**, *19*, 1272. [CrossRef] [PubMed]
252. Cheng, H.-W.; Chen, Y.-F.; Wong, J.-M.; Weng, C.-W.; Chen, H.-Y.; Yu, S.-L.; Chen, H.-W.; Yuan, A.; Chen, J.J. Cancer cells increase endothelial cell tube formation and survival by activating the PI3K/Akt signalling pathway. *J. Exp. Clin. Cancer Res.* **2017**, *36*, 1–13. [CrossRef] [PubMed]
253. Xiong, Y.-Q.; Sun, H.-C.; Zhang, W.; Zhu, X.-D.; Zhuang, P.-Y.; Zhang, J.-B.; Wang, L.; Wu, W.-Z.; Qin, L.-X.; Tang, Z.-Y. Human Hepatocellular Carcinoma Tumor–derived Endothelial Cells Manifest Increased Angiogenesis Capability and Drug Resistance Compared with Normal Endothelial Cells. *Clin. Cancer Res.* **2009**, *15*, 4838–4846. [CrossRef] [PubMed]
254. Hida, K.; Hida, Y.; Amin, D.N.; Flint, A.F.; Panigrahy, D.; Morton, C.C.; Klagsbrun, M. Tumor-Associated Endothelial Cells with Cytogenetic Abnormalities. *Cancer Res.* **2004**, *64*, 8249–8255. [CrossRef] [PubMed]
255. Ohga, N.; Ishikawa, S.; Maishi, N.; Akiyama, K.; Hida, Y.; Kawamoto, T.; Sadamoto, Y.; Osawa, T.; Yamamoto, K.; Kondoh, M.; et al. Heterogeneity of Tumor Endothelial Cells. *Am. J. Pathol.* **2012**, *180*, 1294–1307. [CrossRef]
256. Alessandri, G.; Chirivi, R.G.; Fiorentini, S.; Dossi, R.; Bonardelli, S.; Giulini, S.M.; Zanetta, G.; Landoni, F.; Graziotti, P.P.; Turano, A.; et al. Phenotypic and functional characteristics of tumour-derived microvascular endothelial cells. *Clin. Exp. Metastasis* **1999**, *17*, 655–662. [CrossRef]
257. Ruscetti, M.; Morris, J.P.; Mezzadra, R.; Russell, J.; Leibold, J.; Romesser, P.B.; Simon, J.; Kulick, A.; Ho, Y.-J.; Fennell, M.; et al. Senescence-Induced Vascular Remodeling Creates Therapeutic Vulnerabilities in Pancreas Cancer. *Cell* **2020**, *181*, 424–441.e21. [CrossRef]
258. Zhao, Q.; Eichten, A.; Parveen, A.; Adler, C.; Huang, Y.; Wang, W.; Ding, Y.; Adler, A.; Nevins, T.; Ni, M.; et al. Single-Cell Transcriptome Analyses Reveal Endothelial Cell Heterogeneity in Tumors and Changes following Antiangiogenic Treatment. *Cancer Res.* **2018**, *78*, 2370–2382. [CrossRef]
259. Hida, K.; Maishi, N.; Sakurai, Y.; Hida, Y.; Harashima, H. Heterogeneity of tumor endothelial cells and drug delivery. *Adv. Drug Deliv. Rev.* **2016**, *99*, 140–147. [CrossRef]
260. Maishi, N.; Hida, K. Tumor endothelial cells accelerate tumor metastasis. *Cancer Sci.* **2017**, *108*, 1921–1926. [CrossRef] [PubMed]
261. Adjuto-Saccone, M.; Soubeyran, P.; Garcia, J.; Audebert, S.; Camoin, L.; Rubis, M.; Roques, J.; Binétruy, B.; Iovanna, J.L.; Tournaire, R. TNF-α induces endothelial–mesenchymal transition promoting stromal development of pancreatic adenocarcinoma. *Cell Death Dis.* **2021**, *12*, 1–15. [CrossRef]
262. Choi, K.J.; Nam, J.-K.; Kim, J.-H.; Choi, S.-H.; Lee, Y.-J. Endothelial-to-mesenchymal transition in anticancer therapy and normal tissue damage. *Exp. Mol. Med.* **2020**, *52*, 781–792. [CrossRef]
263. Garcia, J.; Sandí, M.J.; Cordelier, P.; Binétruy, B.; Pouysségur, J.; Iovanna, J.L.; Tournaire, R. Tie1 deficiency induces endothelial–mesenchymal transition. *EMBO Rep.* **2012**, *13*, 431–439. [CrossRef]
264. Issa, Y.; Nummer, D.; Seibel, T.; Müerköster, S.S.; Koch, M.; Schmitz-Winnenthal, F.-H.; Galindo, L.; Weitz, J.; Beckhove, P.; Altevogt, P. Enhanced L1CAM expression on pancreatic tumor endothelium mediates selective tumor cell transmigration. *J. Mol. Med.* **2008**, *87*, 99–112. [CrossRef]
265. Sano, M.; Takahashi, R.; Ijichi, H.; Ishigaki, K.; Yamada, T.; Miyabayashi, K.; Kimura, G.; Mizuno, S.; Kato, H.; Fujiwara, H.; et al. Blocking VCAM-1 inhibits pancreatic tumour progression and cancer-associated thrombosis/thromboembolism. *Gut* **2021**, *70*, 1713–1723. [CrossRef]
266. Nummer, D.; Suri-Payer, E.; Schmitz-Winnenthal, H.; Bonertz, A.; Galindo, L.; Antolovich, D.; Koch, M.; Büchler, M.; Weitz, J.; Schirrmacher, V.; et al. Role of Tumor Endothelium in CD4+CD25+ Regulatory T Cell Infiltration of Human Pancreatic Carcinoma. *J. Natl. Cancer Inst.* **2007**, *99*, 1188–1199. [CrossRef] [PubMed]
267. Harjunpää, H.; Asens, M.L.; Guenther, C.; Fagerholm, S.C. Cell Adhesion Molecules and Their Roles and Regulation in the Immune and Tumor Microenvironment. *Front. Immunol.* **2019**, *10*, 1078. [CrossRef] [PubMed]
268. Klein, D. The Tumor Vascular Endothelium as Decision Maker in Cancer Therapy. *Front. Oncol.* **2018**, *8*, 367. [CrossRef]
269. Orozco, C.A.; Bosch, N.M.; Guerrero, P.E.; Vinaixa, J.; Dalotto-Moreno, T.; Iglesias, M.; Moreno, M.; Djurec, M.; Poirier, F.; Gabius, H.-J.; et al. Targeting galectin-1 inhibits pancreatic cancer progression by modulating tumor–stroma crosstalk. *Proc. Natl. Acad. Sci.* **2018**, *115*, E3769–E3778. [CrossRef]
270. Hotz, H. Angiogenesis inhibitor TNP-470 reduces human pancreatic cancer growth. *J. Gastrointest. Surg.* **2001**, *5*, 131–138. [CrossRef]
271. Kato, H.; Ishikura, H.; Kawarada, Y.; Furuya, M.; Kondo, S.; Kato, H.; Yoshiki, T. Anti-angiogenic Treatment for Peritoneal Dissemination of Pancreas Adenocarcinoma: A Study Using TNP-470. *Jpn. J. Cancer Res.* **2001**, *92*, 67–73. [CrossRef]
272. Martin, L.K.; Li, X.; Kleiber, B.; Ellison, E.C.; Bloomston, M.; Zalupski, M.; Bekaii-Saab, T.S. VEGF remains an interesting target in advanced pancreas cancer (APCA): Results of a multi-institutional phase II study of bevacizumab, gemcitabine, and infusional 5-fluorouracil in patients with APCA. *Ann. Oncol.* **2012**, *23*, 2812–2820. [CrossRef] [PubMed]
273. Gilles, M.-E.; Maione, F.; Cossutta, M.; Carpentier, G.; Caruana, L.; Di Maria, S.; Houppe, C.; Destouches, D.; Shchors, K.; Prochasson, C.; et al. Nucleolin Targeting Impairs the Progression of Pancreatic Cancer and Promotes the Normalization of Tumor Vasculature. *Cancer Res.* **2016**, *76*, 7181–7193. [CrossRef] [PubMed]
274. Viallard, C.; Larrivée, B. Tumor angiogenesis and vascular normalization: Alternative therapeutic targets. *Angiogenesis* **2017**, *20*, 409–426. [CrossRef] [PubMed]

275. Mazzone, M.; Dettori, D.; de Oliveira, R.L.; Loges, S.; Schmidt, T.; Jonckx, B.; Tian, Y.-M.; Lanahan, A.A.; Pollard, P.; de Almodovar, C.R.; et al. Heterozygous Deficiency of PHD2 Restores Tumor Oxygenation and Inhibits Metastasis via Endothelial Normalization. *Cell* **2009**, *136*, 839–851. [CrossRef] [PubMed]
276. Cartier, A.; Leigh, T.; Liu, C.H.; Hla, T. Endothelial sphingosine 1-phosphate receptors promote vascular normalization and antitumor therapy. *Proc. Natl. Acad. Sci.* **2020**, *117*, 3157–3166. [CrossRef] [PubMed]
277. Ivy, S.P.; Wick, J.Y.; Kaufman, B.M. An overview of small-molecule inhibitors of VEGFR signaling. *Nat. Rev. Clin. Oncol.* **2009**, *6*, 569–579. [CrossRef] [PubMed]
278. Ottaiano, A.; Capozzi, M.; De Divitiis, C.; De Stefano, A.; Botti, G.; Avallone, A.; Tafuto, S. Gemcitabine mono-therapy versus gemcitabine plus targeted therapy in advanced pancreatic cancer: A meta-analysis of randomized phase III trials. *Acta Oncol.* **2017**, *56*, 377–383. [CrossRef]
279. Kindler, H.L.; Niedzwiecki, D.; Hollis, D.; Sutherland, S.; Schrag, D.; Hurwitz, H.; Innocenti, F.; Mulcahy, M.F.; O'Reilly, E.; Wozniak, T.F.; et al. Gemcitabine Plus Bevacizumab Compared With Gemcitabine Plus Placebo in Patients With Advanced Pancreatic Cancer: Phase III Trial of the Cancer and Leukemia Group B (CALGB 80303). *J. Clin. Oncol.* **2010**, *28*, 3617–3622. [CrossRef]
280. Annese, T.; Tamma, R.; Ruggieri, S.; Ribatti, D. Angiogenesis in Pancreatic Cancer: Pre-Clinical and Clinical Studies. *Cancers* **2019**, *11*, 381. [CrossRef]
281. Miller, M.O.; Kashyap, P.C.; Becker, S.L.; Thomas, R.M.; Hodin, R.A.; Miller, G.; Hundeyin, M.; Pushalkar, S.; Cohen, D.; Saxena, D.; et al. SSAT State-of-the-Art Conference: Advancements in the Microbiome. *J. Gastrointest. Surg.* **2020**, *25*, 1–11. [CrossRef]
282. Thomas, H. Intra-tumour bacteria promote gemcitabine resistance in pancreatic adenocarcinoma. *Nat. Rev. Gastroenterol. Hepatol.* **2017**, *14*, 632. [CrossRef] [PubMed]
283. Gaiser, R.A.; Halimi, A.; Alkharaan, H.; Lu, L.; Davanian, H.; Healy, K.; Hugerth, L.W.; Ateeb, Z.; Valente, R.; Moro, C.F.; et al. Enrichment of oral microbiota in early cystic precursors to invasive pancreatic cancer. *Gut* **2019**, *68*, 2186–2194. [CrossRef] [PubMed]
284. Ciernikova, S.; Novisedlakova, M.; Cholujova, D.; Stevurkova, V.; Mego, M. The Emerging Role of Microbiota and Microbiome in Pancreatic Ductal Adenocarcinoma. *Biomedicines* **2020**, *8*, 565. [CrossRef]
285. Mitsuhashi, K.; Nosho, K.; Sukawa, Y.; Matsunaga, Y.; Ito, M.; Kurihara, H.; Kanno, S.; Igarashi, H.; Naito, T.; Adachi, Y.; et al. Association ofFusobacteriumspecies in pancreatic cancer tissues with molecular features and prognosis. *Oncotarget* **2015**, *6*, 7209–7220. [CrossRef]
286. Gopalakrishnan, V.; Spencer, C.N.; Nezi, L.; Reuben, A.; Andrews, M.C.; Karpinets, T.V.; Prieto, P.A.; Vicente, D.; Hoffman, K.; Wei, S.C.; et al. Gut microbiome modulates response to anti–PD-1 immunotherapy in melanoma patients. *Science* **2018**, *359*, 97–103. [CrossRef]
287. Matson, V.; Fessler, J.; Bao, R.; Chongsuwat, T.; Zha, Y.; Alegre, M.-L.; Luke, J.J.; Gajewski, T.F. The commensal microbiome is associated with anti–PD-1 efficacy in metastatic melanoma patients. *Science* **2018**, *359*, 104–108. [CrossRef]
288. Routy, B.; Le Chatelier, E.; DeRosa, L.; Duong, C.P.M.; Alou, M.T.; Daillère, R.; Fluckiger, A.; Messaoudene, M.; Rauber, C.; Roberti, M.P.; et al. Gut microbiome influences efficacy of PD-1–based immunotherapy against epithelial tumors. *Science* **2017**, *359*, 91–97. [CrossRef] [PubMed]
289. Kleeff, J.; Whitcomb, D.C.; Shimosegawa, T.; Esposito, I.; Lerch, M.M.; Gress, T.; Mayerle, J.; Drewes, A.; Rebours, V.; Akisik, F.; et al. Chronic pancreatitis. *Nat. Rev. Dis. Prim.* **2017**, *3*, 17060. [CrossRef] [PubMed]
290. Wei, M.-Y.; Shi, S.; Liang, C.; Meng, Q.C.; Hua, J.; Zhang, Y.-Y.; Liu, J.; Bo, Z.; Xu, J.; Yu, X.J. The microbiota and microbiome in pancreatic cancer: More influential than expected. *Mol. Cancer* **2019**, *18*, 97. [CrossRef] [PubMed]
291. Diakos, C.I.; Charles, K.A.; McMillan, D.C.; Clarke, S.J. Cancer-related inflammation and treatment effectiveness. *Lancet Oncol.* **2014**, *15*, e493–e503. [CrossRef]
292. Stone, M.L.; Beatty, G.L. Cellular determinants and therapeutic implications of inflammation in pancreatic cancer. *Pharmacol. Ther.* **2019**, *201*, 202–213. [CrossRef]
293. Pastushenko, I.; Blanpain, C. EMT Transition States during Tumor Progression and Metastasis. *Trends Cell Biol.* **2019**, *29*, 212–226. [CrossRef] [PubMed]
294. Hofman, P.; Vouret-Craviari, V. Microbes-induced EMT at the crossroad of inflammation and cancer. *Gut Microbes* **2012**, *3*, 176–185. [CrossRef]
295. Vergara, D.; Simeone, P.; Damato, M.; Maffia, M.; Lanuti, P.; Trerotola, M. The Cancer Microbiota: EMT and Inflammation as Shared Molecular Mechanisms Associated with Plasticity and Progression. *J. Oncol.* **2019**, *2019*, 1–16. [CrossRef]
296. Goebel, L.; Grage-Griebenow, E.; Gorys, A.; Helm, O.; Genrich, G.; Lenk, L.; Wesch, D.; Ungefroren, H.; Freitag-Wolf, S.; Sipos, B.; et al. CD4+T cells potently induce epithelial-mesenchymal-transition in premalignant and malignant pancreatic ductal epithelial cells–novel implications of CD4+T cells in pancreatic cancer development. *OncoImmunology* **2015**, *4*, e1000083. [CrossRef] [PubMed]
297. Rhim, A.D.; Mirek, E.T.; Aiello, N.M.; Maitra, A.; Bailey, J.M.; McAllister, F.; Reichert, M.; Beatty, G.L.; Rustgi, A.K.; Vonderheide, R.H.; et al. EMT and Dissemination Precede Pancreatic Tumor Formation. *Cell* **2012**, *148*, 349–361. [CrossRef]
298. Vétizou, M.; Pitt, J.M.; Daillère, R.; Lepage, P.; Waldschmitt, N.; Flament, C.; Rusakiewicz, S.; Routy, B.; Roberti, M.P.; Duong, C.P.M.; et al. Anticancer immunotherapy by CTLA-4 blockade relies on the gut microbiota. *Science* **2015**, *350*, 1079–1084. [CrossRef]

299. Tanoue, T.; Morita, S.; Plichta, D.R.; Skelly, A.N.; Suda, W.; Sugiura, Y.; Narushima, S.; Vlamakis, H.; Motoo, I.; Sugita, K.; et al. A defined commensal consortium elicits CD8 T cells and anti-cancer immunity. *Nature* **2019**, *565*, 600–605. [CrossRef] [PubMed]
300. Sivan, A.; Corrales, L.; Hubert, N.; Williams, J.B.; Aquino-Michaels, K.; Earley, Z.M.; Benyamin, F.W.; Lei, Y.M.; Jabri, B.; Alegre, M.L.; et al. Commensal Bifidobacterium Promotes Antitumor Immunity and Facilitates Anti-PD-L1 Efficacy. *Science* **2015**, *350*, 1084–1089. [CrossRef]
301. Froeling, F.; Casolino, R.; Pea, A.; Biankin, A.; Chang, D.; Precision-Panc, O.B.O. Molecular Subtyping and Precision Medicine for Pancreatic Cancer. *J. Clin. Med.* **2021**, *10*, 149. [CrossRef]
302. Ding, D.; Javed, A.A.; Cunningham, D.; Teinor, J.; Wright, M.; Javed, Z.N.; Wilt, C.; Parish, L.; Hodgin, M.; Ryan, A.; et al. Challenges of the current precision medicine approach for pancreatic cancer: A single institution experience between 2013 and 2017. *Cancer Lett.* **2021**, *497*, 221–228. [CrossRef] [PubMed]
303. Dreyer, S.; Jamieson, N.; Cooke, S.; Valle, J.; McKay, C.; Biankin, A.; Chang, D. PRECISION-Panc: The Next Generation Therapeutic Development Platform for Pancreatic Cancer. *Clin. Oncol.* **2020**, *32*, 1–4. [CrossRef]
304. Gore, J.; Korc, M. Pancreatic Cancer Stroma: Friend or Foe? *Cancer Cell* **2014**, *25*, 711–712. [CrossRef]
305. Jiang, H.; Torphy, R.J.; Steiger, K.; Hongo, H.; Ritchie, A.J.; Kriegsmann, M.; Horst, D.; Umetsu, S.E.; Joseph, N.M.; McGregor, K.; et al. Pancreatic ductal adenocarcinoma progression is restrained by stromal matrix. *J. Clin. Investig.* **2020**, *130*, 4704–4709. [CrossRef]
306. Dreyer, S.B.; Pinese, M.; Jamieson, N.B.; Scarlett, C.J.; Colvin, E.K.; Pajic, M.; Johns, A.L.; Humphris, J.L.; Wu, J.; Cowley, M.J.; et al. Precision Oncology in Surgery. *Ann. Surg.* **2018**, *272*, 366–376. [CrossRef] [PubMed]
307. Heredia-Soto, V.; Rodríguez-Salas, N.; Feliu, J. Liquid Biopsy in Pancreatic Cancer: Are We Ready to Apply It in the Clinical Practice? *Cancers* **2021**, *13*, 1986. [CrossRef] [PubMed]
308. Ho, W.J.; Jaffee, E.M.; Zheng, L. The tumour microenvironment in pancreatic cancer—Clinical challenges and opportunities. *Nat. Rev. Clin. Oncol.* **2020**, *17*, 527–540. [CrossRef] [PubMed]
309. Torphy, R.J.; Wang, Z.; True-Yasaki, A.; Volmar, K.E.; Rashid, N.; Yeh, B.; Johansen, J.S.; Hollingsworth, M.A.; Yeh, J.J.; Collisson, E.A. Stromal Content Is Correlated With Tissue Site, Contrast Retention, and Survival in Pancreatic Adenocarcinoma. *JCO Precis. Oncol.* **2018**, *2*, 1–12. [CrossRef]
310. Tripathi, A.; Kashyap, A.; Tripathi, G.; Yadav, J.; Bibban, R.; Aggarwal, N.; Thakur, K.; Chhokar, A.; Jadli, M.; Sah, A.K.; et al. Tumor reversion: A dream or a reality. *Biomark. Res.* **2021**, *9*, 1–27. [CrossRef]
311. Kocher, H.M.; Basu, B.; Froeling, F.E.M.; Sarker, D.; Slater, S.; Carlin, D.; Desouza, N.M.; De Paepe, K.N.; Goulart, M.R.; Hughes, C.; et al. Phase I clinical trial repurposing all-trans retinoic acid as a stromal targeting agent for pancreatic cancer. *Nat. Commun.* **2020**, *11*, 1–9. [CrossRef]